

PERFORMANCE OF GEOTEXTILE-REINFORCED SOIL STRUCTURES

by

Jorge Gabriel Zornberg

B.S. (Universidad Nacional de Córdoba, Argentina) 1987

M. Eng. (Pontifícia Universidade Católica do Rio de Janeiro, Brazil) 1989

A dissertation submitted in partial satisfaction of the

requirements for the degree of

Doctor of Philosophy

in

Engineering-Civil Engineering

in the

GRADUATE DIVISION

of the

UNIVERSITY of CALIFORNIA at BERKELEY

Committee in charge:

Professor James K. Mitchell, Chair

Professor Nicholas Sitar

Professor Neville G. W. Cook

1994

The dissertation of Jorge Gabriel Zornberg is approved:

Chair James K. Mitchell December 9, 1994
Date

Nicholas Sitar December 8, 1994
Date

Neville G. W. Cook December 8, 1994
Date

University of California at Berkeley

1994

Performance of Geotextile-Reinforced Soil Structures

Copyright © 1994

by

Jorge Gabriel Zornberg

Abstract

Performance of geotextile-reinforced soil structures

by

Jorge Gabriel Zornberg

Doctor of Philosophy in Civil Engineering
University of California at Berkeley

Professor James K. Mitchell, Chair

The increasing use of geotextile-reinforced soil systems for important earth structures requires proper understanding of their behavior and validation of the assumptions in their design. Geotextile reinforcement materials are particularly useful in reinforced soil systems built using indigenous backfill soils, which may be finer grained, more plastic and less permeable than fill materials commonly specified in soil reinforcement practice. Four aspects of the performance of geotextile-reinforced soil structures were investigated by performing: (1) An evaluation study of the suitability of poorly draining soils for reinforced soil structures; (2) a finite element study on the deformability and design aspects of geotextile-reinforced soil walls; (3) a centrifuge study on the failure mechanisms and on the suitability of limit equilibrium methods to predict failure of geotextile-reinforced soil slopes; and (4) a field instrumentation study to evaluate the performance of a permanent geotextile-reinforced slope built using decomposed granite as backfill material. Each analysis provides specific lessons useful for understanding the performance of the engineered composite material which is reinforced soil. Collectively, they illustrate that the behavior of reinforced soil structures (and probably of earth structures in general) may defy characterization by a single method of analysis. Instead, by complementing strengths and limitations of different approaches, good understanding of many facets in the performance of a geotechnical structure can be achieved.

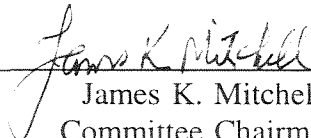
The evaluation of experimental and analytical studies undertaken to investigate the cohesive soil-reinforcement interaction and the reinforcement drainage characteristics shows that permeable inclusions can effectively reinforce clay structures. This conclusion is strengthened by lessons learned from case histories of structures constructed using marginal soils. Benefits and applications of

reinforcing poorly draining backfills are addressed, and research needs aimed at formulating a consistent design methodology for these structures are presented.

The finite element study investigates the deformability of geotextile-reinforced soil structures and the effect of backfill slope on the performance of geosynthetically reinforced walls. The methodology involves initial validation of the numerical model against instrumentation records from a full-scale wall and subsequent parametric study of different wall and surcharge configurations. Good agreement is observed between field and numerical results. For practical purposes, the location of the potential planar failure surface is found to be independent of the presence of a sloping backfill on the top of the wall.

Geotextile-reinforced slope models were tested in a geotechnical centrifuge to identify the possible failure mechanisms and to verify the ability of limit equilibrium methods to predict the experimental results. Failure of the centrifuge models initiated at midheight of the slope, and always occurred due to geotextile breakage without evidence of pullout. Important contribution to the stability of the models was provided by the overlapping geotextile layers. Additionally, the stability of the reinforced slopes was found to be governed by the peak and not by the critical state strength of the soil. Moreover, centrifuge testing provides much needed evidence that existing limit equilibrium methodologies adequately predict the performance of geotextile-reinforced soil structures at failure.

The performance of a permanent geotextile-reinforced slope 15.3 m high is finally investigated. Several characteristics were unique to the slope design: the structure was higher than usual geotextile slopes, it involved the use of both a high modulus composite and a nonwoven geotextile, and it was constructed using indigenous soils (decomposed granite) as backfill material. Small global deflections and low geotextile strain levels occurred both during the construction period and during post-construction, after the spring thaw. Pore water measurements indicate appropriate drainage of seepage water from the backslope of the structure. Overall, the instrumentation results are in agreement with the design assumptions, providing insight into the mechanisms that dominate the slope behavior.


James K. Mitchell
Committee Chairman

To Denise, Giselle, and Leonardo.

TABLE OF CONTENTS

CHAPTER 1

INTRODUCTION	1
1.1 Why reinforcements in earthwork construction?	2
1.2 Why geotextiles as reinforcements?	5
1.3 Methods to investigate the performance of geotextile-reinforced soil structures	7
1.4 Scope of the dissertation	10
References	12

CHAPTER 2

PERFORMANCE OF GEOTEXTILE-REINFORCED SOIL STRUCTURES WITH POORLY DRAINING BACKFILLS: AN EVALUATION STUDY ...	14
2.1 Introduction	14
2.2 Current standards for backfill materials in reinforced soil structures	17
2.3 Interaction mechanisms observed using triaxial tests	19
2.4 Interaction mechanisms observed using shearbox and pullout tests	27
2.4.1 Poorly draining soil-metallic reinforcement interaction	27
2.4.2 Poorly draining soil-geogrid interaction	36
2.4.3 Poorly draining soil-geotextile interaction	39
2.4.4 Poorly draining soil-geomembrane interaction	44
2.5 Hydraulic function of geosynthetic reinforcements	49
2.5.1 Determination of in-plane hydraulic conductivity	50
2.5.2 Analysis of pore water pressure dissipation	53
2.5.3 Effect of lateral drainage on stability	57
2.6 Additional considerations for geosynthetics embedded in poorly draining backfills	61
2.6.1 Confined mechanical properties	61
2.6.2 Durability	63
2.6.3 Creep	65
2.7 Lessons learned from case histories	67
2.7.1 General considerations	67
2.7.2 Pore water pressure generation in reinforced fills	74
2.7.2.1 Structures reinforced using impermeable elements ..	74
2.7.2.2 Structures reinforced using permeable elements ...	81
2.7.3 Modes and causes of failure	85
2.7.3.1 Structures reinforced using impermeable elements ..	85
2.7.3.2 Structures reinforced using permeable elements ...	90

2.7.4	Displacement evaluation	95
2.7.4.1	Structures reinforced using impermeable elements	95
2.7.4.2	Structures reinforced using permeable elements	98
2.8	Benefits and potential applications of poorly draining backfills in reinforced soil construction	102
2.9	Research needs	110
2.10	Conclusions	114
	References	117

CHAPTER 3

	PERFORMANCE OF GEOTEXTILE-REINFORCED SOIL STRUCTURES WITH SLOPING BACKFILLS: A FINITE ELEMENT STUDY	135
3.1	Introduction	135
3.2	Finite element analysis of reinforced soil structures	139
3.2.1	General Considerations	139
3.2.2	Validation of the finite element model used in this study	140
3.2.3	Key issues to be considered for modeling soil structures reinforced with extensible inclusions	146
3.3	Finite element analysis of the Rainier Ave. wall	149
3.3.1	Wall description and available instrumentation records	150
3.3.2	Modeling characteristics	156
3.3.2.1	Mesh layout	158
3.3.2.2	Hyperbolic soil parameters	162
3.3.2.3	Reinforcement material parameters	170
3.3.2.4	Parameters for interface and structural facing elements	173
3.3.2.5	Incremental analysis sequence	175
3.3.3	Results from the analysis	176
3.3.3.1	Calibration process for selection of geotextile parameters	176
3.3.3.2	Tension distribution along the reinforcements	180
3.3.3.3	Lateral wall displacements	181
3.3.3.4	Stress distribution in the soil mass	187
3.3.3.5	Location and magnitude of maximum reinforcement tensions	195
3.3.4	Location of the critical planar surface in the Rainier Ave. wall	199
3.4	Parametric study: Effect of sloping backfills on geosynthetically reinforced soil walls	208
3.4.1	Effect of sloping backfill geometry	208
3.4.2	Effect of wall design characteristics	216
3.5	Conclusions	221
	References	225

CHAPTER 4

PERFORMANCE OF GEOTEXTILE-REINFORCED SOIL STRUCTURES		
AT FAILURE: A CENTRIFUGE STUDY		232
4.1	Introduction	232
4.2	Centrifuge testing of reinforced soil structures	235
4.2.1	General	235
4.2.2	Scaling laws	237
4.2.3	Previous centrifuge studies on reinforced soil structures	246
4.3	Description of the centrifuge testing scheme	253
4.3.1	Geotechnical centrifuge	254
4.3.2	Characteristics of the reinforced slope models	254
4.3.3	Construction of the models	258
4.3.4	Measurements	263
4.3.5	Test procedure	266
4.3.6	Effective radius for evaluation of g-level	268
4.4	Material properties	271
4.4.1	Backfill soil	271
4.4.1.1	Sand characterization	271
4.4.1.2	A note on the estimation of plane strain friction angles	273
4.4.1.3	Shear strength properties	276
4.4.2	Geotextile reinforcements	281
4.4.2.1	Geotextile characterization	281
4.4.2.2	A note on the interpretation of wide width tensile test results	284
4.4.2.3	Tensile strength properties	289
4.4.3	Interface properties	303
4.4.3.1	Test setup	303
4.4.3.2	Interface strength results	306
4.5	Experimental results	311
4.5.1	Scope of the testing program	311
4.5.2	Centrifuge test results	313
4.5.2.1	Baseline B-series	313
4.5.2.2	Denser soil D-series	324
4.5.2.3	Stronger geotextile S-series	331
4.6	Interpretation of the experimental results	334
4.6.1	Normalization of results: Summation of reinforcement forces	336
4.6.2	Characteristics of the failure surfaces	340
4.6.2.1	Development of failure	341
4.6.2.2	Location of the potential failure surfaces	347
4.6.3	Interpretation of the failure mechanisms	349
4.6.4	Additional design aspects	358
4.6.4.1	Displacement evaluation	358
4.6.4.2	Evaluation of pullout safety	363

	4.6.4.3	Selection of soil strength parameters	365
4.7		Limit equilibrium analyses	367
	4.7.1	General	367
	4.7.2	Evaluation of modeling assumptions in limit equilibrium . .	369
		4.7.2.1 Effect of geotextile tensile strength	370
		4.7.2.2 Effect of nonuniform unit weight	375
		4.7.2.3 Effect of orientation of reinforcement forces	377
		4.7.2.4 Effect of geotextile overlaps	380
		4.7.2.5 Effect of wall friction at model boundaries	382
		4.7.2.6 Influence of the selected slope stability method of analysis	390
	4.7.3	Comparison between predicted and experimental results . .	393
		4.7.3.1 Characteristics of the analyses	393
		4.7.3.2 Experimental and predicted g-levels at failure	394
		4.7.3.3 Experimental and predicted location of failure surfaces	395
		4.7.3.4 Evaluation of in-soil geotextile tensile strength . . .	409
	4.7.4	Remarks on the suitability of limit equilibrium for the analysis of reinforced soil slopes	412
4.8		Conclusions	418
		References	421

CHAPTER 5

PERFORMANCE OF GEOTEXTILE-REINFORCED SOIL STRUCTURES UNDER WORKING STRESS CONDITIONS: A FIELD INSTRUMENTATION STUDY

			433
5.1		Introduction	433
5.2		Design considerations	435
	5.2.1	Site description	435
	5.2.2	Use of indigenous soils	437
	5.2.3	Basis for geotextile selection	437
	5.2.4	Design methodology	439
	5.2.5	Reinforcement layout	439
5.3		Construction	443
5.4		Instrumentation program	447
5.5		Instrumentation results	454
	5.5.1	Global structure deformations	456
		5.5.1.1 Construction period	456
		5.5.1.2 Early post-construction period	462
		5.5.1.3 Spring measurements	462
	5.5.2	Geotextile strain distribution	469
		5.5.2.1 Construction period	470
		5.5.2.2 Early post-construction period	474
		5.5.2.3 Spring measurements	479

5.5.3	Cross-check of displacement measurements	481
5.5.4	Pore water pressures	484
5.6	Implications for design	486
5.6.1	Suitability of current design approach	486
5.6.2	Geotextile strain levels	487
5.6.3	Global structure deformation and post-construction performance	489
5.6.4	Ability of geotextile reinforcements to control pore water pressures in the fill	489
5.6.5	Additional considerations	490
5.7	Conclusions	491
	References	493

CHAPTER 6

SUMMARY AND CONCLUSIONS	496
Reference	504

LIST OF FIGURES

Figure 1.1 - Alternative designs for earth retaining structures	4
Figure 2.1 - Effect of reinforcement spacing on strength ratio for rapid shearing of saturated clay specimens with permeable reinforcements (after Ingold and Miller, 1982)	22
Figure 2.2 - Effect of reinforcement spacing on strength ratio for constant volume shearing of kaolin specimens reinforced with porous plastic (after Ingold and Miller, 1982)	22
Figure 2.3 - Stress-strain behavior of reinforced kaolin specimens during drained triaxial loading (cell pressure 250 kPa) (after Ingold and Miller, 1983) . . .	24
Figure 2.4 - Variation of strength ratio with degree of saturation for rapid triaxial tests on kaolin specimens with impermeable reinforcements (after Ingold, 1985)	24
Figure 2.5 - Strip pullout capacity versus normal pressure for soils with different fines content (redrawn after Elias and Swanson, 1983)	33
Figure 2.6 - Strip pullout capacity versus normal pressure for samples at two water contents (redrawn after Elias and Swanson, 1983)	33
Figure 2.7 - Typical load-displacement curves from pullout tests using welded-wire steel grids in weathered clay (after Bergado et al., 1992b)	35
Figure 2.8 - Load-displacement curves from pullout tests on polymer geogrids (after Christopher and Berg, 1990)	40
Figure 2.9 - Direct shear test results for three types of geotextile in a plastic clay (moisture content 40%) (after Lafleur et al., 1987)	40
Figure 2.10 - Effect of water content on the pullout resistance of a woven geotextile in a plastic clay (after Gilbert et al., 1992)	43
Figure 2.11 - Pullout resistance of a woven geotextile versus normal load in clay specimens molded (a) at 26% water content; (b) at 40% water content (after Gilbert et al., 1992)	45
Figure 2.12 - Shear strengths for smooth HDPE-compacted clayey till interfaces: (a) as-compacted samples; (b) samples sheared after initial pre-soaking (after Seed and Boulanger, 1991)	48
Figure 2.13 - Relationship between coefficient of in-plane hydraulic conductivity and effective normal stress for a nonwoven geotextile (after Ling et al., 1993)	52
Figure 2.14 - In-plane hydraulic conductivity of fresh and retrieved nonwoven geotextile specimens (after Ling et al., 1993)	52
Figure 2.15 - Embankment section showing the semi-layer under study (after Auriault et al., 1977)	54
Figure 2.16 - Diagrams of pore water pressure dissipation determined numerically for a silty backfill (after Bourdillon et al., 1977)	55
Figure 2.17 - Multiple strip-sandwich method using geotextile-quicklime composite stripes in a clay embankment (after Yamanouchi et al., 1982) . .	57

Figure 2.18 - Effect of pore water pressures on the stability of a reinforced soil structure	60
Figure 2.19 - Load-extension characteristics of plastic strips tested after eight years of burial in cohesive soil (after Temporal et al., 1989)	64
Figure 2.20 - Transport and Road Research Laboratory (TRRL) experimental reinforced wall (after Boden et al., 1978)	76
Figure 2.21 - Vertical distribution of pore water pressure in the lower cohesive layer of the TRRL experimental wall (after Murray and Boden, 1979)	77
Figure 2.22 - Instrumentation in Devon test fill (after Scott et al., 1987)	78
Figure 2.23 - Field measurements, 3 m above base and at various distances from slope face, within embankment and geogrids of Devon test fill: (a) fill height; (b) horizontal displacements; (c) settlements; (d) pore pressures; (e) geogrid strains (after Sego et al., 1990)	79
Figure 2.24 - Pore water pressures (u) recorded in the Rouen reinforced wall, along a woven and a nonwoven/geogrid composite, at different locations within the silty backfill (redrawn after Perrier et al., 1986)	82
Figure 2.25 - Variation of pore pressure during rainfall in a clay embankment reinforced with nonwoven geotextiles: (a) rainfall recorded; (b) pore water pressures (after Tatsuoka and Yamauchi, 1986)	84
Figure 2.26 - Arrangement of reinforcements in a clay wall model (after Ingold, 1981)	86
Figure 2.27 - Moisture content and percentage fines for damaged and undamaged walls reinforced with metallic strips (after Elias and Swanson, 1983)	88
Figure 2.28 - Configuration of welded wire wall on Interstate 580, California (after Mitchell and Villet, 1987)	89
Figure 2.29 - Horizontal displacements versus depth recorded at a geogrid reinforced wall (after Burwash and Frost, 1991)	90
Figure 2.30 - Sequence of failure for centrifuge models of kaolin clay reinforced with nonwoven geotextiles: (a) lightly reinforced model; (b) intermediate reinforced model; (c) heavily reinforced model (after Goodings, 1990)	92
Figure 2.31 - Cross-section of clay Test Embankment II, observed at dismantling (after Yamauchi et al., 1987)	94
Figure 2.32 - Schematic diagram showing deformation of right-hand slope of Test Embankment II in Figure 2.31 (after Yamauchi et al., 1987)	94
Figure 2.33 - Curve for estimation of lateral displacement anticipated at the end of construction of reinforced walls (after Mitchell and Christopher, 1990)	96
Figure 2.34 - Load-horizontal displacement curves of reinforced and unreinforced clay wall models (after Fabian and Fourie, 1988)	99
Figure 2.35 - Geotextile reinforced wall on Autoroute A15, France (after Puig and Blivet, 1973)	100
Figure 2.36 - Water infiltration in a reinforced slope for road widening projects	105
Figure 2.37 - Flow regime for embankment: (a) on an impermeable base; (b) on a pervious base (after Ingold, 1992)	106

Figure 2.38 - Effect of nonwoven geotextile spacing on compaction curves for reinforced clay specimens (after Indraratna et al., 1991)	109
Figure 3.1 - Reinforced soil wall with sloping backfill showing potential failure surface assumed in conventional design	138
Figure 3.2 - Instrumentation of the Rainier Ave. wall. Dimensions are in meters (after Christopher et al., 1990)	153
Figure 3.3 - Distribution of strains in each instrumented layer on the Rainier Ave. wall (after Christopher et al., 1990)	155
Figure 3.4 - Inclinomater records on the Rainier Ave. wall (after Christopher et al., 1990)	157
Figure 3.5 - Incremental movement of the wall face as determined by optical and photogrammetric surveys at the completion of surcharge fill (after Holtz et al., 1991)	157
Figure 3.6 - Mesh dimensions and boundary conditions	159
Figure 3.7 - Finally selected mesh for the Rainier Ave. wall analysis	160
Figure 3.8 - Final mesh layout. Reinforced soil zone	161
Figure 3.9 - Final mesh layout - Detail of discretization between reinforcement layers	163
Figure 3.10 - Hyperbolic model for stress-strain behavior	164
Figure 3.11 - Reconstitution of triaxial test series#1 using hyperbolic parameters	167
Figure 3.12 - Reconstitution of triaxial test series#2 using hyperbolic parameters	168
Figure 3.13 - Load-deformation relationship for a spun-bonded geotextile at different effective normal stresses (after Ling et al., 1992)	172
Figure 3.14 - Tension distribution along geotextile reinforcements	182
Figure 3.15 - Computed reinforcement tension distribution during different construction stages (layer#9)	183
Figure 3.16 - Lateral displacements at the location of the inclinometer within the reinforced zone	185
Figure 3.17 - Lateral displacements at the wall face after surcharge placement	186
Figure 3.18 - Comparison of predicted and measured vertical stresses at the wall base	188
Figure 3.19 - Predicted and corrected measured vertical stresses	189
Figure 3.20a - Predicted vertical stress distribution (before surcharge). Stress units are in ksf	191
Figure 3.20b - Predicted vertical stress distribution (after surcharge). Stress units are in ksf	192
Figure 3.21a - Predicted vertical stress contours (before surcharge). Stress units are in ksf	193
Figure 3.21b - Predicted vertical stress contours (after surcharge). Stress units are in ksf	194
Figure 3.22 - Detail of the distribution of lateral earth pressure coefficient ($K=\sigma_h/\sigma_v$) before surcharge placement	195

Figure 3.23 - Locus of maximum reinforcement tensions on the Rainier Ave. wall	197
Figure 3.24 - Locus of maximum reinforcement tensions. Interpretation of possible mechanisms	198
Figure 3.25 - Maximum reinforcement tension versus depth	200
Figure 3.26 - Location of maximum reinforcement tension forces assumed in the design of reinforced soil walls	201
Figure 3.27 - Location of the planar surface with maximum Reinforcement Tension Summation (RTS)	204
Figure 3.28 - Location of the coherent gravity surface with maximum Reinforcement Tension Summation (RTS)	205
Figure 3.29 - Wall and sloping surcharge geometry	209
Figure 3.30 - Effect of surcharge height H_s on the location of the critical planar surface	211
Figure 3.31 - Effect of surcharge height H_s on the Reinforcement Tension Summation along the critical planar surface	212
Figure 3.32 - Effect of slope s and surcharge height H_s on the location of the critical planar surface	214
Figure 3.33 - Normalized Reinforcement Tension Summation along the critical planar surface	215
Figure 3.34 - Effect of wall height H_t on the location of the critical planar surface - Normalized curves	217
Figure 3.35 - Effect of wall height H_t on the Reinforcement Tension Summation along the critical planar surface - Normalized curves	219
Figure 3.36 - Effect of reinforcement stiffness J on the location of the critical planar surface - Normalized curves	220
Figure 3.37 - Effect of reinforcement stiffness J on the Reinforcement Tension Summation along the critical planar surface - Normalized curves	222
Figure 4.1 - Limit equilibrium of a reinforced soil slope using a circular failure surface	239
Figure 4.2 - Scaling requirements between model and prototype reinforcements.	246
Figure 4.3 - View of the Schaevitz geotechnical centrifuge	256
Figure 4.4 - Strong box used to house the centrifuge slope models	256
Figure 4.5 - Dimensions of a reinforced slope model with nine geotextile layers	257
Figure 4.6 - Dynamic compaction of foundation layer during construction of a reinforced slope model	259
Figure 4.7 - View of a geotextile reinforcement ready for placement	259
Figure 4.8 - Lining of the geotextile layer over levelled surface of backfill material	261
Figure 4.9 - Placement of the third sand layer during construction of model S9. Dry pluviation was used to achieve the target density	261
Figure 4.10 - Use of vacuum to level recently pluviated sand	262

Figure 4.11 - View of model S9 after the third sand layer has been placed. Geotextile has been wrapped around and the overlap length has been embedded	262
Figure 4.12 - Model S9, still with wooden supports in place, after completion of the construction process	263
Figure 4.13 - Plate holding the linear potentiometers used for monitoring lateral face displacements	265
Figure 4.14 - View of TV camera and centrifuge bucket with model and slant mirror in place	267
Figure 4.15 - Top view of model B12, already placed in the swing bucket, and of its image trough the slant mirror	267
Figure 4.16 - Nonlinear vertical stress distribution in the centrifuge models and linear approximation	270
Figure 4.17 - Gradation curve for Monterey No. 30 sand	272
Figure 4.18 - Influence of intermediate principal stress on soil friction angle (after Kulhawy and Mayne, 1990)	275
Figure 4.19 - Ratio between friction angles under plane strain and triaxial compression conditions for Monterey sand	277
Figure 4.20 - Stress-strain curves for Monterey No.30 sand obtained from triaxial testing at different relative densities	279
Figure 4.21 - Friction angle for Monterey No.30 sand obtained from triaxial testing at different relative densities	280
Figure 4.22 - Stress-strain curves for Monterey No.30 sand obtained from triaxial testing at different confining pressures	282
Figure 4.23 - Friction angle for Monterey No.30 sand obtained from triaxial testing at different confining pressures	283
Figure 4.24 - Effect of testing boundary conditions on the tensile geotextile stiffness J	287
Figure 4.25 - Schematic illustration of the effect of test boundary conditions on the geotextile ultimate strength	288
Figure 4.26 - Standard wide width strip tensile testing of a geotextile specimen	291
Figure 4.27 - Typical wide-width tensile test results for pellow sew-in geotextiles (Test by Geosyntec Consultants)	292
Figure 4.28 - Typical wide-width tensile test results for pellow tru-grid geotextiles (Test by Geosyntec Consultants)	293
Figure 4.29 - Geotextile tensile testing using a small (1.5 mm) gauge length setup	295
Figure 4.30 - View of a geotextile specimen after tensile testing using a small gauge length setup	296
Figure 4.31 - Typical tensile test results obtained for a pellow sew-in geotextile tested using a small gauge length setup (Test by Geosyntec Consultants)	297
Figure 4.32 - Breakage pattern in Pellow sew-in specimens tested using (from left to right) small gauge length setup, centrifuge modeling, and standard wide width testing	298

Figure 4.33 - Typical tensile test results obtained for a pellaon tru-grid geotextile tested using a small gauge length setup (Test by Geosyntec Consultants)	299
Figure 4.34 - Effect of width/length specimen ratio on the ultimate tensile strength of geotextile reinforcements	301
Figure 4.35 - Schematic cross section showing sample configuration in the direct shear device	304
Figure 4.36 - View of direct shear apparatus ready for sand/geotextile interface testing	305
Figure 4.37 - Direct shear test results for the different sand/geotextile interfaces	307
Figure 4.38 - Direct shear test results for sand/teflon and sand/mylar interfaces	310
Figure 4.39 - Model B18 after construction	315
Figure 4.40 - G-level (N) versus time during centrifuge test of model B18	316
Figure 4.41 - Settlements at the crest of reinforced slope B18, indicating the moment of failure	317
Figure 4.42 - View of model B18 after the centrifuge test	318
Figure 4.43 - Geotextile layer retrieved from model B18, showing tensile tears along the primary reinforcement and overlapping layers	319
Figure 4.44 - Geotextile reinforcements retrieved from model B18	320
Figure 4.45 - Location of the failure surface for model B18, as obtained from tears in the reinforcements and from images recorded through the plexiglass wall	322
Figure 4.46 - View of model B9 after centrifuge testing	323
Figure 4.47 - Geotextile reinforcements retrieved from model B9 after centrifuge testing	325
Figure 4.48 - G-level at failure for the different centrifuge models	326
Figure 4.49 - Model D12 ready for testing	328
Figure 4.50 - Model D12 right after the test	328
Figure 4.51 - Geotextile reinforcements retrieved from model D12 after centrifuge testing	329
Figure 4.52 - Location of the failure surface for model D12, as obtained from tears in the reinforcements and from images recorded through the plexiglass wall	330
Figure 4.53 - View of model S9 after centrifuge testing	332
Figure 4.54 - Geotextile reinforcements retrieved from model S9	333
Figure 4.55 - Location of the failure surface for model S9, as obtained from tears in the reinforcements and from images recorded through the plexiglass wall	335
Figure 4.56 - Estimation of normalized Reinforcement Tension Summation (RTS) values from centrifuge test results	339
Figure 4.57 a - Initiation of failure in model B6	343
Figure 4.57 b - Final collapse of model B6	343
Figure 4.58 a - Initiation of failure in model B12	344
Figure 4.58 b - Final collapse of model B12	344
Figure 4.59 a - Initiation of failure in model B18	345

Figure 4.59 b - Final collapse of model B18	345
Figure 4.60 a - Initiation of failure in model D12	346
Figure 4.60 b - Final collapse of model D12	346
Figure 4.61 - Location of tears in reinforcements defining the failure surfaces in B-series models	348
Figure 4.62 - Location of tears in reinforcements defining the failure surface in D-series models	350
Figure 4.63 - Location of tears in reinforcements defining the failure surface in S-series models	351
Figure 4.64 - Location of failure surface obtained from images recorded in-flight for all centrifuge models	352
Figure 4.65 - Reinforcement force distribution with depth assumed for reinforced soil walls	353
Figure 4.66 - Reinforcement force distribution with depth for reinforced slopes at working stresses	356
Figure 4.67 - Alternative distributions of reinforcement tension with depth in reinforced soil slopes	359
Figure 4.68 - Vertical settlements at the crest of the slope, 12.5 mm from the slope face. The moment of failure is indicated by an arrow	361
Figure 4.69 - Vertical settlements at the crest of the slope, 63.5 mm from the slope face. The moment of failure is indicated by an arrow	362
Figure 4.70 - Second reinforcement layer for model B9, showing breakage of the geotextile overlap	364
Figure 4.71 - Effect of geotextile tensile strength on the calculated factor of safety for model B18	372
Figure 4.72 - Comparison between the observed failure surface in model B18 and the critical circle predicted using limit equilibrium	374
Figure 4.73 - Calculated factors of safety for model B18 with increasing centripetal acceleration: Effect of nonuniform unit weight	376
Figure 4.74 - Calculated factors of safety for model B18 with increasing centripetal acceleration: Effect of orientation of reinforcement forces	378
Figure 4.75 - Calculated factors of safety for model B18 with increasing centripetal acceleration: Effect of geotextile overlaps	381
Figure 4.76 - Effect of geotextile overlaps on the predicted critical circles	383
Figure 4.77 - Lateral shear stresses caused by wall friction in a centrifuge slope model	385
Figure 4.78 - Calculated factors of safety for model B18 with increasing centripetal acceleration: Effect of friction on lateral walls	389
Figure 4.79 - Calculated factors of safety with increasing g-level loading for models in the B-series	396
Figure 4.80 - Calculated factors of safety with increasing g-level loading for models in the D-series	397
Figure 4.81 - Calculated factors of safety with increasing g-level loading for models in the S-series	398
Figure 4.82 - Predicted and measured g-levels causing failure for all centrifuge models	399

Figure 4.83 - Predicted and measured location of failure surface for model B12	401
Figure 4.84 - Predicted and measured location of failure surface for model B9	402
Figure 4.85 - Predicted and measured location of failure surface for model B6	403
Figure 4.86 - Predicted and measured location of failure surface for model D12	404
Figure 4.87 - Predicted and measured location of failure surface for model D6	405
Figure 4.88 - Predicted and measured location of failure surface for model S9	406
Figure 4.89 - Predicted and measured location of failure surface for model S6	407
Figure 4.90 - Critical circles for all centrifuge models predicted by limit equilibrium	408
Figure 4.91 - Effect of geotextile strength on the calculated factor of safety for all centrifuge models	410
Figure 4.92 - Design chart for reinforced soil slopes (from Leshchinsky and Boedeker, 1989)	415
Figure 4.93 - Design chart for reinforced soil slopes (from Jewell, 1991)	417
Figure 5.1 - Map showing Highway 93 and the location of the slope under study	436
Figure 5.2 - Cross section of the reinforced slope	440
Figure 5.3 - Nonwoven geotextile PP-20 used in the upper half of the slope	442
Figure 5.4 - Composite geotextile PPC-100 used in the lower half of the slope	442
Figure 5.5 - Rock shear key under construction.	444
Figure 5.6 - View of the reinforced slope after placement of layer 25	444
Figure 5.7 - Top view of the reinforced slope during compaction operations	446
Figure 5.8 - Placement of backfill during construction of the top layer	446
Figure 5.9 - Finished reinforced slope with erosion matting in place	447
Figure 5.10 - Cross section of the reinforced slope showing the instrumentation layout	449
Figure 5.11 - View of inclinometer casing added during construction progress	450
Figure 5.12 - End bearing plate of a mechanical extensometer attached to a geotextile reinforcement	452
Figure 5.13 - Geotextile layer instrumented with extensometers ready for placement in the field	452
Figure 5.14 - Silicon-diaphragm transducer used to monitor pore water pressure	453
Figure 5.15 - Construction progress of the geotextile-reinforced slope	455
Figure 5.16 - Development of lateral displacements measured by inclinometer SI1 with increase in fill height	457
Figure 5.17 - Development of lateral displacements measured by inclinometer SI2 with increase in fill height	458
Figure 5.18 - Horizontal deflections obtained by the inclinometers during the construction period	460
Figure 5.19 - Total face movements at the end of construction as determined from survey measurements	461

Figure 5.20 - Development of lateral displacements measured by inclinometer SI1 with time after construction	463
Figure 5.21 - Horizontal deflections from inclinometer SI1, including early post-construction measurements	464
Figure 5.22 - Development of lateral displacements measured by inclinometer SI2 with time after construction	465
Figure 5.23 - Horizontal deflections from inclinometer SI2, including early post-construction measurements	466
Figure 5.24 - Horizontal deflections obtained by the inclinometers within the reinforced fill during spring runoff	468
Figure 5.25 - Total face movements measured during the spring runoff as determined from survey measurements	469
Figure 5.26 - Lateral displacements measured by extensometers attached to geotextile layer 15 (Extensometer set E2)	471
Figure 5.27 - Development of geotextile Strains at geotextile layer 15 with increasing fill height	473
Figure 5.28 - Lateral displacements measured by extensometers attached to geotextile layer 5 (Extensometer set E1)	475
Figure 5.29 - Lateral displacements measured by extensometers attached to geotextile layer 31 (Extensometer set E4)	476
Figure 5.30 - Distribution of strains in each instrumented geotextile layer	477
Figure 5.31 - Development of lateral displacements measured by extensometers from set E2 with time after construction	478
Figure 5.32 - Distribution of strains in each instrumented geotextile layer obtained from the spring measurements	480
Figure 5.33 - Development of relative displacements with increase in fill height, as measured by inclinometers and extensometers (Relative horizontal displacements between inclinometers SI1 and SI2, at the level of extensometer set E2)	482
Figure 5.34 - Geotextile strain distribution at geotextile layer 15 compared with average soil strains measured between inclinometer tubes	483
Figure 5.35 - Pore water pressure measurements	485

LIST OF TABLES

Table 2.1 - Triaxial tests on reinforced samples using poorly draining soils	20
Table 2.2 - Shearbox and pullout tests using poorly draining soils	28
Table 2.3 - Reduced-scale reinforced soil models constructed using poorly draining backfills	69
Table 2.4 - Full-scale reinforced soil structures constructed using poorly draining backfills	70
Table 3.1 - Previous FE analyses of reinforced soil structures using SSCOMP, validated against instrumentation records	141
Table 3.2 - Rainier Ave. wall characteristics	152
Table 3.3 - Hyperbolic parameters for the backfill material	166
Table 3.4 - Hyperbolic parameters for the foundation soil	170
Table 3.5 - Unconfined parameters from wide width strength data (after Allen et al., 1991)	173
Table 3.6 - In-situ geotextile stiffnesses back calculated from finite element analysis	179
Table 4.1 - Conventional scale factors for centrifuge modeling of static problems	243
Table 4.2 - Scale factors for parameters used in the centrifuge modeling of reinforced soil structures	244
Table 4.3 - Previous centrifuge studies on the performance of reinforced soil structures	247
Table 4.4 - Direct shear test results on interfaces between sand and geotextiles, mylar, and teflon	308
Table 4.5 - Summary of centrifuge tests	314
Table 4.6 - Calculated factors of safety for model B18 using different methods of analysis	392

ACKNOWLEDGEMENTS

I would like to thank Professor James K. Mitchell for his invaluable guidance during the course of my studies and research. It is a high honor for me to have him as a mentor. Not only did he give me the encouragement and strong guidance that I certainly needed during my graduate studies, but he was an exemplary model of a person, engineer, and professor that I will always treasure.

Professor Nicholas Sitar generously offered me his time, patience, and advice. I am profoundly grateful for his unconditional help and insight, which were of great assistance for the development of this research and interpretation of its results.

The entire course of this study benefited significantly from my association with Dr. Barry Christopher of Polyfelt Americas. His exceedingly helpful assistance provided me with understanding and practical perspectives that were a limitless source of motivation. His encouragement and guidance have been immeasurable.

Thanks are also due to Prof. Neville G. W. Cook, who thoroughly reviewed this dissertation.

The centrifuge study presented as part of this study was only possible through the valuable contribution of many colleagues and professors. These contributions include long discussions with Dr. Mike Riemer and precious laboratory assistance by Lili Nova and Stephanos Papadopoulos. I am also grateful to Prof. Bruce L. Kutter and Dr. Gregg Feigel from U.C. Davis for their assistance with my centrifuge testing, and to Prof. Stephen G. Wright from University of Texas for his support in the limit equilibrium analyses.

The success of the field instrumentation study of a FHWA geotextile-reinforced slope presented as part of this dissertation is due in large part to the support and cooperation of Richard J. Barrows from the Federal Highway Administration, Rodney W. Prellwitz, instrumentation contractor of Bitterrot Engineering, and Mark Wayne from Polyfelt Americas. Their invaluable participation is greatly appreciated.

My stay at Berkeley was made very pleasant and rewarding thanks to many graduate colleagues and friends. Particular thanks go to Carlos Lazarte and David Espinoza for their invaluable assistance and helpful discussions.

Thanks are due to Fani Zaborowski for her skillful help in having this dissertation printed on time.

To my wife and children go the deepest thanks of all. Only Denise, Giselle, and Leonardo can truly appreciate the time and effort spent on this dissertation, time and effort that belonged to them.

The different stages of this research were funded by the Brazilian National Council for Development and Research (CNPq), Polyfelt Americas, The Tensar Corporation, the Federal Highway Administration, and the State of California Department of Transportation (Caltrans). This support is gratefully acknowledged. Caltrans funding was provided under project number RTA65T128 and supervised by Gary Garofalo from the Office of Geotechnical Engineering.

CHAPTER 1

INTRODUCTION



Relics of the Great Wall of China, an earth structure built with natural geotextiles about 2000 years ago.

The steering motivation for the research presented in this dissertation is to contribute towards the design of safe, durable, and economical reinforced soil systems built using indigenous backfill soils. Experimental studies on poorly draining soil-reinforcement interactions, as well as lessons learned from case histories show that permeable geotextiles are well suited for reinforcing marginal backfills. Geotextile materials not only provide the required in-plane transmissivity, but they also render an

inexpensive reinforced soil system. In geotextile reinforcement applications, however, practice leads theory, so that optimum designs may not always result, prediction of performance may not be precise, and all aspects of behavior may not be fully understood. Consequently, the use of geotextile-reinforced systems in critical structures should be substantiated by a better understanding of their behavior and by a validation of the assumptions in their design. The research presented in this dissertation seeks to conceptualize and quantify several aspects of the behavior of geotextile-reinforced soil structures by performing:

- an evaluation study on the suitability of poorly draining backfills for reinforced soil structures.
- a finite element study on the deformability and design aspects of geotextile-reinforced soil walls;
- a centrifuge study on the failure mechanisms and on the suitability of limit equilibrium methods to predict failure of geotextile-reinforced soil slopes; and
- a field instrumentation study to evaluate the performance of a permanent geotextile-reinforced slope built using decomposed granite as backfill material.

1.1 Why reinforcements in earthwork construction?

Design and construction of stable slopes and retaining structures within limited right-of-way are aspects of major economical significance in geotechnical engineering projects. When geometry requirements dictate changes of elevation in highway projects, the engineer faces a variety of distinct alternatives for the design of the required earth

structures. Traditional solutions have been either the design of concrete retaining walls (Figure 1.1a) or of conventional embankment slopes (Figure 1.1d). Concrete retaining walls (either gravity or cantilever) have been the conventional choice for many projects involving construction under the constraints of limited access. Although simple to design, standard wall alternatives have generally led to elevated construction and material costs, that often constitute a significant fraction of total project bids. The traditional alternative to concrete retaining walls has been the use of unreinforced slopes. However, the construction of conventional embankments, often with flat slope angles dictated by conventional stability analyses, is precluded on projects in which design is controlled by space constraints.

Soil reinforcement, which involves the use of inclusions in a soil mass to improve its mechanical properties, has become a widely used earthwork construction method that provides technically attractive and cost-effective grade separations at the ground surface. Reinforced soil walls (Figure 1.1b) generally provide vertical grade separations at a lower cost than do traditional cast-in-place concrete construction. Ribbed steel strips, steel bar mats, geogrids, and geotextile sheets, are examples of typical reinforcement elements. Reinforced wall systems additionally involve the use of shotcrete facing protection or of facing elements such as precast or cast-in-place concrete panels. Alternatively, steepened reinforced slopes (Figure 1.1c) may eliminate the use of facing elements, thus saving material costs and construction time in relation to the vertical reinforced wall. The use of reinforced slopes often constitutes the most cost-effective solution in highway projects involving the addition of traffic lanes within the right-of-way of existing embankments.

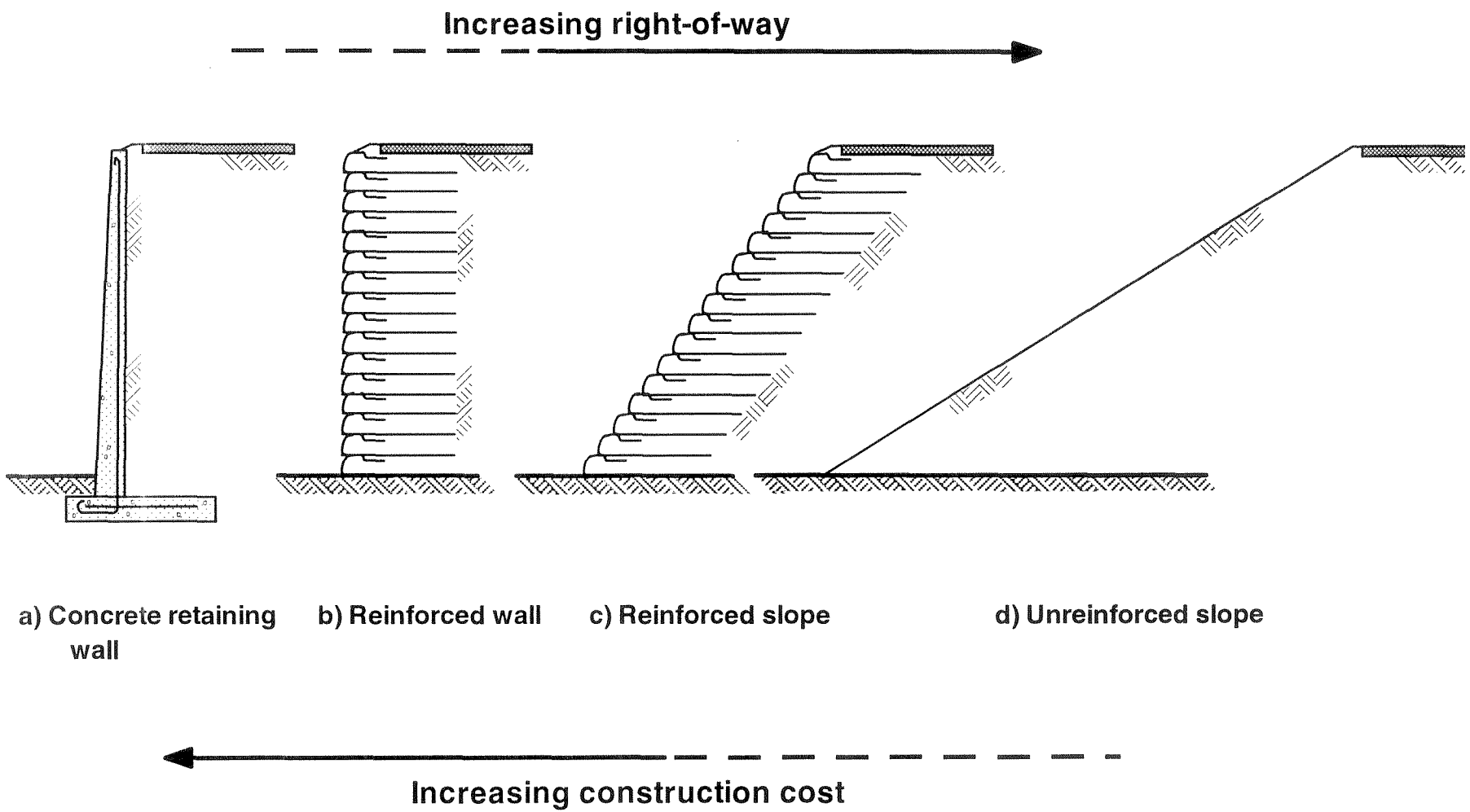


Figure 1.1 - Alternative designs for earth retaining structures

The decision-making process for selecting an earth structure involves a trade off between the imposed space constraints and the construction costs of the retaining structure. The optimum design alternative is to be defined by project-specific conditions, however, the general trends are as shown in Figure 1.1. Depending on the available right-of-way, the figure illustrates that the optimum alternatives for projects involving grade separations are reinforced soil walls and reinforced soil slopes. As indicated by dashed lines in the trends suggested in the figure, both conventional and reinforced retaining walls require equivalent right-of-way and that both conventional and reinforced slopes often result in equivalent construction costs.

The use of inclusions to improve the mechanical properties of soils dates to ancient times. However, it is only within the last quarter of century or so (Vidal, 1969) that analytical and experimental studies have led to the contemporary soil reinforcement techniques, used for a wide range of earthwork construction. Soil reinforcement is now a highly attractive alternative for embankment and retaining wall projects because of the economic benefits it offers in relation to conventional retaining structures. Moreover, its acceptance has also been triggered by a number of technical factors, that include aesthetics, reliability, simple construction techniques, good seismic performance, and the ability to tolerate large deformations without structural distress.

1.2 Why geotextiles as reinforcements?

As the availability of suitable construction sites decreases, there is an increasing need to utilize poor soils for foundation support and earthwork construction (Mitchell, 1981). Although the different soil reinforcement systems have greatly extended the use

of soil as construction material, their use has often been limited by the availability of good-quality granular material which has generally been specified for the backfill. Even though there are several reasons for requiring good quality granular backfill, this specification has restricted the use of reinforced soil structures in cases where such material is not readily available. Undoubtedly, substantial cost savings and new soil reinforcement applications would result if indigenous fine grained soils as well as industrial and mine wastes could regularly be used as backfill materials.

Steel has been the most widely used reinforcement material and, since poorly draining soils are usually saturated, the possibility of corrosion of these reinforcements is high. The inherent low strength, moisture instability, possible volume changes, and creep potential of poorly draining soils are other concerns that have precluded their extensive use as backfills in reinforced soil structures. With the introduction of polymer geotextiles and geogrids, non-corrosive reinforcement systems are now available. Permeable geotextile reinforcements may be especially useful for reinforcing poorly draining soils because their drainage capabilities would help to increase the structure stability by dissipating excess pore water pressures. Although reported results have led to some contradictory conclusions on the use of impermeable reinforcements, there is already strong experimental evidence that permeable inclusions can effectively reinforce poorly draining backfills (Chapter 2).

Metallic reinforcements are not strong reinforcement candidates for poorly draining backfills. Not only do they not provide lateral drainage to the cohesive fill, but also the interface friction of these systems relies on the dilatant characteristics offered by granular fills. Polymeric grid reinforcements provide adequate tensile strength required for the

design of permanent reinforced soil structures. However, since they offer only limited in-plane drainage capacity, a low moisture content in the fill should be guaranteed by appropriate drainage systems throughout the design life of the structure. Geotextile materials with high in-plane hydraulic conductivity are reinforcements that offer the desired drainage capacity for poorly draining fills. Particularly, composite geotextiles, which combine the hydraulic properties of nonwovens with the mechanical characteristics of geogrids or wovens, are probably the most appropriate reinforcement for marginal soils.

1.3 Methods to investigate the performance of geotextile-reinforced soil structures

The performance of geotextile-reinforced soil structures involves many complex soil-structure interactions which defy simple characterization. Current knowledge of most aspects of reinforced soil behavior stem from a combination of testing and modeling that support current design procedures (Jewell, 1993). Testing of the reinforcements, of the backfill soil, and of the interactions between them provides the parameters needed for design. However, it is through numerical modeling, physical modeling, and the instrumentation of field structures, that we are coming to understand the principles of soil reinforcement and the mechanisms that characterize the behavior of reinforced soils structures.

Numerical modeling. Among the different numerical techniques that have been developed to solve problems in computational mechanics, the finite element method has been the one predominantly used in the analysis of geotechnical structures. A rational approach for the use of finite element analyses to aid in geotechnical engineering design involves an initial interpretation of field instrumentation of earth structures, the subsequent validation of the numerical model against the field data, and a final numerical simulation of new design aspects. However, the finite element modeling of failure in frictional materials requires techniques to handle the localization of deformations, such as specific continuum formulations or the use of adaptive mesh refinement to capture slip discontinuities (Zienkiewicz and Taylor, 1991). Consequently, for earth structures which have their design based on limit equilibrium approaches, finite element simulations have been generally unsuitable to validate design procedures. Consequently, the major contribution of finite element studies to the design of reinforced soils structures has been for the analysis of the performance of structures far from failure condition. They are particularly useful for parametric studies of structures under working stress conditions designed with nonstandard geometries or with unusual loading conditions.

Physical modeling. Many physical phenomena can be investigated using scaled models of large prototypes. However, scaled models of geotechnical structures under normal gravity seriously lack similitude because the stress levels, which control the stress-deformation response in the model, do not match those in the full scale prototype. The scaled model can then be tested using a geotechnical centrifuge to replicate both magnitude and distribution of stresses (Schofield, 1980). The principle of centrifuge

testing is to raise the acceleration of the scaled model in order to obtain prototype stress levels in the model. Since similitude criteria for soil and reinforcement strengths can be readily satisfied, centrifuge modeling appears particularly suitable for the investigation of failure mechanisms in geotextile-reinforced structures. Consequently, centrifuge testing can be used to study the validity of current design procedures for reinforced soil slopes based on limit equilibrium.

Instrumentation of field structures. Field instrumentation is vital to the practice of geotechnics, in contrast to the practice of most other branches of engineering in which people have greater control over the materials with which they deal (Peck, 1988). In the case of geotextile-reinforced soil structures, however, much of the field experience to date has provided only a qualitative assessment of the design variables, and there is a major need of quantitative information on the behavior of these structures. Monitoring the performance of full-scale structures using field instrumentation is essential to build confidence on the still new soil reinforcement techniques and to validate the numerical and physical modeling approaches. Although adequate field instrumentation is costly, examination of the performance of full-scale structures constitutes the only true confirmation that the design of reinforced soil structures is, in fact, satisfactory.

The different methods to investigate the performance of geotextile-reinforced soil structures complement each other. While field instrumentation programs offer the more conclusive results, full-scale structures are prohibitively expensive for parametric studies, which are particularly suitable to be performed using finite element and centrifuge

modeling techniques. In order to provide insight into the mechanisms that dominate the performance of geotextile-reinforced soil structures, finite element modeling (Chapter 3), centrifuge modeling (Chapter 4), and interpretation of field instrumentation results from a full-scale structure (Chapter 5) have been performed as part of the research presented in this dissertation.

1.4 Scope of the dissertation

The scope of this research includes an evaluation of the use of poorly draining soils in reinforced soil construction and an investigation of different aspects of the performance of geotextile-reinforced soil structures. Finite elements, centrifuge testing, and field instrumentation are used for this purpose. Given the individual objectives and the specific background of each aspect of the research, a conscious attempt is made to present the information of each chapter in a self-contained manner. Objectives, background, conclusions, and references are presented separately in each chapter.

This first chapter provides the motivations of this study and brief background information. In view of the extensive literature already available related to conventional reinforced soil structures with granular backfill (Mitchell and Villet, 1987; Christopher et al., 1990), the description of different reinforcement systems, the general design procedures for reinforced soil structures, and the evaluation of the soil-reinforcement interactions are not reviewed in this dissertation.

The use and performance of reinforced soil structures constructed using poorly draining and/or cohesive backfills is evaluated in Chapter 2. The evaluation includes experimental and analytical studies undertaken to investigate the cohesive soil-

reinforcement interaction and the reinforcement drainage characteristics, which show that permeable inclusions can effectively reinforce clay structures. This conclusion is supported by lessons learned from case histories of structures constructed using marginal soils. Benefits and applications of reinforcing poorly draining backfills are addressed, and research needs aimed at formulating a consistent design methodology for these structures are presented.

The deformability of geotextile-reinforced soil structures and the effect of backfill slope on the performance of geosynthetically reinforced walls are investigated using the finite element analyses presented in Chapter 3. The methodology involves initial validation of the numerical model against instrumentation records from a full-scale wall and a subsequent parametric study of different wall and surcharge configurations. The effect of sloping backfills on the location of the potential failure surface is of particular interest in these analyses.

A centrifuge study, undertaken to investigate the performance of geotextile-reinforced soil structures at failure, is described in Chapter 4. A series of scaled geotextile-reinforced slopes was tested to evaluate current design procedures, which are based on limit equilibrium. The investigation included studies of the failure mechanisms of reinforced slopes, the effect of confinement on ultimate tensile strength of reinforcements, and the capability of limit equilibrium methods to predict the experimental results.

A field instrumentation study done to investigate the performance of geotextile-reinforced soil structures under working stress conditions is presented in Chapter 5. As part of a highway widening project, the FHWA constructed a 1H:1V permanent

geotextile-reinforced slope 15.3 m high. Several characteristics were unique to the slope design: the structure was higher than usual geotextile slopes, it involved the use of both a high modulus composite and a nonwoven geotextile, and it was constructed using decomposed granite soil as backfill material. Overall structure deformation, geotextile strain distributions, and pore water pressures in the fill are evaluated after analyzing the results of an extensive field instrumentation program.

Finally, a summary of the main conclusions reached in each facet of this study, as well as recommendations for further study, are presented in Chapter 6.

References

- Christopher, B. R., S. A. Gill, J. P. Giroud, I. Juran, J. Mitchell, F. Schlosser and J. Dunicliff. (1990). *Design and construction guidelines for reinforced soil structures - Volume I*, Report No. FHWA-RD-89-043. Federal Highway Administration, U.S. Department of Transportation, 285 p.
- Jewell, R.A. (1993). "Links between the testing, modelling, and design of reinforced soil." *Earth Reinforcement Practice*, Vol. 2, Ochiai et al. (Ed.), A.A. Balkema, Proceedings of the International Symposium held in Fukuoka, Japan in November 1992, pp.755-772.
- Mitchell, J. K. (1981). "Soil Improvement: State-of-the-Art." *Proceedings of the Tenth International Conference on Soil Mechanics and Foundation Engineering*, Stockholm, Sweden, Vol.4, pp. 509-565.

- Mitchell, J. K. and W. C. B. Villet. (1987). *Reinforcement of Earth Slopes and Embankments*, National Cooperative Highway Research Program Report No.290. Washington, D.C.: Transportation Research Board, 323 p.
- Peck, R.B. (1988). Foreword to *Geotechnical Instrumentation for Monitoring Field Performance* by Dunicliff, J., J. Wiley & Sons, 577 p.
- Schofield, A.N. (1980) "Cambridge Geotechnical Centrifuge Operations." 20th Rankine Lecture, *Géotechnique*, Vol. 30, No.3, pp.227-268.
- Vidal, H. (1969). "La Terre Armée." *Annales de l'Institut Technique du Bâtiment et des Travaux Publics*, Series: Materials (38), No. 259-260, pp.1-59.
- Zienkiewicz, O.C. and R.L. Taylor. (1991). *The Finite Element Method*, Fourth Edition, Volume 2, McGraw-Hill, 807 p.

CHAPTER 2

PERFORMANCE OF GEOTEXTILE-REINFORCED SOIL STRUCTURES WITH POORLY DRAINING BACKFILLS: AN EVALUATION STUDY



First geotextile-reinforced wall, built in 1971 along freeway A15 in Rouen, France. This first wall was built using a poorly draining cohesive soil as backfill material.

2.1 Introduction

Reinforced soil, an engineered composite material, is now extensively used for construction of earth retaining walls and embankment slopes, and in the stabilization of embankments placed over soft ground. A number of reinforcement types and proprietary systems have been developed, which offer the advantages of simple design, ease of

construction, low cost, and the ability to tolerate large deformations without structural distress.

Conventionally, free draining granular material is specified for the backfill material of reinforced soil structures. Although there are several reasons for requiring good quality granular backfill, this specification has limited the use of reinforced soil structures in cases where such material is not readily available. Steel has been the most widely used reinforcement material and, since poorly draining soils are usually saturated, the possibility of corrosion of these reinforcements is high. The inherent low strength, moisture instability, possible volume changes, and creep potential of poorly draining soils are other concerns that have precluded their extensive use as backfills in reinforced soil structures. With the introduction of polymer geotextiles and geogrids, non-corrosive reinforcement systems are now available. However, considering the limited experience with cohesive backfills, common practice has been to avoid using lower quality soils in geosynthetically reinforced constructions whenever possible (Mitchell and Christopher, 1990).

Interestingly, however, the first geotextile-reinforced wall ever constructed used poorly draining cohesive soil as backfill material. The purposes of this first geotextile-reinforced structure, built in 1971 by the French Highway Administration in Rouen, were to test its stability and to verify the magnitude of deformations caused by the soil-geotextile interaction (Puig and Blivet, 1973; Puig et al., 1977). The first geotextile-reinforced wall in the United States was built by the U. S. Forest Service in 1974 (Bell and Steward, 1977). This wall used on-site silty sand for the backfill, and was built to reconstruct a road fill above the Illinois River in Oregon. The construction of reinforced

soil structures using poorly draining backfill has been largely restricted, however, to early applications of soil reinforcement. This is probably a consequence of strong recommendations by various design agencies against the use of low-quality backfill for permanent structures.

With the development of improved reinforcement materials and systems, as well as the expanding need for construction using alternative backfills, it is useful to evaluate the present status of reinforced structures with poorly draining backfill. This evaluation was motivated both by the lack of consensus on the mechanisms involved in cohesive soil-reinforcement interaction, and by the belief that proper design and construction can result in stable, durable, and economical reinforced soil structures. With the reassessment of different interpretations that have been put forth to explain the observed behavior, development of a consistent design methodology for reinforced soil structures with poorly draining backfills may then be possible.

The use of backfill soils capable of developing positive pore water pressures either during construction or after rainfall events is evaluated for both reinforced soil walls and slopes. Other applications, such as reinforced foundations and the use of geosynthetics to stabilize embankments over soft soils are outside the scope of this work. Since the poor drainage characteristics of clays and silts are of major concern for the structure design, they are termed "poorly draining backfills" herein. Other terms, such as low-quality, cohesive, fine-grained, or marginal backfills have also been used in the technical literature to refer to these fill materials.

Experimental research done to investigate the cohesive soil-reinforcement interaction and the drainage function of reinforcement elements is initially reviewed in

this chapter. Potential applications of marginal soils in reinforced soil construction and lessons learned from case histories are subsequently addressed. The evaluation presented in this chapter is condensed and updated from a more comprehensive report by Zornberg and Mitchell (1992). Although reported experimental results have led to contradictory conclusions on the effects of impermeable reinforcement layers, there is already strong experimental evidence that permeable inclusions can effectively reinforce poorly draining backfills. There is no general design methodology for reinforced soil structures built with cohesive backfills. Nevertheless, since a number of these types of reinforced structures has already been constructed, many lessons can be learned from past experience. The purpose of this chapter is to provide the results of a review and evaluation of published material related to the use of poorly draining soils in reinforced soil structures. On the basis of this evaluation, research needs required to formulate a consistent design methodology for reinforced structures with poorly draining backfill are identified. Both laboratory studies done to explain the mechanisms involved in the cohesive soil-reinforcement interaction and field case histories on reinforced soil structures with poorly draining backfill materials are covered.

2.2 Current standards for backfill materials in reinforced soil structures

Well graded, free draining granular material is usually specified for construction of reinforced soil walls and embankments. Gradation and soundness limits are given in

the FHWA specifications for mechanically stabilized earth walls, as recommended by AASHTO-AGC-ARTBA, Joint committee Task Force 27 (Christopher et al., 1990):

<u>U.S. Sieve Size</u>	<u>Percent Passing (walls)</u>	<u>Percent Passing (slopes)</u>
4 inch (100 mm)	100	100-75
No. 4 (4.75 mm)		100-20
No. 40 (0.425 mm)	0-60	0-60
No. 200 (0.075 mm)	0-15	0-15

The Plasticity Index for the backfill is also specified ($PI \leq 6$ for walls and $PI \leq 20$ for slopes), and magnesium sulfate soundness loss of less than 30% after four cycles is required. The maximum aggregate size should be limited to 19 mm (3/4 inch) for extensible reinforcement unless field tests are performed to evaluate potential strength reductions due to reinforcement damage during construction.

Some concerns about the use of poorly draining soils for reinforced soil construction have been (Mitchell, 1981; Jewell and Jones, 1981):

- Buildup of pore water pressures may reduce the backfill soil strength. Furthermore, the drained frictional strength of cohesive soils is intrinsically lower than that of cohesionless soils.
- Poorly draining cohesive soils are chemically more aggressive than cohesionless soils, and this can increase the rate of corrosion of metallic reinforcements.
- Post-construction movements may occur under sustained stresses because of the higher creep potential in poorly draining soils.
- Poorly draining soils are usually more difficult to compact.

However, these concerns may represent unrealistic restrictions in actual practice. In fact, many highway embankments are constructed of compacted clays, and to preclude their use when reinforcement is required for stability may be overly conservative. In many cases, buildup of excess pore water pressures can be avoided by adopting suitable construction techniques and drainage systems involving use of permeable reinforcements. In relation to the long-term performance issues of geotextile degradation and creep deformations, the cases reported in the literature have shown encouraging results. Furthermore, the use of geosynthetics such as nonwoven geotextile sheets has been reported to allow better compaction of cohesive soils.

2.3 Interaction mechanisms observed using triaxial tests

A number of experimental studies using triaxial tests have been done to develop an understanding of the interaction between cohesive soil and different reinforcement systems. Characteristics and conclusions drawn from the results of triaxial tests on reinforced specimens using poorly draining soils are summarized in Table 2.1, and an evaluation of many of these studies is presented next in this section. The general approach using triaxial tests has been to determine the strength of the unreinforced soil and the apparent strength of the same soil containing reinforcements placed at various spacings within the cylindrical sample. In this way, the change in strength caused by the reinforcement could be quantified using a *strength ratio*, which is the deviator stress at failure measured in the reinforced sample divided by the deviator stress at failure measured in the unreinforced sample.

Table 2.1 - Triaxial tests on reinforced samples using poorly draining soils.

Research agency	Test type	Soil	Reinforcement	Test variables	Observed behavior	Conclusions	Reference
Ground Engineering Ltd, U.K.	Undrained triaxial	Saturated kaolin clay; London clay	Aluminum foil; porous plastic	Reinforcement spacing was varied	Aluminum foil reduces the sample strength. Permeable plastic reinforcements increased compressive strength in the clay sample	Permeable plastic performs better than impermeable foil. Reduction in strength is due to generation of pore water pressures	Ingold 1979; Ingold & Miller 1982
Ground Engineering Ltd, U.K.	Drained triaxial	Normally consolidated kaolin clay	Porous plastic	Tests on multi-reinforced samples and on unit cells of clay	Decreasing the reinforcement spacing increased both the drained shear strength and the secant deformation modulus	Strength enhancement was attributed to radial strain control mobilized on soil-reinforcement interface	Ingold & Miller 1983
Laing Design Develop. Centre, U.K.	Rapid triaxial tests on unsaturated samples	Kaolin clay	Aluminum foil	Degrees of saturation ranged from 75% to 100%	A linear relationship between strength and degree of saturation, apparently independent of cell pressure, was observed	Conditions very close to drained situations might be expected to prevail for low degrees of saturation	Ingold, 1985
Queensland Inst. of Technology, Australia	UU and CU triaxial tests	Silty clay (PL:14% ; LL:27%)	Geotextiles and geogrids	Eleven different types of geosynthetics were used	Geotextile reinforcement restricted the lateral deformations in the sample. Stress-strain curve of the reinforced sample differs from that of the unreinforced material	Permeable geotextiles increase sample strength. Adhesion factor between clay and reinforcement improves with increasing moisture content	Fabian & Fourie 1986
Scientific Research C., Baghdad	CU triaxial tests	Kaolin clay	Geogrid	Samples had overconsolidation ratio of 3	Enhancement in undrained strength was obtained	Strength improvement was attributed to openings in the geogrid, that cause interlocking	Al-Omari et al. 1987
Scientific Research C., Baghdad	CD and CU triaxial tests	Powdered kaolin clay	Geogrid	Geogrid stiffness, reinforcement spacing, and confining pressure were changed	Geogrid reinforcement enhanced strength in both undrained and drained conditions. The A pore pressure parameter was higher for reinforced than for unreinforced samples	Reinforcement effect in undrained condition is an increase in cohesion. The effect in drained condition is an increase in internal friction	Al-Omari et al. 1989
AIT, Bangkok	UU triaxial, consolidation tests	Soft silty clay	Nonwoven and woven geotextiles	Compactability, strength, and consolidation were investigated	Nonwoven geotextile improved the compactability of clay samples	Nonwoven geotextile performed better than woven geotextile because of its better drainage, particularly at high moisture content	Indraratna et al. 1991
U. of Tokyo, Japan	Drained and undrained plane strain tests	Nearly saturated silty clay	Nonwoven geotextiles	Tests done on isotropically and anisotropically consolidated samples	Improvement in strength and stiffness was more significant for the anisotropically consolidated specimens	Drained tests show greater reinforcement effect than undrained tests.	Ling & Tatsuoka 1993

Note: UU: unconsolidated undrained; CU: consolidated undrained; CD: consolidated drained

Studies on reinforced clay using the triaxial apparatus were first reported by Ingold (1979). Results of undrained compression tests on normally consolidated, cylindrical clay samples reinforced using several disks of reinforcement were subsequently presented by Ingold and Miller (1982). The reinforcement material used was either aluminum foil or porous plastic. The test results showed that reinforcing clay specimens with continuous horizontal layers of aluminum foil caused reductions in undrained axisymmetric compressive strength of more than 50% relative to unreinforced samples. The premature failure of the specimen was attributed to pore water pressures induced in the reinforced specimen which were greatly in excess of those measured in a similar unreinforced specimen. Evidence of pore pressure generation during shear was further substantiated when tests were performed using the same clay, but with continuous horizontal porous reinforcement. In this case, the porous reinforcement was found to partially dissipate the pore water pressures induced in the clay, thus averting premature failure. Indeed, as the porous reinforcement spacing was decreased, the compressive strength of the reinforced specimen was found to increase substantially beyond that of the unreinforced specimen.

Figure 2.1 shows results for rapid shearing of fully saturated clay with permeable reinforcement. These samples were sheared at a strain rate of 2% per minute; this rate being deemed compatible with undrained shear in an unreinforced sample. Figure 2.2 shows test results for constant volume shearing, i.e. true undrained loading, of kaolin reinforced with porous plastic. Unexpectedly, there was also strength increase in this truly undrained condition. A suggested explanation to this phenomenon was that porous reinforcements decreased the Skempton pore pressure parameter A of the cohesive soil

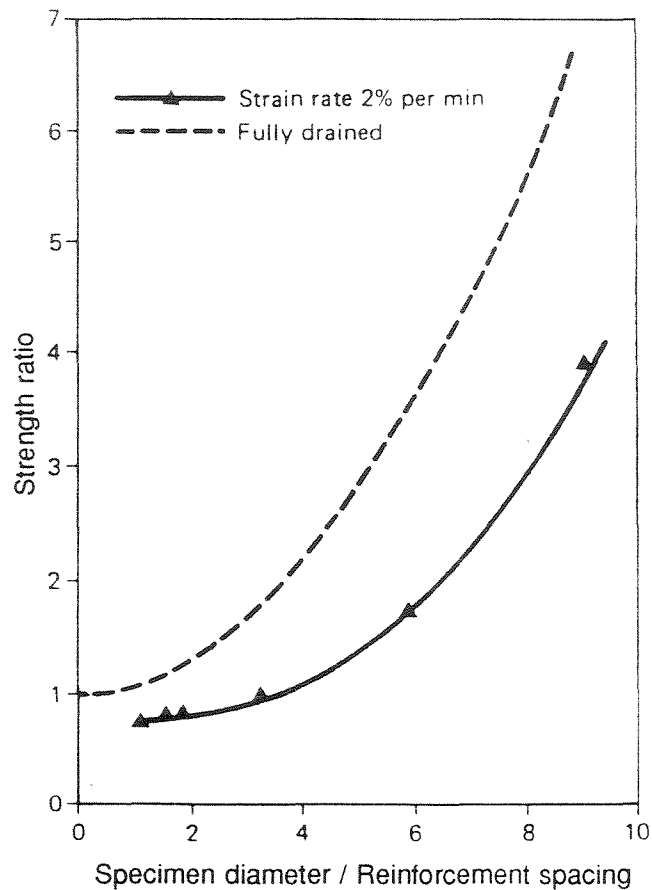


Figure 2.1 - Effect of reinforcement spacing on strength ratio for rapid shearing of saturated clay specimens with permeable reinforcements (after Ingold and Miller, 1982). (Note: Strength ratio = Strength of reinforced specimen / Strength of unreinforced specimen).

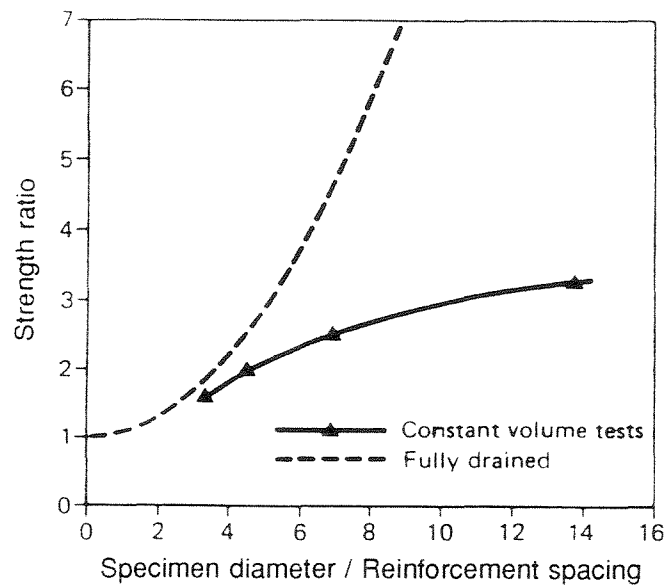


Figure 2.2 - Effect of reinforcement spacing on strength ratio for constant volume shearing of kaolin specimens reinforced with porous plastic (after Ingold and Miller, 1982). (Note: Strength ratio = Strength of reinforced specimen / Strength of unreinforced specimen).

and hence increased the minor effective principal stress giving a higher undrained strength.

If the undrained compressive strength of a clay specimen can be increased by the introduction of porous reinforcement to partially dissipate the pore water pressures induced by shear, then it would be expected that even greater strength increases would be obtained if pore water pressures were allowed to fully dissipate, as occurs in a drained compression test. Ingold and Miller (1983) carried out a number of tests to investigate the drained behavior of normally consolidated clay reinforced with porous plastic disks. Test results showed that the effect of decreasing the spacing between the horizontal layers of reinforcement was an increase in both the drained shear strength and the secant deformation modulus of the reinforced sample. The stress-strain curves for one of the test series on reinforced kaolin clay are given in Figure 2.3. The ratio of sample diameter to reinforcement spacing is indicated as ρ_r in this figure. The unreinforced sample, with a ratio $\rho_r = 0.5$, is also indicated. Based on the results of a radiographic investigation, the strength enhancement was attributed, as in the case of sand reinforcement, to radial strain control arising from shear stress mobilized on the soil-reinforcement interface.

Rapid triaxial tests on partly saturated clay using impermeable reinforcement were also performed by Ingold (1985). As degree of saturation decreased, the strength ratio increased until, at a degree of saturation of approximately 70%, the strength ratio was equal to the one obtained under fully drained conditions. The results for 76 mm high samples with 6 mm reinforcement spacing are given in Figure 2.4, plotted in the form of a strength ratio against degree of saturation. As can be seen, there is a well-defined linear relationship between strength and degree of saturation, which appears to be independent

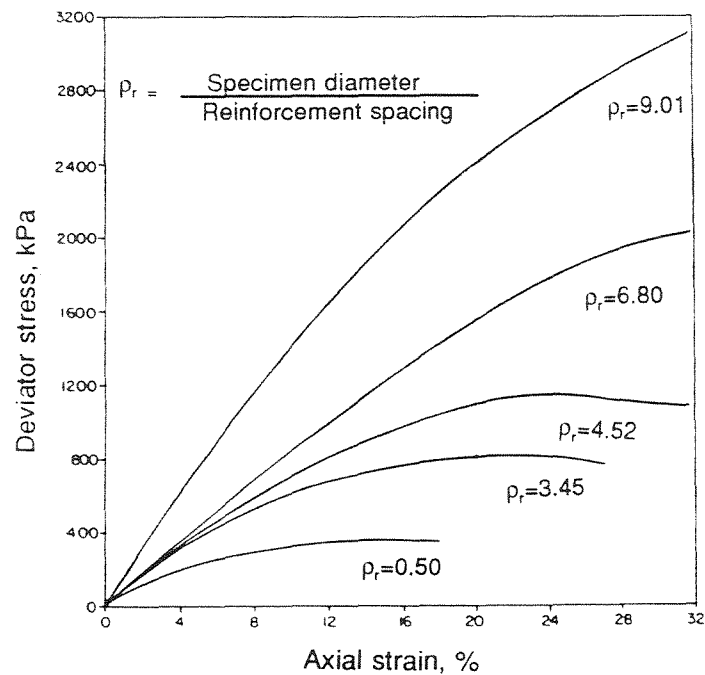


Figure 2.3 - Stress-strain behavior of reinforced kaolin specimens during drained triaxial loading (cell pressure 250 kPa) (after Ingold and Miller, 1983).

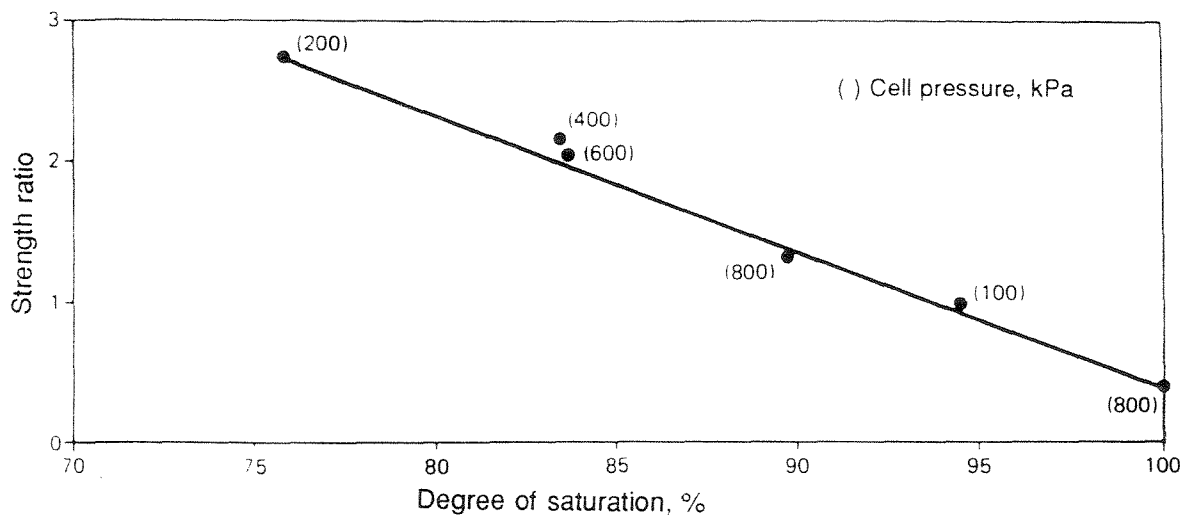


Figure 2.4 - Variation of strength ratio with degree of saturation for rapid triaxial tests on kaolin specimens with impermeable reinforcements (after Ingold, 1985). (Note: Strength ratio = Strength of reinforced specimen / Strength of unreinforced specimen)

of cell pressure. The practical implications of these results are that rapid construction using fully or nearly saturated clay fill could prove unstable if continuous impermeable reinforcements are used.

Fabian and Fourie (1986) presented the results of a series of undrained triaxial tests performed on silty clay samples reinforced with various geosynthetics having different in-plane transmissivities, including woven geotextiles, nonwovens, and geogrids. Unconsolidated undrained and consolidated undrained triaxial tests were done to determine the relationship between geotextile permeability and undrained strength. Their results showed that reinforcements with high transmissivity can increase the undrained strength of the clay by up to almost 40%, while reinforcements with low transmissivity can decrease the undrained strength by a similar magnitude. It was also reported that the strength ratio increased with the moisture content of the sample. This was because the undrained strength of an unreinforced clay sample decreases as moisture content increases, while the undrained strength of a reinforced clay sample was less affected by increases in moisture content. No significant strength increase was observed for samples reinforced with geogrids.

Although results from the above mentioned tests showed a decrease in strength when impermeable reinforcement was used, Al-Omari et al. (1987) obtained encouraging results using geomesh reinforced clay specimens. They presented the strength ratios obtained from 15 undrained triaxial tests on geomesh reinforced kaolin clay specimens having an overconsolidation ratio of three. Depending on the number of reinforcement layers, significant increase in the undrained strength was reported. The harmful effect of pore water pressure generation on the soil-reinforcement interface was considered to be

mitigated. Results from both consolidated undrained and consolidated drained triaxial tests on overconsolidated geomesh reinforced clay were subsequently presented by Al-Omari et al. (1989). The geomesh stiffness, number of reinforcing layers, and the confining pressure were varied. The geomesh reinforcement enhanced the strength in both the undrained and drained conditions. For undrained loading, the effective stress failure envelope of reinforced clay was reported to be parallel to the envelope for unreinforced clay, but with a greater cohesion intercept. For drained loading, the failure envelope of the reinforced clay indicated an increased friction angle.

The use of nonwoven geotextiles for reinforcing a near-saturated silty clay was evaluated by Ling and Tatsuoka (1993) using a plane strain device. The reinforcement effect, in terms of strength and stiffness, was reported to be more significant for anisotropically consolidated specimens than for isotropically consolidated specimens. In both cases, the reinforcement effect was greater in the drained tests than in the undrained tests. At small strain levels, excess pore water pressures adversely affected the stress-strain response of the reinforced soil samples tested under undrained conditions. In the drained tests, tensile stresses were mobilized in the geotextile ensuring a positive reinforcement effect.

Strength improvements measured by triaxial compression tests do not correspond quantitatively to the improvement expected in full-scale reinforced soil structures because triaxial tests do not necessarily duplicate soil stresses and reinforcement tensions developed in the field. Nonetheless, triaxial test results on reinforced samples provide qualitative information on the strength of the soil-reinforcement composite, thus contributing to a better understanding of the nature of improvements that may be expected

in full-scale soil structures. Although results obtained by different investigators using impermeable reinforcement have led to some contradictory conclusions, triaxial test results have clearly shown that poorly draining soils can be reinforced with properly selected permeable geotextiles.

2.4 Interaction mechanisms observed using shearbox and pullout tests

As the backfill material of a reinforced soil structure deforms under load, relative movements develop between the reinforcement and the soil, which mobilize bond stresses on the soil-reinforcement interface. Interface strength test results have been reported both in terms of an equivalent friction angle and an adhesion value. Collios et al. (1980) introduced the concept of *contact efficiency*, which is the ratio of the friction angle or cohesion of the soil-reinforcement interface to the friction angle or cohesion of the soil. Several studies have been conducted with the objective of quantitatively determining the interaction between poorly draining soils and different types of reinforcements. The characteristics and results of these studies, performed using shearbox and pullout tests, are summarized in Table 2.2.

2.4.1 Poorly draining soil-metallic reinforcement interaction

The dilatancy of the compacted granular backfill has been recognized as a major factor in explaining the high interface friction obtained from pullout tests using ribbed metallic strips (Guilloux et al., 1979). The resulting additional vertical stress at the

Table 2.2 - Shearbox and pullout tests using poorly draining soils.

Research agency	Test type	Soil	Reinforcement	Characteristics	Observed behavior	Conclusions	Reference
Reinforced Earth Co.	Pullout and creep tests	Low plastic silts and clay	Ribbed steel strips	Deformation rate was 2.5 mm/min	Peak shear stresses along the strip were considerably less than for granular soils	Additional work is necessary prior to use of fine-grained soil in Reinforced Earth fill	Elias 1979
LRPC, Rouen, France	Direct shear	Phosphogypsum	Woven and nonwoven	Material placed at optimum moisture content	Coefficient of friction decreased with increasing confining stresses	Friction coefficient was in excess of 0.4	Blivet & Gestin 1979
Ground Eng. Ltd, U.K.	Direct shear and pullout tests	Kaolin clay	Polyethylene mesh; metallic reinforcement	Unconsolidated-undrained tests	Inclined reinforcements on clay samples subject to undrained direct shear caused apparent increase in shear strength	Enhanced strength may be induced by resistance of reinforcement to rotation rather than pullout	Ingold 1981; Ingold 1983
Cambridge Univ., U.K.	Undrained direct shear tests	Lightly over-consolidated kaolin clay	Geogrid	Geogrid types, dimensions, and orientation were changed	Short- and long-term shear strength of cohesive soil was increased by reinforcement	Shear strength of reinforced soil may be calculated using a limit equilibrium analysis	Jewell & Jones 1981
Reinforced Earth Co.	Pullout tests	Residual low-plastic silts	Ribbed steel strips	Soils with different % of fines were tested	Apparent friction coefficient decreased with fines content. Samples compacted wet of optimum showed reduced pullout capacity	Fines content and moisture content should be carefully evaluated in structures reinforced with steel strips	Elias & Swanson 1983
Illinois Inst. of Technology	Direct shear tests	Sandy clay	Woven and nonwoven geotextiles	Shear box was placed into saturation tank	Peak shear strength was reached at relatively large displacements. Residual strength did not vary from peak strength	Soil-geotextile interface strength for woven geotextile was lower than for nonwoven fabric	Saxena & Budiman 1985
Drexel Univ., Philadelphia	Direct shear tests	Cohesive soils	Five geomembranes	Geomembrane was placed in lower box portion	Adhesion of soil to geomembrane was smaller than the soil cohesion. Friction angles at geomembrane interfaces were relatively high	Geomembranes placed directly on clay should have low slopes (e.g. 4H to 1V)	Koerner et al. 1986
Arizona State Univ.	Pullout and creep tests	Wyoming bentonite	Polymeric geogrids	Expansive clay was placed at low moisture content	Pullout force versus normal force was linear	Pullout resistance of geogrids in low moisture content clays is rather insensitive to geogrid strength or configuration	Brand & Duffy 1987
Ecole Polytechnique de Montreal	Direct shear tests	Plastic clay (PI: 30%)	Woven and nonwoven geotextiles	Clay samples were molded at different water contents	Contact efficiency for nonwoven geotextiles exceeded 100%, and for wovens decreased to 60%	The better frictional characteristic of nonwoven geotextile were attributed to the presence of randomly oriented fibers	Lafleur et al. 1987

Table 2.2 (Cont.)

Research agency	Test type	Soil	Reinforcement	Characteristics	Observed behavior	Conclusions	Reference
Georgia Inst. of Technology	Direct shear tests	Gulf coast clay; glacial till	Nonwovens wovens, PVC, HDPE	A large shear box was used	For geosynthetics with moderately rough surfaces, the sliding did not occur along the interface, but within the soil	Adhesion is primarily a function of soil type, moisture content, and the surface roughness of the geosynthetic	Williams & Houlihan 1987
Univ. of Queensland, Australia	Shearbox and pullout	Silty clay (PL: 14%; LL: 27%)	Wovens, nonwoven, geogrids	Drained and undrained tests	Shear strength of clay was increased by geotextile reinforcement in both undrained and drained loading	For high transmissivity geotextiles or for geogrids, pullout resistance is limited by the tensile strength and relaxation of the material	Fourie & Fabian 1987
Lakehead U., Canada	Direct shear	Plastic and non-plastic silty clays	Woven and nonwoven geotextiles	Samples were saturated for testing	Efficiencies were approximately 60% for woven geotextiles and 70% for nonwoven geotextiles	Direct shear tests are appropriate to determine shear strength values at soil-geosynthetic interfaces for low stress level applications	Eigenbrod & Locker 1987
AIT, Bangkok	Direct shear and pullout	Clayey sand, weathered clay	Polymer geogrid, bamboo	Samples were tested at optimum moisture	Bamboo grids showed higher pullout resistance than the polymer geogrids	Reinforcement interaction results from soil reinforcement adhesion and from bearing capacity by the geogrid transverse members	Bergado et al. 1987
Univ. of Queensland, Australia	Pullout	Silty clay. Saturation of 95%	Woven and nonwoven geotextiles	In-soil tensile strength of geotextiles was determined	Geotextile modulus greatly increased due to confinement. This increase was considerable larger for nonwoven geotextiles	Soil confinement increases the tensile modulus of geotextiles due to improved interfiber friction and interlocking	Fabian & Fourie 1988
Nihon University, Japan	Direct shear	Volcanic ash clay (Kanto loam)	Woven and nonwoven geotextiles	Soil at optimum water content	No peak friction observed during shearing. Similar friction-displacement response observed for all geotextiles	Mobilized interface friction is generally a small portion of soil friction	Makiuchi & Miyamori 1988
I.I.T., Madras, India	Direct shear	Kaolin, silty clay	Woven geotextile	Samples were tested dry and wet of optimum	Molding water content significantly affected the strength of samples	At low water content, geotextile does not affect kaolin samples, but produced loss in strength in silty clay	Krishnaswamy & Raghavendra 1988
Univ. of Alberta, Canada	Direct shear tests	Silty clay	Four geogrids, one woven geotextile	Samples were compacted dry of optimum	Reinforced and unreinforced clay exhibited similar stress-deformation relationships	Construction method and geometry of reinforcement strongly influence the shear strength behavior	Richards et al. 1989
STS Consultants Ltd.	Pullout tests	Four cohesive soils	Geotextiles; geogrids	Tests performed under drained and undrained conditions	Differences in as-placed water content resulted in significant variations in undrained strength.	Current evaluations of pullout resistance are generally conservative	Christopher & Berg 1990

Table 2.2 (Cont.)

Research agency	Test type	Soil	Reinforcement	Characteristics	Observed behavior	Conclusions	Reference
Warsaw Agricultural Univ.	Direct shear and pullout tests	Organic mud soils (silty clay)	Nonwoven geotextiles	Pullout tests performed in modified triaxial apparatus	Pullout tests gave frictional resistance 30% smaller than obtained from direct shear tests	Pullout and direct shear test results showed linear relationship between shear and normal stress	Garbulew-ski 1990
Univ. of California, Berkeley	Direct shear and pullout tests	Compacted clay	HDPE, geotextile, geonet	Components of a clay liner system were investigated	Minimum residual frictional resistance was fully mobilized at small deformations	Critical interfaces were those between HDPE and geotextile, HDPE and geonet, and HDPE and saturated compacted clay	Mitchell et al. 1990
Univ. of California, Berkeley	Direct shear tests	Compacted clay (soil-bentonite)	Smooth HDPE geomembranes	As-compacted and unconsolidated undrained tests	Contours of strength values could be drawn in zones roughly parallel to the zero air voids curve	As compacted HDPE-clay interface friction angles can change by factor of two as a result of minor variations in compaction conditions content	Seed & Boulanger 1991
Scientific Research Council, Baghdad	Pullout tests; swelling tests in oedometer apparatus	Mixtures of kaolinite and bentonite	Nonwoven polymer geogrids	Geogrid stiffness, soil plasticity index, and applied surcharge were varied	Reinforcements reduced both the final swell, and the rate of swell	Reduction in swell due to reinforcement increases with increasing stiffness of the geogrid	Al-Omari & Hamodi 1991
Indian Inst. of Science, Bangalore	Pullout tests	Sawdust and Kaolin clay	Steel bars and flats	Thin zone of sand was placed around the reinforcement	Using fine-grained backfill soil with 15-mm of sand around the reinforcement increased the interface strength to that obtained using only sand as bulk material	The required thickness of sand layer depends on the surface roughness of the reinforcement and the strength of the fine-grained medium	Sridharan et al. 1991
AIT, Bangkok	Pullout tests	Clayey sand, lateritic soil, weathered clay	Steel grid	Large pullout box was used	Pullout resistance increased with increasing overburden pressure (soil compacted dry of optimum)	Laboratory pullout tests were a conservative approximation of the field pullout resistance	Bergado et al. 1992a
AIT, Bangkok	Pullout tests	Weathered Bangkok clay	Steel grid	Soil compacted both dry and wet of optimum	Pullout resistance was much higher for backfill compacted dry of optimum	As-compacted moisture content has a significant effect on pullout resistance	Bergado et al. 1992b
Korea Institute of Construction Technology	Pullout tests	Weathered granite (CL)	Protruded members attached to reinforcements	Soils tested as compacted	Coefficient of passive resistance decreased with increasing width and/or length of reinforcements	Results are influenced by the three dimensional nature of shear failure surface and by the progressive nature of the pullout failure	Sohn et al. 1992
Univ. Fed. de Ouro Preto, Brazil	Shearbox tests	Kaolin clay	Woven and nonwoven geotextiles	Large direct shearbox was used	Clay-nonwoven interface friction was higher than soil friction	Clay-geotextile interaction mechanisms are similar to those obtained using sand backfill	Gomes 1992

Table 2.2 (Cont.)

Research agency	Test type	Soil	Reinforcement	Characteristics	Observed behavior	Conclusions	Reference
WES, Corps of Engineers	Pullout and shearbox tests	Clay, silty clay, silty sand	Woven geotextiles	Tests were performed at various normal stresses and water contents	Increase of pullout rate caused increase in apparent pullout resistance. Water submergence decreased the apparent pullout resistance	Increase of normal stress causes increase in pullout resistance only in unsaturated samples	Gilbert et al. 1992
AIT, Bangkok	Large scale pullout and direct shear	Weathered Bangkok clay	Steel, bamboo, polymeric geogrids	Samples were tested dry of optimum water content	During pullout tests, steel and bamboo grids moved as rigid body, while polymer grids elongated along the reinforcement length	For steel grids, most pullout resistance were from the passive-bearing resistance of transverse members. Opposite results were obtained for bamboo grid and polymer geogrids	Bergado et al. 1993

reinforcements mobilizes substantial friction in spite of the narrowness of the reinforcements. Consequently, the use of granular backfill in these reinforcement systems is not only important to prevent an undrained condition, but also to induce dilatant behavior in the compacted backfill.

A laboratory study was performed by Elias (1979) to analyze the possibility of using fine grained backfills in Reinforced Earth structures. This study focused on the determination of fine soil-reinforcement friction parameters and on a qualitative evaluation of creep characteristics of ribbed reinforcements in fine grained soils. Pullout tests were performed using samples compacted at or near their optimum moisture contents. All the tested soils were either non-plastic or of low plasticity and exhibited relatively large values of undrained shear strength. The apparent friction coefficient (average peak shear stress along the strip divided by the normal pressure on the strip) was, contrary to pullout results obtained using cohesionless soils, less than the drained friction angle of the soil as measured by direct shear tests. Figure 2.5 shows the results of pullout tests using ribbed reinforcing strips in residual soils with different fines content. The apparent friction coefficient varies considerably with the normal pressure applied to the strip and, at all pressures, there is a drastic reduction in the coefficient magnitude with increasing fines content (Elias and Swanson, 1983). The effect of compaction moisture content on the apparent friction coefficient can be observed in Figure 2.6, which shows a significant decrease when compaction moisture content was only 2% above optimum.

Ingold (1981) carried out shear box tests to investigate the undrained behavior of inclined reinforcements embedded in clay. Metallic reinforcements (mild steel Z-plate, plain plate, and corrugated plate), as well as polythene and polyethylene meshes were

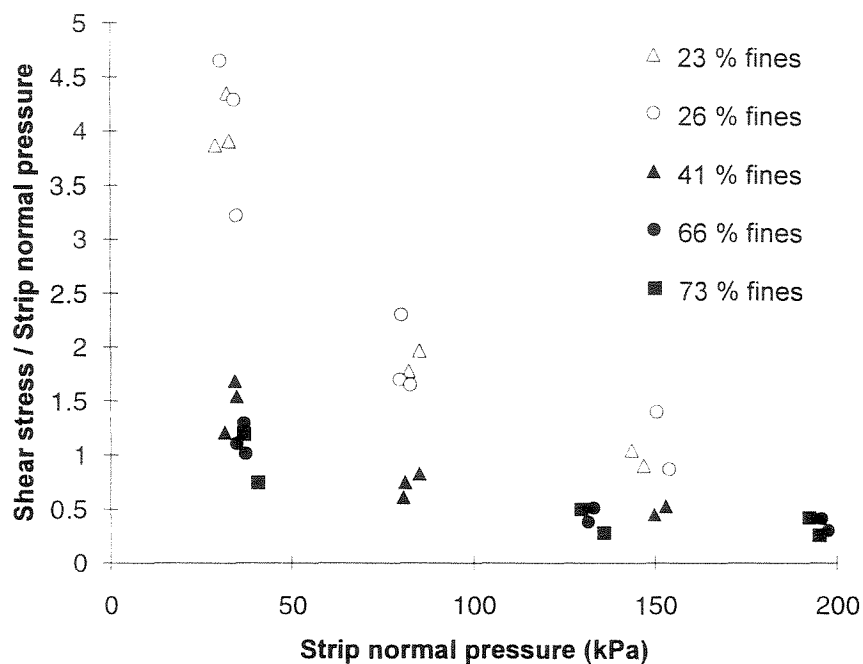


Figure 2.5 - Strip pullout capacity versus normal pressure for soils with different fines content (redrawn after Elias and Swanson, 1983).

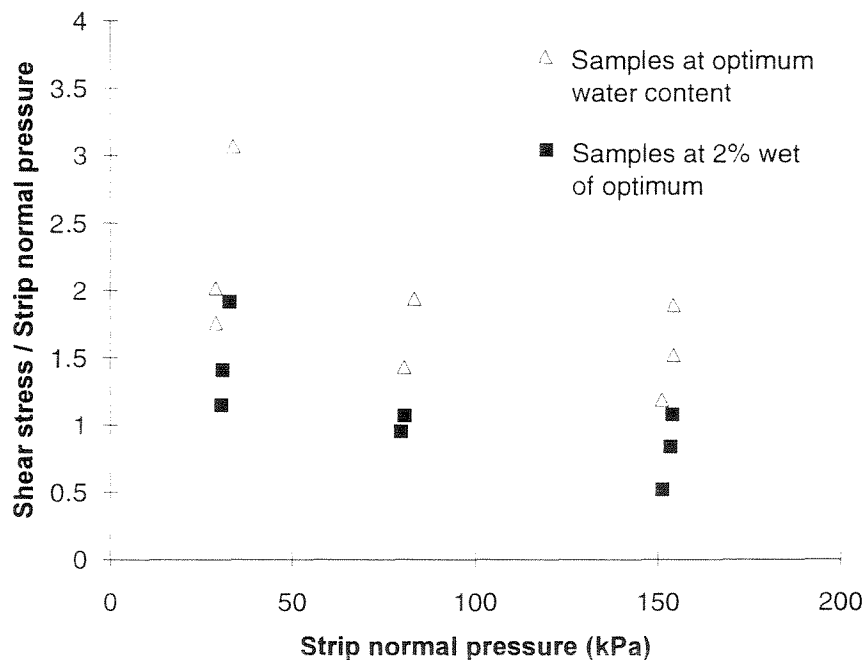
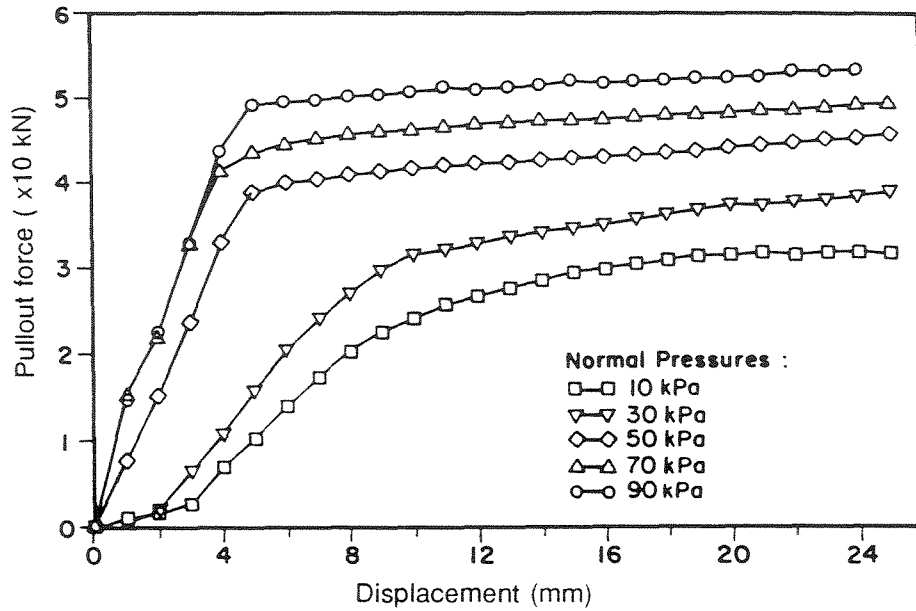


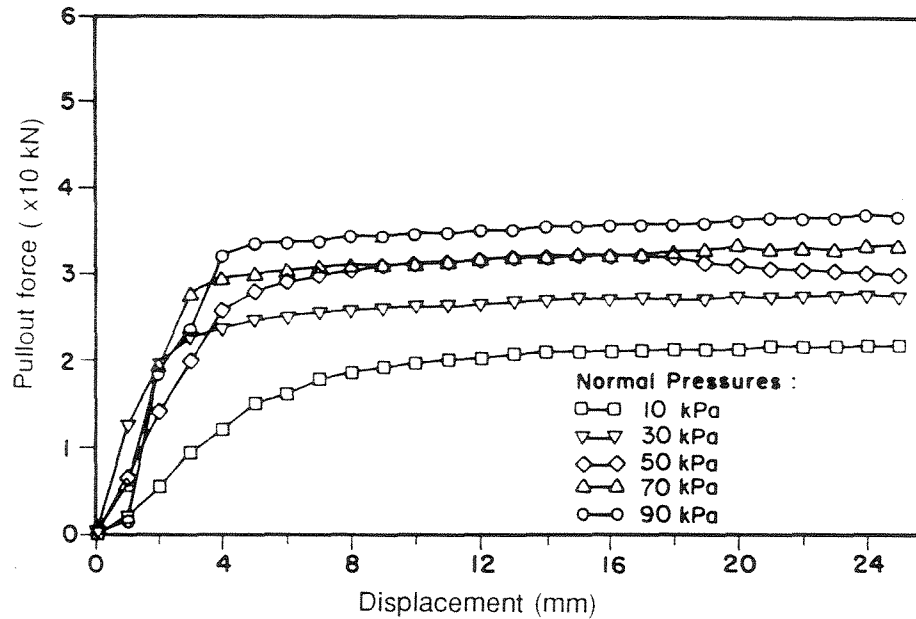
Figure 2.6 - Strip pullout capacity versus normal pressure for samples at two water contents (redrawn after Elias and Swanson, 1983).

used in this study. Test results were compared using adhesion factor values that relate the apparent undrained shear strength of the reinforced clay to the true undrained shear strength of the unreinforced clay. Although the corrugated steel plate was found to perform better than the other metallic inclusions, the polyethylene mesh was the most efficient of all the reinforcements tested.

Laboratory and field pullout tests were conducted using steel grid reinforcements with cohesive-frictional backfill soils (Bergado et al., 1992a). The laboratory pullout tests were performed using a large scale pullout apparatus, and the field pullout tests were done on dummy welded-wire reinforcements embedded in a full-scale reinforced test structure. Three different low-quality backfill soils, namely, clayey sand, lateritic soil, and weathered Bangkok clay were used. The backfill material was compacted to densities of about 95% of the Standard Proctor maximum density, on the dry side of the optimum moisture content. The laboratory pullout test results were reported to provide a conservative approximation of the field pullout resistance of the grid reinforcements. Additional pullout tests were carried out using welded-wire mild steel grids embedded in weathered Bangkok clay, after compacting the backfill material both dry and wet of optimum moisture content (Bergado et al., 1992b). Typical load-displacement relationships for dry and wet side of optimum compaction, shown in Figure 2.7, indicate that the pullout resistance is significantly higher for backfill compacted dry than wet of optimum. Tests performed using reinforcements with their transverse members removed showed that the pullout resistance was carried mainly by the passive component mobilized by transverse members of the welded-wire grid, with only a minimal frictional contribution from the longitudinal bars.



(a) Samples compacted dry of optimum water content



(b) Samples compacted wet of optimum water content

Figure 2.7 - Typical load-displacement curves from pullout tests using welded-wire steel grids in weathered clay (after Bergado et al., 1992b).

This review of published results on the interaction between poorly draining soils and metallic reinforcements shows that, although some metallic reinforcements were observed to effectively reinforce poorly draining soils if moisture content was low, the results were very dependent on the compaction water content. The effect of backfill saturation requires further study and the concern of metal corrosion should be addressed prior to the long-term use of metallic reinforcements in poorly draining soils.

2.4.2 Poorly draining soil-geogrid interaction

The adhesion between kaolin clay and polymeric and other reinforcements was investigated by Ingold (1981) using both unconsolidated undrained direct shear and pullout tests. Contact efficiency was initially investigated using a direct shear box with the reinforcements inclined across the two halves of the box. In these tests, performed with kaolin clay compacted at a moisture content close to its plastic limit, polyethylene geogrids were the most efficient reinforcements. The inclined reinforcements caused an apparent shear strength increase in the clay samples, which was interpreted as induced by the resistance of the reinforcement to rotation rather than pullout. Consequently, the bending stiffness of the reinforcement was considered to have a significant effect. Tests were then performed using horizontal polyethylene geogrids. The contact efficiencies were markedly dependent on test method, with generally higher values being obtained from the shear box and lower values from the pullout apparatus. An undrained pullout resistance equation based on these results was formulated by Ingold (1983), suggesting that geogrid pullout resistance is a function of the area of geogrid members normal and parallel to the direction of applied load rather than the embedded plan area.

Direct shear tests on samples of lightly over-consolidated kaolin, also using geogrid reinforcements inclined across the two halves of the box, were performed by Jewell and Jones (1981). Results from both drained and quick direct shear tests showed that the reinforced kaolin was both stronger and stiffer than the unreinforced clay. Thin vertical threads of fine lead powder were introduced into each sample, and the prints of radiographs showed that reinforcement caused a wider zone of kaolin to be deformed. The deformation pattern is similar to that obtained by Shewbridge and Sitar (1989) on reinforcement-sand composites.

Brand and Duffy (1987) performed additional pullout tests on four types of polymeric geogrids. An expansive smectite clay was placed with a low moisture content, approximately 10%, to simulate initial placement conditions. Since similar pullout resistance values were obtained using the different geogrids, the authors concluded that pullout resistance of geogrids in low moisture content clays was relatively insensitive to the geogrid characteristics. Direct shear and pullout tests on polymer geogrid embedded in cohesive soils (clayey sand and weathered clay) were also performed by Bergado et al. (1987). Based on the results from tests performed on soil specimens compacted to 95% of standard Proctor density at optimum moisture content, they concluded that cohesive soils can be effective backfill material for geogrid reinforced embankments. The pullout resistance of the geogrids using cohesive backfill was interpreted to be due to adhesion between the soil and the reinforcement on the plan area of the geogrids as well as passive resistance of the soil in front of all transverse members. The interaction of weathered clay with steel, bamboo, or polymeric geogrids was compared by Bergado et al. (1993). Soil specimens were compacted at the dry side of optimum to 95% of

standard Proctor density. While the steel grids moved as a rigid body during the pullout tests, the polymeric grids showed varying resistance mobilization along the reinforcement.

Results from both short- and long-term pullout tests on polymeric geogrids and geotextiles, performed in cohesive soils, were reported by Christopher and Berg (1990). The short-term tests were performed to evaluate the influence of pore water pressure generation, while the long-term pullout tests were used to investigate the soil-geogrid creep response. Consistent test procedures in a large pullout box were used for all tests, with loading rates to failure varying from several hours to several months. Although different cohesive soils were used in the test programs, the soil characteristics were similar in terms of liquid limits and plasticity indices. The main variation between the soils was the as-placed water content, which resulted in a significant variation in undrained shear strength. Drained pullout resistances were not necessarily greater than the undrained ones. Figure 2.8 shows displacement measurements at the front and back of a sample compacted wet of optimum for both the undrained and drained conditions. The nearly constant movements of the front and rear gages observed in this particular test indicate failure by pullout. Pullout resistance values calculated using the interaction coefficients recommended by the manufacturers were conservative in relation to the experimental test results.

The reported results from shearbox and pullout tests performed using geogrids embedded in poorly draining backfills generally showed encouraging results. Most tests were performed on samples with moisture contents that simulate typical initial field placement conditions, that is, at optimum water content or dry of optimum. However, the field placement conditions of the backfill material may not correspond to the worst case

scenario over the life of the structure. Consequently, the effect of fill water content changes on the performance of reinforced structures should be further investigated. Drainage and collection systems should be used to help maintain a low moisture content in the structure backfill.

2.4.3 Poorly draining soil-geotextile interaction

Direct shear tests using three geotextiles (a thick nonwoven, a thin nonwoven, and a woven) were performed by Lafleur et al. (1987) to evaluate the contact efficiency of geotextiles in medium plasticity lateritic gravels and highly plastic clays. The shear testing program was undertaken to justify the choice of a geotextile in reinforced fill applications involving lateritic gravel embankments laid over a soft clay foundation. The soil strength and the soil-geotextile adherence parameters were obtained using strain rates slow enough to create a drained condition. The contact efficiency was up to 1.0 in the case of nonwovens and 0.5-0.6 for wovens. The smooth surface of the woven geotextiles did not permit particle penetration and the creation of strong adhesion between the soil and the geosynthetic. However, as indicated in Figure 2.9, the relative displacement between the reinforcement and the soil required to mobilize the total shearing resistance was significantly larger in the tests performed with the lower-stiffness nonwoven geotextiles. Lafleur et al. concluded that the nonwoven geotextiles offer superior performance because the adherence values are higher and, in cases where the loads are applied at a fast rate, they can convey water coming out of the soil from consolidation.

The contact efficiencies for five geosynthetics and seven soils, measured using a modified direct shear device, were reported by Williams and Houlihan (1987). Test

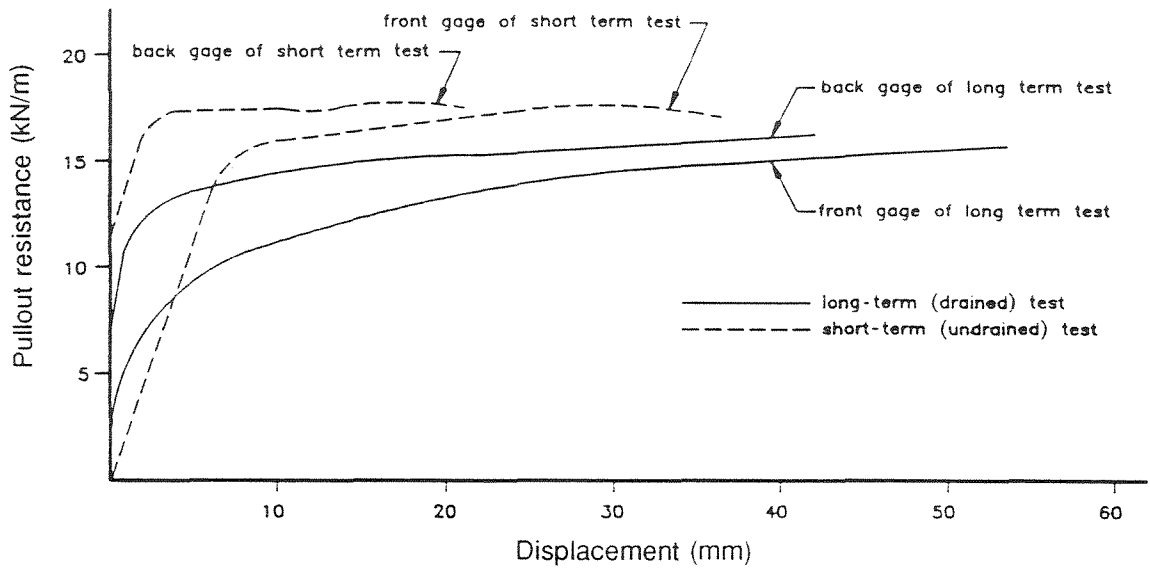


Figure 2.8 - Load-displacement curves from pullout tests on polymer geogrids (after Christopher and Berg, 1990).

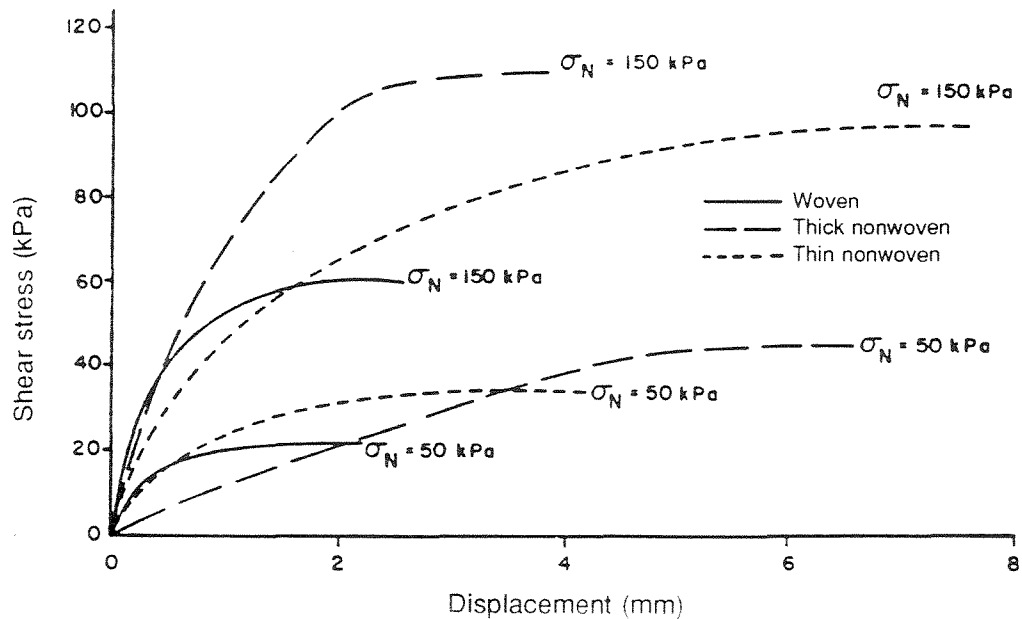


Figure 2.9 - Direct shear test results for three types of geotextile in a plastic clay (moisture content 40%) (after Lafleur et al., 1987).

results indicated three primary modes of failure: sliding along the interface between the soil and the geosynthetic; failure along a surface in the soil parallel to the geosynthetic layer, and failure along a surface between two adjacent layers of geosynthetics. The location of the sliding surface and magnitudes of the interface friction parameters were found to be a function of the soil type, the soil water content and density, and the surface roughness of the geosynthetics. Sliding along a failure surface which develops within the soil, parallel to the geosynthetics, was reported for tests performed with nonwoven and woven geotextiles with cohesive soils. In contrast, sliding occurred on the interface between the soil and the geosynthetic in tests performed to evaluate the interface friction of cohesive soils with smooth sheets of polyvinyl chloride (PVC) and high density polyethylene (HDPE).

Fourie and Fabian (1987) performed shearbox and pullout tests to investigate the major factors governing the clay-geotextile interaction in both undrained and drained conditions. The undrained tests were actually rapid tests with shearing and pullout displacement rates of 0.9 mm/min. Woven and nonwoven geotextiles were used in the tests, performed in a small shearbox apparatus using a silty clay (CL) with a plasticity index of 13%. The authors identified the stiffness, the surface roughness and the transmissivity of the geotextile as the main factors affecting the undrained shearing interaction. The shearing strength of the clay was increased by the high-transmissivity nonwoven geotextile. At any stress level, the nonwoven reinforcement was reported to have a higher contact efficiency than the woven reinforcement. The pullout resistance was found to be strongly related to the shearing interaction, but it was also affected by the stiffness and the tensile strength of the geotextile. Load-displacement curves of

undrained pullout tests showed that, in the pullout mode, the nonwoven and the woven geotextile performed equally well. However, the ultimate load in tests performed using the nonwoven material was generally limited by the geotextile tensile strength and not by the pullout resistance.

In drained conditions, the clay-geotextile interaction observed by Fourie and Fabian (1987) was similar to sand-geotextile interaction. However, the pullout resistance was influenced by the relaxation of the geotextile during long-term testing. This reduced the tensile strength of the geotextile, producing a lower ultimate pullout resistance than in the undrained tests. Load-displacement curves showed that the maximum pullout resistance required significantly more displacement than that required to mobilize full shearing resistance. The authors concluded that high-transmissivity nonwoven geotextiles can effectively reinforce clay in both undrained and drained shear. The pullout resistance of high-transmissivity geotextiles is limited by the tensile strength and the relaxation properties of the reinforcement. Woven geotextiles can effectively reinforce clay in drained conditions because of their rough surface, which induces dilation during shearing, but these materials do not perform as well in undrained conditions due to their low transmissivity.

The pullout resistance of woven geotextiles in cohesive soils was investigated by Gilbert et al. (1992) using 0.6 m by 0.6 m test specimens. Laboratory parameters were compared with prototype field tests. Three high-strength woven polyester geotextiles were tested using clays, silty clay, and silty sand specimens. The effect of increasing the rate of pullout deformation was to increase the apparent pullout resistance of the system. This increase was observed at water contents between the liquid and plastic limits and

was attributed to viscosity mechanisms. Submergence below water decreased the apparent pullout resistance as a result of the loss of capillary tension. Slippage was not observed at the clay/geotextile interface, but within the soil mass, and it was interpreted that pore water pressures generated by shear strains were partly dissipated through the woven geotextiles.

Although an increase in pullout resistance was obtained by increasing the normal stress, this effect was dependent on the soil water content. Figure 2.10 shows how pullout resistance decreases with increasing water content and appears to reach a limiting value at about 40% water content for all normal loads. Results from laboratory pullout tests as well as full-size prototype field tests performed using low water content (26%) specimens showed increasing pullout resistance with increasing normal stress (Figure 2.11a). On the other hand, laboratory and full-size tests using soil at 40% water content

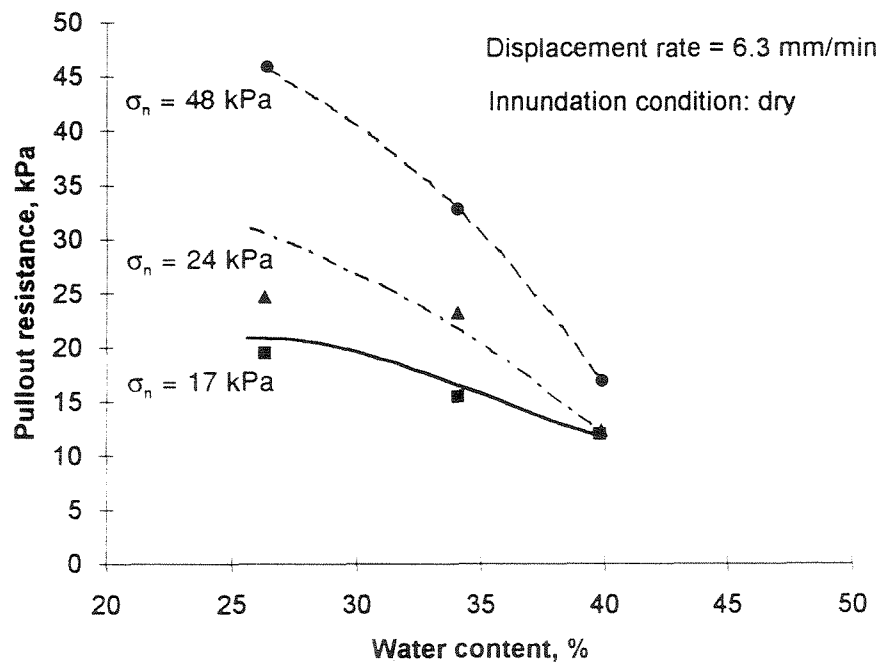


Figure 2.10 - Effect of water content on the pullout resistance of a woven geotextile in a plastic clay (after Gilbert et al., 1992).

showed that pullout resistance is affected by induced pore water pressures. This may be observed in Figure 2.11b, in which strength appears to be essentially constant and unaffected by normal stress.

Additional studies were done to investigate the clay-geotextile interaction for different applications and systems (Saxena and Budiman, 1985; Eigenbrod and Locker, 1987; Fabian and Fourie, 1988; Makiuchi and Miyamori, 1988; Garbulewski, 1990; Gomes, 1992). Test details and conclusions are summarized in Table 2.2.

This evaluation of shearbox and pullout tests done with geotextiles highlights the different results obtained using low permeability woven and permeable nonwoven reinforcements. Geotextiles with adequate in-plane transmissivity, namely nonwoven geotextiles, can be effectively used to reinforce clay structures under both rapid and fully drained conditions. Reinforcement of marginal soils might be enhanced by combining the high tensile strength of woven geotextiles with the high transmissivity of nonwovens in a composite geotextile.

2.4.4 Poorly draining soil-geomembrane interaction

Even though geomembranes are not ordinarily used as reinforcement elements, evaluation of shearing resistance between various geomembranes and cohesive soils is important for other applications. Geomembranes used in solid waste disposal systems are often placed directly on low permeability compacted clay soils. Direct shear and pullout tests have been performed to evaluate the shear strength along clay-geomembrane interfaces, which may be critical to the stability of multilayered liner systems. A clear evidence of this hazard was the slope-stability failure of a Class I hazardous-waste landfill

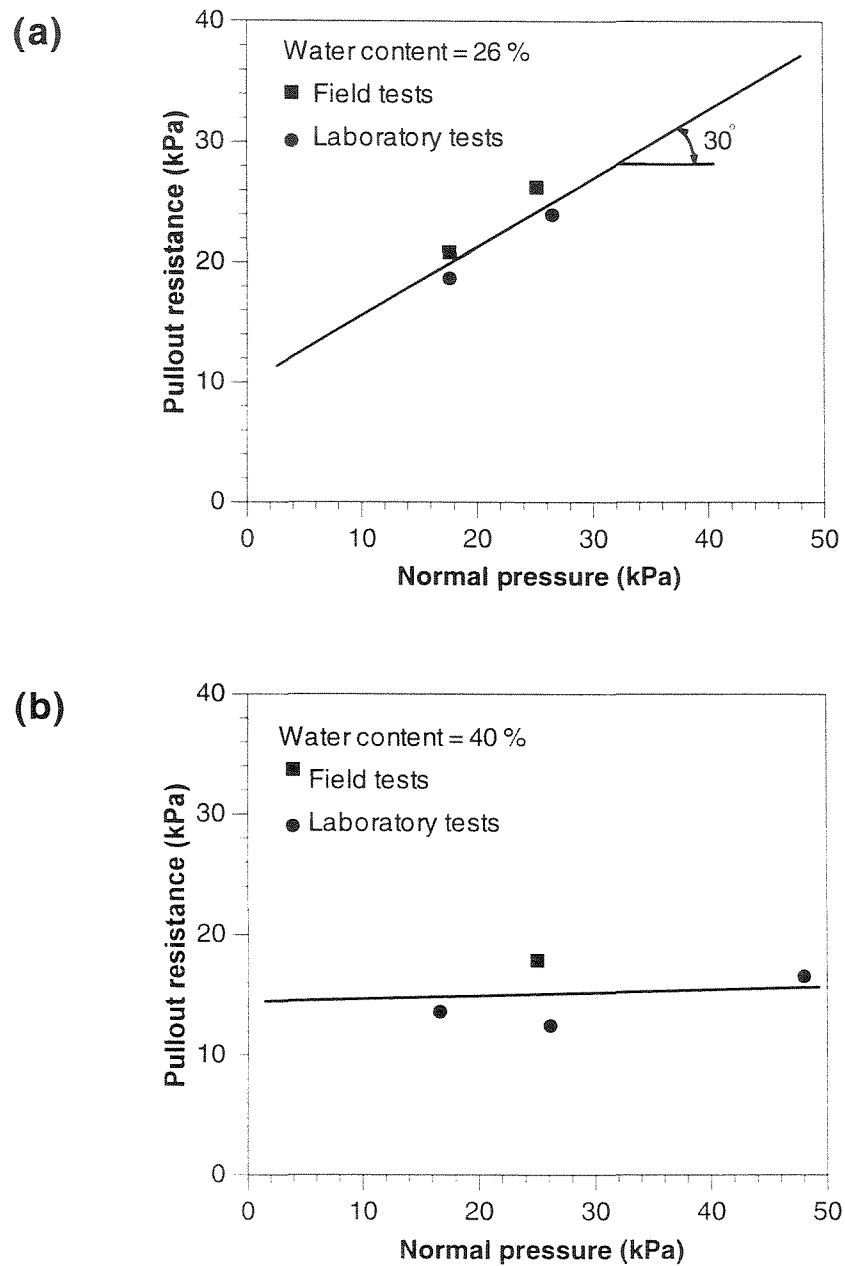


Figure 2.11 - Pullout resistance of a woven geotextile versus normal load in clay specimens molded (a) at 26% water content; (b) at 40% water content (after Gilbert et al. 1992).

at Kettleman Hills (Mitchell et al., 1990; Seed et al., 1990) that resulted from slippage along interfaces within a multilayered liner system. Accordingly, a few significant references regarding geomembrane-cohesive soil interaction are reviewed herein.

Koerner et al. (1986) determined the interface shear strength between various geomembranes and a number of cohesive soils using direct shear tests. Despite the low permeability of the soils, the tests were considered to be drained, as the soils were less than fully saturated (75-85%). A standard direct shear apparatus was considered to be useful for obtaining site-specific data on a production basis. The adhesion of geomembrane to soil was significantly lower than the cohesion value obtained for the soil. Conversely, the friction angle at the soil-geomembrane interface was reasonably high. Interface friction was as high as the soil friction angle for the case of soft (chlorinated polyethylene, ethylene propylene diene monomer) and textured (HDPE) geomembranes, being somewhat lower for harder (PVC, HDPE) geomembranes. The data base of adhesion and friction values for interfaces between common liner materials can be used for practical design considerations, such as preliminary assessments of stability.

A testing program performed to evaluate the shear resistances along different interfaces in a composite liner system was described by Mitchell et al. (1990). Both direct shear tests and pullout tests were carried out, and the obtained interface parameters were used for the stability analyses of the Kettleman Hills waste landfill slope failure. The interfaces between the various geosynthetics, and between these materials and the compacted clay in the liner system, were characterized by low frictional resistance, with interface friction angles as low as 8° for some combinations. The direct shear tests on HDPE-compacted clay liner interface samples were performed under two sets of

conditions. The first test series was done on unsaturated as-compacted samples, that showed residual friction angles between 11° and 14° . The second series was performed on samples initially compacted to field conditions and then submerged and soaked under light surcharges. In this case, the resulting interface-shear strengths were independent of the applied normal stress, exhibiting residual interface strengths of between 39 and 49 kPa. Shear tests on geotextile-compacted clay liner interfaces were performed using clay liner material first compacted to field conditions and then soaked under light surcharge. These direct shear tests were intended to represent unconsolidated undrained testing conditions, though the geotextile probably facilitated pore pressure dissipation at the geotextile-clay interface contact. A residual friction angle of 24° was obtained for this interface.

A wide range of interface shear strengths has been reported by different laboratories for apparently similar combinations of geomembranes and soil conditions. In order to investigate the causes of such differences, Seed and Boulanger (1991) analyzed shear strength data for smooth HDPE-compacted clay interfaces. Direct shear tests results, performed on smooth HDPE in contact with two different clay liner materials, showed that the interface strength varies greatly over the range of possible as-compacted conditions. Some of the test results, expressed as equivalent friction angles (ϕ_r), are shown in Figure 2.12. Two sets of results are shown: samples sheared as-compacted, and samples soaked under a small normal stress (12 kPa) prior to application of surcharge and undrained shear. As shown in Figure 2.12a, the interface shear strengths for samples sheared in as-compacted conditions are strongly influenced by compaction conditions (as-compacted density and water content). Interface friction angles may differ

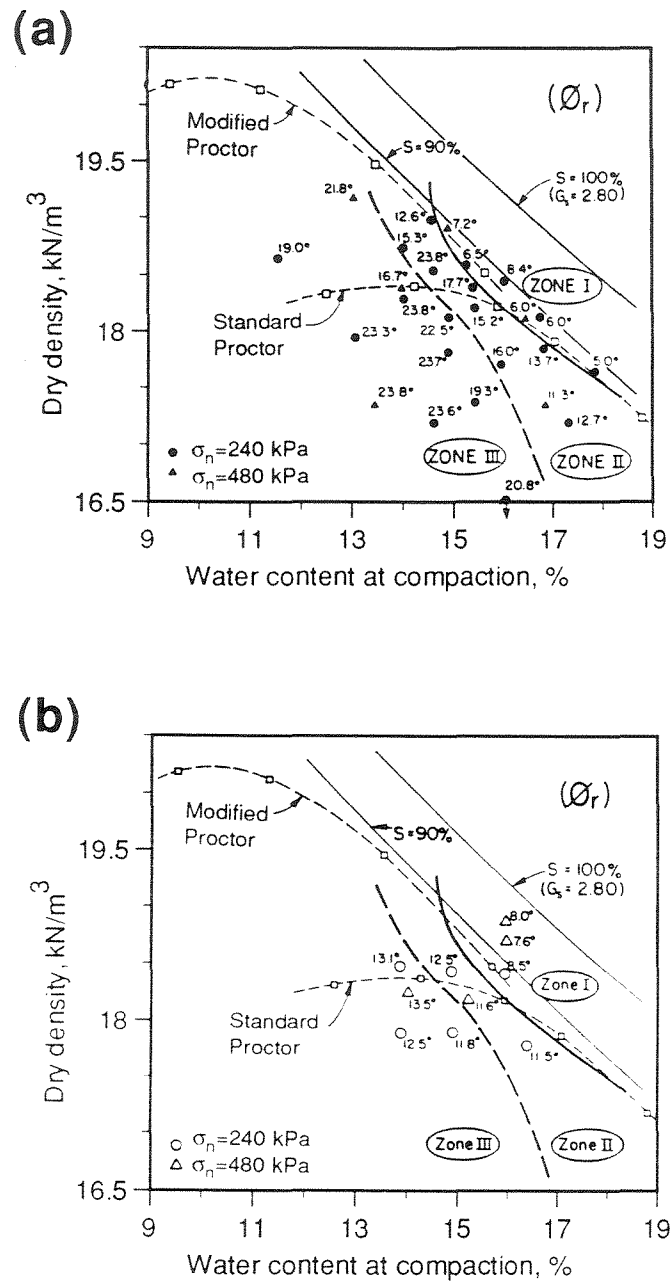


Figure 2.12 - Shear strengths for smooth HDPE-compacted clayey till interfaces: (a) as-compacted samples; (b) samples sheared after initial pre-soaking (after Seed and Boulanger, 1991).

by a factor of two or more as a result of relatively minor variations in as-compacted dry density and water content. Zones roughly parallel to the zero air voids curve can be defined by drawing contours of shear strength values. The probable reasons for different shear strength zones were reported to be the degree-of-saturation and soil fabric effects (e.g. flocculated versus dispersed fabric). As shown in Figure 2.12b, the differences in strength among the zones are reduced as a result of pre-soaking. However, this is primarily a result of significant reductions in the strengths for samples in Zones II and III since the strengths of samples compacted in Zone I are not appreciably changed.

The results presented by Seed and Boulanger (1991) for cohesive soil-geomembrane interfaces suggest that compaction conditions and pre-soaking would greatly influence the interface strength between cohesive soils and other geosynthetics. Shearbox and pullout tests on metallic, geogrid, and geotextile reinforcements have not yet been done to fully address the effects of these conditions.

2.5 Hydraulic function of geosynthetic reinforcements

Permeable geosynthetic reinforcements may be especially useful for soil structures with poorly draining backfills because the drainage capabilities may help increase the structure stability by dissipating excess pore water pressures. In this way, the geosynthetic layers may work not only as reinforcements but also as lateral drains. In order to formulate a rational design that takes into account the in-plane transmissivity of the geosynthetic reinforcements, their hydraulic characteristics must be evaluated. Such evaluation includes the correct determination of the reinforcement drainage capacity, the

analysis of the pore water pressure dissipation in the fill, and the assessment of the effect of pore water pressures on the structure stability.

2.5.1 Determination of in-plane hydraulic conductivity

Relatively little study has been made of the in-plane hydraulic conductivity of geotextiles as compared to the cross-plane conductivity. The test methods commonly used for measuring the in-plane hydraulic conductivity of geotextiles are the parallel flow test (ASTM Standard D 4716), and the radial flow test. In the parallel flow device, flow occurs parallel to and between two rigid plates by applying a constant head difference across the specimen. The in-plane hydraulic conductivity is then measured by monitoring the flow rate while the geotextile is under confinement. The radial flow test uses a circular disk-shaped geotextile specimen that allows flow to enter the geotextile specimen at the inner circumference. The stream lines of the flow therefore radiate from the center of the circular disk outward in all directions.

However, the common tests used to determine the in-plane hydraulic conductivity do not always reproduce the geosynthetic field conditions. A test apparatus, capable of measuring geotextile transmissivities under specified constant hydraulic heads and under confinement, was described by Ling et al. (1990, 1993). Using this apparatus, a nonwoven geotextile and a woven/nonwoven composite geotextile were tested to measure their in-plane hydraulic conductivity under various normal stresses. Three methods of geotextile confinement were used to simulate the in-soil condition: rigid blocks, flexible membranes, and soil. Soil-confinement tests were performed by placing compacted cakes of volcanic ash clay on each side of the geotextile. Figure 2.13 shows the relationship

between in-plane hydraulic conductivity and confining stress for the nonwoven geotextile. As would be expected, the in-plane hydraulic conductivity is strongly dependent upon the effective normal stress. Similar behavior was observed for the composite geotextile. As shown in the figure, the hydraulic conductivity of the geotextiles was influenced by the method of confinement. Differences in the measured hydraulic conductivity were attributed to interface flow, mainly under rigid block confinement, and to soil penetration and retention that occurs under soil confinement. Based on these results, it was concluded that in-plane hydraulic conductivity for a geotextile embedded in soil could be overestimated if the test is performed using block or membrane confinement.

Soil-confinement tests were also performed to determine the in-plane hydraulic conductivity of geotextile specimens retrieved from the field after several years of installation. The geotextile specimens were extracted from a test embankment built at the University of Tokyo (Tatsuoka and Yamauchi, 1986). Figure 2.14 shows the in-plane hydraulic conductivities of the fresh and the exhumed nonwoven geotextiles. It can be observed that the field-retrieved specimens gave several times smaller in-plane hydraulic conductivity than fresh specimens. The primary reason for the reduction of in-plane hydraulic conductivity was attributed to clogging of the geotextile by fine soil particles. A direct relationship was observed between the amount of soil retained in a geotextile and the reduction in its in-plane hydraulic conductivity. However, the reduction in in-plane hydraulic conductivity did not affect the performance of the embankment, which was satisfactory in terms of mechanical and hydraulic behavior. An equation proposed by Ling et al. (1993) shows that the reciprocal of hydraulic conductivity varies in a linear

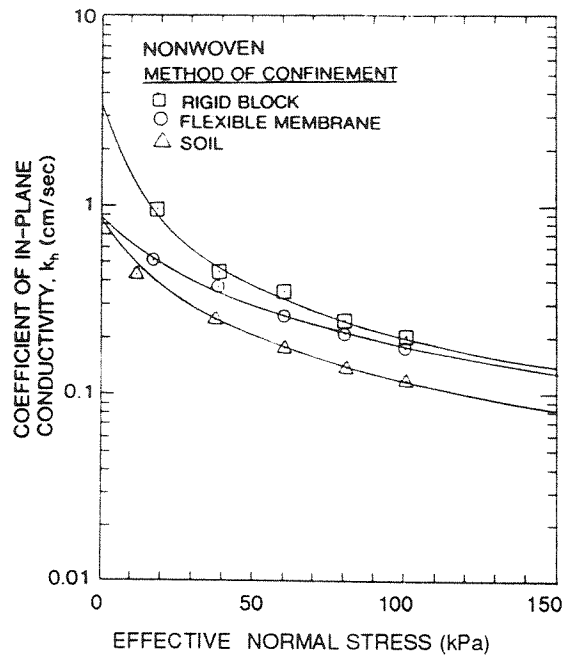


Figure 2.13 - Relationship between coefficient of in-plane hydraulic conductivity and effective normal stress for a nonwoven geotextile (after Ling et al., 1993).

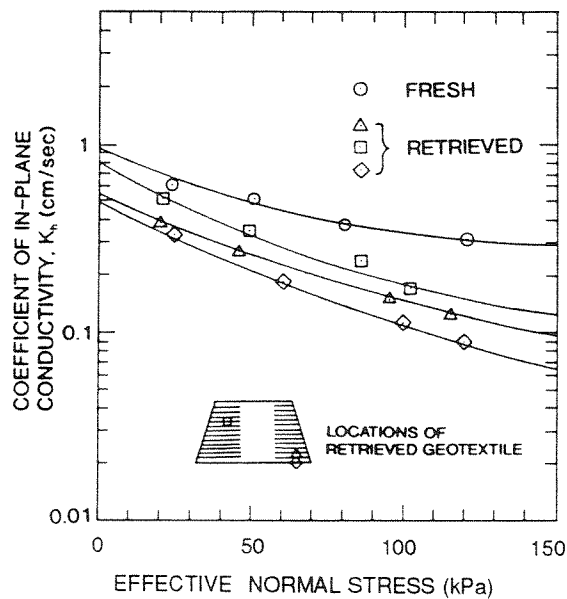


Figure 2.14 - In-plane hydraulic conductivity of fresh and retrieved nonwoven geotextile specimens (after Ling et al., 1993).

manner with effective normal stress. Additionally, a reduction factor was introduced to account for the long-term reduction in hydraulic conductivity due to soil-particle retention.

Additional field experience should be collected to further evaluate the possible clogging of geotextiles that function as reinforcement in marginal backfills. However, a preliminary assessment of the long-term equilibrium flow rate could be made using the clogging resistance criteria already designed to evaluate geotextile filters (e.g. Christopher and Fisher, 1992). Different approaches to assess the long-term flow rate behavior and research needs for geotextiles used in filtration applications are addressed by Koerner et al. (1992).

2.5.2 Analysis of pore water pressure dissipation

Pore water pressure may be generated in a cohesive backfill during the construction process or after rainfalls. Since the compacted fill is generally unsaturated, the pore water pressure distribution in the soil mass is difficult to predict. A conservative estimate of such a distribution can be made if the backfill material is assumed to be fully saturated. This conservative assumption has led to theoretical methods to estimate the geotextile transmissivity requirements and the pore water pressure dissipation after construction of a reinforced clay structure.

Auriault et al. (1977) presented a theoretical treatment for the consolidation of a saturated fill placed between horizontal layers of permeable geotextile. The calculations assumed that the height of the fill was small as compared to its width. The geometry considered in this study is a layer of soil located between two nonwoven geotextile layers as shown in Figure 2.15. One-dimensional consolidation was assumed, and the system

of partial differential equations that models the problem was solved analytically. The calculated rates of consolidation were considered assuming two different cases: constant thickness of the draining geotextile, and taking into account the geotextile compressibility. Numerical examples showed that a typical nonwoven geotextile (with a transmissivity of $6.6 \times 10^{-6} \text{ m}^2/\text{s}$) placed with 2 m vertical spacing would work as a perfect drain in a clay backfill, but would not prevent the generation of positive pore pressures in a silt backfill.

A similar approach, but without the simplifying one-dimensional consolidation assumption, was presented by Bourdillon et al. (1977). The problem was formulated considering two-dimensional consolidation, and solved using finite differences. Parametric studies were carried out by varying the soil layer thickness, drain thickness, embankment width, loading method, and soil and drain hydraulic conductivities. An example of the analysis results is presented in Figure 2.16, where the rate of pore water pressure dissipation obtained using perfect drains is compared to the rate obtained using geotextiles with non-ideal draining capabilities in a silty backfill. A parametric analysis was made to investigate the time required to dissipate 90% of the pore water pressure generated in the center of a soil layer. The minimum drain thickness and the ratio

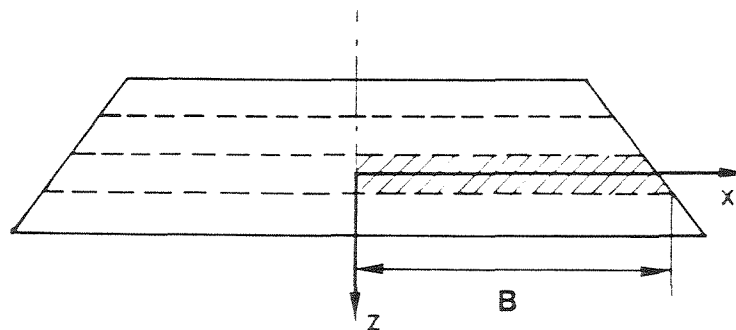


Figure 2.15 - Embankment section showing the semi-layer under study (after Auriault et al., 1977).

between the hydraulic conductivities of the drain and the soil were found to be critical parameters. Other variables investigated in the parametric study, such as the geotextile vertical spacing and the embankment length, were reported to have comparatively less influence on the results. The parametric study showed that a nonwoven geotextile over 2 mm thick will provide perfect drainage if its hydraulic conductivity is 10^4 to 10^5 times higher than the hydraulic conductivity of the soil.

A homogenization method, consisting of replacing the soil-geotextile system by an anisotropic equivalent material, was proposed by Auriault et al. (1982). This approach was considered to be more attractive for practical purposes, since it does not require numerical or analytic treatment as in the method presented by Auriault et al. (1977). Rapid evaluation of the efficiency of the geotextile layers in the embankment consolidation can be made using nondimensional charts. To validate the proposed

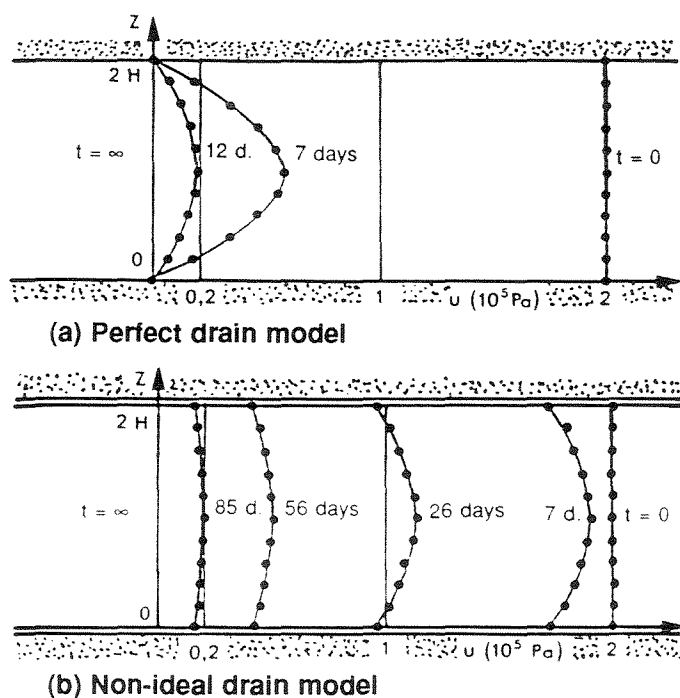


Figure 2.16 - Diagrams of pore water pressure dissipation determined numerically for a silty backfill (after Bourdillon et al., 1977).

homogenization simplification, the obtained results were compared to those obtained using previously proposed analytic methods. The cases for which the homogenization simplification is valid were established in terms of nondimensional parameters.

Giroud (1983) investigated the parameters governing the selection of a geotextile to be used as a horizontal drainage layer. The theoretical study assumed purely vertical flow (one-dimensional consolidation). As a design requirement, it was considered that the water pressure in the geotextile should be small compared to the applied pressure. Additional assumptions led to simple formulas to estimate the required geotextile transmissivity. The controlling factors are the rate of construction, the geotextile width, and the hydraulic conductivity and consolidation coefficients of the soil. The thickness of the soil being consolidated is not always a controlling parameter in the geotextile selection since, for the case of clayey soils, the geotextile spacing governs the consolidation rate but it has no influence on the required geotextile transmissivity. Based on the proposed formulation, it was concluded that the required transmissivity of a geotextile is higher if the soil to be consolidated is a silt rather than a clay. The reason for this result is that water is expelled faster from a consolidating silt than from a clay fill. These conclusions are consistent with the findings of Auriault et al. (1977) and Bourdillon et al. (1977). The criteria presented for selection of geotextiles to be used as draining layers can be easily implemented in practical design applications.

The hydraulic function of geotextiles used to reinforce saturated fine soils was studied by Blivet et al. (1986) using finite element calculations. Displacements, stresses and hydraulic heads were calculated as a function of time using a coupled elastic-plastic formulation. Stiffness and transmissivity of the geotextile layers are the required

parameters for the reinforcement layers, modelled using one-dimensional elements. The dissipation, with the aid of geotextiles, of pore water pressures generated during an embankment construction was calculated. The lowest geotextile transmissivity that avoids generation of positive pore water pressure could also be determined.

The theoretical methods examined in this section were developed to evaluate the rate of settlement due to the fill consolidation rather than to investigate the structure stability. Nonetheless, the formulations can also be used to conservatively estimate the effect of pore water pressure dissipation on the structure stability as consolidation progresses.

2.5.3 Effect of lateral drainage on stability

Some reinforced soil structures have already been constructed using poorly draining backfills reinforced using permeable inclusions (Section 2.7). The effect of lateral drainage on the stability of a reinforced clay structure is twofold: it will produce an increasing soil resistance to shearing along the failure surface, and will result in a pullout resistance that increases with time. However, most reported cases have not taken into account the time-dependent increase in stability provided by the permeable

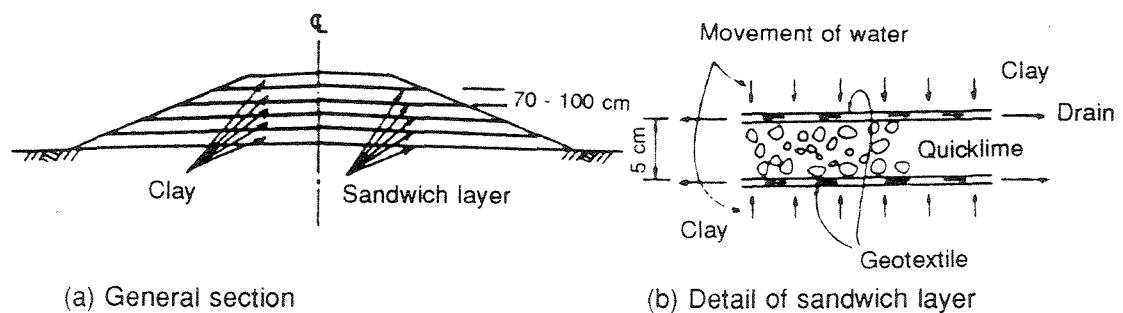


Figure 2.17 - Multiple strip-sandwich method using geotextile-quicklime composite stripes in a clay embankment (after Yamanouchi et al., 1982).

reinforcements. Generally, the analyses have either assumed drained behavior of the unsaturated backfill material or considered total stress soil parameters representative of placement conditions.

Few reported stability analyses take into account the increase in stability that occurs in a clay structure due to consolidation of the backfill. One such case is the analysis of a 32 m high embankment constructed using a specially devised technique, named the multiple strip-sandwich method, that used layers of quicklime and geotextile filter layers (Yamanouchi et al., 1982). Although the stability analysis did not incorporate any tensile resistance for the filter layers, the strength of the cohesive soil was considered to increase during consolidation. Quicklime layers 50 mm thick, sandwiched between two sheets of geotextile, were placed in horizontal layers within the cohesive fill (Figure 2.17). Owing to combined actions resulting from the hydration of quicklime, particularly the absorption of water, the cohesive soil was effectively dewatered. The shear strength of the strongly weathered tuff used as backfill increased due to consolidation. Stability was calculated using the method of slices assuming circular failure surfaces, and taking into account the increase in undrained shear strength of the cohesive soil with time as consolidation progresses. The time-dependent strength gain was estimated using the average degree of consolidation formulated for drain wells. After completing the embankment work, borings were carried out on the embankment to ascertain the effectiveness of the multiple strip-sandwich method. Good improvement of the fill material was observed. Also, inclinometer measurements indicated no horizontal movements in the embankment even during unusually heavy rains.

The strength gain in a cohesive backfill material due to consolidation was also reported by Yunoki and Nagao (1988) for a 20 m high fill slope built in Japan using cohesive soil. Nonwoven geotextiles were used to accelerate consolidation of the fill material and to reinforce the fill slope. The authors employed the method of slices on circular failure surfaces to analyze the stability of the slope. The analysis considered, in a simplified way, the strength gain of the backfill material due to the consolidation process. The shear strength on the base of each slice was calculated as a function of a given degree of consolidation. The formulation used to define the degree of consolidation was not reported.

Limit equilibrium methods have been commonly used in the analysis of reinforced soil slopes composed of free draining granular material. These methods are techniques for conventional slope stability analysis, adapted to take into account the stabilizing moment created by the reinforcements. In structures reinforced with permeable inclusions that used cohesive backfill placed at high water content, the generation and time-dependent dissipation of pore water pressures should be considered in the design. In this case, the permeable reinforcements work not only as reinforcements but also as drains, dissipating excess pore water pressures and enhancing stability. The lateral drainage provided by this system will enhance the structure stability by increasing both the soil shear resistance along the potential failure surface, and the pullout resistance along the soil-geosynthetic interface.

Figure 2.18 shows a possible pore water pressure distribution, at two different times after construction of a reinforced slope, along a segment of the shear surface and along one of the reinforcement layers. The dissipation of excess pore water pressures (u_s

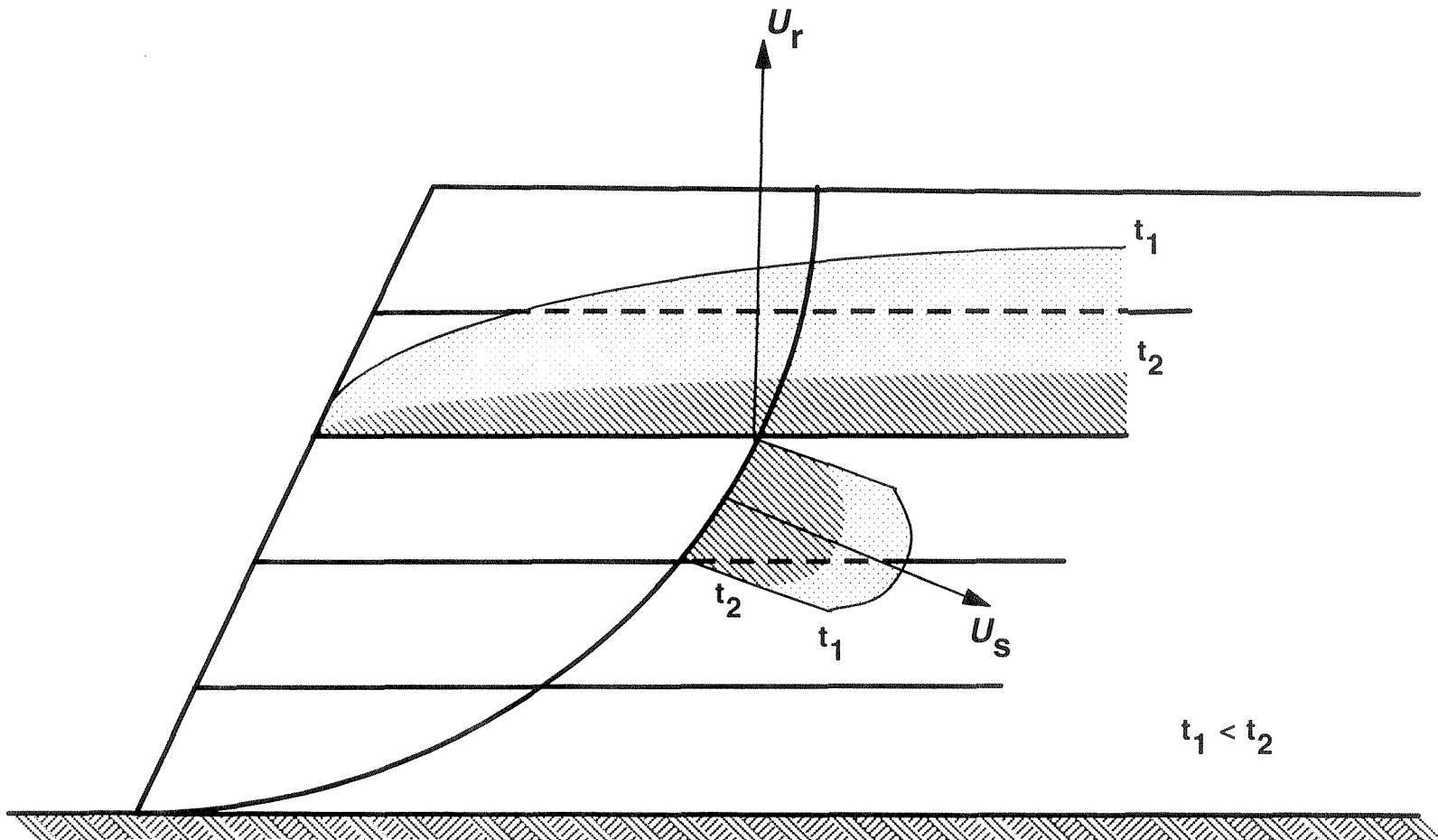


Figure 2.18 - Effect of pore water pressures on the stability of a reinforced soil structure.

in the figure) causes an increase in effective stresses along the potential shear surface that results in higher resisting shear stresses and, consequently, a higher factor of safety with time. Pore water pressure dissipation along the reinforcement (u_r in the figure) will increase the effective stress along the geotextile anchorage length, increasing the pullout resistance. Moreover, as described in the following section, the increasing effective stresses along the geotextile will result in improved reinforcement mechanical properties, particularly for the case of nonwoven geotextiles.

2.6 Additional considerations for geosynthetics embedded in poorly draining backfills

For the safe design of a reinforced soil structure with poorly draining backfill, it is necessary to evaluate the influence of these backfills on geosynthetic mechanical properties, durability, and creep characteristics.

2.6.1 Confined mechanical properties

Correct determination of the modulus and tensile strength of geosynthetics is of fundamental importance for the design of reinforced structures. The geosynthetic mechanical properties should be measured in a manner that simulates the field conditions. This is not the case for some methods of testing, such as the grab tensile test and the wide-width test, which are commonly used in the textile industry. Several investigators have already focused on the tensile characteristics of geosynthetics under the soil-confinement condition. Among them, McGown et al. (1982) found that the mechanical

properties of nonwoven and composite geotextiles significantly improve when tested under sand confinement. Christopher et al. (1986) developed a zero span test which mechanically models the confinement provided by granular soil. This test, while quick and simple to perform, yielded stress-strain information which compared favorably with the in-soil results obtained by McGown et al. (1982). Ling et al. (1992) developed a test apparatus for measuring the load-deformation properties of geotextiles under in-air, in-membrane, and in-soil conditions. They found that using a membrane for confinement of the geotextile specimen is as effective as using soil confinement, and concluded that this test is a superior alternative for determining the load-deformation properties of geotextiles under typical operational conditions.

In-soil tensile tests have also been performed under confinement by cohesive soils. Fabian and Fourie (1988) carried out tensile tests on woven and nonwoven needle-punched geotextile specimens confined in clay. They found that the geotextile modulus greatly increased due to the confinement. Due to the different mechanism of the clay-geotextile interaction, the modulus increase for the nonwoven geotextile was considerably larger (up to ten times) than for the woven geotextile (up to three times). Additional tensile tests under confinement by fine soils were performed by Chang et al. (1993). Although differing in the testing methodology, all previous studies show that there is a significant increase in stiffness and strength of geotextiles under soil confinement, in comparison to values obtained in unconfined conditions. The tests results show that improvement in geotextile mechanical properties occurs under confinement by both granular and cohesive soils.

2.6.2 Durability

The design of geosynthetic reinforced structures must ensure that long-term stresses in the reinforcement do not exceed the strength of the reinforcement at any time during the design life of the structure. The service life of a reinforced soil structure depends on the durability of the reinforcing elements. Although not susceptible to corrosion, polymeric reinforcements may degrade by a number of different actions. These include ultraviolet light, high energy radiation, oxidation, hydrolysis, and some chemical reactions (Allen, 1991; Koerner et al., 1992). In addition, they are susceptible to construction damage. The issue of long-term geosynthetic strength is currently the subject of continuous research, and the experience already gained is generally based on case histories of structures built using granular backfill. However, reported cases in which geosynthetics have been used in cohesive fills have indicated satisfactory long-term performance.

Reinforcement samples were retrieved from the Transport and Road Research Laboratory experimental structure, a full-scale embankment built with cohesive fill. These samples have been used for evaluation of the long-term durability of the reinforcements (Temporal et al., 1989). Preliminary data have been reported for plastic strips and, as shown in Figure 2.19, no loss of strength had occurred in the first eight years of burial. However, some increase in stiffness may have developed.

A geotextile reinforced embankment was built for test purposes in 1981 and had already been exposed to three years of extreme climatic fluctuations and environmental influences by the time it was loaded in early 1984 (Werner and Resl, 1986). A nonwoven needle-punched polypropylene geotextile was used as reinforcement, and the backfill

material was a silty sand. After loading, nonwoven samples were taken from the interior and surface of the embankment. Tensile tests were performed on the nonwoven polypropylene samples retrieved from the embankment to determine any strength losses or material changes, showing no changes from the original mechanical characteristics. For the case of nonwoven polyesters, Colin et al. (1986) reported no significant degradation for geotextiles buried for seven years in moist organic rich soil.

The performance of two reinforced slopes, the M4 at Yattendon and the A45 Cambridge Northern bypass, were described by O'Reilly et al. (1990). The M4 Yattendon cutting was constructed with about 1% quicklime added to the excavated clay material and reinforced with layers of high density polyethylene mesh. The A45 Cambridge Northern bypass was constructed of Gault clay using polypropylene geogrid reinforcements. Both slopes and geotextile reinforcements have performed well over periods of nine and six years respectively. Also, samples of polymer reinforcement from

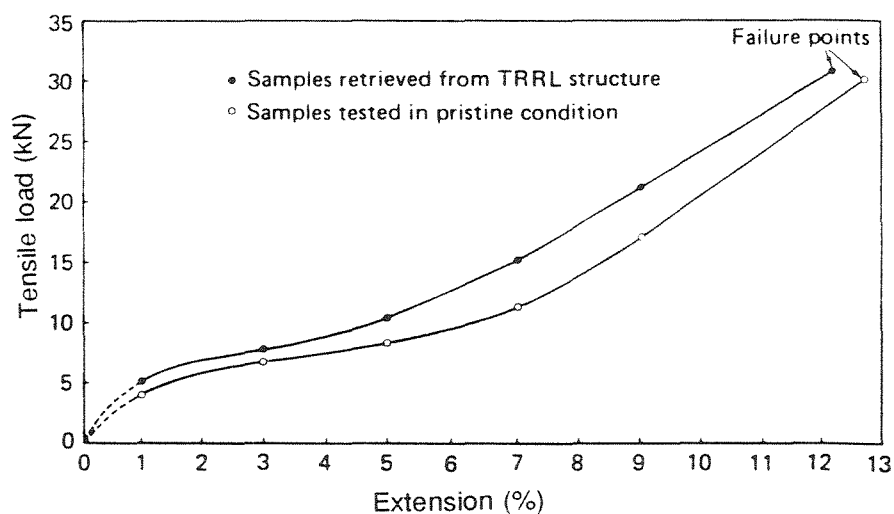


Figure 2.19 - Load-extension characteristics of plastic strips tested after eight years of burial in cohesive soil (after Temporal et al., 1989).

both sites were recovered and have been tested. No significant degradation of either the mesh or the geogrid has apparently occurred, although the materials recovered from the field probably had been subjected to site damage and ultra-violet weathering prior to installation as well as aging in-situ.

2.6.3 Creep

Creep is the response of the reinforcement to sustained load, resulting in time-dependent deformations that may continue as long as the reinforcement is loaded. Early studies of tensile creep behavior of geotextiles found that geotextiles in unconfined tests exhibit instantaneous recoverable primary creep, long-term nonrecoverable secondary creep and tertiary creep to rupture. Although there is concern of higher creep potential for the case of structures built with poorly draining backfills, geosynthetic creep response observed in reported case histories has been encouraging.

Soil creep has been a concern for the use of marginal backfills using metallic reinforcement systems. Elias (1979) carried out creep pullout tests on ribbed steel strips buried in a wide variety of cohesive soils at optimum moisture content and in the range of 95% of the maximum density. During conventional pullout tests, strips were subjected to creep testing using a constant pullout force, 50 to 60% of the ultimate pullout load, acting for 175 hours. The test results indicated little or no tendency to creep for any of the typical soils involved in the program. Surprisingly, even kaolin clay did not exhibit creep.

Soil confinement has been found to substantially reduce the magnitude of geotextile macrostructure creep. This is because confinement tends to restrict movement

of individual filaments preventing their realignment in the direction of the load. McGown et al. (1982) found the reduction in primary creep to be especially large (on the order of 40 to 60%) for nonwoven geotextiles confined in sand. They also found that the secondary creep rate is substantially reduced due to soil confinement. It was concluded that unconfined creep testing grossly overestimates the long-term creep deformations that would occur under soil confinement. The reduced geotextile creep deformations could explain the small long-term deformations observed on actual geotextile-reinforced walls.

The effect of cohesive soil confinement on the creep response of geotextiles was investigated by Fourie and Fabian (1987) by performing drained pullout tests on geotextiles in a silty clay. Drained pullout tests are not only long-term interaction tests, but long-term geotextile tensile tests as well. The pullout resistance in drained conditions was influenced by the time-dependent rearrangement of polymer molecules at a constant strain less than failure strain. Although relaxation reduced the geotextile tensile strength, producing a lower ultimate pullout resistance in the drained condition than in the undrained one, the mechanism of drained resistance developed at the clay-geotextile interface was considered not to differ from that at sand-geotextile interfaces. Christopher and Berg (1990) performed pullout tests on geogrids over extended periods of time using cohesive soils. Differences in the displacement measurements obtained at the front and back of the geosynthetic sample, as shown in Figure 2.8, were interpreted after evaluating the creep response of geogrid during testing. It was concluded that stress dissipation along the length of the sample, and not creep deformations, was the main cause of differences in the monitored movements of the front and rear gages of the sample.

Field monitoring of creep deformations in reinforced soil structures with granular fill has shown that deformations predicted based on laboratory tests of unconfined geotextiles have not occurred. This was the case for several portions of the geotextile-reinforced wall built at Glenwood Canyon in Colorado, that were expected to experience substantial creep deformations. However, Bell et al. (1983) reported that no significant creep deformations were measured, even though many of the wall segments had factors of safety with respect to creep rupture much less than 1.0. Acceptable creep performance may also be expected for the case of structures with marginal backfills since, as for the case of granular backfills, geotextile mechanical properties are improved under the confinement of cohesive soils. An example is the acceptable long-term performance reported for two geotextile-reinforced soil structures built with cohesive backfill and reinforced with nonwoven geotextile layers (Test Embankments I and II reported by Tatsuoka and Yamauchi, 1986). Although the creep potential of nonwoven geotextiles is larger than for other kinds of geotextiles, the horizontal creep deformation of the two test embankments was found to be slight except in the first year. The creep strain rate of the nonwoven geotextile at the measurement location decreased from about 3×10^{-3} %/day, one week after construction, to 3×10^{-5} %/day 200 days after construction.

2.7 Lessons learned from case histories

2.7.1 General considerations

Several aspects of the performance of those reinforced marginal soil structures for which data are available are reviewed individually in this section, including generation

of pore water pressures in the fill, possible modes and causes of failure, and structure deformability.

Reduced-scale models of reinforced soil structures have been built to help define the mechanisms of soil-reinforcement interaction. Behavior and conclusions drawn from the performance of models that used poorly draining soils as backfill material are summarized in Table 2.3. Additionally, several full-scale mechanically stabilized structures have been built using low-quality backfills, and the performance of these structures is noted in Table 2.4. Full-scale experimental reinforced soil structures proved to be unique sources of information. Although generally built with a more limited instrumentation, the performance of actual (non-experimental) reinforced clay structures also supplied valuable information. Complete details about each of the cases summarized in these tables may be found in the indicated references.

Relatively few of the reported small-scale models and full-scale structures contained metallic reinforcements (e.g. Elias and Swanson, 1983; Hannon and Forsyth, 1984; Bergado et al., 1991). This may be a consequence of concerns about corrosion and pore water pressure generation. Most of the reported case histories relied either on the high tensile strength offered by geogrids (e.g. Segó et al., 1990; O'Reilly et al., 1990; Burwash and Frost, 1991; Hayden et al., 1991), or on the drainage capabilities of nonwoven geotextiles (e.g. Puig et al., 1977; Tatsuoka and Yamauchi, 1986; Yunoki and Nagao, 1988).

Silts or low plasticity clays were used as backfill material for many structures; e.g. Boden et al. (1978), Hannon and Forsyth (1984), Perrier et al. (1986), Segó et al. (1990), Burwash and Frost (1991). However, more difficult to compact plastic clays were used

Table 2.3 - Reduced-scale reinforced soil models constructed using poorly draining backfills.

Research agency	Test type	Soil	Reinforcement	Characteristics	Observed behavior	Conclusions	Reference
TRRL, U.K.	Experimental wall	Silty clay	Glass reinforced plastic strips	3 m high model with hexagonal facing panels	Good vertical profile was obtained by providing temporary support of facing units	Tension in the reinforcements appear to be highly influenced by compaction procedures	Boden et al. 1978
Ground Eng. Ltd., U.K.	Small-scale reinforced clay walls	Kaolin clay	polyethylene mesh	Walls were failed by application of vertical surcharge	Surcharge load at failure increased linearly with the number of reinforcement layers	Wall performance could be explained by total stress analysis	Ingold 1981
Geotextile Consultants Ltd., U.K.	Reinforced clay cube, reinforced foundations	Remolded London clay, kaolin	Plastic geogrid	Undrained plane-strain conditions were simulated	Tests on reinforced clay showed reasonable agreement with proposed theory to model plane strain compression	Reinforcements impart an equivalent undrained shear strength higher than the clay shear strength	Ingold & Miller 1982
Queensland Inst. of Technology, Australia	Large geotextile reinforced clay wall models	Silty clay, basically kaolinite	Nonwoven needle-punched geotextile	Uniformly distributed & discrete strip loads were applied. Soil moisture content was 19%	Vertical surcharge to failure increased nearly two times with geotextile reinforcement	Geotextile reinforcement laterally confined the wall models developing tensile stresses in reinforcement. Geotextile strains were small	Fabian & Fourie 1988
Univ. of California, Berkeley	Centrifuge tests	Low plasticity clay	Nonwoven geotextile, plastic strips	Walls were 15 cm high	Vertical cracks appeared 10 to 12 cm behind the wall facing	Reinforcement improved wall stability. Further research is needed to fully explain test behavior	Jaber 1989
TRRL, U.K.	Four half-scale embankments	Overconsolidated London Clay	Geogrid	Applied surcharge loading was monitored	Deformations on the unreinforced embankment were high. Reinforcement significantly improved the ultimate strength	Reinforcements forced the redistribution of strains such that the development of the slip surface was inhibited	Irvin et al. 1990
Univ. of Maryland	Centrifuge tests	Kaolin, kaolin-sand mix, natural soils	Nonwoven geotextile	Reinforcement spacing and length varied	Lightly reinforced models failed by overturning. Heavily reinforced models developed a sliding failure	In all tested soils reinforcement had a significant beneficial effect	Goodings 1990
Dames & Moore, Darwin	Reinforced clay wall models	Silty clay	Nonwoven geotextile	CU loading conditions were simulated	Nonwoven geotextile effectively drained the clay backfill. Long term deformability of reinforced clay was less critical than that of unreinforced clay	High transmissivity geotextile increased undrained strength of the cohesive backfill. Time required for primary consolidation is reduced	Fabian 1990
Univ. of Colorado at Denver	Reinforced clay wall	Sand and clay mixture	Nonwoven geotextile	Wall was 3 m high with timber facing	Overall shear failure was not attained at the maximum surcharge pressure of 234 kPa	Observed wall movements were smaller in the clay wall than in a sand wall of similar dimensions	Wu 1991
Univ. of Maryland	Centrifuge models	lime stabilized kaolin	Nonwoven geotextile	Various reinforcement lengths were used	Three failure modes were identified depending on the reinforcement length	Lime improved wall stability substantially even with short geotextile length	Güler & Goodings 1992

Table 2.4 - Full-scale reinforced soil structures constructed using poorly draining backfills.

Name	Location	Date	Structure	Height (m)	Reinforcing method	Backfill	Facing	Construction	Comments	Reference
Autoroute A15	Rouen, France	1971	Highway embankment wall	4.0	Nonwoven geotextile	Weathered chalk, silt, and fire stone	Wrapped vertical	Berm on passive side partly removed after construction	First geotextile-reinforced wall. Unprotected facing geotextile. Satisfactory behavior	Puig & Blivet 1973; Puig et al. 1977
Illinois River Wall	Oregon	1974	Reinforced soil wall	3.5	Nonwoven, geotextile	silty sand and angular gravel	gunnite facing	0.3 m geotextile spacing at top, and 0.22 m at the base	First full-scale geotextile reinforced soil wall in U.S.	Bell & Steward 1977
Barrage de Maraval	Pierrefeu, France	1976	Dam spillway weir	6.5	Polyester woven geotextile	Compacted clay and schist (gravel at face)	Wrapped resin coated	Vertical face made up with polyester woven bags filled with loam	Withstood three overtoppings before end of construction without damage	Kern 1977
TRRL Experimental wall	Crowthorne, U.K.	1978	Reinforced soil wall	6.0	Several steel and plastic strips	Sandy clay, sand, silty clay	Facing panels	Vertical reinforcement spacing was 0.5 m	High pore water pressures developed in clay fill during construction, causing large deformations	Boden et al. 1978; Murray & Boden 1979
Yokohama residential complex	Tokyo, Japan	1978	Reinforced Retaining Wall	8.7	Metal strips	Volcanic clay	Facing panels	Reinforcement tension was monitored	Final settlements of up to 91 cm were observed	Hashimoto 1979
Industrial structure	U.K.	?	Industrial structure	3.2	Plastic geogrid	Mine waste	Rigid facing	Structure built on a mine waste tip	Plastic reinforcement exhibits low creep and high strength	Jewell & Jones 1981
Railway engine spur	U.K.	?	Mine waste reinforced structure	6.0	Glass fibre reinforced plastic strips	Mine waste	Rigid facing	A rigid full-height facing was used	Reinforcements were connected to facing with sliding connections	Jewell & Jones 1981
Shimonoseki Sanitary Facility	Shimonoseki, Japan	1979	Embankment	32.0	Multiple strip-sandwich method	Cohesive soil of strongly weathered tuff	Crib retaining wall	Quicklime layers placed in triangular configuration	Water content decreased about 7% after ten months. No significant movement during heavy rains	Yamanouchi et al. 1982
Virginia wall	Virginia	1978-79	Reinforced wall	up to 7.0	Ribbed steel strips	Residual low-plasticity silts	Concrete panels	Tilting 250 to 300 mm out of plumb occurred after precipitations	Areas of backfill with more than 25% fines were excavated and replaced with selected backfill	Elias & Swanson 1983
Highway wall at Koper	Slovenia	1982	Reinforced wall	3.5	Polyester strips	clayey silt	Reinforced concrete panels	A 50 cm wide sand drain was built along the facing panels	Facing lateral displacements reached 40 mm 152 days after end of construction	Battelino 1983
Interstate 80	Baxter, California	1982	Four embankment walls	5.0	Bar mat	Silt 49% passing #200 sieve	Prefabricated concrete facing	Construction forced to stop due to rainfalls	Extensive instrumentation showed no significant wall movements	Hannon & Forsyth 1984

Table 2.4 (Cont.)

Name	Location	Date	Structure	Height (m)	Reinforcing method	Backfill	Facing	Construction	Comments	Reference
Test Embankment I	Univ. of Tokyo, Japan	1982	Clay embankment	4.0	Polypropylene nonwoven geotextile	Volcanic Ash Clay (Kanto loam)	Geotextile sheet	One of the embankment sides had larger geotextile vertical spacing	The slope with the larger vertical spacing (80 cm) moved considerably	Tatsuoka & Yamauchi 1986
Test Embankment II	Univ. of Tokyo, Japan	1984	Clay embankment	5.2	Nonwoven geotextile	Volcanic Ash Clay (Kanto Loam)	Gabions at the face	One of the embankment sides had smaller geotextile length	Steep clay slopes reinforced with short geotextile sheets were stable during heavy artificial rainfall	Tatsuoka & Yamauchi 1986
Chemie Linz embankment	Austria	1984	Reinforced embankment	2.5	Nonwoven geotextile	Silty sand	Geotextile facing	Embankment exposed 3 years before loading	Embankment did not fail when loaded up to 1.7 times the theoretical failure load. No evidence of geotextile creep	Werner & Resl 1986
Otto-Graff-Institute reinforced wall	Germany	?	Geotextile reinforced wall	4.8	Polyester fabric	Weathered marl	Geotextile facing	Unit weight of 2.0 t/m ³ reached by compaction	In spite of the high loading, wall failure was not reached	Wichter et al. 1986
LCPC Experimental Embankment	Rouen, France	1984	Geotextile-reinforced embankment	6.4	3 woven geotextiles; 1 nonwoven/grid composite	Silt, compacted 5% wet of optimum	geotextile, geotextile gabions	Four sections with different geotextiles. Vertical spacing was 0.8 m	Positive pore water pressures generated in sections reinforced with woven geotextiles. Negative pore pressures recorded in composite sections	Perrier et al. 1986
Kami-Onda Experimental Embankment	Yokohama city, Japan	1985	Clay embankment	5.4	Polypropylene nonwoven geotextile	Kanto Loam Volcanic Ash Clay	Concrete panels, gabions	1V:0.2H slope with 0.5 m geotextile vertical spacing	Slope was stable after heavy artificial rainfall	Tatsuoka et al., 1987
Test Embankment III	Univ. of Tokyo, Japan	1986	Clay embankment	5.5	Nonwoven geotextile	Kanto Loam Volcanic Ash Clay	Different facing systems	Longer reinforcements were used at the embankment base	Facing system should provide local rigidity	Tatsuoka et al. 1987
Devon test fill	Alberta, Canada	1988	Reinforced embankment	12.0	Geogrids	Silty clay (Activity=1.0)	Secondary and tertiary grids	1V:1H slopes. Embankment was heavily instrumented	Geogrid strains are in direct response to both horizontal and vertical deformations in the embankment	Scott et al. 1987; Sego et al. 1990
Interstate 580 Wall	Hayward, California	1982	Vertical faced wall	1.8 to 9.1	Welded wire mesh	Sandy clay with potential expansibility	Facing panels	There was poor drainage of surface water	Wall showed excessive movement and cracking	Mitchell & Villet 1987
Ashigara parking area	Tomei way, Japan	1988	Fill slope	20.0	Nonwoven fabric	Soft loam	No structural facing	Geometric constrains imposed a 1V:1.8H slope	Soil strength increase by consolidation was taken into account in the analysis	Yunoki & Nagao 1988

Table 2.4 (Cont.)

Name	Location	Date	Structure	Height (m)	Reinforcing method	Backfill	Facing	Construction	Comments	Reference
Paulsgrove experimental wall	Hampshire, U.K.	1985	Experimental wall	5.6	Steel strips	Three types of local chalk	Concrete facing panels	Negative pore water pressures were generated during construction	Horizontal wall movements were up to 15 mm 3 months after construction. No later movement	Temporal et al. 1989
JR No.2 Experimental embankment	Japan	1988	Clay embankment	5.0	Nonwoven and composite geotextiles	Kanto loam volcanic ash clay	Continuous rigid facing	Six test segments were constructed	Good performance observed two years after construction	Tatsuoka et al. 1990
AIT Experimental wall	Thailand	?	Experimental wall	5.7	Welded wire mats	Clayey sand, lateritic soil, weathered clay	Vertical wire mesh	Wall was stable. Large settlements and lateral movements occurred	Subsoil movement greatly influenced vertical pressure beneath the wall and reinforcement tensions	Bergado et al. 1991
M4 Yattendon Cutting	U.K.	1980	Reinforced slope	20.0	HDPE mesh	Clay fill with 1% quicklime	No structural facing	Reinforcement vertical spacing was 0.5 m and 1.0 m	Slope and geotextile reinforcement performed well over period of 9 years	O'Reilly et al. 1990
A45 Cambridge Northern Bypass	U.K.	1983	Reinforced embankment	7.0	Polypropylene geogrid	Gault Clay	No structural facing	Slope was 1V:2H	Good performance after 6 years. Recovered geotextiles showed no degradation	O'Reilly et al. 1990
Annan Bypass Retaining Wall	U.K.	1989	Retaining wall	23.0	Concrete half discs used as anchors	Clayey till	Facing panels	Anchors were connected to facing polymeric straps	Pore pressures during construction ranged between -1 and +1 m head of water	Brady & Masterton 1990
Calgary parking lot	Alberta, Canada	1984	Reinforced retaining wall	9.0	Geogrid	Low plastic clay till	H-pile and timber	Upper 6 m of wall were replaced 3 years after construction	Wall suffered distress due to saturation of the backfill	Burwash & Frost 1991
Cannon Creek embankment	Arkansas	1988	Highway embankment	23.2	Geogrid	Highly plastic and expansive clay	Intermediate geogrids	Long-term loading conditions governed the design	Good performance was observed during the first 24 months of service	Hayden et al. 1991
Experimental wall of Lezat	France	1992	Experimental wall	6.0	Woven/ non-woven composite	Silt	LCPC patented facing	Geotextile strains were measured during construction	Experimental wall will be saturated until failure	Delmas et al. 1992
Reinforced slopes	Taiwan	?	Three reinforced slopes	Up to 10 m	Geogrid	Clayey silt	No structural facing	Failure by reinforcement breakage, pullout, and overall sliding were reported	Only qualitative description of failure mechanisms was given	Huang 1992

Table 2.4 (Cont.)

Name	Location	Date	Structure	Height (m)	Reinforcing method	Backfill	Facing	Construction	Comments	Reference
Waste disposal facility	Japan	?	1:1 reinforced slope	Up to 25 m	Geogrid	Cohesive soil	No structural facing	Cohesive soil was cement stabilized	Geogrid strains and slope displacements were measured during construction	Toriihara et al. 1992
Hengyang wall	China	1988	Retaining wall	Up to 6.83 m	Polypropylene strips	Silty clay	Concrete blocks	Soil was compacted to 95 % Standard Proctor	Vertical pressures at the base was bilinear increasing and then decreasing from the face to the back of the wall.	Wang & Wang 1993
Pingshi wall	China	1988	Retaining walls	Up to 10 m	Polypropylene strips	Local cohesive soils	concrete blocks	Soil was compacted to 95 % Standard Proctor	Lateral earth pressure coefficient decreased with depth from a maximum at the top of backfill	Wang & Wang 1993
Waterworks Corner Slope	London, U. K.	1986	Reinforced slope	8.0	Geogrid	Overconsolidated clay	Secondary geogrid	A 300 mm thick granular drainage layer was built	No movements have been noted since construction	Dixon 1993
Lawrence Berkeley Laboratory slope	Berkeley, California	1986	Geogrid reinforced slope	24.0	Geogrid	Silty clays, clayey sandy gravels	Intermediate geogrid	Soil used as backfill was more cohesive than assumed in the initial design	Reinforced slope has performed as intended	Lucia & Blair 1993
Barren River Plaza Shopping Center	Glasgow, Kentucky	1990	Reinforced wall	3.0 to 6.4	Geogrid	Cohesive soil	Keystone block facing	Clay backfill was poorly compacted. Geogrid layers were misplaced/omitted during construction	The structure failed. Deficiencies in design and construction quality control explain the observed modes of failure	Leonards et al. 1994

in some cases; e.g. Hashimoto (1979), Yamanouchi et al. (1982), Tatsuoka and Yamauchi (1986), Hayden et al. (1991). In a few cases, industrial or mine wastes were used as embankment fill (Jewell and Jones, 1981).

Although there is usually a tendency to report only successful case histories, some unsuccessful cases are also described in the literature (Elias and Swanson, 1983; Mitchell and Villet, 1987; Burwash and Frost, 1991; Huang, 1992).

2.7.2 Pore water pressure generation in reinforced fills

Only a small number of the reported case histories included monitoring of the generation and dissipation of pore water pressures in a cohesive backfill. Since many of these structures were constructed using unsaturated compacted clay, the fill material was often considered to have a drained behavior. Analytic prediction of the generation or dissipation of pore pressures has generally not been done. Some theoretical methods have been proposed for the analysis of consolidation between horizontal geotextiles (Section 2.5.2). Although they assume full saturation in the fill, this conservative assumption could be eventually used to estimate the pore water pressure dissipation in a reinforced clay structure reinforced with permeable inclusions.

2.7.2.1 Structures reinforced using impermeable elements

To investigate the feasibility of using cohesive fills, a full-scale experimental reinforced wall was constructed by the Transport and Road Research Laboratory (TRRL), U.K. . The construction and instrumentation are described by Boden et al. (1978), and the early performance by Murray and Boden (1979). This structure was a vertical sided

6 m high embankment, with three layers of different fill materials, each occupying about one-third of the height (Figure 2.20). A wet cohesive fill was placed at the lowest level, granular fill was used for the central layer, and a cohesive fill at lower moisture content was placed in the upper part of the structure. A range of different types of impermeable reinforcing elements, basically plastic and steel strips were used. Pore water pressures were monitored during construction of the embankment. An indication of the relatively high excess pore water pressures generated in the lower clay layer can be observed in Figure 2.21, which shows the excess pore water pressure condition immediately after construction, and six months later at a distance of 3 m from the facing. Higher pore pressures were measured at a location 5 m from the facing, and negligible pore pressures were recorded at distances less than 1 m from the facing. Pore water dissipation was reported to agree well with that predicted using the coefficients of consolidation from laboratory tests. No preferential drainage along the reinforcements (plastic and metal strips) appears to have occurred.

Four half-scale embankments, including a control and three geogrid reinforced embankments, were constructed in stiff overconsolidated clay soils (London Clay) and loaded to failure (Irvin et al., 1990). The response of the embankments to vertical surcharge loading applied through hydraulic jacks was monitored by extensive instrumentation. Piezometers were installed to monitor the effect of geogrid layers on the distribution of pore water pressures, showing that changes in the pore water pressures generally reflected the changes in applied load. Some piezometers in the upper part of the embankment showed increasingly negative pore water pressures as the load increased. It was suggested that dilation of the clay, associated with widespread shearing of the soil,

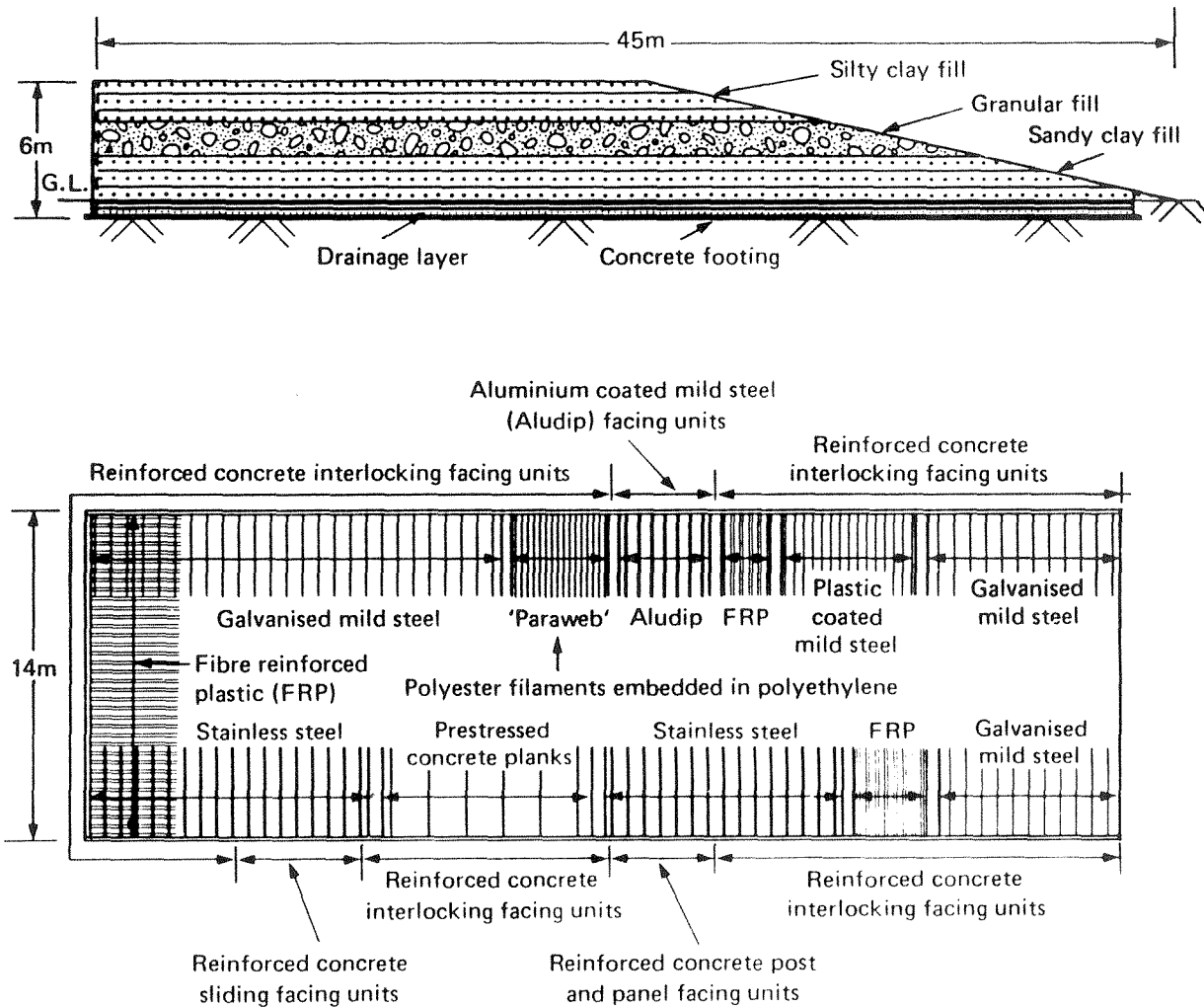


Figure 2.20 - Transport and Road Research Laboratory (TRRL) experimental reinforced wall (after Boden et al., 1978).

may have occurred. The response of piezometers at the level of geogrid layers and midway between them was similar, indicating that geogrid layers did not provide preferential drainage paths.

An insight into the interaction between pore water pressure generation, soil displacements, and geogrid strains may be gained from the analysis of the field measurements done at the Devon test fill. This test fill, built near Devon (Alberta, Canada), is a 12 m high test embankment with three sections reinforced with different geogrid materials and one unreinforced test section (Scott et al., 1987). The fill material is a silty clay that was compacted wet of optimum moisture content to ensure significant deformations and straining of the reinforcements.

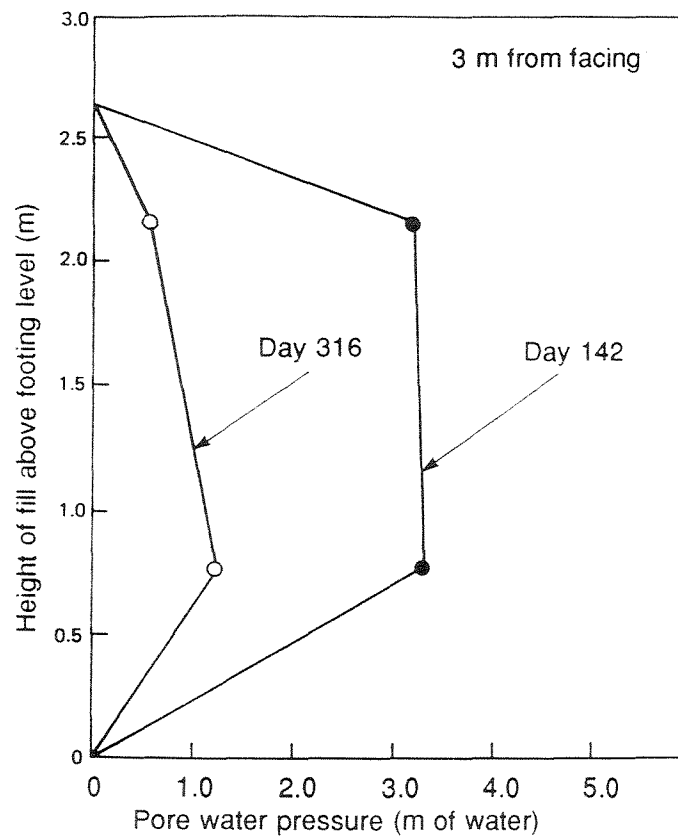


Figure 2.21 - Vertical distribution of pore water pressure in the lower cohesive layer of the TRRL experimental wall (after Murray and Boden, 1979).

The location of instruments installed within the embankment is shown in Figure 2.22. A series of field measurements has been reported for one of the test sections, showing the effect of the pore water pressures on the deformations within the embankment (Sego et al., 1990). The reported field data are from instrumentation located in the fill, 3 m above the foundation level, where the second level of primary reinforcement was installed. Figure 2.23a shows the fill height versus time throughout the construction period. Inclement weather and short construction seasons caused the fill to take 26 months to be constructed. Figures 2.23b and 2.23c present the horizontal and vertical displacement recorded at the 3 m level within the embankment and at various distances (2, 6, 10, and 14 m) behind the slope face. Pore pressures measured 5 m from the slope face at the 3 m elevation (Figure 2.23d) increased in direct response to the loading during the fill placement periods.

Figure 2.23e illustrates the geogrid strains at various distances from the slope face, also 3 m above the base of the fill. The geogrid began to strain as the embankment underwent vertical and horizontal deformation during embankment construction. After

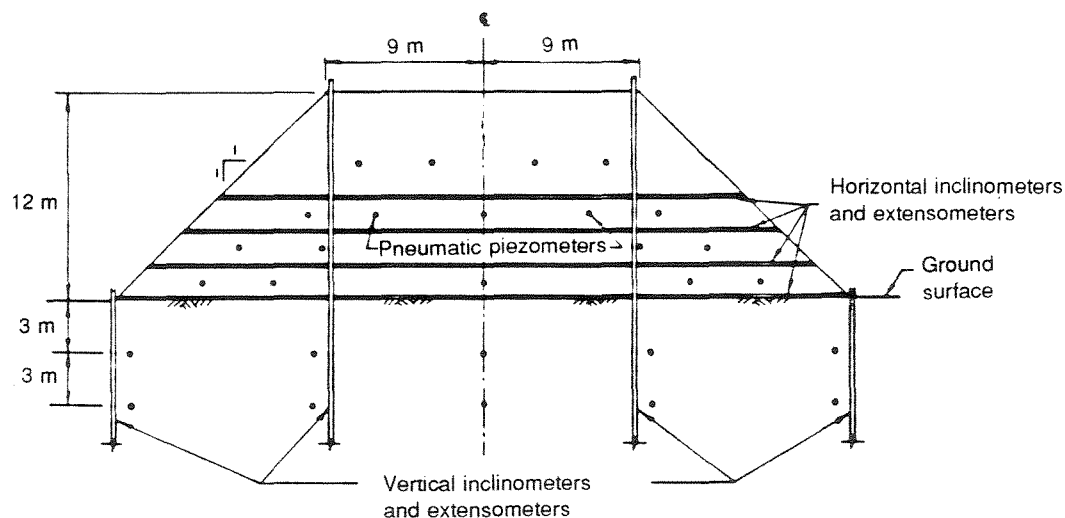


Figure 2.22 - Instrumentation in Devon test fill (after Scott et al., 1987).

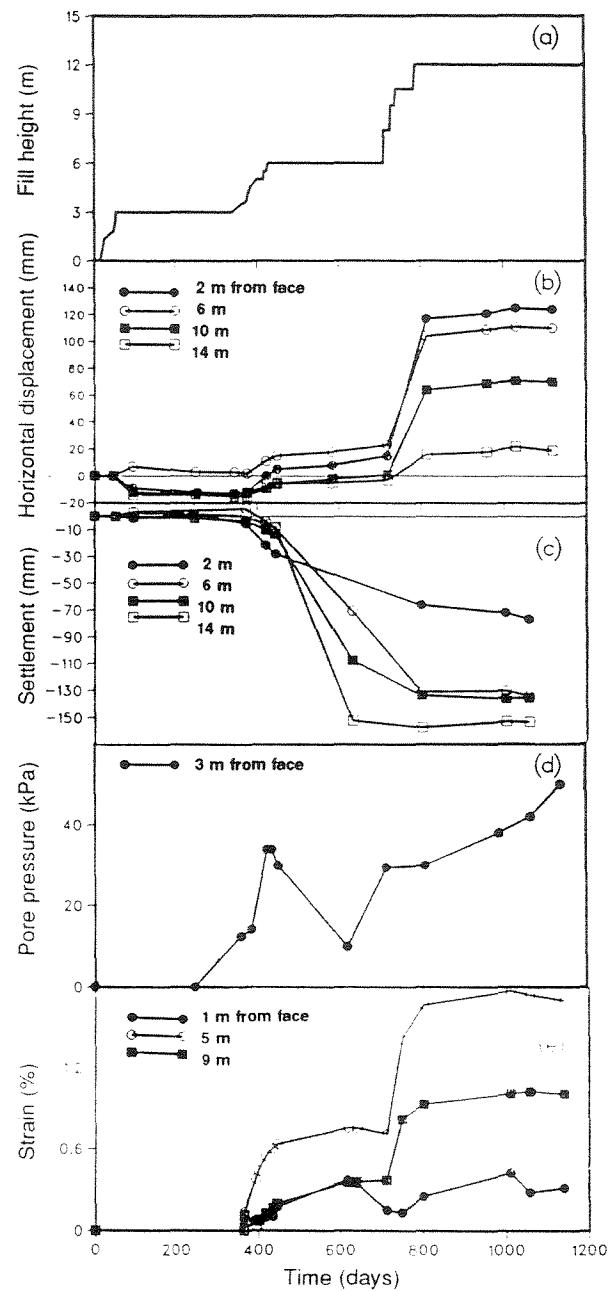


Figure 2.23 - Field measurements, 3 m above base and at various distances from slope face, within embankment and geogrids of Devon test fill: (a) fill height; (b) horizontal displacements; (c) settlements; (d) pore pressures; (e) geogrid strains (after Sego et al., 1990).

the first 3 m of fill were placed above the geogrids, the reinforcement strains measured 5 m from the slope face were about 0.6%. Also, up to 20 and 15 mm of horizontal and vertical deformations occurred 3 m above the base during the same period, while the pore water pressure increased from 0 to 34 kPa. During the winter shut down (after day 430), significant settlements occurred as the pore pressures dissipated from 34 to 10 kPa. Since the soil was becoming stronger as effective stresses increased, the geogrids were not required to carry much additional load, and the measured strains decreased slightly.

The placement of an additional 6 m of fill caused the geogrid strains and the horizontal and vertical displacements to increase, and pore pressures within the fill increased from 10 to 30 kPa. After the embankment reached the fill height of 12 m, pore pressures at the 3 m level continued to increase from 30 to 50 kPa. This increase was attributed to shear deformations occurring within the embankment, and to pore pressure migration from the center of the embankment towards the slope face. During the year following completion of the fill the geogrids gradually strained as the pore pressures increased. Although full understanding of the interaction between the geogrid reinforcement and the soil may require further analysis, it was clear that the increase in strain within the geogrid, and thus load in the reinforcements, was in direct response to both horizontal and vertical deformations in the embankment soil. The measured deformations, in turn, can be interpreted in terms of the generation and dissipation of pore water pressures.

In the previously described monitored case histories, the pore water pressures were generated during construction of the reinforced soil structures. Another critical situation results from water infiltration after rainfall events, but no case histories have been found

that monitored this condition. However, failure cases of reinforced soil structures with poorly draining backfills were reported to have been caused by the saturation of the backfill due to water infiltration (Elias and Swanson, 1983; Mitchell and Villet, 1987; Burwash and Frost, 1991; Huang, 1992). These structures, some of them described in Section 2.7.3.1, were constructed with marginal backfill soils reinforced using impermeable inclusions.

2.7.2.2 Structures reinforced using permeable elements

An experimental embankment at Rouen, France, provided information on the combined mechanical and hydraulic functions of permeable geotextiles (Perrier et al., 1986). Pore water pressures were monitored in this 5.6 m high experimental structure, built with a silt backfill having a water content 5% wet of optimum. The structure consisted of three sections reinforced with different types of woven geotextiles and one section reinforced with a composite nonwoven bonded to a polyester geogrid. Figure 2.24 shows positive and negative pore water pressures as a function of time recorded at different locations within the fill. The pressure sensor inside the embankment and beyond the reinforcement region, indicated as location (4) in the figure, recorded placement excess pore water pressures of as much as 60 kPa at the end of construction. Along the woven geotextile, positive pore water pressures on the order of 20 kPa were registered at the end of construction, 3.5 m from the wall face. These pore water pressures were dissipated in 350 days, becoming finally negative near the facing. Along the composite geotextile, on the other hand, negative pore water pressures were registered over the whole length of the reinforcement even at the end of construction. As indicated in the

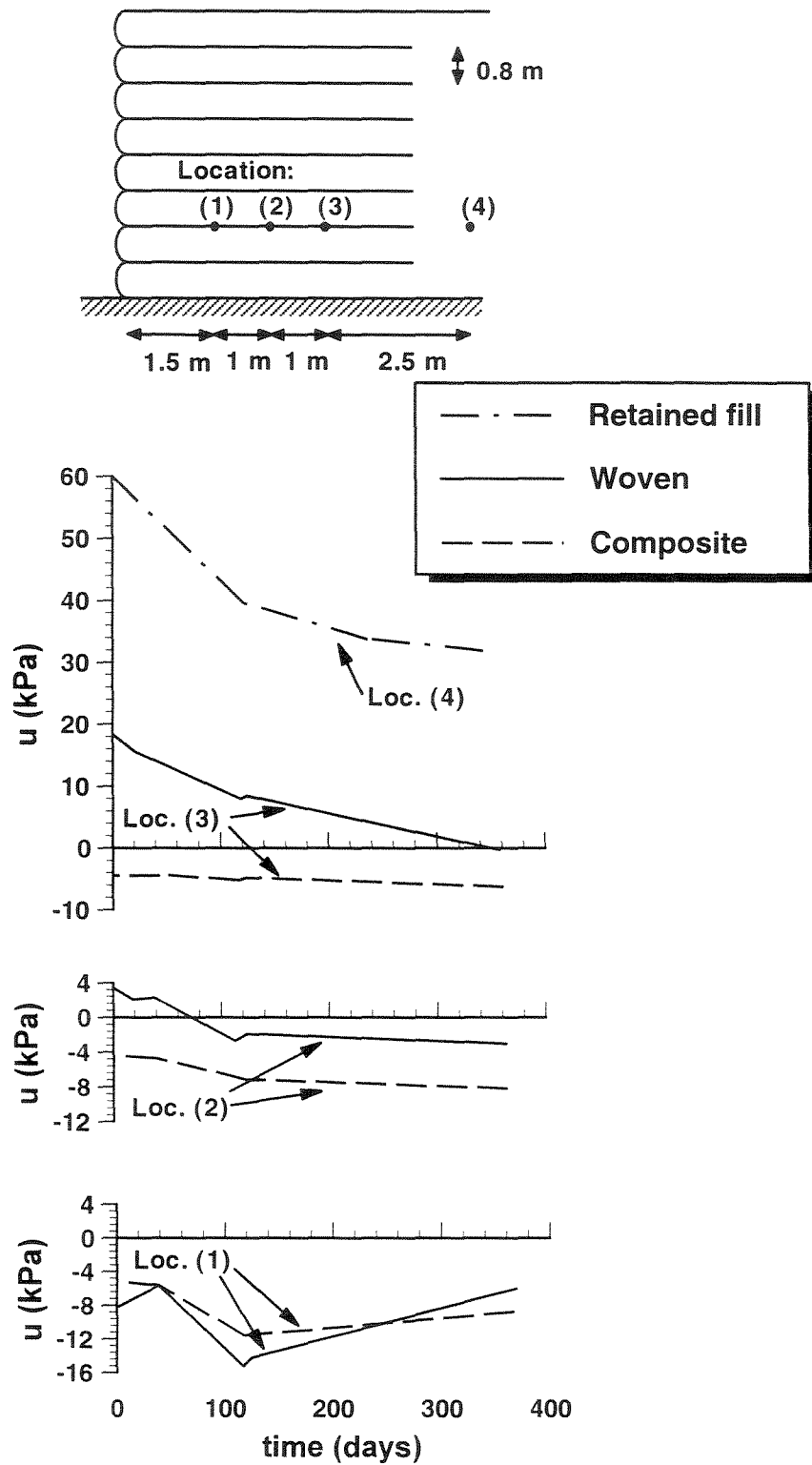


Figure 2.24 - Pore water pressures (u) recorded in the Rouen reinforced wall, along a woven and a nonwoven/geogrid composite, at different locations within a silty backfill (redrawn after Perrier et al. 1986)

figure, pore water pressures along the composite geotextile were systematically lower than those recorded along the non-draining woven textile. The limited drainage provided by the woven geotextiles affected the structure stability, since water pressure along these reinforcing layers may result in sliding along the interface. As an example, anchorage failure was observed in a nearby test section reinforced with woven polyester (Delmas et al., 1988).

The effect of nonwoven geotextile reinforcements on the stability and deformation of clay embankments was investigated through a series of field tests in Japan (Tatsuoka and Yamauchi, 1986, Tatsuoka et al., 1990). A sensitive volcanic ash clay called Kanto loam was used as backfill for these geotextile reinforced embankments which ranged in height from 4 to 5.5 m. The Kanto loam had a degree of saturation of 83 to 90%, and the as-constructed water content was 100 to 120%. Even though the test embankments have been subjected to heavy rainfalls and earthquakes, they have performed satisfactorily. Figure 2.25 shows the pore pressure changes in a test embankment 5.2 m high (Test Embankment II) during a heavy rainfall. When the rainfall occurred, the geotextile-reinforced zones at both sides of the embankment (U1, U3, U4, and U6) were able to maintain a high degree of suction (negative pore pressure), whereas positive pore pressure was generated in the unreinforced zones (U2 and U5) as water infiltrated into the soil. After the rainfall, the excess pore pressure dissipated rapidly through the geotextile layers. These results indicate that the nonwoven geotextile was effective as a drainage layer. Limit equilibrium analyses, in which the beneficial effect of suction was taken into account, showed that suction in the backfill material contributes significantly to the stability of the clay slopes (Yamauchi et al., 1987).

As part of a highway widening project, the U. S. Federal Highway Administration designed and supervised the construction of a permanent geotextile-reinforced slope 15.3 m high. Analysis of the instrumentation results from this structure is presented in Chapter 5 of this dissertation. The reinforced structure is a 1H:1V (45°) slope located in Idaho's Salmon National Forest along Highway 93. Several characteristics were unique to the design: the structure was higher than usual for geotextile-reinforced slopes; it involved the use of high strength woven/nonwoven composites; and it was constructed using indigenous soil (decomposed granite) as backfill material. Consequently, the reinforced slope was considered experimental, and an extensive program of instrumentation and

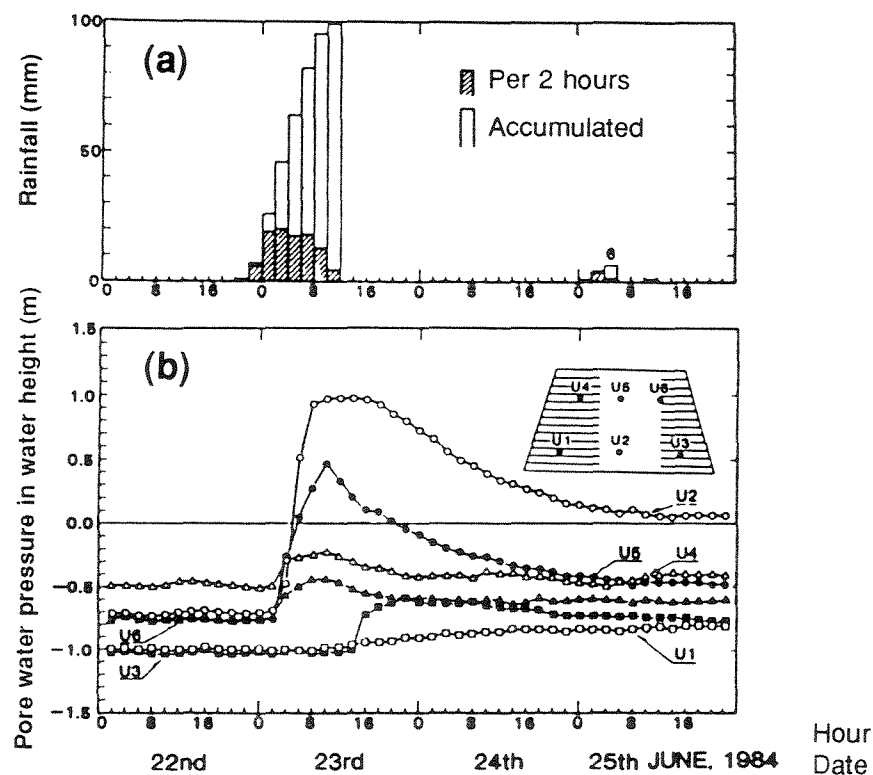


Figure 2.25 - Variation of pore pressure during rainfall in a clay embankment reinforced with nonwoven geotextiles: (a) rainfall recorded; (b) pore water pressures (after Tatsuoka and Yamauchi, 1986).

construction monitoring was implemented to evaluate its performance. Piezometers were installed to evaluate generation and dissipation of pore water pressures that could develop either during construction or after rainfall events. Of particular concern was the possibility of seepage during the spring thaw from the fractured rock mass at the backslope of the reinforced fill. Slope construction took place during the summer of 1993. Based on the pore water pressures monitored since construction of the reinforced slope and through the following spring, it can be inferred that destabilizing flow is not occurring within the reinforced soil mass and that, as considered in the design, a separate drainage system was not necessary at the back of the slope.

2.7.3 Modes and causes of failure

Reduced-scale models have been constructed with the purpose of studying the failure modes in reinforced soil structures using either impermeable or permeable reinforcement elements. Some experimental full-scale structures were also brought to failure to investigate the failure mechanisms and, although without instrumentation records, a few failure cases of real (non-experimental) reinforced structures have also been reported.

2.7.3.1 Structures reinforced using impermeable elements

To assess the possibility of using clay fill in the construction of reinforced soil structures, a series of model wall tests was carried out by Ingold (1981) using kaolin clay reinforced with polyethylene meshes. Due to the impracticality of bringing a laboratory model to failure by self-weight only, the walls were failed under the application of a

vertical surcharge as shown in Figure 2.26. The surcharge was applied using a rigid platen that had the effect of inducing failure along a preselected plane. Results from these tests were interpreted using total stress analyses which related the surcharge intensity at failure to the geometry and strength parameters of the clay and reinforcement. Reasonable agreement was obtained between observed and calculated values of failure surcharge loads, which were found to increase linearly with the number of layers of reinforcement in the wall.

The failure behavior of reduced-scale structures was also reported by Irvin et al. (1990) for half-scale embankments constructed with London Clay and loaded to failure with a vertical surcharge. Failure loading was characterized by large internal displacements, large slope face movements, and development of a near horizontal shear plane above the geogrid layers. The information obtained during sectioning of the embankments, together with the measured displacements, confirmed that the clay fill sheared adjacent to the geogrid layers. After comparing the performance of reinforced and unreinforced embankments, the authors concluded that the geogrid reinforcement

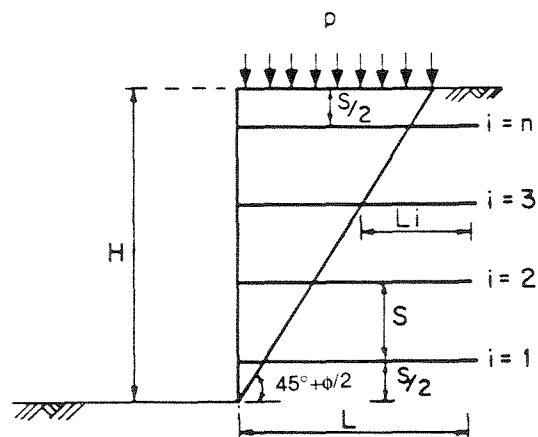


Figure 2.26 - Arrangement of reinforcements in a clay wall model (after Ingold, 1981).

modified the mode of deformation, improving the overall stability of the structure and limiting failures to localized areas.

The failures of some full-scale reinforced soil structures constructed with low-quality backfill have been reported. Elias and Swanson (1983) reported on problems that evolved in Reinforced Earth walls constructed during the winter of 1978-1979 in Virginia. The walls varied in height, with a maximum section of approximately 7 m, and specifications required that the backfill be nonplastic with less than 15% passing the no. 200 sieve (0.075 mm). Earthwork was halted due to adverse weather conditions, and significant wall movements were later observed after above normal precipitation. Typical movements consisted of tilting 250 to 300 mm out of plumb, which caused the wall facing to apply a lateral force on some adjacent piers.

To investigate the probable cause of the movements, test borings and hand-dug excavations of the backfill were performed, and detailed tests were conducted (field sampling, moisture contents, compaction tests, and grain size analyses). The cause of the problem is shown in Figure 2.27, which indicates that the reinforced walls with the most severe damage were composed of excessively wet fill with a high fines content. The investigation revealed that a significant portion of the backfill was not within the project gradation specifications since, in the areas of severe wall distress, the backfill contained well over 30% and up to 50% fines. Plasticity limits were also outside of project specifications. Based on this investigation, the areas of reinforced backfill with more than 25% fines were identified, excavated, and replaced with select backfill. Elias and Swanson concluded that backfill with high percentage of fines in structures reinforced

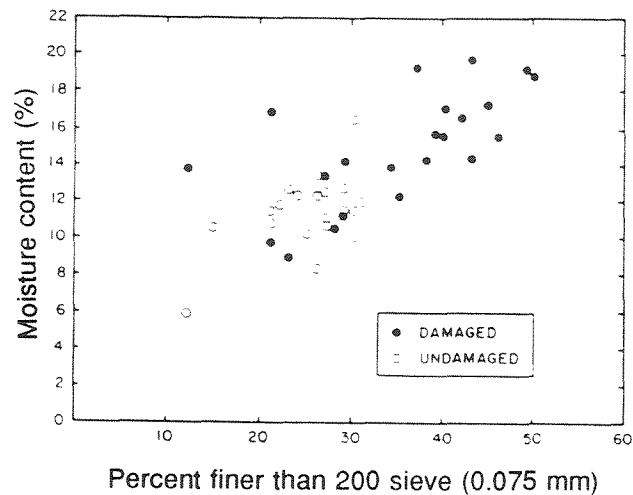


Figure 2.27 - Moisture content and percentage fines for damaged and undamaged walls reinforced with metallic strips (after Elias and Swanson, 1983).

with steel strips may result in a significant reduction in pullout capacity, decreasing the internal stability of the wall.

A welded wire wall was constructed in 1982 on Interstate 580, near Hayward, California (Mitchell and Villet, 1987). This vertical faced wall ranged in height from 1.8 m to 9 m and was about 137 m long. The reinforcing mats in the top section were substantially shorter than those in the bottom section of the wall, as shown in Figure 2.28. Following construction, a section of the upper portion of the wall was gradually tilting outward, and cracks began appearing at the back of the wall. A 600 mm wide fissure was observed, and remedial backfilling did not solve the problem. Testing of representative soils indicated that, instead of the specified granular backfill, a sandy clay with a moderate potential for expansion had been used. The soil was found to have a water content generally well in excess of optimum and above the plastic limit. The primary cause of the problem was considered to be poor drainage of surface water. Although the original plans called for positive drainage on top of the wall, water was allowed to saturate the backfill material. Remedial measures involved removal of the top layers of

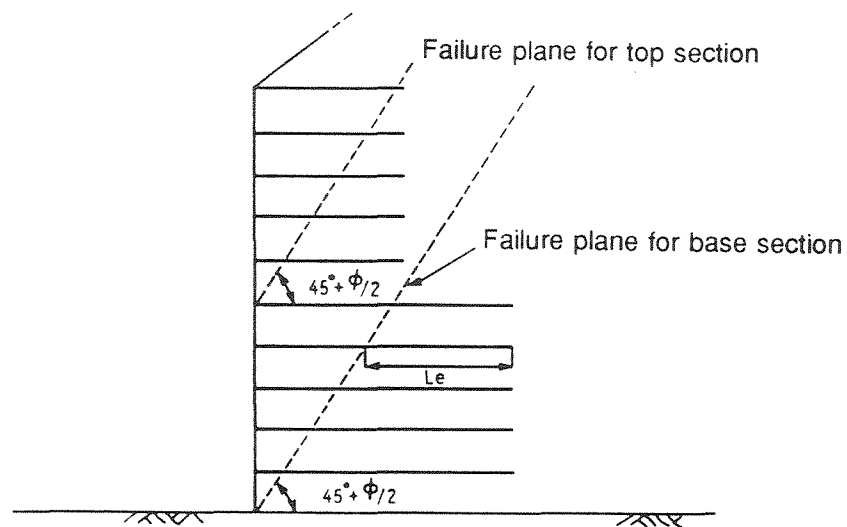


Figure 2.28 - Configuration of welded wire wall on Interstate 580, California (after Mitchell and Villet, 1987).

mats, their replacement with longer mats and select backfill, and improved surface drainage to prevent water migration into the wall. The wall has performed satisfactorily since completion of this work.

A 9 m high retaining wall reinforced with polymeric geogrids and backfilled with cohesive soil was constructed in Calgary, Canada, in 1984 (Burwash and Frost, 1991). The wall performed satisfactorily for 16 months when signs of settlement were first observed in the fill behind the wall. Conditions gradually deteriorated and, over the next 22 months, settlement of the backfill approached 900 mm in one area. The top of the retaining wall rotated outward about the toe and a deflection of 310 mm was recorded with a slope indicator over a 17 month period (Figure 2.29). The rates of displacement were, in general, constant. The post-construction site investigation showed that the moisture content of the clay backfill had increased significantly from that measured during construction of the wall. The upper 3 m of the fill appeared to be saturated and

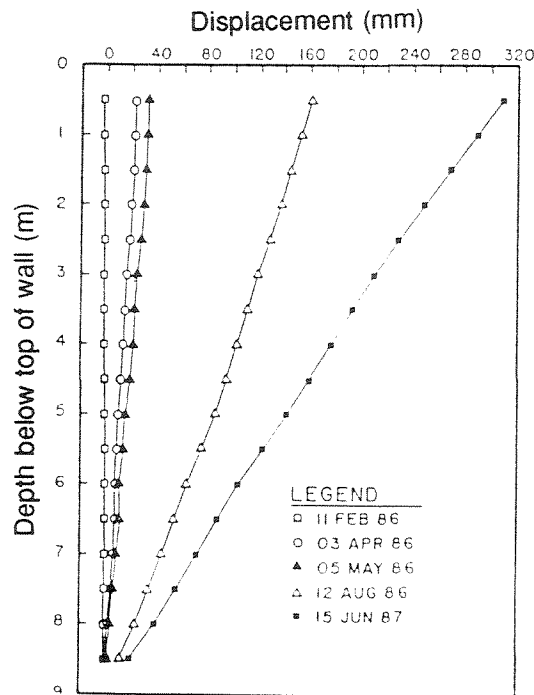


Figure 2.29 - Horizontal displacements versus depth recorded at a geogrid reinforced wall (after Burwash and Frost, 1991).

was much softer than when placed. The poor performance of this retaining wall was then believed to be related to saturation of the clay backfill which was placed 4% dry of optimum. Saturation occurred by ponding of surface run-off near the face of the wall and, consequently, the geogrids were subjected to increased loads to compensate for the resulting loss in soil strength. Approximately 3 years after completion of construction, the upper 6 m of wall was replaced with a free standing 2H:1V slope.

2.7.3.2 Structures reinforced using permeable elements

Reduced-scale models were constructed by Fabian and Fourie (1988) to study failure modes in walls reinforced using permeable nonwoven geotextiles. The clay wall models were tested by applying a vertical load using a rigid plate, while strains in the

geotextile reinforcements were monitored. The peaks on the strain distribution curves indicated the location of the failure surface. The authors considered that even in undrained loading conditions the true failure surface should be inclined at $45^\circ + \phi'/2$. A good agreement was reported between the inclination of the observed failure plane and the theoretical one.

Centrifuge models of geotextile reinforced and unreinforced vertical walls were reported by Goodings (1990). Models were built of kaolin clay placed at its plastic limit and compressed using a pressure of 200 kPa applied to each layer of soil. The models were reinforced with nonwoven geotextiles with variable vertical spacings and lengths. Two modes of failure were observed in the models after centrifuge loading until catastrophic failure. In lightly reinforced walls, the characteristic mode of failure was the opening of a tension crack followed by overturning and geotextile breakage (Figure 2.30a). In intermediate to heavily reinforced models (Figures 2.30b and 2.30c), failure was characterized by opening of a tension crack followed by development of an inclined sliding failure surface that emerged on the face of the wall. Failure occurred by geotextile breakage in all cases, never by pullout. Models were also built using mixes of kaolin with different percentages of sand as well as different natural soils. The equivalent prototype height of the reinforced walls at failure was compared to the equivalent height of unreinforced walls at failure showing that, in all tested models, reinforcement had a significant beneficial effect. The reinforcement effectiveness increased with the number of reinforcement layers and, for models reinforced with sixteen layers, an equivalent height at failure approximately three times higher than for unreinforced models was achieved.

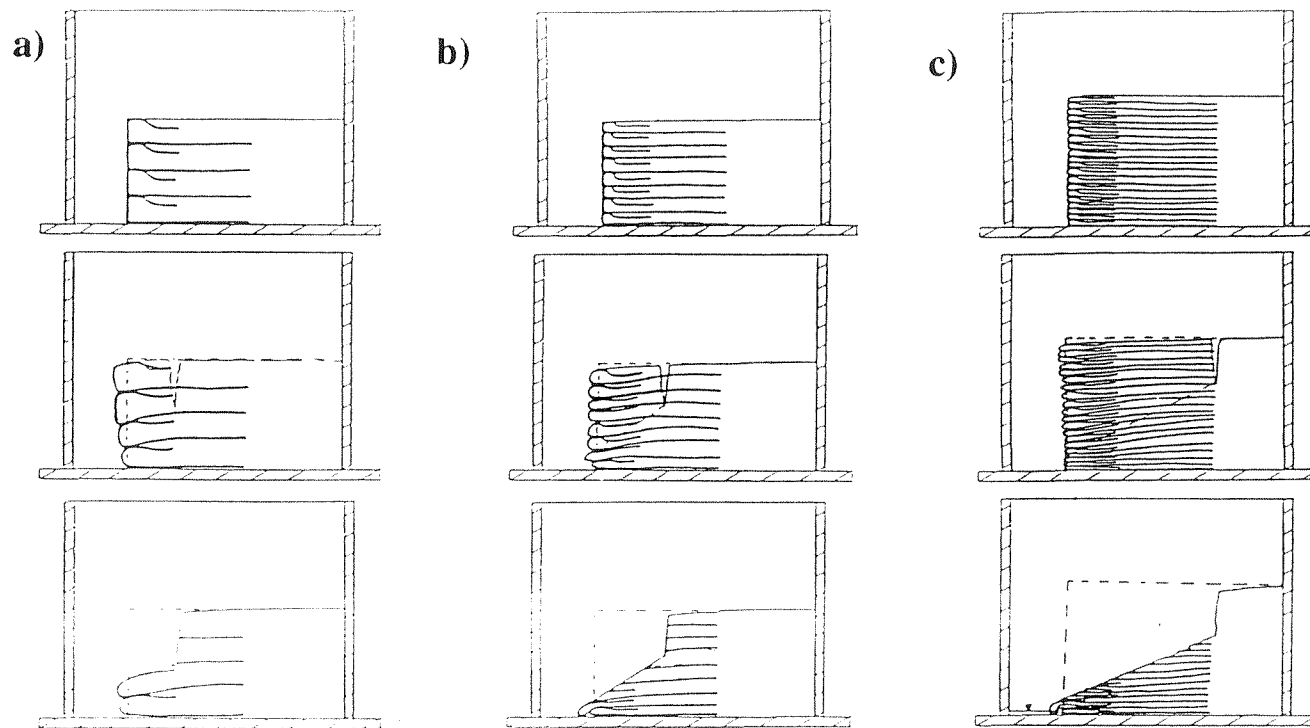


Figure 2.30 - Sequence of failure for centrifuge models of kaolin clay reinforced with nonwoven geotextiles: (a) lightly reinforced model; (b) intermediate reinforced model; (c) heavily reinforced model (after Goodings, 1990).

Five full-scale test embankments, having near-vertical slopes and using permeable reinforcements, were constructed using a nearly saturated clay (Tatsuoka and Yamauchi, 1986; Yamauchi et al., 1987). The embankments were made using a volcanic ash clay with a high natural water content and high sensitivity (4 to 5). Test Embankment II was constructed using two layers of gabions that were placed at the edge of each previous layer of the slope, before placing the soil layer. These gabions helped to achieve better compaction of the soil near the slope faces and prevented local failures during and after filling. A spun-bonded polypropylene nonwoven geotextile that showed good in-plane drainage capabilities was used as reinforcement for this embankment.

Two years after construction, the slopes of Test Embankment II did not show any noticeable displacements. It was concluded that the slopes would not displace under natural heavy rainfall. Subsequently, a total supply of about 70 m³ of water was allowed to percolate from the crest of the embankment over a period of eight days. After the artificial rainfall, several large cracks appeared in the embankment, as shown in Figure 2.31. The cracks appeared only in the unreinforced fill behind the reinforced zones. Moreover, in spite of the large deformations experienced during the wetting, the long-term deformations observed after the artificial rainfall were very small. Analysis of the cross-section in Figure 2.31 obtained after dismantling of Test Embankment II indicated that three modes of deformation took place. They are rotation about the toe, sliding along a shear band, and local compression near the toe (Figure 2.32). Displacements due to the rotational mode were considered to be the largest of the three modes. Since the reinforced zone at the right hand slope rotated as a monolith about the toe and no cracks

or slip surfaces were observed in the reinforced zones, it was concluded that the nonwoven geotextiles were effective in reinforcing the cohesive backfill.

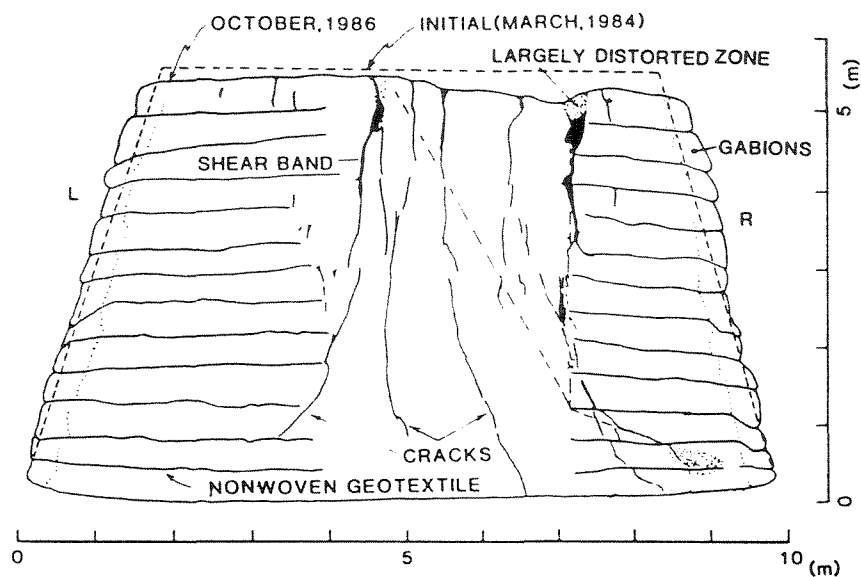


Figure 2.31 - Cross-section of clay Test Embankment II, observed at dismantling (after Yamauchi et al., 1987).

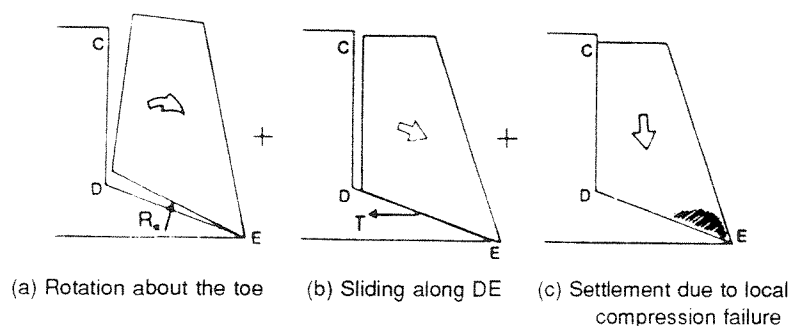


Figure 2.32 - Schematic diagram showing deformation of right-hand slope of Test Embankment II in Figure 2.31 (after Yamauchi et al., 1987).

2.7.4 Displacement evaluation

The magnitude of displacements that occur during and after construction are important considerations in the performance of reinforced soil structures. However, even for reinforced soil structures using good-quality backfill, there is no standard method for prediction of the lateral displacements. Horizontal movements depend on compaction effects, reinforcement extensibility, reinforcement length, reinforcement to facing connection details, and deformability of the facing system (Mitchell and Christopher, 1990). Finite element analyses have shown that while reinforcement length has only little effect on the maximum tensions in the reinforcements, its effect on lateral deformation is large. Based on the ratio of reinforcement length to wall height, an estimate of the lateral displacements that may occur during construction of simple structures with granular backfill can be made using Figure 2.33.

Considering the difficulty involved in the analytic prediction of movements in reinforced soil structures, displacement predictions rely heavily on the reported performance of similar structures. Relevant information about reported displacements on reinforced clay structures is reviewed in this section.

2.7.4.1 Structures reinforced using impermeable elements

The TRRL embankment, one of the first full-scale embankments constructed using cohesive fill, incorporated seven types of reinforcement (basically plastic strips and steel), four types of facing panel, and three different soils (Boden et al., 1978; Murray and Boden, 1979). The layout of this 6 m high trial structure is shown in Figure 2.20. Because the sandy clay at the bottom of the structure was placed very wet, excess pore

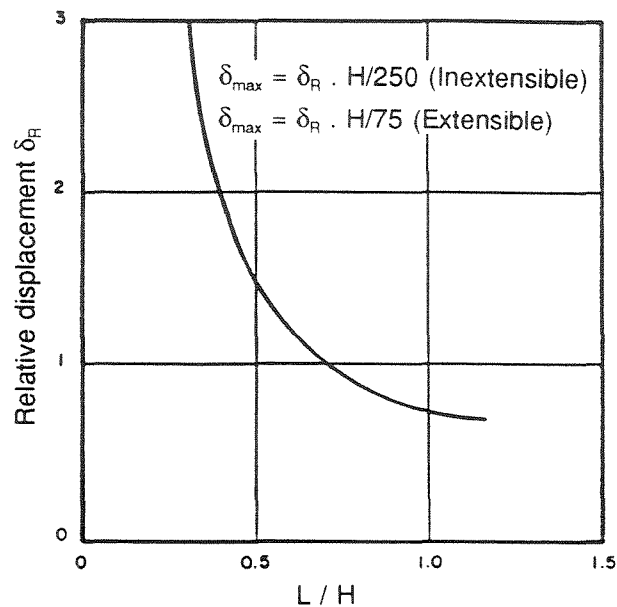


Figure 2.33 - Curve for estimation of lateral displacement anticipated at the end of construction of reinforced walls (after Mitchell and Christopher, 1990).

(Note: Based on a 6 m high wall, the relative displacement increases approximately 25% for every 19 kPa of surcharge. Experience indicates that for higher walls the surcharge effect may be greater).

water pressures were generated during construction in the bottom layer (see Section 2.7.2.1), and large horizontal movements and vertical settlements occurred over the first two years after placement of this fill material. Maximum values of vertical settlement of up to 50 mm were recorded just behind the facing panels, and up to 40 mm were measured near the center of the structure. Deviations of the facing panels from vertical were large, with typical values of about 200 mm and extreme values up to 400 mm. Little difference was seen in the vertical profiles between comparable sections of the wall supported by metallic and non-metallic reinforcements.

The performance of a Reinforced Earth wall built in Japan using as backfill material a volcanic clay at a water content greater than 50% is described by Hashimoto

(1979). Lateral displacements of 40 mm were measured in this 8.7 m high, while maximum vertical displacements reached 910 mm at the top of the wall.

Battelino (1983) reported the performance of a 3.5 m high wall, reinforced with polyester strips, that used a clayey silt backfill material at a water content of about 20%. Lateral displacements were monitored and reached 35 mm 152 days after the end of construction. The rate of deformation decreased rapidly and was negligible at the end of this period.

To prevent significant movements when impermeable reinforcements are used, water content conditions should be controlled during construction, and appropriate drainage systems should be adopted. An example of reinforced soil structures where appropriate drainage systems were used with impermeable bar-mat reinforcements was reported by Hannon and Forsyth (1984). Four mechanically stabilized embankment walls were constructed for the widening of Interstate 80, near Baxter, California. Two of the four walls were instrumented with strain gauges, pressure cells, reference monuments, plumb points, and piezometers, to monitor the effects of using a low-quality backfill. Maximum wall height was 4.9 m. The material used for the embankments was a sandy silt with about 50% of the material passing the no. 200 sieve (0.075 mm), which is considered excessive for most reinforced soil walls. Since this on-site material was not free-draining and was subject to considerable strength loss when saturated, a subsurface drainage system was constructed. Because of intermittent rains, the fine-grained backfill material became excessively saturated, and construction was forced to stop more than once since additional time was required to dry out the material before work could be resumed. The wall was completed in the fall of 1982. Monitoring of the wall during and

after the record rainfall of the 1982-1983 winter showed no significant lateral or vertical wall movements.

Field measurements reported by Sego et al. (1990) for a geogrid reinforced slope constructed with silty clay showed that generated pore water pressures had a significant effect on the performance of the monitored reinforced structure (see Section 2.7.2.1). As indicated in Figure 2.23, lateral and vertical displacements were closely related to the generation and subsequent dissipation of pore water pressures.

Displacements in walls and embankments reinforced using either metallic or polymeric impermeable inclusions were also reported by Ingold (1981), Perrier et al. (1986), Temporal et al. (1989), Irvin et al. (1990), Bergado et al. (1991), and Hayden et al. (1991), as described in Tables 2.3 and 2.4. Although large movements were observed in some of the structures having a cohesive backfill placed at high water content, an acceptable performance was generally reported if no increase in water content occurred in the backfill after construction. However, as described in Section 2.7.3.1, the increase in water content because of heavy rains has been critical to structures reinforced with impermeable inclusions.

2.7.4.2 Structures reinforced using permeable elements

Fabian and Fourie (1988) measured deformations in wall models built using a silty clay soil as backfill material and nonwoven needle-punched geotextile as reinforcements. Models with and without geotextile reinforcements were failed under the application of a vertical surcharge. The results showed that the vertical load-bearing capacity of the wall can be significantly increased with the geotextiles. Figure 2.34 shows curves of load

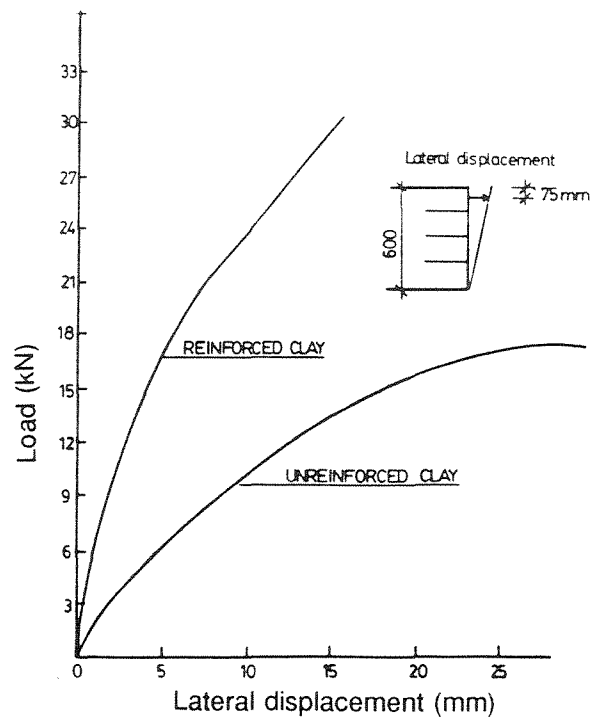


Figure 2.34 - Load-horizontal displacement curves of reinforced and unreinforced clay wall models (after Fabian and Fourie, 1988).

versus horizontal displacement, at the location of the top geotextile layer, for geotextile-reinforced and unreinforced wall models. Since failure was reached in less than 20 minutes in most of the tests, the loading condition was regarded as undrained. Clearly, the reinforced wall model did not reach failure at the displacement that caused failure in the unreinforced wall.

The first geotextile-reinforced wall was built by the French Highway Administration in Rouen (Puig and Blivet, 1973; Puig et al., 1977). Weathered chalk, silt and fire stone were used as backfill material, and a surcharge load was placed on top of the vertical faced wall. The structure, 4 m high and 20 m long, was founded on very compressible peat that has a natural moisture content of 300%. As illustrated in Figure 2.35, layers of polyester needle-punched nonwoven geotextile were placed extending 5

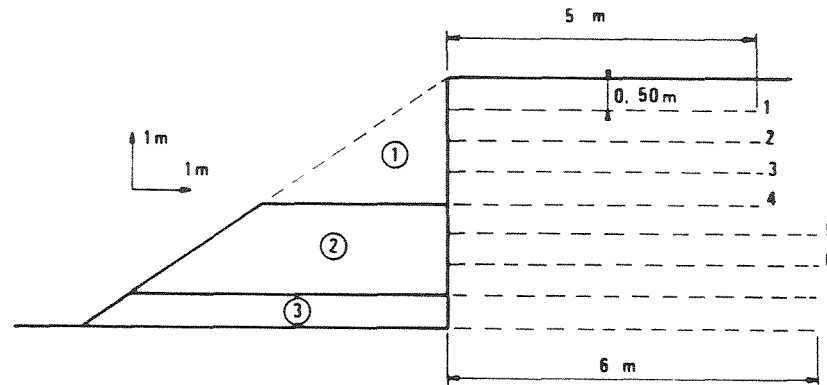


Figure 2.35 - Geotextile reinforced wall on Autoroute A15, France (after Puig and Blivet, 1973).

(Note: zones 1 and 2 were removed after construction).

to 6 m behind the wall face, and the wall face was formed by wrapping geotextile layers around 0.5 m thick backfill layers. A berm was raised on the passive side of the wall as construction proceeded and was partially removed after the end of construction. The purposes of this berm were to provide stability for the wall and its compressible foundation, and to support a temporary wood-form system used for the facing. Lateral deformations on the order of 20 mm were recorded on the wall face, and were confirmed by an inclinometer located in the reinforced fill. A total settlement of 1.1 m, and differential settlements of about 250 mm over a length of 3 m were observed. The drainage action of the geotextiles in this structure was later confirmed by traces of deposited calcite found on nonwoven samples taken from the wall in 1986 (Delmas et al., 1988).

The stabilizing function of structural facing elements in steep reinforced clay embankments was examined based on the behavior of five full-scale test embankments

constructed using a nearly saturated clay (Tatsuoka et al., 1990). The performance of one of these structures, Test Embankment II, was partly described in Sections 2.7.2.2 and 2.7.3.2 . Based on the behavior of these nonwoven geotextile-reinforced embankments, the authors concluded that facing structures with various kinds of rigidities should be used to increase the stability of steep slopes. These various kinds of rigidities were classified as local rigidity, overall axial rigidity, and overall bending rigidity. The slope faces of the different structures were either wrapped around with nonwoven geotextile, covered with discrete concrete panels, or constructed with the aid of gabions. The deformations in the slopes wrapped around with nonwoven geotextiles were generally larger than those in the other two slopes. It was concluded that the use of full height continuous rigid facing would be effective in reducing the deformations in clay reinforced walls. Based on the results of this study, the authors proposed that steep clay slopes be designed using relatively short nonwoven geotextile sheets, but using structural facing elements to prevent large lateral movements.

The lateral drainage provided by nonwoven geotextiles has proved effective in reducing or eliminating pore water pressures in the backfill material. The use of geotextile composites with higher tensile strength than that of nonwovens, would expand the use of geotextiles as reinforcement for more critical, permanent structures.

2.8 Benefits and potential applications of poorly draining backfills in reinforced soil construction

Although there are no design guidelines for reinforced soil structures using marginal soils, good performance was observed for reinforced soil structures that adequately prevented the generation of pore water pressures in the fill. Thus, it is clear that proper design can lead to the use of fine grained marginal soils as backfill material for reinforced soil construction, providing important cost savings and new soil reinforcement applications.

One potential solution for reinforcing marginal soils is the use of permeable geosynthetics that function not only as reinforcements but also as lateral drains. This would lead to a number of benefits:

- reduced cost of structures that would otherwise be constructed with expensive select backfill;
- improved performance of compacted clay structures that would otherwise be constructed without reinforcements; and
- use in civil engineering construction of materials, such as nearly saturated cohesive soils and mine wastes, that would otherwise require disposal.

The generally specified granular material may lead to high costs for transportation of the backfill, and the disposal of unused cohesive soils may also lead to substantial costs. While the reinforcement materials generally account for a relatively small portion of the total cost of the structure, the cost of granular backfill may be as much as half the

total cost. For example, Hollinghurst and Murray (1986) reported that from the total cost of a 6 m high reinforced earth wall only 17% corresponded to the reinforcement elements, while 25% corresponded to the facing, 40% to the granular fill, 15% to parapets and foundation, and 3% to earthwork. Hayden et al. (1991) reported that constructing a geogrid reinforced clay embankment costed a total of \$2.1 million, resulting in about \$1.1 million savings over conventional alternatives such as the importation of granular fill.

In the case of free-draining granular backfill, rate of construction is not a design consideration since, even for rapid loading, the fully-drained condition will prevail. This is not necessarily the case for poorly draining fills, where rapid construction is likely to be associated with undrained loading. In this case, permeable reinforcements, such as nonwoven geotextiles, could be used to increase the rate of consolidation and, consequently, speed the embankment construction. The dissipation of pore water pressure will increase both the shear strength of the cohesive backfill and the pullout resistance along the soil-reinforcement interface.

The controversial issue of what type of stability analysis should be used to design staged construction projects and to check stability during actual construction was addressed by Ladd (1991). Staged construction uses controlled rates of loading to enable soil strengthening via consolidation in order to increase the foundation stability of structures such as dams, embankments, landfills, and tanks founded on soft cohesive soils. It is also used for the operation of many tailings waste storage dams. A reinforced soil wall or embankment with poorly draining backfill and permeable reinforcements is another structure type to be added to the list of geotechnical structures requiring staged construction. In this case, however, it is the strengthening due to consolidation of the fill

material, and not of the foundation soil, that may require controlled rates of loading to guarantee stability. The speed of construction of this particular type of staged construction will be governed by the drainage capabilities of the reinforcement layers.

Permeable reinforcements would not only be useful to dissipate pore water pressures generated during construction, but can also prevent the formation within the embankment fill of flow configurations with destabilizing seepage forces. Transient and steady state seepage conditions in natural and artificial slopes have a significant effect on the slope stability. An infinite slope analysis gives an indication of the potentially adverse effect of seepage forces in slope stability: while in an infinite slope without seepage the maximum stable angle is equal to the soil friction angle, in a slope with seepage forces parallel to the surface the maximum stable angle is approximately half the soil friction angle. Although the adverse effect of seepage forces in engineered slopes could be prevented by designing special drainage systems, a more economical design alternative could be to combine drainage and reinforcement capabilities by using permeable geosynthetics as reinforcement elements. Internal drainage is of particular concern in road widening projects, because of the potential water seepage from cut slopes in fractured rock into the reinforced fill, as shown in Figure 2.36. Geotextile layers have already been used to provide basal drainage of unreinforced embankments placed on compressible and saturated soils. Ingold (1992) analyzed the stability of an embankment where surface water infiltration threatened long-term stability (Figure 2.37a), showing that the flow regime obtained using a basal geotextile layer (Figure 2.37b) led to a substantial increase in the embankment stability. Multiple permeable reinforcement layers would also be effective in preventing destabilizing flow regimes caused by infiltrating water.

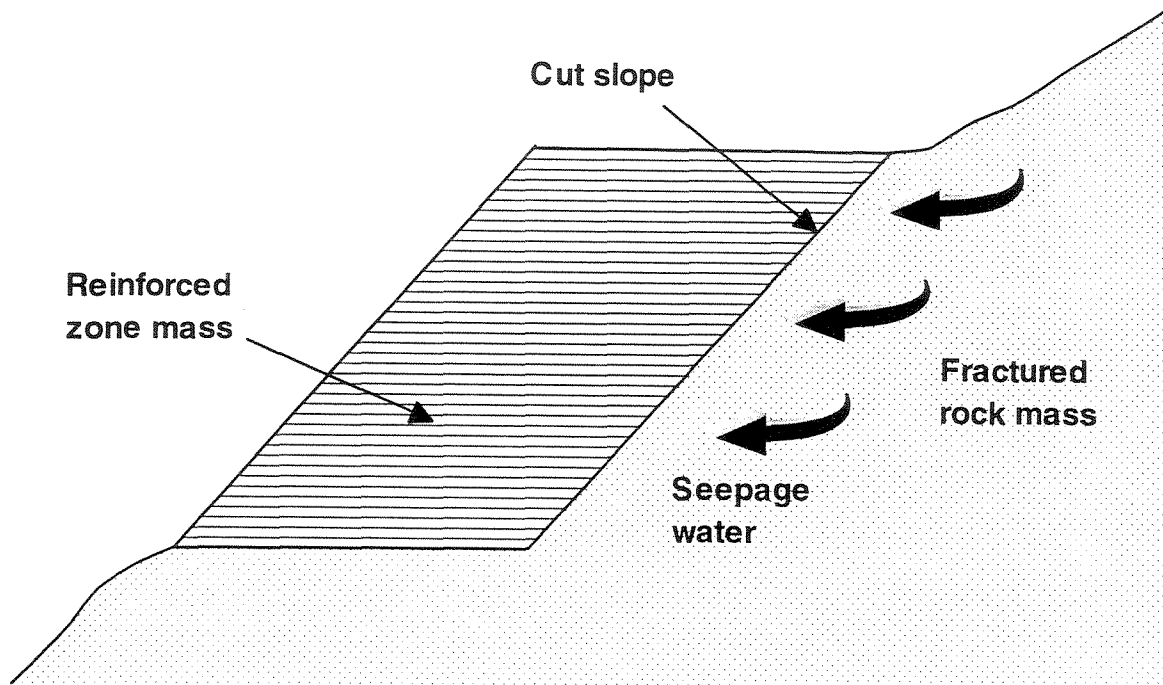


Figure 2.36 - Water infiltration in a reinforced slope for road widening projects.

The performance of properly designed and constructed reinforced soil walls during earthquakes has been excellent (Mitchell and Christopher, 1990). Qualitative assessment has been made on the performance of structures reinforced with inextensible elements and geosynthetic reinforcements that have actually experienced earthquake excitation during the Loma Prieta earthquake (The Reinforced Earth Company, 1990; Collin et al., 1992) and during the recent 1994 Northridge earthquake (Stewart et al., 1994). No significant signs of structural distress or movements have been observed during these events. Good performance was also reported for an embankment built using a clay backfill, reinforced with nonwoven geotextiles, that experienced relatively large earthquake motion (Nakamura et al., 1988). Any amplification of accelerations in structures with extensible reinforcements, should be compensated by the greater damping in less stiff systems and

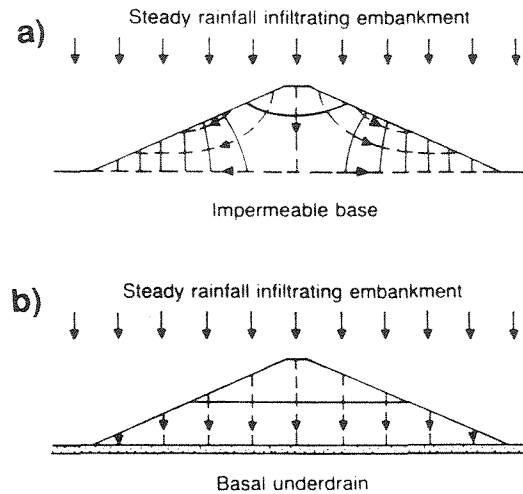


Figure 2.37 - Flow regime for embankment: (a) on an impermeable base; (b) on a pervious base (after Ingold, 1992).

by the higher factors of safety adopted on the reinforcement tensile strength to allow for creep under long term static loads. It may also be speculated that lateral drainage provided by permeable reinforcements would be beneficial in dissipating excess pore water pressures generated during seismic events in a reinforced fill.

There are potentially new applications of soil reinforcement using on-site, generally marginal soils for waste landfill construction. For waste repository construction in which the waste is to be placed in an excavation, steep sidewall slopes help maximize the available waste storage volume for a given site area. However, the repository must be designed considering several failure modes and mechanisms that are possible for the landfills during excavation, during filling, and after closure (Mitchell and Mitchell, 1992). Among them, sidewall slope failures can occur during the excavation of a repository and during the placement of liner systems prior to the commencement of filling operations. Use of reinforcements to provide stable steep sidewall slopes would be an economic

design alternative. These reinforced slopes could be designed as temporary structures since the reinforcement function of the geosynthetics would be required only until filling of the basin is completed. The low reduction factors (creep, durability) on the geosynthetic tensile strength required for temporary structures, would lead to an economic design. Instead of steepening the sidewall slopes, the construction of vertical reinforced sidewalls would be another potential alternative design. Besides maximizing the storage volume, a vertical excavated wall would eliminate other potential failure modes such as pullout of liner system components from anchor trenches, and sidewall failure along interfaces within the composite liner system. Current landfill design accounts for these failure modes by using flat side slopes, that can result in considerable reduction of waste storage volume.

If the strength of industrial and mine wastes could be increased by reinforcement, the range of civil engineering uses for these materials would be greatly broadened. Embankment construction using mine waste as backfill materials has already been reported by Jewell and Jones (1981). The range of particle size distributions found for mine waste materials is highly variable and depends on many factors including the method of handling and placement. Many materials are predominantly fine-grained, but include sand and gravel sized particles. Although plasticity characteristics of mine wastes vary substantially, there are strong similarities to inorganic clays of medium plasticity. Reinforcement of waste materials, not only for their use in construction but to facilitate their placement in storage systems, is another potential alternative. The use of cheap geotextiles could be effective in preventing failures through the waste pile, a critical failure mode for low-strength waste materials.

The use of admixture stabilizers, while not yet fully investigated, may enhance the range of materials that can satisfactorily be used for reinforced soils. The addition of lime to stabilize cohesive soil for use as fill in geotextile reinforced walls was investigated by Güler (1990). A successful performance was obtained by using quicklime and a filter geotextile for embankments in a difficult cohesive soil in Japan (Yamanouchi et al., 1982). Additionally, good performance was reported for a geogrid reinforced slope constructed at Yattendon, U.K., where clay fill was stabilized with lime (O'Reilly et al., 1990), and for a geogrid reinforced slope in Japan built for a waste disposal facility using cement-stabilized cohesive backfill (Toriihara et al., 1992). Centrifuge models of geotextile reinforced soil retaining walls using lime stabilized kaolin have been tested to failure by increasing self-weight (Güler and Goodings, 1992), showing that lime improved wall stability substantially.

The usefulness of consolidation by electro-osmosis as a technique for stabilization has been recognized in a number of geotechnical applications (Mitchell, 1991). The use of electro-osmosis for accelerating the consolidation process in reinforced structures with cohesive backfill may deserve some speculation. If cohesive soil with high as-placed water content is used as backfill material, a time-dependent gain in both soil strength and pullout resistance occurs as pore water pressures dissipate. However, if slow rate of pore water dissipation rate compromises either the stability of the embankment or the construction speed, electrically driven flow could be generated by placing electrodes along the reinforcements. A mathematical representation of the coupled flow generated by electro-osmosis would need to be formulated. Implementation, practicality, and costs involved in using this stabilization method are yet to be evaluated.

The advantages of using nonwoven geotextiles in clay embankments are not just limited to their reinforcement and drainage functions. Two problems frequently reported for embankments of (unreinforced) compacted clay are the development of surface tension cracks and compaction difficulties. In a reinforced soil structure, any surface tension cracks in the cohesive fill will be limited to the region above the first geosynthetic layer. Moreover, the use of nonwoven geotextiles has been reported to help in the compaction of the fill, by allowing a better distribution of the compaction effort and by draining excess pore water pressure induced during compaction (Yamauchi et al., 1987). The compaction characteristics of a geotextile-reinforced soft marine clay have been investigated by applying to reinforced soil samples a known compactive effort, equivalent to that of the Standard Proctor test (Indraratna et al., 1991). Figure 2.38 shows the compaction results for specimens reinforced with an increasing number of nonwoven

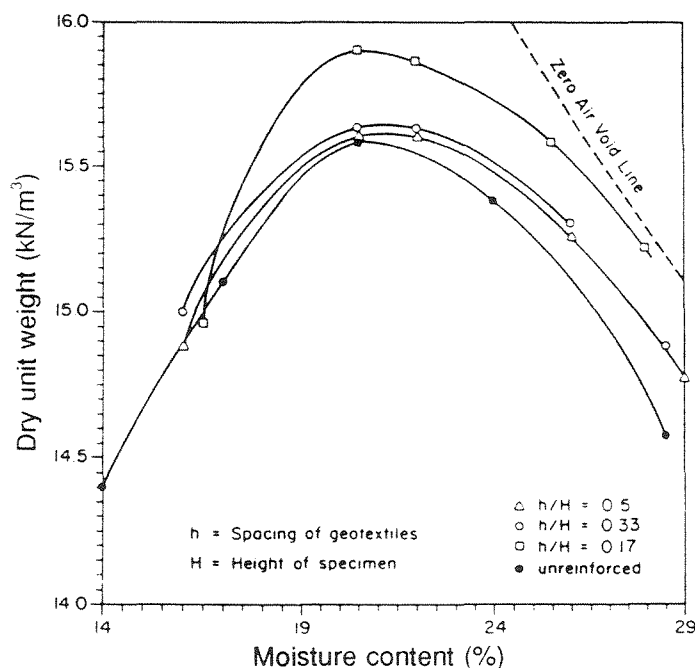


Figure 2.38 - Effect of nonwoven geotextile spacing on compaction curves for reinforced clay specimens (after Indraratna et al., 1991).

geotextile layers. The increase in dry unit weight was significant for the reinforced specimens, particularly at a close geotextile spacing, with no significant change in the optimum moisture content. In contrast, woven geotextiles were reported to hardly contribute to the compaction of the clay specimens.

The use of geosynthetics in cohesive soils has also been suggested for purposes other than reinforcement. For example, a geosynthetic based solution to the problem of expansive clays was investigated by Al-Omari and Hamodi (1991). Experimental results revealed a significant reduction in swell due to geogrid reinforcement.

2.9 Research needs

The results of experimental studies and the performance of several reported case histories have shown that poorly draining fills can be efficiently improved if appropriate reinforcement systems are used. Nevertheless, soil-reinforcement interactions in cohesive backfills are still not fully understood and no generally accepted design methodologies are currently available. On the basis of the review done in this chapter, aspects that require further insight to achieve safer and more economical designs of reinforced soil structures with poorly draining backfills are identified. They are:

- *Analysis of poorly draining soil-geosynthetic interaction.* Although different mechanisms have been proposed to explain soil-reinforcement interactions, more detailed understanding is needed in order to better define the load transfer mechanisms. The influence of confinement on the stress-strain characteristics and on the transmissivity of geosynthetics requires special consideration.

- *Analytic treatment of pore water pressure.* The effect of geosynthetic transmissivity and reinforcement spacing on the pore water pressure dissipation within a reinforced clay fill should be further investigated. As pore water pressures dissipate, there is a coupled increase in both soil shear strength and pullout resistance that requires analytic formulation. Not only the effect of permeable inclusions on the dissipation of pore pressures generated during construction, but also their effect on preventing permanent and transient flow configurations should be addressed.
- *Selection of design methods and failure criteria.* Even though some geosynthetics have been shown to effectively dissipate excess pore water pressures, design methods and failure criteria that take into consideration the combined effects of geosynthetic transmissivity and reinforcement have not been developed. Practical methods for predicting the increase with time of the stability factor of safety as consolidation proceeds, as well as the speed of construction required to keep a minimum factor of safety, should be developed.
- *Deformation analysis of reinforced soil structures with poorly draining backfills.* The use of cohesive backfills in reinforced soil construction produces less stiff structures than those constructed with conventional granular backfill. Consequently, reinforcements will play an even more relevant role in preventing excessive lateral deformations. The influence of reinforcement stiffness and length, intensity of soil compaction, and types of facing structures on the lateral deformations and on the reinforcement tension distribution should be addressed.

The ability of permeable reinforcements stiffer than nonwoven geotextiles to prevent large lateral deformations should be specifically investigated.

- *Selection of reinforcements.* The most appropriate geosynthetic types to be selected for these reinforced structures need better definition. When interface friction is a controlling factor in the choice of a reinforcement material, nonwoven geotextiles offer good characteristics because of their high contact efficiency and because they can convey water coming out of the soil due to consolidation. However, if tensile strength controls the design, the use of composite geosynthetics or high strength nonwoven geotextiles should be considered.
- *Dynamic response analysis.* Reinforced soil structures constructed using granular fill materials have shown excellent performance during earthquakes. Greater damping may be expected in less stiff structures constructed using cohesive backfills. Nevertheless, further verification of the seismic stability of structures with poorly draining backfills is needed.
- *Evaluation of geosynthetic durability in cohesive materials.* Since poorly draining soils constitute a more aggressive environment than cohesionless soils, there remains some concern about geosynthetics durability. Reported tests on retrieved geosynthetic samples showed encouraging results (Section 2.6.2). Nevertheless, accumulation of field data on different exposure conditions and in different soils is essential, since durability predictions are based primarily on observations of buried materials used for other purposes. A method for classification of polymers regarding their ability to resist chemical degradation is needed.

- *Estimation of geosynthetic-cohesive soil creep potential.* Reinforced soil structures using sand backfill, as well as confined laboratory creep tests, have shown only very limited creep deformations. Reinforced structures with poorly draining backfill have also been reported to behave successfully in relation to long-term creep deformations (Section 2.6.3). Nevertheless, caution should be taken due to the higher creep potential of cohesive soils. Long-term pullout tests in cohesive soils would provide valuable information related to clay-geosynthetic creep response.
- *Use of admixture stabilization and electro-osmosis for fill improvement.* The possibility of using admixture stabilizers, such as cement and lime, for improving poor or marginal backfill soils should be further investigated. Stabilization of reinforced clay structures by electro-osmosis should be analyzed. Economical and technical viability of these backfill improvement techniques require careful examination.
- *Study of the potential use of poorly draining wastes as backfill materials.* If the strength of industrial, domestic, and mine wastes could be improved by reinforcement, then the range of civil engineering uses for these materials would be greatly increased. In view of the rapidly increasing production of mine wastes in industrialized countries, new potential applications of these materials such as in reinforced tailings dams or embankments should be considered.

2.10 Conclusions

The requirement of granular backfill has been a major limitation to the selection of reinforced soil for many retaining wall and embankment projects. The purpose of this chapter is to provide the results of a review and evaluation of published material related to the suitability of poorly draining soils for reinforced soil structures.

Although the interaction mechanisms between poorly draining soils and metallic and polymeric reinforcements could not be clearly elucidated, triaxial test results have shown that poorly draining soils can be reinforced with properly selected permeable geosynthetics. The bond strength between the permeable reinforcement and the soil can be higher than the undrained soil strength soil if the geosynthetic transmissivity is high enough to drain the soil-reinforcement interface.

The results of shearbox and pullout tests using metallic reinforcements, geogrids, geotextiles, and geomembranes with poorly draining backfill soils are consistent with those from triaxial tests, showing that soil-reinforcement contact efficiencies are higher with permeable geosynthetics than with impermeable reinforcements. Consequently, in addition to the required tensile strength, geosynthetics in poorly draining backfills should also have adequate drainage capabilities.

If permeable geosynthetics are used to reinforce poorly draining backfills, the geosynthetic layers can function not only as reinforcements but also as lateral drains. The hydraulic function of reinforcements should be incorporated in a rational design approach that takes into account the geosynthetic transmissivity. Laboratory procedures have already been developed to determine the reinforcement drainage capacity under operational conditions, and theoretical methods have been proposed to evaluate the

dissipation of pore water pressures generated during construction using a saturated backfill. The challenge now is to account for the hydraulic function of reinforcements in the structure design and to validate the design assumptions against field monitoring results.

There is already experimental evidence that, as for the case of granular soils, the mechanical properties of geotextiles are improved under the confinement of cohesive soils. Moreover, although the long-term performance of geosynthetics embedded in marginal soils has been of major concern, experimental results so far have shown adequate durability and creep characteristics for the tested geotextile samples.

The use of fine-grained poorly draining materials in reinforced soil structures would reduce the cost of projects that would otherwise require granular material to satisfy current specifications, and would broaden the range of use of soil reinforcement to new applications. Geosynthetic reinforcements with high in-plane transmissivity not only provide mechanical reinforcement to the marginal fill, but their drainage properties can prevent destabilizing water flow configurations in a reinforced slope. In addition, the reinforcement limits the development of tension cracks in the cohesive fill, and may simplify soil compaction operations. It may also be speculated that lateral drainage would be beneficial during seismic events. The use of geosynthetic reinforcements to strengthen industrial and mine wastes for use as backfill materials, instead of disposing them in a landfill, and the reinforcement of sidewall slopes in waste repository systems are examples of potentially new applications.

No consistent design methodology for reinforced soil structures containing poorly draining backfills has been developed. Nevertheless, a number of structures has been

constructed, and the performance of some of them has been reported. Reduced and full-scale reinforced soil structures with poorly draining backfills were evaluated, focusing particularly on the generation of pore water pressures in the fill, on the possible modes and causes of failure, and on the structure deformability. Analysis of these case histories shows that large movements were generally recorded in reinforced structures when pore water pressures were generated in the fill, especially in those containing metallic reinforcements. Thus, good performance strongly depends on prevention of excess pore water pressure development within the fill material. This conclusion is strengthened by the fact that the failure cases reported so far involved poorly draining backfills that became saturated due to surface run-off, and were reinforced with impermeable inclusions.

Metallic reinforcements are not strong reinforcement candidates for poorly draining backfills. Not only do they not provide lateral drainage to the cohesive fill, but also the interface friction of these systems relies on the dilatant characteristics offered by granular fills. An additional concern is the higher rate of corrosion of metallic reinforcements when embedded in cohesive soils. Polymeric grid reinforcements and woven geotextiles provide adequate tensile strength required for the design of permanent reinforced soil structures. However, since they offer a limited in-plane drainage capacity, a low moisture content in the fill should be guaranteed by appropriate drainage systems throughout the design life of the structure. Nonwoven geotextiles, having a high in-plane hydraulic conductivity, offer the desired drainage capacity both during construction and after rainfall events. However, the generally lower strength and stiffness of these materials have limited their use to low or temporary structures. In order to reinforce marginal soils, it

is apparent that new synthetic materials with both high in-plane drainage capacity and high tensile strength and stiffness will be valuable. Composite geosynthetics, that combine the hydraulic properties of nonwovens with the mechanical characteristics of geogrids or wovens, are probably the most appropriate reinforcement for marginal soils.

A number of research needs should be addressed in order to formulate a consistent design methodology for reinforced soil structures with poorly draining backfill materials. They include the analytic treatment of pore water pressures in the fill taking into account the reinforcement transmissivity, a better understanding of marginal soil-geosynthetic interactions, the development of methods for deformation prediction, and further evaluation of durability and creep potential of geosynthetics embedded in cohesive soils. Due to an increasing demand for structures constructed using indigenous soils, current needs go beyond the fundamental understanding of the problem, and a consistent design methodology for walls and embankments with poorly draining backfills should be formulated.

References

- Al-Omari, R.R., Al-Dobaissi, H.H., and Al-Wadood, B.A., 1987, "Inextensible Geomesh Included in Sand and Clay", *Prediction and Performance in Geotechnical Engineering*, Proceedings of a symposium held in Calgary, Canada, pp. 155-160.
- Al-Omari, R.R., Al-Dobaissi, H.H., Nazhat, Y.N., and Al-Wadood, A.A., 1989, "Shear Strength of Geomesh Reinforced Clay", *Geotextiles and Geomembranes*, Vol. 8, No. 4, pp. 325-336.

- Al-Omari, R.R. and Hamodi, F.J., 1991, "Swelling Resistant Geogrid - A New Approach for the Treatment of Expansive Soils", *Geotextiles and Geomembranes*, Vol. 10, No. 4, pp. 295-317.
- Allen, T.M., 1991, "Determination of Long-Term Tensile Strength of Geosynthetics: A State-of-the-Art Review", *Proceedings of Geosynthetics '91*, Atlanta, USA, pp. 351-379.
- ASTM Standard D 4716-87, 1989, "*Standard Test Methods for Constant Head Hydraulic Transmissivity (In-Plane Flow) of Geotextiles and Geotextile Related Products*", Vol. 04.08, pp. 874-877.
- Auriault, J.L., Borne, L., and Cordary, D., 1982, "Consolidation des Remblais au Moyen de Textiles: Etude par Homogénéisation", *Proceedings of the Second International Conference on Geotextiles*, Las Vegas, Vol. 1, pp. 31-42, (in French)
- Auriault, J.L., Cordary, D., Giroud, J.P., and Gourc, J.P., 1977, "Etude Théorique du Rôle des Drains Textiles dans la Consolidation des Remblais", *Proceedings of the International Conference on the Use of Fabrics in Geotechnics*, Paris, Vol. 2, pp. 273-278.
- Battelino, D., 1983, "Some Experience in Reinforced Cohesive Earth", *Proceedings of the Eighth European Conference on Soil Mechanics and Foundation Engineering*, Vol. 2, Helsinki, pp. 463-468.
- Bell, J.R., Barrett, R.K., and Ruckman, A.C., 1983, "Geotextile Earth-Reinforced Retaining Wall Tests: Glenwood Canyon, Colorado", *Transportation Research Record* 916, pp. 59-69.

- Bell, J.R. and Steward, J.E., 1977, "Construction and Observation of Fabric Retained Soil Walls", *Proceedings of the International Conference on the Use of Fabrics in Geotechnics*, Vol.1, Paris, pp. 23-128.
- Bergado, D.T., Bukkanasuta, A., and Balasubramaniam, A.S., 1987, "Laboratory Pull-out Tests using Bamboo and Polymer Geogrids Including a Case Study", *Geotextiles and Geomembranes*, Vol. 5, No. 3, pp. 153-189.
- Bergado, D.T., Lo, K.H., Cai, J.C., Shivashankar, R., Alfaro, M.C. and Anderson, L.R., 1992a, "Pullout Tests Using Steel Grid Reinforcements with Low-Quality Backfill", *Journal of Geotechnical Engineering, ASCE*, Vol. 118, No.7, July, pp. 1047-1063.
- Bergado, D.T., Hardiyatimo, H.C., Cisneros, C.B., Chun C.J., Alfaro, M.C., Balasubramaniam, A.S., and Anderson, L.R., 1992b, "Pullout Resistance of Steel Geogrids with Weathered Clay as Backfill Material", *Geotechnical Testing Journal*, Vol. 15, No. 1, pp. 33-46.
- Bergado, D.T., Macatol, K.C., Amin, N.U., Chai, J.C., Alfaro, M.C., and Anderson, L.R., 1993, "Interaction of Lateritic Soil and Steel Grid Reinforcement", *Canadian Geotechnical Journal*, Vol. 30, No. 2, pp. 376-384.
- Bergado, D.T., Shivashankar, R., Sampaco, C.L., Alfaro, M.C. and Anderson, L.R., 1991, "Behavior of a Welded Wire Wall with Poor Quality, Cohesive-Friction Backfills on Soft Bangkok Clay: a Case Study", *Canadian Geotechnical Journal*, Vol. 28, No. 6, pp. 860-880.

- Blivet, J.C., and Gestin, F., 1979, "Etude de l'adhérence entre le Phosphogypse et Deux Géotextiles", *Colloque International sur le Renforcement des Sols*, Paris, Vol. 2, pp. 403-408 (in French).
- Blivet, J.C., Jouve, P., and Maillot, R., 1986, "Modelisation Numerique du Renforcement des Sols par Geotextiles: Fonction Hydraulique", *Proceedings of the Third International Conference on Geotextiles*, Vienna, Austria, Vol. 1, pp. 249-253.
- Boden, J.B., Irwin, M.J. and Pocock, R.G., 1978, "Construction of Experimental Reinforced Earth Walls at the TRRL", *Ground Engineering*, Vol. 11, No. 7, pp. 28-37.
- Bourdillon, M., Didier, G., and Gielly, J., 1977, "Utilisation des Produits Non-tissés pour le Drainage", *Proceedings of the International Conference on the Use of Fabrics in Geotechnics*, Paris, Vol. 2, pp. 279-284.
- Brady, K.C. and Masterton, G.G.T., 1990, "Design and construction of an Anchored Earth Wall at Annan", *Performance of Reinforced Soil Structures*, McGown, A., Yeo, K., and Andrawes, K.Z., Eds., Thomas Telford Ltd., London, pp. 127-134.
- Brand, S.R. and Duffy, D.M., 1987, "Strength of Pull-out Testing of Geogrids", *Proceedings of Geosynthetics '87*, New Orleans, USA, Vol. 1, pp. 226-236.
- Burwash, W.J. and Frost, J.D., 1991, "Case History of a 9 m High Geogrid Reinforced Retaining Wall Backfilled with Cohesive Soil", *Proceedings of Geosynthetics '91*, Vol.2, Atlanta, USA, pp. 485-493.
- Chang, D.T.T., Wey, W.T., and Chen, T.C., 1993, "Study on Geotextile Behaviors of Tensile Strength and Pull-out Capacity under Confined Condition", *Proceedings of Geosynthetics '93*, Vol. 2, Vancouver, Canada, pp. 607-618

- Christopher, B.R. and Berg, R.R., 1990, "Pullout Evaluation of Geosynthetics in Cohesive Soils", *Proceedings of the Fourth International Conference on Geotextiles, Geomembranes and Related Products*, The Hague, Netherlands, Vol. 2, pp. 731-736.
- Christopher, B.R., and Fisher, G.R., 1992, "Geotextile Filtration Principles, Practices and Problems", *Geotextiles and Geomembranes*, Vol. 11, Nos. 4-6, pp. 337-353.
- Christopher, B.R., Gill, S.A., Giroud, J.P., Juran, I., Mitchell, J.K., Schlosser, F., and Dunicliff, J., 1990, "*Design and Construction Guidelines for Reinforced Soil Structures - Volume I*", Report No. FHWA-RD-89-043. Federal Highway Administration, U.S. Department of Transportation, 285 p.
- Christopher, B.R., Holtz, R.D., and Bell, D., 1986, "New Tests for Determining the In-Soil Stress-Strain Properties of Geotextiles", *Proceedings of Third International Conference on Geotextiles*, Vienna, Vol. 3, pp. 683-688.
- Colin, G., Milton, M.T., Carlsson, D.J., and Wiles, D.M., 1986, "The Effect of Soil Burial Exposure on some Geotechnical Fabrics", *Geotextiles and Geomembranes*, Vol. 4, No. 1, pp. 1-8.
- Collin, J.G., Chouery-Curtis, V.E. and Berg, R.R., 1992, "Field Observation of Reinforced Soil Structures under Seismic Loading", *Earth Reinforcement Practice*, Proceedings of a symposium held in Fukuoka, Vol. 1, Japan, pp. 223-228.
- Collios, A., Delmas, P., Gourc, J.P., and Giroud, J.P., 1980, "Experiments on soil reinforcement with geotextiles", *Use of Geotextiles for Soil Improvement*, ASCE, Proceedings of a symposium held in Portland, OR, USA pp. 53-73.

- Delmas, P., Gotteland, P., Gourc, J.P. and Haidar, S., 1992, "Two Full Size Structures Reinforced by Geotextiles", *Grouting, Soil Improvement and Geosynthetics*, Geotechnical Special Publication No.30, ASCE, Vol. 2., New Orleans, pp. 1201-1212.
- Delmas, P., Blivet, J.C. and Matichard, Y., 1988, "Geotextile-Reinforced Retaining Structures: A Few Instrumented Examples", *The Application of Polymeric Reinforcement in Soil Retaining Structures*, Kluwer Academic Publishers, pp. 285-311.
- Dixon, J.H., 1993, "Geogrid Reinforced Soil Repair of a Slope Failure in Clay. North Circular Road, London, United Kingdom", *Geosynthetics Case Histories*, Raymond, G.P. and Giroud, J.P., Eds., pp. 236-237.
- Eigenbrod, K.D. and Locker, J.G., 1987, "Determination of Friction Values for the Design of Side Slopes Lined or Protected with Geosynthetics", *Canadian Geotechnical Journal*, Vol. 24, No. 4, pp. 509-519.
- Elias, V., 1979, "Friction in Reinforced Earth Utilizing Fine Grained Backfills", *Colloque International sur le Renforcement des Sols*, Paris, Vol. 2, pp. 435-438.
- Elias, V. and Swanson, P., 1983, "Cautions of Reinforced Earth with Residual Soils", *Transportation Research Record* 919, pp. 21-26.
- Fabian, K.J., 1990, "Time Dependent Behaviour of Geotextile Reinforced Clay Walls", *Proceedings of Fourth International Conference on Geotextiles, Geomembranes and Related Products*, Vol.1, The Hague, Netherlands, pp. 33-38.

- Fabian, K.J. and Fourie, A.B., 1986, "Performance of Geotextile-Reinforced Clay Samples in Undrained Triaxial Tests", *Geotextiles and Geomembranes*, Vol. 4, No. 1, pp. 53-63.
- Fabian, K.J. and Fourie, 1988, "Clay Geotextile Interaction in Soil-Tensile Tests", *Theory and Practice of Earth Reinforcement*, Proceedings of a symposium held in Fukuoka Kyushu, Japan, pp. 81-86.
- Fabian, K.J. and Fourie, A.B., 1988, "Clay-Geotextile Interaction in Large Retaining Wall Models", *Geotextiles and Geomembranes*, Vol. 7, No. 3, pp. 179-201.
- Fourie, A.B., and Fabian K.J., 1987, "Laboratory Determination of Clay Geotextile Interaction", *Geotextiles and Geomembranes*, Vol. 6, No. 4, 275-294.
- Garbulewski, K., 1990, "Direct Shear and Pullout Frictional Resistance at the Geotextile-Mud Interface", *Proceedings of the Fourth International Conference on Geotextiles, Geomembranes and Related Products*, The Hague, Netherlands, Vol.2, pp. 737-742.
- Gilbert, P.A., Oldham, J.C., and Coffing, L.R., 1992, "*Laboratory Measurement of Pullout Resistance of Geotextiles against Cohesive Soils*", Technical Report GL-92-6, Waterways Experiment Station, Corps of Engineers, New Orleans, 67 p.
- Giroud, J.P., 1983, "Geotextile Drainage Layers for Soil Consolidation", *Civil Engineering for Practicing and Design Engineers*, Vol. 2, pp. 275-295.
- Gomes, R.C., 1992, "Mecanismos de Interação Solos-Geotêxteis" , *Proceedings of Geossintéticos '92*, Brasília, Brazil, pp. 35-60, (in Portuguese).
- Goodings, D.J., 1990, "Research on Geosynthetics in Reinforced Cohesive Soil Retaining Walls at the University of Maryland", *Geotechnical News*, June, pp. 23-25.

- Guilloux, A., Schlosser, F., and Long, N.T., 1979, "Etude du Frottement Sable-Armature en Laboratoire", *Colloque International sur le Renforcement des Sols*, Paris, Vol. 1, pp. 35-40 (in French).
- Güler, E., 1990, "Lime Stabilized Cohesive Soil as a Fill for Geotextile Reinforced Retaining Structures", *Proceedings of Fourth International Conference on Geotextiles, Geomembranes and Related Products*, Vol. 1, The Hague, Netherlands, pp. 39-44.
- Güler, E. and Goodings, D.G., 1992, "Centrifuge Models of Clay-Lime Reinforced Soil Walls", *Grouting, Soil Improvement and Geosynthetics*, Geotechnical Special Publication No.30, ASCE, Vol. 2, New Orleans, pp. 1249-1260.
- Hannon, J.B. and Forsyth, R.A., 1984, "Performance of an Earthwork Reinforcement System Constructed with Low Quality Backfill", *Transportation Research Record* 965, pp. 55-66.
- Hashimoto, Y., 1979, "Comportement d'un Mur en Terre Armée Construit Avec le Limon de Kanto", *Colloque International sur le Renforcement des Sols*, Vol. 2, Paris, pp. 545-550.
- Hayden, R.F., Schmertmann, G.R., Qedan, B.Q. and McGuire, M., 1991, "High Clay Embankment over Cannon Creek Constructed with Geogrid Reinforcement", *Proceedings of Geosynthetics '91*, Vol. 2, Atlanta, pp. 799-822.
- Hollinghurst, E. and Murray, R.T., 1986, "Reinforced Earth Retaining Wall at A3/A322 Interchange: Design, Construction and Cost", *Proceedings of the Institution of Civil Engineers, Transportation*, Vol. 80, Part 1, pp.1327-1341.

- Huang, C.C., 1992, "Report on Three Unsuccessful Reinforced Walls", *Recent Case Histories of Permanent Geosynthetic-Reinforced Soil Retaining Walls*, Tatsuoka, F. and Leshchinsky, D., Eds., Balkema 1994, Proceedings of the symposium held in Tokyo, Japan, November 1992, pp. 219-222.
- Indraratna, B., Satkunaseelan, K.S., and Rasul, M.G., 1991, "Laboratory Properties of a Soft Marine Clay Reinforced with Woven and Nonwoven Geotextiles", *Geotechnical Testing Journal*, Vol. 14, No. 3, pp. 288-295.
- Ingold, T.S., 1979, "Reinforced Clay - A Preliminary Study Using the Triaxial Apparatus", *Colloque International sur le Renforcement des Sols*, Paris, Vol.1, pp. 59-64.
- Ingold, T.S., 1981, "A Laboratory Simulation of Reinforced Clay Walls", *Géotechnique*, Vol. 31, pp. 399-412.
- Ingold, T.S., 1983, "A Laboratory Investigation of Grid Reinforcements in Clay", *Geotechnical Testing Journal*, Vol. 6, No. 3 , pp. 112-119.
- Ingold, T.S., 1985, "Fully and Partially Saturated Reinforced Clay under Undrained Axisymmetric Loading", *Ground Engineering*, Vol. 18, No. 6 , pp. 27-31.
- Ingold, T.S., 1992, "Geotextiles used in Basal Drainage of Embankments: a Case History", *Proceedings of the Institution of Civil Engineers, Transportation*, Vol. 95, pp. 193-196.
- Ingold, T.S. and Miller, K.S., 1982, "Analytical and Laboratory Investigation of Reinforced Clay", *Proceedings of Second International Conference on Geotextiles*, Vol. 2, Las Vegas, pp. 587-592.

- Ingold, T.S. and Miller, K.S., 1982, "The Performance of Impermeable and Permeable Reinforcement in Clay Subject to Undrained Loading", *Quarterly Journal of Engineering Geology*, Vol.15, pp. 201-208.
- Ingold, T.S. and Miller, K.S., 1983, "Drained Axisymmetric Loading of Reinforced Clay", *Journal of the Geotechnical Engineering Division, ASCE*, Vol. 109, No. 7 , pp. 883-898.
- Irvin, R.A., Farmer, I.W. and Snowdon, R.A., 1990, "Performance of Reinforced Trial Embankments in London Clay - Undrained Loading", *Performance of Reinforced Soil Structures*, McGown, A., Yeo, K., and Andrawes, K.Z., Eds., Thomas Telford Ltd., London, pp. 119-126.
- Jaber, M. B., 1989, "*Behavior of Reinforced Soil Walls in Centrifuge Model Tests*", Thesis submitted in partial satisfaction of the requirements for the degree of Doctor of Philosophy. Department of Civil Engineering, University of California, Berkeley, California, 239 p.
- Jewell, R.A. and Jones, C.J., 1981, "Reinforcement of Clay Soils and Waste Materials Using Grids", *Proceedings of the Tenth International Conference on Soil Mechanics and Foundation Engineering*, Stockholm, Sweden, Vol. 2, pp. 701-706.
- Kern, F., 1977, "Realisation d'um Barrage en Terre avec Parement Aval Vertical au Moyen de Poches en Textile", *Proceedings of the International Conference on the Use of Fabrics in Geotechnics*, Vol. 1, Paris, pp. 91-94.
- Koerner, R.M., Hsuan, Y., and Lord, A.E., 1992, "Remaining Technical Barriers to Obtain General Acceptance of Geosynthetics", *Grouting, Soil Improvement and*

- Geosynthetics*, ASCE Geotechnical Special Publication No.30, Vol. 1, Proceedings of a symposium held in New Orleans, pp. 63-109.
- Koerner, R.M., Martin, J.P., and Koerner, G., 1986, "Shear Strength Parameters between Geomembranes and Cohesive Soil", *Geotextiles and Geomembranes*, Vol. 4, No. 1, pp. 21-30.
- Krishnaswamy, N.R., and Raghavendra, H.B., 1988, "Behaviour of Reinforced Earth under Direct Shear Test", *Proceedings of the First Indian Geotextiles Conference on Reinforced Soil and Geotextiles*, pp. c47-c52.
- Ladd, C.C., 1991, "Stability Evaluation during Staged Construction", *Journal of Geotechnical Engineering, ASCE*, Vol. 117, No. 4, pp. 537-615.
- Lafleur, J., Sall, M., and Ducharme, A., 1987, "Frictional Characteristics of Geotextiles with Compacted Lateritic Gravels and Clays", *Proceedings of Geosynthetics '87*, New Orleans, Vol. 1, pp. 205-215.
- Leonards, G.A., Frost, J.D. and Bray, J.D., 1994, "Collapse of geogrid-reinforced retaining structure", *Journal of Performance of Construction Facilities, ASCE*, Vol. 8, No.4 , pp. 274-292.
- Ling, H.I and Tatsuoka, F., 1993, "Laboratory Evaluation of a Nonwoven Geotextile for Reinforcing On-site Soil", *Proceedings of Geosynthetics '93*, Vancouver, Canada, pp. 533-546.
- Ling, H.I., Tatsuoka, F., and Wu, J.T.H., 1990, "Measuring In-Plane Hydraulic Conductivity of Geotextiles", *Geosynthetic Testing for Waste Containment Applications*, ASTM STP 1081, pp. 257-272.

- Ling, H.I., Tatsuoka, F., Wu, J.T.H., and Nishimura, J., 1993, "Hydraulic Conductivity of Geotextiles under Typical Operational Conditions", *Geotextiles and Geomembranes*, Vol. 12, No. 6, pp. 509-542.
- Ling, H.I., Wu, J.T.H., and Tatsuoka, F., 1992, "Short-term Strength and Deformation Characteristics of Geotextiles under Typical Operational Conditions", *Geotextiles and Geomembranes*, Vol. 11, No. 2, pp. 185-219.
- Lucia, P.C. and Blair, S.A., 1993, "Geogrid Reinforcement for a Soil Slope. Lawrence Berkeley Laboratory, California, USA", *Geosynthetics Case Histories*, Raymond, G.P. and Giroud, J.P., Eds., pp. 238-239.
- Makiuchi, K., and Miyamori, T., 1988, "Mobilization of Soil-geofabric Interface Friction", *Theory and Practice of Earth Reinforcement*, Proceedings of a symposium held in Fukuoka Kyushu, Japan, pp. 129-134.
- McGown, A., Andrawes, K.Z., and Kabir, M. H., 1982, "Load-extension Testing of Geotextiles Confined in Soil", *Proceedings of Second International Conference on Geotextiles*, Las Vegas, Vol. 3, pp. 793-798.
- Mitchell, J.K., 1981, "Soil Improvement: State-of-the-Art", *Proceedings of Tenth International Conference on Soil Mechanics and Foundation Engineering*, Stockholm, Sweden, Vol. 4, pp.509-565.
- Mitchell, J.K., 1991, "Conduction Phenomena: from Theory to Geotechnical Practice", *Géotechnique*, Vol. 41, No. 3, pp. 299-340.
- Mitchell, J.K. and Christopher, B.R., 1990, "North American Practice in Reinforced Soil Systems", *Design and Performance of Earth Retaining Structures*, ASCE

- Geotechnical Special Publication No.25, Proceedings of a symposium held in Ithaca, NY, June 1990, pp. 322-346.
- Mitchell, R.A. and Mitchell, J.K., 1992, "Stability Evaluation of Waste Landfills", *Stability and Performance of Slopes and Embankments II*, Geotechnical Special Publication No.31, ASCE, Vol. 2, Berkeley, California, pp. 1152-1187.
- Mitchell, J.K. and Villet, W.C.B., 1987, *Reinforcement of Earth Slopes and Embankments*, National Cooperative Highway Research Program Report No.290, Transportation Research Board.
- Mitchell, J.K., Seed, R.B., and Seed, H.B., 1990, "The Kettleman Hills Waste Landfill Slope Failure. I: Liner Interface Properties", *Journal of the Geotechnical Engineering Division, ASCE*, Vol. 116, No. 4 , pp.647-668.
- Murray, R.T. and Boden, J.B., 1979, "Reinforced Earth Wall Constructed with Cohesive Fill", *Colloque International sur le Renforcement des Sols*, Vol. 2, Paris, pp. 569-577.
- Nakamura, K., Tamura, Y., Tatsuoka, F., Iwasaki, K. and Yamauchi, H., 1988, "Roles of Facings in Reinforcing Steep Clay Slopes with a Non-Woven Geotextile", *Theory and Practice of Earth Reinforcement*, Proceedings of a symposium held in Fukuoka Kyushu, Japan, pp. 553-558.
- O'Reilly, M.P., Boden, D.G. and Johnson, P.E., 1990, "Long-Term Performance of Repairs to Highway Slopes using Geotextiles", *Performance of Reinforced Soil Structures*, McGown, A., Yeo, K., and Andrawes, K.Z., Eds., Thomas Telford Ltd., London, pp. 159-162.

- Perrier, H., Blivet, J.C., and Khay, M., 1986, "Stabilization de Talus par Renforcement tout Textile: Ouvrages Experimental et Reel", *Proceedings of the Third International Conference on Geotextiles*, Vol. 2, Vienna, pp. 313-318.
- Puig, J. and Blivet, J.C., 1973, "Remblai à Talus Vertical Armé avec un Textile Synthétique", *Bulletin de liaison des Laboratoires des Ponts et Chaussées*, Vol. 64, pp. 13-18. (in French)
- Puig, J., Blivet, J.C. and Pasquet, P., 1977, "Remblai Armé avec un Textile Synthétique", *Proceedings of the International Conference on the Use of Fabrics in Geotechnics*, Paris, pp. 85-90. (in French)
- Richards, E.A., Scott, J.D., Bobey, L.W.M., and Diyaljee, V. 1989, "Shear Resistance between Cohesive Soil and Geogrids", *Proceedings of Geosynthetics '89*, San Diego, Vol. 2, pp. 365-372.
- Saxena, S.K. and Budiman, J.S., 1985, "Interface Response of Geotextiles", *Proceedings of the Eleventh International Conference on Soil Mechanics*, San Francisco, USA., Vol. 3, pp. 1773-1775.
- Scott, J.D., Sego, D.C., Hofmann, B.A., Richards, E.A. and Burch, E.R., 1987, "Design of the Devon Geogrid Test Fill", *Proceedings of Geosynthetics '87*, Vol. 1, New Orleans, pp. 157-168.
- Seed, R.B., and Boulanger, R.W., 1991, "Smooth HDPE-Clay Liner Interface Shear Strengths: Compaction Effects", *Journal of the Geotechnical Engineering Division*, ASCE, Vol. 117, No. 4 , pp. 686-693.

- Seed, R.B., Mitchell, J.K. and Seed, H.B., 1990, "The Kettleman Hills Waste Landfill Slope Failure. II: Stability analyses", *Journal of the Geotechnical Engineering Division, ASCE*, Vol. 116, No. 4 , pp. 669-690.
- Sego, D.C., Scott, E.A., Richards, E.A. and Liu, Y., 1990, "Performance of a Geogrid in a Cohesive Soil Test Embankment", *Proceedings of Fourth International Conference on Geotextiles, Geomembranes and Related Products*, Vol. 1, The Hague, Netherlands, pp. 67-72.
- Shewbridge, S. and Sitar, N., 1989, "Deformation Characteristics of Reinforced Sand in Direct Shear", *Journal of Geotechnical Engineering, ASCE*, Vol. 115, No. 8 , pp. 1134-1147.
- Sohn, J., Kim, S., Kim, Y., and Yoon, D., 1992, "Factors Influencing Passive Pull-out Resistance", *Grouting, Soil Improvement and Geosynthetics*, ASCE Geotechnical Special Publication No.30, Vol. 2, Proceedings of a symposium held in New Orleans, pp. 1153-1162.
- Sridharan, A., Srinivasa Murthy, B.R., Bindumadhava, and Revanasiddappa, K., 1991, "Technique for Using Fine-grained Soil in Reinforced Earth", *Journal of the Geotechnical Engineering Division, ASCE*, Vol. 117, No. 8 , pp. 1174-1190.
- Stewart, J., Seed, R.B., Riemer, M. and Zornberg, J.G., 1994, "Geotechnical Aspects of the Northridge Earthquake of January 17, 1994 - Geotechnical Structures", *Geotechnical News*, June 1994.
- Tatsuoka, F., Murata, O., Tateyama, M., Nakamura, K., Tamura, Y., Ling, H.I., Iwasaki, K. and Yamauchi, H., 1990, "Reinforcing Steep Clay Slopes with a Non-woven

- Geotextile", *Performance of Reinforced Soil Structures*, McGown, A., Yeo, K. and Andrawes, K.Z., Eds., Thomas Telford Ltd., London, pp. 141-146.
- Tatsuoka, F., Nakamura, K., Iwasaki, K. and Yamauchi, H., 1987, "Behavior of Steep Clay Embankments Reinforced with a Non-Woven Geotextile Having various Face Structures", *Proceedings of Post Vienna on Geotextiles*, Singapore, pp. 387-403.
- Tatsuoka, F. and Yamauchi, H., 1986, "A Reinforcing Method for Steep Clay Slopes using a Non-woven Geotextile", *Geotextiles and Geomembranes*, Vol. 4, Nos. 3-4, pp. 241-268.
- Temporal, J., Craig, A.H., Harris, D.H., and Brady, K.C., 1989, "The use of Locally Available Fills for Reinforced and Anchored Earth", *Proceedings of the Twelfth International Conference on Soil Mechanics and Foundation Engineering*, Rio de Janeiro, Brazil, Vol. 2, pp. 1315-1320.
- The Reinforced Earth Company, 1990, "*Seismic Design of Reinforced Earth Retaining Walls and Bridge Abutments*", 12 p.
- Toriihara, M., Matsumoto, S. and Hiramama K., 1992, "Construction and Measurement of Embankment Reinforced with Geogrid using In-situ Cohesive Soil", *Recent Case Histories of Permanent Geosynthetic-Reinforced Soil Retaining Walls*, Tatsuoka, F. and Leshchinsky, D., Eds., Balkema 1994, Proceedings of the symposium held in Tokyo, Japan, November 1992, pp. 295-299.
- Wang, Y.H. and Wang, M.C., 1993, "Internal Stability of Reinforced Soil Retaining Structures with Cohesive Backfills", *Transportation Research Record* 1414, pp. 38-48.

- Werner, G. and Resl, S., 1986, "Stability Mechanism in Geotextile Reinforced Earth Structures", *Proceedings of the Third International Conference on Geotextiles*, Vol. 2, Vienna, pp. 465-469.
- Wichter, L., Risseuw, P. and Gay, G., 1986, "Large Scale Test on the Bearing Behavior of a Woven Reinforced Earth Wall", *Proceedings of the Third International Conference on Geotextiles*, Vol. 2, Vienna, pp. 301-306.
- Williams, N.D. and Houlihan, M.F., 1987, "Evaluation of Interface Friction Properties between Geosynthetics and soils", *Proceedings of Geosynthetics '87*, New Orleans, Vol. 2, pp. 616-627.
- Wu, J.T.H., 1991, "Measured Behavior of the Denver Walls", *Geosynthetic-Reinforced Soil Retaining Walls*, Wu, J.T.H., Ed., Balkema 1992, Proceedings of the International Symposium on Geosynthetic-Reinforced Soil Retaining Walls, Denver, CO, USA, August 1991, pp.31-41.
- Yamanouchi, T., Miura, N., Matsubayashi, N., and Fukuda, N., 1982, "Soil Improvement with Quicklime and Filter Fabric", *Journal of the Geotechnical Engineering Division, ASCE*, Vol. 108, No. GT7, July, pp. 953-965.
- Yamauchi, H., Tatsuoka, F., Nakamura, K. and Iwasaki, K., 1987, "Stability of Steep Clay Embankments Reinforced with a Non-Woven Geotextile", *Proceedings of the Post Vienna on Geotextiles*, Singapore, pp. 370-386.
- Yunoki, Y. and Nagao, A., 1988, "An Application of Non-woven Fabrics to Embankment of Cohesive Soil", *Theory and Practice of Earth Reinforcement*, Proceedings of a symposium held in Fukuoka Kyushu, Japan, pp. 491-496.

Zornberg, J.G. and Mitchell, J.K., 1992, *Poorly Draining Backfills for Reinforced Soil Structures - A State of the Art Review -*, Geotechnical Research Report No. UCB/GT/92-10, Department of Civil Engineering, University of California, Berkeley, CA, USA, 101 p.

CHAPTER 3

PERFORMANCE OF GEOTEXTILE-REINFORCED SOIL STRUCTURES WITH SLOPING BACKFILLS: A FINITE ELEMENT STUDY



View of the 12.6 m high Rainier Ave. wall supporting a more than 5 m high surcharge fill. This extensively instrumented structure is considered the highest geotextile-reinforced wall.

3.1 Introduction

There is now considerable experience in using approximate methods of analysis and design of reinforced soil walls. In conjunction with the normally adopted soil properties and safety factors, current design guidelines (Mitchell and Christopher, 1990;

Christopher et al., 1990) generally provide safe structures and acceptably small deformations under working stress conditions. These methods, however, were developed for walls of simple geometry. Consequently, the wide range of wall geometry, facings, backfill materials, and reinforcement characteristics now being used may result in a wall behavior different from that assumed in the design.

The construction and monitoring of a large number of full-scale field test walls could resolve many uncertainties, particularly when requirements dictate wall structures with nonstandard geometry or loadings that fall outside the range considered by the empirical design methods. However, instrumenting and adequately monitoring full-scale wall tests is costly.

Numerical simulations are an alternative for predicting the behavior of nonstandard projects, provided field test data are available for validation of parameters and procedures used in the analyses. A rational approach involves initial interpretation of instrumentation results, subsequent validation of the numerical model against the field data, and then numerical simulation of new design aspects. One of the purposes of this chapter is to describe the validation of the finite element representation of a soil structure having two distinctive characteristics: extensible geotextile reinforcements, and a sloping backfill on top of the wall.

Although a number of successful finite element analyses of metallic- and geogrid-reinforced soil retaining walls have been validated against field records, this is not the case for the more flexible geotextile-reinforced structures. A review by Yako and Christopher (1987) identified approximately 200 reinforced walls and slopes that had been constructed in North America using polymeric reinforcements. The number has certainly

grown significantly since then. However, of the reviewed projects, only 13 had well-documented instrumentation. Of these, only five provided stress-strain information, and these were all geogrid-reinforced structures. Consequently, much of the field experience to date has provided only qualitative assessment of the design variables in geotextile-reinforced structures, and quantitative data is needed to substantiate design modifications. The finite element analysis of a 12.6 m high geotextile-reinforced wall with a sloping backfill presented in this study, referred to as the Rainier Ave. wall, adds quantitative information to the existing instrumentation records and provides a calibrated modeling procedure for future parametric studies.

While sloping backfills behind geosynthetically reinforced soil walls are common, some aspects of their design and performance have not been fully investigated. The state-of-practice for design of soil walls reinforced with extensible inclusions and having horizontal backfills has been to consider a Rankine failure surface as the locus of maximum tensile forces (Mitchell and Christopher, 1990). In the case of reinforced soil walls with surcharges induced by sloping backfills (Figure 3.1), the same potential failure surface defined by an angle of $45^\circ + \phi/2$ from the horizontal has also been generally considered suitable for design. Since the anchorage length for pullout resistance verification is the reinforcement length behind this surface, correct location of the potential failure surface has major implications on the verification of the wall internal stability.

Although only few instrumented case histories of full-scale geosynthetically reinforced walls with sloping backfills are available (Zornberg and Mitchell, 1993), these records suggest that the theoretical Rankine surface appropriately represented the

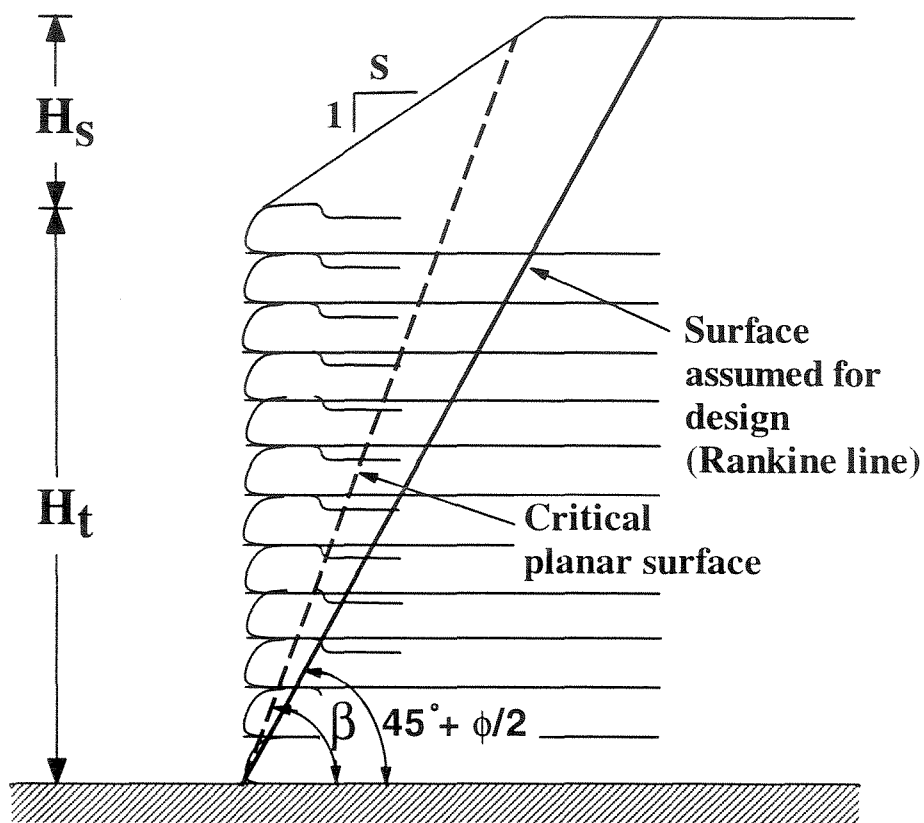


Figure 3.1 Reinforced soil wall with sloping backfill showing potential failure surface assumed in conventional design.

reinforcement maximum tension line. However, further verification of the location of the potential failure surface is necessary to extend current design methods to different wall and backfill characteristics. Accordingly, a second purpose of this study is to undertake a finite element parametric analysis to investigate the validity of current design assumptions for geosynthetically reinforced soil walls with sloping backfills. The study involves two steps: (1) the finite element prediction of the behavior of an actual instrumented geosynthetically reinforced soil wall with sloping backfill surcharge, and (2) a parametric study, using calibrated input parameters obtained from the previous step, to

investigate the effect of surcharge geometry and wall design characteristics on the location of the potential failure surface.

After describing the Rainier Ave. wall and its instrumentation, the characteristics of its finite element modeling (geometry definition, soil and reinforcement material parameters, incremental sequence of analysis) are presented. Results from the analysis, interpretation of mechanisms that dominated the wall behavior, and location of the potential failure surface are addressed. Subsequently, the results of a finite element parametric study are presented to investigate the influence of the sloping surcharge geometry (fill slope and surcharge height) and of wall design characteristics (wall height and reinforcement stiffness) on the location of the potential planar surface.

3.2 Finite element analysis of reinforced soil structures

3.2.1 General Considerations

The finite element analyses in this study were performed using the code SSCOMP developed originally by Seed and Duncan (1984), and subsequently modified by Collin (1986) and Jaber (1989) for the analysis of reinforced soil structures. Additional modifications were implemented for the purposes of this study. SSCOMP is a general, plane strain, soil-structure interaction program for static analyses of geotechnical structures including consideration of compaction-induced stresses and deformations.

Nonlinear stress-strain and volumetric strain behavior of soil is modeled in SSCOMP using the hyperbolic formulation proposed by Duncan et al. (1980). The program allows the modeling of compaction induced stresses using a hysteretic model for stresses resulting from cyclic loading under condition of no lateral deformations.

Reinforcements are modeled using elastic bar elements. Soil-structure interaction is modeled using interface elements capable of transferring shear stresses between the soil and the reinforcement.

Details of the algorithms and capabilities of SSCOMP are not discussed in this report. The reader is referred to well documented previous publications such as Seed and Duncan (1984), Schmertmann et al. (1989), and Boulanger et al. (1991). The program version used for this study is based on the version 'SSCOMP90' used by Schmertmann et al. (1989) in their parametric study. Some of the results were postprocessed using the program Feapplot available for the PC version of SSCOMP (Boulanger et al., 1991; Bray et al., 1992). The revised code used in this study is a UNIX version that handles problems with a larger number of degrees of freedom, generates output files used for postprocessing of results, and deals slightly differently with soil elements in tension state of failure. In order to generate plots efficiently and reduce chances for transcription errors, postprocessing programs were either developed or adapted.

3.2.2 Validation of the finite element model used in this study

Confidence on the accuracy of results obtained with a numerical model is gained after favorable comparison of numerically predicted responses against actual structure behavior, as quantified by instrumentation records. SSCOMP has been used successfully by previous investigators to predict the behavior of large model walls in centrifuge tests and full-scale instrumented reinforced soil walls. A summary of the reinforced soil structures modeled using SSCOMP which have been validated against instrumentation records is presented in Table 3.1. Predicted reinforcement tensions generally agree very

Table 3.1 - Previous FE analyses of reinforced soil structures using SSCOMP, validated against instrumentation records

Structure	System name	Backfill material	Foundation material	Height (ft)	Reinforcement	Validated instrumentation data	Surcharge	Facing	Reference
Hayward wall	VSL	gravelly sand	Soft to medium sandy clay	20	Bar mat	Reinforcement tension distribution	Sloping backfill surcharge (26° up to 50 ft)	Concrete panels	Collin (1986); Seed et al (1986)
Baxter wall	MSE	sandy silt	Sandy silt	16	Bar mat	Reinforcement tension distribution	No surcharge	Concrete panels	Collin (1986); Seed et al (1986)
Dunsmuir wall	Reinforced Earth	granular aggregate (SM)	Compacted fill (gravel in silty clay matrix)	15	Metal strips	Reinforcement tension distribution	No surcharge	Concrete panels	Collin (1986); Seed et al (1986)
Wall 1	Reinforced Earth	Gravelly sand	Medium dense sand	20	Steel strips	Reinforcement tension distribution Face deformation	No surcharge	Precast concrete panels	Adib (1988); Adib et al (1990)
Wall 2	Tensar SR2	Gravelly sand	Medium dense sand	20	geogrid	Reinforcement tension distribution Lateral deformation (14 ft wall height)	No surcharge	Precast concrete panels	Adib (1988); Adib et al (1990)
Wall 3	VSL	Gravelly sand	Medium dense sand	20	Bar mat	Reinforcement tension distribution Lateral deformation (10 ft wall height) Vertical pressure	No surcharge	Precast concrete panels	Adib (1988); Adib et al (1990)
Wall 4	VSL	Cobbles	Medium dense sand	20	Bar mat	Reinforcement tension distribution Lateral deformation (14 ft fill height)	No surcharge	Precast concrete panels	Adib (1988); Adib et al (1990)
Wall 5	VSL	Clayey silt	Medium dense sand	20	Bar mat	Reinforcement tension distribution	No surcharge	Precast concrete panels	Adib (1988); Adib et al (1990)
Wall 6	Quline 160	Gravelly sand	Medium dense sand	20	Non-woven geotextile	No reliable measurements available	No surcharge	Wrap-around geotextile	Adib (1988)
Wall 7	Gabion	Gravelly sand	Medium dense sand	21	Gabion mesh	Reinforcement tension distribution Lateral deformations	No surcharge	Gabion baskets	Adib (1988)

Table 3.1 (cont.)

Structure	System name	Backfill material	Foundation material	Height (ft)	Reinforcement	Validated instrumentation data	Surcharge	Facing	Reference
Wall 8	Gabion	Gravelly sand	Medium dense sand	21	Gabion mesh	Reinforcement tension distribution Lateral deformation (9 ft fill height)	No surcharge	Gabion baskets	Adib (1988)
Embankment 1	Signode TNX 250	Clayey silt	Medium dense sand	20	Geogrid	Reinforcement tension distribution Lateral deformation	No surcharge	No facing	Adib (1988); Adib et al (1990)
Embankment 2	Amoco 2006	Clayey silt	Medium dense sand	20	Woven geotextile	Reinforcement tension distribution	No surcharge	No facing	Adib (1988); Adib et al (1990)
Embankment 3	Signode TNX 250	Clayey silt	Medium dense sand	25	Geogrid	Reinforcement tension distribution	No surcharge	No facing	Adib (1988); Adib et al (1990)
Embankment 4	Amoco 2006	Clayey silt	Medium dense sand	25	Woven geotextile	Reinforcement tension distribution	No surcharge	No facing	Adib (1988); Adib et al (1990)
Centrifuge Wall Model 1	VSL model	Sand	Sand	1.67	Bar mat	Reinforcement tension distribution. Face movement	No surcharge	Cruciform Aluminum panels	Jaber (1989)
Centrifuge Wall Model 2	Reinforced Earth model	Sand	Sand	1.67	Steel strip	Reinforcement tension distribution. Face movement	No surcharge	Cruciform Aluminum panels	Jaber (1989)
Centrifuge Wall Model 3	Tensar model	Sand	Sand	1.67	Geogrid	Reinforcement tension distribution. Face movement	No surcharge	Cruciform Aluminum panels	Jaber (1989)
Centrifuge Wall Model 4	Geotextile model	Sand	Sand	1.67	Geotextile	Reinforcement tension distribution. Face movement	No surcharge	Wrapped geotextile	Jaber (1989)
Bridge approach embankment	-	Silty sand	H-section steel base	5	Geogrid	Wall deformation. Geogrid strains. Vertical earth pressure.	Imposed differential settlements	Rigid box wall	Schmertmann(1991)

well with measured values, whereas predicted wall facing deformations are qualitatively reasonable, but deviate from the actual values in some cases. The code has been mainly validated against structures with horizontal backfills that are reinforced with inextensible inclusions.

Collin (1986) predicted reinforcement tensions and lateral wall displacements for three walls constructed with different types of steel reinforcements and soil backfills. Analyses were performed both with and without modeling the effects of soil compaction in order to investigate the influence of compaction on the stresses within these reinforced soil walls. The importance of modeling compaction-induced soil stresses on the analysis of these steel reinforced soil walls was emphasized by Seed et al. (1986). The three walls modeled by Collin ranged in height from 16 to 20 ft. One of the studied cases, a bar mat reinforced soil wall (Hayward wall), had a sloping backfill surcharge. Predicted reinforcement tensions on the performed analyses matched very well with the measured values, both in magnitude and distribution, indicating the ability of the model to simulate steel reinforced structures.

Adib (1988) predicted reinforcement tensions and lateral wall deformations for eight full-scale walls and four full-scale reinforced embankments using SSSCOMP. These 20 ft high test structures were constructed as part of the FHWA "Behavior of Reinforced Soil" research project (Christopher et al., 1990) using three soil types, seven reinforcement materials, and three facing types. Comparisons were made between the finite element predictions and the measured values of soil stresses, deformations, location of the maximum tension, and distribution of tensile forces along the reinforcement. Adib

concluded that the analyses correctly estimated the distribution and maximum values of reinforcement tension and qualitatively matched the lateral wall deformations.

Jaber (1989) predicted the response of four 20 in high model reinforced soil walls using SSCOMP, and compared the results to measured values during centrifuge testing. These walls were scale models of four of the FHWA test structures considered by Adib (1988). Reinforcement materials ranged from steel to non-woven geotextile. Gravity turn-on loading was used to simulate the centrifuge testing via finite element analysis. There was reasonably good agreement between predicted and observed values of reinforcement tension, but poor quantitative agreement for lateral wall displacements. The good tension distribution predictions obtained under gravity turn-on loading indicated that finite element analyses can be successfully used for predicting reinforcement tensions.

A parametric study on the response of steel reinforced soil walls to variations in wall geometry, material properties, external loading, and soil compaction was reported by Schmertmann et al. (1989). A reference wall, representative of a typical reinforced soil wall for highway applications was chosen, and selected wall variations were modeled using SSCOMP. No prototype structure existed for this reference wall. Nevertheless, the model predictions for reinforcement tension, facing displacements, and vertical soil stresses were found to be in reasonable ranges. The results showed that both the magnitude of tension that develops in the reinforcements and the lateral deformation of the wall facing may be strongly influenced by factors such as the degree of soil compaction, the type of wall facing material, and the reinforcement length.

Schmertmann (1991) investigated the response of reinforced soil walls to the presence of uncompacted zones within the backfill, and to post-construction backfill

wetting collapse. SSCOMP was modified to allow updating of nodal point coordinates in order to simulate large-strain behavior. The modified code was used to model a 5 ft high geogrid reinforced bridge approach embankment, and a 30 ft long buried pipeline subjected to differential subsidence. Finite element predictions were reasonably close to the responses measured during the experiments. Results from the analyses indicated that wetting collapse in the backfill causes reductions in reinforcement tension stress, increases in reinforcement bending stresses, and increases in lateral wall facing deformations. Also, analyses showed that walls with uncompacted backfill zones adjacent to the wall facing have reduced reinforcement tension stresses, increased reinforcement bending stresses, and reduced lateral wall facing deformations.

Bray et al. (1993) investigated the use of fill-reinforcement materials in a development project located in a zone containing minor subsidiary faults. Differential movement of underlying bedrock faults dissipates as the shear rupture plane propagates through overlying compacted fill materials. In order to mitigate the hazard associated with earthquake fault rupture propagation through compacted fill, the possibility of using geosynthetics within a smaller thickness of compacted fill was investigated using SSCOMP. The numerical results indicated that the reinforcement is effective in spreading the differential movement across a wider zone in the reinforced compacted fill. Differential settlement and tensile strains in the fill are sufficiently reduced to allow the construction of building foundations within an acceptable level of risk.

Overall, results obtained from reinforced soil wall modeling by previous investigators have shown that SSCOMP is an accurate tool for analysis of walls constructed of a variety of soil types, reinforcement materials and wall facing types. The

considerable experience gained in simulating a range of wall geometries, reinforcement layouts, and external loadings is useful for the numerical simulations performed in this study.

3.2.3 Key issues to be considered for modeling soil structures reinforced with extensible inclusions

A number of finite element analyses of soil structures reinforced with geosynthetics (mainly with geogrids) has been reported in the literature. Some of these studies investigated the performance of hypothetical reinforced soil structures (e.g., Chalaturnyk et al., 1990; Ho and Rowe, 1993), while others validated finite element analyses of geogrid-reinforced structures against field records (e.g., Adib, 1988; Bathurst et al., 1992). Only a limited number of finite element studies of the more flexible geotextile-reinforced structures were identified in the technical literature (e.g., Adib, 1988). Considering this limited modeling experience, extra care was required in the determination of appropriate mesh layout, material parameters, and analysis sequence for the geotextile-reinforced structure under study.

The finite element modeling of soil structures reinforced with extensible reinforcements differs from the modeling of structures with inextensible reinforcements. Some modeling aspects are actually simpler in the first case:

- *Two-dimensional reinforcement layout.* Reinforcement layers and soil/reinforcement interfaces should be modeled as continuous sheets when using a plane-strain analysis program. Geosynthetic reinforcements are generally continuous layers and, consequently, they can be naturally assumed as plane strain

structural elements. This is generally not the case for inextensible reinforcements, such as steel strips or bar mats, which have a three dimensional layout. There is no agreement in the technical literature on how to distribute reinforcement and interface strength and stiffness properties into a two-dimensional representation.

- *Less influence of facing modeling on the analysis results.* This applies for the common case of structures using flexible facing system, like wrap-around geotextiles. Selection of material parameters and boundary conditions of facing structures is not straight forward, and generally involves the use of parameter values from previously validated case histories. While rigid facing structures can play an important role in the overall wall behavior, in the case of more flexible structures the wall response is dominated by soil and reinforcement characteristics. The selection of facing parameters in these analyses is consequently less important.

On the other hand, several modeling aspects are more complex in the finite element analysis of geosynthetically reinforced soil structures:

- *Uncertain stress-strain-strength relationship for the geosynthetic.* The effect of confinement and time effects on the tensile strength and stiffness of geosynthetics is not fully understood. The available information generally consists of results from wide width tensile tests. These data, obtained by testing unconfined geosynthetic samples under high strain rates, are certainly not representative of in-service conditions and merely represent index properties. Choosing an appropriate

in-soil stiffness value for the geosynthetic reinforcement is probably the single most critical selection to be made in the numerical modeling of the structure.

- *Finer mesh discretization.* Since geosynthetically reinforced soil structures generally have smaller reinforcement vertical spacing than structures reinforced with inextensible inclusions, a finer mesh discretization is required. Moreover, due to the high contact efficiency between soil and geosynthetics, pullout failure may conceivably occur within the soil layer and not at the soil-reinforcement interface. Consequently, an accurate representation requires a finer mesh discretization of the soil backfill between reinforcement layers.
- *Higher dependency on soil stress-strain relationship.* Finite element results are expected to be more sensitive to the stress-strain-strength behavior of the backfill soil than in the case of soil structures reinforced with inextensible reinforcements. The stiffer reinforcements and facing structures used in those structures dominate the wall response behavior. A careful evaluation of soil parameters is then of more relevance in the analysis of the less stiff geosynthetically reinforced structures.
- *Modeling of soil compaction effects.* Analytical procedures were developed to estimate compaction-induced earth pressures for situations in which geostatic soil stresses represent conditions of no lateral deformation (Seed and Duncan, 1983). These estimations were extended to situations such as embankments, deflecting soil structure interfaces, and soil structures with inextensible reinforcements (Seed and Duncan, 1983; Collin, 1986) by incorporating the developed procedures into a finite element framework. However, the ability of the model to simulate

compaction-induced pressures on soil structures with extensible inclusions and flexible facing may require additional investigation.

- *Highly mobilized shear stresses.* The backfill material in geosynthetically reinforced soil walls experiences larger lateral deformations than in structures reinforced with inextensible elements. Consequently, zones of highly mobilized shear stresses and possibly zones of failed elements may develop. Although the accuracy with which the hyperbolic model represents the soil behavior may be compromised, the presence of zones with highly mobilized shear stresses is not so adverse as in nonreinforced earth structures. This is because, in reinforced earth structures, zones of highly mobilized soil shear stresses do not imply a failure mechanism if ultimate tensile strength has not been reached also in the reinforcements.

3.3 Finite element analysis of the Rainier Ave. wall

The finite element analysis of a 12.6 m high wall constructed at the SR-90, Rainier Avenue Interchange project in Seattle, Washington (Christopher et al., 1990; Allen et al., 1991) is presented in this section. Results obtained from the numerical study are compared with the wall instrumentation records at the end of construction and after placement of a sloping backfill surcharge. Modeling procedures validated from this Class C, after the event, prediction (Lambe, 1973) are the basis for the parametric study presented in Section 3.4.

3.3.1 Wall description and available instrumentation records

To provide for a preload fill in an area of limited right-of-way, the Washington State Department of Transportation designed and supervised the construction of a 12.6 m (41.25 ft) high geotextile-reinforced retaining wall. As the wall was higher than any geotextile-reinforced wall built previously and supported a 5.3 m (17.4 ft) high surcharge fill, an extensive instrumentation program was developed to evaluate its performance (Christopher et al., 1990; Allen et al., 1991). The objectives of the monitoring program were to observe the stress and strain distributions within the reinforced soil wall, and to evaluate the wall response due to the inclined surcharge fill.

Geotechnical investigations at the site indicated an upper layer about 6 m thick of fairly dense granular materials overlying up to 15 m of soft lacustrine silty clays and clayey silts. Although these soft deposits were slightly overconsolidated, they were sufficiently compressible that settlements up to 150 mm in the area of abutments were anticipated. Thus the need for temporary surcharge fills. Traffic and site geometric constraints dictated that some type of retaining structures would be required, and geotextile reinforced retaining walls were chosen because of their economy and ease of construction.

Reinforcement requirements for the Rainier Ave. wall were determined based on a conventional tieback wedge analysis (Mitchell and Christopher, 1990), and a reinforcement spacing of 0.38 m was adopted. The specified geotextile strength was varied with the height of the wall to more closely match theoretical design strength requirements. Accordingly, four different polypropylene slit film woven and polyester

multifilament woven geotextiles were selected as reinforcements. A summary of the characteristics of this wall is indicated in Table 3.2.

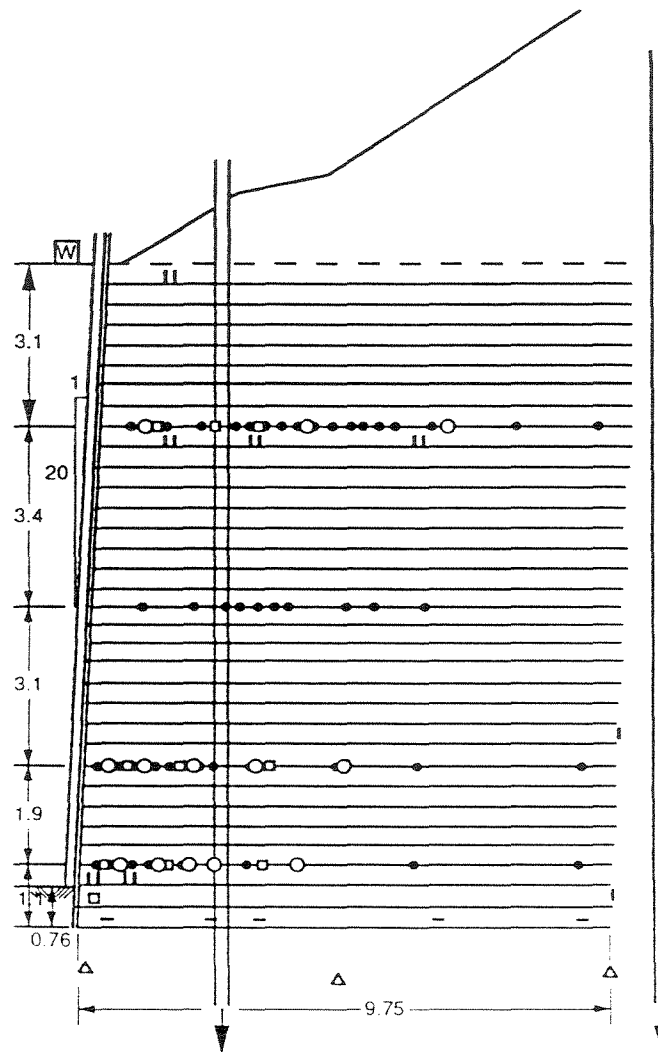
The following parameters, suitable for comparison against results from finite element analyses, were monitored during construction and subsequent surcharging:

- Strain and stress distribution in the geotextile and, particularly, the magnitude and location of maximum stress;
- Vertical and horizontal movement of the instrumented section;
- Horizontal movement of the wall face;
- Lateral earth pressure at the back of the reinforced section;
- Stress distribution at the base of the reinforced section;
- Changes in the stress distribution and displacements due to the surcharge load;

Figure 3.2 shows the type and location of the installed instruments. Bonded resistance strain gage sets were installed on the geotextile reinforcement to evaluate the local stress and strain distribution as well as the location and magnitude of the maximum stress within the four instrumented layers of reinforcement. A total of 45 bonded resistance strain gage points was used. They were concentrated in the area of the theoretical Rankine and a bilinear (or coherent gravity) failure surfaces. To evaluate the global strain and stress state in the geotextile and to provide additional redundancy for the bonded strain gage data, 14 mechanical extensometers were mounted on three of the reinforcement layers.

Table 3.2 - Rainier Ave. wall characteristics:

	Rainier Ave. wall
Location	Interstate Highway 90, Seattle, Washington
Height	41.25 ft (12.6 m)
Length	approx. 200 ft
Vertical batter	1:20
Purpose	Preload fill for Rainier Interchange (SE wall)
Backfill material	gravelly sand. $\phi=43^\circ$ to 47° at field densities (from Triaxial tests)
Foundation	20 ft thick dense granular material (deltaic deposits and recent fills) overlying 50 ft of soft lacustrine silty clays and clayey silts.
Reinforcement type	<ul style="list-style-type: none"> •Polypropylene woven (Exxon GTF 200; Tensile strength: 177 lbs/in) •Polypropylene woven (GTF 375; Tensile strength: 354 lbs/in) •Polypropylene woven (GTF500; Tensile strength: 527 lbs/in) •Polyester woven (GTF1225; Tensile strength: 1064 lbs/in)
Reinf. spacing	constant 1.25 ft (0.38 m)
# Reinf. layers	33 (four 10 ft vertical zones)
Reinf. length	32 ft (9.75 m)
Instrumented layers	Layers #4, #9, #17, #26 (3.8, 10.0, 20.0, and 31.3 ft high)
Surcharge slope	1-3/4H:1V
Surcharge height	17.4 ft (5.3 m)
Compaction characteristics	w.opt.:7% Average dry density: 124.5 pcf (97% of the maximum dry density). Average moisture content: 7.5% Field compaction with small vibratory rollers or larger roller for static compaction
Facing	Wrap around geotextile



LEGEND

- Bonded resistance strain gage
- Mechanical extensometer
- Earth pressure cell
- || Inclinometer casing
- Thermistor
- △ Remote settlement gage
- || Inductance coil strain gage
- W Weather station

Figure 3.2 - Instrumentation of the Rainier Ave. wall. Dimensions are in meters (after Christopher et al, 1990).

Figure 3.3 shows the final tensile strain distribution in each instrumented reinforcement layer based on the strain gage and the extensometer measurements. Strain distribution is shown at the end of construction, immediately after placement of the surcharge, and six months later (Christopher et al., 1990). The Rankine failure plane is indicated by a dashed line in Figure 3.3. It was defined based upon the friction angle of the backfill material of 43° , as obtained from consolidated drained, triaxial tests. The data show that the maximum tensile strains are mostly located along the theoretical Rankine failure plane. The sloping backfill surcharge caused relatively small increases in strain (usually less than 0.05%) in the lower reinforcement layers, but relatively greater increases (0.1 to 0.2%) in the upper layers.

To evaluate the horizontal movement of the wall, inclinometer tubes were installed at the face of the wall, within the reinforced soil section, and behind the reinforced section. Figure 3.4 shows the deflection perpendicular to the wall face, as measured by the inclinometer located within the reinforced section. The kink at elevation 26 m was interpreted to correspond to the intersection with the theoretical Rankine failure plane. The effect of the surcharge is also indicated in Figure 3.4. Inclinometer data from the middle location showed 28 mm (1.1 inches) of deflection towards the top of the wall after loading. The front inclinometer indicated 43 mm (1.7 inches) of deflection.

To provide additional redundancy, both optical and photogrammetric surveys were made of the wall face during and after construction. The inclinometers measured the total movement relative to the bottom of the inclinometer casing, which is a fixed reference. The optical survey readings as well as the photogrammetric measurements are relative to the initial readings taken for each specific optical or photogrammetric target.

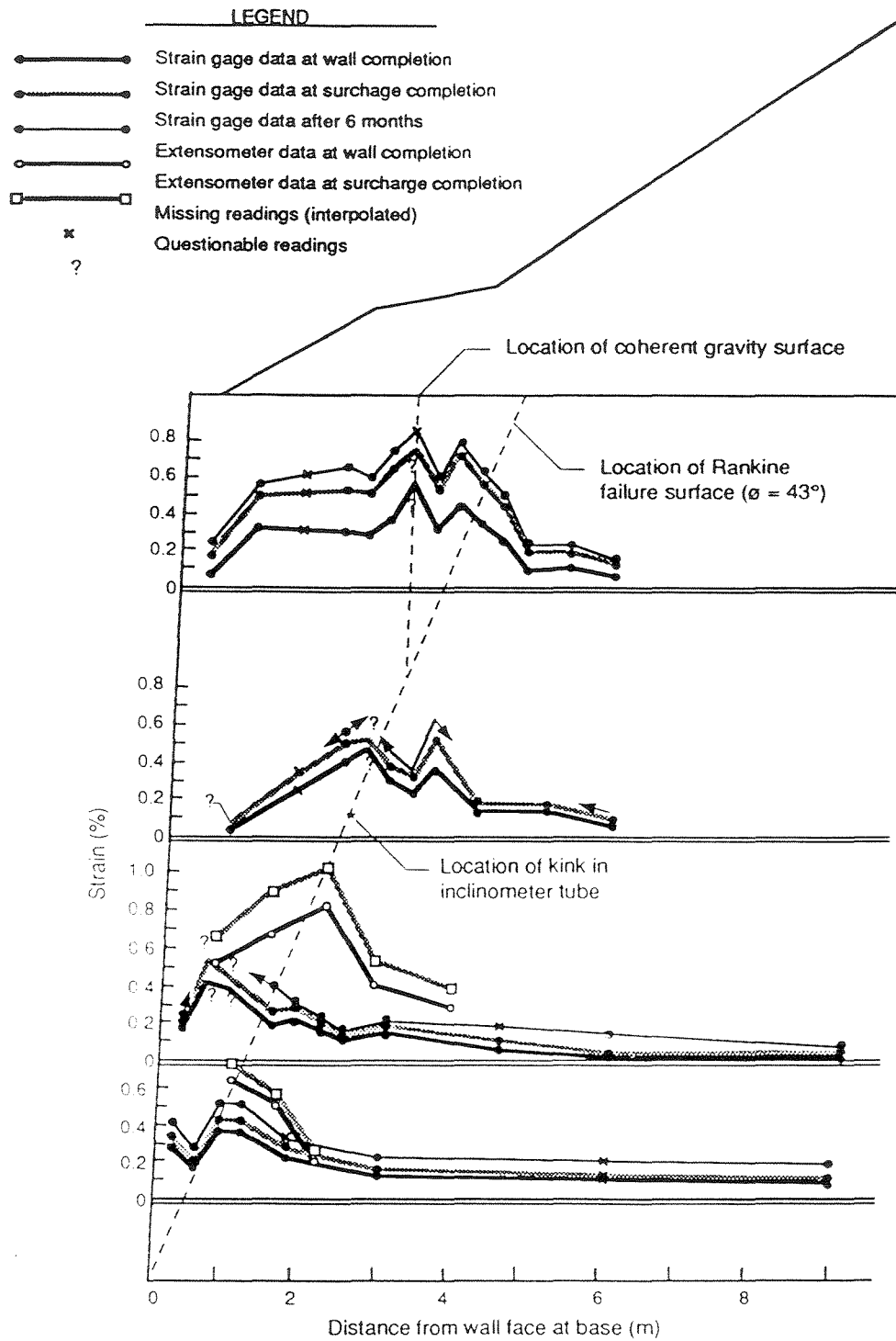


Figure 3.3 - Distribution of strains in each instrumented layer on the Rainier Ave. wall (after Christopher et al, 1990).

Comparison of the optical and photogrammetric face deflections at the completion of the wall and surcharge is shown in Figure 3.5 (Holtz et al., 1991). Incremental deflections can be compared with measured geotextile strains, while total deflections from inclinometer measurements can be used to estimate overall wall face movements.

Vertical stresses beneath the wall were measured using Glötzl stress cells. Stresses at the toe were approximately 20% higher than in the middle or back of the wall. However, the measured stresses were lower than the average overburden pressure, and this discrepancy was under investigation (Allen et al., 1991). Additional instrumentation included Bison inductance coil soil strain gages, placed in the backfill soil, and earth pressure cells, placed behind the reinforced soil mass.

Reinforcement strains and long-term creep rates were much lower than expected, showing that current design methodologies are conservative, even for very high walls. Since the geotextile wall was built to temporarily retain preload fills for bridge abutments founded on soft deposits, the structure was torn down after approximately one year of service. During that time, the measured deflections were low and the overall wall performance was considered excellent (Allen et al., 1991).

3.3.2 Modeling characteristics

Final geometry configuration and material parameters used in the finite element analysis of the Rainier Ave. wall were defined after careful interpretation of available information, followed by a study of the sensitivity of the finite element results to the selected values. Considerations made for selecting different modeling aspects is presented next. The two major modeling issues for this analysis ended up being the large number

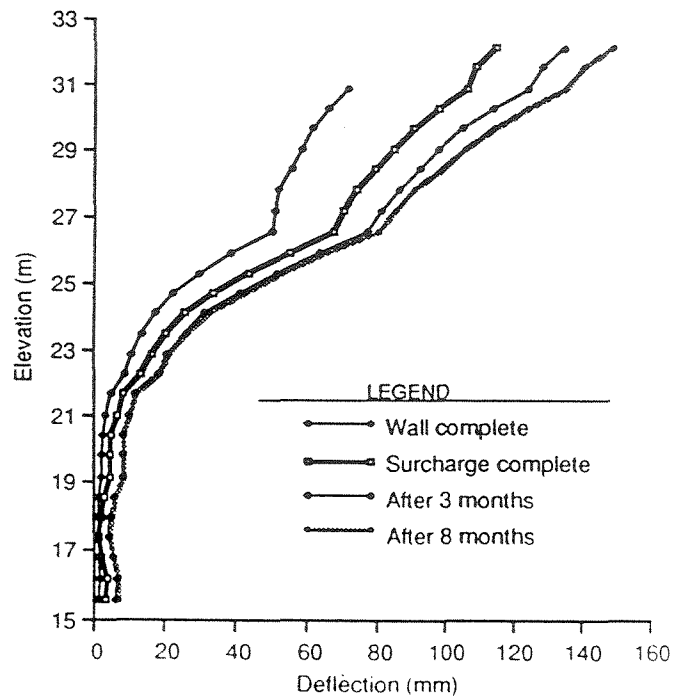


Figure 3.4 - Incliner records on the Rainier Ave. wall (after Christopher et al, 1990).

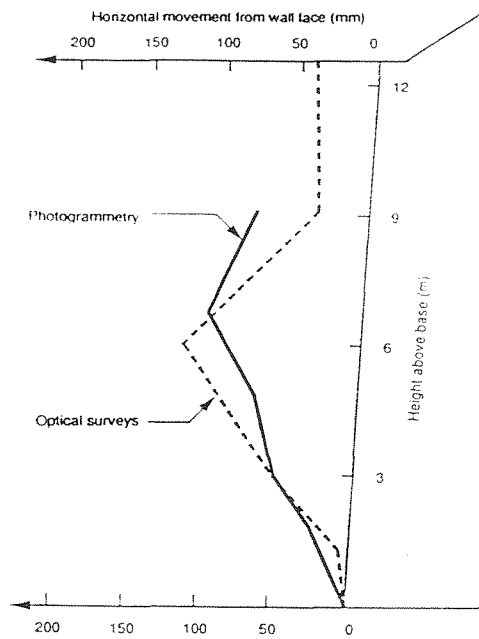


Figure 3.5 - Incremental movement of the wall face as determined by optical and photogrammetric surveys at the completion of surcharge fill (after Holtz et al, 1991).

of degrees of freedom required for the final analysis, and the uncertainty in the value of the geotextile in-situ stiffness.

3.3.2.1 Mesh layout

The finite element mesh for the analysis of the Rainier Ave. wall was established based on the following considerations:

- a) a sensitivity study of the mesh discretization, mainly in zones of high stress gradients, required to render accurate and convergent results;
- b) the need of retrieving numerical results at the location of instrumentation devices (strain gauges in reinforcements, inclinometers, earth pressure cells); and
- c) practical limitations of program capacity and run times.

The finite element mesh selected for the final analysis consisted of 1698 nodes, 1661 plane strain elements for soil representation, and 561 bar elements for numerical simulation of the reinforcements. The location of the two soil material types used in the analysis, the origin of coordinates selected for the nodal points, and the boundary conditions for the final layout are indicated in Figure 3.6. Final mesh configuration is shown in Figure 3.7. The total dimensions of the mesh were set considering previous experience in the analysis of nonreinforced and reinforced earth structures (Dunlop and Duncan, 1970; Collin, 1986; Adib, 1988). A scale drawing of the mesh layout in the reinforced zone is shown in Figure 3.8. Vertical alignment of the nodes was selected at a horizontal distance of 2.7 m (9 ft) from the toe, instead of keeping the facing batter, in order to accommodate the mesh layout to the location of the inclinometer. Although

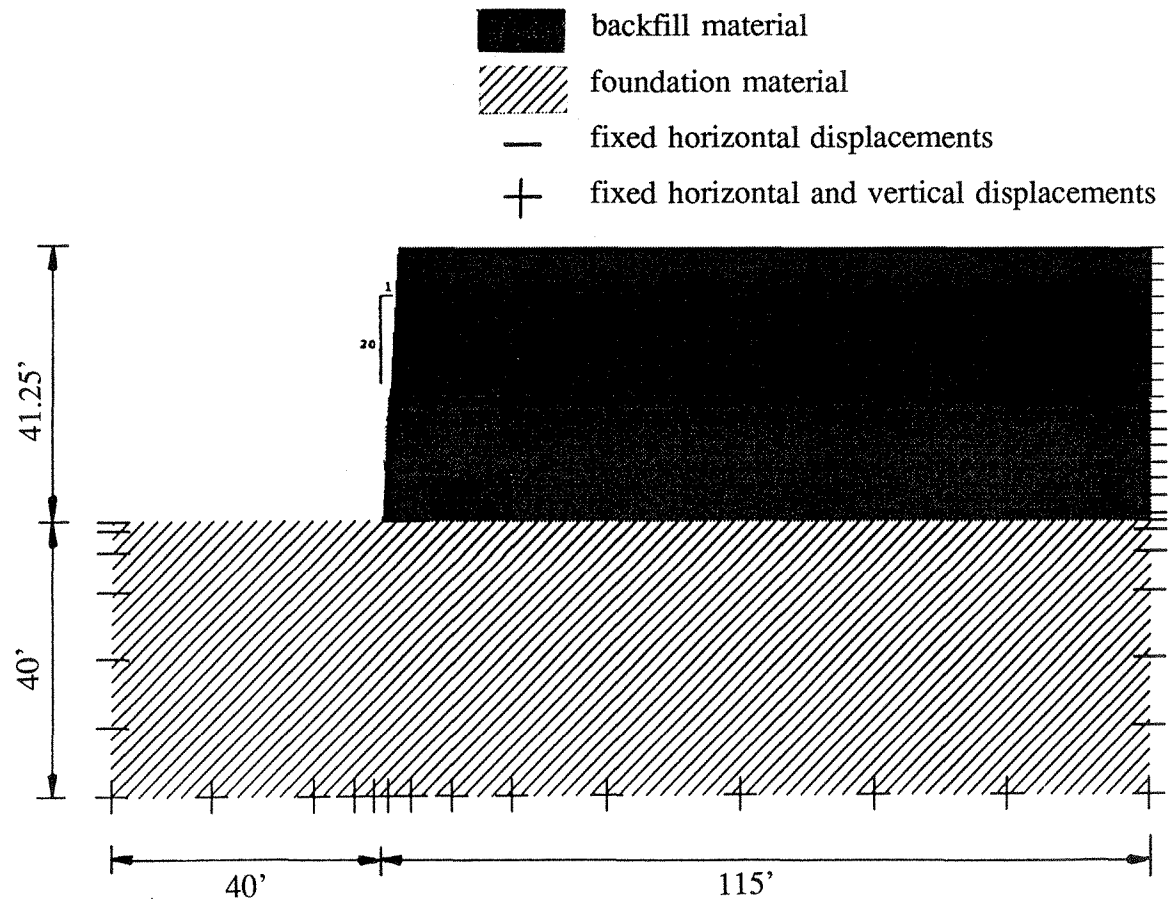


Figure 3.6 - Mesh dimensions and boundary conditions

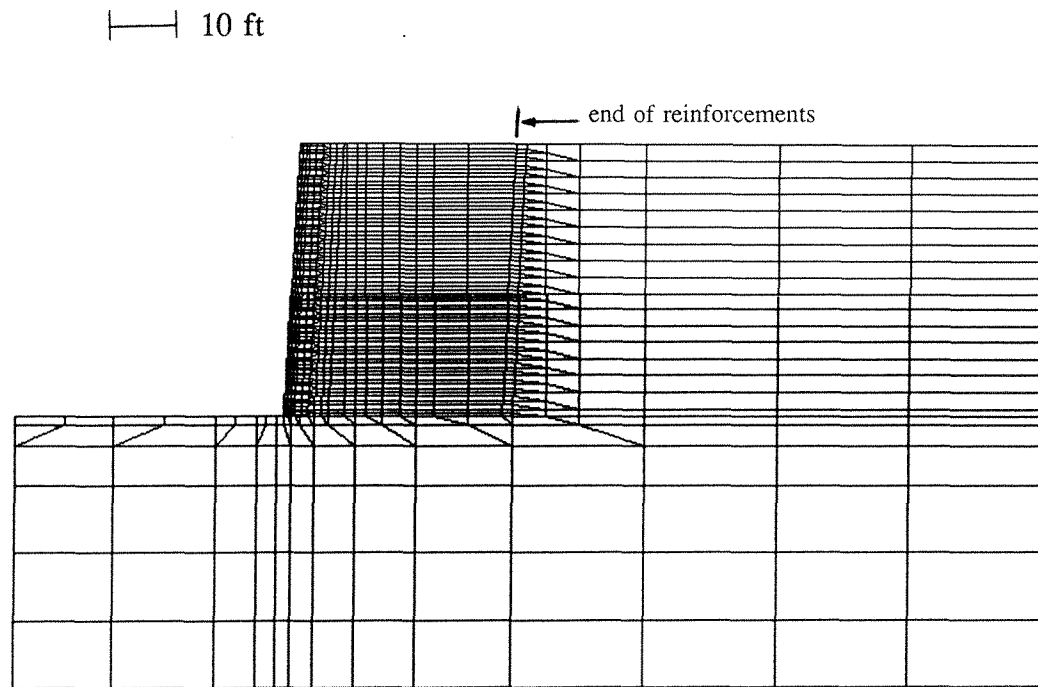


Figure 3.7 - Finally selected mesh for the Rainier Ave. wall analysis

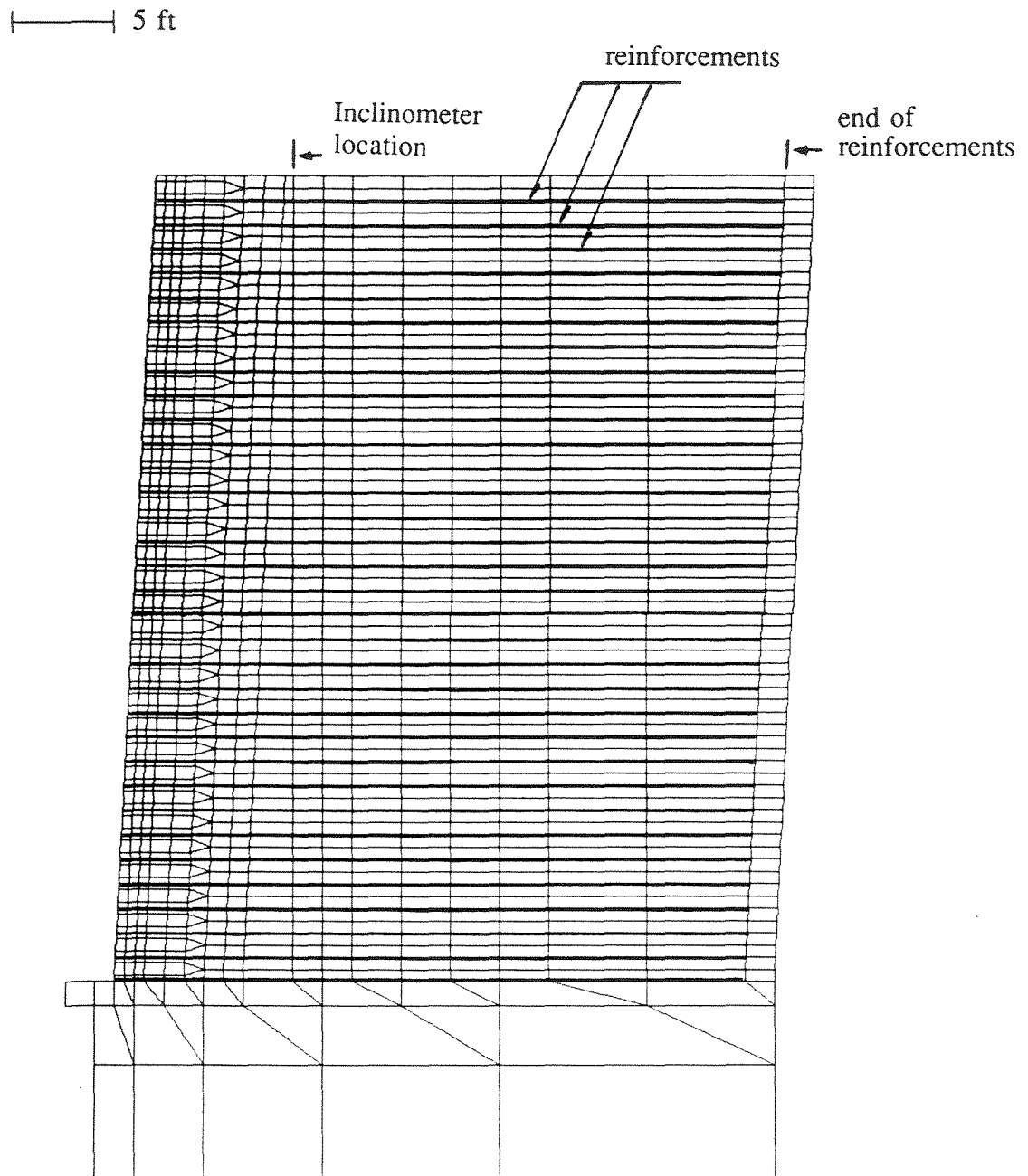


Figure 3.8 - Final mesh layout. Reinforced soil zone

triangular elements are also used, they were not placed right at the end of the bar elements, since quadrilateral elements will certainly perform numerically better in this zone of high stress gradients.

Mesh discretization between reinforcement layers was found essential for the proper representation of the soil layer behavior. As contact efficiency between geotextiles and soil is high, displacement compatibility between soil and reinforcement elements is a reasonable assumption. Even during pullout, failure would probably occur within the soil mass and not along the soil/reinforcement interface. Consequently, a fine discretization of the backfill soil between reinforcement layers was used in the analysis. A detail of the selected discretization near the face of the wall is shown in Figure 3.9.

3.3.2.2 Hyperbolic soil parameters

The stress-strain-strength characterization of the backfill soil plays a more relevant role in geosynthetically reinforced soil walls than in stiffer metallic-reinforced structures. Triaxial compression tests were available for the backfill material used in the Rainier Ave. wall (STS Consultants, 1990), and special care was taken in estimating the parameters for the hyperbolic model.

The soil constitutive relationship implemented in SSCOMP is a modified version of the hyperbolic model proposed by Duncan, et al. (1980). Soil element material properties at any increment during the finite element analysis are based on the current stress state and the previous stress history of each element. The non-linear, stress-dependent model assumes that stress-strain curves for soils can be approximated with hyperbolas, as shown in Figure 3.10a . The slope of the hyperbolic stress-strain curve is

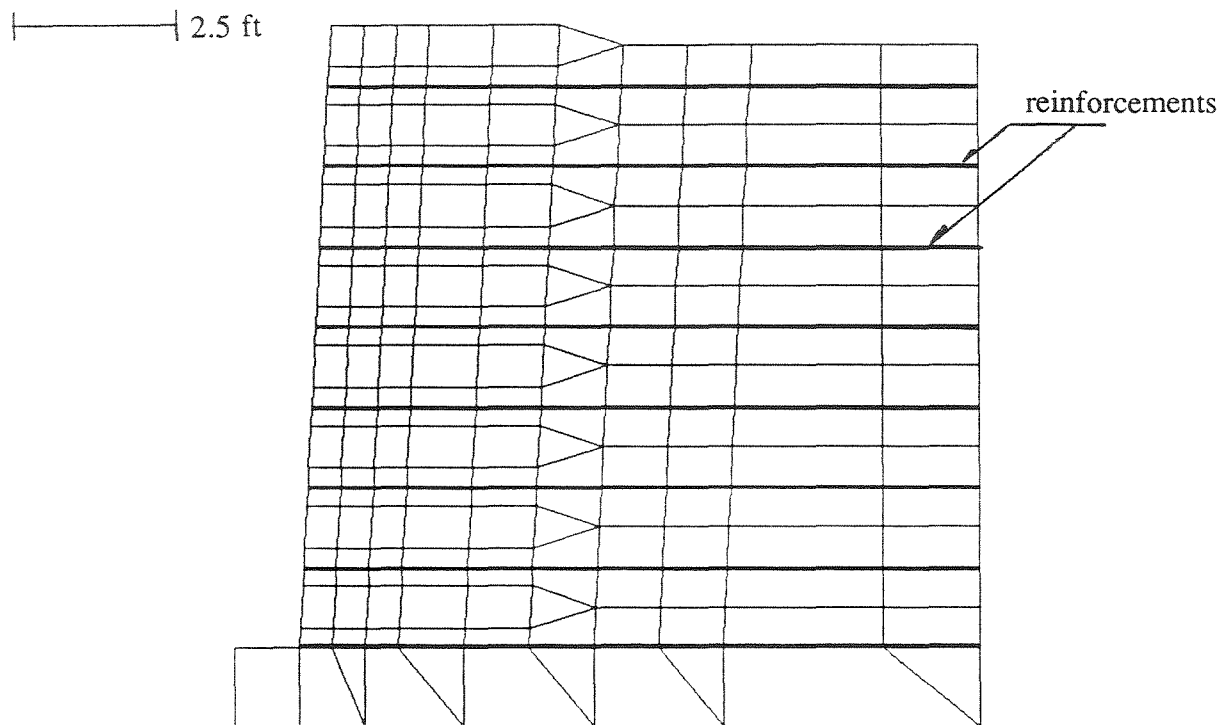
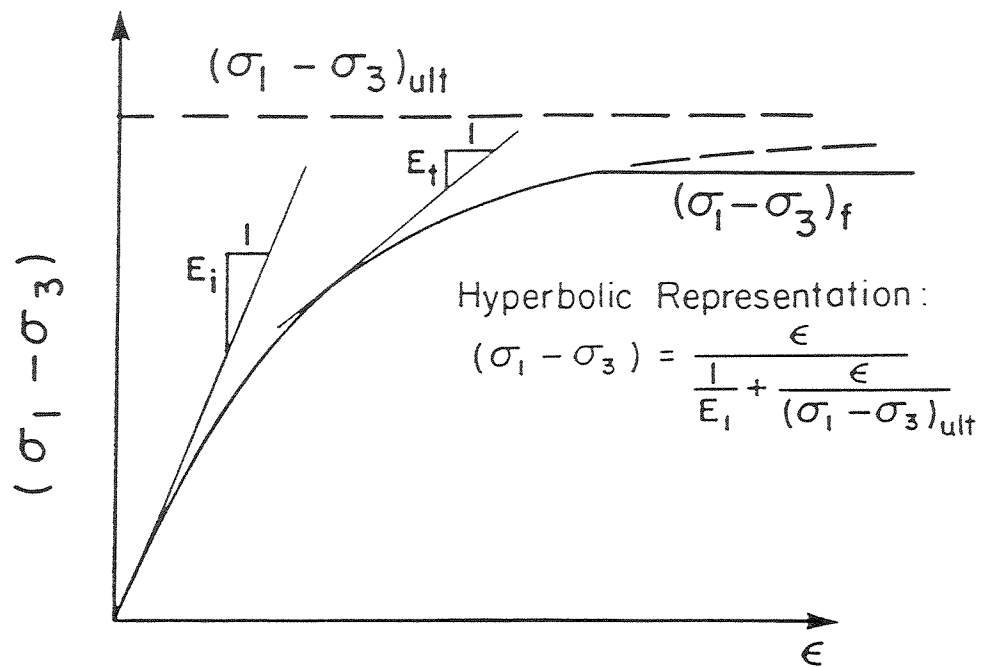
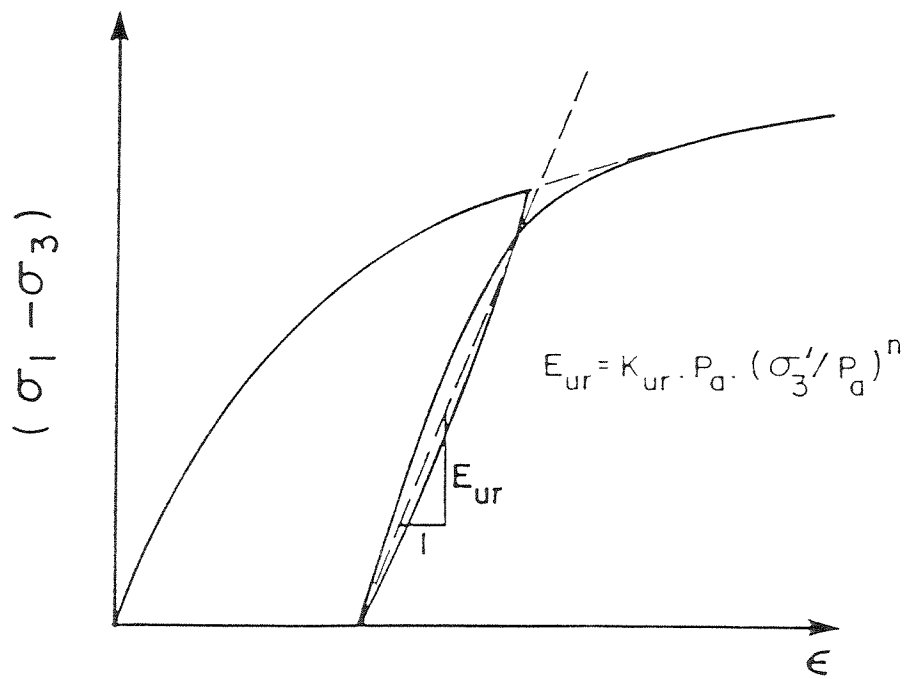


Figure 3.9 - Final mesh layout - Detail of discretization between reinforcement layers.

the tangent modulus, E_t , which is a function of confining stress, σ'_3 , and stress level, SL . The Mohr-Coulomb criterion is used to define failure conditions. The soil stiffness modeled in this manner increases with increasing confining stress and decreases with increasing stress level. A very small stiffness is assigned to elements with stress conditions at failure. Under unload-reload conditions, the soil modulus used in the model is only a function of confining stress (Figure 3.10b). The volumetric strain behavior of the soil is controlled by the soil bulk modulus, which is assumed to be a function of confining stress but independent of stress level. Details on the characteristics of the model, the calibration process, and typical parameter values can be found in Duncan et al. (1980).



(a) Hyperbolic Representation of Stress-Strain Curve for Primary Loading.



(b) Linear Unloading-Reloading Stress-Strain Relationship.

Figure 3.10 - Hyperbolic model for stress-strain behavior.

A relatively clean subrounded to subangular gravelly sand was selected for the backfill and preload fill by the contractor of the Rainier Ave. wall. The soil had an average moist unit weight of 134 pcf, which corresponds to 97% relative compaction with respect to standard Proctor. Two consolidated drained triaxial test series were performed on backfill obtained from the wall. The triaxial samples (4.0 in diameter) were compacted as closely as practical to field density and moisture content. Samples were tested at four confining pressures for each test series, simulating pressures anticipated in the wall. A friction angle of 36° had been assumed for design, but triaxial testing indicated that the actual soil friction angle in the wall backfill varied from 43° to 47° .

Calibration of the backfill soil to obtain the hyperbolic parameters was performed using data from the two triaxial test series, following the procedures suggested by Duncan et al. (1980). The parameters obtained from each of the two triaxial test series are presented in Table 3.3. Similar values were obtained from the two test series, indicating good representativeness of the samples. Model predictions of the actual experimental data showed very good results. Figure 3.11 shows the model prediction of the triaxial test series#1, using parameters obtained from the calibration. The model is able to capture the pre-failure stress strain behavior, as well as the stress level that corresponds to the failure condition in each test. Figure 3.12 shows the prediction of the second triaxial test series. The good representation of the soil behavior by the hyperbolic model is evident. Although a good hyperbolic representation of soil stress-strain relationship under axial compression stress paths does not guarantee good characterization under different stress paths, axial compression is a dominant stress path in embankments and retaining wall

constructions. Consequently, a good representation of the soil stress-strain is expected in the finite element modeling.

Table 3.3 - Hyperbolic parameters for the backfill material

Parameter	Parameter definition	Triaxial series#1	Triaxial series#2	SW 95%RC (Boscardin, 1990)	Selected Values
K	Young's modulus number	832	913	950	913
n	Young's modulus exponent	0.7	0.6	0.60	0.6
R_f	Failure ratio	0.62	0.64	0.70	0.64
c (ksf)	Cohesion	0.0	0.0	0.0	0.0
φ₀ (°)	Friction angle at 1 atm conf. press.	45.4	46.1	48	46.1
Δφ (°)	Reduction in friction angle for 10x increase in conf. press.	4.6	5.3	8	5.3
K_B	Bulk modulus number	-	-	250	250
m	Bulk modulus exponent	-	-	0.8	0.8
K_{ur}	Unload-reload modulus number	-	-	-	1485
γ	Unit weight (kef)	-	-	-	0.134
K₀	At rest lateral Earth pressure coefficient	-	-	-	0.35

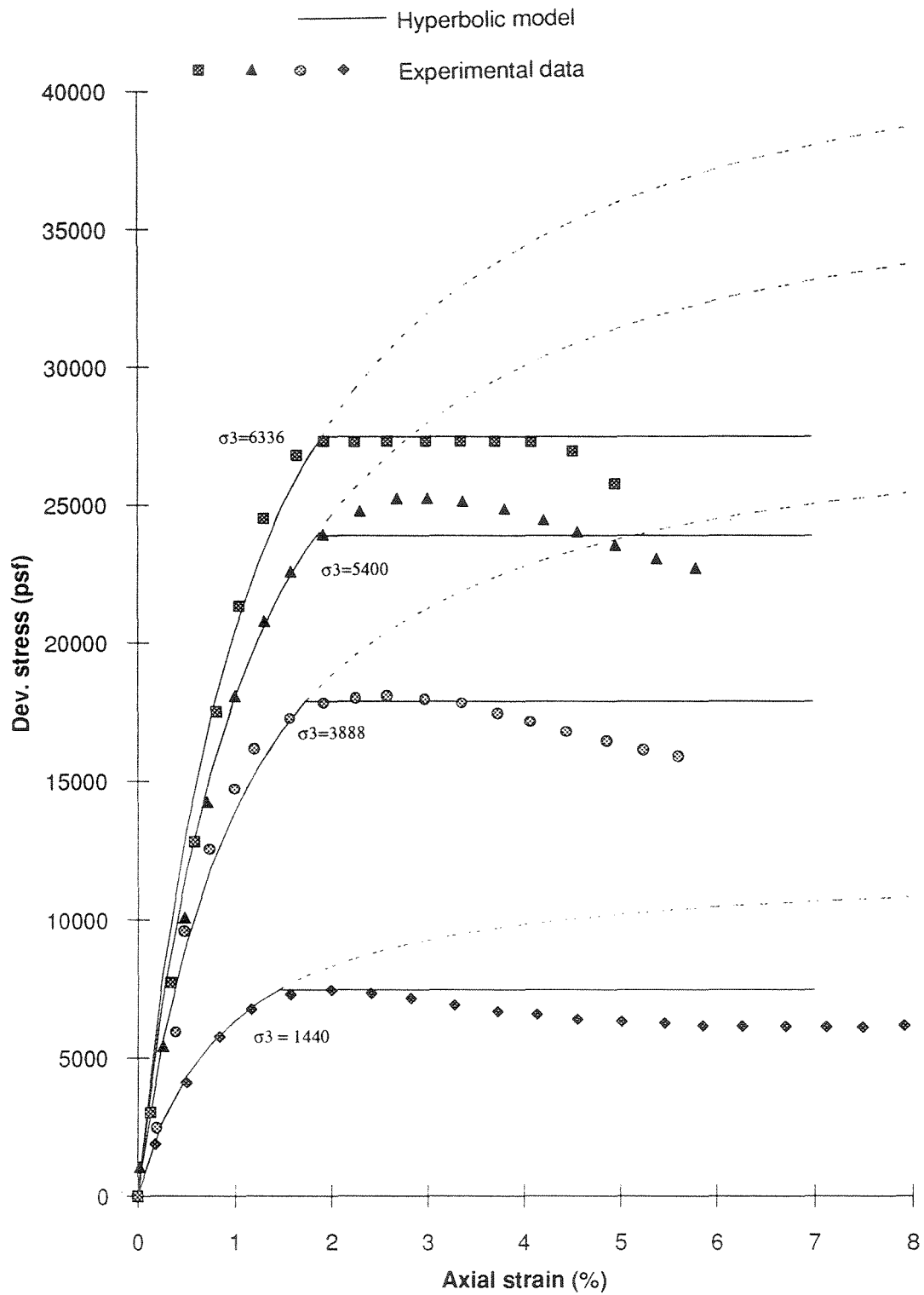


Figure 3.11 - Reconstitution of triaxial test series#1 using hyperbolic parameters

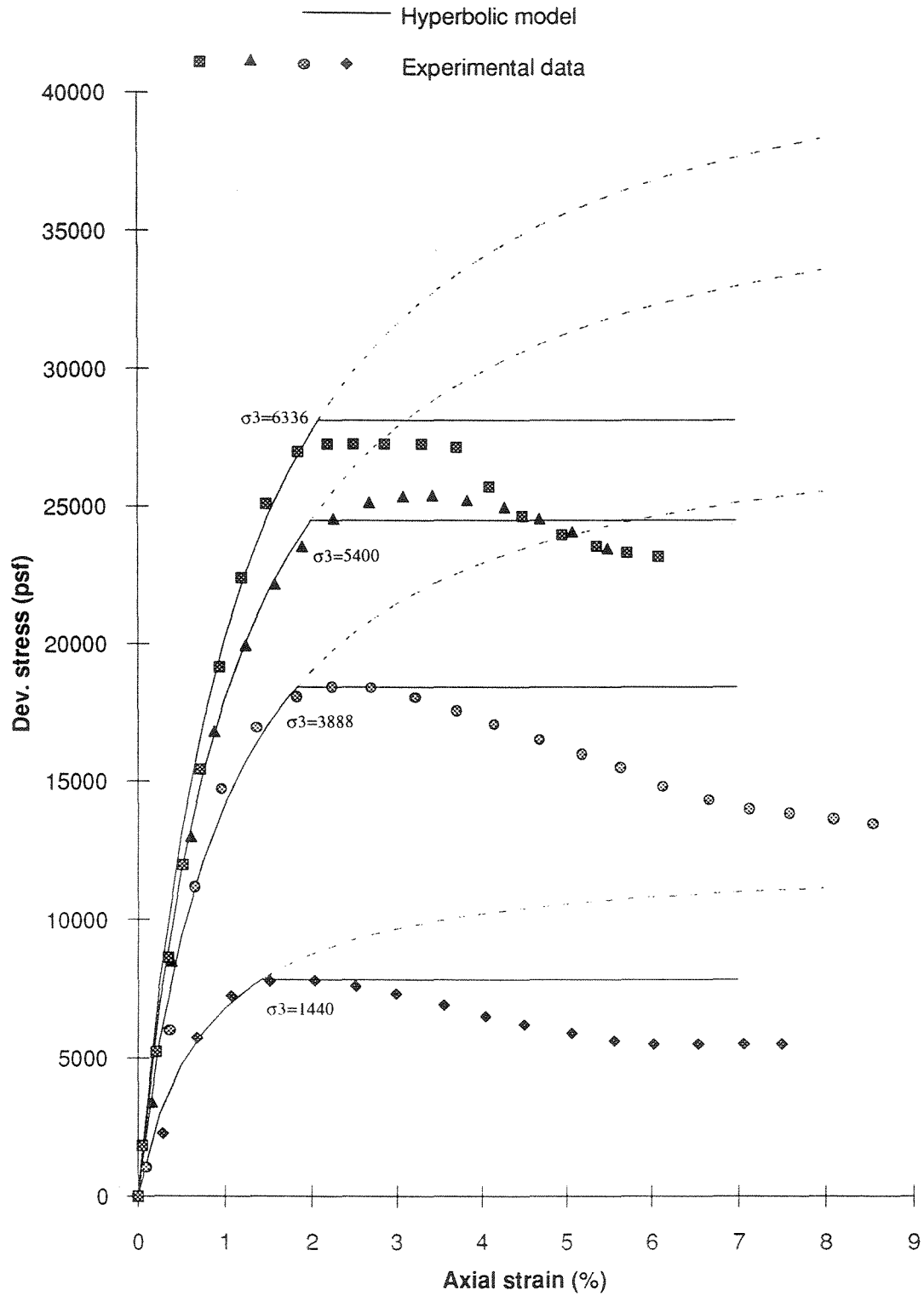


Figure 3.12 - Reconstitution of triaxial test series#2 using hyperbolic parameters

Volume change data are required for determination of bulk modulus. However, since the compacted soils were tested in unsaturated conditions, volume change data was not available. Thus, bulk modulus parameters for the analyses performed in this study were selected based on results reported by Boscardin et al. (1990) for a similar compacted granular material. The hyperbolic soil parameters determined by Boscardin for a SW soil compacted to 95% relative compaction, based on experimental tests on unsaturated specimens, are indicated in Table 3.3. The values obtained for the backfill material of the Rainier Ave. wall are similar to those obtained by Boscardin, especially those obtained for the second triaxial test series.

As shown in the last column of Table 3.3, the hyperbolic stress-strain parameters finally selected for this study were those obtained from the triaxial test series#2. The adopted bulk modulus parameters were those determined by Boscardin for a similar compacted granular material.

Hyperbolic parameters for the foundation soil were estimated from a review prepared by Duncan et al. (1980), which lists hyperbolic parameters for 80 different soils. The selected values are listed in Table 3.4. Only the fairly dense granular deltaic deposits were modeled. The sensitivity of the finite element results to the selected foundation soil properties was studied. The parametric investigation essentially showed no influence of the selected foundation parameters on the reinforcement tension distribution. The selected foundation parameters was observed to cause lateral displacements on the foundation soil that affected the lateral displacement at the base of the structure. However, besides a constant shift displacement at the base of the wall, the effect of foundation parameters on the lateral wall face displacements was negligible, and essentially did not affect the

deflection pattern. Similar effects were observed by Schmertmann et al. (1989) in a parametric study on bar mat reinforced walls.

Table 3.4 - Hyperbolic parameters for the foundation soil

Parameter	Parameter definition	Selected Values
K	Young's modulus number	1900
n	Young's modulus exponent	0.25
R_f	Failure ratio	0.7
c (ksf)	Cohesion	1.022
φ₀ (°)	Friction angle at 1 atm conf. press.	40.0
Δφ (°)	Reduction in friction angle for 10x increase in conf. press.	0.0
K_B	Bulk modulus number	450
m	Bulk modulus exponent	0.0
K_{ur}	Unload-reload modulus number	2850
γ	Unit weight (kcf)	0.13
K₀	At rest lateral Earth pressure coefficient	0.41

3.3.2.3 Reinforcement material parameters

One of the most important parameters to be selected in a finite element analysis of a reinforced soil wall is the in-situ tensile stiffness of the geotextiles. However, methods commonly used for determination of deformation and strength properties of geosynthetics, do not replicate the operational condition of the geotextile in the field. Researchers have suggested that the tensile characteristics of geotextiles should be

measured under the soil-confinement condition. Results from unconfined wide width strength tests, available for the geotextiles used in the structure under study, may grossly underestimate the in-situ tensile stiffness. Consequently, among the input parameters to be adopted for the finite element analysis, there is a major uncertainty in the in-situ geotextile stiffness to be selected.

Laboratory determination of deformation and strength properties of geotextiles under confinement has been attempted using specially devised tests. McGown et al. (1982) found that highly structured non-woven and composite geotextiles significantly change the shape of their load-strain curves when tested in soil. Christopher et al. (1986) developed a "zero span" test which models the mechanical confinement provided by granular soil. Reported results indicated that this test, while quick and simple to perform, yielded stress-strain information which compared favorably with McGown's results. Fabian and Fourie (1988) reported modulus increases of up to ten times in non-woven geotextiles and of up to three times in woven materials. Ling et al. (1992) developed a test apparatus for measuring the load-deformation properties of geotextiles under in-air, in-membrane, and in-soil conditions. Figure 3.13 shows typical load-deformation relationships obtained for different effective normal stresses applied on a geotextile during in-membrane testing. Gomes (1992) reported substantial stiffness increases, mainly in nonwoven geotextiles, in tensile tests performed under soil confinement. Chang et al. (1993) also studied the confined behavior of four types of woven geotextiles and reported that soil confinement increases significantly the geotextile stiffness, but only at low elongation strains. Increase in geotextile modulus due to confinement was also reported

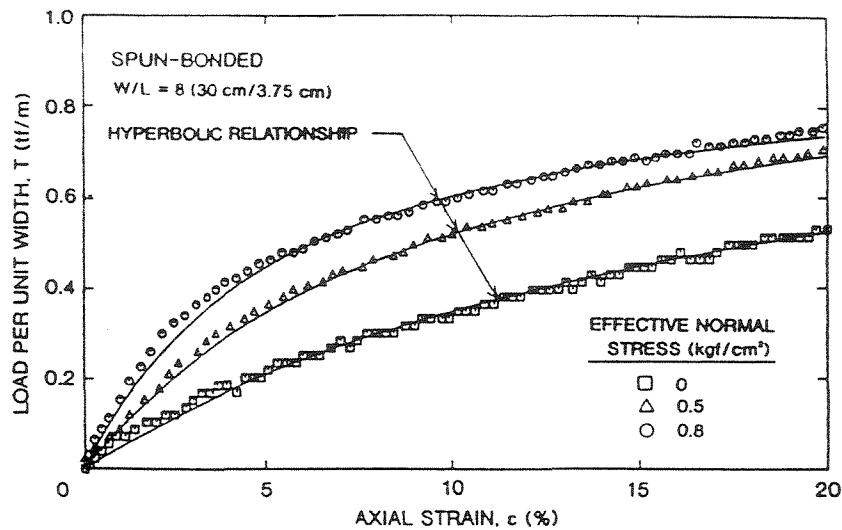


Figure 3.13 - Load-deformation relationship for a spun-bonded geotextile at different effective normal stresses (after Ling et al, 1992)

by El-Fermaoui and Nowatzki (1982), Tatsuoka et al. (1986), Leshchinsky and Field (1987), and Kokkalis and Papacharisis (1989).

Although differing in testing methodology, all previous laboratory studies concluded that there is a significant increase in stiffness and strength of geotextiles confined in soil, in comparison to values obtained under unconfined conditions. There is also clear field evidence of the improvement of geotextile mechanical properties under confinement. The performance of structures such as the FHWA geotextile walls in Glenwood Canyon, Colorado (Bell et al., 1983), showed that current design procedures are conservative. Unfortunately, it is essentially impossible to determine in-situ geotextile stiffness directly from the instrumentation data. However, numerical backcalculation offers an alternative for this determination, and the in-situ geotextile stiffness was estimated in this way for this study.

The unconfined modulus values at 5% strain obtained from wide width strength tests for the four geotextile reinforcements used in the Rainier Ave. wall are summarized

in Table 3.5. These moduli are the lower bound for the in-situ stiffness values of the geotextiles used in the wall under study. Additionally, confined geotextile stiffness values were estimated based on the results of pullout tests (Zornberg and Mitchell, 1993). Stiffness values from pullout testing provided upper bound reference values for geotextile moduli under working stress conditions.

Table 3.5 - Unconfined parameters from wide width strength data (after Allen et al., 1991)

Distance from top of the wall (ft)	Geotextile type	Wide width tensile strength (kips/ft)	Elongation at Peak Tension (%)	Modulus at 5% strain (kips/ft)
0 -10	Polypropylene slit film woven (GTF200)	2.12	21	13.57
10 -20	Polypropylene stitch-bonded (2 layers) slit film woven (GTF375)	4.25	16	31.04
20 -30	Polypropylene stitch-bonded (3 layers) slit film woven (GTF500)	6.30	17	45.36
30 - 40	Polyester multifilament woven (GTF1225T)	12.74	18	73.18

3.3.2.4 Parameters for interface and structural facing elements

SSCOMP incorporates zero thickness interface elements capable of representing soil/structure interface conditions by modeling the relative movement between the soil and the structure. This element is made up of a normal spring and a non-linear stress

dependent shear spring. The use of interface elements incorporates additional degrees of freedom in the finite element analysis. For the finally adopted mesh, 1188 additional nodes would have been required if interface elements were used, representing a 70% increase on the number of degrees of freedom. Since a parametric study showed that the use of interface elements had only a minor influence on the results, the final analysis was performed without interface elements. The assumption of displacement compatibility between soil and reinforcements is justified by the following considerations:

- High interface shear strength, as measured by a high interface contact efficiency has been reported for polymeric reinforcements. The assumption that interface slippage will occur only after interface failure is then appropriate. For the case under study, interfacial shear stresses developed between the soil and the planar reinforcement were found to be too small to cause interface failure.
- Extensible reinforcements like geotextiles can tolerate large strains, of the same order of magnitude or greater than the soil, without failure. Consequently, displacement compatibility between soil and reinforcement is expected.
- Previous investigations using SSCOMP have already modeled the interface behavior considering a reduction in the interface slippage. This was done by adopting actual interface properties (no-distribution approach) in structures with a three dimensional reinforcement layout (Schmertmann et al., 1989). Parametric studies performed to justify this reduction showed a better distribution in maximum reinforcement tension. Also, studies using either SSCOMP (Schmertmann, 1991) or other finite element programs (Chalaturnyk, 1990) have been successfully performed without using interface elements.

- Additional pullout test results would have been required for the correct determination of interface material properties.

Beam elements have been used previously to simulate the facing of reinforced soil structures. These elements are formulated in SSCOMP as linear elastic materials with no limiting failure stress. A parametric analysis was performed to evaluate the sensitivity of the finite element results to the use of beam elements in the face. Different boundary conditions (location of pin connections), as well as different moments of inertia were considered. Only minor influence was observed in the results if beam elements are used to represent the flexible face. Based on this parametric study, beam elements were not used in the final analysis of the Rainier Ave. wall.

3.3.2.5 Incremental analysis sequence

Non-linear and stress dependent material properties are modeled in SSCOMP by using an incremental analysis procedure that follows the actual construction sequence of the earth structure. An increment of an analysis may consist of placement of a soil layer, compaction of a soil layer, or application of loads to the soil mass.

Selection of the number of analysis increments is a trade off between improved representation of the non-linear stress-dependent modulus values and increased computation time. After a study of sensitivity, the placement of soil layers 0.38 m (1.25 ft) thick was adopted. A total of 33 soil placement increments were then used in the final study.

Sloping backfill surcharge load was modeled by applying equivalent distributed loads on the top of the wall. Surcharge loads applied in each analysis increment were kept always smaller than 0.38 m of fill. Since the surcharge loading was applied in 17 increments, a total number of 50 solution increments were considered in the analysis. For the final mesh adopted in this study, the selected number of analysis steps gave typical computer run times of 6 hours per case, on a Digital Equipment Company DECstation.

3.3.3 Results from the analysis

3.3.3.1 Calibration process for selection of geotextile parameters

More than 60 finite element analyses were performed during the calibration process of the Rainier Ave. wall. Being a numerical approximation, the accuracy of finite element results depends on the selected geometry layout. Consequently, some cases consisted of studies of sensitivity of the results to mesh fineness. Since a non-linear constitutive model was used to represent the soil behavior, other analyses were made to determine the sensitivity of the results to the number of layers per construction step and number of surcharge loading steps. As previously indicated, other modeling characteristics such as the structure facing representation, the soil/reinforcement interface characteristics, and the soil foundation properties were also adopted based on results obtained from parametric studies.

The final step in the calibration process consisted on selecting appropriate values of in-situ stiffness for the different geotextiles used in the wall. The unconfined modulus obtained from wide width testing was considered to be the lower bound for the trial

values. The stiffnesses obtained from interpretation of pullout testing provided the upper bound values. The calibration process consisted basically of three stages:

- a) Selection of in-situ geotextile stiffnesses for use in a FE analysis of the wall. These confined moduli were selected so that the numerical results matched the monitored geotextile strain distribution, as recorded by strain gauges in four reinforcement layers of the Rainier Ave. wall.
- b) Evaluation of the quality of the selection made in (a) by comparing lateral displacements, obtained from the finite element solution, with records obtained from the inclinometer located within the reinforced zone. The selected in-situ geotextile stiffness values are considered to be accurate, based on the reliability of inclinometer information, and on the very good simultaneous agreement of instrumented data with numerical results.
- c) The quality of the numerical representation was further evaluated by quantitatively comparing the numerical results with additional instrumentation records (pressure cells, face displacements), and by qualitatively assessing non-instrumented responses of the wall behavior with available numerical results.

Backcalculated in-situ geotextile stiffness values obtained after the described calibration process are indicated in Table 3.6. Modulus values obtained from interpretation of laboratory testing are restated along with the ratios between the backcalculated finite element results and the laboratory estimates.

Ratios between numerically backcalculated and experimentally obtained unconfined stiffness values are also shown in Table 3.6. For the reasons noted earlier, the

backcalculated values are higher than the results obtained from unconfined wide width testing. The increase is expected to be dependent on both the material type of the woven geotextiles and the in-situ confining pressures. For polypropylene materials, a consistent increase in the ratio can be observed. Confined stiffness increases from roughly twice the unconfined value in the upper reinforced zone (0 to 3 m from top of the wall) to roughly four times the unconfined value in the third zone (6 to 9 m from top). The increase in stiffness of the only polyester material used as reinforcement (in the zone from 9 to 12 m from top of the wall) is less than four times the unconfined modulus.

The backcalculated values are lower than the stiffnesses determined using the stress-strain relationships based on pullout testing. In this case, the ratio between numerical and laboratory values is not expected to be a function of in-situ confining pressures, since pullout tests were performed under representative confinement. The most reliable pullout test was performed on the GTF375 material (instrumented both with strain gauges and mechanical extensometers). For this test, the backcalculated in-situ stiffness is 65% of the value interpreted from the laboratory pullout test. Differences between field and laboratory conditions (e.g., field construction damage, geotextile degradation) may be pointed out as possible causes of the discrepancy. The comparison, however, is encouraging considering the difficulties involved in the confined stress-strain determination and the preliminary character of the laboratory results. The in-soil stress-strain behavior of geosynthetics is currently being investigated at the University of Washington (Allen, 1993). The geotextiles used at the Rainier Ave. wall are under study as a part of this research.

Table 3.6 - In-situ geotextile stiffnesses back calculated from finite element analysis

Distance from top of the wall (ft)	Geotextile type	Stiffness back calculated from FEM (kips/ft)	Stiffness from wide width testing (kips/ft)	Stiffness from pullout testing (kips/ft)	Back calculated / wide width testing	Back calculated / pullout testing
0 -10	Polypropylene slit film woven (GTF200)	30	13.57	79	2.21	0.38
10 -20	Polypropylene stitch-bonded (2 layers) slit film woven (GTF375)	85	31.04	130	2.73	0.65
20 -30	Polypropylene stitch-bonded (3 layers) slit film woven (GTF500)	190	45.36	(*)	4.18	(*)
30 - 40	Polyester multifilament woven (GTF1225T)	260	73.18	417	3.55	0.62

(*) Not available

Backcalculated values of in-situ geotextile moduli obtained in this study are consistent with results published in the literature (Section 3.3.2.3). In the case of nonwoven geotextiles, stiffness increase has been reported to occur even at high geotextile elongations. For the case of woven materials, however, reported results suggest that the increase in confined stiffness occurs only at low geotextile strains (Chang et al, 1993). The finite element results of the analyses performed using the in-situ geotextile stiffnesses

indicated in Table 3.6, are presented in sections 3.3.3.2 to 3.3.3.5. Zornberg and Mitchell (1993) show additional results, obtained from analyses performed using geotextile moduli defined from wide width unconfined tensile tests and from confined pullout testing.

3.3.3.2 Tension distribution along the reinforcements

As indicated in Section 3.3.1, bonded resistance strain gauges and mechanical extensometers were installed on four geotextile layers to evaluate the strain distribution as well as the location and magnitude of maximum tensile stress. Differences were observed between the strain gauge and the extensometer records. Maximum geotextile strains obtained from strain gauge measurements were approximately 0.5%, while maximum strains measured by the extensometers were on the order of 0.7 to 1.0%. The extensometers incorporate strain occurring in the geotextile macrostructure, including local effects such as creases and folds. Additionally, since the extensometers were not rigidly fixed to the fabric, but were only wired to the geotextile, it was possible for the extensometer to move relative to the geotextile (Christopher et al., 1990; Allen et al., 1991). Based on these considerations, only strain gauge records were considered in this study. Nevertheless, since the glue used to fix the gauges is often stiff relative to the geotextile, measured strains are expected to be lower than the actual field strains.

The finite element analysis provided reinforcement tension values at several points along the reinforcement length. Reinforcement tensions predicted from the finite element analysis are shown in Figure 3.14, where they are compared with tension distributions obtained from the strain gauge measurements. Since these field measurements represent a lower bound of the actual strains, in-situ reinforcement stiffness was selected so that

predicted values represent an upper envelope (and not an average) of field strain records. Geotextile strains from instrumentation records were transformed into tensile stress by multiplying the measured strain value by the same confined stiffness used in the finite element analysis. The matching is good, and both numerical and field results reflect a similar tension increase after surcharge placement. Figure 3.15 shows the load distribution predicted in one of the layers (layer 9, the second instrumented layer from the bottom) at different stages during the construction of the wall. It may be observed that at early stages after placement of the reinforcements the load distribution does not show the pattern observed at later stages.

3.3.3.3 Lateral wall displacements

An inclinometer tube was installed within the reinforced section 2.7 m behind the wall face as measured from the toe (Figure 3.2). Measurements from this inclinometer are considered the most reliable record available for lateral displacements. Lateral displacement measurements from this inclinometer were not subject to the measurement difficulties reported for the displacements monitored at the wall facing (Holtz et al., 1991; Allen et al., 1991).

The lateral displacements computed using SSCOMP were corrected to account for the fact that the incremental sequence of reinforced wall construction causes each new soil layer to be placed on material that has already undergone some displacement. The SSCOMP code does not recognize this situation and sets all element displacements to zero at the time of their initial placement. Thus, the corrected displacements at each nodal point represent total displacements relative to the initial position of the node.

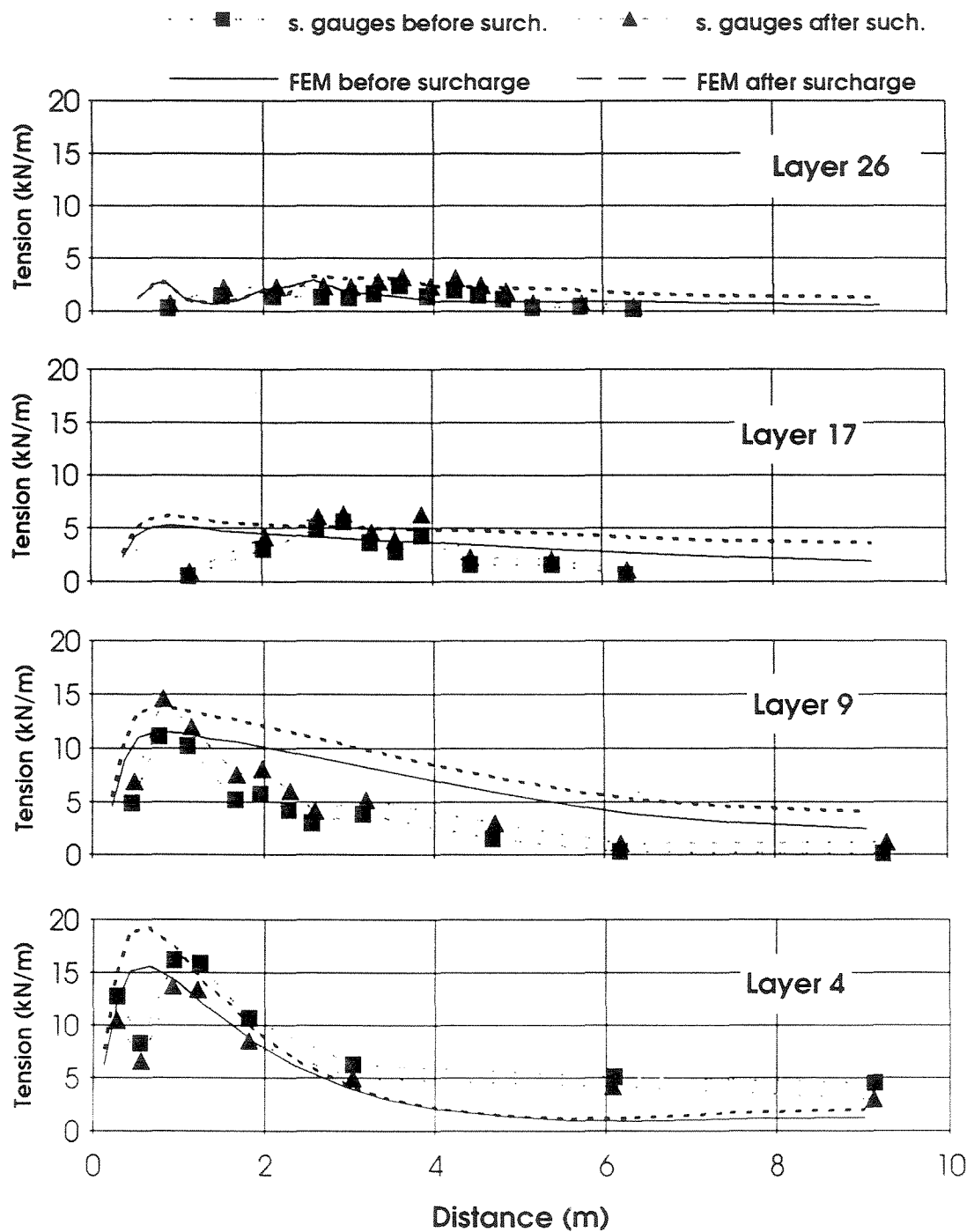


Figure 3.14 - Tension distribution along geotextile reinforcements

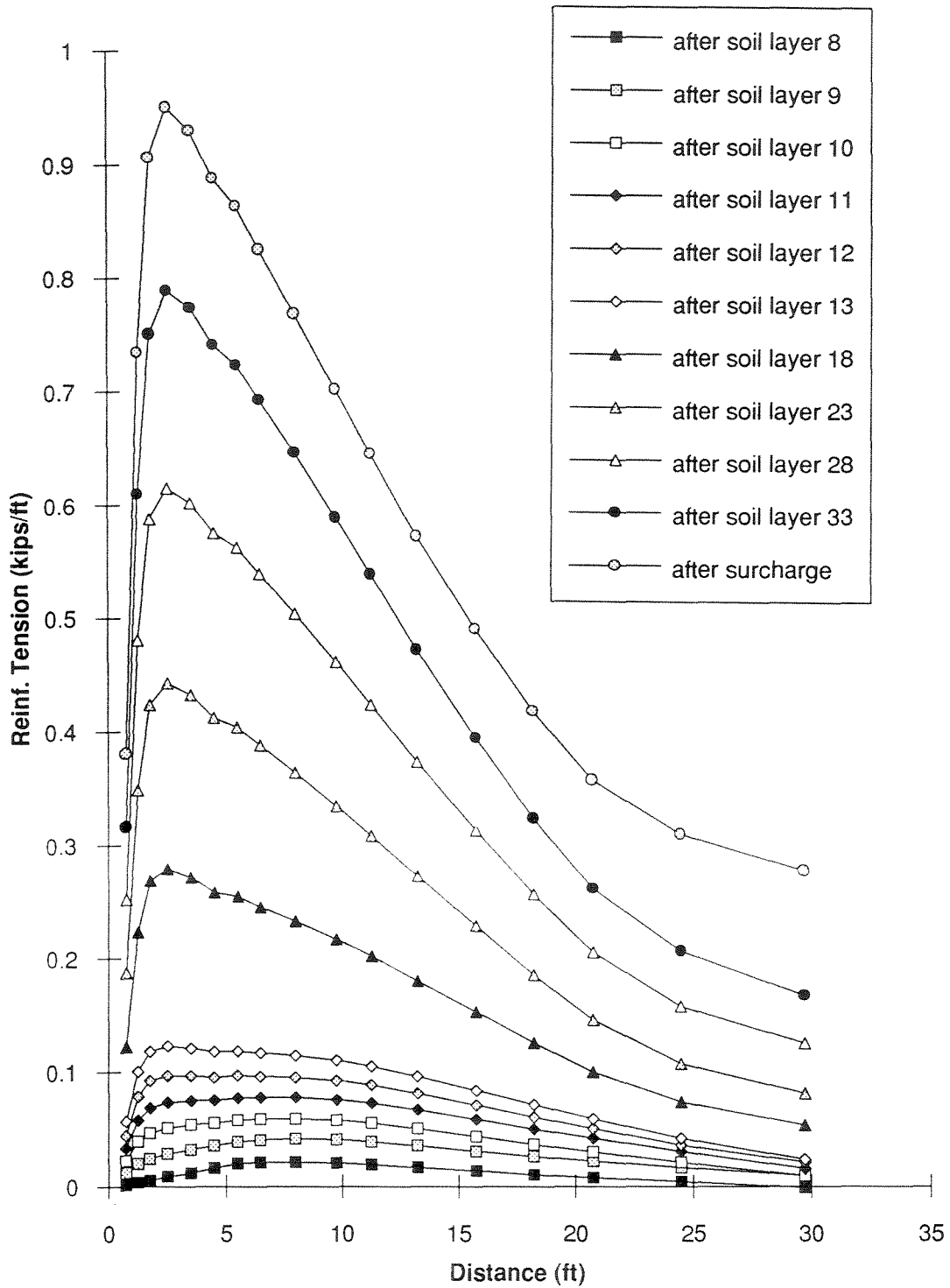


Figure 3.15 - Computed reinforcement tension distribution during different construction stages (layer#9)

Lateral deformations at the location of the inclinometer within the reinforced section are presented in Figure 3.16. The agreement between the numerically obtained displacements and inclinometer measurements is very good. Both numerical results and measured field values show a lateral displacement increase of roughly 25 mm (one inch) caused by the surcharge. The good agreement between the numerical results and the different instrumented responses of the wall supports the selection of parameters and procedures made for the analysis.

Face movements were monitored by means of photogrammetric evaluation, optical surveys and an inclinometer tube placed at the face of the wall. The optical survey readings as well as the photogrammetric measurements are relative to the initial readings taken for each specific optical or photogrammetric target (Figure 3.5). This is the basic reason for the different shapes of the curves observed for the lateral displacements at the face and at the inclinometer within the reinforced zone (Figure 3.4). A complicating factor for the photogrammetric measurements was reported to be the lack of a suitable fixed reference target for the top of the wall (Christopher et al., 1990). Figure 3.17 shows the comparison between optical survey readings, photogrammetric measurements and finite element results obtained for the stage of construction immediately after placement of the surcharge. Numerically predicted lateral displacements are relative to the face location at the moment of layer placement (uncorrected displacements). Although lateral displacement show a similar pattern, the numerical prediction underestimates instrumentation results. There is, however, controversy on the instrumentation results obtained to monitor lateral displacements at the wall face (Allen, 1991).

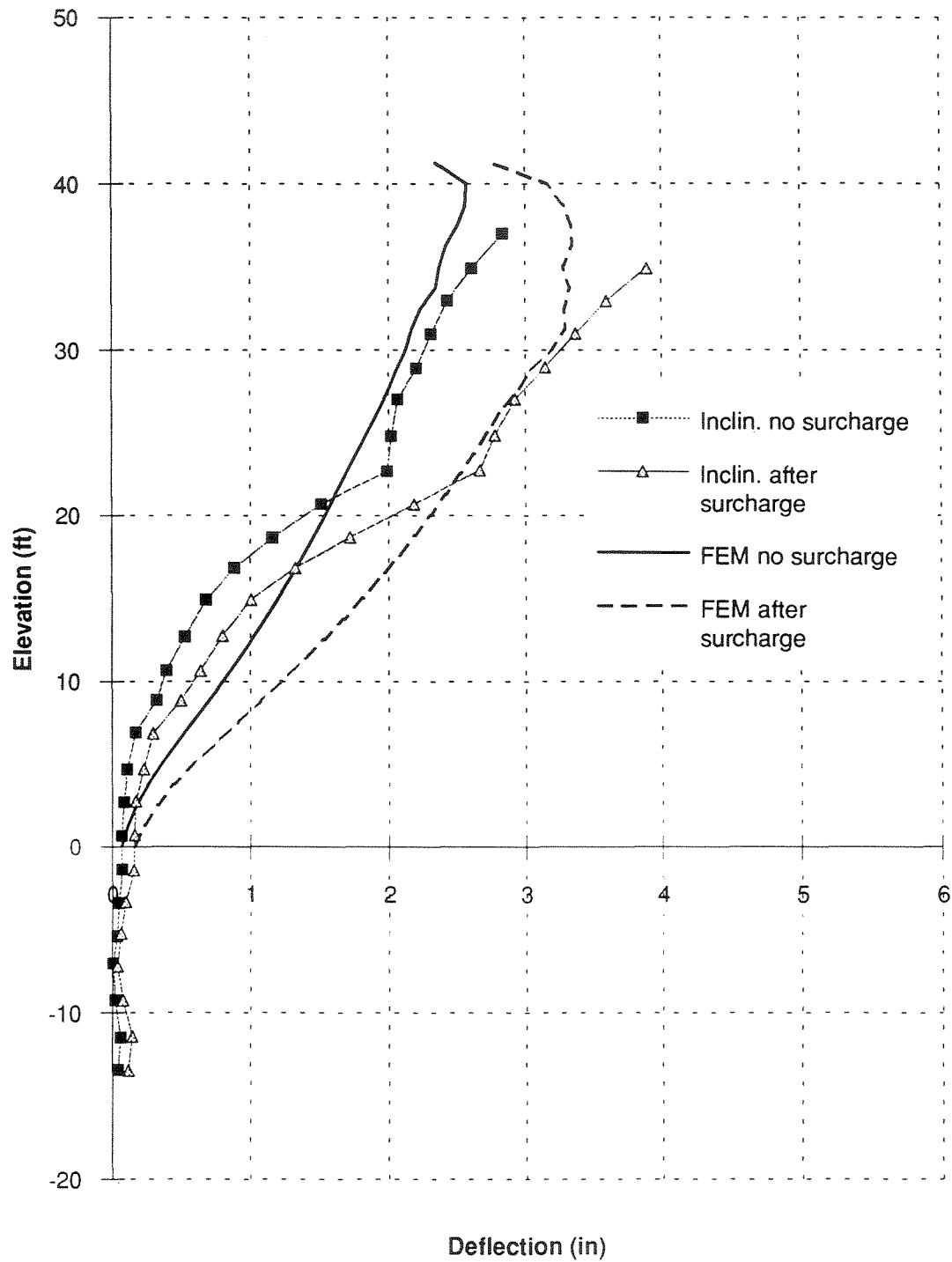


Figure 3.16 - Lateral displacements at the location of the inclinometer within the reinforced zone

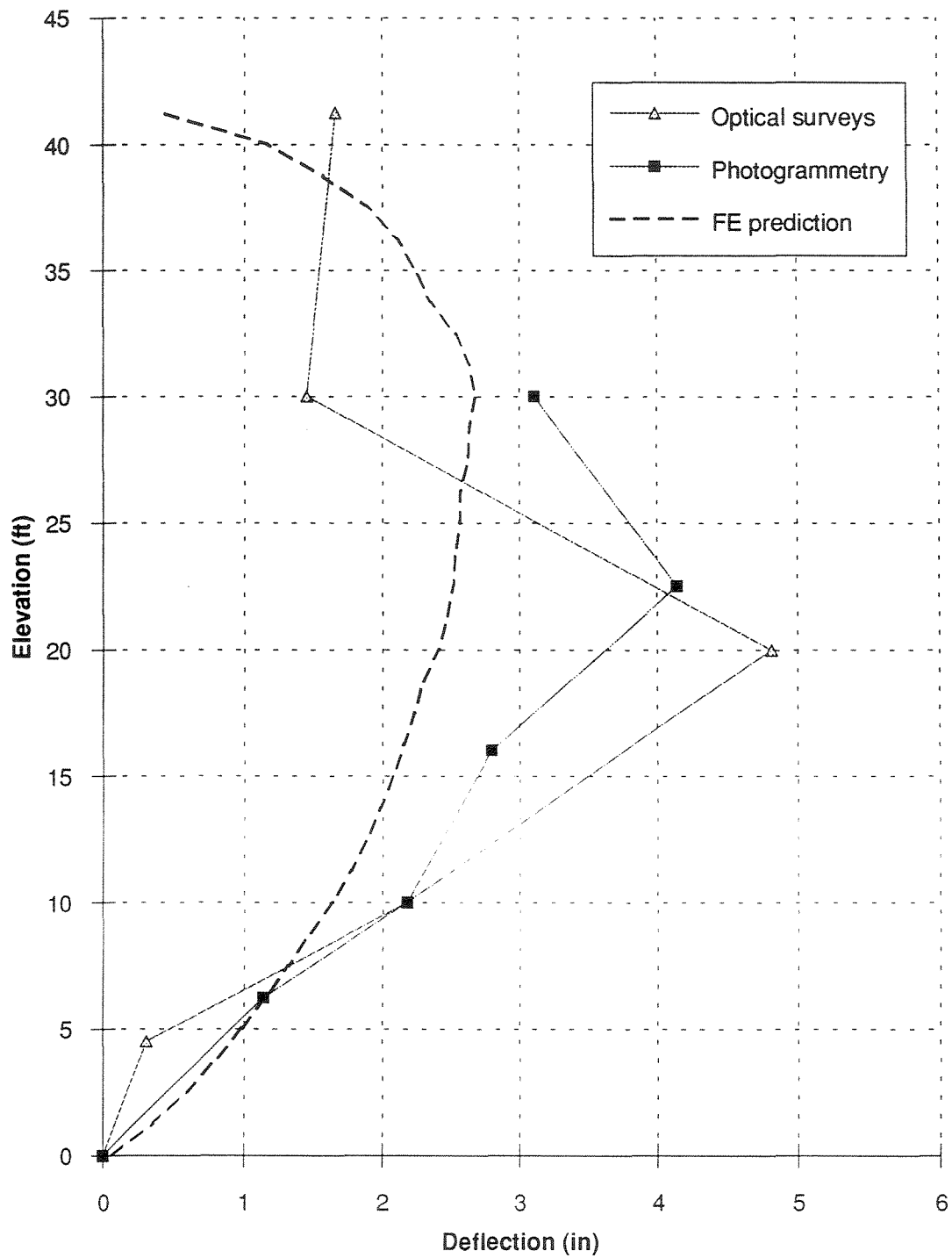


Figure 3.17 - Lateral displacements at the wall face after surcharge placement

3.3.3.4 Stress distribution in the soil mass

Vertical stresses beneath the wall, measured using Glötzl stress cells, showed that the stresses at the toe were approximately 20% higher than in the middle and the back of the wall. However, the measured vertical stresses were inconsistently lower than the average overburden pressure, both before and after placement of the sloping backfill surcharge (Allen, 1991).

Measured vertical stresses are shown in Figure 3.18. Vertical stresses predicted by the finite element analysis and, as a reference, theoretical average overburden pressures before and after the surcharge are also indicated. The numerical results show a pattern very similar to the distribution obtained from cell pressures. Moreover, predicted values are consistent with the average overburden pressure at both construction stages. The vertical pressures measured by the stress cells was shifted until the average measured vertical stress matched the average overburden pressure. The corrected vertical stress values are shown in Figure 3.19. The agreement between the corrected field measurements and the numerical prediction is very good. This suggests that the finite element solution correctly represents vertical soil stress distributions, even for walls higher than conventional.

Numerical prediction of the vertical stress distribution on the Rainier Ave. wall is shown in Figures 3.20a and 3.20b for the construction stages before and after placement of the sloping backfill surcharge. Vertical stress information at each reinforcement layer is required in conventional wall design both for estimating the maximum reinforcement tension and for verification of pullout safety requirements. Figures 3.21a and 3.21b show vertical stress contours. Contour values were selected so

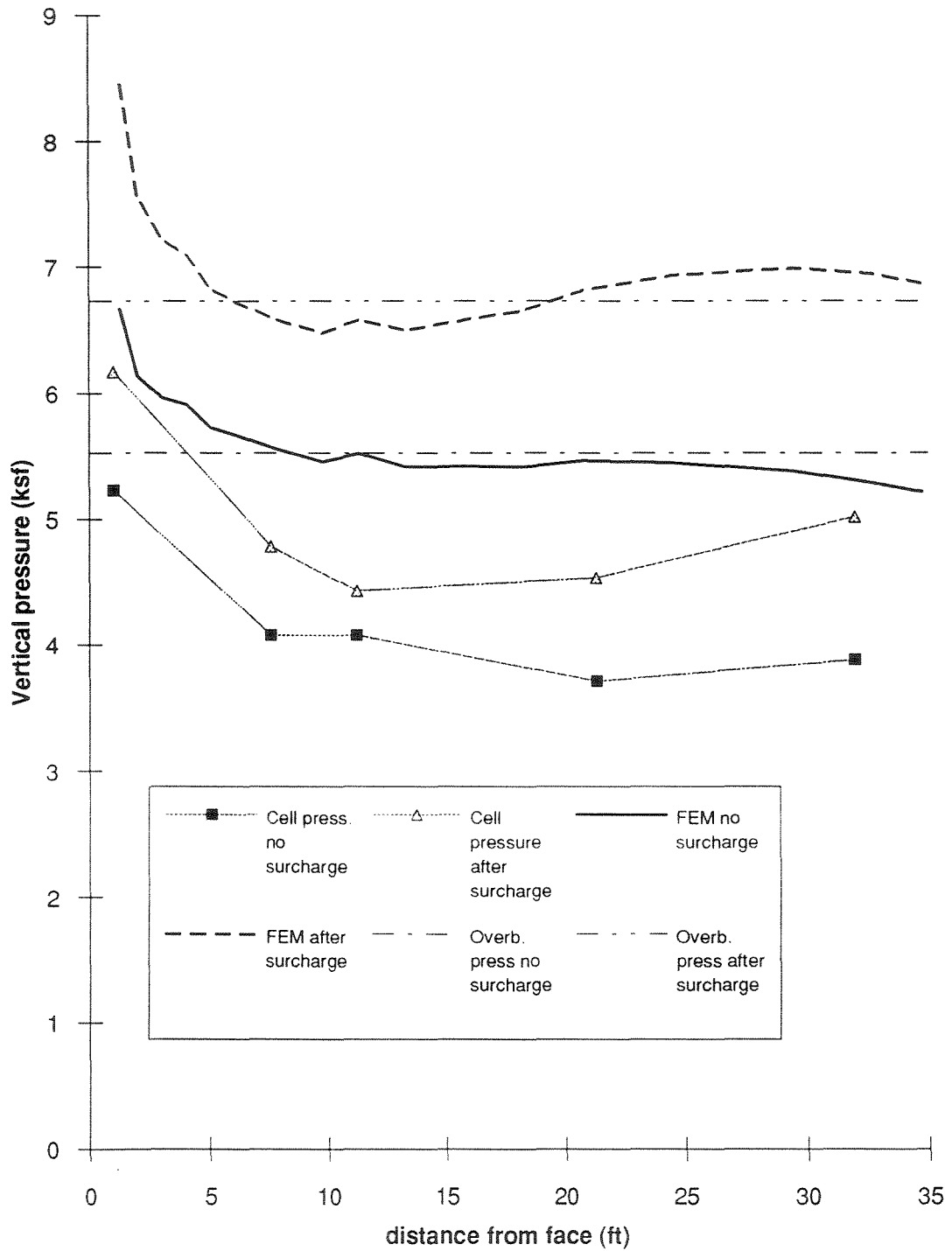


Figure 3.18 - Comparison of predicted and measured vertical stresses at the wall base

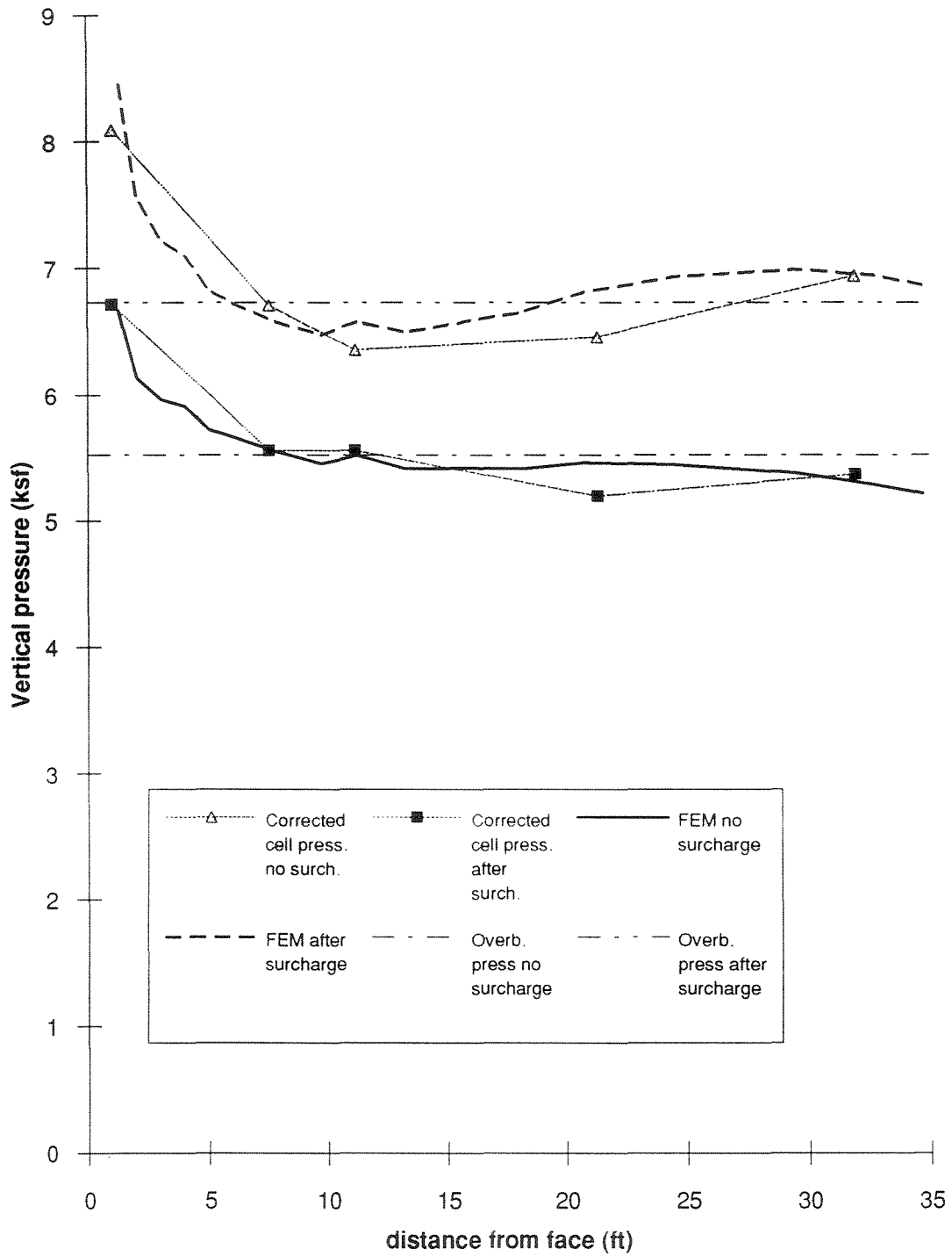


Figure 3.19 - Predicted and corrected measured vertical stresses

that they correspond to the theoretical overburden pressure at each of the reinforcement layers indicated in the figure. Contour values in Figure 3.21b (sloping backfill case) correspond to the overburden pressure at the back of the reinforced zone. The pattern shows that predicted vertical stresses in the reinforced soil mass are lower than average overburden stresses both near the structure facing and at the beginning of the retained soil. On the other hand, predicted vertical stresses in the reinforced zone away from the facing were higher than overburden pressures, suggesting that frictional resistance along reinforcement anchorage length is higher than that calculated assuming overburden pressures. The numerical results also showed that just behind the reinforced zone predicted horizontal stresses were in agreement with pressures estimated by the active Rankine coefficient. Figure 3.22 shows a detail of the computed distribution of lateral stresses near the face of the structure. The distribution is presented in terms of the lateral earth pressure coefficient, $K = \sigma_h / \sigma_v$. There is a clear increase in horizontal stresses in the soil elements located around a geotextile layer, with a lateral distress in soil elements between two reinforcements. Mobilized shear stresses near the facing were high due to the large lateral displacements undergone by the reinforced soil mass. However, the presence of zones with highly mobilized shear stresses did not cause an imminent state of failure. The complete distribution of vertical stresses, lateral earth pressure coefficients, and mobilized shear stresses is presented by Zornberg and Mitchell (1993).

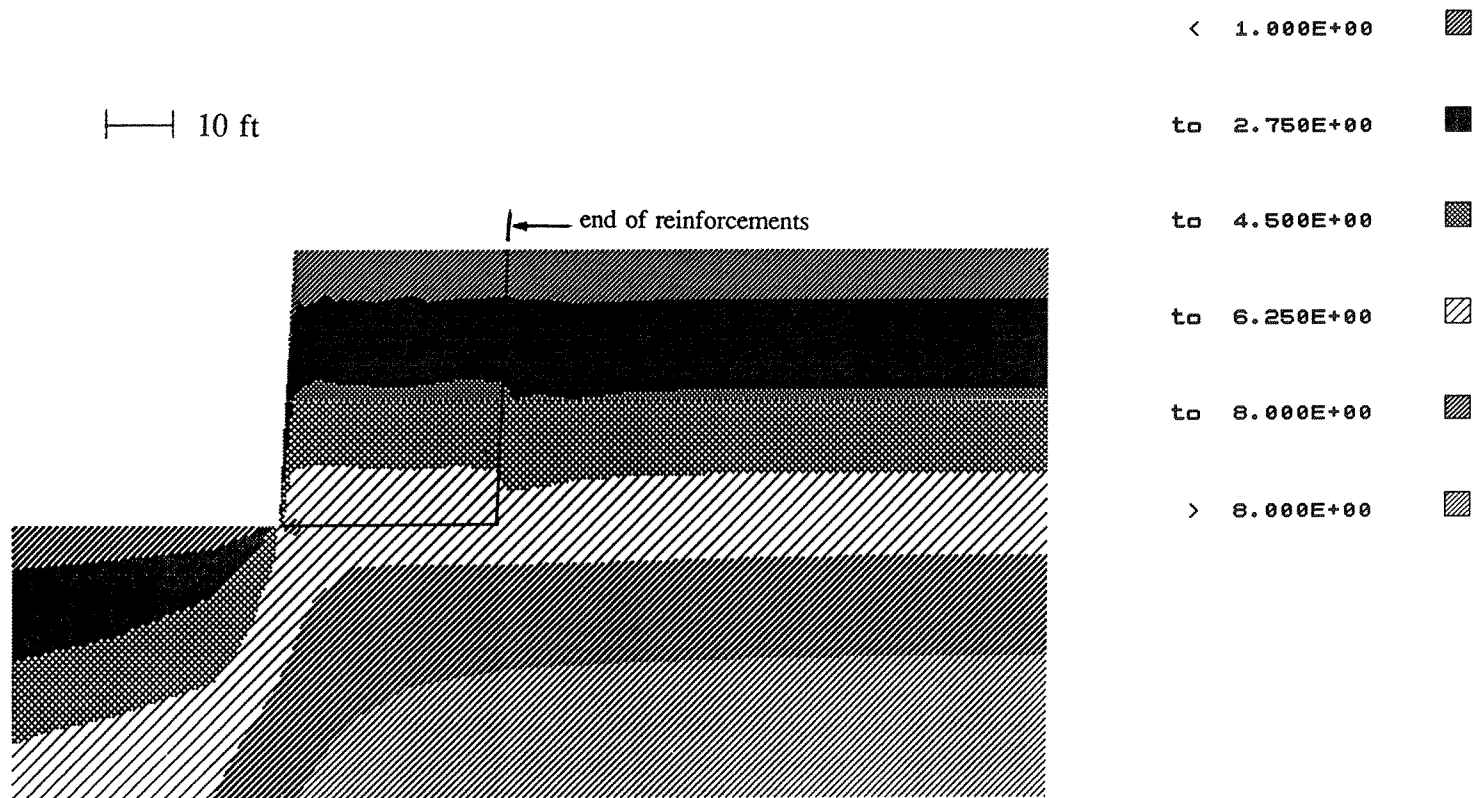


Figure 3.20a - Predicted vertical stress distribution (before surcharge). Stress units are in ksf

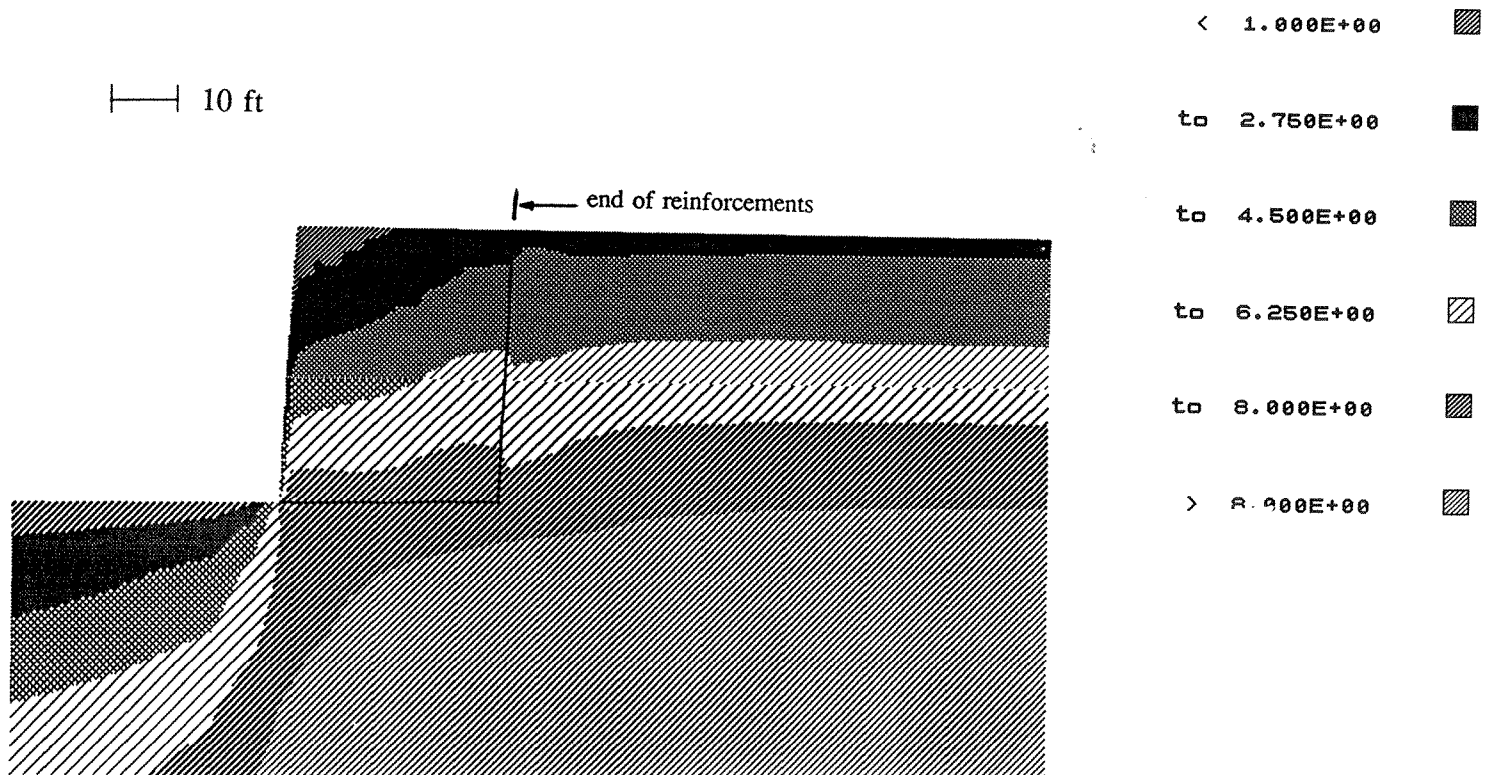


Figure 3.20b - Predicted vertical stress distribution (after surcharge). Stress units are in ksf

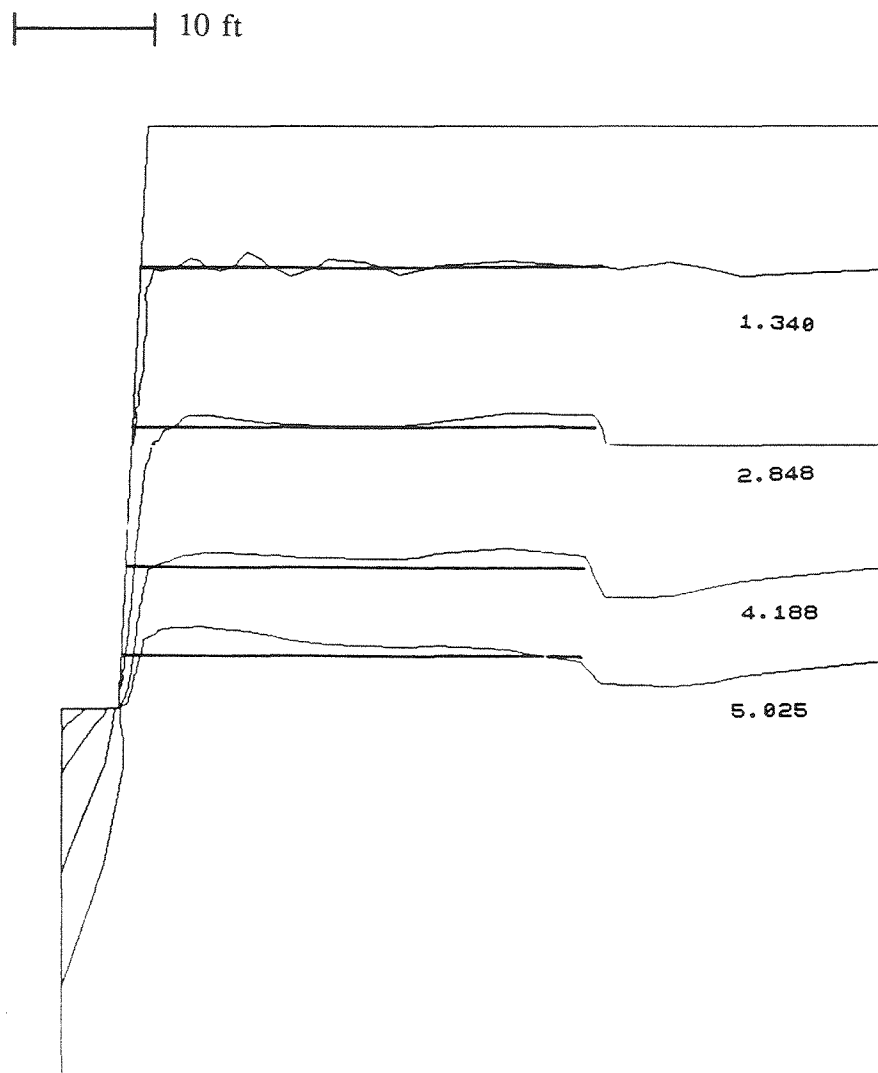


Figure 3.21a - Predicted vertical stress contours (before surcharge). Stress units are in ksf

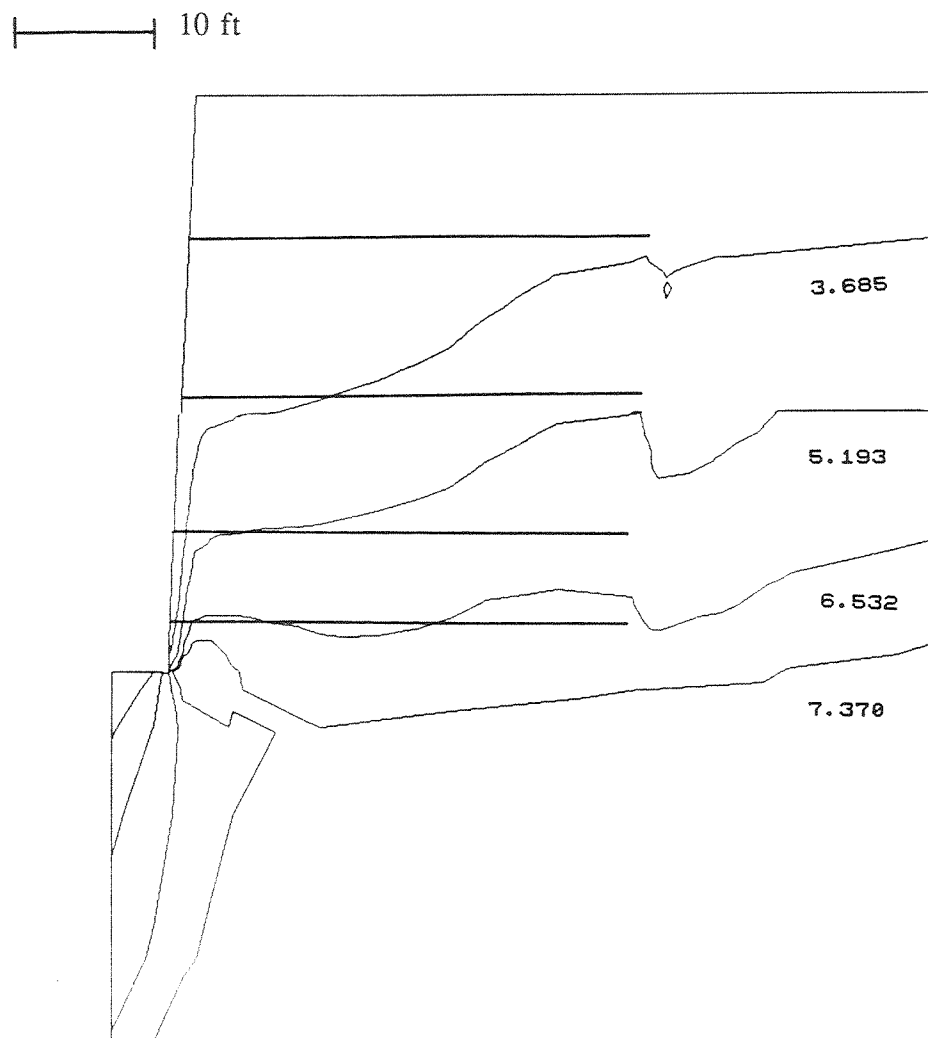


Figure 3.21b - Predicted vertical stress contours (after surcharge). Stress units are in ksf

2.5 ft

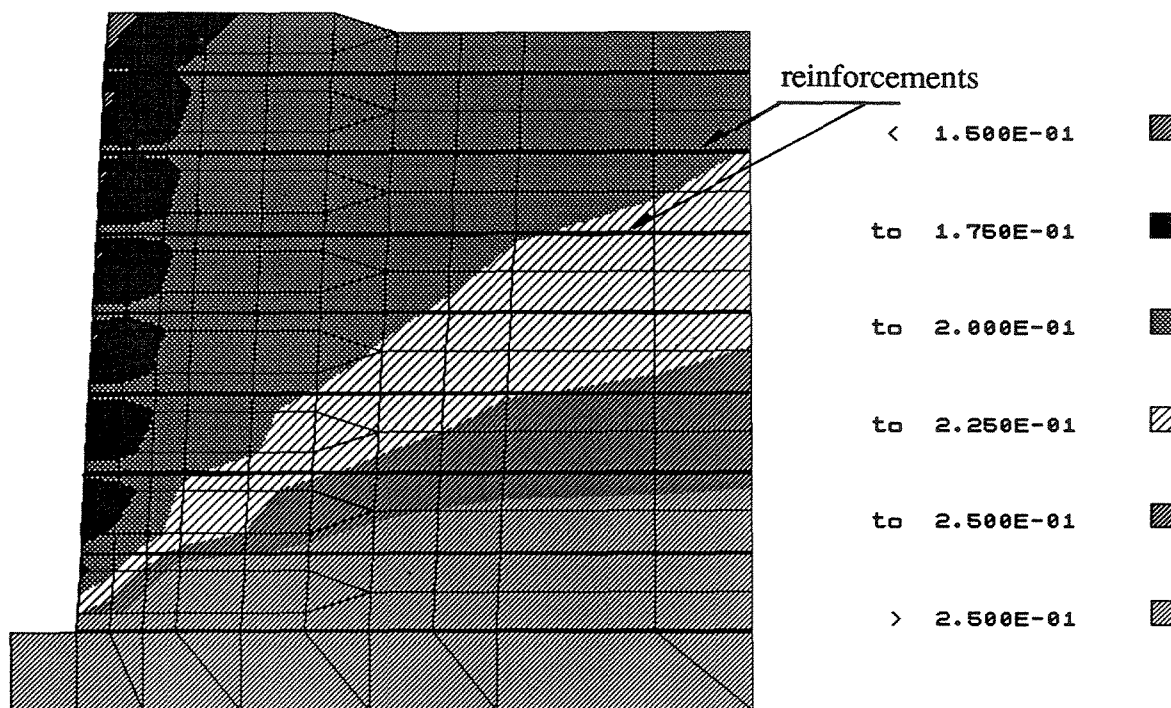


Figure 3.22 - Detail of the distribution of lateral earth pressure coefficient ($K=\sigma_H/\sigma_v$) before surcharge placement

3.3.3.5 Location and magnitude of maximum reinforcement tensions

The location of the maximum reinforcement tension in each of the 33 geotextile layers on the Rainier Ave. wall can be defined from the numerically predicted axial forces in the reinforcements (Section 3.3.3.2). The location of the maximum geotextile tension defines the beginning of reinforcement anchorage length needed to satisfy pullout requirements. The locus of the maximum reinforcement tension, obtained numerically for each geotextile layer, is shown in Figure 3.23. Results obtained before and after placement of the sloping backfill surcharge are indicated in the figure. The Rankine line,

which is the conventionally assumed locus for walls with geosynthetic reinforcements, is also indicated. Two observations can be made based on the observed distribution:

- a) although there is some scatter near the top of the wall, there is no significant change in position of maximum reinforcement tension is observed after the surcharge is placed; and
- b) the Rankine line is a conservative approximation for the actual position of the maximum reinforcement tensions; i.e., the actual maximum tension locus is inside the plane defined by an angle of $45^\circ + \phi/2$ from the horizontal.

Reinforced soil structures with sloping backfill surcharges are generally designed assuming the same design failure surface as walls with level backfill. As shown in Figure 3.23, numerical results obtained for the Rainier Ave. wall verify that actual failure surface is inside the Rankine plane, both before and after surcharge placement. This locus does not show, however, a smooth configuration. An interpretation of the mechanism that may have originated the observed pattern is suggested with dotted lines in Figure 3.24. Since the Rainier Ave. wall was designed with four vertical zones of different reinforcement strength, each zone can be interpreted as a composite material placed on a stiffer base. Different potential failure surfaces appear to develop at the interfaces between the zones. This pattern is favorable to pullout safety, resulting in a steep composite maximum reinforcement tension line. Walls with several vertical reinforced zones may then be especially advantageous for projects in which the design is controlled by pullout requirements.

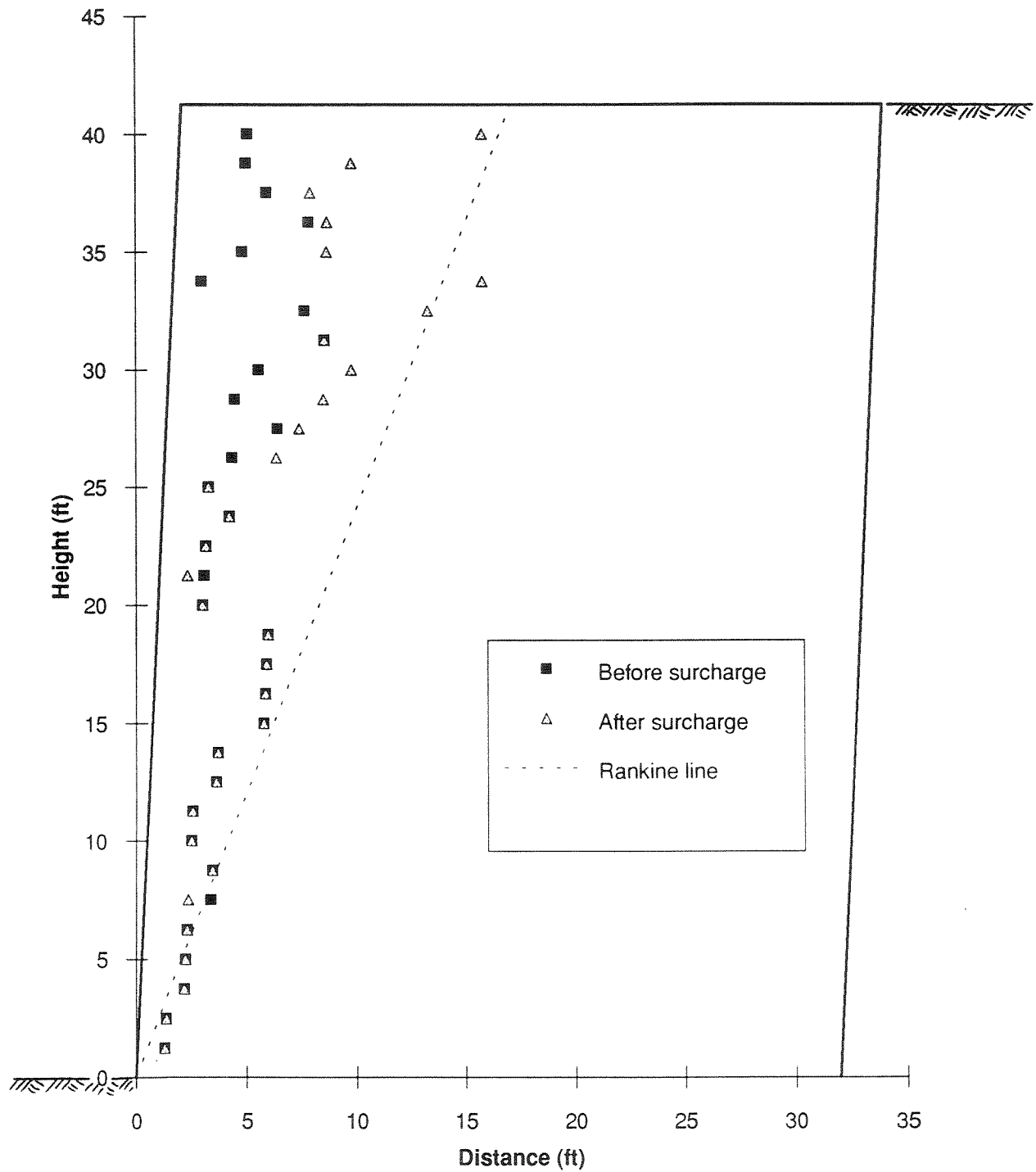


Figure 3.23 - Locus of maximum reinforcement tensions

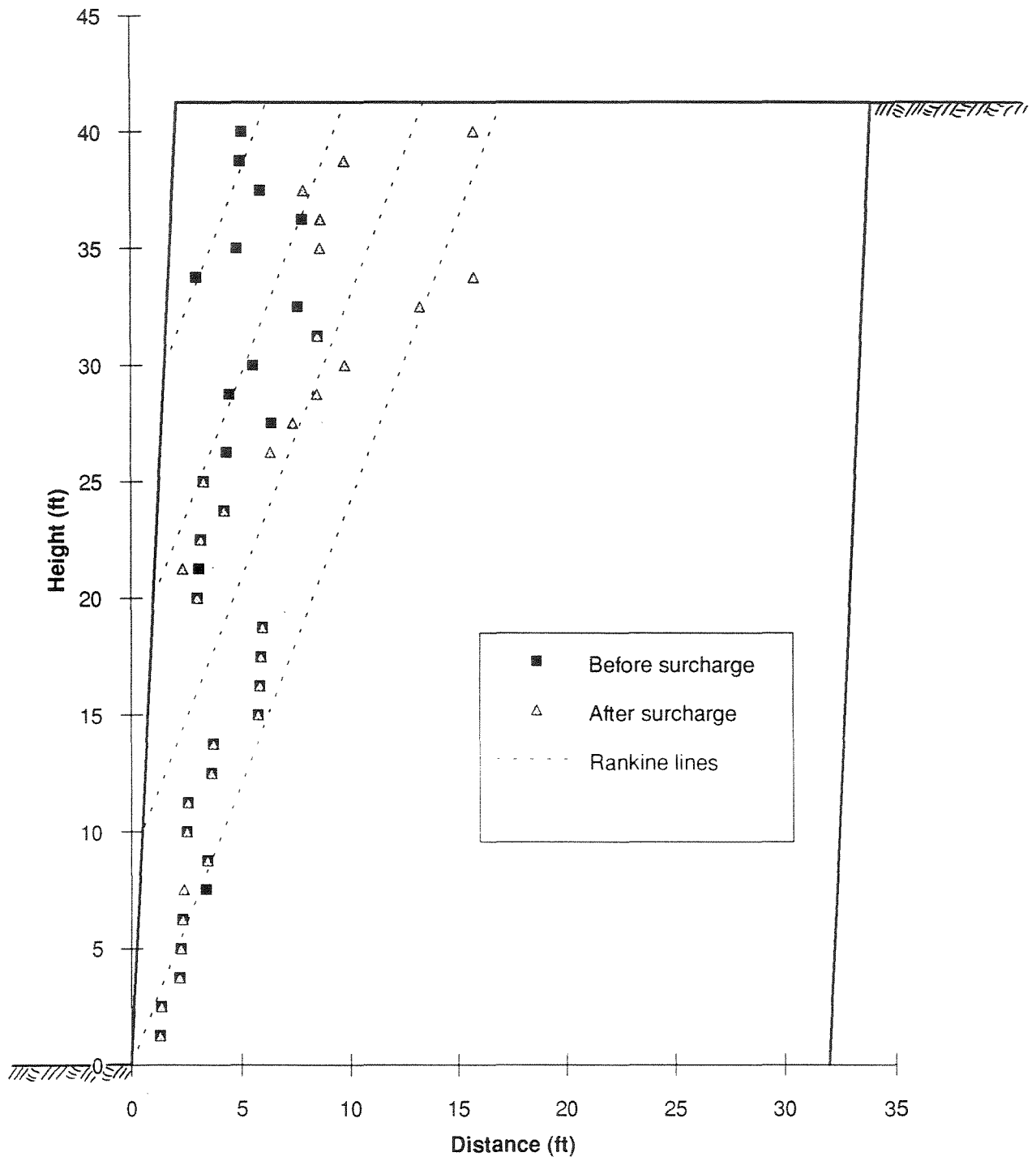


Figure 3.24 - Locus of maximum reinforcement tensions. Interpretation of possible mechanisms

The maximum reinforcement tensions with depth, as predicted by the finite element analysis of the Rainier Ave. wall, is indicated in Figure 3.25. The straight lines in the figure represent reinforcement tensions estimated using either the active Rankine coefficient for the case with level backfill ($K_a=0.19$ for $\phi = 45^\circ$), the active coefficient considering infinite sloping backfill ($K_{as}=0.23$), or using the at-rest lateral earth pressure coefficient (assuming $K_0=0.35$). The active stress state for the sloping backfill case was calculated considering the Coulomb approximation for infinite slope (Bowles, 1988):

$$K_{as} = \left[\frac{\cos\phi}{1 + \sqrt{\frac{\sin\phi \sin(\phi-\beta)}{\cos\beta}}} \right]^2$$

where ϕ is the soil friction angle ($\phi = 45^\circ$) and β is the fill slope ($\beta=29.7^\circ$).

The predicted maximum tensions for the horizontal backfill (no surcharge) case match reasonably well the Rankine line, while maximum tensions for the sloping surcharge case are conservatively estimated by the active coefficient for infinite slope. The sudden changes observed in the maximum tensions correspond to the boundaries between different reinforced zones.

3.3.4 Location of the critical planar surface in the Rainier Ave. wall

The potential slip surface in a reinforced soil wall is assumed to coincide with the locus of maximum tension forces in the reinforcements (Mitchell and Villet, 1987). This locus has been assumed to be approximately bilinear in the case of inextensible reinforcements, approximately linear in the case of extensible reinforcements, and passes through the toe of the wall in both cases (Figure 3.26). The locus of maximum reinforcement tension forces, obtained from the finite element analysis of the Rainier Ave

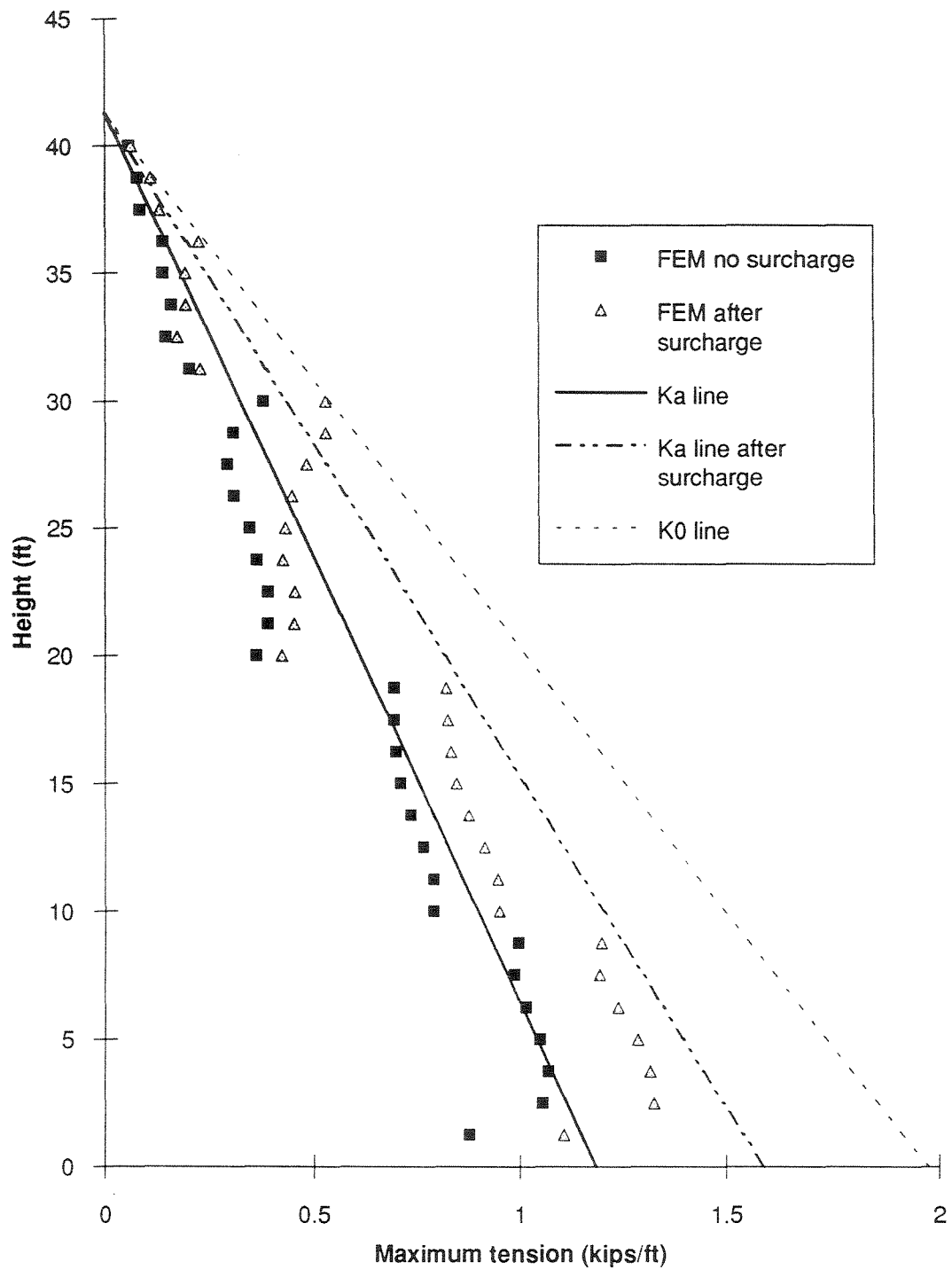


Figure 3.25 - Maximum reinforcement tension versus depth obtained from the Rainier Ave. wall analysis

wall, is indicated in Figure 3.23. A parametric study on the location of the potential failure surface would be simplified if the failure surface is assumed to be planar. However, such a planar failure surface is difficult to define from the data observed in Figure 3.23. A systematic methodology is then used to determine this critical plane.

The location of potential failure surfaces in nonreinforced soil structures has already been investigated using finite element analyses (Dunlop and Duncan, 1970; Duncan, 1992; Deschamps and Leonards, 1992). In these studies, the numerically predicted shear stresses along a trial surface are compared to the ultimate shear stresses available along that surface. In studies performed using limit equilibrium analysis, the factor of safety is assumed to be constant along the potential failure surface. However, local factors of safety can be defined along a critical surface if the analysis is performed using finite elements. This is particularly useful for the study of progressive failure problems.

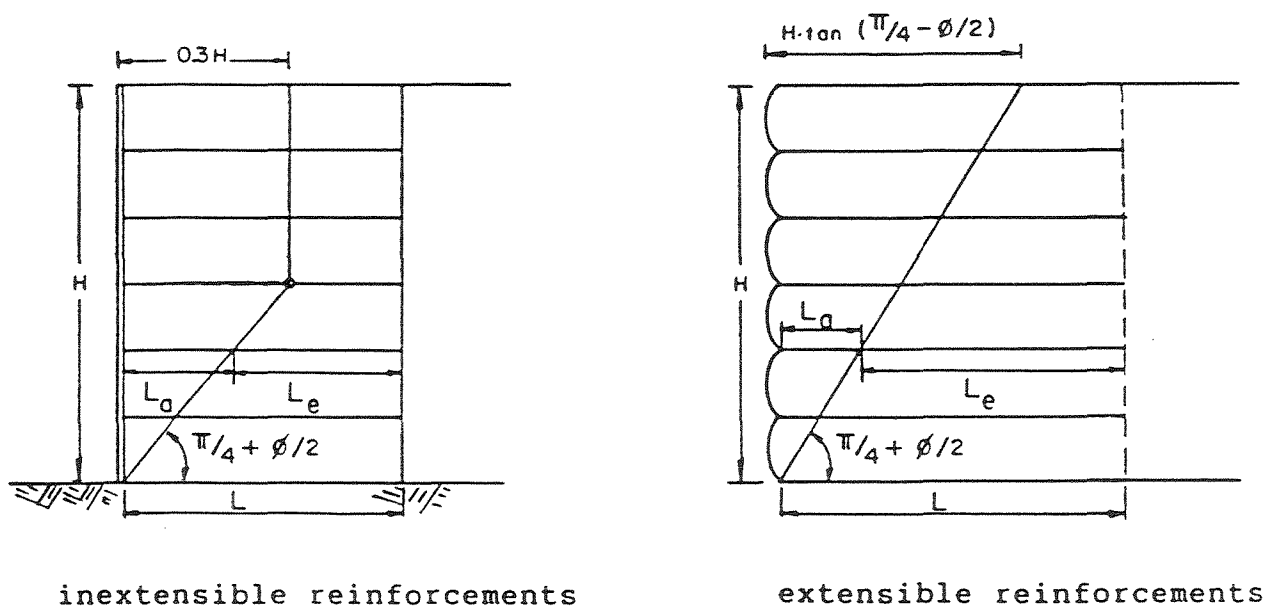


Figure 3.26 - Location of maximum reinforcement tension forces assumed in the design of reinforced soil walls

Limit equilibrium slope stability analysis procedures have been adapted and used for analyses of reinforced slopes. In these analyses, the reinforcement force is considered to be known and is prescribed for purposes of the analysis, introducing no additional unknowns (Wright and Duncan, 1991). The investigation of the location of the critical failure surface using finite element results, on the other hand, does not assume reinforcement forces to be known. In fact, instead of prescribing reinforcement forces by adopting a factor of safety on the ultimate reinforcement tensile strength, these forces are obtained from the finite element analysis. The methodology used in this study to determine the location of the critical failure surface relies on the finite element results to investigate the different trial surfaces.

The adopted search methodology assumes planar trial surfaces forming an angle β from the horizontal. The Reinforcement Tension Summation (RTS) was determined at each of these trial surfaces. The determination of the RTS value involved:

- a) determination of the intersection of the trial plane with each reinforcement layer,
- b) determination, at each location defined in (a), of the reinforcement tension by interpolating the reinforcement forces predicted in the finite element analysis at the center of each reinforcement element, and
- c) addition of tension contributions at each reinforcement layer to obtain the Reinforcement Tension Summation at the trial surface under investigation.

These calculations were performed using a postprocessor (rkine.f) developed for this study. The trial surface with the maximum RTS was assumed to be the critical planar surface. The value of the Factor of Safety along each trial surface can also be

determined using numerically obtained soil stresses and reinforcement tensions. The surface with the maximum RTS is the critical planar surface since, considering simplifying assumptions, it can be demonstrated that the plane with a minimum Factor of Safety corresponds to the surface with a maximum RTS (Zornberg and Mitchell, 1993).

The critical surfaces, before and after surcharge placement, obtained after the search process are shown in Figure 3.27. Reinforcement Tension Summation values at each plane forming an angle β from the horizontal are also indicated in the figure. The critical plane before surcharge placement forms an angle $\beta=70.75^\circ$ from the horizontal, while the critical plane after surcharge placement forms an angle $\beta=68.60^\circ$. The Rankine plane, defined using the friction angle obtained from triaxial tests on backfill specimens ($\phi=45^\circ$), forms an angle $\beta=67.50^\circ$ from the horizontal. Thus, for the wall under study, the anchorage length for pullout safety can be conservatively estimated both before and after surcharge using a potential failure surface defined by the theoretical Rankine line.

Search of critical coherent gravity surfaces, defined as the bilinear surfaces with a maximum RTS, was also performed (Figure 3.28). The critical coherent gravity surface before surcharge is located at $0.07 H_t$ from the wall face, where H_t is the height of the wall. After surcharge placement, the maximum RTS location is less clearly defined, being approximately at $0.16 H_t$ from the wall face. The critical planar surfaces are also indicated for reference in this figure. These results also indicate the selection of the theoretical Rankine line to define reinforcement anchorage lengths for design purposes is a conservative assumption.

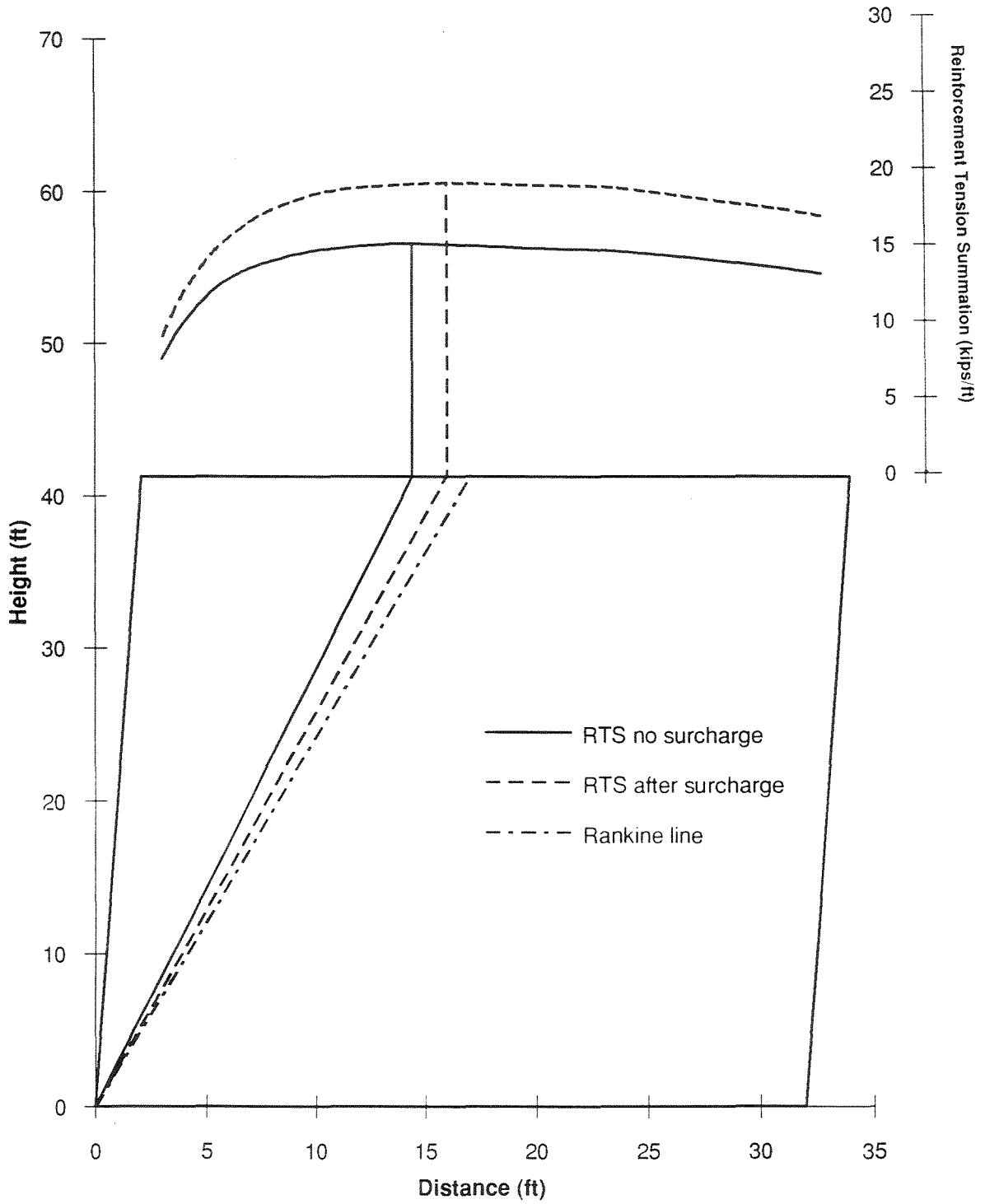


Figure 3.27 - Location of the planar surface with maximum Reinforcement Tension Summation (RTS)

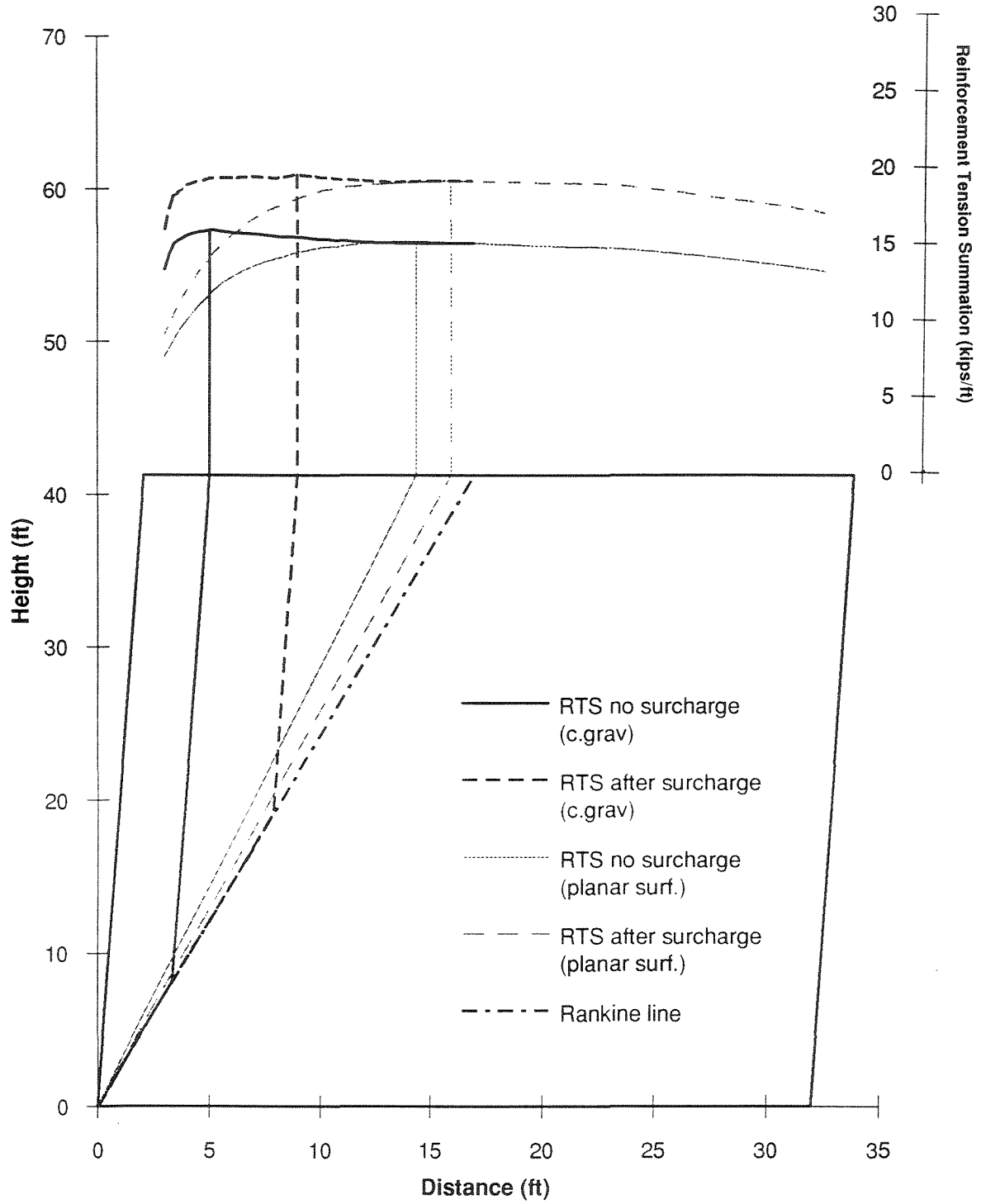


Figure 3.28 - Location of the coherent gravity surface with maximum Reinforcement Tension Summation (RTS)

Field observations on the location of the potential failure surfaces reported by other investigators agree with the finite element results shown in Figure 3.27. Field data reported by Adib (1988) showed the locus of the maximum tensile forces in a geogrid reinforced wall to be inclined at 72° from the horizontal. This value agrees with the critical surface inclination obtained in this study ($\approx 71^\circ$). Finite element analysis performed by Adib predicted a locus that fell about 2 ft behind the measured one. In two model geogrid reinforced soil walls constructed at the Royal Military College, Ontario, peak strain locations were observed to form an angle $\beta=71.5^\circ$ from the horizontal (Bathurst et al., 1989; Bathurst and Benjamin, 1990). The actual failure surface was also investigated by excavating the failure zone, and was observed to form approximately 72° from the horizontal.

Using calibrated input parameters and modeling procedures obtained from the analysis of the Rainier Ave. wall, a parametric study was performed to investigate the effect of sloping backfill surcharges on the performance of geosynthetically reinforced soil walls. Results from this parametric study will be described in Section 3.4. A Factor of Safety on the order of 3 was calculated for the Rainier Ave. wall along the critical planar surface (Zornberg and Mitchell, 1993). Such a high factor shows that current design procedures for geotextile-reinforced structures are conservative.

Results from this finite element study provide insight into the internal stability evaluation of reinforced soil walls. To provide an internally stable mass, the reinforcement is required to resist horizontal stresses so that it will not break, elongate excessively, or pullout (Mitchell and Christopher, 1990). Current design methodologies verify stability with respect to reinforcement pullout on an individual layer basis, i. e., the

pullout resistance that can be developed along the embedment length in each individual reinforcement shall be at least 1.5 times the maximum tension estimated in the same reinforcement layer. Pullout failure is assumed to develop if there is not enough reinforcement anchorage in a passive reinforced zone to prevent the sliding of an active reinforced wedge along a potential failure surface. This pullout mechanism is then related to a generalized sliding that, from the results obtained in this study, shows a very high factor of safety. A global verification of reinforcement anchorage requirements is probably more consistent with the wedge sliding mechanism than a layer by layer verification. A global evaluation of pullout safety would render a less conservative internal stability design.

Determination of a global pullout factor of safety would involve estimation of the summation of the ultimate resisting forces that can be developed along all the reinforcement embedment lengths. This value should then be compared to the summation of the maximum tensile forces in the reinforcements under in-service conditions. In this study, the Reinforcement Tension Summation (RTS) along the critical failure surface was determined from the finite element analysis results. This value could also be estimated from procedures currently used in the design of geosynthetically reinforced walls, i. e., by using the active K_a coefficient to estimate in-service maximum tensile forces in the reinforcements.

3.4 Parametric study: Effect of sloping backfills on geosynthetically reinforced soil walls

The results of a finite element parametric study of geosynthetically reinforced soil retaining walls, performed to investigate the effect of sloping backfills, are presented in this section. Particularly, these analyses investigate aspects of the wall response relevant to the pullout verification. The influence of the sloping surcharge geometry (fill slope and surcharge height) is initially evaluated in Section 3.4.1. This parametric study is performed on a structure designed as the Rainier Ave. wall, that is, using four vertical zones with different geotextile stiffnesses. Subsequently, the effect of sloping backfill surcharges on walls with different design characteristics (wall height and reinforcement stiffness) is investigated (Section 3.4.2). These last analyses are performed on walls designed using a single geosynthetic type and constant vertical spacing. Identification of the location of the potential failure surface is important for pullout verification purposes. Particular attention is also given to the analysis of Reinforcement Tension Summation along the critical planar surfaces, since this value is relevant in a global pullout verification, as already outlined in Section 3.3.4.

3.4.1 Effect of sloping backfill geometry

Two variables were used to define the surcharge geometry, namely, the slope $s:l$ of the backfill behind the top of the wall (Figure 3.29), and the surcharge height H_s (or the ratio with the wall height, H_s / H_t). The parametric study was performed on a structure with the dimensions, reinforcement characteristics, and backfill soil properties

of the Rainier Ave. wall. Reinforcement Tension Summations were determined along the critical planar surfaces.

For a given surcharge geometry (defined by H_s / H_t and s), the critical planar surface is defined as the plane along which the Reinforcement Tension Summation, obtained from the finite element analyses, reaches a maximum. Although the locus of the numerically obtained maximum reinforcement tensions does not necessarily correspond to a planar surface, the plane with the maximum RTS was generally a good linear fit of the actual locus. For this parametric study a linear fit is particularly suitable since the effect of surcharge loadings on the location of the critical surface can be easily quantified. In this case, a straight forward index to measure the effect of the sloping surcharge is the ratio β/β_0 , where β is the angle from the horizontal of the critical planar surface after placement of a given surcharge, and β_0 is the inclination of the critical plane before surcharge.

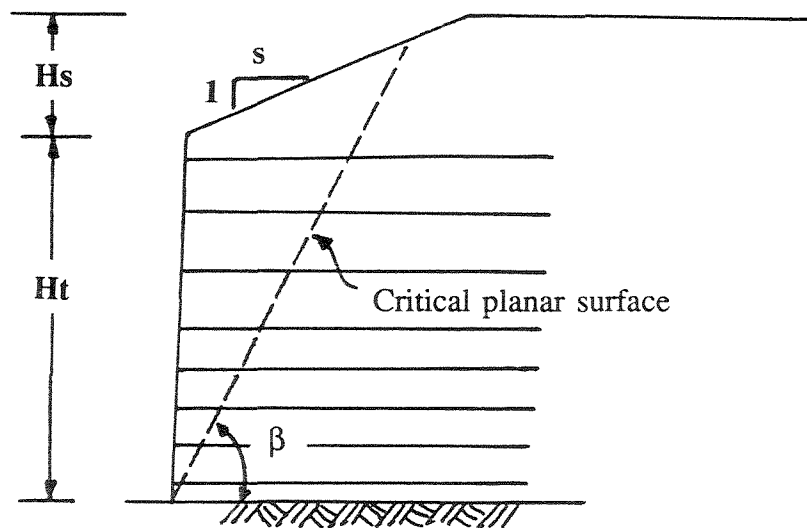


Figure 3.29 - Wall and sloping surcharge geometry

In the case of the Rainier Ave. wall ($H_s / H_f = 0.42$, $s = 1.75$), the inclination of the critical planar surface decreased about 2° , which corresponds to a ratio $\beta/\beta_0 = 0.97$. It is considered that this small change in the location of potential failure surface can be neglected for practical design purposes. Overall, the numerical results are consistent with reinforcement strain records obtained at the Rainier Ave. wall, which showed no change in the location of the maximum reinforcement tensions after surcharge placement.

Figure 3.30 shows the effect of sloping backfill height on the location of the critical planar surface considering a surcharge slope equal to that of the Rainier Ave. wall ($s = 1.75$). The figure shows that the slight changes in the location of the critical planar surface ($\approx 2^\circ$) occur after placement of relatively low surcharges ($H_s / H_f \approx 0.2$). Then, the location of the critical planar surface remains constant with additional surcharge placement. Numerical results obtained considering placement of sloping backfill surcharges up to the wall height ($H_s / H_f = 1.0$) are indicated in the figure. For any sloping surcharge height H_s , the inclination of the critical planar surfaces was always greater than the angle formed by the theoretical Rankine line. Thus, it is apparent that both before and after surcharge placement, the state-of-practice use of the Rankine line as internal failure surface is a conservative design assumption for determination of pullout resistance.

Figure 3.31 shows the effect of sloping backfill height on the Reinforcement Tension Summation. As would be expected, RTS values increase with increasing surcharge heights. However, the tension summation achieves a maximum value at $H_s / H_f \approx 0.30$ and no further increase is observed with additional surcharge beyond this value. The Reinforcement Tension Summation after placement of 12.6 m of surcharge ($H_s / H_f = 1.0$) is only 26% higher than the RTS value before surcharge.

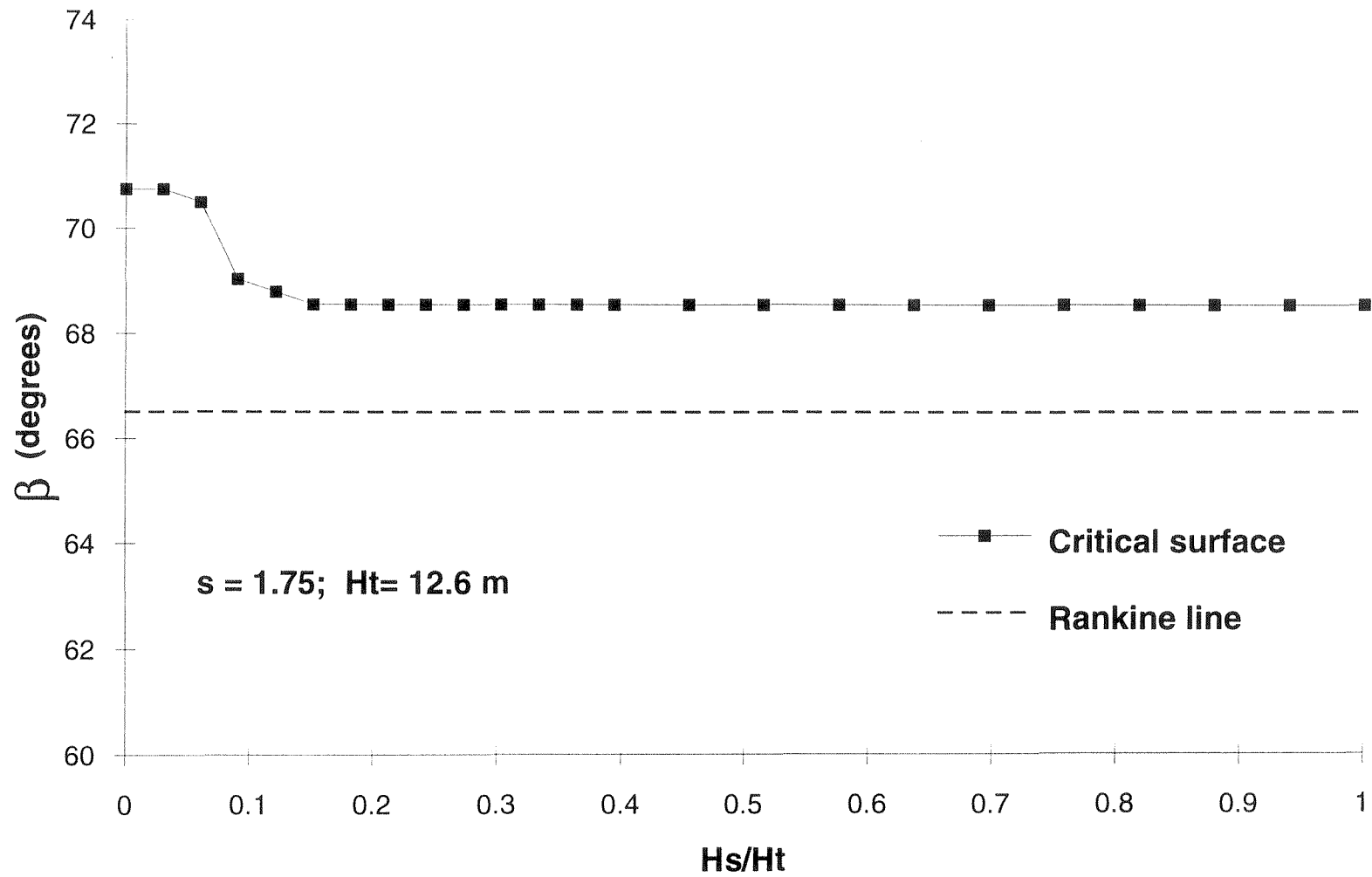


Figure 3.30 - Effect of surcharge height H_s on the location of the critical planar surface

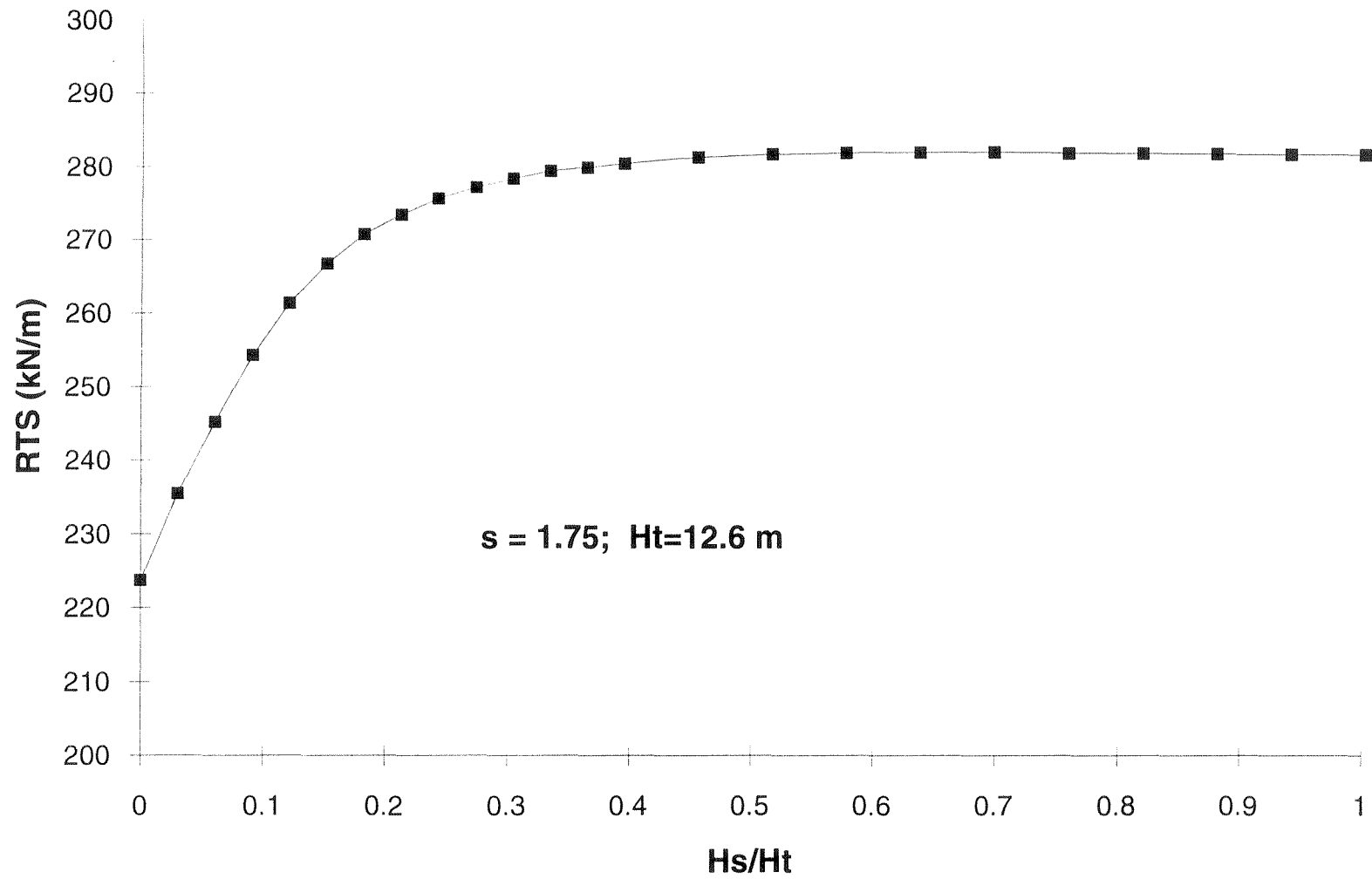


Figure 3.31 - Effect of surcharge height H_s on the Reinforcement Tension Summation along the critical planar surface

The influence of the surcharge slope s on the location of the critical planar surface was investigated by performing a series of finite element analyses on a reinforced wall designed as the Rainier Ave wall, but with surcharges placed at different slope angles. Slopes varying from $s=1.0$ to $s=3.0$ and surcharge heights up to 12.6 m ($H_s / H_t=1.0$) were considered in these analyses. The normalized inclinations β/β_0 of the critical planar surface are indicated in Figure 3.32 showing that the surcharge effect on the location of the potential failure surface is basically independent of the slope s . In all cases, the surcharge causes only a slight decrease in the angle β of the critical surface. This decrease always occurs after placement of relatively low surcharges, from $H_s / H_t \approx 0.10$ (for the case $s=3.0$) to $H_s / H_t \approx 0.20$ (for the case $s=1.0$).

The influence of the surcharge slope s on the Reinforcement Tension Summation, calculated along the critical planar surface, is indicated in Figure 3.33. RTS values are normalized in relation to RTS_0 , the Reinforcement Tension Summation before surcharge placement. As expected, there is an increase in the calculated RTS values with increasing surcharge slopes. In all cases, and particularly for the cases with lower surcharge slopes, the maximum RTS is achieved at relatively low surcharges. The increase in RTS values due to the surcharge goes from 14% for a slope $s=3.0$ to 47% for a surcharge slope $s=1.0$.

In conclusion, the effect of the sloping backfill surcharge on the location of the potential failure surface was observed to be very small, and can be neglected for practical design purposes. This observation is found valid independently of the geometry of the sloping surcharge. Although the magnitude of the Reinforcement Tension Summation after surcharge placement depends on the inclination and height of the surcharge, the maximum RTS value is achieved at relatively low surcharge heights. The implication of

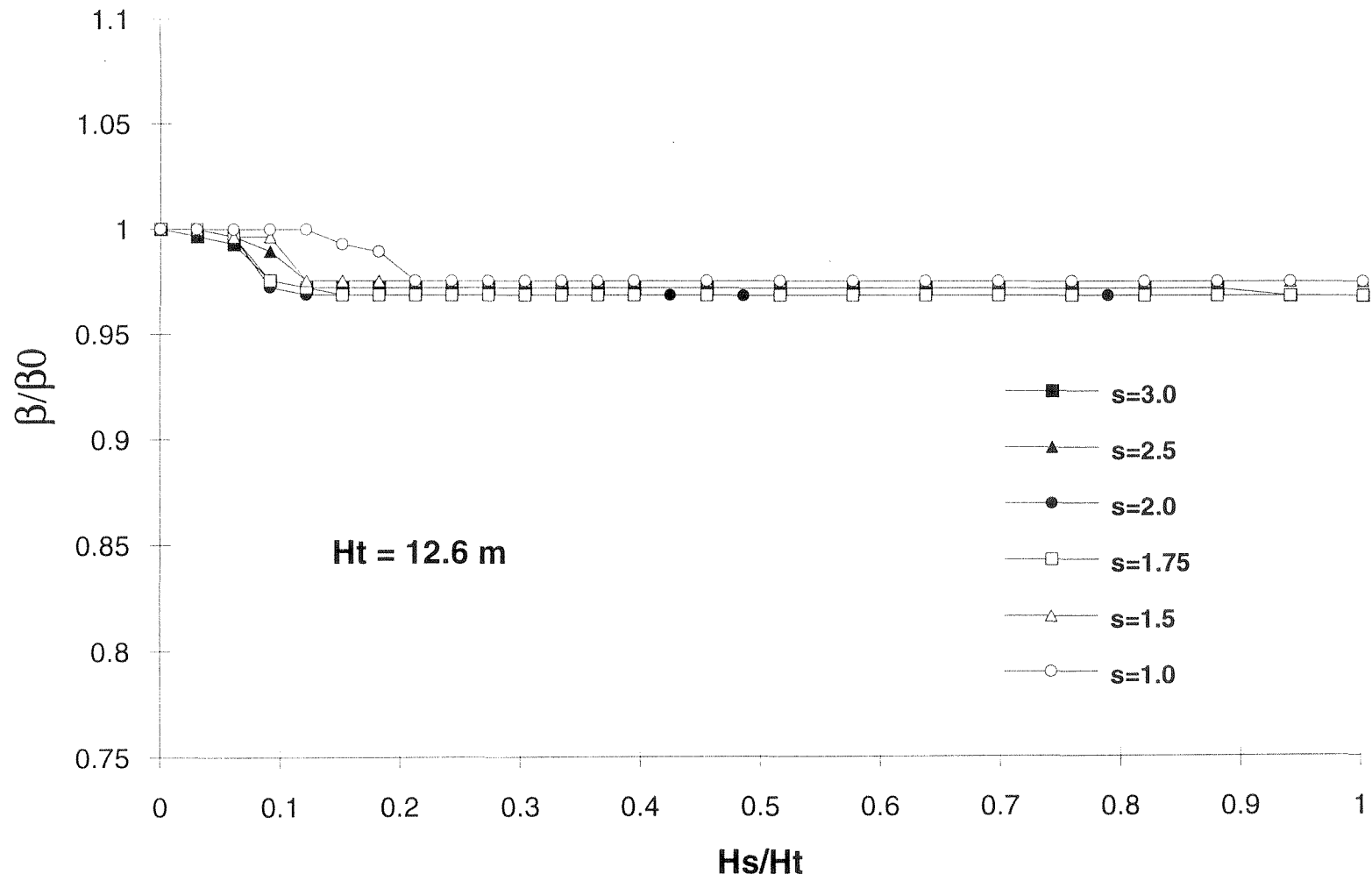


Figure 3.32 - Effect of slope s and surcharge height H_s on the location of the critical planar surface

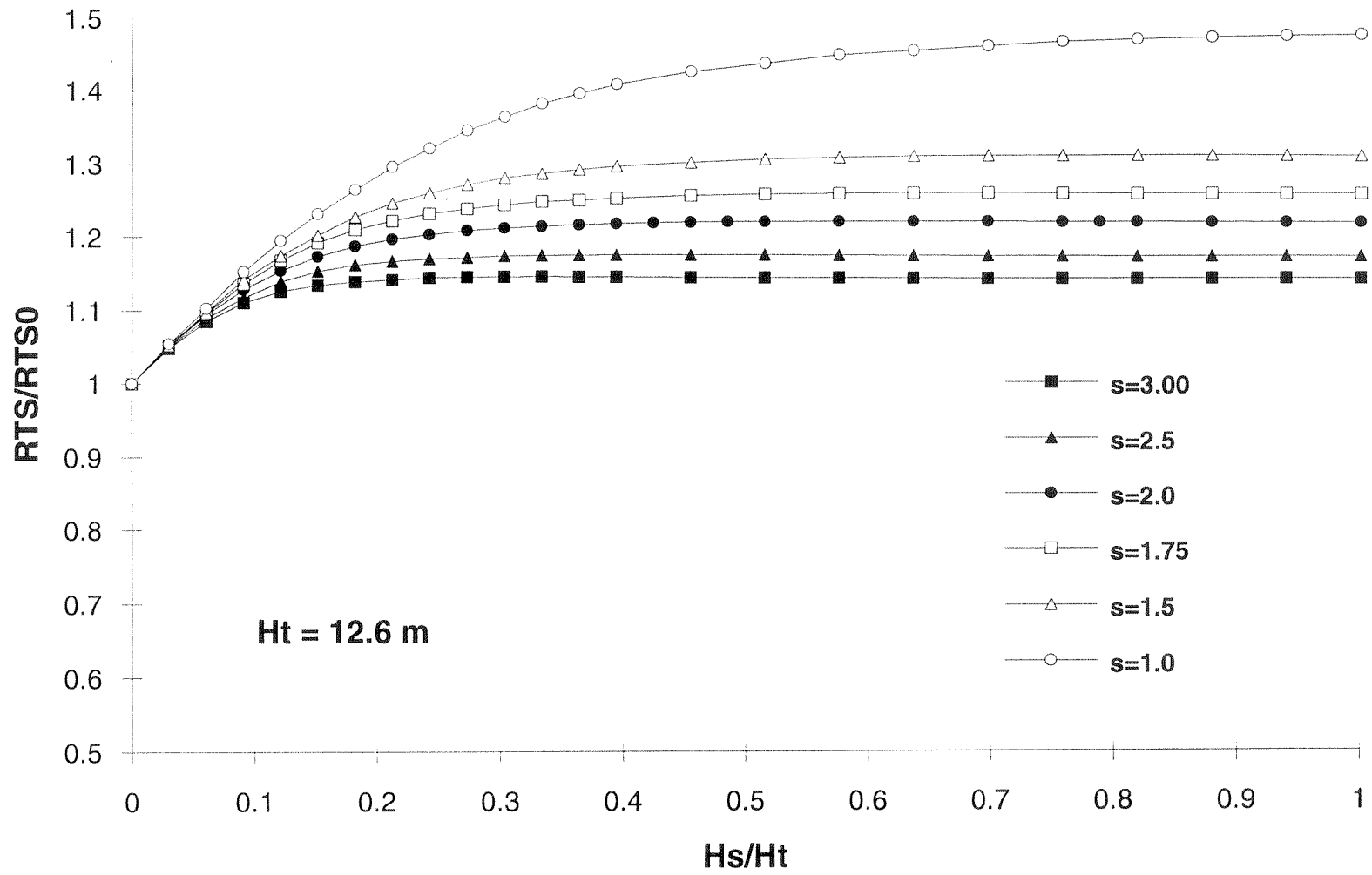


Figure 3.33 - Normalized Reinforcement Tension Summation along the critical planar surface

this observation is that, beyond a certain surcharge height H_s , there are no additional reinforcement requirements with further surcharge loads; e.g., the height of the surcharge fill becomes of no importance once H_s / H_t exceeds about 0.2 for a backfill slope defined by $s=2.0$

3.4.2 Effect of wall design characteristics

The parametric analyses in the previous section showed that the location of the critical planar surface is almost independent of the geometry of the sloping surcharge. The validity of this observation for different wall design characteristics, namely, wall height and reinforcement stiffness is investigated in this section.

The effect of wall height was evaluated by a parametric finite element study of generic 6.5, 9.5, and 12.6 m high walls. A constant reinforcement spacing of 0.38 m, a constant reinforcement stiffness of 1820 kN/m, and a reinforcement length of 80% of the wall height were adopted. Selected soil properties were those obtained for the Rainier Ave wall.

Figure 3.34 shows the effect of wall height on the inclination β of the critical planar surfaces after surcharge placement (slope $s=2.0$). The pattern of the results is similar to that obtained for the analyses performed to investigate different surcharge geometries. The general observation that the surcharge has only a small effect on the location of the potential failure surface is valid, independent of the height of the reinforced soil wall. Almost no change at all is observed in the slope of the potential failure surface for the 6.5 m high wall.

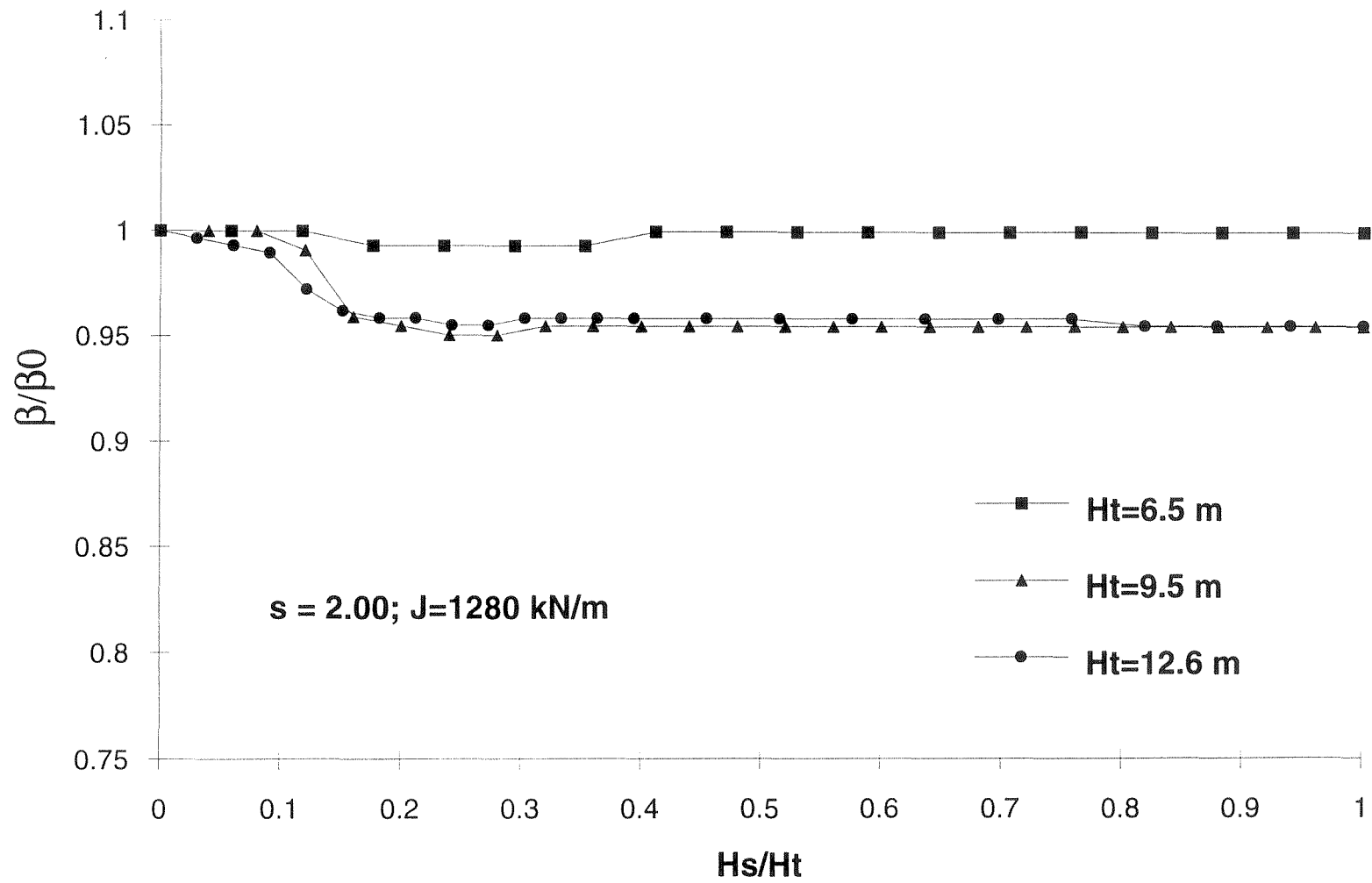


Figure 3.34 - Effect of wall height H_t on the location of the critical planar surface - Normalized curves

The influence of the wall height H_t on the normalized Reinforcement Tension Summation calculated along each critical planar surface is indicated in Figure 3.35. The maximum RTS is always achieved at relatively small surcharge heights. The calculated RTS values collapse into a single normalized RTS curve, showing that the normalized values are essentially independent of the height of the wall.

The effect of reinforcement stiffness on the location of the critical planar surface was also investigated. These analyses were performed on 6.5 and 9.5 m high walls. A constant reinforcement stiffness was adopted for the full vertical section of the walls, with selected values ranging from 364 to 2912 kN/m. This range encompasses confined stiffness values of commonly used geosynthetic reinforcements. The reinforcement layout in these generic walls was based on that used in the Rainier Ave. wall analysis, with constant reinforcement spacing of 0.38 m and reinforcement length 80% of the wall height. Soil parameters were those obtained for the Rainier Ave. wall, and the surcharge slope in these analyses was $s=2.0$.

The effect of surcharge placement on the location of the critical planar surface in 9.5 m high walls reinforced using different reinforcement stiffnesses J is shown in Figure 3.36. The figure shows the normalized inclination of the critical planar surface (β/β_0) as a function of the sloping surcharge height. It may be observed that the influence of the surcharge on the location of the potential failure surface is small for the range of reinforcement stiffnesses considered in the study. The observed trend is that the more flexible reinforced soil walls show less change in the location of the critical planar surface as a result of surcharge placement. For the 6.5 m high wall, the location of the critical

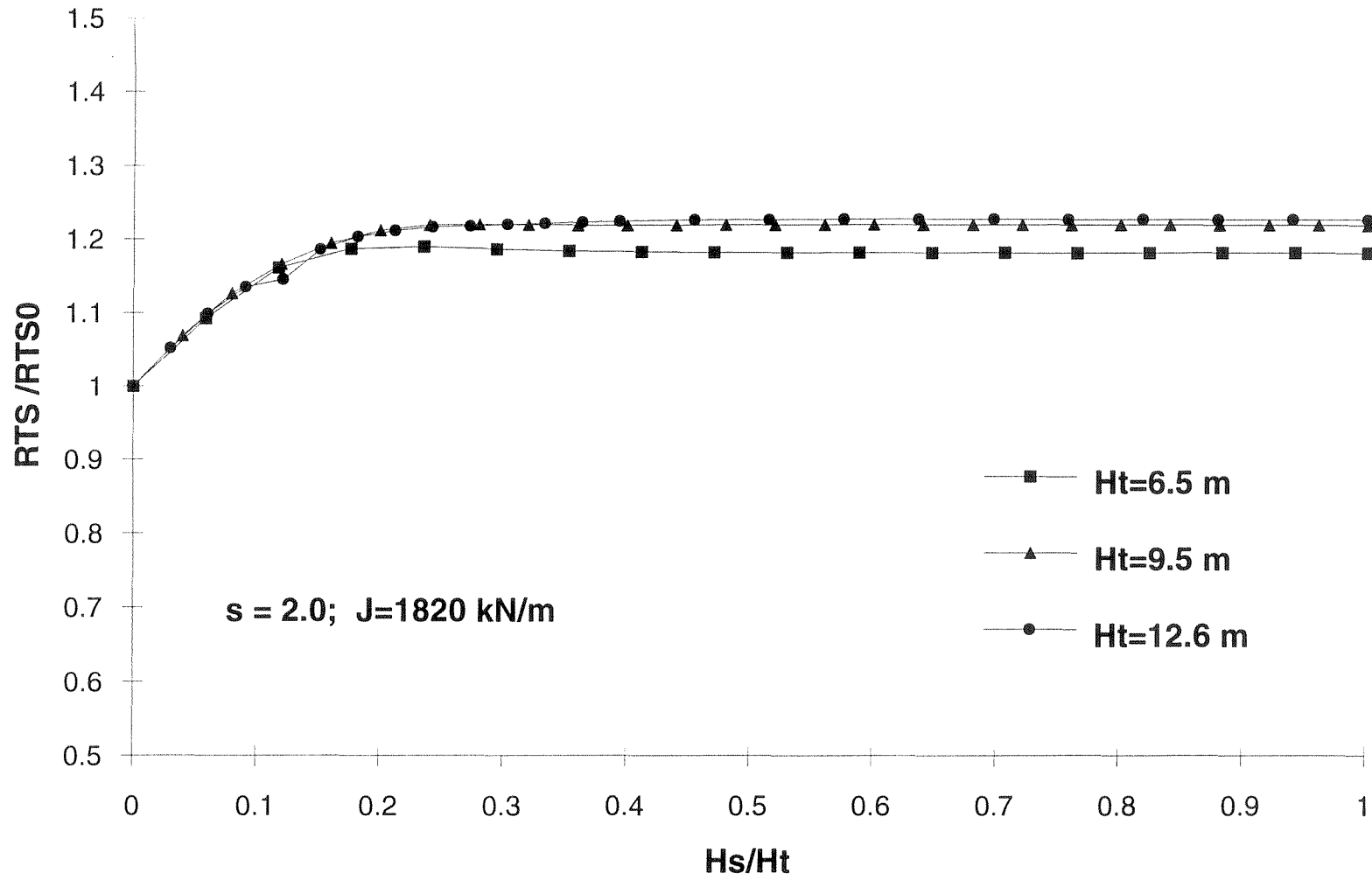


Figure 3.35 - Effect of wall height H_t on the Reinforcement Tension Summation along the critical planar surface - Normalized curves

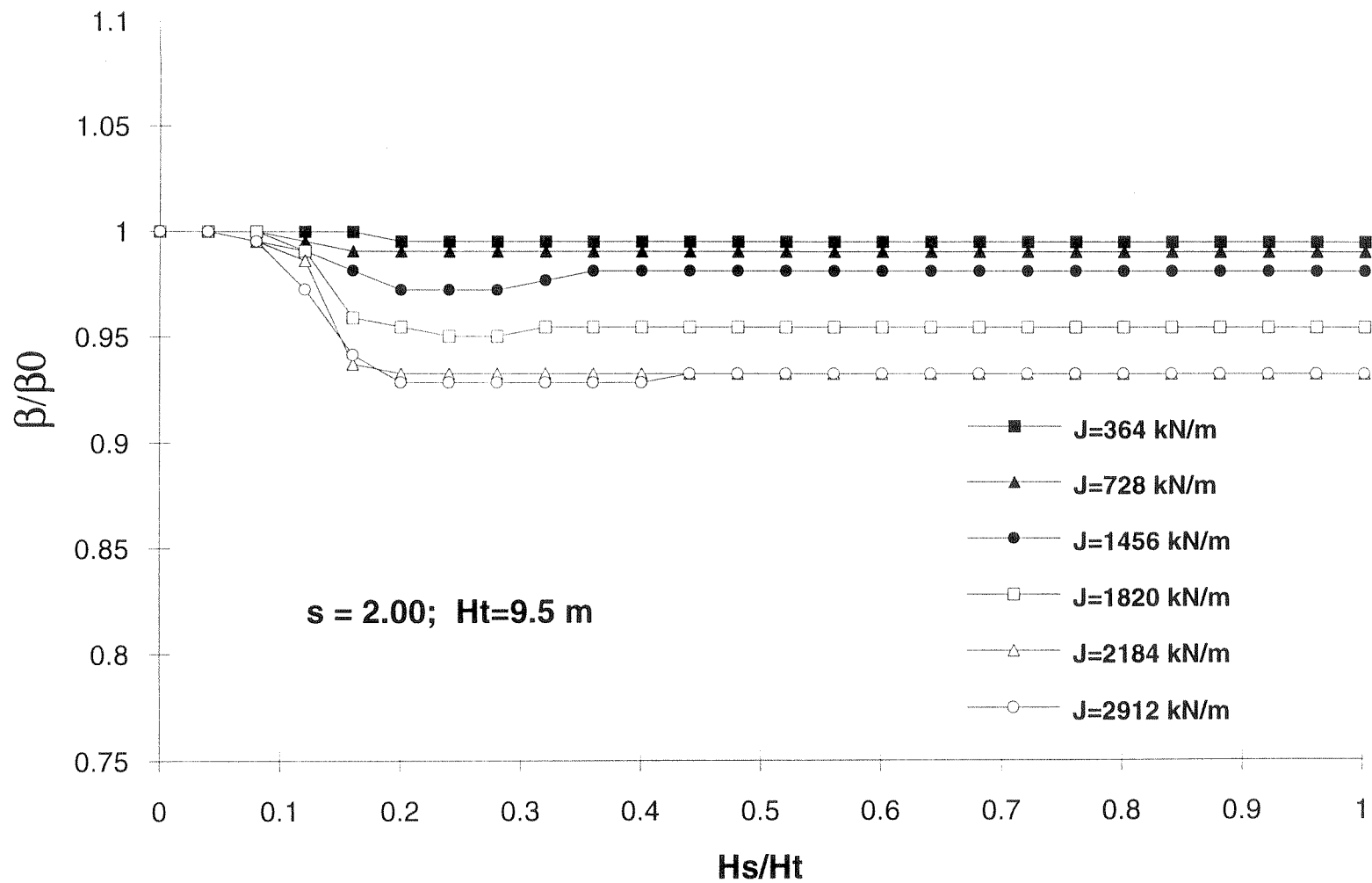


Figure 3.36 - Effect of reinforcement stiffness J on the location of the critical planar surface - Normalized curves

planar surface was essentially unchanged after surcharge placement, independent of the reinforcement stiffness.

The influence of reinforcement stiffness J on the normalized Reinforcement Tension Summation, calculated along each critical planar surface is indicated in Figure 3.37. The maximum RTS is always achieved under relatively low surcharges ($H_s / H_f \approx 0.2$). Since all RTS curves essentially collapse into a single normalized curve, it may be inferred that the normalized Reinforcement Tension Summation is independent of the reinforcement stiffness. Results from the analysis of a 12.6 m high wall designed having four vertical sections with different reinforcement stiffnesses (as the Rainier Ave. wall, but with a surcharge slope $s=2.0$) also fit very well into the normalized RTS curve. Moreover, it may be observed that the normalized RTS curves in Figures 3.35 and 3.37 essentially collapse into a unique plot. This suggests that the normalized Reinforcement Tension Summations depend only on the surcharge geometry (Figure 3.33), and are independent of the wall height (Figure 3.35) and of the reinforcement stiffness (Figure 3.37).

3.5 Conclusions

The finite element analysis of a well instrumented geotextile-reinforced soil wall with a sloping backfill surcharge, the Rainier Ave. wall, was performed in this study. The finite element results added information to the available field records that monitored the wall response, and several lessons were learned on the behavior of geosynthetically reinforced soil structures. They are:

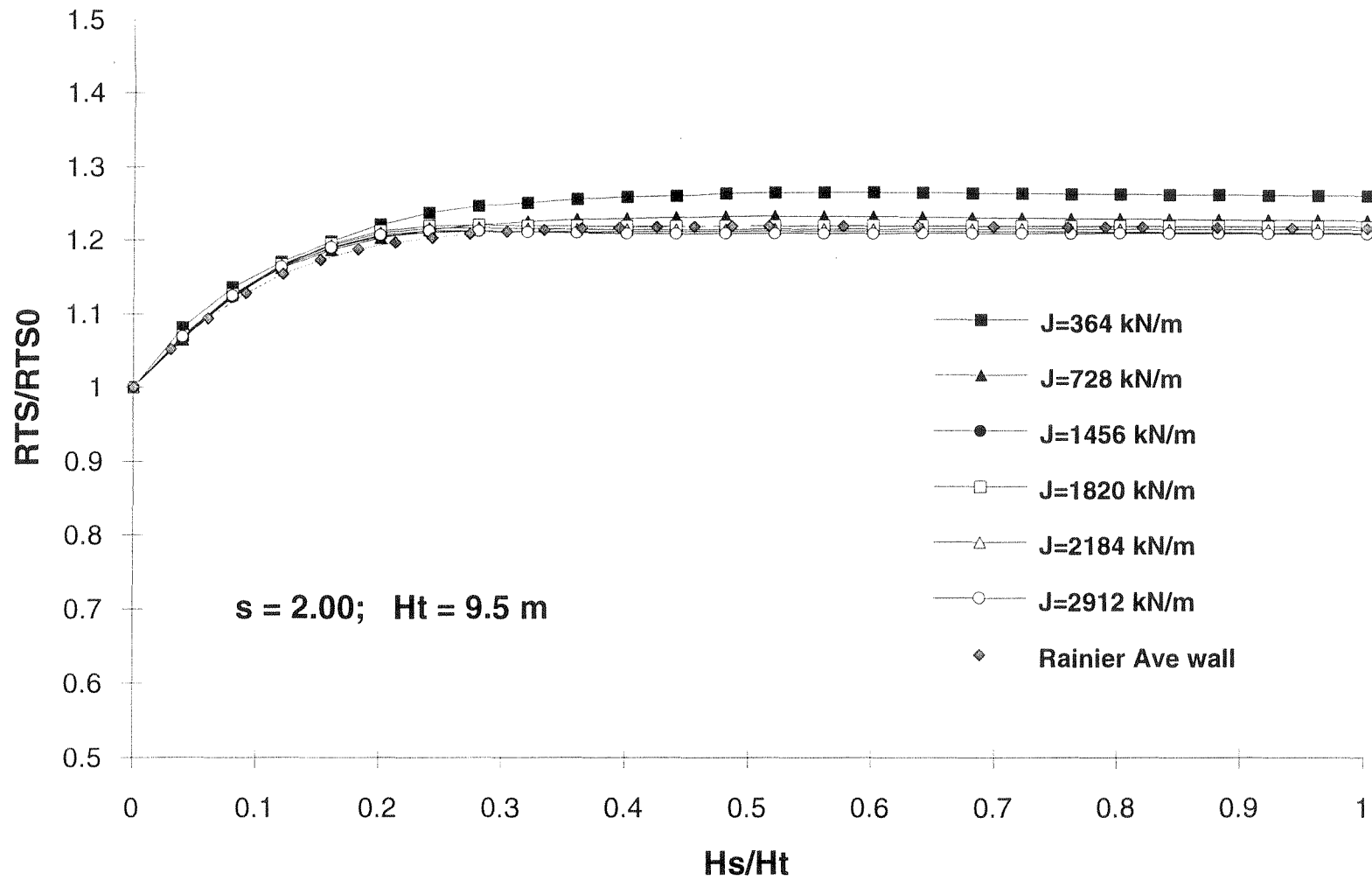


Figure 3.37 - Effect of reinforcement stiffness J on the Reinforcement Tension Summation along the critical planar surface - Normalized curves

- The numerical results are in agreement with the different instrumented responses of the wall (geotextile tension distribution, lateral displacements, vertical stresses).
- In-situ geotextile stiffness, backcalculated by matching the available instrumentation records to the finite element results, was found to vary from twice to four times the values determined from unconfined wide width tensile tests.
- Numerical results showed that maximum reinforcement forces can be appropriately estimated using the Rankine active coefficient for the horizontal backfill case. The use of the Coulomb active coefficient for infinite backfill slope conservatively predicts the maximum reinforcement forces after surcharge placement.
- The locus of the maximum reinforcement tensions suggests the development of multiple potential failure surfaces when the wall is designed with zones of different reinforcement strengths.
- The locus of the maximum reinforcement tensions for the Rainier Ave. wall, both before and after surcharge placement, is inside the conventionally assumed Rankine line.
- A high factor of safety, calculated along the critical planar surface using reinforcement tensions and soil stresses from the finite element analysis, reflects conservatism in the wall design.

Using calibrated input parameters and modeling procedures obtained from the back analysis of the Rainier Ave. wall, a parametric study was performed to investigate the effect of sloping backfill surcharges on the performance of geosynthetically reinforced soil walls. Emphasis was placed on aspects relevant to pullout verification during wall design,

namely, location of the potential failure surface and Reinforcement Tension Summation along this surface. The following conclusions can be drawn from this parametric finite element study:

- For practical purposes, the location of the critical planar potential failure surface is independent of the presence of a sloping backfill surcharge on the top of the wall. This was found to be true independently of the geometry of the surcharge (surcharge slope and surcharge height), and of wall design characteristics (wall height and reinforcement stiffness).
- Reinforcement Tension Summation (RTS) values under surcharge loading can be normalized to the RTS value before surcharge placement. Normalized RTS values are only a function of the surcharge geometry, being independent of the wall height and of the reinforcement stiffness. The maximum RTS value is achieved at relatively low surcharge fill heights.
- The Rankine failure surface provides a conservative, however suitable, design basis for separation of the active and resistant zones within geosynthetically reinforced walls with sloping backfills. The required reinforcement length for pullout resistance purposes can be taken as the reinforcement length behind this surface at each reinforcement level.

References

- Adib, M. E. (1988). *Internal lateral earth pressure in earth walls*, Thesis submitted in partial satisfaction of the requirements for the degree of Doctor of Philosophy. Department of Civil Engineering, University of California, Berkeley, California.
- Adib, M., J. K. Mitchell and B. Christopher. (1990). "Finite element modeling of reinforced soil walls and embankments." *Design and performance of earth retaining structures*, Geotechnical Special Publication No.25, ASCE, 409-423.
- Allen, T. M. (1993). Personal communication.
- Allen, T. M., B. R. Christopher and R. D. Holtz. (1991). "Performance of a 12.6 m high geotextile wall in Seattle, Washington." *Proc., International Symposium on Geosynthetic-Reinforced Soil Retaining Walls*, J. T. H. Wu, eds. Denver, Colorado: A.A. Balkema, August, 81-100.
- Bathurst, R. J. and D. J. Benjamin. (1990). "Failure of a geogrid reinforced soil wall." *Transportation Research Record* 1288, 109-116.
- Bathurst, R. J., D. J. Benjamin and P. M. Jarrett. (1989). "An instrumented geogrid reinforced soil wall." *Proc., Twelfth International Conference on Soil Mechanics and Foundation Engineering*. Rio de Janeiro, Brazil, 1223-1226.
- Bathurst, R. J., R. Karpurapu and P. M. Jarrett. (1992). "Finite element analysis of a geogrid reinforced soil wall." *Grouting, Soil Improvement and Geosynthetics*, Borden R.H., R. Holtz and I. Juran, eds., Geotechnical Special Publication No.30, ASCE, vol. 2. New Orleans, 1213-1224.

- Bell, J. R., R. K. Barrett and A. C. Ruckman. (1983). "Geotextile earth-reinforced retaining wall tests: Glenwood Canyon, Colorado." *Transportation Research Record* 916, 59-69.
- Boulanger, R. W., J. D. Bray, S. H. Chew, R. B. Seed, J. K. Mitchell and J. M. Duncan. (1991). *SSCOMPPC: A finite element analysis program for evaluation of soil-structure interaction and compaction effects*, Geotechnical Engineering Report No. UCB/GT/91-02. Department of Civil Engineering, University of California, Berkeley.
- Boscardin, M. D., E.T Selig, R.S. Lin and G.R. Yang. (1990). "Hyperbolic parameters for compacted soils." *Journal of the Geotechnical Engineering Division, ASCE* 116(1), 88-104.
- Bowles, J. E. (1988). *Foundation Analysis and Design*. Fourth Ed. McGraw-Hill Inc.
- Bray, J. D., R. W. Boulanger, S. H. Chew and R. B. Seed. (1992). "Finite element analysis in geotechnical engineering." *Proc., Eighth Conf. on Computing in Civil Engineering and Geographic information Systems Symposium*. Dallas, Texas, June, 410-417.
- Bray, J. D., A. Ashmawy, G. Mukhopadhyay and E. M. Gath (1993). "Use of geosynthetics to mitigate earthquake fault rupture propagation through compacted fill." *Proc., Geosynthetics'93 Conference*. Vancouver, British Columbia, 379-392.
- Chalaturnyk, R. J., J. D. Scott, D. H. K. Chan and E. A. Richards. (1990). "Stresses and deformations in a reinforced soil slope." *Canadian Geotechnical Journal* 27, 224-232.

- Chang, D. T. T., W. T. Wey and T. C. Chen (1993). "Study on geotextile behaviors of tensile strength and pull-out capacity under confined condition." *Proc., Geosynthetics'93 Conference*. Vancouver, British Columbia, 607-618.
- Christopher, B. R. (1987). "Geogrid reinforced soil retaining wall to widen an earth dam and support high live loads." *Proc., Geosynthetics'87 Conference*. New Orleans, 145-156.
- Christopher, B. R., R. D. Holtz and D. Bell. (1986). "New tests for determining the in-soil stress-strain properties of geotextiles." *Proc., Third International Conference on Geotextiles*. Vienna, 683-688.
- Christopher, B. R., R. D. Holtz and T. M. Allen. (1990). "Instrumentation for a 12.6 m high geotextile-reinforced wall." *Performance of Reinforced Soil Structures*, A. McGown, K. Yeo and K. Z. Andrawes, eds. London: Thomas Telford Ltd., 73-78.
- Christopher, B. R., S. A. Gill, J. P. Giroud, I. Juran, J. K. Mitchell, F. Schiosser and J. Dunnycliff. (1990). *Design and construction guidelines for reinforced soil structures*, Report No.FHWA-RD-89-043. Federal Highway Administration, U. S. Department of Transportation.
- Collin, J. G. (1986). *Earth wall design*, Thesis submitted in partial satisfaction of the requirements for the degree of Doctor of Philosophy. Department of Civil Engineering, University of California, Berkeley, California.
- Deschamps, R. J. and G. A. Leonards. (1992). "A study of slope stability analysis." *Stability and Performance of Slopes and Embankments II*, Geotechnical Special Publication No.31, ASCE. Berkeley, California, June, 267-291.

- Dunlop, P. and J. M. Duncan. (1970). "Development of failure around excavated slopes." *ASCE Journal of the Soil Mechanics Division* 96(SM2), 471-493.
- Duncan, J. M. (1992). "State-of-the-Art: Static stability and deformation analysis." *Stability and Performance of Slopes and Embankments II*, Geotechnical Special Publication No.31, ASCE. Berkeley, California, June, 222-266.
- Duncan, J. M., P. Bryne, K. S. Wong and P. Mabry. (1980). *Strength, stress-strain and bulk modulus parameters for finite element analyses of stresses and movements in soil masses*, Report No. UCB/GT/80-01. Department of Civil Engineering, University of California, Berkeley.
- El-Fermaoui, A. and E. Nowatzki. (1992). "Effect of confining pressure on performance of geotextiles in soil." *Proc., Second International Conference on Geotextiles*. Las Vegas, vol.3, 799-804.
- Fabian, K. J. and A. B. Fourie. (1988). "Clay geotextile interaction in soil-tensile tests." *Proc., Int. Geot. Symposium on Theory and Practice of Earth Reinforcement*, Fukuoka Kyushu, Japan. Rotterdam: A.A.Balkema, 81-86.
- Gomes, R. C. (1992). "Soil-geotextile interaction mechanisms." (in Portuguese) *Proc., Geossintéticos'92, Brazilian Symposium on Geotechnical Applications of Geosynthetics*, Brasília, Brazil, 35-60.
- Ho, S. K. and R. K. Rowe (1993). "Finite element analysis of geosynthetics-reinforced soil walls." *Proc., Geosynthetics'93 Conference*. Vancouver, British Columbia, 203-216.

- Holtz, R. D., T. M. Allen and B. R. Christopher. (1991). "Displacement of a 12.6 m high geotextile-reinforced wall." *Proc., Tenth European Conference on Soil Mechanics and Foundation Engineering*. Florence, Italy: A. A. Balkema, Rotterdam, 725-728.
- Jaber, M. B. (1989). *Behavior of reinforced soil walls in centrifuge model tests*, Thesis submitted in partial satisfaction of the requirements for the degree of Doctor of Philosophy. Department of Civil Engineering, University of California, Berkeley, California.
- Kokkalis, A. and N. Papacharisis. (1989). "A simple laboratory method to estimate the in-soil behaviour of geotextiles." *Geotextiles and Geomembranes* 8, 147-157.
- Lambe, T. W. (1973). "Predictions in soil engineering." *Geotechnique* XXIII(2), June, 149-202.
- Leshchinsky, D. and D. A. Field. (1987). "In-soil load elongation, tensile strength and interface friction of non-woven geotextiles." *Proc., Geosynthetics'87 Conference*. New Orleans, 238-249.
- Ling, H. I., J. T. H. Wu and F. Tatsuoka. (1992). "Short-term strength and deformation characteristics of geotextiles under typical operational conditions." *Geotextiles and Geomembranes* Vol.11, 185-219.
- McGown, A., K. Z. Andrawes and M. H. Kabir. (1982). "Load-extension testing of geotextiles confined in soil." *Proc., Second International Conference on Geotextiles*. Las Vegas, 793-798.
- Mitchell, J. K. and B. R. Christopher. (1990). "North American practice in reinforced soil systems." *Design and Performance of Earth Retaining Structures*, June 1990, ASCE Geotechnical Publication No.25, 322-346.

- Mitchell, J. K. and W. C. B. Villet. (1987). *Reinforcement of Earth Slopes and Embankments*, National Cooperative Highway Research Program Report No.290. Washington, D.C.: Transportation Research Board.
- Schmertmann, G. R. (1991). *Effects of variable backfill compaction and settlement on reinforced soil wall behavior*, Thesis submitted in partial satisfaction of the requirements for the degree of Doctor of Philosophy. Department of Civil Engineering, University of California, Berkeley, California.
- Schmertmann, G. R., S. H. Chew and J. K. Mitchell. (1989). *Finite Element Modeling of Reinforced Soil Wall Behavior*, Report No. UCB/GT/89-01. Department of Civil Engineering, University of California, Berkeley.
- Seed, R. B., J. G. Collin and J. K. Mitchell. (1986). "FEM analyses of compacted reinforced soil walls." *Proc., Second International Symposium on Numerical Models in Geomechanics*. Ghent, 553-562.
- Seed, R. B. and J. M. Duncan. (1983). *Soil-structure interaction effects of compaction-induced stresses and deflections*, Geotechnical Engineering Research Report No. UCB/GT/83-06. Department of Civil Engineering, University of California, Berkeley.
- Seed, R. B. and J. M. Duncan. (1984). *SSCOMP: A finite element analysis program for evaluation of soil-structure interaction and compaction effects*, Report No. UCB/GT/84-02. Department of Civil Engineering, University of California, Berkeley.

- STS Consultants Ltd. (1990). *Final Report of SR-90 Rainier Avenue interchange geotextile wall instrumentation project*, Project no. 25280. Final report to Washington State Department of Transportation.
- Tatsuoka, F., H. Ando (Yamauchi), K. Iwasaki and K. Nakamura. (1986). "Performances of clay test embankments reinforced with a non-woven geotextile." *Proc., Third International Conference Geotextiles*. Vienna, 355-360.
- Wright, S. G. and J. M. Duncan. (1991). "Limit equilibrium stability analyses for reinforced slopes." *Transportation Research Record* 1330, 40-46.
- Zornberg, J.G. and J.K. Mitchell (1993). *Finite Element Analysis of Geosynthetically Reinforced Soil Walls with Sloping Backfills*, Report No. UCB/GT/93-04. Department of Civil Engineering, University of California, Berkeley.

CHAPTER 4

PERFORMANCE OF GEOTEXTILE-REINFORCED SOIL STRUCTURES AT FAILURE: A CENTRIFUGE STUDY



Failure of a geotextile-reinforced slope model, as obtained after testing in a geotechnical centrifuge.

4.1 Introduction

Limit equilibrium analysis methods have been traditionally used to analyze the stability of slopes with and without reinforcements. The accuracy of these methods depends on whether or not the assumed mode of failure adequately represents the conditions actually leading to the collapse of a geotechnical structure. Back analyses of structures at failure may be used to substantiate the assumptions in design. However, to

date, limit equilibrium predictions of the performance of geosynthetically reinforced slopes have not been fully validated against monitored failures, and conservatism may have prevailed in their design. Consequently, further investigation was deemed necessary to evaluate the assumptions and selection of parameters for the design of these structures.

Small-scale physical modeling of engineered earth structures has provided insight into failure mechanisms (Lee et al., 1973; Holtz and Broms, 1977; Juran and Christopher, 1989). However, the usefulness of scaled physical models is limited because the stress levels in the models are much smaller than in the full scale structures, thus leading to different soil properties. Finite element analyses have also been made (Hird et al., 1990; San et al., 1994). Although this numerical technique proved useful for analysis of the performance of structures under working stress conditions, finite element modeling of failure in frictional materials requires techniques to handle the localization of deformations, such as specific continuum formulations or the use of adaptive mesh refinement to capture slip discontinuities (Zienkiewicz and Taylor, 1991).

The centrifuge provides a tool for geotechnical modeling in which prototype structures can be studied as scaled-down models while preserving the stress states required to develop the appropriate soil properties (Avgherinos and Schofield, 1969). The principle of centrifuge testing is to raise the acceleration of the scaled model in order to obtain prototype stress levels in the model. Although modeling limitations are often difficult to overcome when seeking a comparison between the performance of centrifuge models and full scale prototype structures, many of these limitations can be taken into account when the purpose is to validate analytic or numerical tools. Thus, the combination of experimental centrifuge modeling results with analytic limit equilibrium

predictions is a useful approach to investigate the performance of reinforced soil structures at failure. Consequently, a centrifuge testing program has been performed as part of this study in order to investigate the performance of geotextile-reinforced soil structures at failure.

The results of eight geotextile-reinforced slope models tested to failure in a geotechnical centrifuge are presented herein. The variables considered in the study (reinforcement spacing, reinforcement tensile strength, and soil strength) can all be taken into account using conventional limit equilibrium analyses. Although data was also collected for a deformability evaluation, only the evaluation of failure is considered here. Centrifuge modeling of reinforced soil structures, including an evaluation of previous studies, is presented in Section 4.2. The characteristics of the centrifuge testing program, including the construction procedures followed in this study, are described in Section 4.3. Properties of the geotextiles, backfill soil, and several interfaces that could influence the performance of the reinforced slope models are addressed in Section 4.4. After describing the results from this experimental study in Section 4.5, the lessons learned from the performance of the centrifuge models at failure, including interpretation of the failure mechanisms, are discussed in Section 4.6. Finally, Section 4.7 presents the results of a comprehensive limit equilibrium study of the reinforced slope models that includes a parametric investigation of the variables that affect the stability of the reinforced slopes and an evaluation of the ability of the limit equilibrium technique to predict the experimental results.

The major objectives of this work were to investigate the failure mechanisms in geotextile-reinforced slopes and to evaluate the validity of limit equilibrium for their

failure. However, the overall aim for this centrifuge study is to address the underlying concepts and methods of analysis for reinforced soil slopes so that the testing of materials, the selection of material properties, and the choice of safety allowances can be placed within a single framework.

4.2 Centrifuge testing of reinforced soil structures

4.2.1 General

The stress dependent behavior of soils poses a problem when testing of small-scale geotechnical models is performed in the laboratory under a normal gravity field. In some cases, the use of appropriate surface loading can provide reasonable representation of the stresses created by body forces in a prototype structure. However, if body forces are to be properly represented a model of a total structure, it is necessary to turn to centrifuge testing.

Besides predicting the performance of prototype structures, which is not a goal pursued in this work, centrifuge testing can be performed for at least two other important purposes, both of which are of interest in this study:

- *The investigation of failure mechanisms*, in which the centrifuge is used as a tool to induce, in a model structure, levels of stress that are comparable to those usually found in prototypes. Such studies are often used to generate new kinematically admissible collapse mechanisms and new statically admissible stress distributions (Schofield, 1980; Mitchell et al., 1988); and

- *the validation of predictive tools*, in which the centrifuge is used to investigate the ability of numerical or analytical tools to predict the response of the small-scale model under prototype-like levels of stress (Shen et al., 1982; Liang et al., 1984). Simple geometries can be used in the models, and the analyses can incorporate the material properties, stress history, boundary loading conditions, and curved acceleration field that prevail in a centrifuge test.

As any experimental technique in geotechnical engineering, centrifuge testing does not reproduce exactly the conditions at which soil exists in an earth structure. This is due to the non-homogeneity and anisotropy of soil profiles, both in natural deposits and in man-made earth structures, and due to the limitations of the modeling tool. Some of the factors that cause differences between the behavior of model and prototype are:

- *Acceleration field in the centrifuge*, which is directly proportional to the radius of rotation in a centrifuge model. As a consequence, the resulting stress distribution is curved, and deviates from the linear distribution of stress in a real structure under 1 g earth gravity.
- *Stress paths in the model*, that are not necessarily identical to those of a structure built sequentially in the field. Compaction effects cannot be replicated as the model is constructed at 1 g prior to centrifuging. Moreover, while placement of a compacted soil layer induces deformations only on soil layers that have been built prior to that stage, the pre-constructed centrifuge model responds in its entirety as it is brought up to scale speed.

- *Boundary effects*, such as friction and adhesion between the walls of the model box and the soil, can affect the results of the tests designed to represent plane strain conditions. Solutions proposed to minimize the deviation from plane strain conditions include the use of wide models and/or treating the boundaries to minimize friction and adherence.
- *Scale effects*, caused by the relative size of sand grains between model and prototype, that may introduce a distortion in situations where either geotextiles or the soil no longer behave as a continuum. Apart from using scaled sand gradations, with the risk of changing the properties of the soil itself, experimental assessment of scale effects have been done by performing modeling of model tests. For example, early centrifuge studies verified that the width of a contact zone should be larger than about 15 particle diameters (Ovesen, 1975).

Although relevant for dynamic and seepage problems, other effects such as coriolis acceleration or time scaling, are not present in the centrifuge tests performed in this study. Identification of the effects listed above helps in the selection of model construction procedures that minimize their influence. More importantly, these effects can often be quantified and taken into account in the analytic tools used to evaluate the centrifuge test results.

4.2.2 Scaling laws

The principle of centrifuge modeling is based upon the requirement of similarity by model and prototype. If a model of the prototype structure is built with dimensions

reduced by a factor $1/N$, then an acceleration field of N times the acceleration caused by gravity g is required for the stresses in the model caused by self-weight to be the same as those of the prototype structure. The additional scaling relationships can be determined either by analysis of governing differential equations or by dimensional analysis and the theory of models.

The conditions for similarity in the problem under study, failure of reinforced soil slopes, can be obtained assuming the validity of limit equilibrium. In this case, similitude requirements should be established in order to guarantee that identical factors of safety are obtained in model and prototype structures. For simplicity, instead of adopting a more rigorous formulation, the limit equilibrium expressions stated below consider the Ordinary Method of Slices (Fellenius, 1936) in a reinforced cohesionless slope, that only satisfies equilibrium of moments for a circular failure surface. In this case, the Factor of Safety is calculated as:

$$FS = \frac{\sum \text{Moments resisting slope failure}}{\sum \text{Moments driving slope failure}} \quad (4.1)$$

For a prototype reinforced cohesionless slope, the factor of safety FS_p can be estimated as (Figure 4.1):

$$FS_p = \frac{\sum (A_i \cdot \rho \cdot g) \cos \theta_i \tan \phi R + \sum T_j Y_j}{\sum (A_i \cdot \rho \cdot g) \sin \theta_i R} \quad (4.2)$$

where:

$(A_i \cdot \rho \cdot g)$ = weight of slice i per unit length;

A_i = Area of slice i ;

ρ = Soil density;

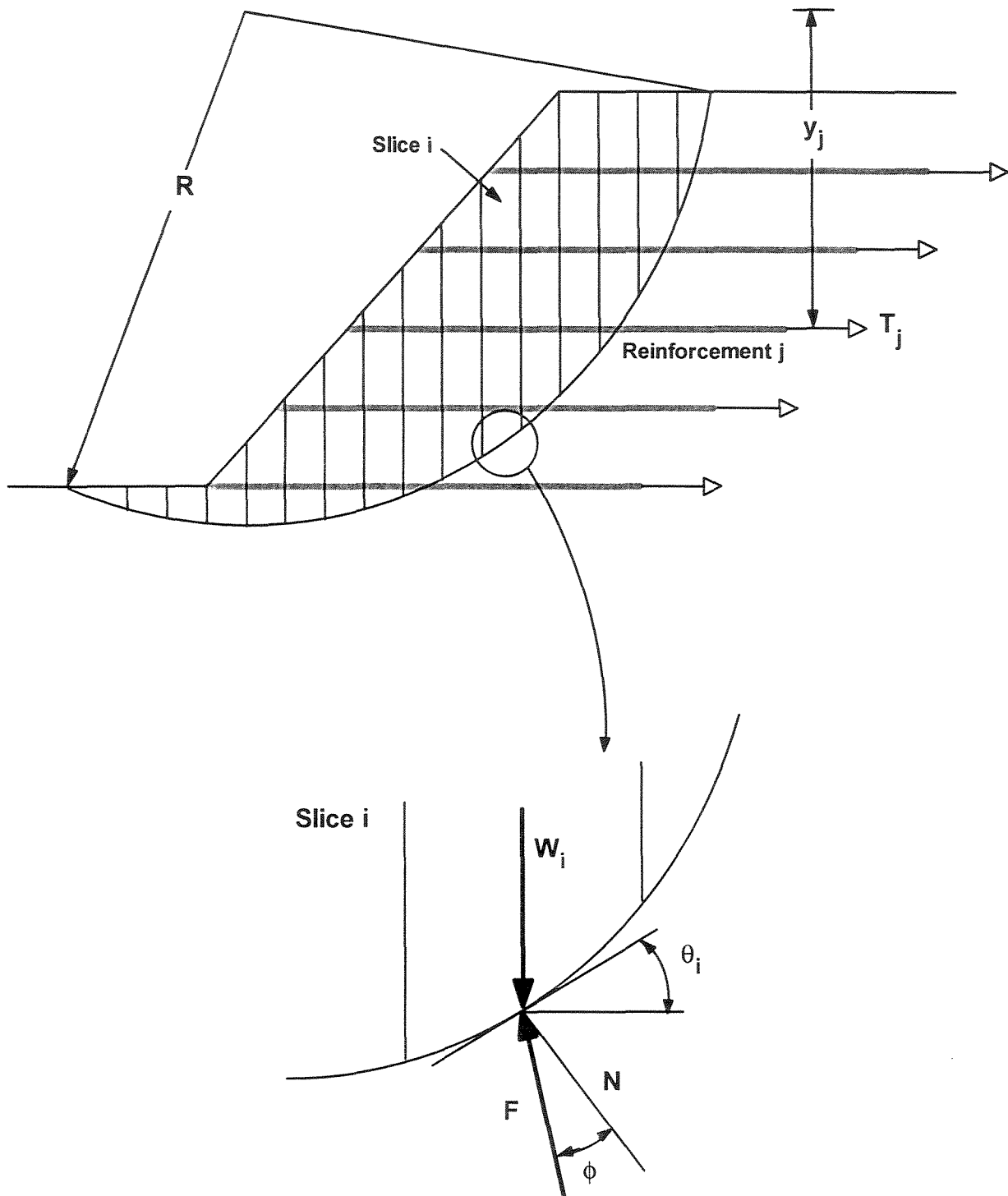


Figure 4.1: Limit equilibrium of a reinforced soil slope using a circular failure surface

g = Acceleration;

θ_i = Angle from horizontal to tangent at center of slice i ;

R = Radius of the failure circle;

ϕ = Soil friction angle;

T_j = Tensile strength of reinforcement j ;

y_j = Moment arm for reinforcement j

A similar expression can be written for the factor of safety FS_m of the slope model:

$$FS_m = \frac{\sum (A_{i_m} \cdot \rho_m \cdot g_m) \cos \theta_i \tan \phi_m R_m + \sum T_{j_m} Y_{j_m}}{\sum (A_{i_m} \cdot \rho_m \cdot g_m) \sin \theta_i R_m} \quad (4.3)$$

where the subscript m is for the model and no subscript designates the prototype. The following relationships exist between the model and prototype quantities:

$$A_{i_m} = (\alpha_L)^2 A_i \quad (4.4)$$

$$g_m = \alpha_g \cdot g \quad (4.5)$$

$$R_m = \alpha_L \cdot R \quad (4.6)$$

$$Y_{j_m} = \alpha_L \cdot Y_j \quad (4.7)$$

where α_L is the scale factor for the linear dimensions, and α_g is the scale factor for acceleration. Notice that a model built with a scale $\alpha_L=1/N$ requires that the acceleration caused by gravity be scaled by $\alpha_g=N$ in order to bring the model to prototype stress levels. Incorporating the expressions above into (4.3), the Factor of Safety for the model can be rewritten as:

$$FS_m = \frac{\sum (A_i \cdot \rho_m \cdot g) \cos \theta_i \tan \phi_m R + \sum \left(\frac{T_{jm}}{(\alpha_L)^2 \alpha_g} \right) Y_j}{\sum (A_i \cdot \rho_m \cdot g) \sin \theta_i R} \quad (4.8)$$

Since similarity between the failure responses of model and prototype requires that:

$$FS_m = FS_p \quad (4.9)$$

the scaling relationships for the analysis of reinforced soil slopes can then be established by comparing expressions (4.2) and (4.8). Consequently, the following similitude requirements should be satisfied in order to get same factors of safety in model and prototype slope:

$$\rho_m = \rho \quad (4.10)$$

$$\tan \phi_m = \tan \phi \quad (4.11)$$

$$T_{jm} = (\alpha_L)^2 \alpha_g T_j = (1/N)^2 N T_j = (1/N) T_j \quad (4.12)$$

Scaling requirements (4.10) and (4.11) establish that same soil density and soil friction angle should be used in model and prototype. They can be naturally satisfied by building the model using the same backfill soil used in the prototype structure. Condition (4.12) requires that the scaling factor α_T for the reinforcement tensile strength be equal to $1/N$. That is, an N th-scale reinforced slope model should be built using a planar reinforcement N times weaker than the prototype reinforcement elements.

Although the expressions (4.10), (4.11), and (4.12) govern the modeling of reinforced slope failures, other scaling relationships in geotechnical centrifuge modeling are based upon analysis of the governing differential equations. This approach has led to a list of relations partially shown in Table 4.1 (Scott and Morgan, 1977). Of particular

importance is the scale factor of unity for stress. Thus, the stress dependency of friction angle and dilatancy is accounted for by testing the model in a centrifuge.

Based on the general similitude conditions in Table 4.1, similitude requirements for the modeling of reinforced soil structures can be inferred. Table 4.2 summarizes the similitude conditions for soil, reinforcement, and interface parameters, which have been inferred from the general conditions in Table 4.1. These scaling relations assume that the same soil is used in model and prototype and that planar inclusions are used as reinforcement elements. Notice that the soil and reinforcement strength requirements are the same as those obtained specifically for the problem under study by assuming validity of limit equilibrium.

Scaling relationships for soil strength and soil stress-strain behavior in Table 4.2 result directly from the unity scale factors for stress and strains in Table 4.1. The scaling relationships for the case of planar reinforcements also stem from considering that stresses and strains in these elements should satisfy the unity scale factors $\alpha_\sigma=1$ and $\alpha_\epsilon=1$. However, ultimate tensile strength in planar reinforcement elements is not expressed as ultimate force per unit area (σ_{ult}), but as ultimate force per unit length (T_{ult}). This can be stated as:

$$T_{ult} = \sigma_{ult} \cdot t \quad (4.13)$$

where t is the thickness of the planar reinforcement.

Table 4.1 - Conventional scale factors for centrifuge modeling of static problems *

Quantity	<u>Model dimension</u> Prototype dimension
<i>For static events</i>	
Stress, σ	1
Strain, ϵ	1
Lenght, L	1/N
Mass, m	1/N ³
Density, ρ	1
Force, F	1/N ²
Gravity, g	N
<i>For dynamic events</i>	
Time	1/N
Frequency	N
Acceleration	N
Strain rate	N
<i>For diffusion events</i>	
Time	1/N ²
Strain rate	1/N ²

* Assuming that same soils are used in model and prototype

Table 4.2 - Scale factors for parameters used in the centrifuge modeling of reinforced soil structures

Quantity	<u>Model dimension</u> <u>Prototype dimension</u>
<i><u>Soil parameters</u></i>	
Strength parameters (c, ϕ)	1
Stress-strain behavior	1
<i><u>Reinforcement parameters</u></i>	
Tensile strength (T_{ult})	1/N *
Modulus (J)	1/N *
<i><u>Interface properties</u></i>	
Interface strength ($\tan \delta$)	1
Interface stress-strain behavior	1 †

* For the case of planar reinforcements (units for T_{ult} and J are: Force/Length).

† The scaling factor would be N if a shear stress-displacement relationship is considered to represent the actual interface behavior

Considering the scaling factors for σ_{ult} and t , we obtain that the scaling factor α_T for the tensile strength T_{ult} is:

$$\alpha_T = \alpha_\sigma \cdot \alpha_L = 1 \cdot 1/N = 1/N \quad (4.14)$$

Similarly, instead of considering the conventional Young modulus E (units: F/L^2), a stiffness parameter J (units: F/L) is used to characterize the deformability of planar reinforcements. The stiffness J can be defined as:

$$J = E \cdot t \quad (4.15)$$

which implies the following scaling relationship:

$$\alpha_J = \alpha_\sigma \cdot \alpha_L = 1 \cdot 1/N = 1/N \quad (4.16)$$

The constitutive behavior that a model reinforcement should have in order to satisfy all load-strain-strength scaling requirements is shown in Figure 4.2 . Notice that the tensile strength requirement of a geotextile model reinforcement could be satisfied by using the same prototype geotextile material with a thickness N times smaller.

The scaling relationships governing the interfaces between soil and reinforcements are also indicated in Table 4.2. These relationships can also be inferred from the general scaling laws for stresses and strains indicated in Table 4.1. Interfaces in model and prototype should have the same interface strength parameters, as deduced from considering $\alpha_\sigma=1$. However, the scaling requirements that should be adopted to properly model the interface stress-strain behavior are not without controversy. If the behavior of the soil reinforcement interfaces is characterized by a shear stress-shear *strain* relationship, the scale factor of unity indicated in Table 4.2 is inferred so that $\alpha_\sigma=1$ and $\alpha_\epsilon=1$ are satisfied along the interfaces. However, if the behavior of the soil

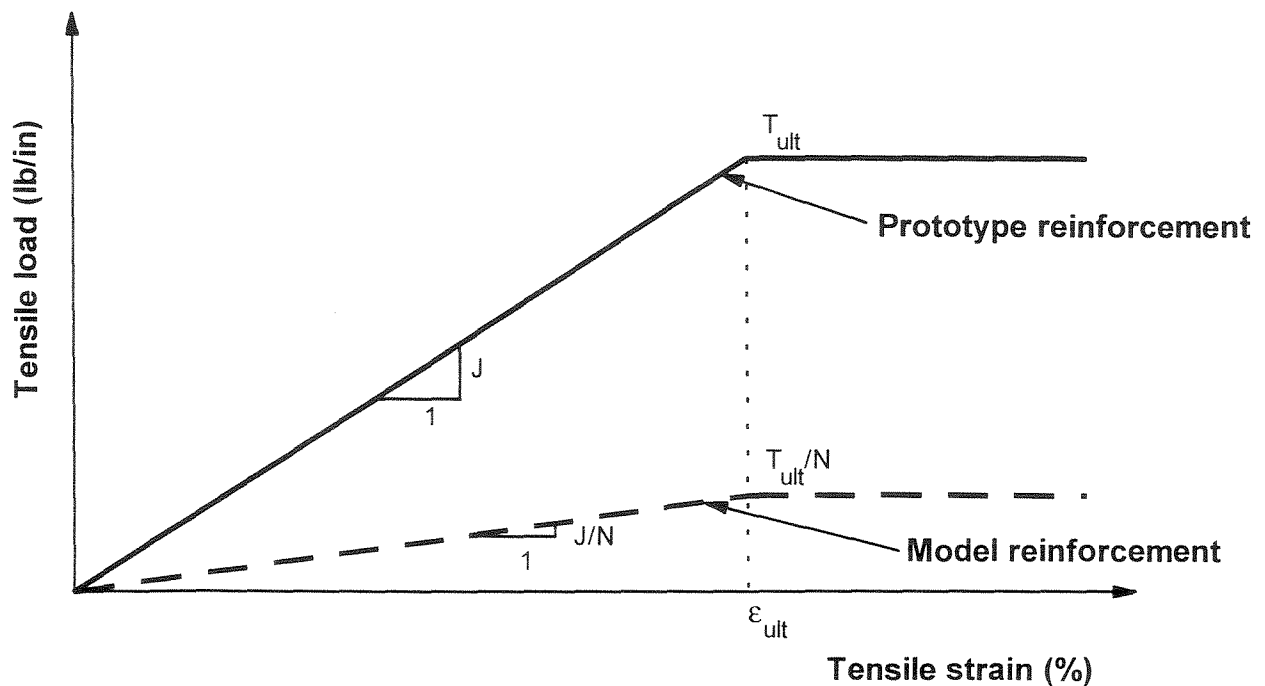


Figure 4.2 - Scaling requirements between model and prototype reinforcements

reinforcement interface is characterized by a shear stress-shear *displacement* relationship (Blivet et al., 1986), the soil-reinforcement interfaces in the model should be stiffer (N times) than the interfaces in the prototype structure.

4.2.3 Previous centrifuge studies on reinforced soil structures

Experimental studies have been performed on geotechnical centrifuges to investigate the behavior of reinforced soil structures. A summary of the main aspects of these previous centrifuge studies is listed in Table 4.3, and an overview of their characteristics and main findings is presented herein.

Bolton et al. (1978) and Bolton and Pang (1982) performed a large number of centrifuge tests on model walls in which metallic strips and rods, and foil or plate facings, were used to support dense dry sand. They suggested a "simple anchor theory" for design

Table 4.3 - Previous centrifuge studies on the performance of reinforced soil structures

Structure	Reinforcement type	Height (mm)	Centrifuge location	Analytic method used for prediction of failure	Reference
Reinforced walls	Metallic strips and rods	200	Manchester, U.K.	Simple anchor method	Bolton et al., 1978
Soil nailed walls	Nails	150	U.C. Davis	Limit equilibrium of nailed wall	Shen et al., 1982
Reinforced walls	Metallic strips and rods	200	Manchester, U.K.	Simple anchor method	Bolton & Pang, 1982
Reinforced walls	Nonwoven geotextile	600	LCPC, France	Models did not reach failure	Blivet et al., 1986; Matichard et al., 1988
Reinforced walls	Aluminum foil; plastic strips; nonwoven; plastic grids	150	U.C. Davis	Tie-back type analysis	Mitchell et al., 1988; Jaber, 1989
Reinforced walls and slopes	Nonwoven geotextile	100	Tsukuba, Japan	Simplified stability analysis (Fellenius)	Taniguchi et al., 1988
Embankments on soft ground	Nonwoven geotextile	up to 48	Yokosuka, Japan	Simplified stability analyses (Fellenius)	Terashi & Kitazume, 1988
Reinforced walls	Aluminum foil strips	144; 80	Maryland	Dimensionless safety index	Goodings & Santamarina, 1989
Reinforced walls	Steel strips, steel mesh, geogrid, nonwoven	500	U.C. Davis	Models did not reach failure	Jaber et al., 1990; Jaber, 1989
Reinforced wall	Aluminum strips	500	U.C. Davis	Global safety against reinforcement rupture	Jaber & Mitchell, 1990; Jaber, 1989
Reinforced walls	Nonwoven geotextile	114 to 191	Maryland	Failure prediction not reported	Goodings, 1990

Table 4.3 (Cont.)

Structure	Reinforcement type	Height (mm)	Centrifuge location	Analytic method used for prediction of failure	Reference
Reinforced walls	Wire mat	150	U.C. Davis	Yield acceleration of sliding block (seismic study)	Kutter et al., 1990; Casey et al., 1991
Anchored walls	Steel anchors	280	Manchester, U.K.	Pullout capacity of anchors	Craig et al., 1991
Embankments on soft ground	Geotextile	100	China	Semi-empirical bearing capacity	Liu et al., 1991
Reinforced walls	Aluminum strips	200	Boulder	Tie-back type analyses	Yoo & Ko, 1991
Reinforced walls	Steel strip	300	RPI	Failure prediction not reported	Ragheb & Elgamal, 1991
Reinforced wall	Woven geotextile	240	China	Model did not reach failure	Shi & Sun, 1992
Reinforced walls	Nonwoven geotextile	190	Maryland	Failure prediction not reported	Güler & Goodings, 1992
Reinforced walls and slopes	Geogrid?	150	Japan	Stability analysis using planar surface	Abe et al., 1992
Reinforced walls	Nonwoven geotextile	550	LCPC, Nantes	Failure prediction not reported	Matichard et al., 1992a; 1992b
Reinforced walls	Nonwoven geotextile	590	Boulder	Failure prediction not reported	Law et al., 1992
Soil nailed walls	Nails	152	RPI	Seismic study	Tufenkjian & Vucetic, 1992
Reinforced walls and slopes	Nonwoven geotextile	152	Maryland	Failure prediction not reported	Porbaha & Goodings, 1994
Soil nailed walls	Nails	up to 150	Israel	Pullout capacity of nails	Frydman et al., 1994
Reinforced walls	Woven geotextile	150	Cambridge, U.K.	Failure prediction not reported	Springman & Balachandran, 1994
Embankments on soft clay	Geotextile, geogrid	≈150	Cambridge, U.K.	Models did not reach failure	Bolton & Sharma, 1994

of reinforced soil walls based on active pressures exerted on the facing area attributable to a strip, wherein the vertical stresses used to compute the active pressures included a contribution from the overturning effect of the backfill. Their main conclusions were that the distribution of vertical stress under the reinforced soil mass was close to being uniform, and that the use of the active earth pressure coefficient to estimate failure accelerations underestimated the capacity of the model walls.

Centrifuge tests at the LCPC (Nantes, France) were performed on 600 mm high geotextile-reinforced walls with five or six layers of reinforcement, tested at 15 g to represent a 9 m high prototype (Matichard et al., 1988; Blivet et al., 1986). A vertical surcharge was applied in-flight in order to investigate the performance of bridge abutments. Up to 10% strain was recorded in one test, but rupture was not achieved.

Numerous centrifuge tests were performed using the geotechnical centrifuge at U.C. Davis to investigate the performance of reinforced soil model walls at failure (Mitchell et al., 1988; Jaber, 1989). An extensive parametric study investigated the effects of reinforcement extensibility, type of facing, compressibility of foundation, creep of geotextile reinforcement, and surface loading. Orientation of the initial failure surface was observed not to be affected by the type of reinforcement. It was concluded that current design procedures for reinforced soil walls may be conservative since the centrifugal accelerations at which rupture failures occurred were up to twice the values computed based on the assumption of Rankine active pressures developing in the soil mass.

Most centrifuge studies on reinforced soil structures have concentrated on parametric studies and validation of design methods without comparing their results to the

behavior of actual prototypes. An exception is the study presented by Jaber et al. (1990) that compared the stresses and displacements of four centrifuge models to those measured on four similar full-scale soil walls. The 500 mm high models were tested at 12 g on the large beam centrifuge at U.C. Davis. A variety of reinforcement types was used, including bar mats, steel strips, geogrids, and nonwoven geotextiles, each instrumented with strain gauges. Reinforcement tensions showed a good agreement between models and prototypes, lending credibility to the centrifuge modeling technique for the study of reinforced soil structures. The outward movements in the centrifuge models were smaller than those observed in the corresponding prototypes.

In addition, a wall model reinforced with aluminum strips was specifically underdesigned so as to collapse (Jaber and Mitchell, 1990). The stresses measured in the reinforcements seemed to indicate that significant stress redistribution occurred within the wall near failure, which may explain the over conservatism of currently used design methods for reinforced walls. A simple design approach for internal stability based on a global factor of safety against reinforcement rupture was proposed, which accounts for stress redistribution within the wall. This approach was able to correctly predict the failure of reinforced soil model walls described by Mitchell et al. (1988).

Several studies were performed at the University of Maryland to evaluate the effect of backfill characteristics and foundation soils on the performance of reinforced soil structures. Goodings and Santamarina (1989) examined the effect of foundation soil and retained fill on the behavior of reinforced soil walls using centrifuge modeling. They observed that the effect of the retained soil on the overall stability of the walls was small, and that soft foundations led to superior wall performance. The behavior of geotextile-

reinforced walls using cohesive backfill soil, instead of conventional granular material was investigated by Goodings (1990). She concluded that cohesive soils can be successfully used to construct reinforced walls, and that failure of the reinforced soil models was always by geotextile breakage and never by pullout. Porbaha and Goodings (1994) reported results from additional tests, performed to investigate geotextile-reinforced walls and slopes using cohesive backfill founded on weak soils. They found that longer reinforcement improved the structure performance, and that excessive deformations or failure were caused by geotextile rupture or straining without evidences of pullout. Also using centrifuge modeling, Güler and Goodings (1992) investigated the use of lime stabilization to improve the properties of clayey backfills. The use of lime was found to substantially improve wall stability even when geotextile length was equal to only one half of wall height.

A number of the studies summarized in Table 4.3 focused on the performance of reinforced soil structures in which deformations or failure were triggered by mechanisms other than selfweight. Among them, Taniguchi et al. (1988) investigated the performance of reinforced soil models that were either tilted in order to simulate lateral acceleration in an earthquake, or subjected to a surcharge loading applied behind the wall crest. Smaller displacements were observed for models with increasing reinforcement length. The performance of bar mat reinforced walls subject to seismic excitations was investigated by Kutter et al. (1990) and Casey et al. (1991). Yield accelerations deduced from the experimental results were found to be lower than those determined from conventional sliding block models.

Ragheb and Elgamal (1991) investigated the effect of deteriorated metallic strip reinforcements on the performance of reinforced soil walls. They found that a strong interlocking in the facing panels attached to compromised strips was effective in delaying or even preventing wall failure. The performance of a series of model walls reinforced with metallic strips subjected to self weight loading and to vertical surcharge to simulate bridge abutments was reported by Yoo and Ko (1991). A series of 1/5 scale reinforced wall models were brought to failure by applying increasing surcharge (Law et al., 1992). Results were obtained for comparison with the collapse load of a full-scale prototype loaded to failure. Matichard et al. (1992a, 1992b) reported centrifuge results on the behavior of a geotextile-reinforced abutment loaded on top until failure. The data showed a qualitative agreement with the results from a full-scale prototype test, in which failure occurred by breakage of the upper geotextile reinforcements and pullout of the top layer. Springman and Balachandran (1994) investigated the behavior of two model walls, reinforced using woven geotextiles, and loaded with a strip surcharge. Maximum tension in the reinforcements under working stress conditions agreed with predicted values.

For completeness, Table 4.3 also includes information on centrifuge studies done to investigate the performance of soil nailed walls (Shen et al., 1982; Tufenkjian and Vucetic, 1992; Frydman et al., 1994), anchored walls (Craig et al., 1991), and embankments over soft foundations (Terashi and Kitazume, 1988; Liu et al., 1991; Bolton and Sharma, 1994).

Two main observations can be drawn from the evaluation of previous centrifuge studies on the performance of reinforced soil structures, and summarized in Table 4.3: (1) that the majority of previous works focused on the performance of vertically faced

reinforced walls; and (2) that limit equilibrium approaches have rarely been used to predict the failure of the centrifuge models.

Several of the previous studies did not focus specifically on validating analytic tools for prediction of failure. Some of them performed comparative evaluations on the relevance of different design variables on the g -level at failure (e.g., Santamarina and Goodings, 1989); while others investigated the performance of models at working stress conditions without reaching failure (e.g., Jaber et al., 1990). However, among those studies in which observed failure conditions were used to validate analytical tools, the methods generally used were tie-back like semi-empirical procedures currently used for reinforced wall design (e.g., Bolton and Pang, 1982; Mitchell et al., 1988). However, the working stress design methods used for reinforced wall design are not generally used for design of reinforced soil slopes, which is generally based on limit equilibrium approaches. There is consequently a lack of centrifuge experimental data suitable for validating design procedures for reinforced soil slopes.

4.3 Description of the centrifuge testing scheme

All reinforced slope models had the same geometry and were built within the same strong box. The models were subjected to a gradually increasing centrifugal acceleration until failure occurred. Details of the geotechnical centrifuge, model characteristics, model construction, measurements, and testing procedures are presented in this section.

4.3.1 Geotechnical centrifuge

The centrifuge tests were performed using the Schaevitz type B-8-D rotary accelerator at the University of California at Davis. This centrifuge is designed to apply controlled centrifugal accelerations up to 175 g and has a limit of 4,500 g-kg at a nominal radius of 100 cm. The payload of the testing package can be as heavy as 45 kg. The centrifuge, capable of reaching a maximum speed of 390 rpm, is enclosed in a protective shell. Sixteen electrical channels are available to send power and to receive signals from transducers which monitor behavior of the models. The models were placed on a swing-up bucket, so that the soil surface remains always perpendicular to the direction of acceleration. For safety reasons, strict operation procedures including both static and dynamic balancing of the rotating arm is enforced. A general view of the centrifuge is shown in Figure 4.3.

4.3.2 Characteristics of the reinforced slope models

A strong box with inside dimensions of 419 mm x 203 mm in plan x 300 mm in height (16.5 in x 8 in x 11.75 in) was used to contain the model. The same box has been previously used by Jaber (1989) in his centrifuge study on the performance of reinforced soil walls. A transparent plexiglass plate was used as one of the side walls of the box to enable side viewing of the model during testing. The other walls of the box were aluminum plates lined with teflon to minimize side friction. The plexiglass was lined with a mylar sheet overprinted with a square grid pattern, which was used as a reference frame for monitoring displacements within the backfill. In order to prevent scratches and to minimize side friction, a second mylar sheet was placed over the one with square grid

pattern. A view of the strong box is shown in Figure 4.4. The box was sufficiently rigid to maintain plane strain conditions in the model (Liang et al., 1984).

All models were built with a total height of 254 mm (10 in). They consisted of 228 mm (9 in) high geotextile-reinforced slopes built on a 25 mm (1 in) thick foundation layer. The slope in all models was 1H:2V, and air dried Monterey No.30 sand was used both as backfill material and foundation soil. The sand was pluviated through air under controlled conditions to give uniform backfill relative densities of 55% and 75%. Sand was pluviated in excess at the level of each reinforcement layer, which was subsequently vacuumed to achieve the target backfill level. A denser foundation layer was reached by vibratory compaction. The overall dimensions of the geotextile-reinforced slope models are given as shown in Figure 4.5 for the case of a model with nine reinforcement layers. The location of the displacement transducers is also indicated in the figure. A temporary wooden support, shaped to give a 1H:2V slope was used to provide support during construction.

The number of reinforcement layers in the models varied from six to eighteen, giving reinforcement spacings from 37.5 mm (1.5 in) to 12.5 mm (0.5 in). All models were built using the same reinforcement length of 203 mm (8 in). The use of a reasonably long reinforcement length was deliberate, since this study focused on the evaluation of internal stability against breakage of the geotextile reinforcements. By selecting long enough geotextile reinforcements, external or compound failure surfaces were expected not to develop during testing. The geotextile layers were wrapped at the slope face in all models. Current design procedures (Christopher et al., 1990) recommend a minimum overlap length of 1.2 m (4 ft). All models but one (B12) were built using a

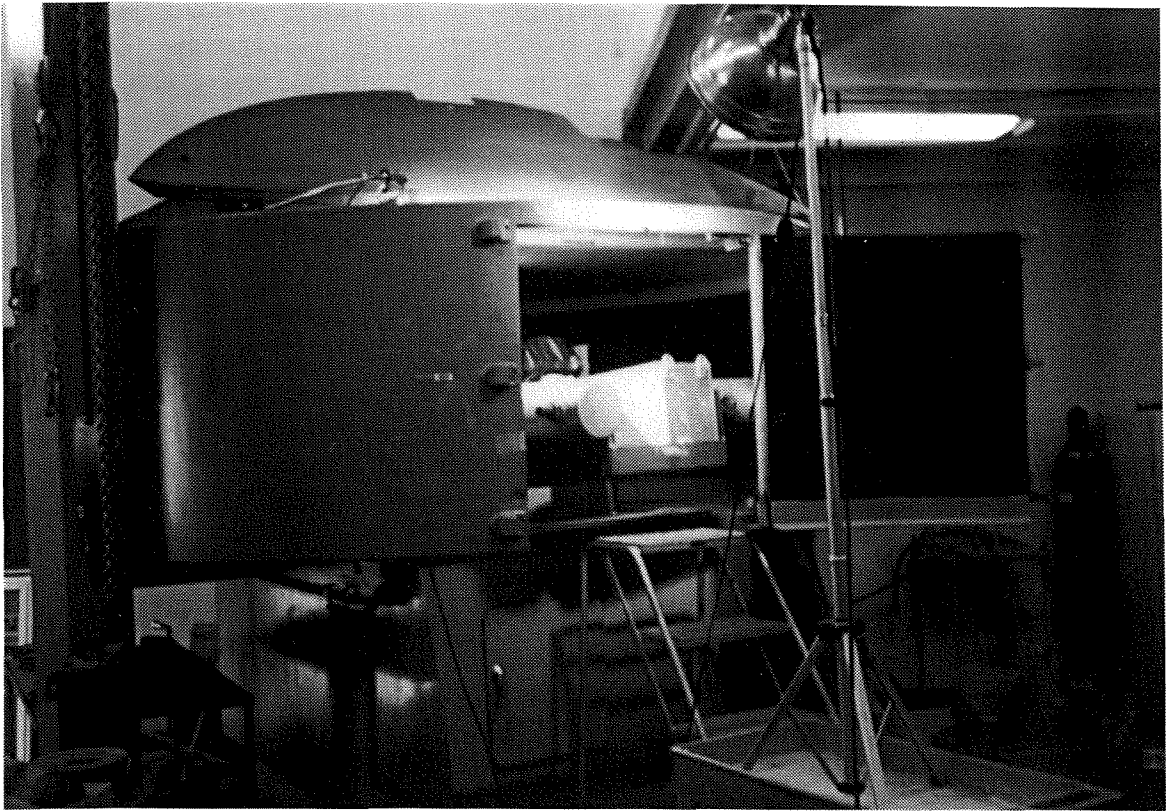


Figure 4.3 - View of the Schaevitz geotechnical centrifuge

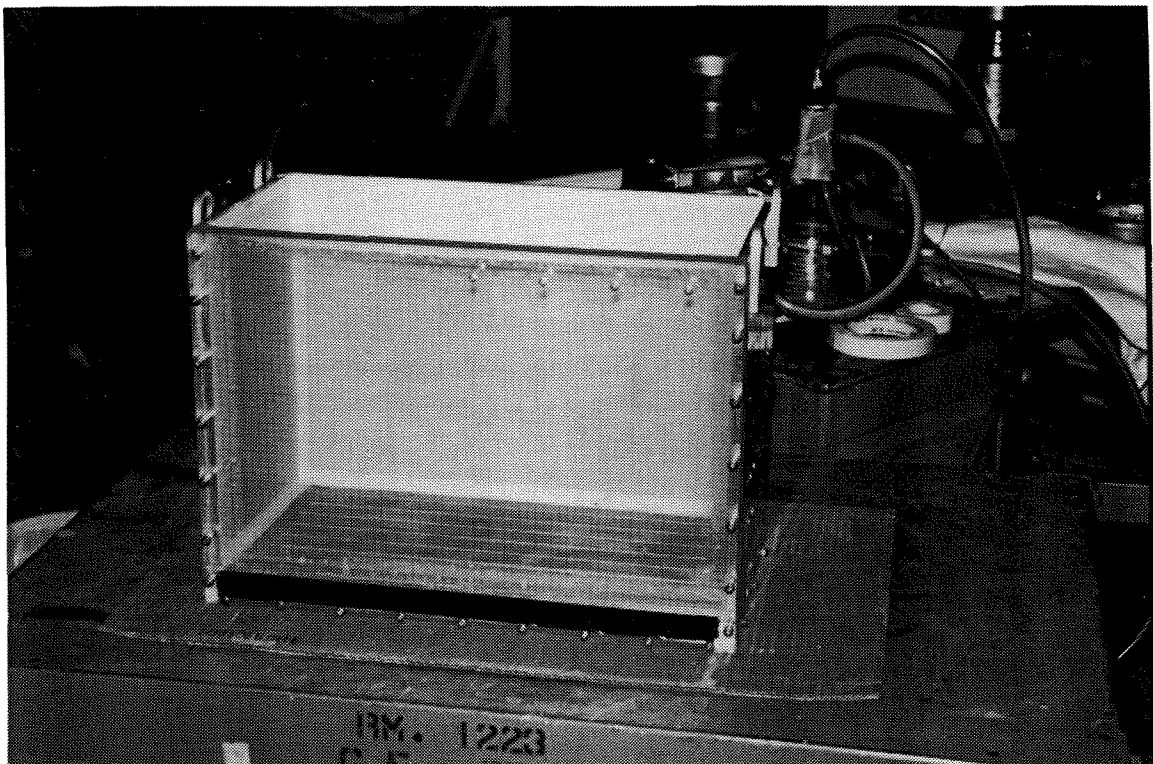


Figure 4.4 - Strong box used to house the centrifuge slope models

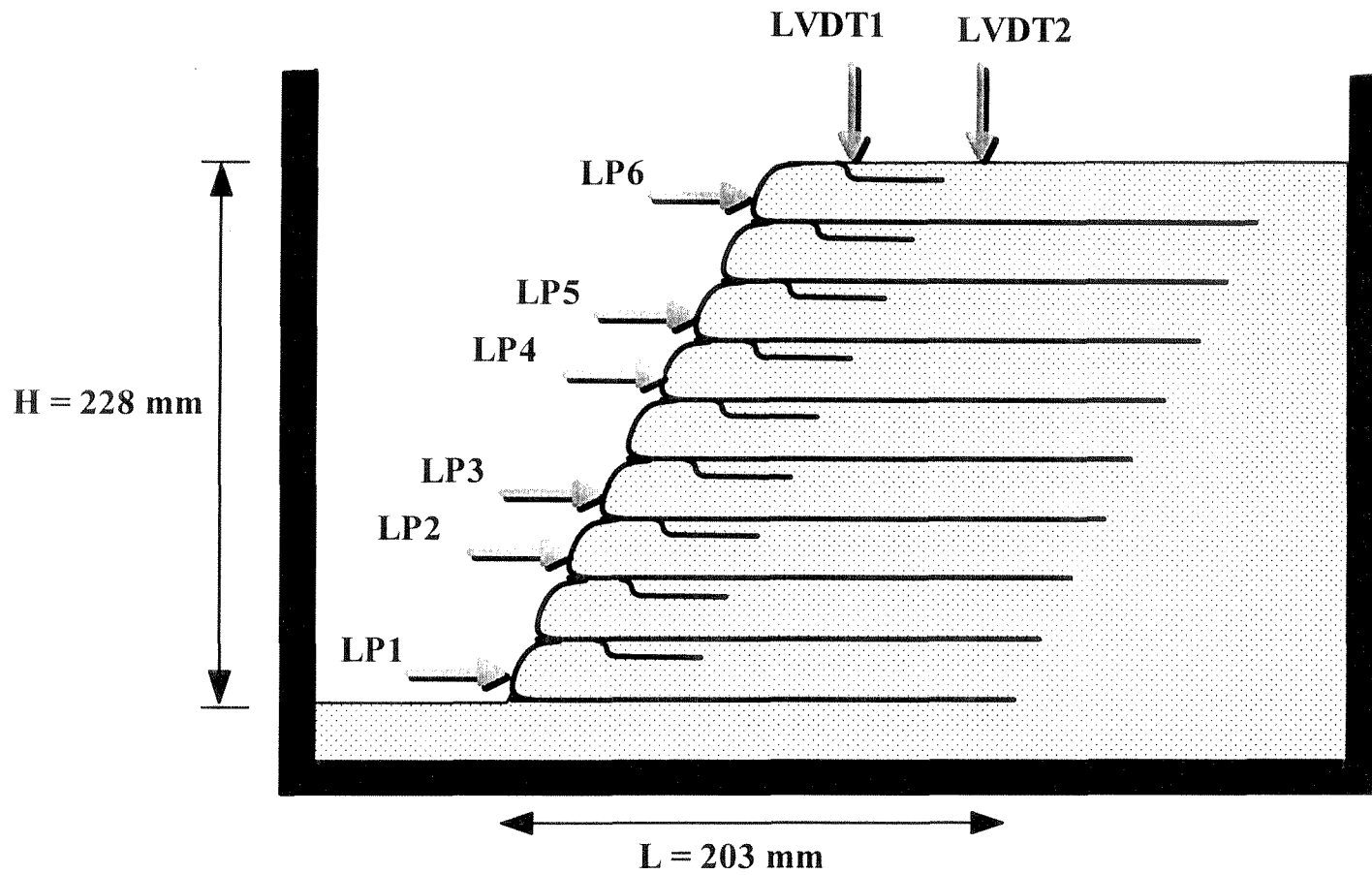


Figure 4.5 - Centrifuge model with 2.5 cm reinforcement spacing

50 mm (2 in) long geotextile overlap, which satisfied the minimum overlap requirements for a prototype structure at g-levels higher than $N=24$. Model B12 was built using overlaps 2.5 in long.

Green colored sand was placed along the plexiglass wall at each level of geotextile reinforcements in order to better identify the location of the potential failure surface. Moreover, black colored sand markers were placed at a regular horizontal spacing (25 mm) in order to monitor lateral displacements within the backfill material.

4.3.3 Construction of the models

In order to guarantee consistent soil densities and placement conditions in the reinforced soil models, carefully controlled construction procedures were followed during model preparation. The models were constructed as follows:

- The 25 mm thick sand foundation layer was placed and compacted dynamically to achieve high density in the foundation material (Figure 4.6).
- Fabrics were cut using cardboard molds. Figure 4.7 shows a fabric layer ready for placement. Lateral flaps were used at the slope face in order to prevent lateral sloughing of the sand during testing. Marks were placed every 12.5 mm along the centerline of each geotextile reinforcement in order to monitor permanent deformations on the fabrics after testing.
- The temporary wooden support with height equivalent to the vertical reinforcement spacing was used during the construction of each layer to provide support during construction.



Figure 4.6 - Dynamic compaction of foundation layer during construction of a reinforced slope model

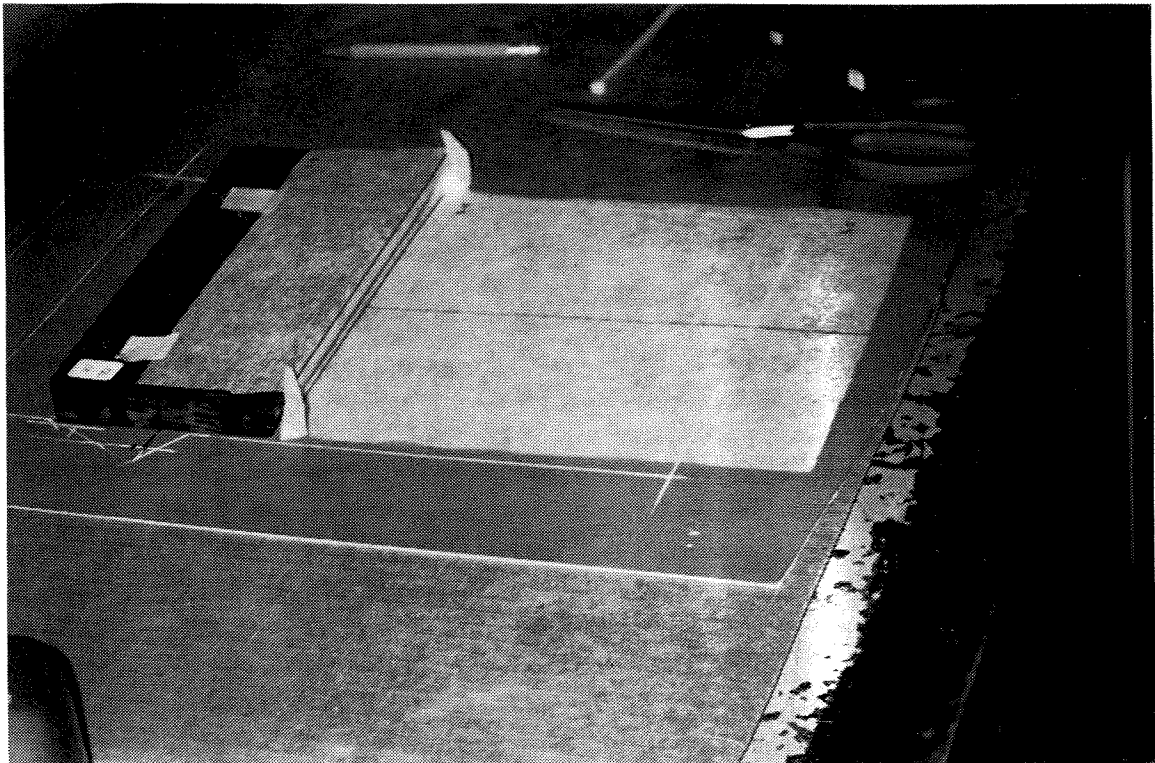


Figure 4.7 - View of a geotextile reinforcement ready for placement

- The geotextile layer was aligned on the levelled backfill surface (Figure 4.8), and geotextile facing and overlap were temporarily attached to the wooden support.
- Green colored sand was placed at the surface along the plexiglass wall to help identify the location of the failure surface during the tests. Moreover, black colored sand markers were placed at a regular spacing (25 mm) in order to monitor lateral displacements on the backfill material.
- Sand was pluviated using a pvc tube using controlled discharge rate and discharge height in order to achieve the target density. The pluviation tube was raised after placement of each sand layer in order to maintain a constant height of sand discharge. A calibrated support and a metallic frame were used for this purpose. Relative densities of 55% and 75% were achieved by pluviating from heights of 62.5 mm and 125 mm respectively. Figure 4.9 shows the pluviation process during placement of the third sand layer for model S9.
- Excess sand was vacuumed in order to reach the target backfill height. Figure 4.10 shows the vacuuming process. The vacuum pressure and the height of the vacuum tube were calibrated to achieve the target height at each reinforcement level. After the target level had been achieved, a ditch was carefully vacuumed parallel to the slope face in order to embed the geotextile overlaps.
- The geotextile overlaps were detached from the wooden support, folded, and placed over the vacuumed ditch. Sand was subsequently pluviated over the geotextile overlap length. Vacuum was used again in order to achieve the target backfill level at the location of the geotextile overlap. Figure 4.11 shows a view of model S9 after placement of the third geotextile reinforcement layer.

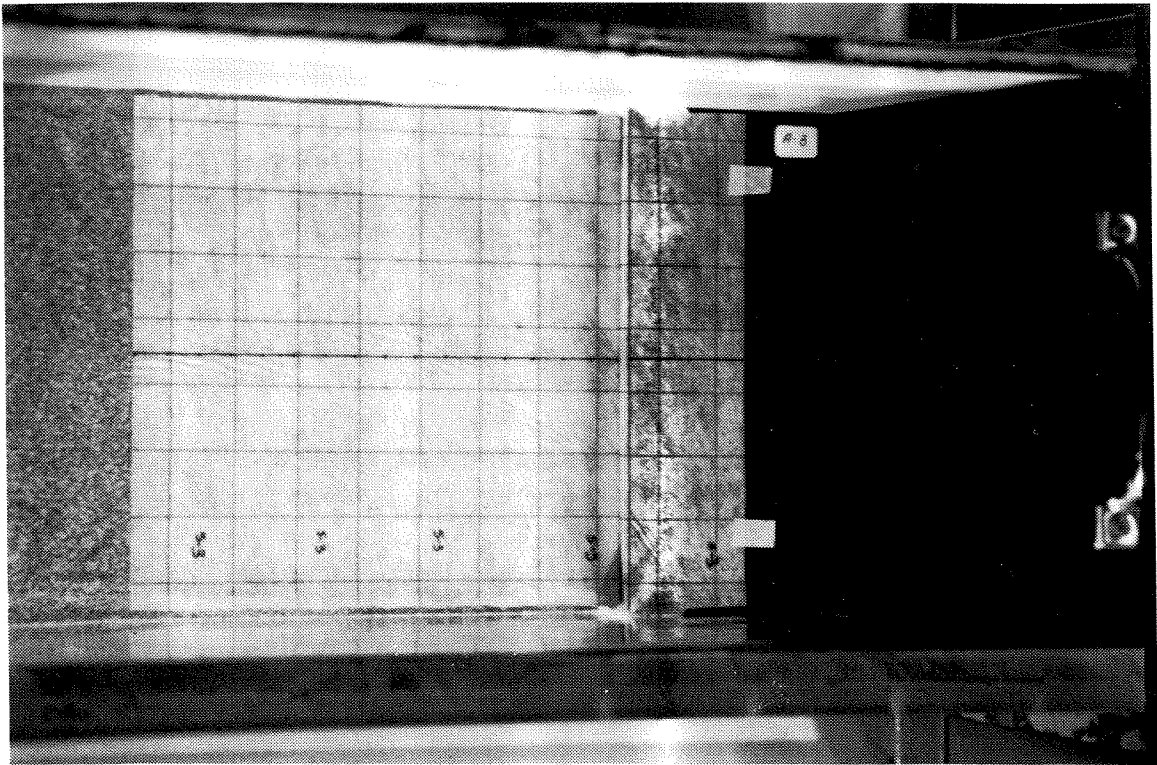


Figure 4.8 - Lining of the geotextile layer over levelled surface of backfill material

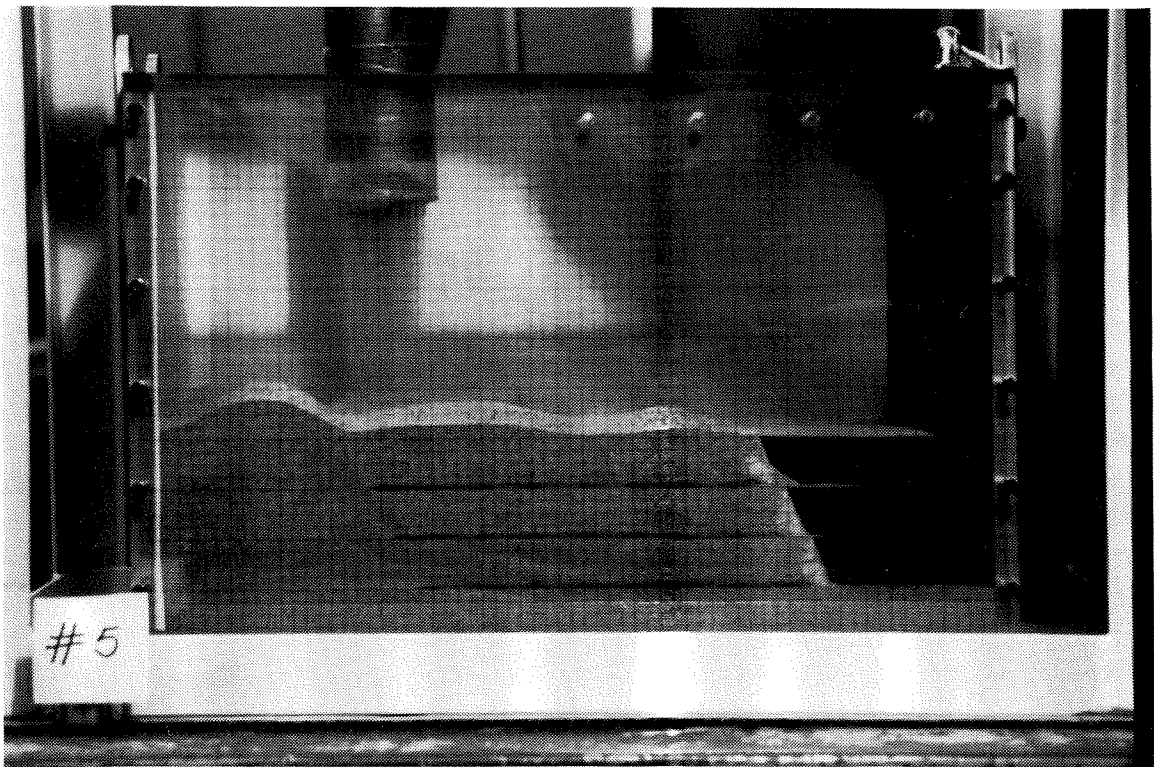


Figure 4.9 - Placement of the third sand layer during construction of model S9. Dry pluviation was used to achieve the target density

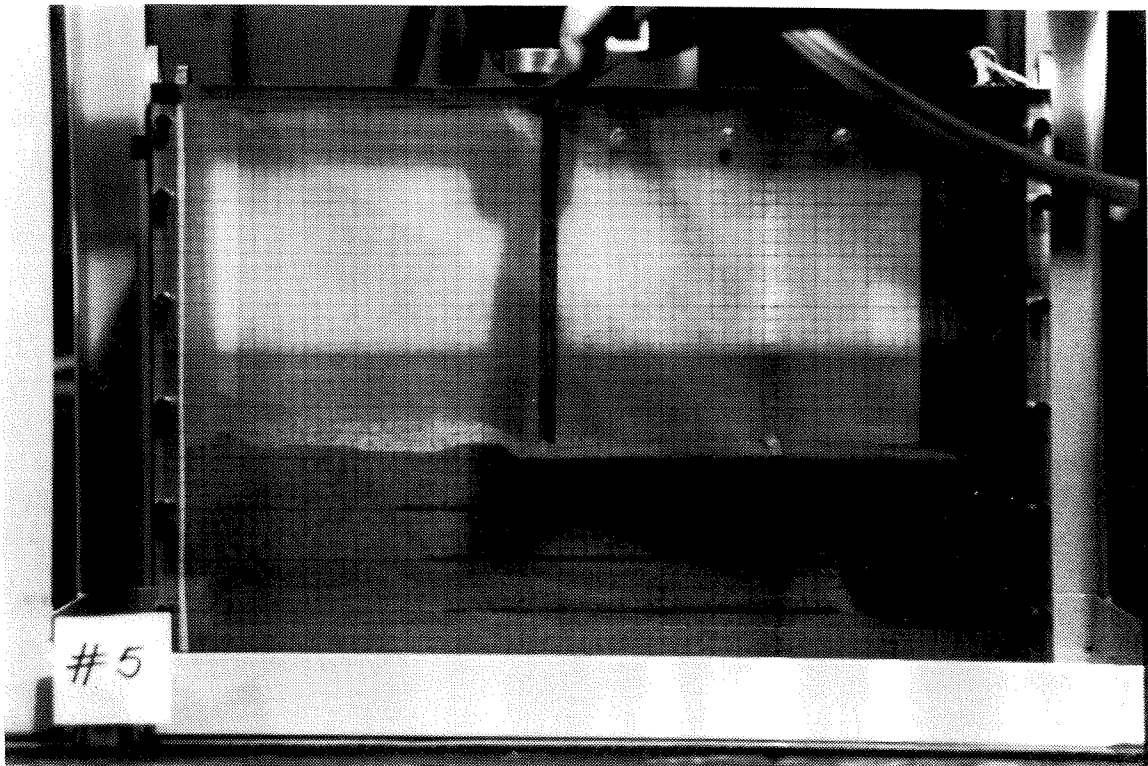


Figure 4.10 - Use of vacuum to level recently pluviated sand

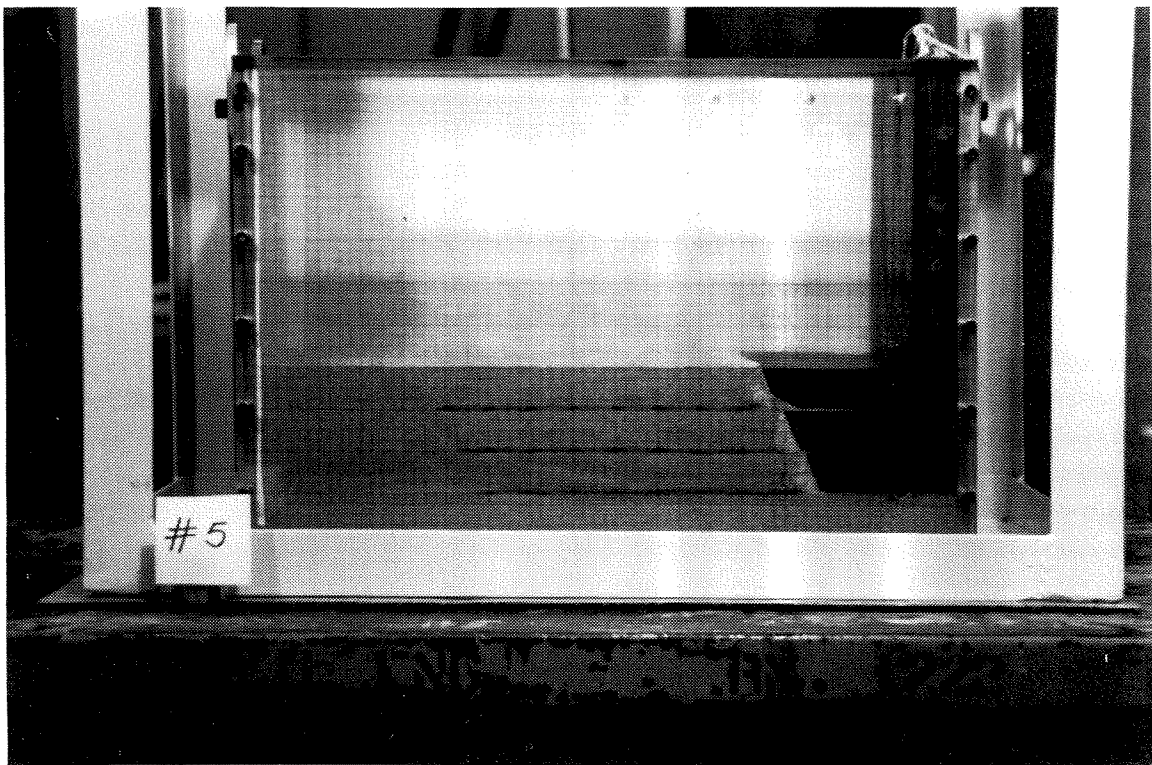


Figure 4.11 - View of model S9 after the third sand layer has been placed. Geotextile has been wrapped around and the overlap length has been embedded

- The next layer of reinforcement was lowered into place and the procedure was repeated until completion of the reinforced slope model.

Figure 4.12 shows a view of model S9 after completion of the construction process. The wooden mold supports which are still in place were removed after placement of the model in the centrifuge bucket.

4.3.4 Measurements

Sixteen electrical channels were available at the geotechnical centrifuge to send power and receive signals from transducers which monitor the behavior of the model.

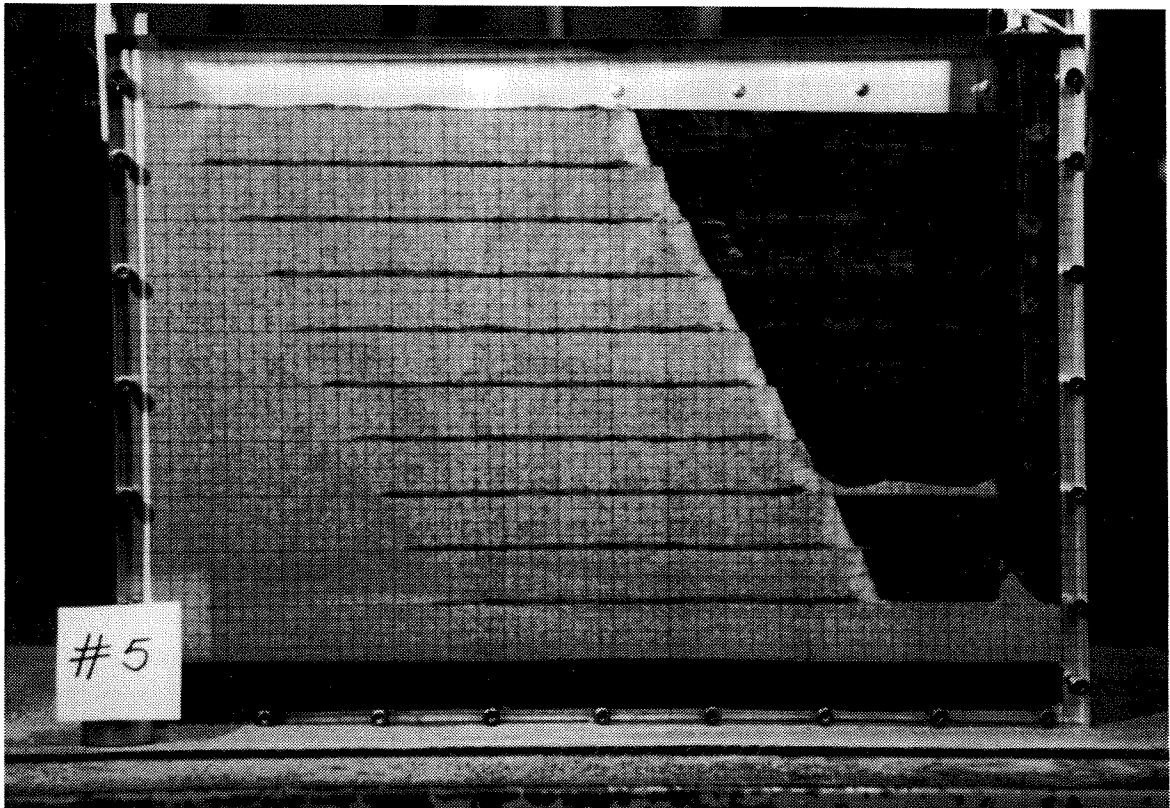


Figure 4.12 - Model S9, still with wooden supports in place, after completion of the construction process

Both electrical signals and hydraulic services are transmitted to the centrifuge rotor and then to the model in-flight through a stack of slip rings.

Six linear potentiometers were used to monitor the lateral displacements of the slope face. The linear potentiometers were supported by an aluminum plate, as shown in Figure 4.13 . The location of the linear potentiometers was adjusted for each model so that they were always placed at midheight between two reinforcement layers. Two linear variable displacement transducers (LVDTs) were used to monitor vertical settlement at the crest of the geotextile-reinforced models. They were located 12.7 mm and 63.5 mm, respectively, from the crest of the geotextile-reinforced slopes. As discussed in Section 4.6.4.1, readings from these transducers proved very useful to accurately identify the moment of failure of the centrifuge models. One electrical channel was additionally used to record directly the angular velocity (rpm) during centrifuge testing. Due to the small size of the model walls, internal instrumentation could not be included to monitor all relevant quantities at working stress levels. It was, for example, impossible to instrument the reinforcing layers due to their small width and fragility.

A television camera and video recording device were used as an additional monitoring system. The television camera was mounted on the center of the rotating structure of the centrifuge. This system provided not only a continuous and instantaneous monitoring of the tests while it was in progress, but also a permanent record of the model tests. A 45° mirror was used to view the model in-flight through the plexiglass side wall. The recorded images were used to examine the initiation of failure and to identify the probable failure mechanisms. Figure 4.14 shows a view of the centrifuge arm showing the TV camera, slant mirror, and slope model already placed in the bucket.

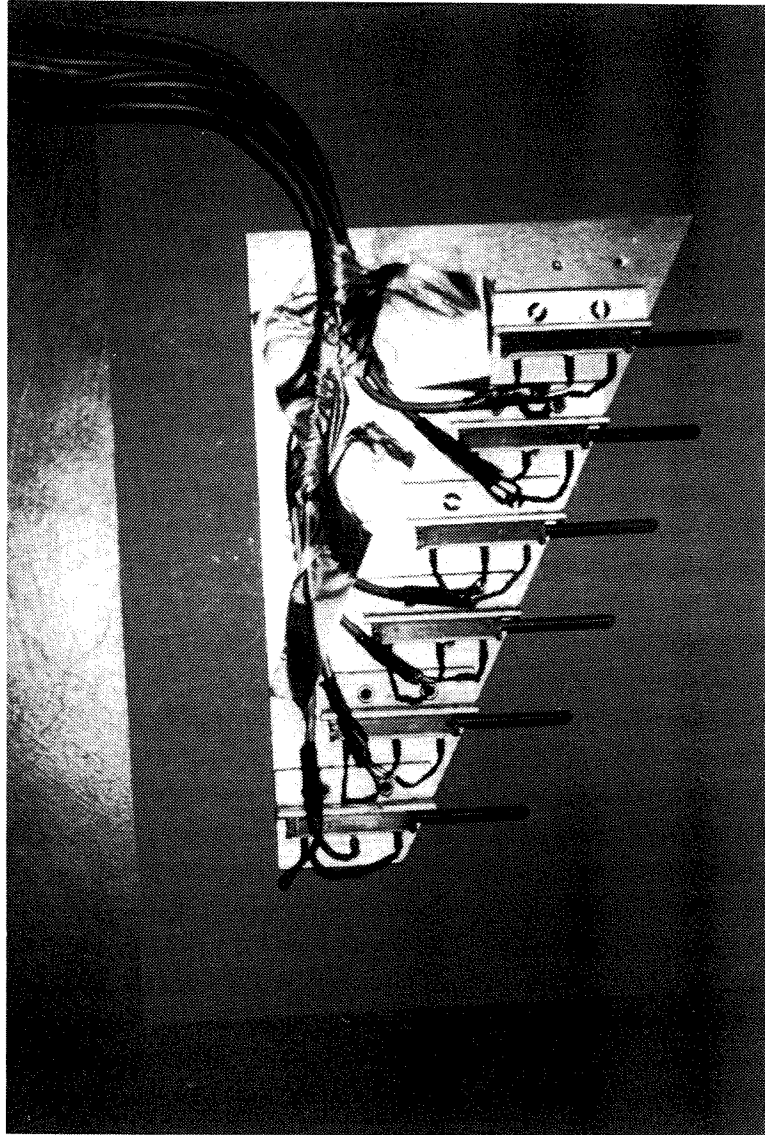


Figure 4.13 - Plate holding the linear potentiometers used for monitoring lateral face displacements

Model displacement under increasing g-level loadings can be retrieved after image processing of the video tape records of the different tests. The black colored sand markers were carefully matched during construction with the corners of the square grid. The movement of the markers under different g-levels can be used to determine the displacement and strain distributions within the reinforced soil mass.

4.3.5 Test procedure

After construction, the reinforced slope models were weighted and placed in the swing bucket of the centrifuge. The temporary support molds were removed, and both static and dynamic balancing of the rotating arm was performed. The 45° inclined mirror was placed adjacent to the plexiglass so that the model could be observed in-flight by the closed circuit TV camera. Figure 4.15 shows a view of model B12 already placed in the swing bucket. The figure shows a top view of the reinforced soil model and its image through the slant mirror before placement of the displacement transducers. As the arm of the centrifuge spun, the buckets supported by hinged pins swung upward so that the top surface of the model was almost perpendicular to the plane of rotation.

The models were subjected to a gradually increasing centrifugal acceleration until failure occurred. Acceleration levels were increased by 5 g-level increments during the initial stages and by approximately 2 g-level increments in the final stages of the test. After reaching each acceleration level, the model was held at a constant acceleration for approximately two minutes to allow equalization of the load. As the model deformed, the black colored markers moved with the adjacent soil. Since these markers were originally matched with the corners of the square grid, their movement under increasing

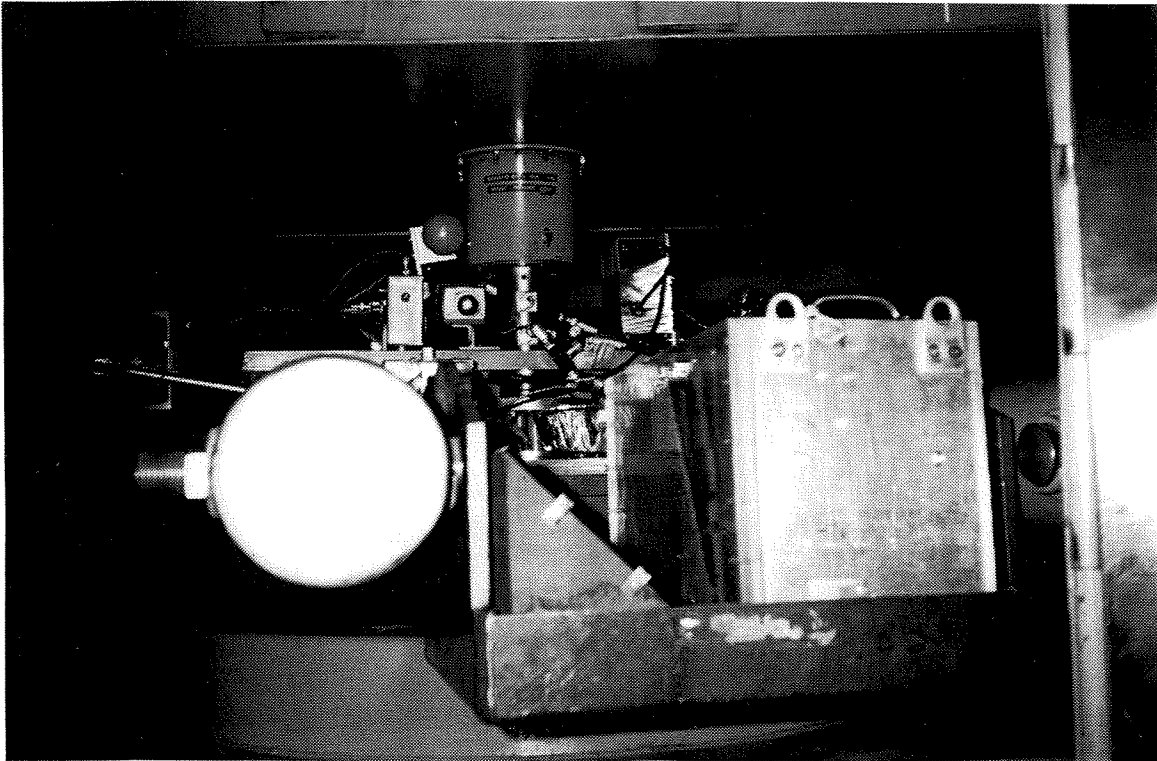


Figure 4.14 - View of TV camera and centrifuge bucket with model and slant mirror in place

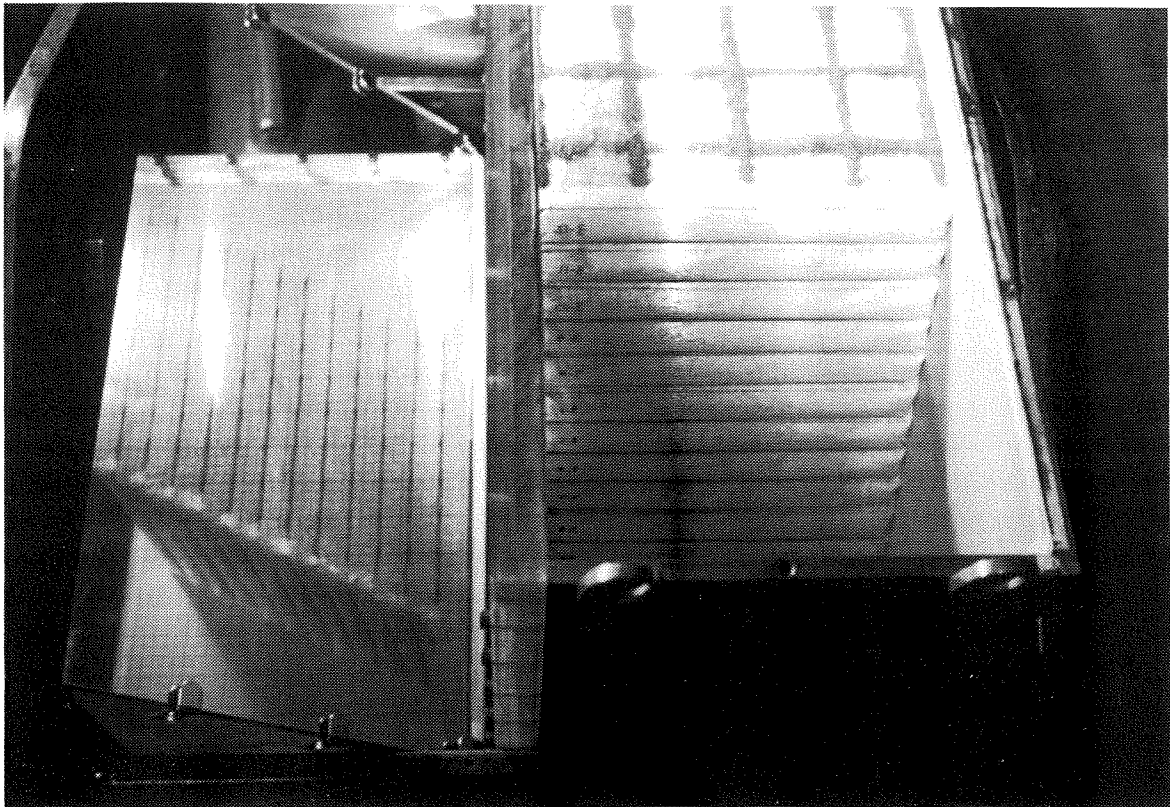


Figure 4.15 - Top view of model B12, already placed in the swing bucket, and of its image through the slant mirror

g-levels could be used to monitor the model deformations during progress of the centrifuge test. Testing progressed until failure of the model occurred. All centrifuge slope models reached failure within the capacity of the centrifuge.

After each test, the backfill was carefully vacuumed out and the geotextile reinforcements were retrieved. The retrieved geotextiles were used to locate the failure surface from the observed tears and to evaluate the breakage pattern. The retrieved geotextile samples always showed breakage in a direction perpendicular to the direction of loading.

4.3.6 Effective radius for evaluation of g-level

The increased g-level, N , during centrifuge testing can be calculated by estimating the centripetal acceleration exerted in the model during centrifuge testing. If the mass of the model is assumed to be concentrated at a radius R_{eff} from the centrifuge axis, the increased acceleration a_r exerted on the model can be calculated as:

$$a_r = N \cdot g = R_{eff} \omega^2 \quad (4.17)$$

where ω is the angular velocity of the centrifuge arm.

However, acceleration within a centrifuge model increases linearly with depth, as it is directly proportional to the radius of rotation. Consequently, the resulting vertical stress distribution within the model is curved, and deviates from the linear distribution of stress in a real structure under 1 g earth gravity. The nonlinear vertical stress distribution σ_v in a centrifuge model can be calculated as:

where ρ is the soil density, r the generic radius, and r_0 the radius to the top surface of the model. On the other hand, the vertical stresses can be approximated by a linear

$$\sigma_v = \rho \omega^2 \int_{r_0}^r r \, dr = \frac{1}{2} \rho \omega^2 (r^2 - r_0^2) \quad (4.18)$$

distribution using a uniform acceleration $N.g$:

$$(\sigma_v)_{lin} = \rho N g (r - r_0) \quad (4.19)$$

where $N.g$ is a uniform acceleration estimated using an effective radius R_{eff} , as indicated by Equation (4.22).

In this study, the effective radius was estimated so that it minimizes the differences between the actual nonlinear stress distribution in the model (Equation 4.23) and the approximate linear one (Equation 4.24). For the dimensions of the models used in this study, the effective radius was calculated as $R_{eff}=873$ mm (34.375 inches). Figure 4.16 shows the nonlinear vertical stresses in the 9-inch high models and the linear approximation estimated using calculated radius R_{eff} . The vertical stresses in the figure are normalized in relation to the g-level N . The figure shows that the linear distribution calculated using R_{eff} approximates the actual nonlinear stresses in the model very well. A procedure commonly used to define the effective radius is to estimate R_{eff} as the distance from the centrifuge axis to the center of the model. The linear stress distribution estimated using such radius (36.375 inches for the models in this study) would not approximate the actual stress distribution in the models as closely as the one shown in Figure 4.16.

Although the difference between the actual vertical stress distribution and the linear approximation is small, the limit equilibrium calculations (Section 4.7) were performed taking into account the nonuniform centripetal acceleration in the models by

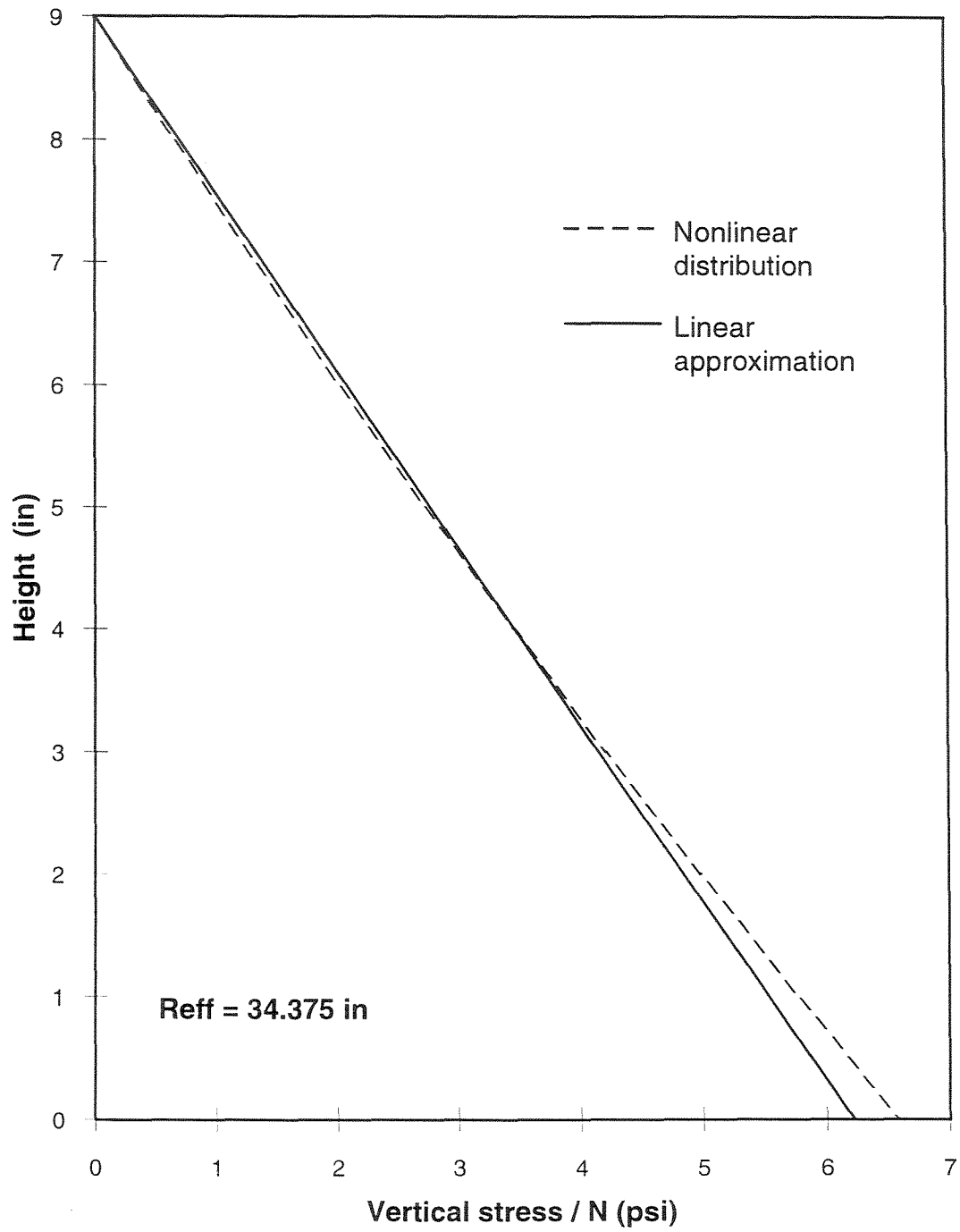


Figure 4.16 - Nonlinear vertical stress distribution in the centrifuge models and linear approximation

considering several backfill layers with increasing unit weights. The main purpose of accurately estimating the effective radius is to be able to precisely report the g-levels at failure.

4.4 Material properties

An extensive testing program was performed in order to evaluate the strength properties of the sand used as backfill material, of the geotextile reinforcements, and of several interfaces that could influence the performance of the slope models. The properties were estimated for conditions likely to be most representative of those in the structure. Accordingly, an effort has been made for estimating the soil shear strength under plane strain conditions and the geotextile tensile strength under embedment conditions. Selection of these parameters, which would be unconservative for design purposes, will more accurately characterize resistance to failure of the geotextile-reinforced slope models.

4.4.1 Backfill soil

4.4.1.1 Sand characterization

The centrifuge models were built using Monterey No. 30 sand, which is a clean, uniformly graded sand classified as SP in the Unified System. The particles are rounded to subrounded, consisting predominantly of quartz with a smaller amount of feldspars and other minerals. Monterey No. 30 has a uniform gradation curve, as shown in Figure 4.17. D_{50} for the material was 0.4 mm, coefficient of uniformity was 1.3, and coefficient of curvature was about 1.1.

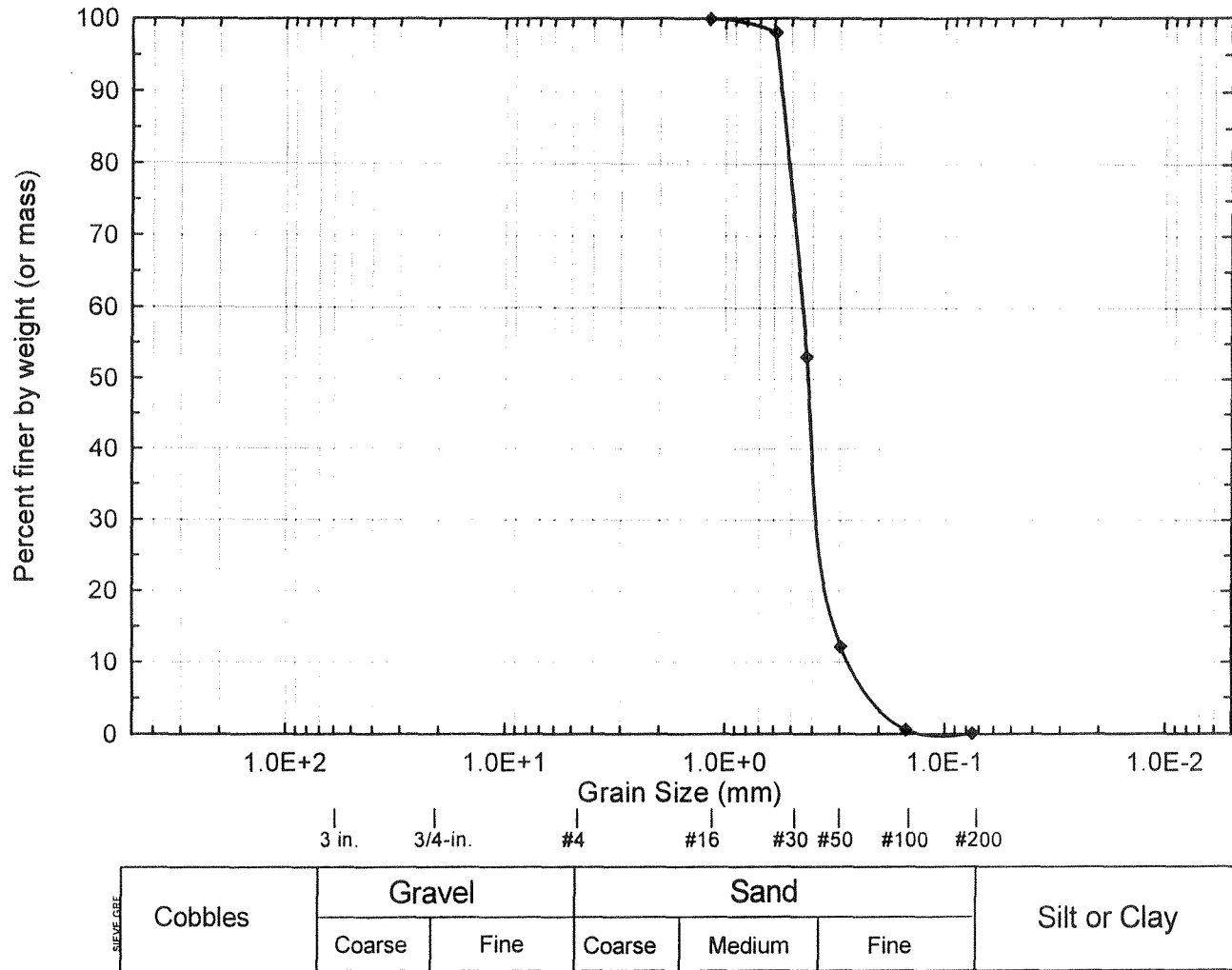


Figure 4.17 - Gradation curve for Monterey No. 30 sand

The maximum void ratio, $e_{\max}=0.83$, was determined by careful dry tipping of the sand in a large graduated cylinder, while the minimum void ratio, $e_{\min}=0.53$, was determined by the Modified Japanese method. The grain properties of a strong, rounded sand such as Monterey No.30 can be assumed to be essentially constant over a large range of stresses, undergoing negligible breakage when tested under moderate stresses. Monterey sand was pluviated through air under controlled conditions to obtain the target dry densities in the model slopes. The target densities were achieved by pluviating the sand at controlled combinations of sand discharge rate and height of sand discharge. The unit weights for the Monterey No.30 sand at the relative densities of 55 and 75 percent used in the centrifuge slope models were 15.64 kN/m^3 (99.5 pcf) and 16.21 kN/m^3 (103.2 pcf). The overburden pressures at the base of the 229 mm (9 inches) high models varied between 3.7 kPa and 370 kPa as the centrifugal acceleration increased from 1 g to a maximum of 100 g.

4.4.1.2 A note on the estimation of plane strain friction angles

Most analyses assume that the peak friction angle is independent of direction of loading, independently of effect of the intermediate effective principal stress (σ_2). Of particular interest is the effect of the intermediate effective principal stress under conditions of plane strain ($\epsilon_2=0$), which has been found to increase the peak friction angle of sand relative to that measured in conventional triaxial compression tests (Cornforth, 1964; Ladd, 1977). Plane strain is the prevailing condition in reinforced soil structures (e.g., Jewell, 1990), and friction angles for this condition had been considered in previous studies that evaluated the performance of reinforced soil walls (Jaber, 1989). To evaluate

the influence of the intermediate principal stress, the intermediate effective principal stress factor b has been defined as:

$$b = \frac{\sigma_2 - \sigma_3}{\sigma_1 - \sigma_3} \quad (4.20)$$

where σ_1 , σ_2 , and σ_3 represent the maximum, intermediate, and minor principal stresses. For triaxial compression and extension, $b=0$ and 1 respectively and for plane strain compression b ranges from 0.3 to 0.4.

Considering the experimental difficulties involved in accurately evaluating plane strain friction angles, the approach followed in this study has been to thoroughly evaluate the friction angle under triaxial compression condition (ϕ_{tc}) and, based on these results, infer the plane strain friction angles (ϕ_{ps}). The estimation of the plane strain friction angles from triaxial results can be done based in general correlations that had been established for a wide variety of sands (Bolton, 1986, Kulhawy and Mayne, 1990). Moreover, specific correlations for the sand used in this study can be obtained from previous research on plane strain testing that has been performed using Monterey No. 0 and Monterey No. 20 sands.

Normalized test data shown in Figure 4.18 illustrate the importance of the intermediate effective principal stress factor b . For plane strain compression, the strength increase in relation to results from triaxial compression ranges from 7 to 18 percent, with higher values for denser sands. Based on these normalized data, an average strength increase ratio was recommended as (Kulhawy and Mayne, 1990):

$$\phi_{ps} = 1.12 \phi_{tc} \quad (4.21)$$

In order to get a more specific relationship for this study, the ratio ϕ_{ps}/ϕ_{tc} was investigated from previous studies involving plane strain testing of Monterey sand. Lade and Duncan (1973) reported plane strain friction angles for Monterey No. 0 sand ($D_{50}=0.43$ mm, $C_u=1.53$), obtained utilizing true triaxial equipment in which the three principal stresses acting on a cubical specimen could be independently varied. Additionally, Marachi et al. (1981) reported the results of a series of tests on Monterey No. 20 sand ($D_{50}=0.55$ mm, $C_u=1.25$) performed using triaxial and plane strain devices

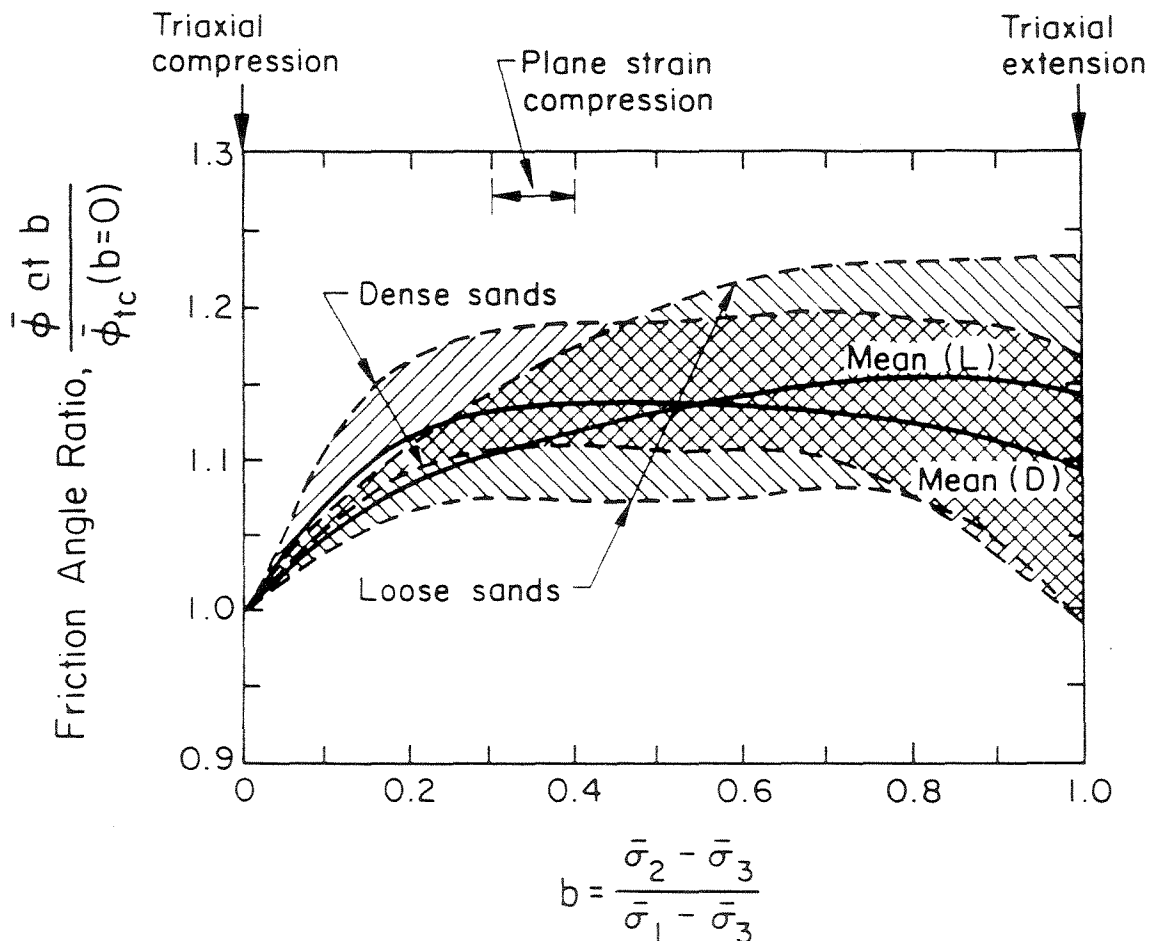


Figure 4.18 - Influence of intermediate principal stress on soil friction angle (after Kulhawy and Mayne, 1990)

in a wide range of confining pressures, considering a variety of specimen sizes and shapes.

The friction angle ratio ϕ_{ps}/ϕ_{tc} for test results obtained for Monterey No. 0 sand on dense and loose samples tested at 58.8 kPa confining pressure are indicated in Figure 4.19. Test results from Monterey No. 20 sand specimens at three different relative densities tested at 70 kPa are also indicated in the same graph. The figure shows that the friction angle ratios from these two different Monterey sands are similar and increase linearly with increasing sand relative densities. The magnitude of the strength ratio obtained for Monterey sands is in good agreement with the average ratio recommended by Kulhawy and Mayne (1990). Based on these correlations, the selected strength increase ratios ϕ_{ps}/ϕ_{tc} for the backfill of the centrifuge models are 1.13 and 1.14 for sand at 55% and 75% relative densities, respectively.

4.4.1.3 Shear strength properties

In order to obtain strength parameters for the Monterey No.30 sand, two series of triaxial tests were performed to evaluate (1) the friction angles for increasing sand relative density; and (2) the effect of confining pressure on the friction angle of Monterey No.30 sand. The tests were performed using a modified form of the automated triaxial testing system developed and described by Li et al. (1988). In addition to data acquisition, the current system utilizes computer control of the chamber pressure and deviatoric load. In the test series performed using sand at increasing relative densities, vertical stresses were applied by an air actuator. In the case of the series of tests done under increasing confining pressures, vertical stresses were applied by a dual pressure actuator, with one

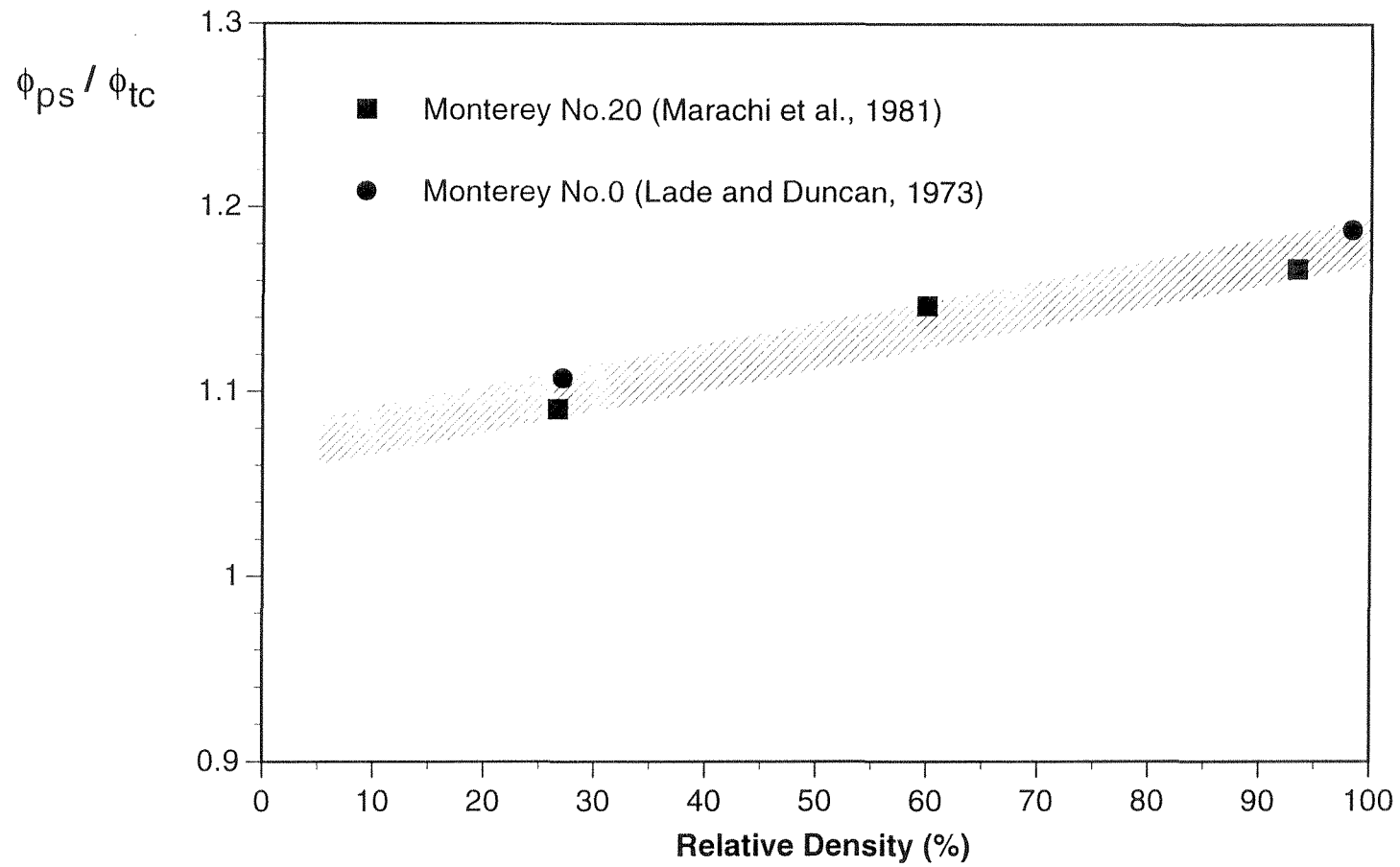


Figure 4.19 - Ratio between friction angles under plane strain and triaxial compression conditions for Monterey sand

chamber of the actuator filled with oil and linked to an oil reservoir by a needle valve with adjustable aperture. This last setup allows limiting the maximum rate at which the piston can descend, thereby limiting the strain rate of the sample during the strain softening portion of the test. All of the specimens had nominal dimensions of 70 mm in diameter and 150 mm in height and were prepared by dry tamping.

Figure 4.20 shows the deviatoric stress-axial strain curves for the test series performed on Monterey No.30 sand at increasing relative densities. All these tests were performed at a confining pressure of 100 kPa. The peak strain at failure increases with decreasing relative densities. Figure 4.21 shows the friction angle results obtained for the tests performed in this series. The figure shows a continuous increase of friction angle with increasing relative density. Of particular interest are the friction angles obtained at relative densities of 55% and 75% that correspond to backfill material in the centrifuge models. The adopted triaxial compression friction angles at these relative densities are $\phi_{tc}=35^\circ$ and $\phi_{tc}=37.5^\circ$, respectively. Although the tests do not achieve large enough strain values to guarantee a critical state condition, the friction angles at large strains appear to converge to a critical state value of approximately $\phi_{cs}=32.5^\circ$. This value agrees with the critical state friction angle for Monterey No.0 sand that has been extensively tested (Riemer, 1992). Since critical state angle of shearing resistance of soil which is shearing at constant volume is principally a function of mineralogy (Bolton, 1986), Monterey No.0 and Monterey No.30 sands should show similar ϕ_{cs} values.

Figure 4.22 shows the deviatoric stress-axial strain curves for the tests series performed on Monterey No.30 sand at increasing confining pressures. The tests were performed at an approximately constant relative density of 60% that corresponds to an

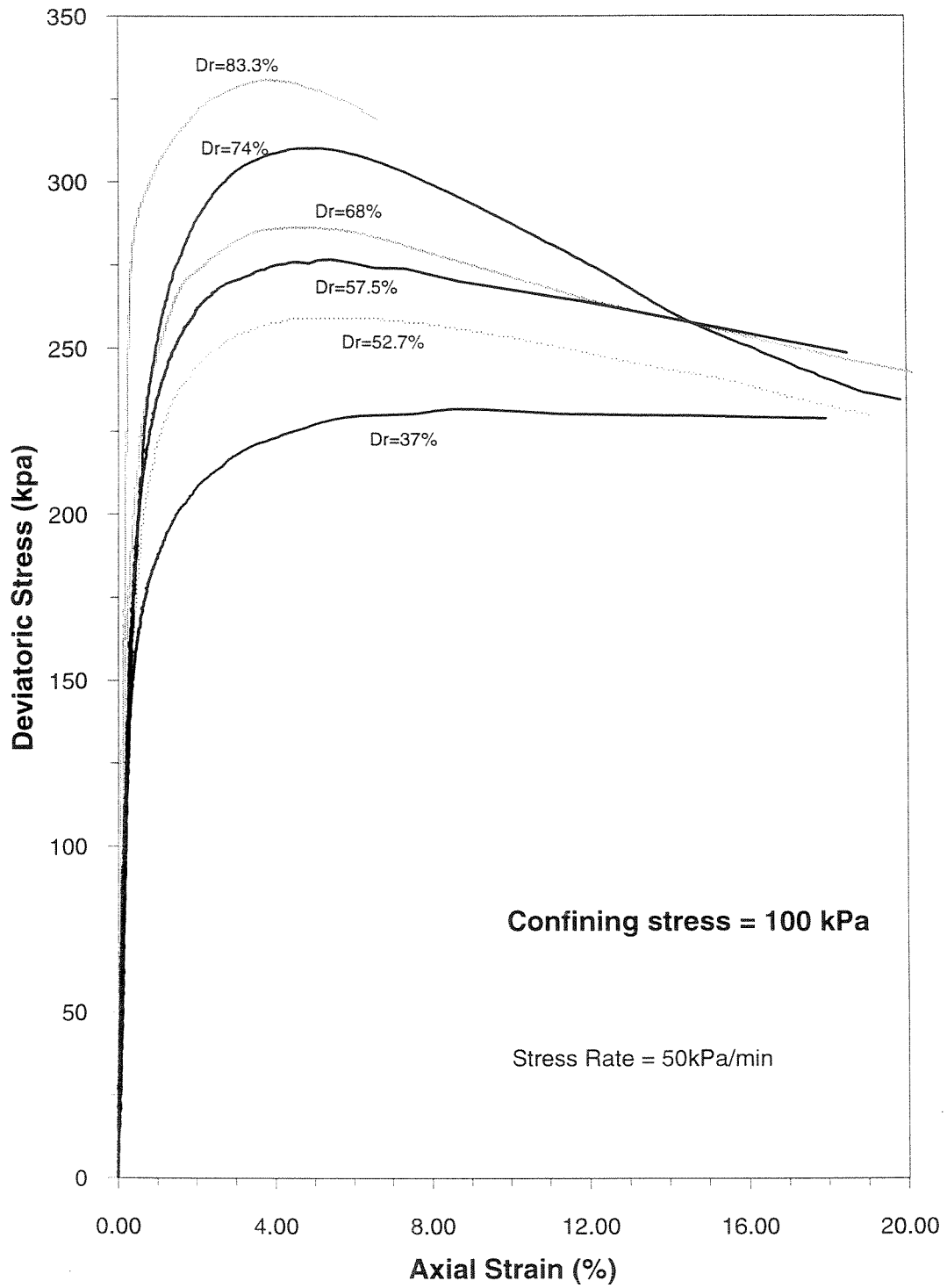


Figure 4.20 - Stress-strain curves for Monterey No.30 sand obtained from triaxial testing at different relative densities

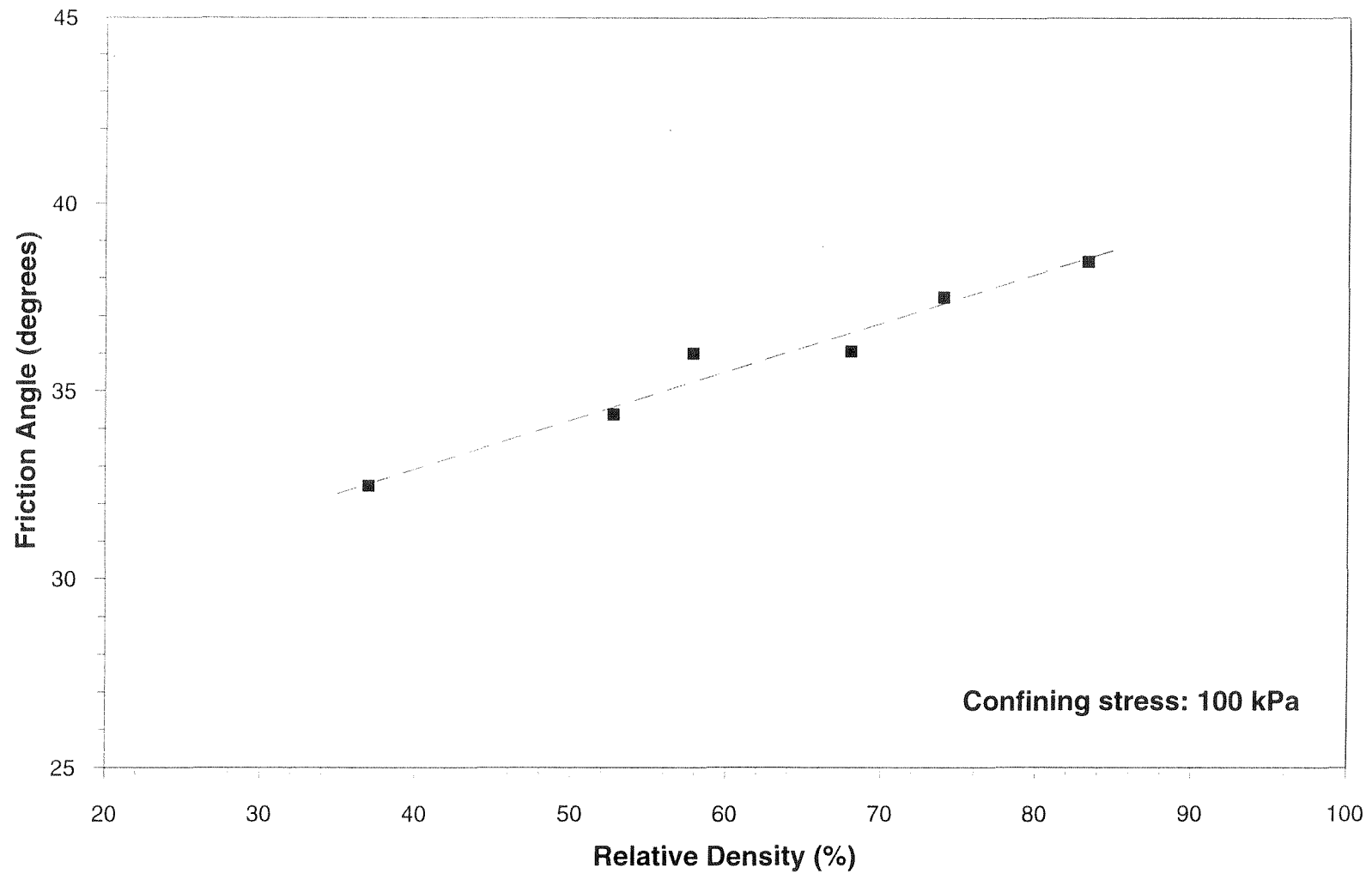


Figure 4.21 - Friction angle for Monterey No.30 sand obtained from triaxial testing at different relative densities

initial void ratio $e_0=65$. Peak axial strain at failure was reached at approximately 4% in all tests. The effect of confining pressure σ_3 on the frictional strength of the sand is indicated in Figure 4.23. The figure shows that the strength of Monterey No.30 shows a slight decrease with increasing confinement. One of the reasons for selecting Monterey sand for this study was that the use of a sand that does not exhibit much normal-stress dependency of the friction angles will avoid an additional complicating factor to the interpretation of the centrifuge model tests. Also in this series of tests, the large strain friction angles appeared to converge to a final value of approximately $\phi_{cs} = 32.5^\circ$.

4.4.2 Geotextile reinforcements

4.4.2.1 Geotextile characterization

According to the scaling relationships in Section 4.2.2, the model geotextiles should have $1/N$ the ultimate tensile strength of prototype geotextile reinforcements. Two types of nonwoven interfacing fabrics with small enough tensile strength were selected to be used as reinforcements for the centrifuge slope models. The fabrics are manufactured by Pellon Division of Freudenberg Nonwovens. The weaker of these fabrics, Pellon Sew-in nonwoven, is a white, 100% polyester fabric with a unit weight of 24.5 g/m^2 . The stronger geotextile used in this study, Pellon Tru-grid nonwoven, is a white 60% polyester/40% rayon fabric with blue 1 inch square grid prints and a unit weight of 28 g/m^2 .

The tensile strength of both fabrics is highly anisotropic, with the lower strength along the cross-machine direction. All centrifuge models were built using the fabrics

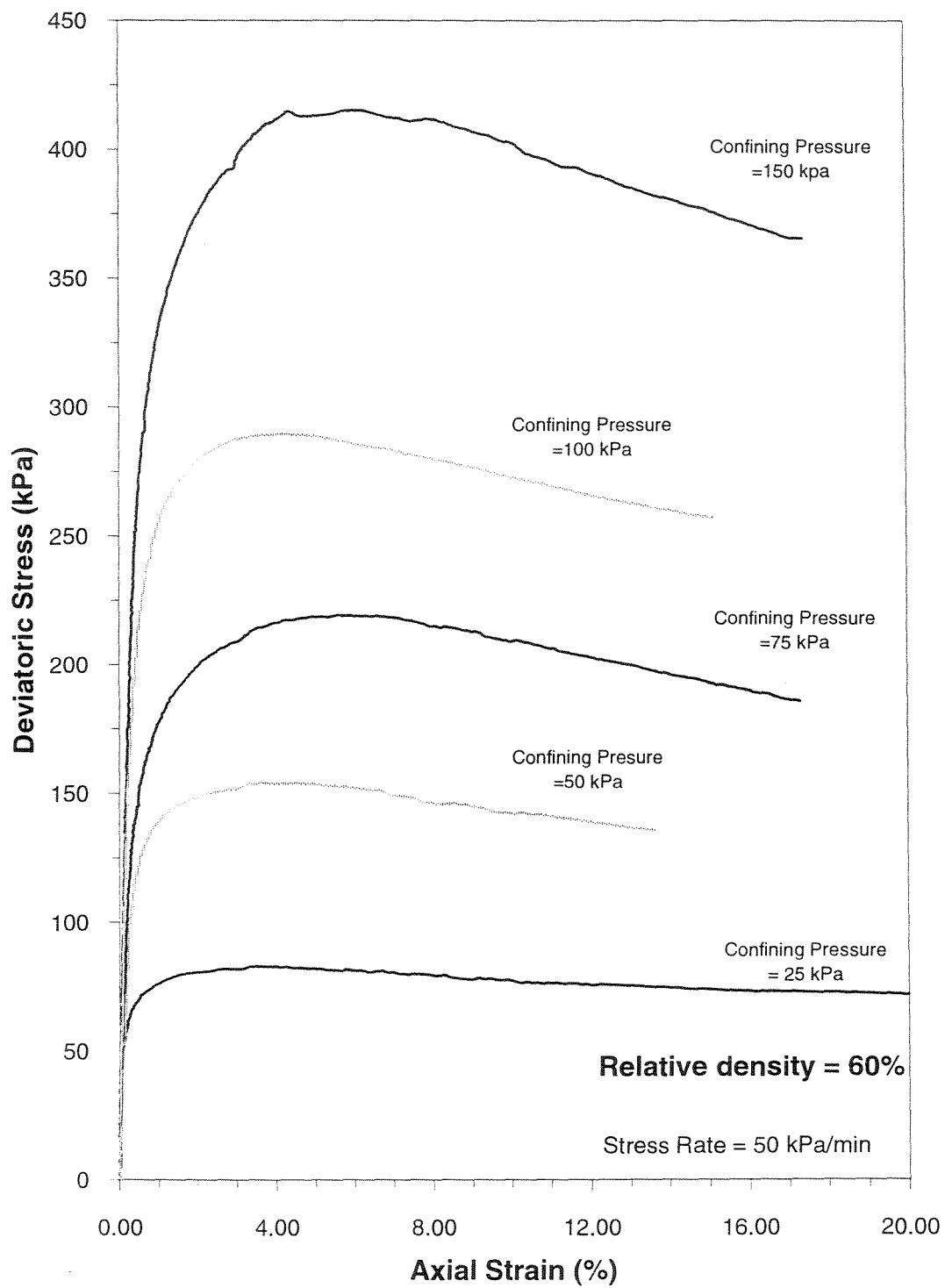


Figure 4.22 - Stress-strain curves for Monterey No.30 sand obtained from triaxial testing at different confining pressures

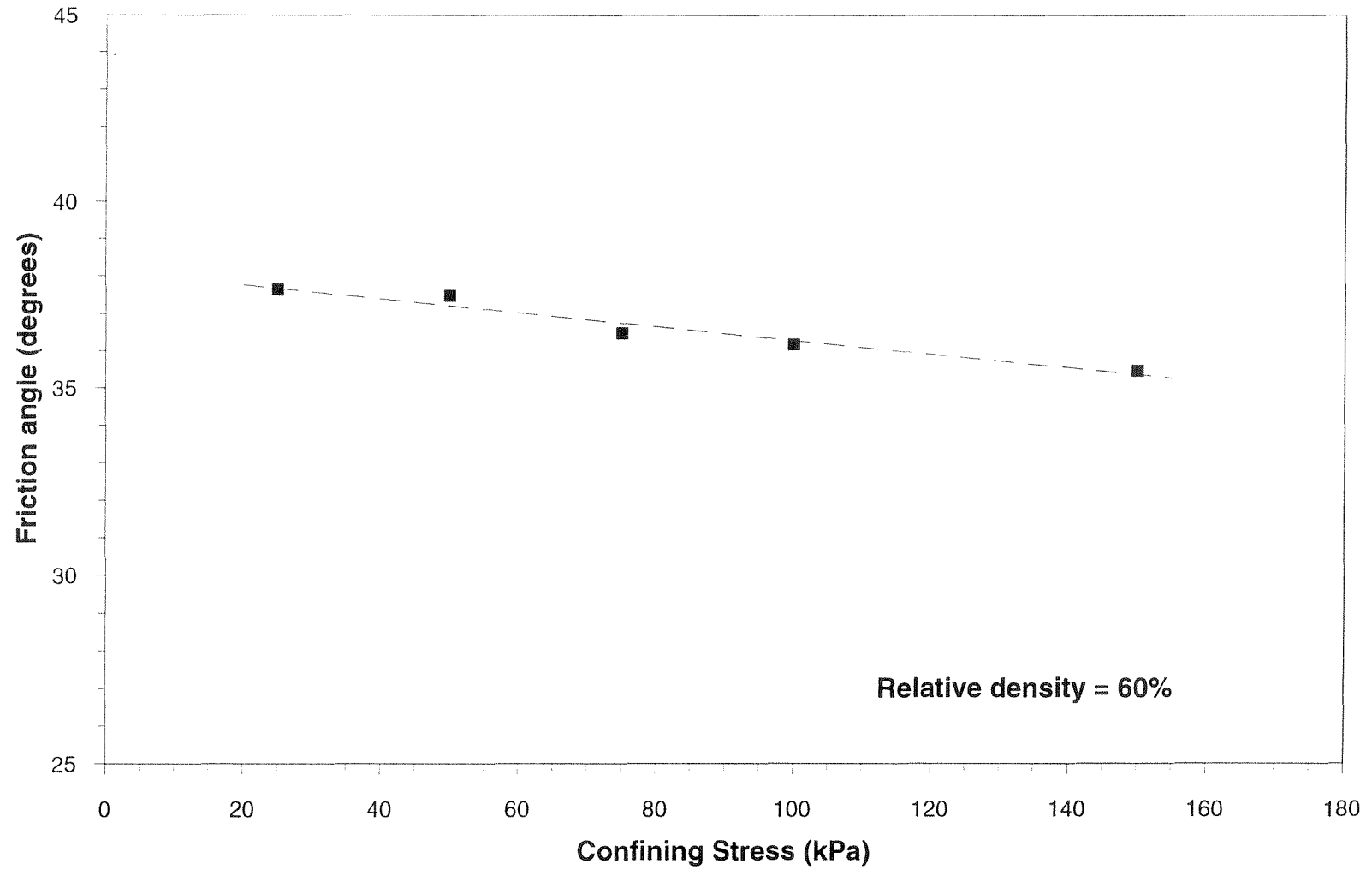


Figure 4.23 - Friction angle for Monterey No.30 sand obtained from triaxial testing at different confining pressures

oriented in the cross-machine direction and, consequently, the geotextile tensile strength tests were also performed with fabrics oriented in the weaker direction.

4.4.2.2 A note on the interpretation of wide width tensile test results

Perhaps the single most important property of a geotextile is its tensile strength (Koerner, 1994). The basic idea of a tensile strength test is to place the geotextile within a set of clamps or jaws, place this assembly in a mechanical testing machine, and stretch the geotextile in tension until failure occurs. The most common wide-width test is ASTM D4595, which uses a 200 mm (8 in) wide specimen which is 100 mm (4 in) long between the faces of the opposing grips.

However, the geosynthetic mechanical properties should be measured in a manner that simulates the field conditions and this is often not the case for unconfined tensile tests such as the wide-width test. Many investigators have already focused on the tensile characteristics of geosynthetics under the soil-confinement condition (e.g., McGown et al., 1982; Christopher et al., 1986; Ling et al., 1992; Boyle and Holtz, 1994; Gomes et al., 1994). This issue has also been indicated as a major problem that requires further investigation in the finite element study presented in Chapter 2 and in the evaluation study presented in Chapter 3. Although differing in the testing methodology, the different studies have shown that there is a significant increase in stiffness and strength of several geotextiles under soil confinement, in comparison to values obtained in unconfined conditions.

Most studies have identified the normal pressure exerted on the geotextiles as the main cause for the improvement in its mechanical properties. However, there are two possible causes of mechanical improvement of geotextiles when tested embedded in soil:

- The embedment of geotextiles in soil provides additional normal stresses or confinement; and
- the embedment of geotextiles in soil provides boundary conditions representative of field conditions by restraining geotextile deformations in the direction perpendicular to loading.

The boundary conditions in unconfined wide-width testing are probably not representative of field conditions since, due to Poisson's ratio effect, the specimens may undergo severe "necking" under increased loading. Although wide enough specimens may be considered to provide negligible lateral deformations, the appropriate dimensions for geotextile testing appears to be still undetermined. While the 2:1 width/length ratio has been considered reasonable for unconfined tests by some studies (Shrestha and Bell, 1982), larger 5:1 ratios have also been recommended (Leflaive et al., 1982), and tests have been even performed using a gauge length of only 3 mm (Resl, 1990). In general, lightweight nonwoven geotextiles have been found to be more sensitive to the width/length ratio of the specimen.

Boundary conditions on the tensile test will affect the estimated value for the stiffness of the geotextiles. Assuming a linear elastic constitutive behavior before failure,

the conventional wide-width tensile test setup with boundary conditions indicated in Figure 4.24a will lead to an estimated "wide-width" stiffness J_{ww} :

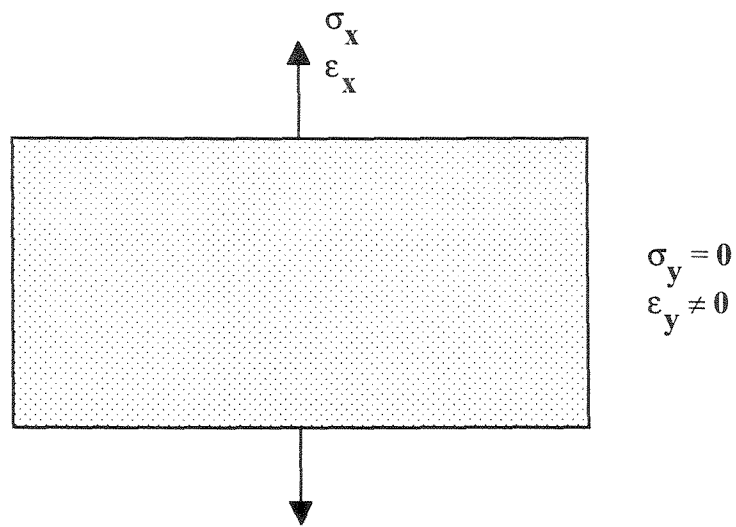
$$J_{ww} = \frac{\Delta\sigma_x}{\Delta\varepsilon_x} = E \cdot t \quad (4.22)$$

where E is the Young modulus of the geotextile and t is the geotextile thickness. On the other hand, a test in which geotextile lateral deformations are prevented (Figure 4.24b) will lead to a more realistic "field" stiffness J :

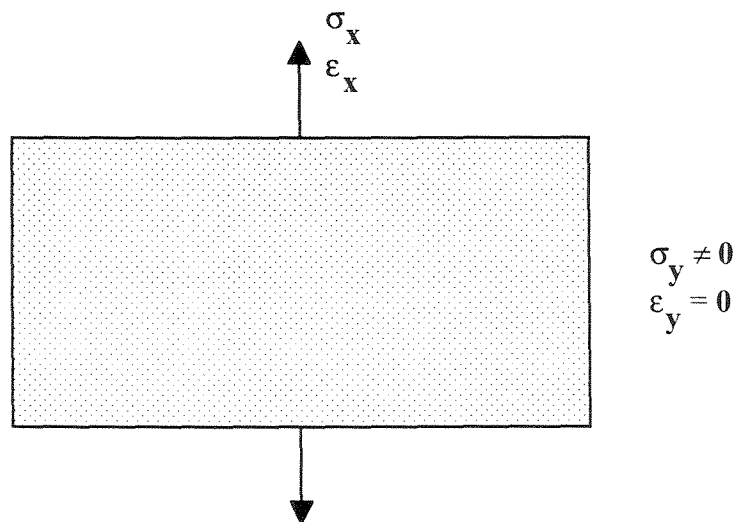
$$J = \frac{\Delta\sigma_x}{\Delta\varepsilon_x} = \frac{E \cdot t}{1 - \nu^2} = \frac{J_{ww}}{1 - \nu^2} \quad (4.23)$$

where ν is the Poisson's ratio of the geotextile. Since the range of possible values for ν is from 0 to 0.5, the stiffness J estimated when lateral deformations are prevented is higher than the one estimated if lateral deformations occur.

The boundary conditions of the tensile test may also affect the measured tensile strength of the geotextiles. Assuming that geotextiles have an elastic-perfectly plastic behavior, a qualitative evaluation of the effect of test boundary conditions on the estimated tensile strength is presented in Figure 4.25. For illustration purposes, the figure shows a geotextile yield surface having a classic Von Mises type shape. The figure shows the "wide width" tensile strength $\sigma_{x, ww}$ obtained from an unconfined tensile test loaded in the x direction, assuming a boundary condition $\sigma_y=0$. A more representative test, however, would be one performed with a boundary condition $\varepsilon_y=0$, which implies that $\sigma_y=\nu\sigma_x$ ($\sigma_y>0$). As indicated for the yield surface indicated in the figure, the strength $\sigma_{x, ult}$ obtained in this case would be higher than the value obtained from a typical wide width test.



a) Boundary conditions in unconfined tensile test



b) More representative field boundary conditions
(no lateral strains)

Figure 4.24 - Standard and ideal geotextile testing boundary conditions

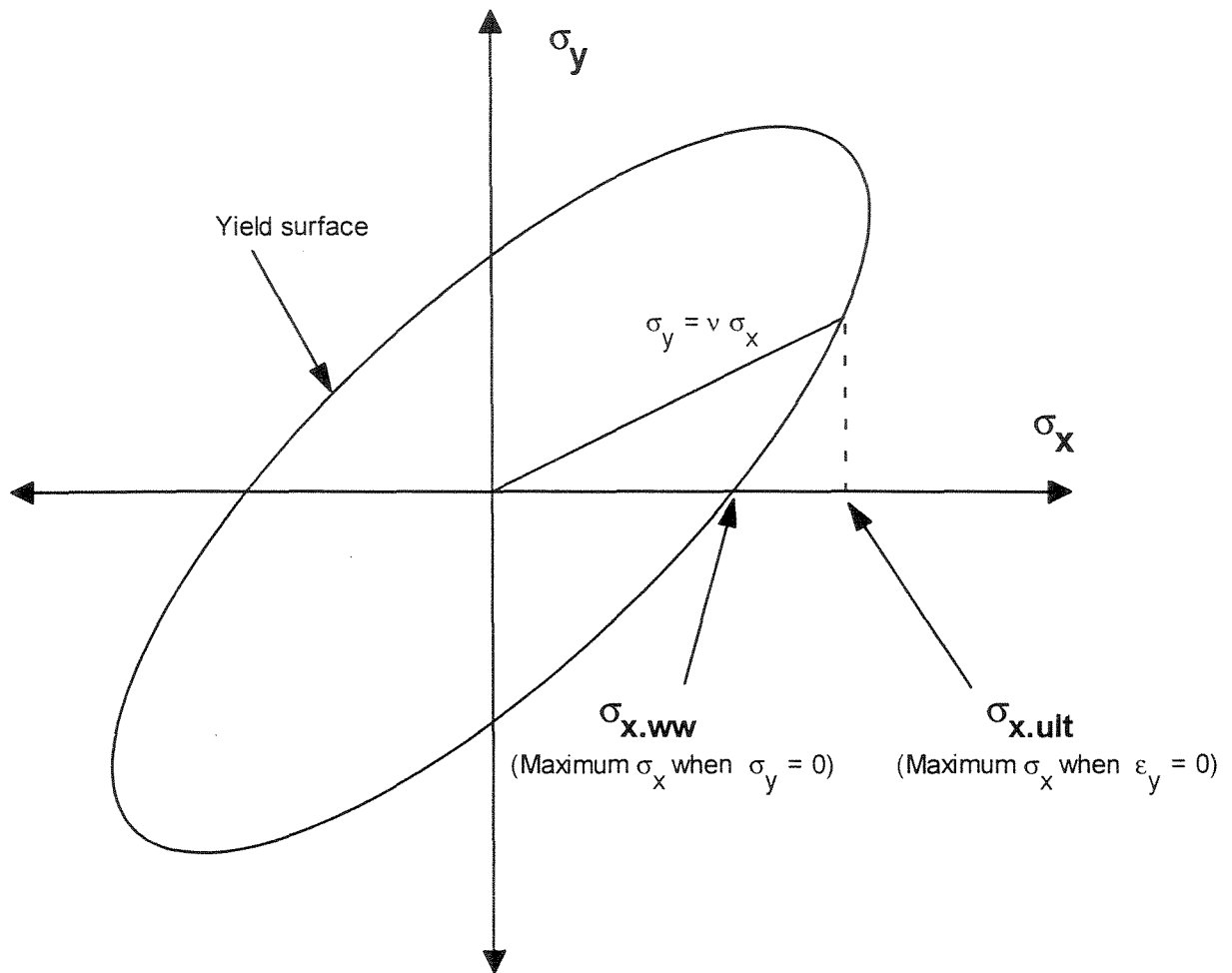


Figure 4.25 - Schematic illustration of the effect of test boundary conditions on the estimated geotextile tensile strength

The actual effect of test boundary conditions on the measured geotextile tensile strength will depend on the actual shape of the yield surface, which has not been investigated herein. However, the underlying message of the preceding discussion is that test boundary conditions different than those prevailing in the field may affect the mechanical properties of geotextiles. To provide actual strength properties, rather than mere quality control values, the tensile tests should be done in a manner that duplicates field operational conditions.

In-soil geotextile testing is still a topic of active research and, considering the difficulties in performing such tests in lightweight fabrics, a thorough study on the confined mechanical properties of the geotextile reinforcements used in this study was not possible. However, a simplified evaluation of the effect of testing boundary conditions on the tensile strength was performed, as described in the next section. The estimated tensile strength values obtained from the geotextile testing program can eventually be refined using results from the centrifuge testing of reinforced slope models. In fact, a centrifuge test can also be considered as a special geotextile tensile test in which field conditions are realistically reproduced.

4.4.2.3 Tensile strength properties

A series of wide-width strip tensile tests ASTM D4595-86 was performed to evaluate the unconfined strength properties of the geotextiles in the cross-machine direction. A series of additional tests was performed to evaluate the effect of testing boundary conditions on the estimated strength values. Most tests were performed by the Material Testing Laboratory of Geosyntec Consultants, Boca Raton, Florida. Additional

tests were performed at the laboratory of Polyfelt Americas, Evergreen, Alabama. Very good agreement was obtained between the results of tests performed in both laboratories.

Figure 4.26 shows the setup for wide-width tests, performed on 200 mm (8 in) wide specimens which are 100 mm (4 in) long between the faces of the opposing grips. The conventionally specified crosshead speed of 10 mm/min (0.4 in/min) was used in all tensile tests. The unconfined tensile strength for the Pellon Sew-in geotextile, obtained from standard wide-width testing, was 0.063 kN/m (0.361 lb/in) with an average strain at ultimate strength of 17.7%. Figure 4.27 shows the unit tension versus strain curve obtained from one of these tests. For the Pellon Tru-grid geotextile, the ultimate tensile strength obtained from wide-width testing was 0.119 kN/m (0.679 lb/in) with an average strain at ultimate strength of 29.3%. Figure 4.28 shows the unit tension versus strain curve obtained after testing one of the Pellon Tru-grid specimens. A softening post-peak behavior can be observed in the unit tension versus strain curves for both geotextile types.

In order to evaluate the effect of testing boundary conditions, a series of tensile tests was performed by decreasing the gauge length in the tested geotextile specimens. The effect of an increasing width/length ratio can then be evaluated and, for very large width/length ratios, the tests approximate a condition in which lateral deformations are prevented. All tests were performed on 200 mm wide specimens, and the gauge length was decreased from the standard 100 mm length to as little as 1.5 mm. Besides guaranteeing that lateral deformations are prevented, the adoption of a very small gauge length was motivated by observation of the failure pattern in geotextile reinforcements retrieved after centrifuge testing. The retrieved geotextiles showed clear breakage

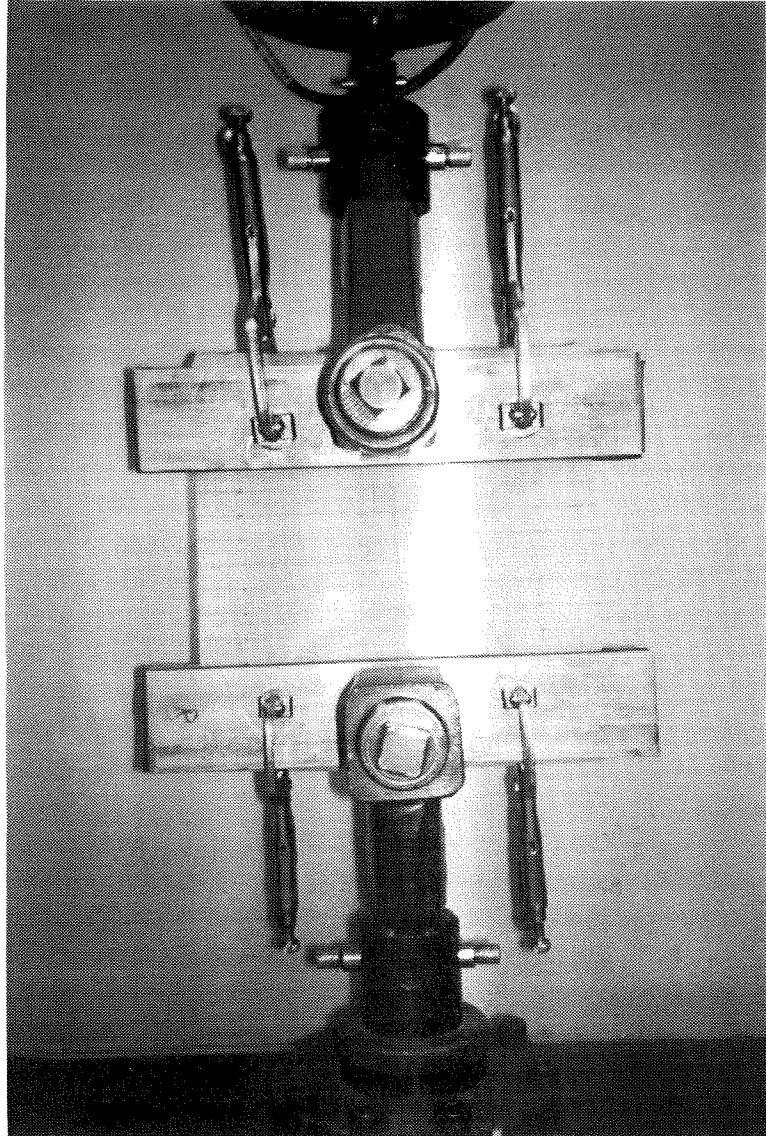


Figure 4.26 - Standard wide width strip tensile testing of a geotextile specimen

WIDE-WIDTH TENSILE TEST RESULTS
FLQ5754 / UNIVERSITY OF CALIFORNIA, BERKELEY

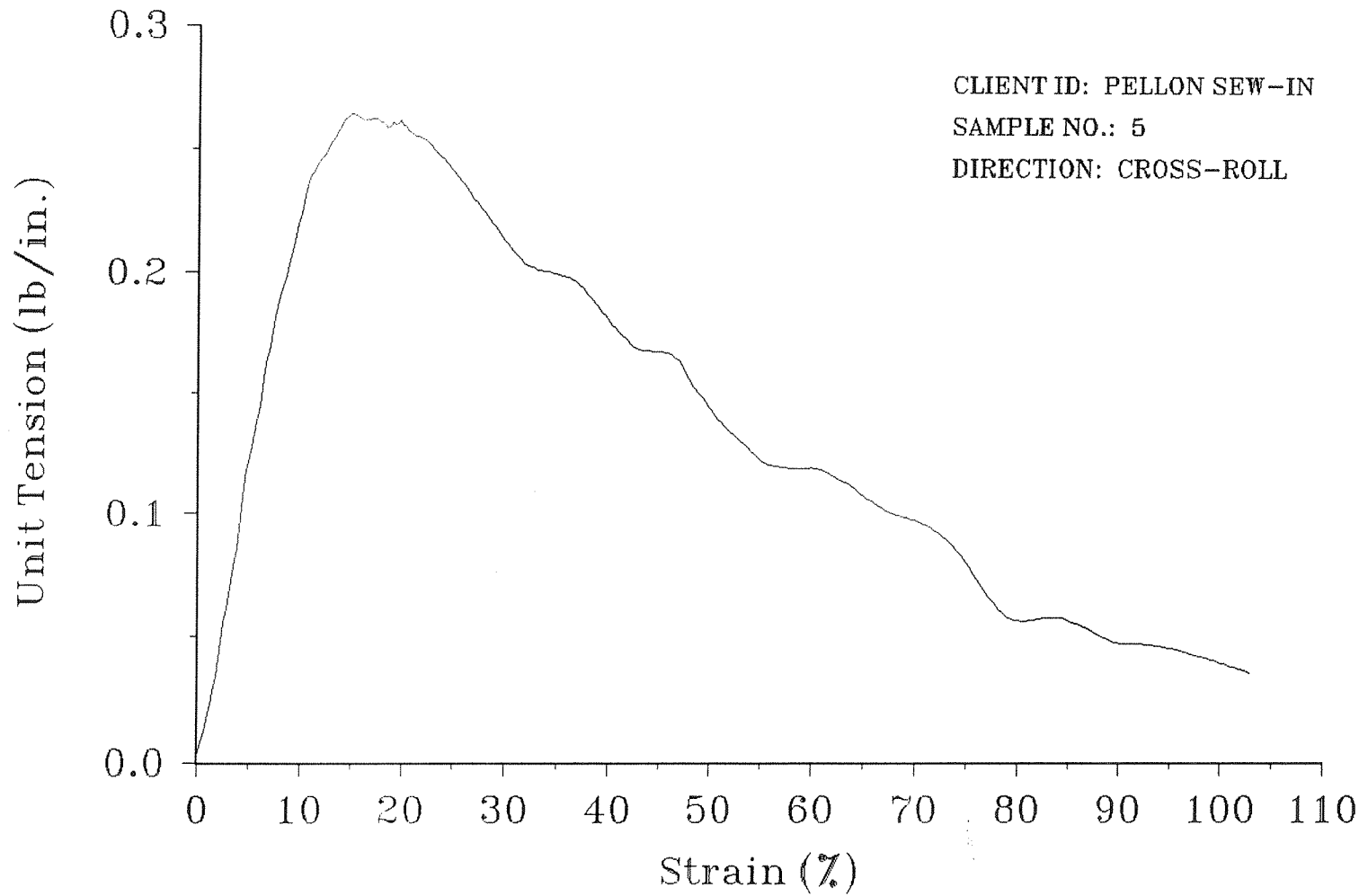


Figure 4.27 - Typical wide-width tensile test results for pellon sew-in geotextiles (Test by Geosyntec Consultants)

WIDE-WIDTH TENSILE TEST RESULTS
FLQ5751 / UNIVERSITY OF CALIFORNIA, BERKELEY

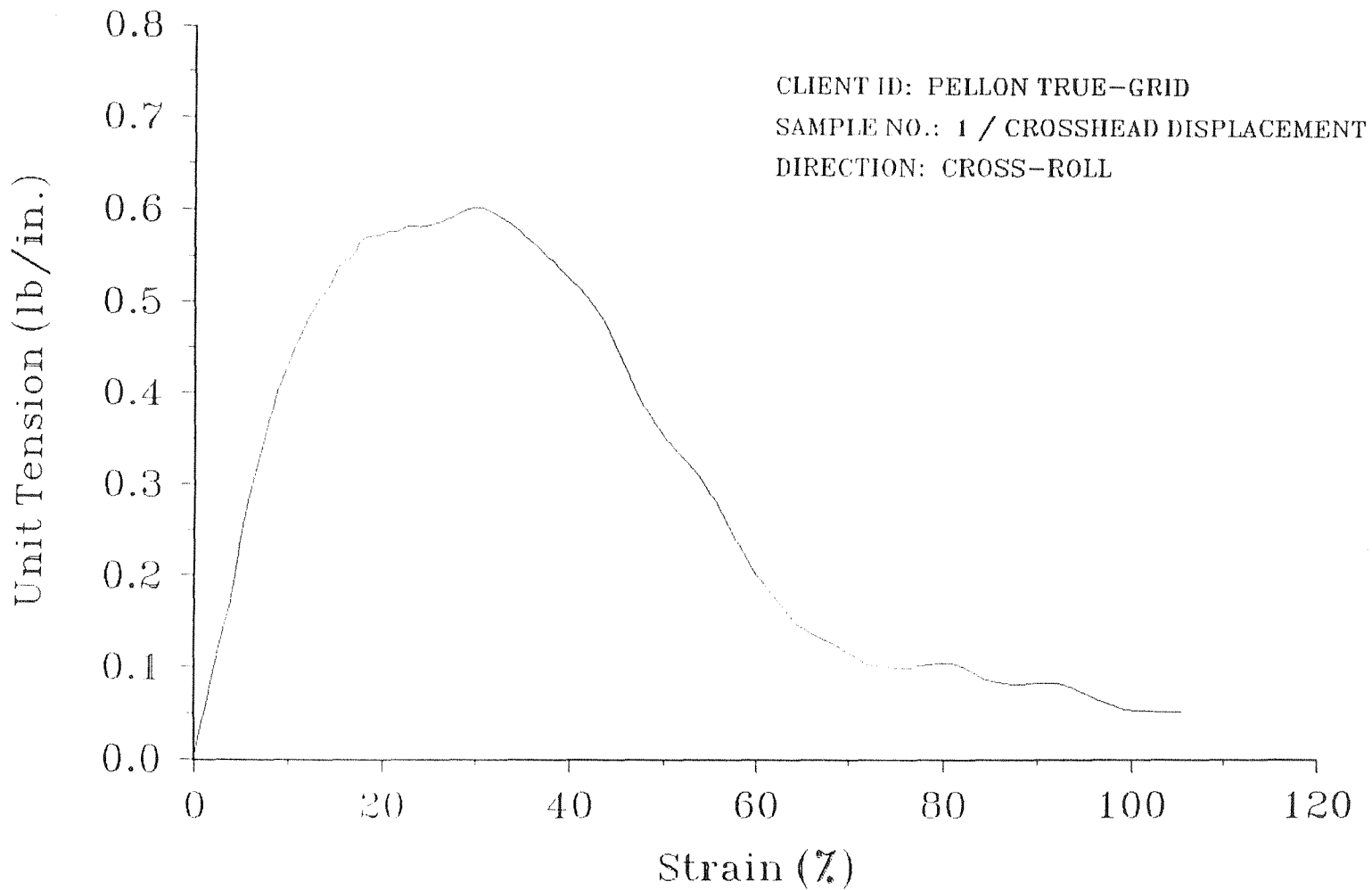


Figure 4.28 - Typical wide-width tensile test results for pellon tru-grid geotextiles (Test by Geosyntec Consultants)

perpendicular to the loading direction without signs of visible stretching at either side of the tear.

Figure 4.29 shows the setup during tensile testing using a 1.5 mm gauge length. The same grips for the conventional D4595 wide-width test were used in this case. Figure 4.30 shows a geotextile specimen before and after tensile testing using a small gauge length. The tensile strength obtained for the Pellon Sew-in geotextile when tested using a 1.5 mm gauge length setup, was 0.150 kN/m (0.858 lb/in) with an approximate displacement at peak tension of 1.3 mm (0.05 in). This value represents a 137% increase in relation to the strength obtained from standard wide-width testing. Figure 4.31 shows the unit tension versus displacement curve for one of the Pellon Sew-in samples. As was also observed from the wide width results, a marked post-peak softening behavior could be observed in these tests. Figure 4.32 shows a Pellon Sew-in geotextile retrieved after centrifuge testing (center of the figure), as well as geotextile specimens obtained after standard wide-width testing, and after testing using the 1.5 mm gauge length setup. It appears that the breakage pattern in the geotextile retrieved from the slope model resembles the specimen tested using the smaller gauge length.

For the Pellon Tru-grid geotextile, the ultimate tensile strength obtained using a 1.5 mm gauge length was 0.234 kN/m (1.337 lb/in) with an average displacement at peak tension of 2.5 mm (0.1 in). The strength increase is of 97% in relation to the ultimate strength from standard wide-width testing. Figure 4.33 shows the unit tension versus displacement curve for one of the Pellon Tru-grid samples. While a softening behavior was observed in the results from wide-width tests using this geotextile, such post-peak softening behavior is not observed when this fabric is tested using a small gauge length.

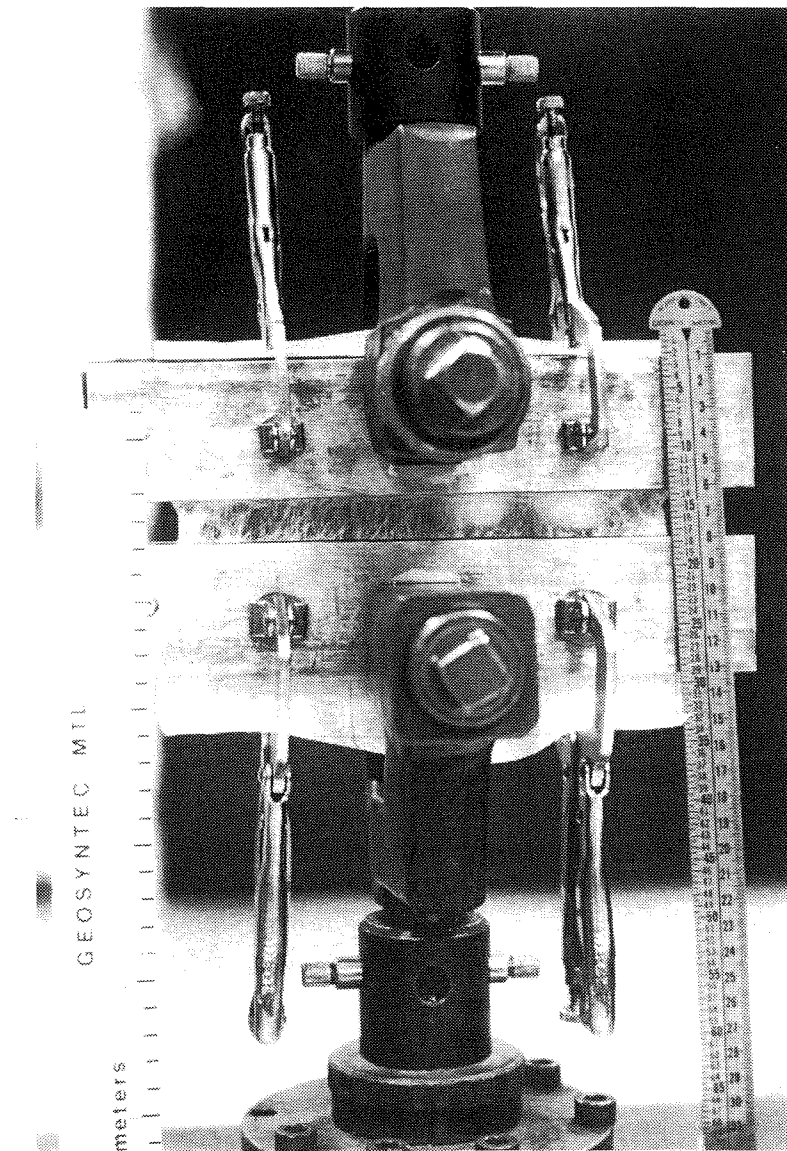


Figure 4.29 - Geotextile tensile testing using a small (1.5 mm) gauge length setup

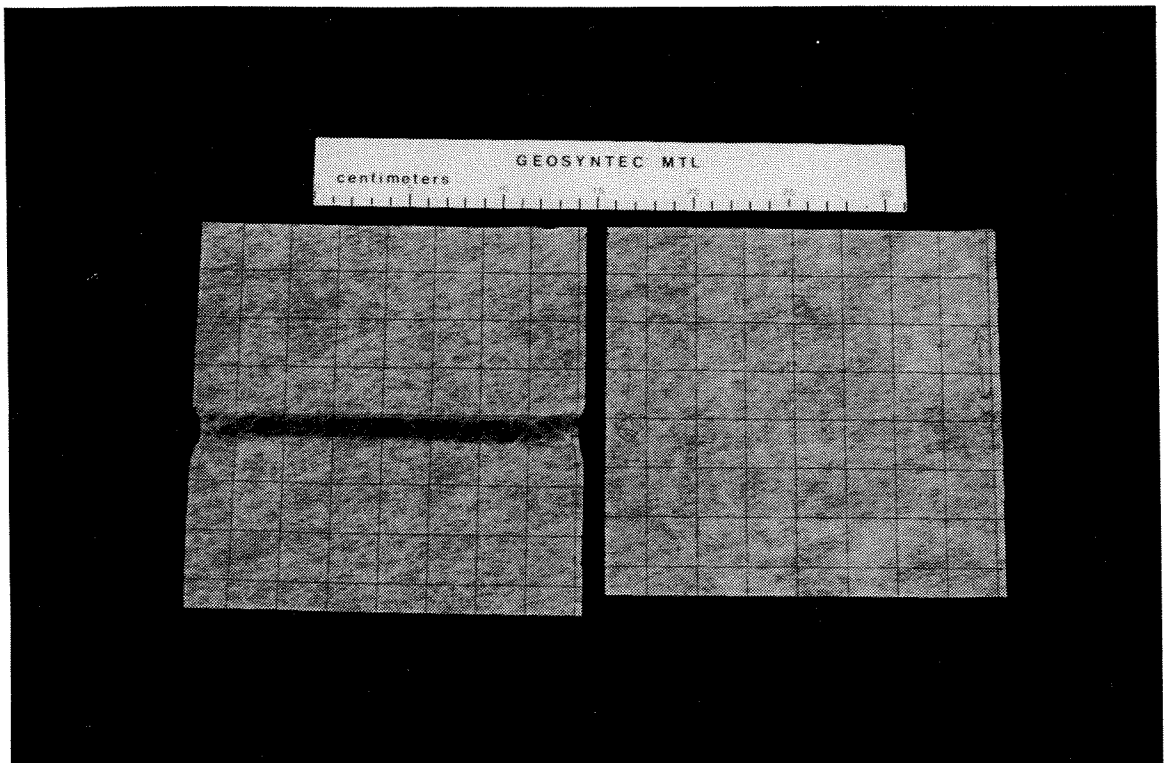


Figure 4.30 - View of a geotextile specimen after tensile testing using a small gauge length setup

WIDE-WIDTH TENSILE TEST RESULTS
FLQ5754 / UNIVERSITY OF CALIFORNIA, BERKELEY

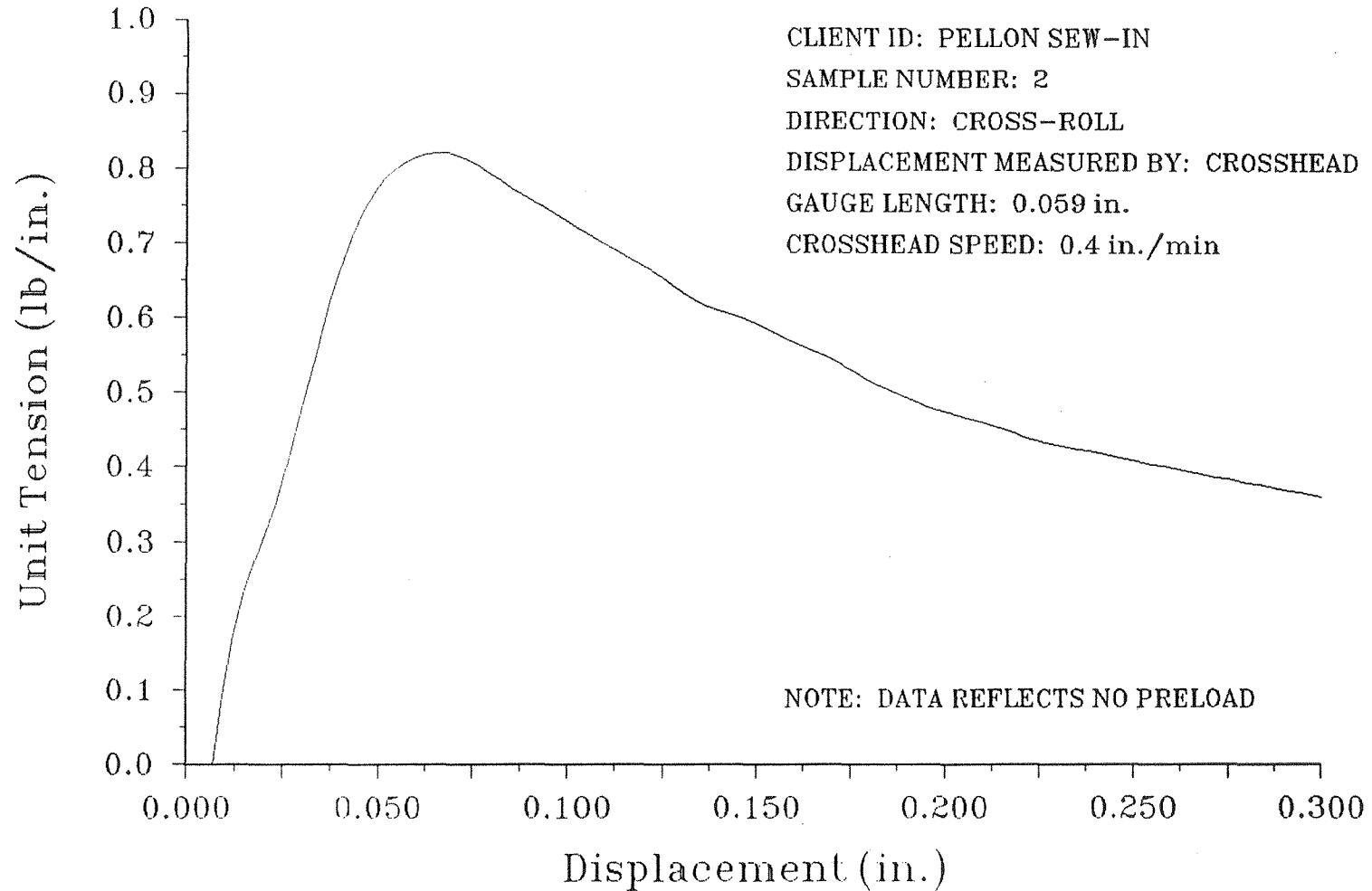


Figure 4.31 - Typical tensile test results obtained for a pellan sew-in geotextile tested using a small gauge length setup (Test by Geosyntec Consultants)

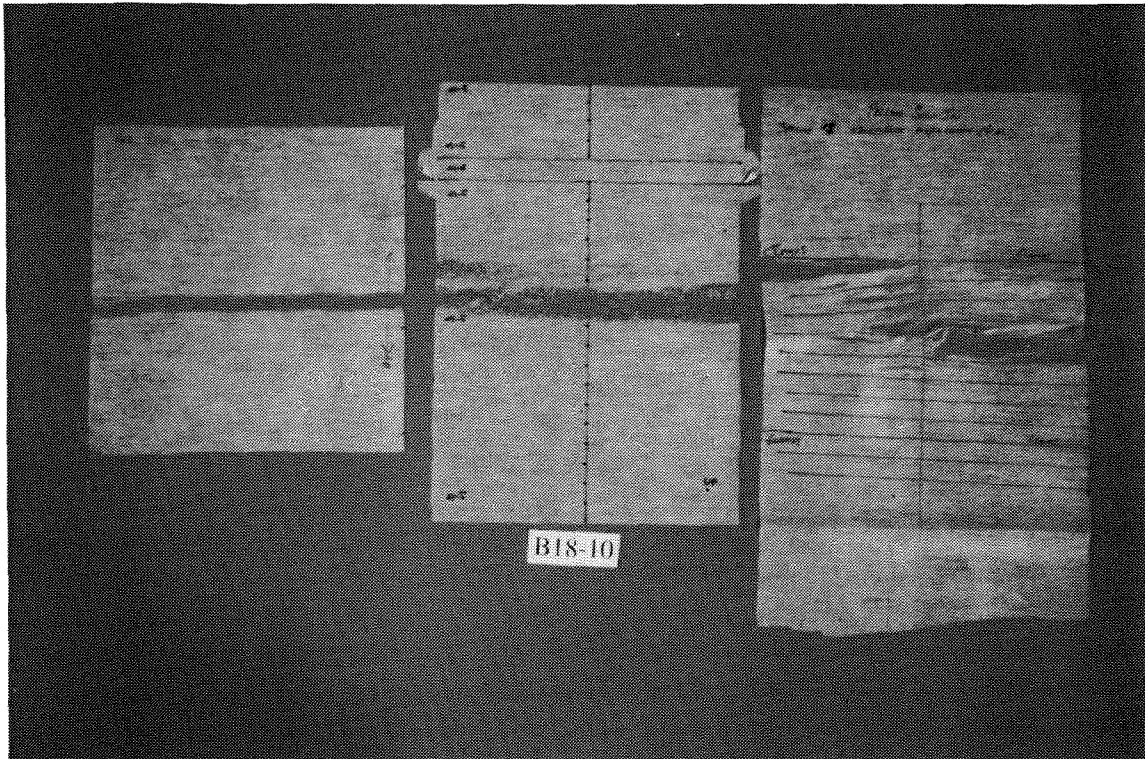


Figure 4.32 - Breakage pattern in Pellon sew-in specimens tested using (from left to right) small gauge length setup, centrifuge modeling, and standard wide width testing

WIDE-WIDTH TENSILE TEST RESULTS
FLQ5754 / UNIVERSITY OF CALIFORNIA, BERKELEY

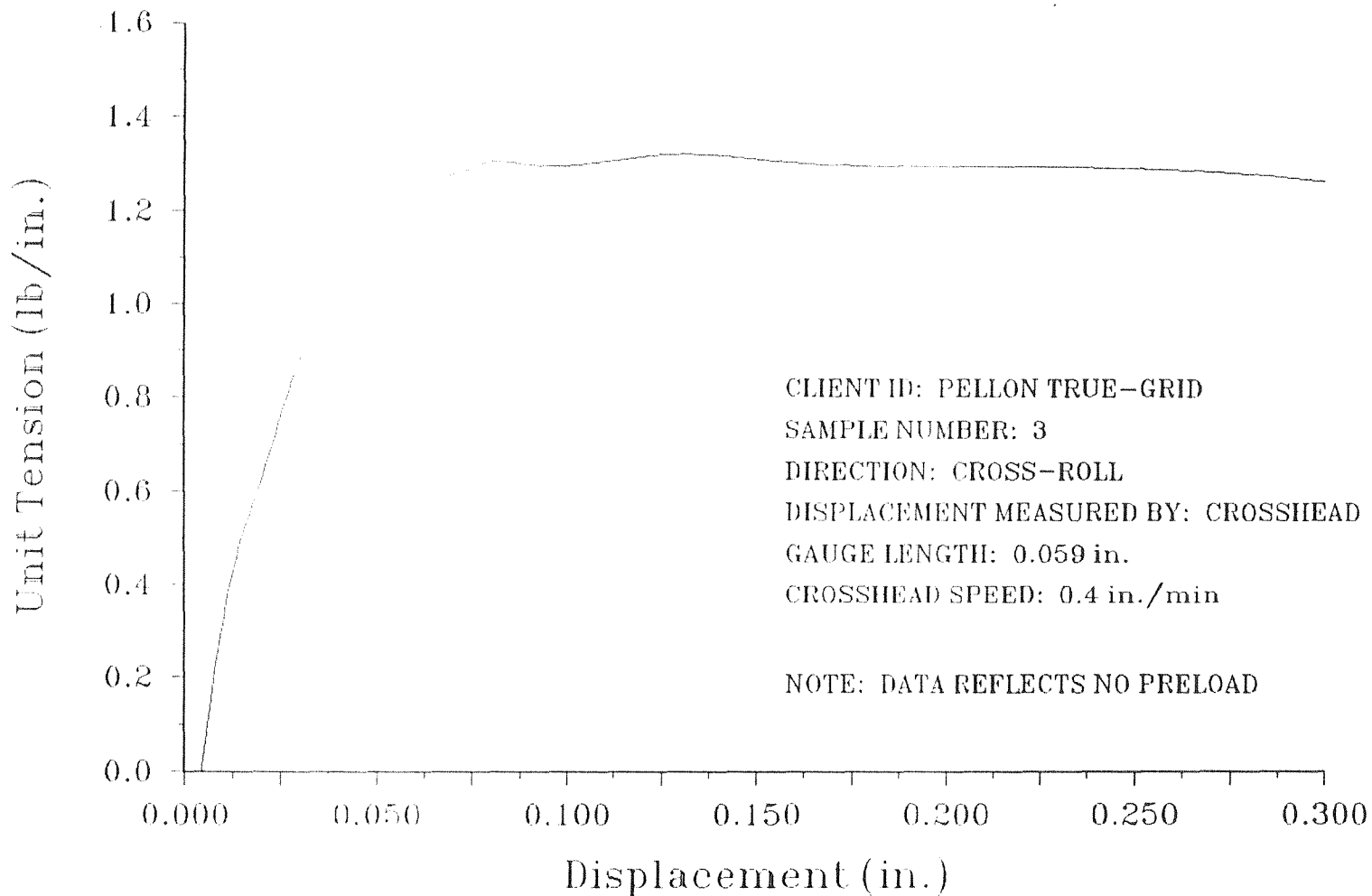


Figure 4.33 - Typical tensile test results obtained for a pellan tru-grid geotextile tested using a small gauge length setup (Test by Geosyntec Consultants)

The difference in post-peak behavior between Pellon Sew-in and Pellon-Tru-grid geotextiles, which is observed only from tensile tests performed using small gauge length appears to explain the post-failure performance of the centrifuge slope models as will be discussed in Section 4.6.2 .

Figure 4.34 shows the tensile strength results obtained for different width/length ratios for both the Pellon Tru-grid and Pellon-sew in geotextiles. The results for the width/length ratios of 2 and 133 (standard and 1.6 mm gauge length tests) are the average results obtained from three tensile tests. The intermediate results were obtained from a single test. All tests were performed at a crosshead speed of 10 mm/min. The figure shows that there is a sharp increase in ultimate tensile strength at lower width/length ratios, and that the strength values tend to stabilize at larger ratios.

The results of the geotextile testing program summarized in Figure 4.34 provided a range of possible strength values that could be adopted in the analysis of the reinforced slope models. However, the finally selected geotextile strength values were adopted from backcalculation of one centrifuge slope built using each geotextile type. The backcalculated strength values, also indicated in Figure 4.34, are $T_{ult}=0.123$ kN/m (0.7 lb/in) for the Sew-in geotextiles and $T_{ult}=0.183$ kN/m (1.05 lb/in) for the Tru-grid geotextiles. As will be discussed in Section 4.7.2.2 , these values were obtained using limit equilibrium analysis assuming that all geotextile reinforcements contribute with their peak tensile strength to the stability of the slope models. Good agreement can be observed between the backcalculated geotextile strengths and the range of values defined in the tensile testing program.

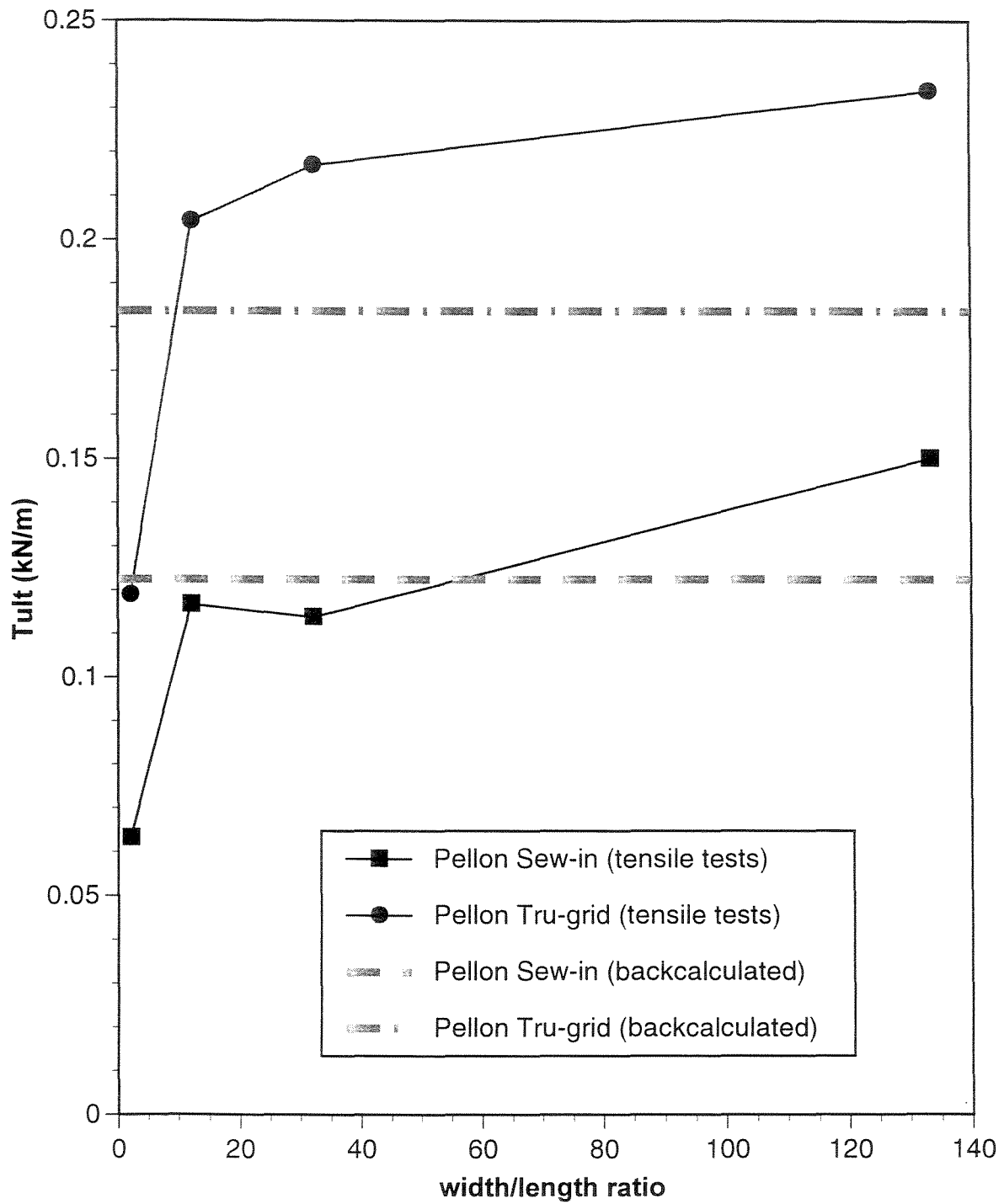


Figure 4.34 - Effect of width/length specimen ratio on the ultimate tensile strength of geotextile reinforcements

The backcalculated values are lower than those obtained using the 1.5 mm gauge length tensile tests. Although further investigation should be pursued in order to appropriately characterize geotextile strength properties, two different explanations can be offered to decide about the which is the "actual" in-soil geotextile strength:

- The actual in-soil strength is the value obtained from tensile testing using a small gauge length. The smaller strength backcalculated from centrifuge testing accounts for the fact that the distribution of reinforcement forces is not completely uniform with depth as assumed in the performed limit equilibrium analyses (see Section 4.6.3 for further discussion).
- The actual in-soil geotextile strength is the one obtained from backanalysis of centrifuge tests considering uniform reinforcement force distribution. The higher strength obtained from tensile tests with small gauge length is caused by high testing strain rates. In this case, a width/length ratio for geotextile specimens of approximately 10 would account for the effect of boundary conditions without inducing high loading strain rates. Notice that all tests indicated in Figure 4.34 were performed at the same displacement rate. The effect of decreasing the displacement rate in tests using 1.5 mm gauge length was preliminary evaluated, and decreasing tensile strengths which appeared to converge to the values backcalculated from the centrifuge tests were obtained.

A final evaluation of these issues can not be provided at this point. However, geotextile tensile strength results obtained from tensile and centrifuge testing provide

insight into the possible causes of strength increase of geotextiles under the confinement of soil. Moreover, although the issues above remain unsolved, the good agreement between the backcalculated geotextile strength and the range of strength values from the geotextile testing program provides confidence in the geotextile properties selected for the limit equilibrium analyses.

4.4.3 Interface properties

A series of direct shear tests was performed to evaluate the interface friction between different interfaces relevant to the interpretation of the centrifuge slope model results. As part of the testing program, the interface strength between the sand and each of the two geotextiles used as reinforcements was determined in order to evaluate the pullout resistance in the slope models. Moreover, the interface strength between the sand and the materials that lined the vertical walls of the centrifuge box (teflon and mylar) was investigated in order to evaluate the influence of the lateral friction on the stability of the centrifuge models.

4.4.3.1 Test setup

Direct shear tests of the different interface combinations were performed at the Geotechnical Laboratory of the University of California at Berkeley, using a modified Karol-Warner direct shear testing apparatus. Load cells were used to monitor shear forces applied to test specimens, while shear displacements were monitored by evaluating the constant displacement rate of the test using dial gauge readings.

Figure 4.35 is a schematic cross section illustrating the typical sample configuration used for direct shear testing of the different interfaces. The geotextile, teflon, and mylar specimens were cut to a diameter of approximately 100 mm, and mounted using two sided adhesive tape to a 100 mm diameter steel base platen. The sand material was then placed above this base platen within a 50 mm x 50 mm square steel forming mold.

Immediately prior to shearing, the steel forming mold was raised approximately 1 mm using four screw jacks, and a vertical (normal) load was applied to the top of the sand specimen. The screw jacks were then withdrawn so the slightly elevated forming mold had no contact with the base interface specimen, and was suspended by the lateral contact force on the sides of the clay specimen. Normal stresses acting on the sample interfaces were corrected to account for the weights of all overlying test system components. Figure 4.36 shows a view of the direct shear apparatus setup in preparation

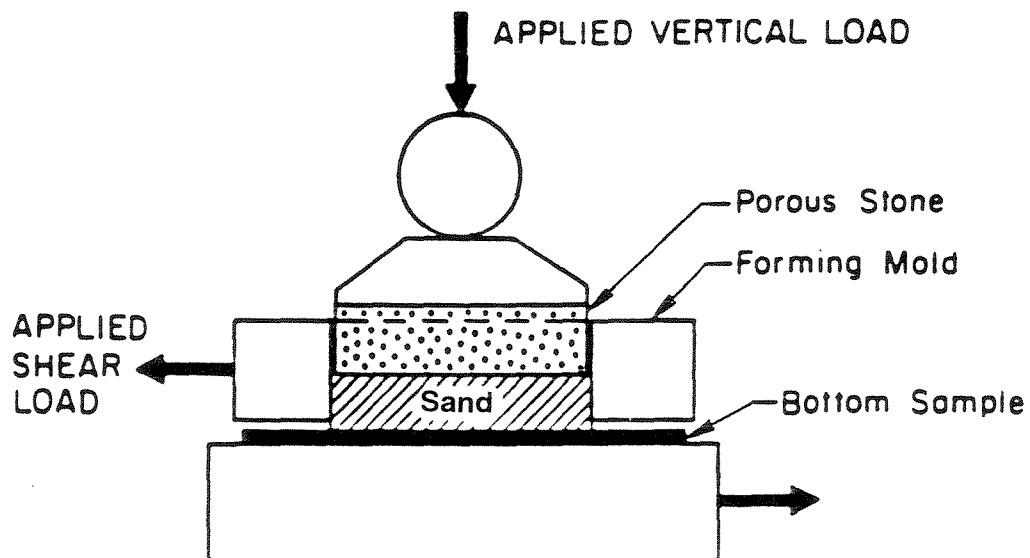


Figure 4.35 - Schematic cross section showing sample configuration in the direct shear device

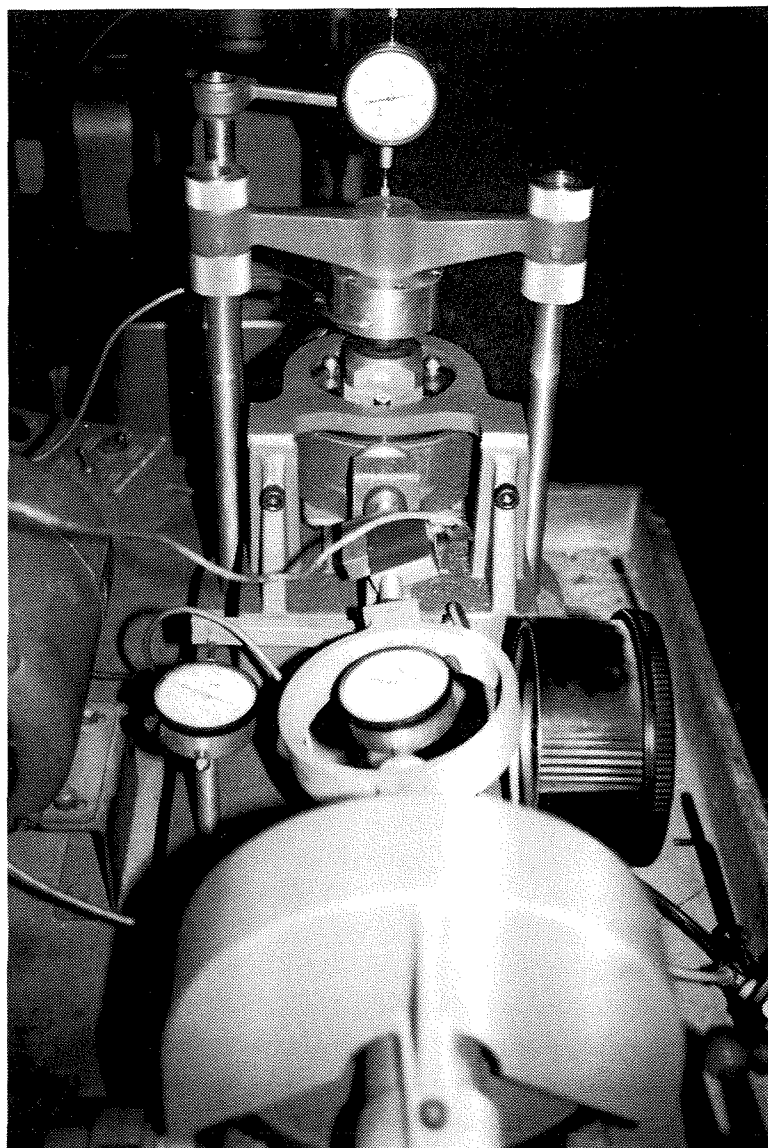


Figure 4.36 - View of direct shear apparatus ready for sand/geotextile interface testing

for a sand/geotextile interface test. The procedures for direct shear testing were based on those followed during investigation of interface strength parameters for the Kettleman Hills waste landfill slope failure (Mitchell et al., 1990). In that study, good agreement was found between the residual interface shear strength properties measured in the small direct shear apparatus and in larger pullout-box tests. This adds confidence to the use of the simpler direct shear box tests for determination of interface strength.

4.4.3.2 Interface strength results

Interface-shear tests were performed by shearing the interface samples under strain-controlled loading at rates of shear displacement of between 0.05 mm/min and 0.08 mm/min. Normal stresses on the sample interfaces during testing were selected to be representative of the range of values experienced in the centrifuge tests.

The interface strength tests between sand and the two geotextiles used in the centrifuge slope models were performed at two different normal pressures. Although the sand relative density is more difficult to control in the direct shear device than in the triaxial apparatus, a target sand relative density of about 60% was obtained in all tests. Figure 4.37 shows the interface test results for the Sew-in and Tru-grid geotextiles, tested at a normal pressure of 85 kPa. The results are indicated as mobilized friction angle (arctan of interface shear stress/normal pressure) versus shear displacement. The interfaces between Monterey No. 30 sand and both geotextile materials show a similar behavior, achieving a peak strength at approximately 1.5 mm of shear displacement. No marked post-peak softening behavior is observed in any of the two interfaces. Table 4.4 summarizes the results obtained from direct shear testing of the sand/geotextile interfaces.

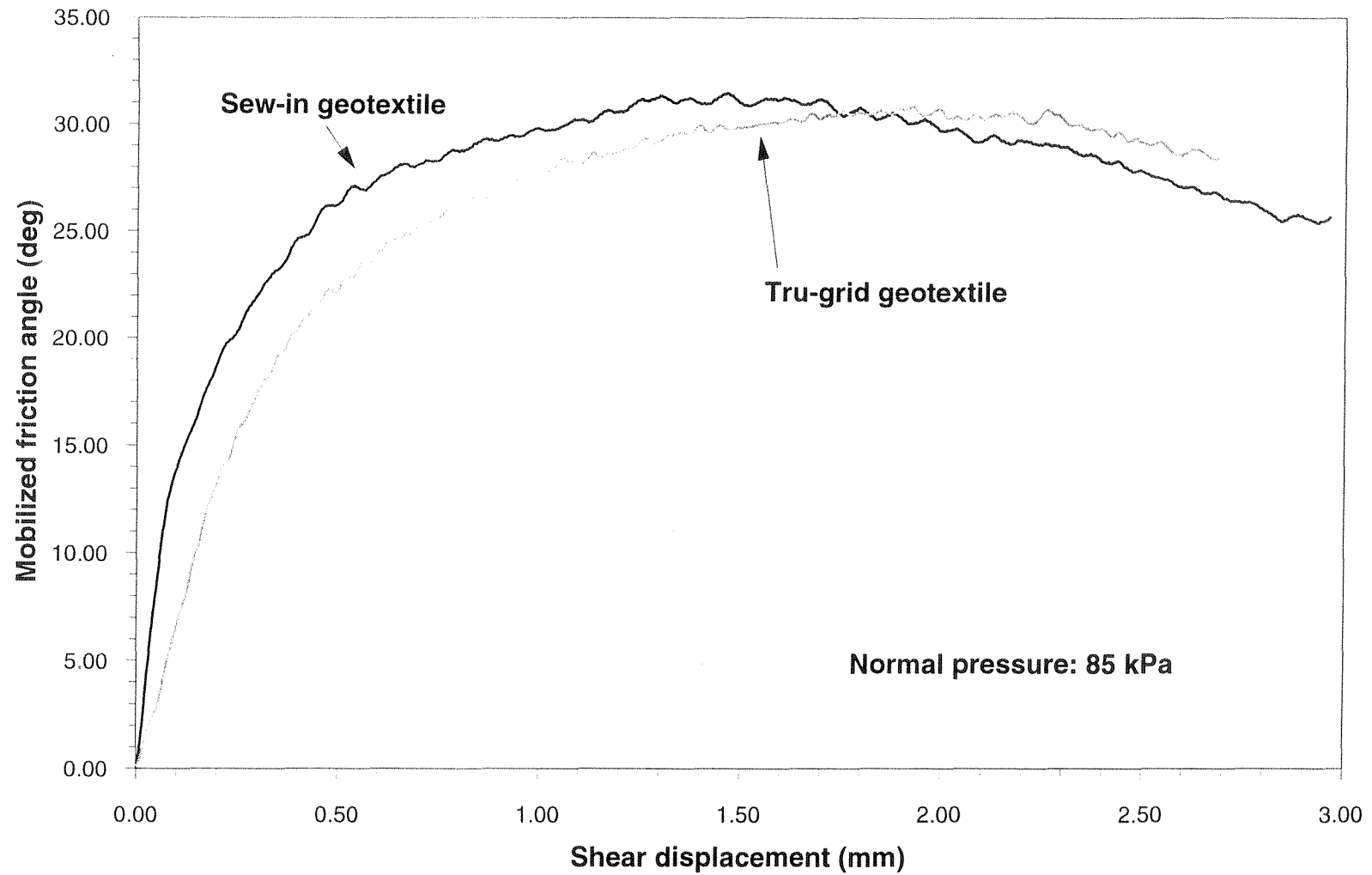


Figure 4.37 - Direct shear test results for the different sand/geotextile interfaces

Table 4.4 - Direct shear test results on interfaces between sand and geotextiles, mylar, and teflon

Interface	Normal stresses (kPa)	Peak friction angle (degrees)	Shear displacement at peak strength (mm)	Residual friction angle (degrees)
Sand / Sew-in geotextile	61	33.5	1.78	-
	85	31	1.37	-
Sand / Tru-grid geotextile	71	30.5	1.27	-
	85	30.5	1.68	-
Sand / Mylar	49 to 89	13.5	0.15	11
Sand / Teflon	63 to 82	19	0.23	18

For plane sheet materials such as geotextiles the direct sliding resistance obtained from direct shear tests is equal to the bond capacity that governs the anchorage length required to mobilize the allowable reinforcement force. Thus the interaction for the geotextiles may be measured either in a pullout test or in a modified direct shear test (Jewell, 1990). The strength of the sand/geotextile interfaces can be characterized by the interface friction factor f , defined as:

$$f = \frac{\tan\delta}{\tan\phi} \quad (4.24)$$

where δ is the interface friction angle and ϕ is the soil friction angle. The interface friction factor for the geotextiles in this study is approximately equal to 0.9 . High interface friction factors generally characterize the interfaces of nonwoven geotextiles.

The interface strength between the sand and the teflon and mylar materials used to line the vertical walls of the centrifuge box was investigated to evaluate the influence of these interfaces on the stability of the models. Normal pressure was increased during the direct shear tests in order to evaluate its effect on the residual interface friction. Sand at 60% relative density was also used in this series of tests. Figure 4.38 shows the mobilized friction angle versus shear displacement for the interfaces between sand and the mylar and teflon materials. The changes in normal pressures are indicated in the figure. The results of tests on both interfaces show a peak strength at very small shear displacements (less than 0.25 mm), with the sand/teflon interface showing a higher strength than the sand/mylar interface. The teflon interface behavior after peaking showed only a slight shear-strength reduction to a residual friction value, while the mylar interface showed a rapid decrease in shear strength to a lower residual (and fairly constant) strength. A summary of the direct shear test results obtained for the sand/mylar and sand/teflon interfaces is presented in Table 4.4. The effect of these interfaces on the performance of the centrifuge slopes is evaluated in Section 4.7.2.5.

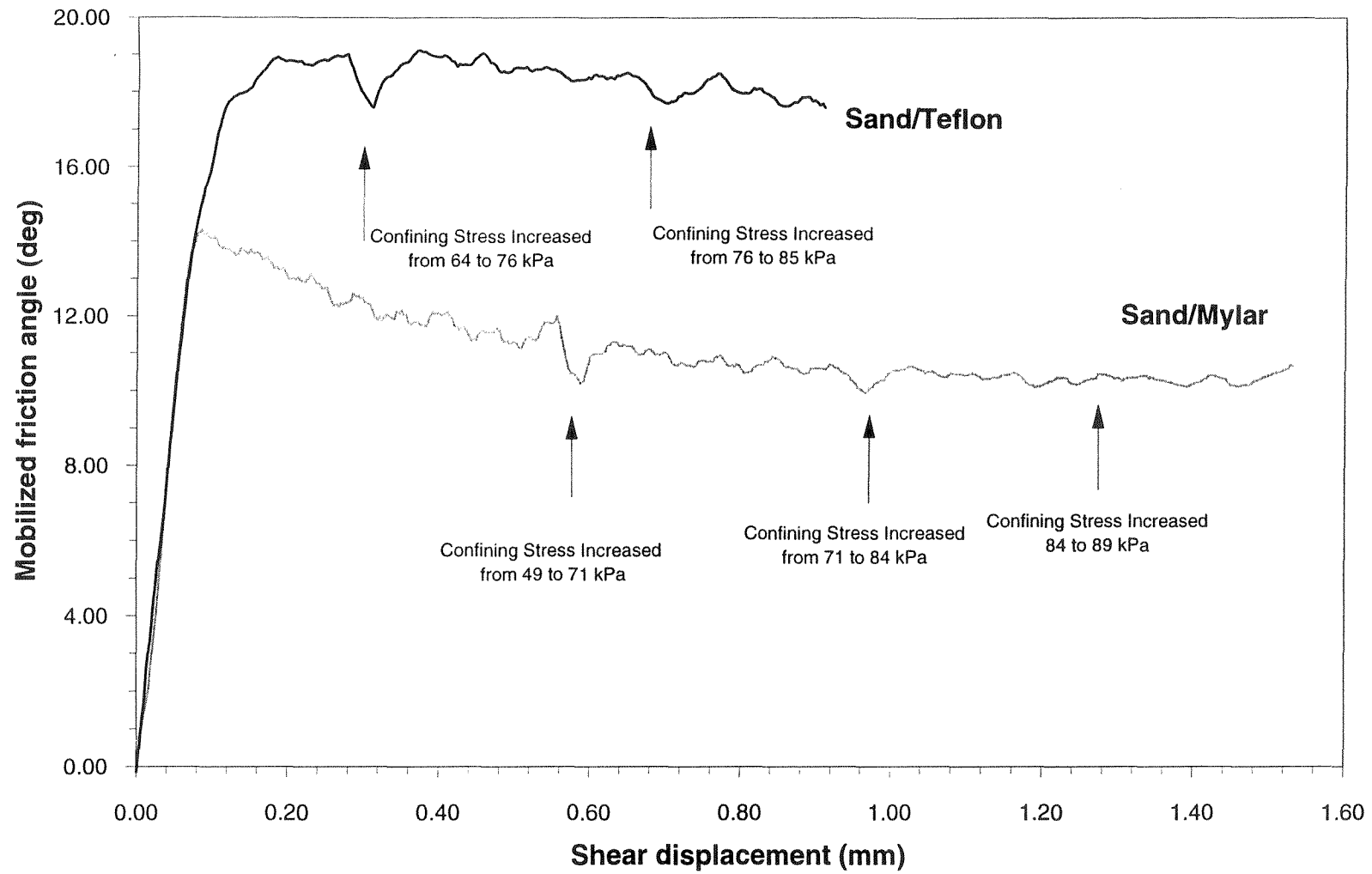


Figure 4.38 - Direct shear test results for sand/teflon and sand/mylar interfaces

4.5 Experimental results

4.5.1 Scope of the testing program

One of the main purposes of this study is the evaluation of limit equilibrium methods used as design procedures for geotextile-reinforced soil slopes. Consequently, all variables were selected so that they can be taken into account in a limit equilibrium framework. Accordingly, the selected variables are:

- Vertical spacing of the geotextile reinforcements: four different reinforcement spacings were adopted;
- soil shear strength parameters: the same sand at two different relative densities were used; and
- ultimate tensile strength of the reinforcements: two geotextiles with different ultimate tensile strength were selected.

All models were built with the same slope, 1H:2V, and the same total height, 9 inches. Since flexible facing (wrapped geotextile) was adopted in all models, possible contribution to stability provided by rigid facing structures is not an issue. The centrifuge tests performed in this study are grouped into three test series, each aimed at investigating the effect of one of the variables:

Baseline, B-series: performed to investigate the effect of reinforcement spacing. Four centrifuge models with six, nine, twelve, and eighteen reinforcement layers were

used in this series. Monterey No.30 sand at 55% relative density and Pellon Sew-in geotextiles were used in all the models in this series.

Denser soil, D-series: performed to investigate the effect of soil strength parameters on the stability of geotextile-reinforced slopes. Monterey No.30 sand at a higher relative density (75%) than in the Baseline series was used. As in the case of the models in the B-series, Pellon-Sew-in geotextiles were used as reinforcements.

Stronger geotextile, S-series: performed to investigate the effect of geotextile ultimate tensile strength on the performance of reinforced slopes. These models were reinforced with Pellon Tru-grid geotextile, which is stronger than the geotextile used in the other series. As in the case of the models in the B-series, Monterey No.30 sand at 55% relative density was used as backfill material.

Each reinforced slope model in this study is named using a letter that identifies the test series (B, D, or S), followed by the number of reinforcement layers used in the model. For example, Model B12 is the reinforced slope model from the B-series (Baseline), reinforced using twelve geotextile layers.

It should be noted that the stability evaluation addressed in this study accounts only for one failure mechanism of reinforced soil walls, namely, breakage of the reinforcements. The safety of the structure against external failure mechanisms (i.e. sliding, foundation bearing capacity) and against pullout of the reinforcements should also be satisfied in the design of reinforced soil slopes.

4.5.2 Centrifuge test results

A summary of the results from the eight centrifuge tests performed in this study is presented next. Interpretation of these results and discussion of their significance for the design of geotextile-reinforced soil slopes is presented in Section 4.6.

4.5.2.1 Baseline B-series

The characteristics of the models in this test series and the g-levels at failure obtained after centrifuge testing are presented in Table 4.5. All models in this series (B18, B12, B9, and B6) were tested using the same backfill density ($D_r=55\%$) and the same geotextile fabric (Pellon Sew-in), but different reinforcement spacing.

Typical results obtained after centrifuge testing of one of the models from the Baseline series (model B18) are first discussed in order to illustrate the type of data which was obtained throughout the study. A view of model B18 after construction, before removal of the wooden supports is shown in Figure 4.39. The gradual increase in centrifugal acceleration with time during centrifuge testing is plotted in Figure 4.40. The acceleration was increased until sudden failure occurred after approximately 50 min of testing when the acceleration imparted to the model was 76.5 times the acceleration of gravity.

Failure development in the reinforced slope could be identified from the TV images. However, settlements at the crest of the slope, monitored by LVDTs, proved to be invaluable to more accurately identify the moment of failure. Figure 4.41 shows the increasing settlements at the top of the reinforced slope during centrifuge testing, monitored at locations 12.5 mm and 62.5 mm from the crest of the slope. The sudden

Table 4.5 - Summary of centrifuge tests

Series:	Baseline (B)				Denser backfill (D)		Stronger geotextile (S)	
Model	B18	B12	B9	B6	D12	D6	S9	S6
# geotextile layers	18	12	9	6	12	6	9	6
Vertical spacing (in)	0.5	0.75	1.0	1.5	0.75	1.5	1.0	1.5
Geotextile	Pellon sew-in	Pellon sew-in	Pellon sew-in	Pellon sew-in	Pellon sew-in	Pellon sew-in	Pellon tru-grid	Pellon tru-grid
Sand Rel. Dens. (%)	55%	55%	55%	55%	75%	75%	55%	55%
g-level at failure (N_f)	76.5	60	37	21	66	29	52.5	32
Failure type	Catastrophic	Catastrophic	Catastrophic	Catastrophic	Catastrophic	Catastrophic	Not catastrophic	Not catastrophic

increase in the monitored settlements indicate the moment of failure, when the reinforced active wedge slid along the failure surface.

Recorded images showing the development of failure of the models were an effective way of identifying the actual shape of the failure surface and the possible failure mechanisms. An evaluation of the images retrieved during centrifuge testing progress is presented in Section 4.6.2 as part of a discussion of the characteristics of the failure surfaces. Figure 4.42 shows the failure surface that developed in model B18, as observed after unloading the model from the centrifuge bucket. As can be observed in the figure, the failure surface is clearly defined and goes through the toe of the reinforced slope.

Following the experiment, each model was carefully disassembled in order to examine the breaks in the geotextile layers. Figure 4.43 shows one of the geotextile

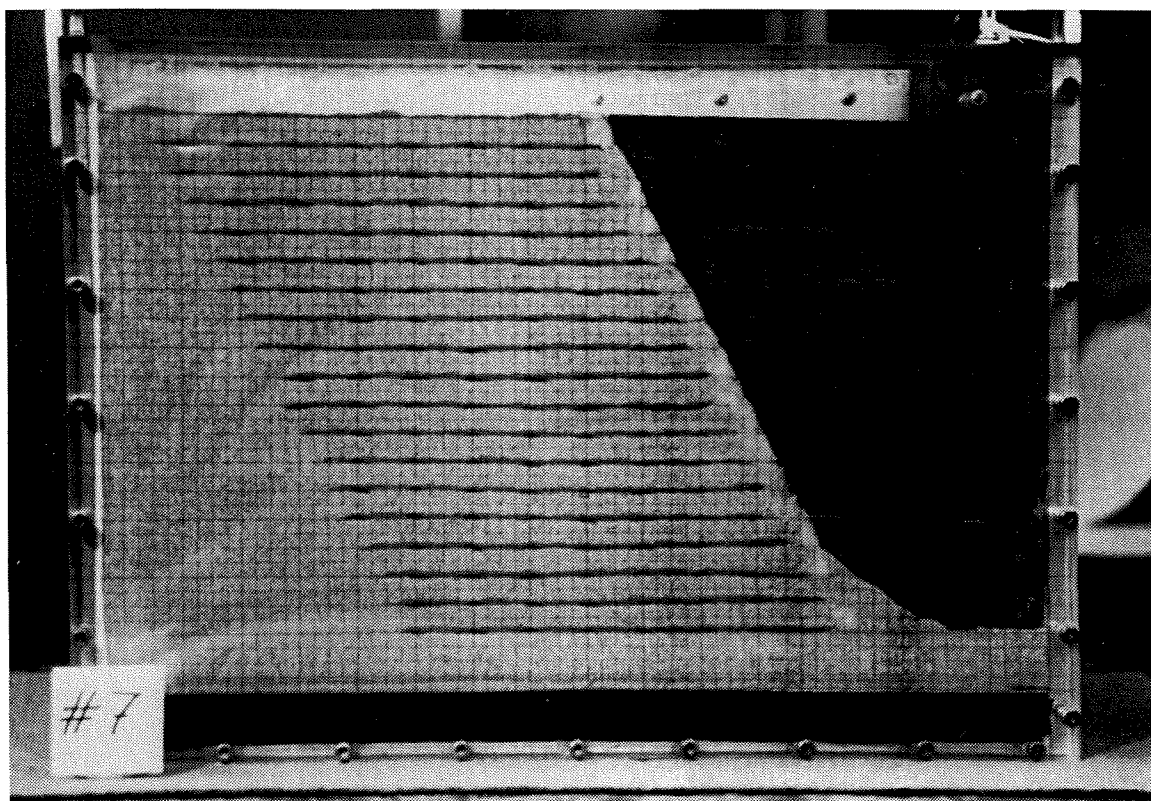


Figure 4.39 - Model B18 after construction

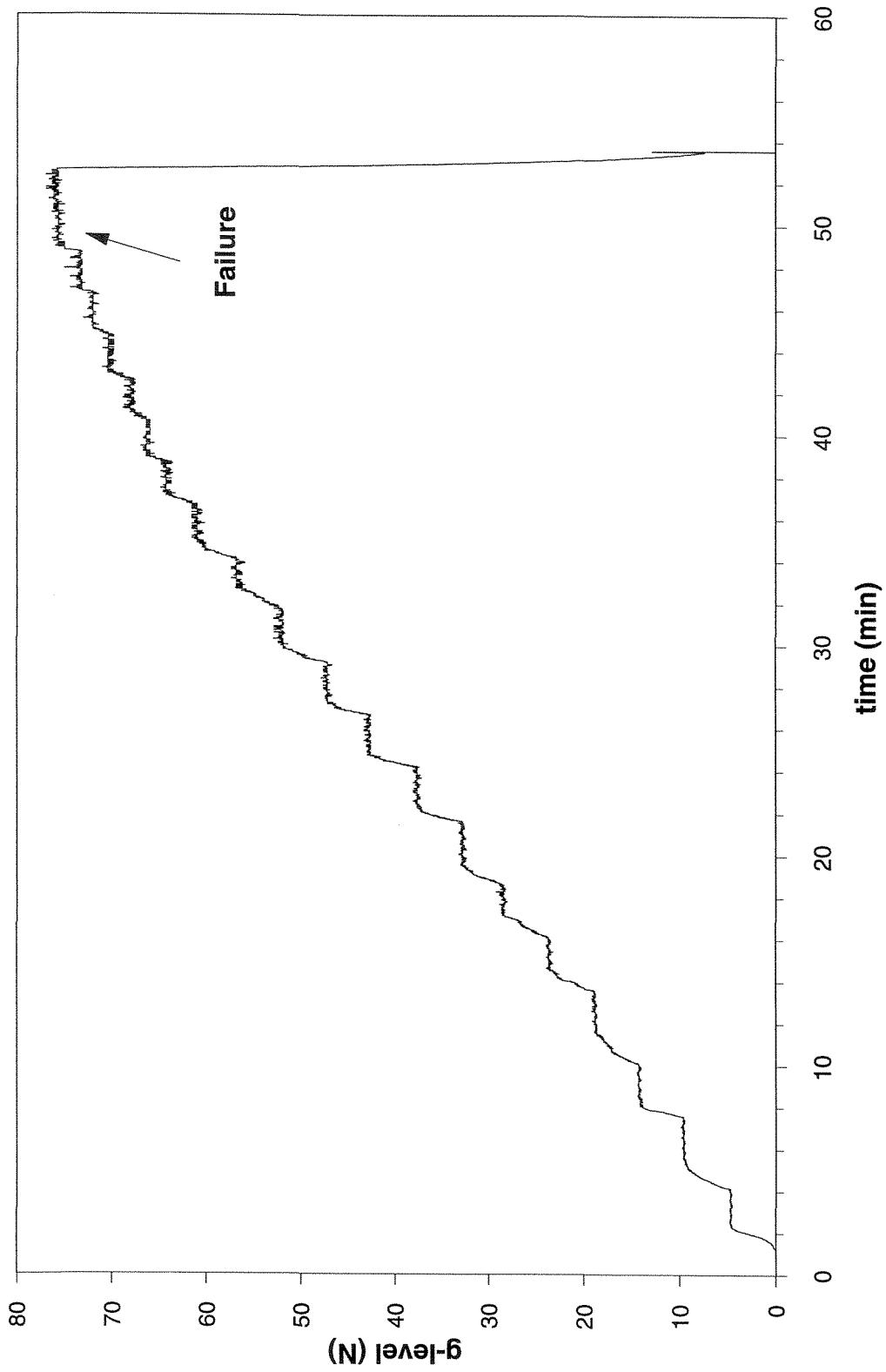


Figure 4.40 - G-level (N) versus time during centrifuge test of model B18

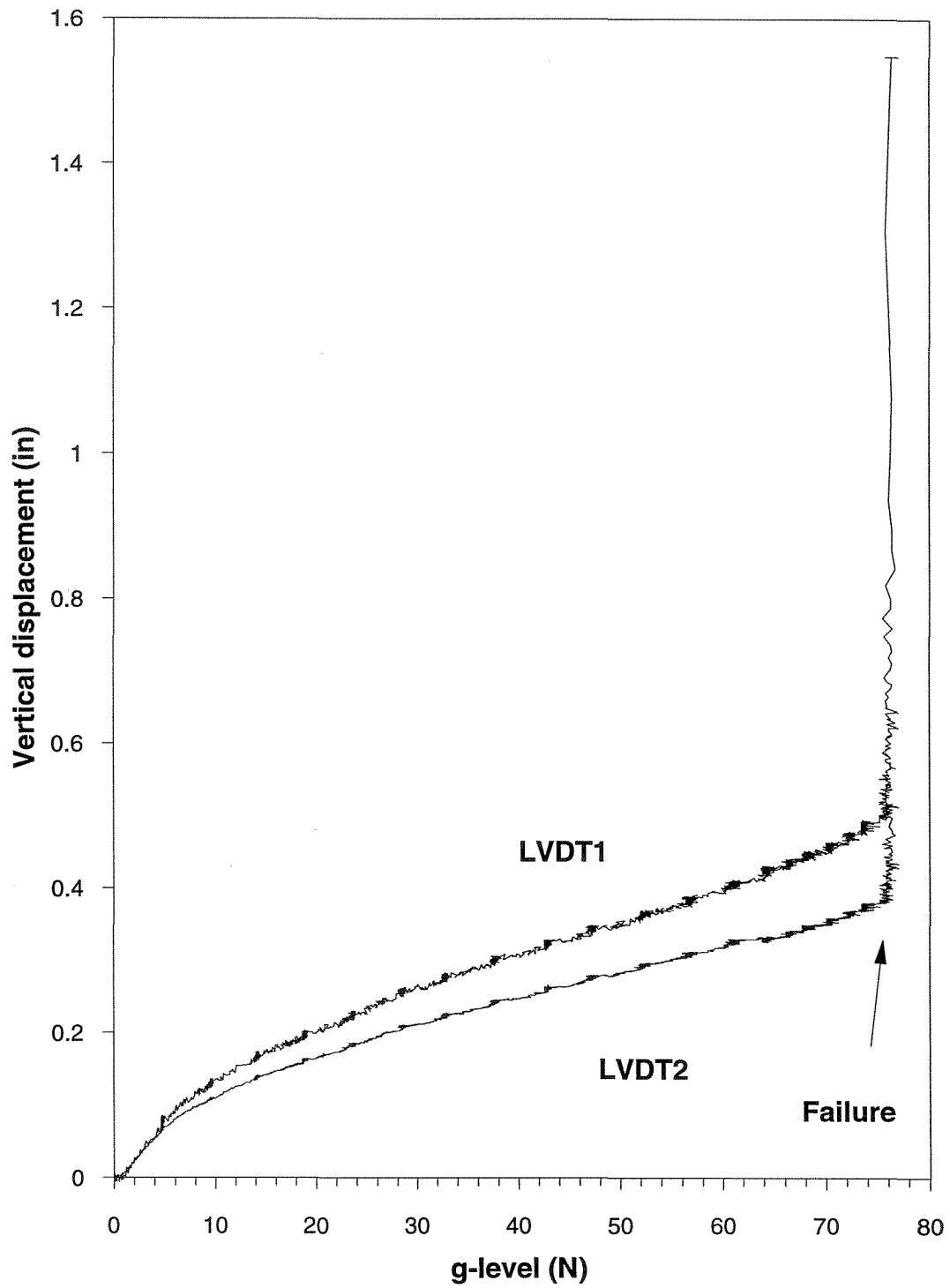


Figure 4.41 - Settlements at the crest of reinforced slope B18, indicating moment of failure

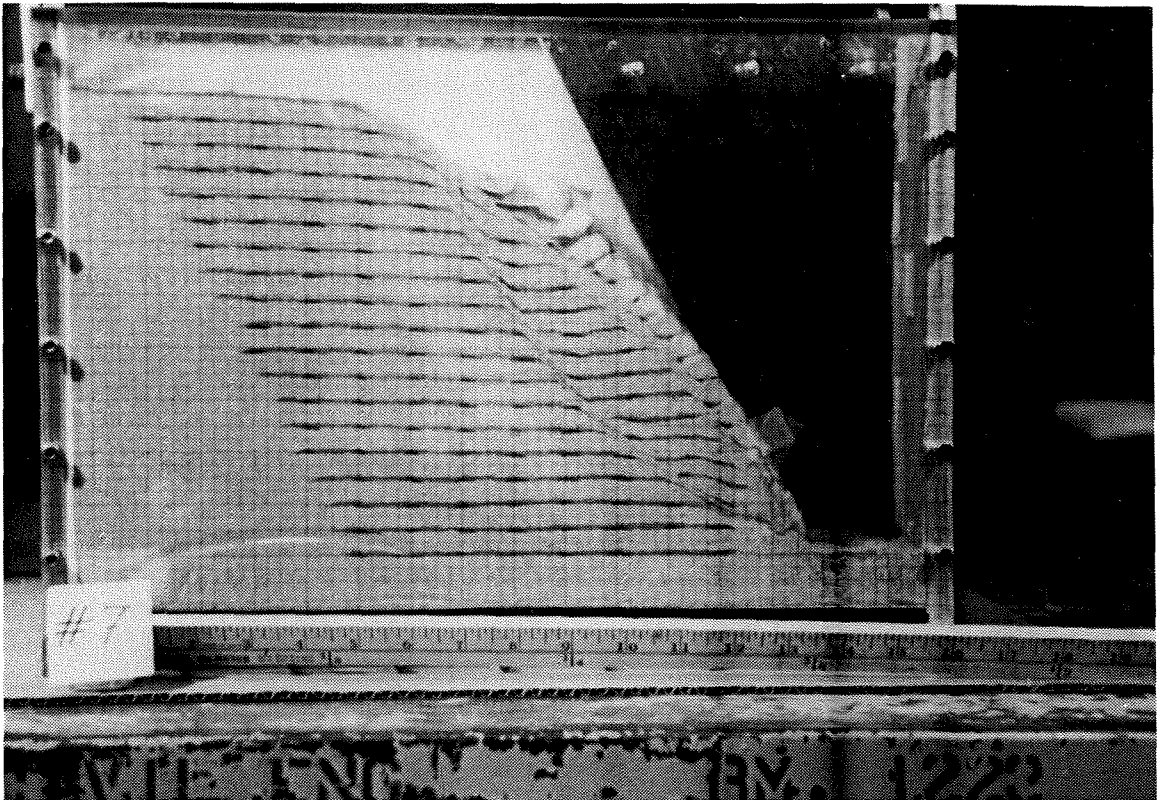


Figure 4.42 - View of model B18 after the centrifuge test

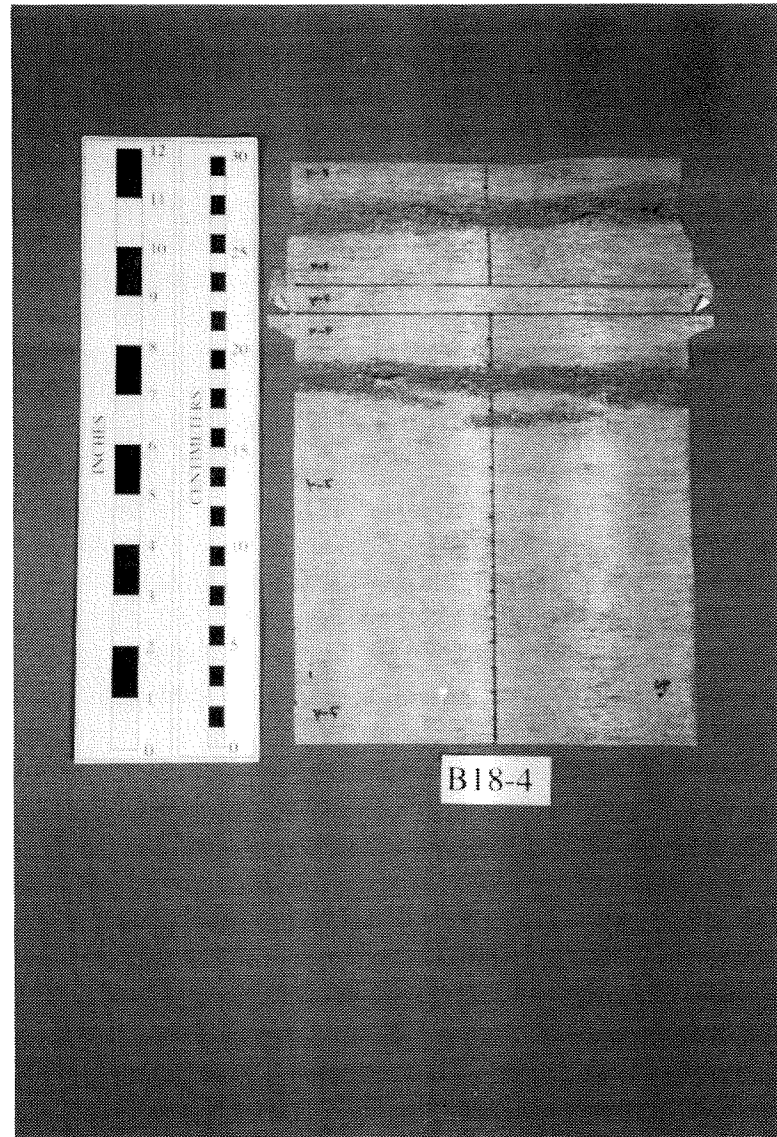


Figure 4.43 - Geotextile layer retrieved from model B18, showing tensile tears along the primary reinforcement and overlapping layers

layers retrieved from model B18 after centrifuge testing (fourth layer the base of the slope). Since this particular layer was located towards the base of the slope, the failure surface intersected the geotextile both on the primary reinforcement and on the overlapping length. Figure 4.44 shows the eighteen geotextiles retrieved after centrifuge testing of model B18. The geotextile shown at the top left corner of the figure is the first reinforcement layer retrieved from the base of the reinforced slope model. The geotextile at the bottom right corner is the reinforcement retrieved from the top of the model. All retrieved geotextiles show clear breaks at the location of the failure surface. The breakage pattern observed from the retrieved geotextiles is clear evidence that internal failure was caused only by breakage of the reinforcements. The geotextile layers located towards the base of the slope model also showed breakage of the geotextile overlaps,

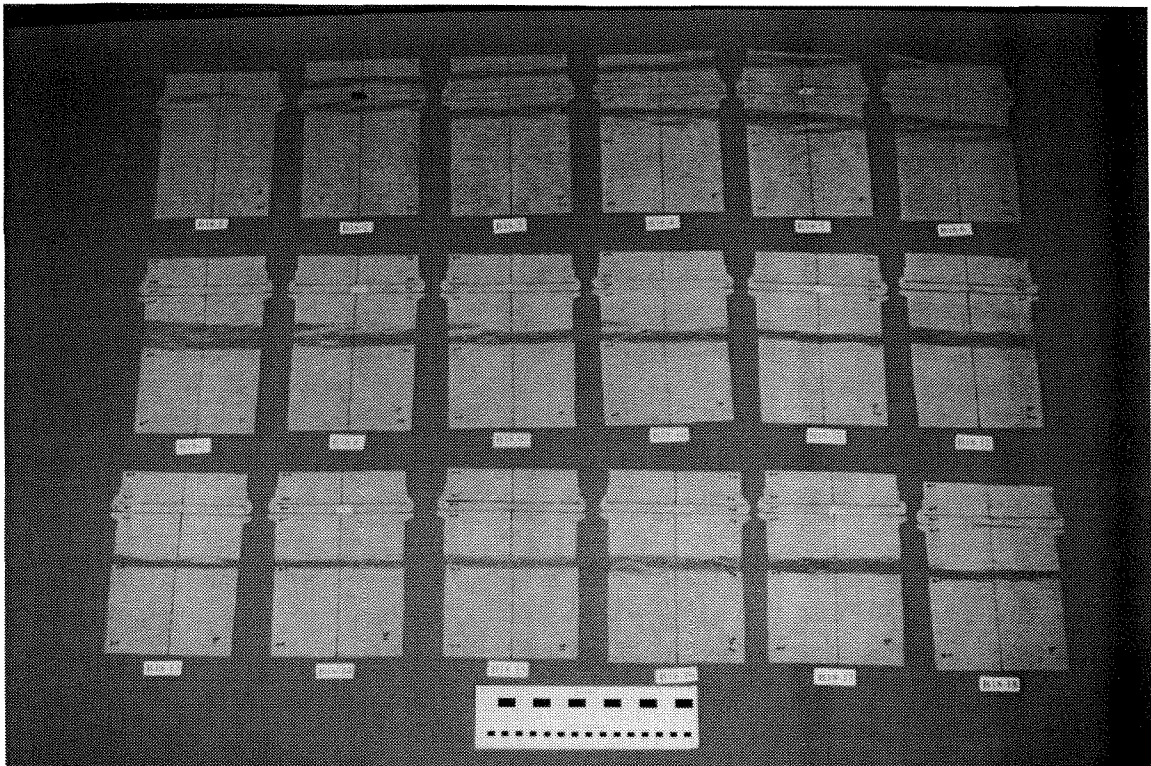


Figure 4.44 - Geotextile reinforcements retrieved from model B18

which clearly contributed to the stability of the slope. No evidence of pullout was observed, even on the short overlapping layers.

Geotextile breakage was always perpendicular to the direction of loading, showing no evidence of edge effects caused by lateral friction between the model and the walls of the centrifuge box. If side friction had significant influence, the shape of the geotextile breakage would have been expected to be curved. Additional evidence that edge effects were small was obtained by dissecting one of the models (model B6) after centrifuge testing. Apparent cohesion was added to the initially dry sand by wetting the backfill after centrifuge testing. Dissection of the model was then performed in order to compare the pattern of displacements observed through the plexiglass wall with those at the center of the model. Displacements observed in colored sand markers were essentially identical.

The location of the failure surface could be determined after the test by measuring the location of the tears in the retrieved geotextile primary reinforcements and overlaps. Figure 4.45 shows the location of the failure surface for model B18, as measured from the retrieved geotextiles. The figure also shows the location of the failure as digitized from the video images recorded at the moment of failure during the test. The top layers of the models were outside the range of view of the images observed with the TV camera. There is a clear agreement between the two sets of experimental data used to estimate the location of the failure surface in the reinforced slope model. This good agreement is further evidence that the edge effects during centrifuge testing were negligible.

Figure 4.46 shows a view of the failure of another model from the B-series, model B9, which is shown on the centrifuge bucket right after centrifuge testing. A clearly defined failure surface through the toe of the reinforced soil model can be observed.

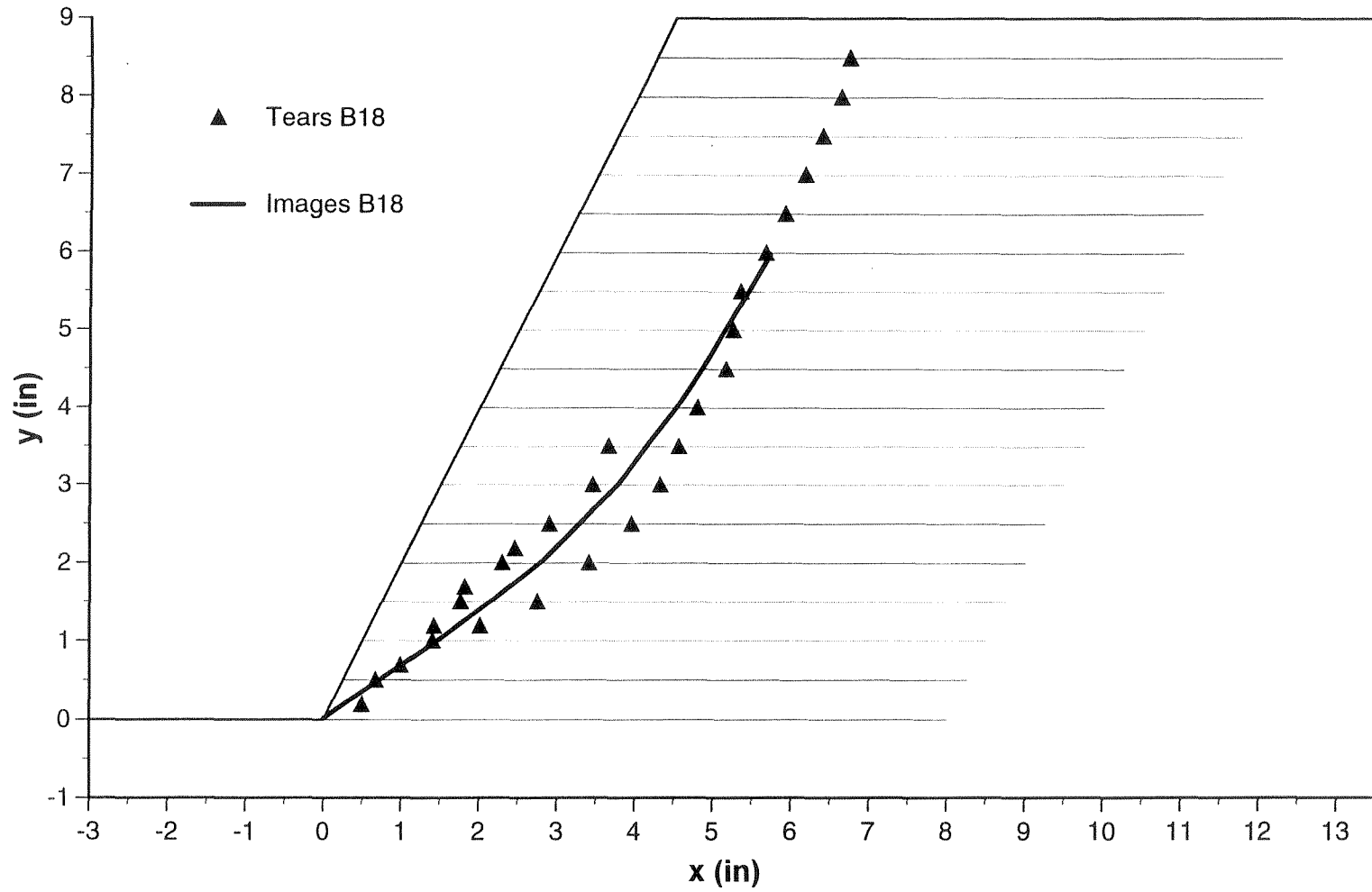


Figure 4.45 - Location of the failure surface for centrifuge model B18, as obtained from tears in the reinforcements and from images recorded through the plexiglass wall

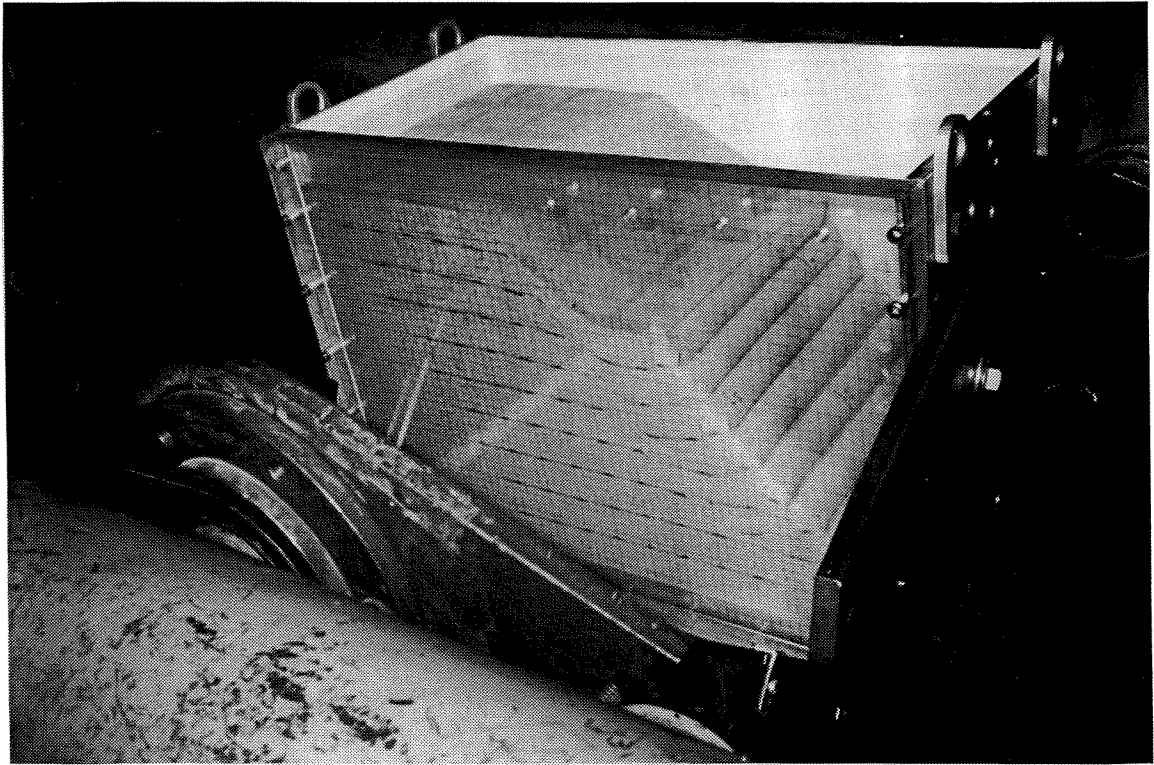


Figure 4.46 - View of model B9 after centrifuge testing

Figure 4.47 shows that the pattern of breakage in the geotextiles retrieved from this model is quite similar to that observed in model B18. Tensile failure is observed both in the primary reinforcements and in the overlap layers, clearly indicating internal failure of model B18 due to breakage of the reinforcements.

The effect of reinforcement spacing on the stability of the reinforced slope models, evaluated by the measured g-level at failure, can be observed in Figure 4.48. The figure indicates the g-level reached at the moment of failure (N_f) for each centrifuge test versus the number of reinforcement layers (n). The number of reinforcement layers in the figure considers all the geotextile layers intersected by the failure surface. This includes not only the primary reinforcement layers, but also the number of geotextile overlapping layers that were intersected by the failure surface. The reason for this consideration is that, as observed on the retrieved geotextiles after testing, the overlaps cut by the failure surface developed tensile forces and eventually failed by breakage and not by pullout (see Sections 4.6.4.2 and 4.7.2.4). The figure shows that a clear linear relationship can be established between the number of reinforcement layers and the g-level at failure. As the fitted line passes through the origin, all tests in the Baseline series can be characterized by a single n/N_f ratio ($n/N_f=0.281$ for series B). The other two series of centrifuge tests can also be represented by constant n/N_f values. The rationale behind this apparent normalization of the centrifuge test results is further discussed in Section 4.6.1.

4.5.2.2 Denser soil D-series

The characteristics of the two slope models tested to failure to investigate the effect of soil strength properties are summarized in Table 4.5. Models D6 and D12 were

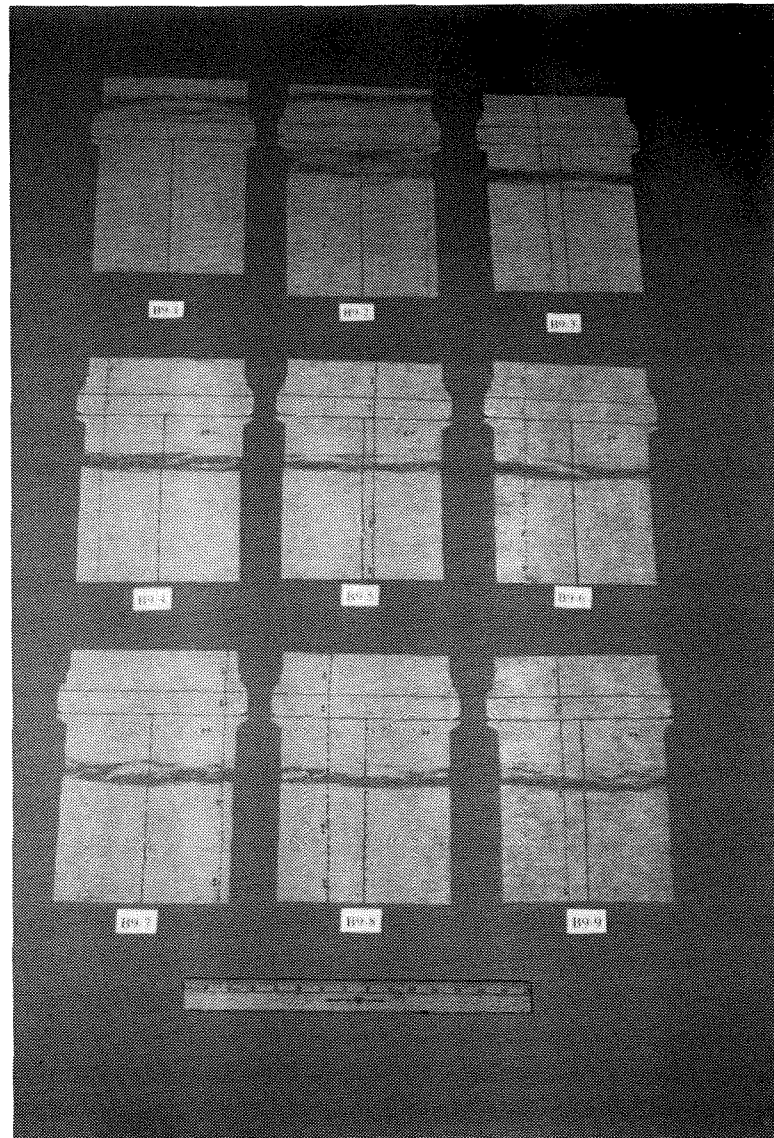


Figure 4.47 - Geotextile reinforcements retrieved from model B9 after centrifuge testing

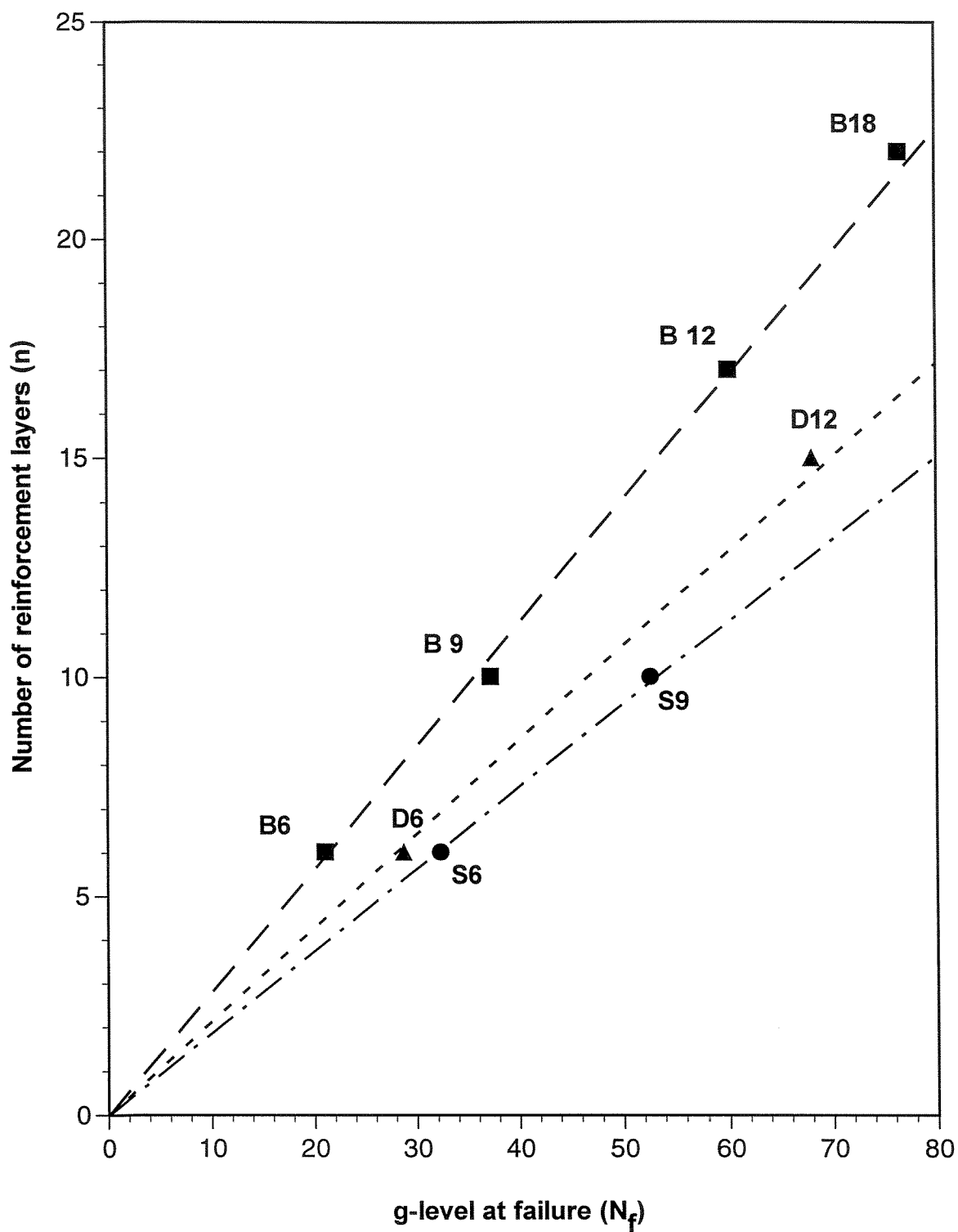


Figure 4.48 - G-level at failure for the different centrifuge models

identical to models B6 and B12, respectively, but built using a denser Monterey No.30 sand ($D_r=75\%$).

Figure 4.49 shows one of the models in this series, model D12, already placed in the centrifuge bucket and ready for testing. Catastrophic failure occurred after approximately 60 min of testing, when the acceleration imparted to the model was 66 times the acceleration of gravity. Figure 4.50 shows a view of the failure obtained in model D12 after centrifuge testing. A clearly defined failure surface developing through the toe of the slope can also be observed for the models from the D-series.

Figure 4.51 shows the twelve geotextile reinforcements retrieved from the model after testing. The geotextile at the top left corner of the picture is the reinforcement layer retrieved from the base of the slope. As was also the case for the models tested in the Baseline series, clear breakage of the reinforcements occurred in model D12 at the location of the failure surface. Internal failure occurred only by geotextile breakage, without any evidence of pullout. Moreover, geotextile overlaps towards the base of the slope also worked as additional reinforcements.

Figure 4.52 shows the location of the potential failure surface developed in model D12, as observed from the location of the tears in the retrieved reinforcements. The figure also shows the location of the failure as digitized from video images recorded during the centrifuge test at the moment of failure. Also in this case, there is a very good agreement between these two sets of data.

The effect of the higher soil strength on the stability of the centrifuge models can be observed in Figure 4.48. The figure shows that for a given number of reinforcement layers n , models from the Denser soil D-series failed at higher accelerations than models

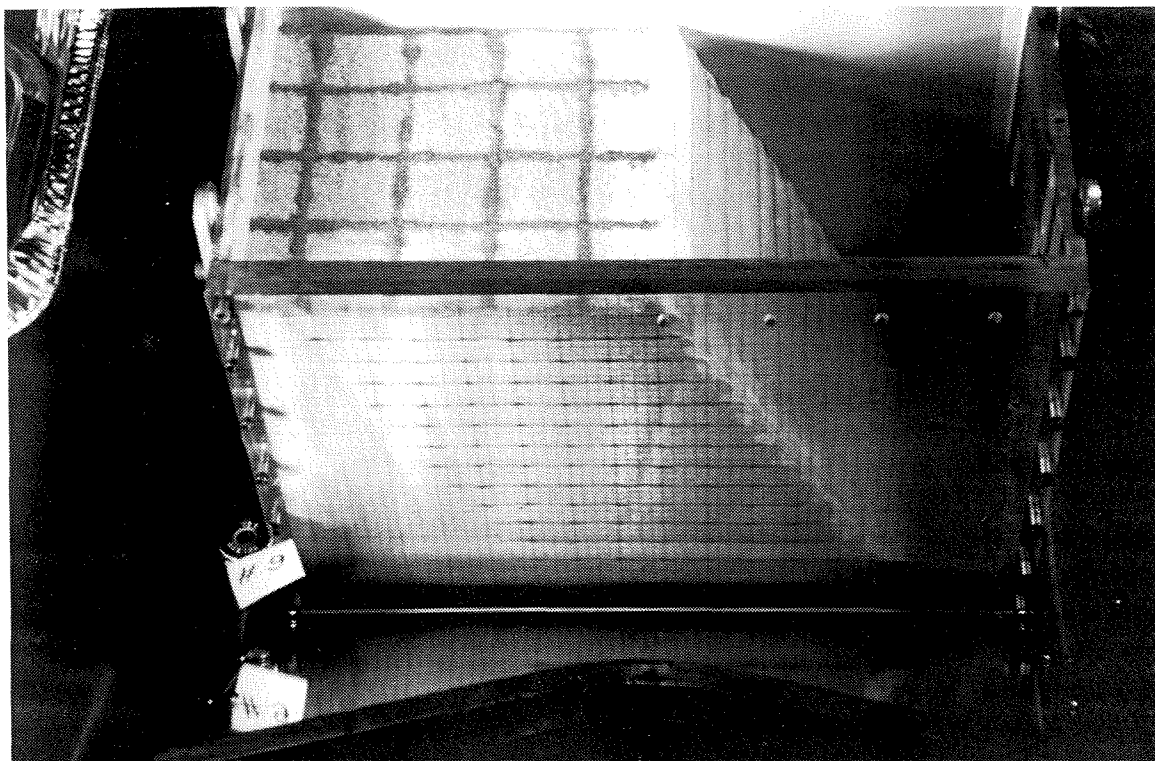


Figure 4.49 - Model D12 ready for testing

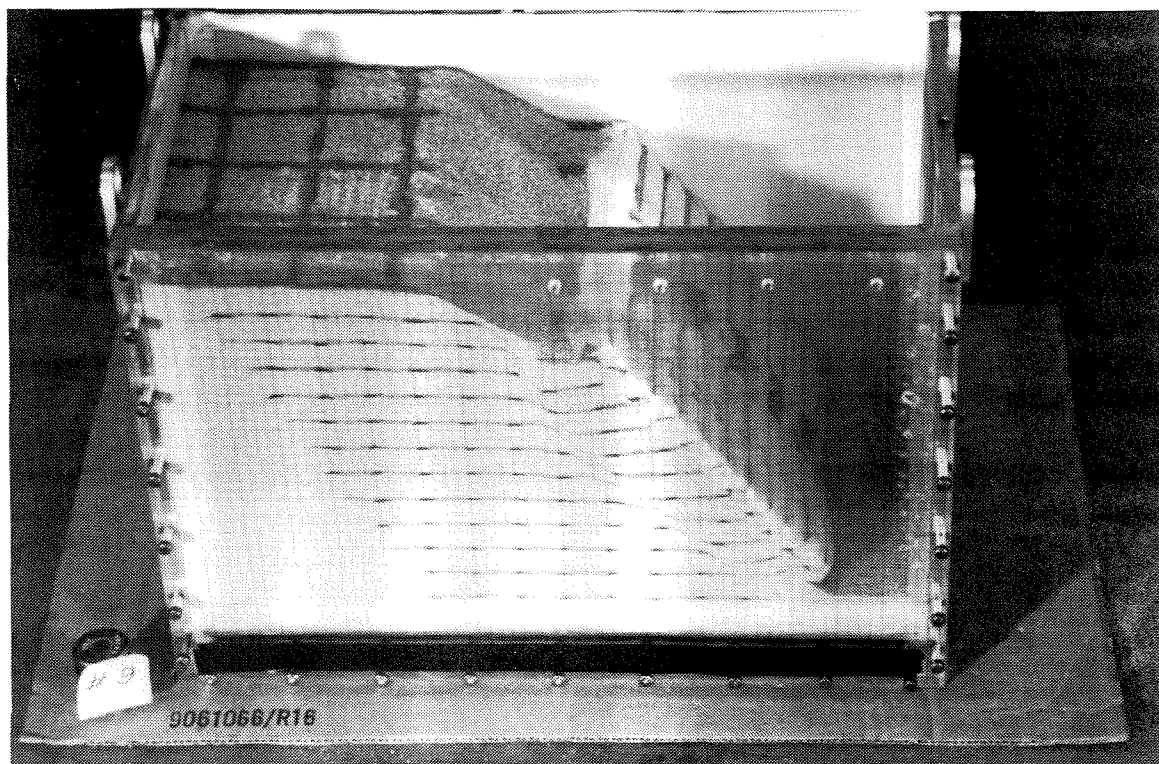


Figure 4.50 - Model D12 right after the test

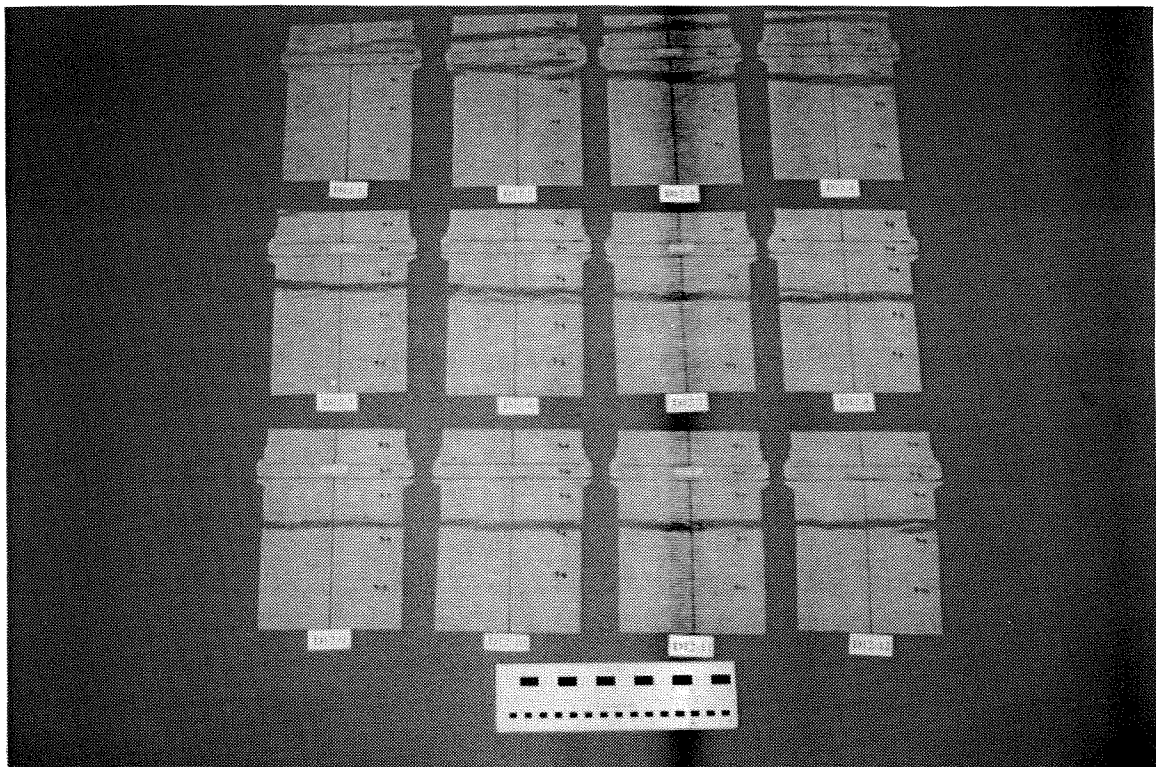


Figure 4.51 - Geotextile reinforcements retrieved from model D12 after centrifuge testing

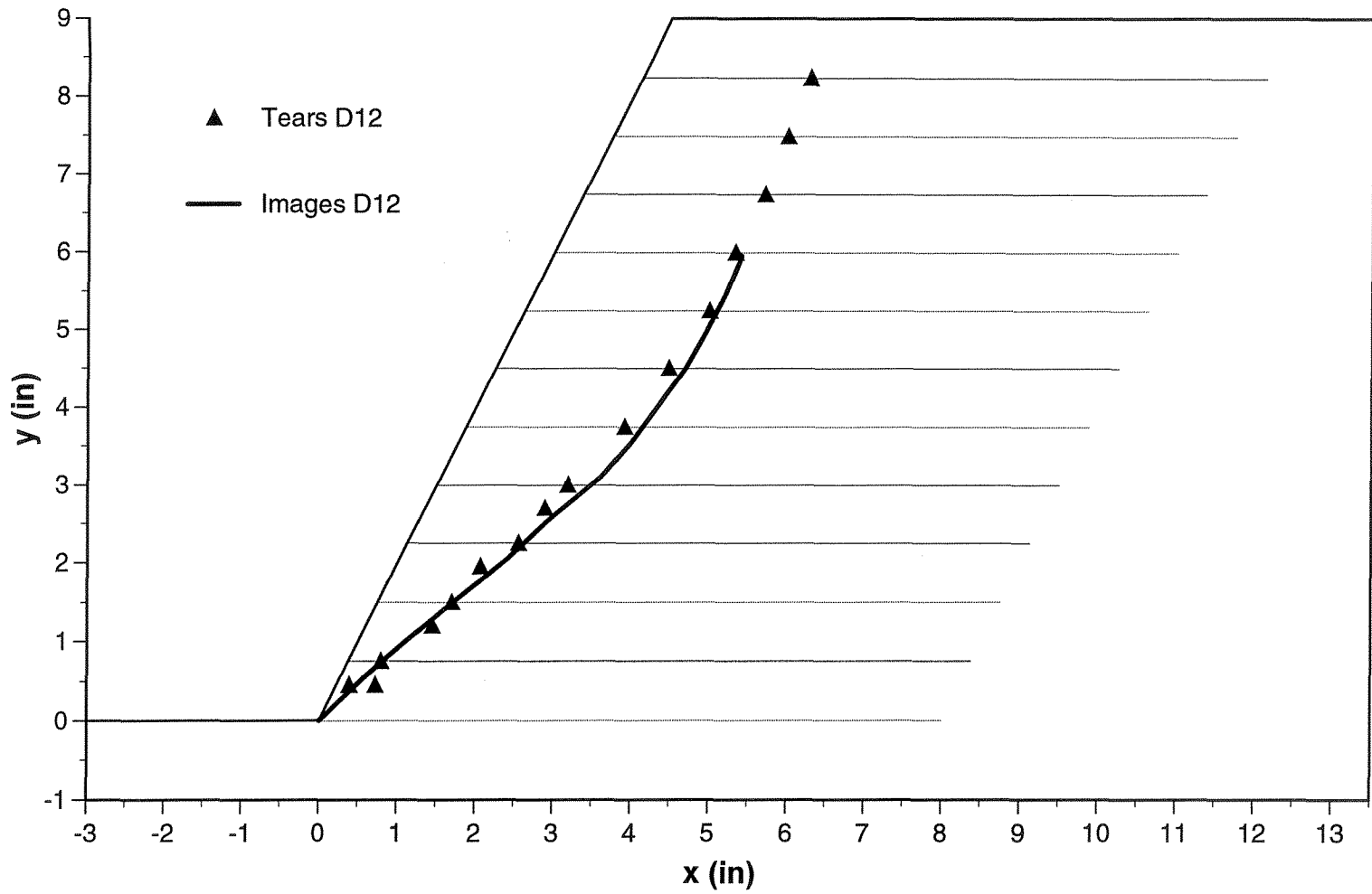


Figure 4.52 - Location of the failure surface for centrifuge model D12, as obtained from tears in the reinforcements and from images recorded through the plexiglass wall

form the Baseline B-series. It is also apparent from the figure that the results from these centrifuge tests define a line through the origin, characterized by a constant value of $n/N_f = 0.215$.

4.5.2.3 Stronger geotextile S-series

Table 4.5 shows the characteristics of the two models in this series, performed to investigate the effect of geotextile tensile strength on the stability of reinforced slopes. Models S6 and S9 were identical to models B6 and B9, respectively, but reinforced using the Pellon Tru-grid geotextile, which has a higher tensile strength than the Sew-in fabric used in the Baseline series.

The construction process for model S9 was described in Section 4.3.3, and figure 4.12 shows the model reinforced with nine geotextile reinforcement layers, ready for centrifuge testing. Failure occurred when the acceleration in the centrifuge reached 52.5 g. Although models reinforced using the Pellon Tru-grid geotextile also failed along a clearly defined surface, they did not exhibit the sudden collapse observed in models built using the weaker Pellon Sew-in fabric. Figure 4.53 shows the failure surface that developed in model S9 after testing. The photograph shows that the failure zone is wider than in the case of models built using the Pellon-Sew-in geotextile.

The geotextile reinforcements retrieved after the test are shown in Figure 4.54. Although the nine reinforcements show severe straining at the location of the failure surface, complete separation breakage did not occur as in the models built with the Pellon-Sew-in fabric. However, the presence of tears and the magnitude of the localized permanent deformations in the geotextiles clearly indicates that the reinforcements did

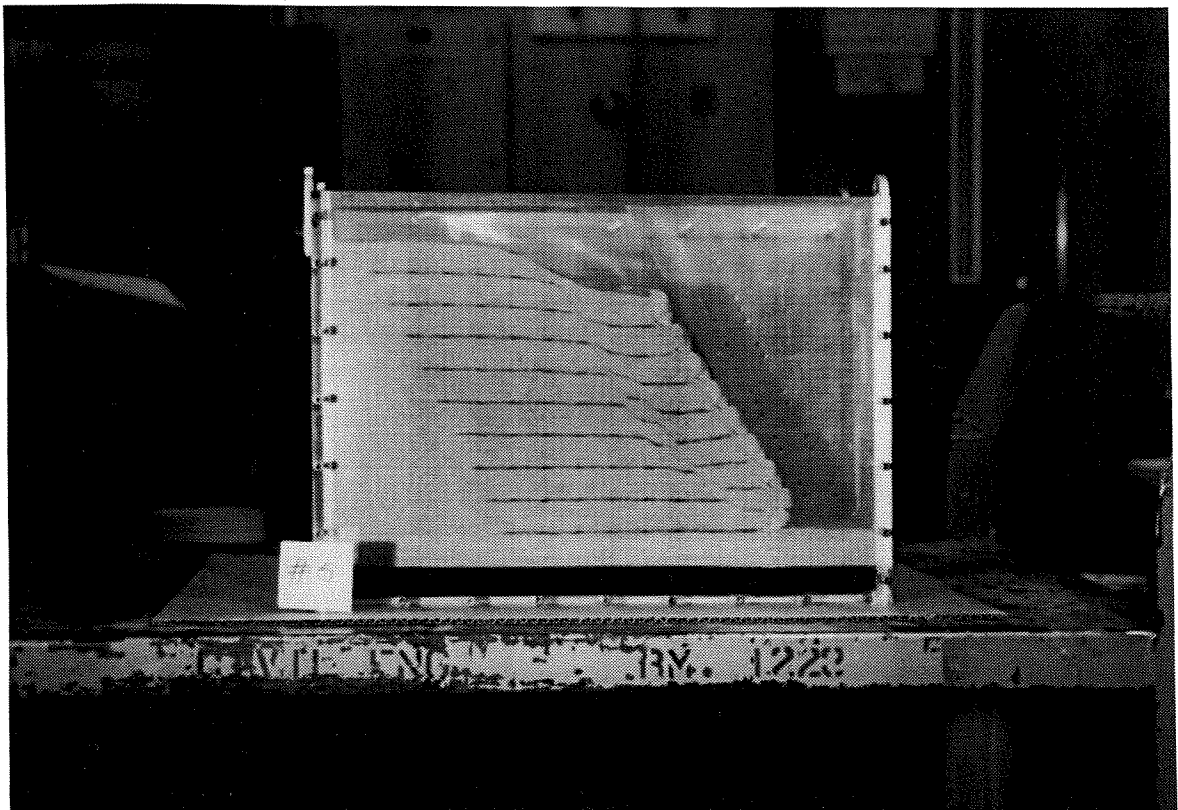


Figure 4.53 - View of model S9 after centrifuge testing

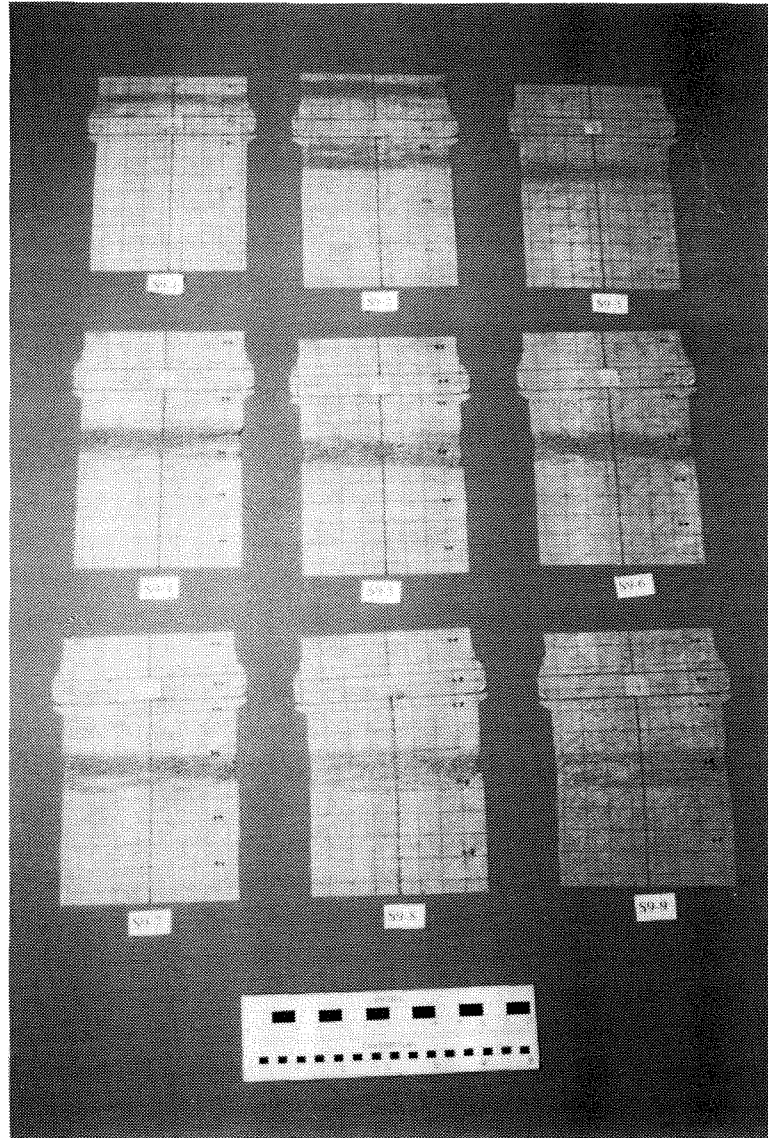


Figure 4.54 - Geotextile reinforcements retrieved from model S9

reach their ultimate strength. As was also the case for the models in the other two test series, no evidences of pullout were observed and the overlaps towards the base of the models worked as additional reinforcements.

Figure 4.55 shows the location of the potential failure surface developed in model S9, as observed from the location of the tears in the reinforcements and the zone of large strains in the retrieved geotextiles. The figure also shows the location of the failure as obtained after digitizing the images recorded at the moment of failure during centrifuge testing. The wider shear zone observed along the failure surface, in comparison with the tests in B- and D-series, is indicated in the figure. Also in this case, there is good agreement between the location of the failure surface defined using the retrieved geotextile layers and the images observed during testing through the plexiglass wall.

The effect of using a stronger geotextile reinforcement is also shown in Figure 4.48. As expected, slope models with the same number of reinforcement layers n , fail at higher accelerations when reinforced with the geotextiles used in the S-series than when using the lower strength fabrics as in the B-series. Also in this case, results from the S-series tests fit on a line through the origin. The constant ratio obtained for this series is $n/N_f=0.188$.

4.6 Interpretation of the experimental results

Lessons learned from the performance of the centrifuge slope models at failure are presented in this section. The g -levels at failure and the location of the failure surfaces obtained from centrifuge testing are evaluated. The experimental data provide insight into the possible failure mechanisms in geotextile-reinforced slopes. Moreover, design

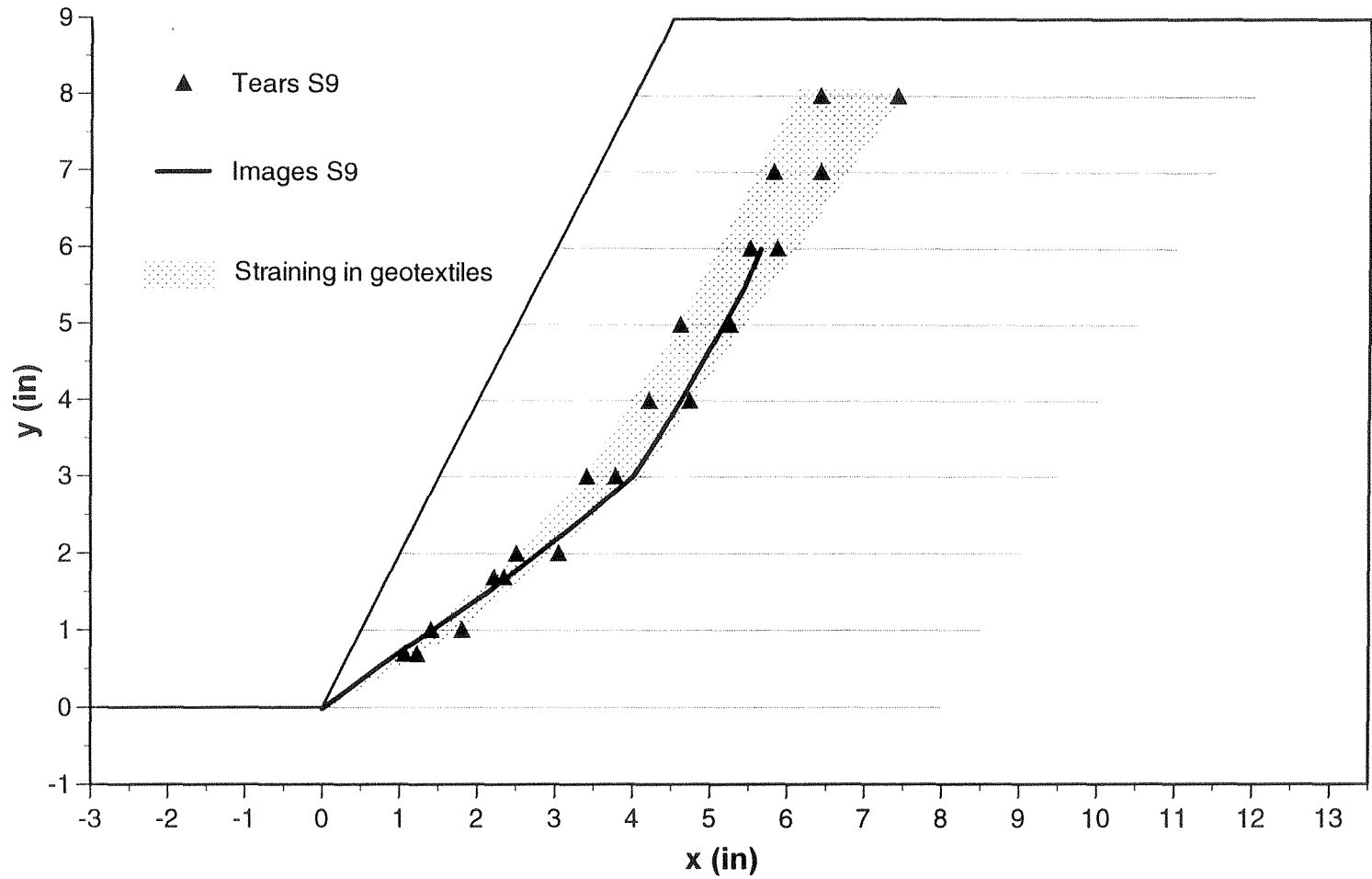


Figure 4.55 - Location of the failure surface for centrifuge model S9, as obtained from tears in the reinforcements and from images recorded through the plexiglass wall

considerations in relation to pullout safety, structure displacements, and soil strength parameters can also be drawn from evaluation of the centrifuge test results.

4.6.1 Normalization of results: Summation of reinforcement forces

Working stress design methods have been developed for the analysis of reinforced soil structures, and are particularly used for the design of reinforced soil walls. They basically rely upon assumptions with regard to the state of stress in the soil. Although the design of geotextile-reinforced slopes is commonly based on limit equilibrium methods, the concepts on which working stress design methodologies are founded may provide insight into the evaluation of the reinforced slope models.

In working stress design of reinforced soil walls, the horizontal soil stress distribution along the potential failure surface is defined based on the knowledge of an earth pressure coefficient, K . Tension in the reinforcements can then be determined from the analysis of local equilibrium between horizontal soil stresses and reinforcement forces. The value of the coefficient K has been determined semi-empirically and, for the case of walls reinforced using inextensible reinforcements, it has been observed to depend on factors like the reinforcement stiffness. However, for the case of walls with extensible reinforcements, the coefficient K has been found to be equal to the active earth coefficient K_a , depending only on the soil friction angle ϕ .

In the case of reinforced soil slopes, equilibrium should also be satisfied between reinforcement forces and horizontal soil stresses along the potential failure surface. It could then be assumed that there is a global earth pressure coefficient K which defines the total force caused by the horizontal soil stresses, and which satisfies equilibrium with

the reinforcement forces. Such coefficient K would not only be dependent on the soil friction angle ϕ , but also on the reinforced soil slope angle β . In this case, the following global equilibrium equation should apply at the moment of failure:

$$RTS_{ult}(\phi, \beta) = \frac{1}{2} K(\phi, \beta) \gamma H^2 \quad (4.25)$$

where $RTS_{ult}(\phi, \beta)$ is the Reinforcement Tension Summation at the moment of failure, γ is the soil unit weight, and H is the slope height. The earth pressure coefficient $K(\phi, \beta)$ can also be interpreted in terms of a normalized Reinforcement Tension Summation (RTS) expressed as:

$$K(\phi, \beta) = RTS_{ult}(\phi, \beta) \left(\frac{2}{\gamma H^2} \right) \quad (4.26)$$

The concept of Reinforcement Tension Summation has already been used in the finite element study presented in Chapter 3 of this dissertation. Equation (4.25) incorporates the traditional assumption of a triangular distribution of horizontal stresses. However, independently of the assumed distribution of horizontal stresses with depth, Equation (4.25) more generally states that the Reinforcement Tension Summation is proportional to the unit weight γ and to the square of the slope height H .

Based on the observations made from the centrifuge slope models that all reinforcements appear to achieve the ultimate load simultaneously (Section 4.6.3), the normalized Reinforcement Tension Summation can be estimated as:

$$K(\phi, \beta) = n T_{ult} \left(\frac{2}{\gamma H^2} \right) \quad (4.27)$$

Nondimensional coefficients similar to $K(\phi, \beta)$ have been used previously in order to develop design charts for geosynthetically reinforced soil slopes (Schmertmann et al., 1987; Leshchinsky and Boedeker, 1989; Jewell, 1991). The validity of the proposed normalization of the summation of reinforcement forces can be investigated using the results obtained in this centrifuge study. For a reinforced slope model that failed at an acceleration equal to N_f times the acceleration of gravity, the coefficient $K(\phi, \beta)$ can then be estimated considering the increased unit weight as:

$$K(\phi, \beta) = n T_{ult} \cdot \left(\frac{2}{\gamma H^2} \right) \cdot \frac{1}{N_f} \quad (4.28)$$

All centrifuge slope models have been built with the same slope β . Consequently, if the suggested normalization holds true, a single coefficient $K(\phi, \beta)$ should be obtained for all six models built using Monterey sand at 55% relative density. Equivalently, another unique value should be obtained from the two models built using a sand backfill at 75% relative density.

Figure 4.56 shows a plot of the centrifuge results in terms of $(n T_{ult}) (2 / \gamma H^2)$ versus the g-level at failure N_f . The geotextile tensile strength T_{ult} has been obtained from backcalculation as previously discussed in Section 4.4.2.3. The results in the figure clearly show that a linear relationship can be established for all models built using the same sand relative density. The slope of the fitted line corresponds to the normalized Reinforcement Tension Summation $K(\phi, \beta)$ defined by Equation 4.28. Consequently, the centrifuge results are consistent with the assumption that the Reinforcement Tension

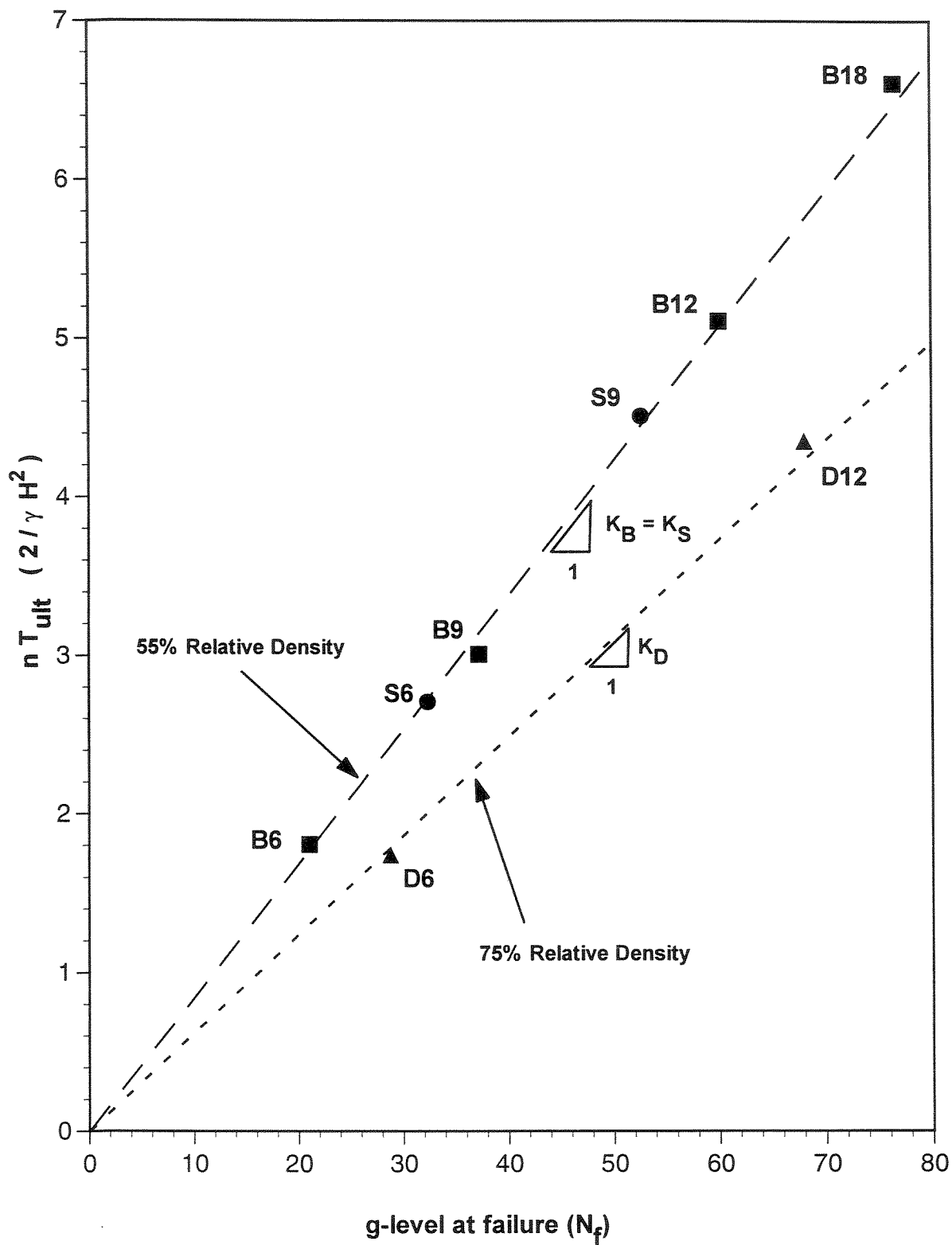


Figure 4.56 - Estimation of normalized Reinforcement Tension Summation (RTS) values from centrifuge test results

Summation can be normalized and that its value depends on the soil friction angle ϕ and on the slope angle β . The results obtained using all centrifuge models from the B- and S-series, built using Monterey sand at 55% relative density, define a normalized coefficient $K(\phi,\beta)=K_B=K_S=0.084$. Similarly, centrifuge results from the D-series models, built using Monterey sand at 75% relative density, define a normalized coefficient $K(\phi,\beta)=K_D=0.062$.

4.6.2 Characteristics of the failure surfaces

4.6.2.1 Development of failure

Failure of all centrifuge models in this study was characterized by the development of a well-defined shear surface approximately through the toe of the slope. The failure surfaces developed in different models (Section 4.5) can probably be fitted using either circular, logarithmic spiral, or bilinear surfaces, which are commonly used in limit equilibrium analyses of reinforced slopes. The moment of failure was defined by a sudden change in the rate of settlements at the crest of the slope, as monitored from transducers placed on top of the centrifuge models. This moment of failure was found to agree very well with the visual observation of the initiation of failure through the plexiglass side wall of the models.

However, some differences in the development of failure were observed in the different test series. In the B-series, the time elapsed between the initiation of failure and the final model collapse was relatively short. After initiation of failure, collapse generally occurred without an additional increase of the g-level. The time elapsed between the initiation of failure and structure collapse appeared to be even shorter in the D-series

experiments. This may be attributed to a more rapid drop in soil strength after the soil peak strength has been reached the denser backfill. The models built using a stronger geotextile, S-series, had a longer elapsed time between initiation of failure and final structure collapse. Although initiation of failure could be estimated with reasonable accuracy, and failure surface was clearly defined, the moment of final structure collapse was more difficult to identify. This post-failure performance may be attributed to the large displacements that the Tru-grid fabric is able to sustain after reaching the ultimate tensile strength, as indicated from the tensile tests performed using a 1.5 mm gauge length (Figure 4.33). This behavior is different than that of the weaker Sew-in geotextiles, which shows a rapid drop in tensile strength after the peak tensile strength. Thus, it appears that the post-failure behavior of the slope models until final structure collapse depends on the post-peak behavior of the backfill soil and, mainly, of the geotextile reinforcements.

Figures 4.57a, 4.58a, 4.59a, and 4.60a show the in-flight view of models B6, B12, B18, and D12, at the moment of initiation of failure during centrifuge testing. The testing time at which these images were grabbed corresponds to the moment of failure defined by the transducers that monitored the settlements at the crest of the model. The images were recorded using the TV camera located inside the centrifuge, and the selected frames were grabbed to obtain a hardcopy of the images. As can be observed in all figures, the initiation of failure occurs approximately in the middle of the slope. This can be observed by kinks in the horizontal colored sand layers that were placed during construction at the levels of the reinforcements. Although the kinks initially appeared at approximately the midheight of the slope, additional kinks rapidly developed in the layers

of the upper half of the model as observed in the figures. The lower geotextile layers showed no evidence of kinking until the moment of ultimate structure collapse. The development of failure observed in the centrifuge slope models indicates that the lower reinforcement layers are not the most tensioned ones, which is in direct opposition to the distribution of reinforcement forces that is generally assumed in the design of reinforced soil slopes. Current design methodologies assume that reinforcement tension increases linearly with depth, which would be expected to result in a progressive failure mechanism starting at the toe of the reinforced slope for uniformly spaced reinforcements of equal strength.

Figures 4.57b, 4.58b, 4.59b, and 4.60b show the final structure collapse of centrifuge slope models B6, B12, B18, and D12. The frames were also grabbed from the TV images recorded in-flight during centrifuge testing. These images were used to locate the failure surfaces previously shown in Section 4.5.3. There was a very good agreement between the location of the failure surfaces obtained from the images on the plexiglass wall and from the measurements of the geotextile reinforcement tears. An interpretation of the possible failure mechanism that explains the development of failure observed in the figures is presented in Section 4.6.3.

Internal monitoring of the reinforcement strains was not possible due to the fragility of the geotextiles. Consequently, in order to verify the location of failure initiation, the testing progress for one of the centrifuge models (model D6) was stopped right after failure occurred, as monitored by the displacement transducers, but before the final collapse. The common testing procedure, followed in all the other models, was to continue the progress of centrifuge testing until collapse. Analysis of the retrieved

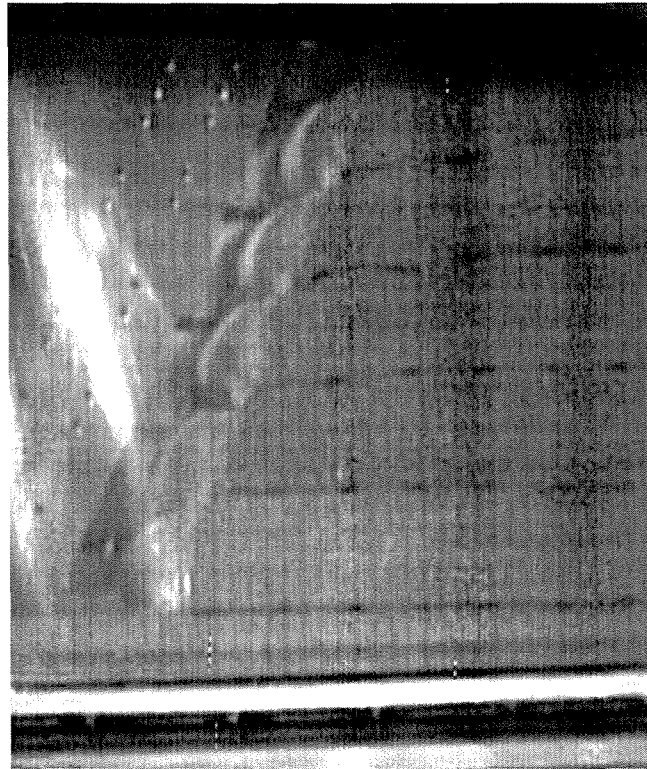


Figure 4.57 a - Initiation of failure in model B6

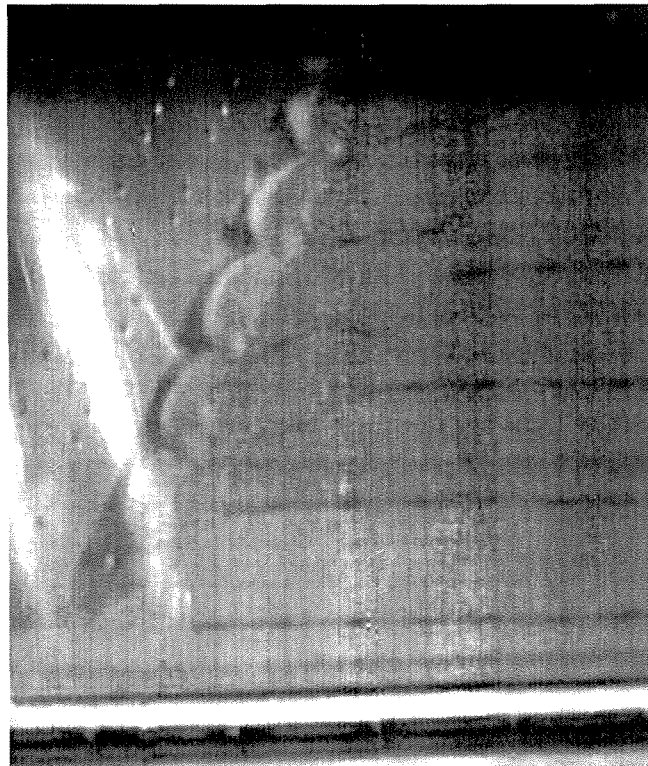


Figure 4.57 b - Final collapse of model B6

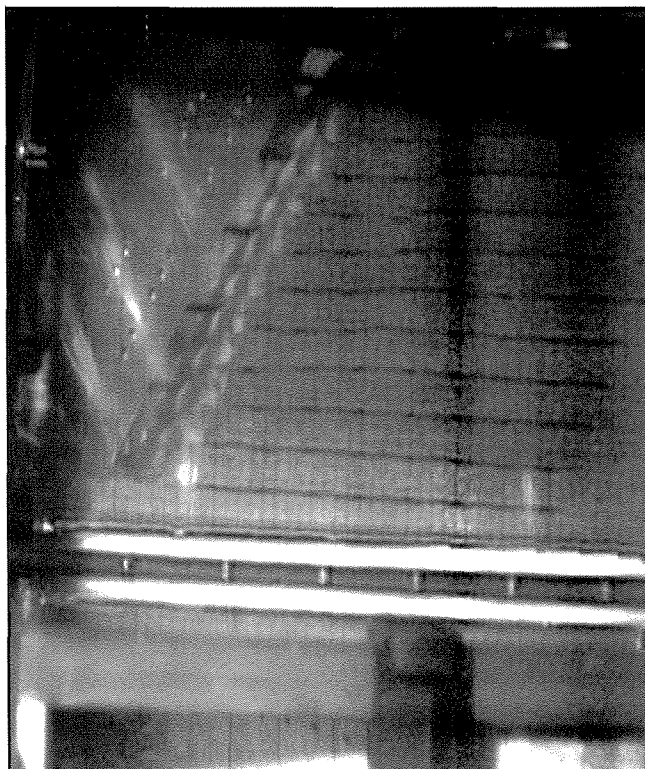


Figure 4.58 a - Initiation of failure in model B12

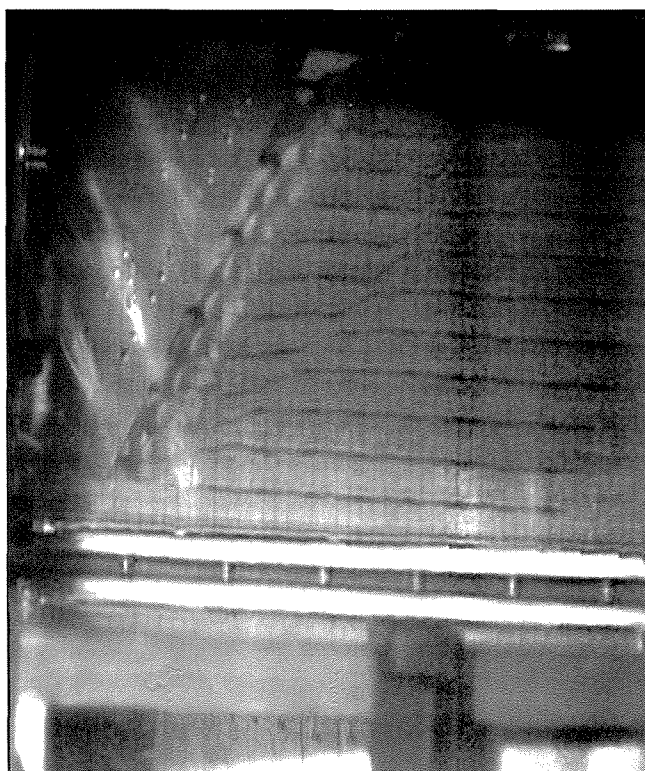


Figure 4.58 b - Final collapse of model B12

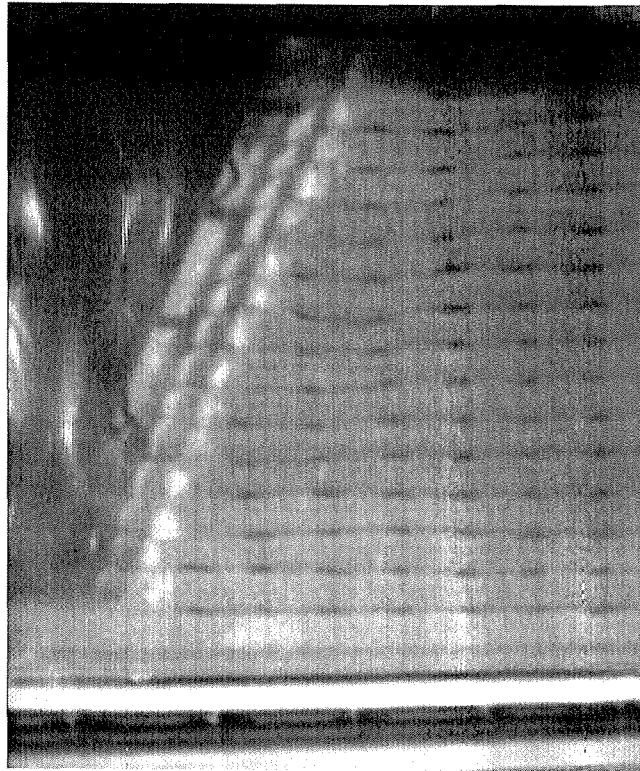


Figure 4.59 a - Initiation of failure in model B18

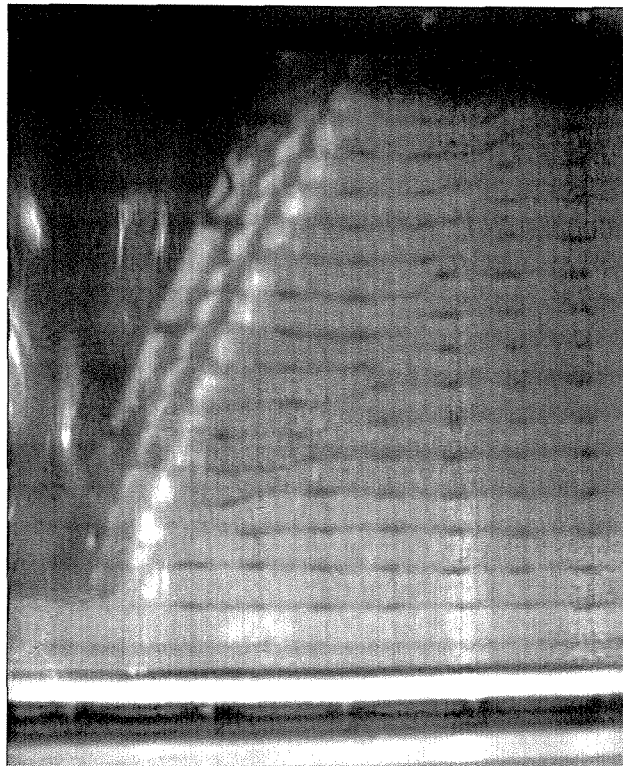


Figure 4.59 b - Final collapse of model B18

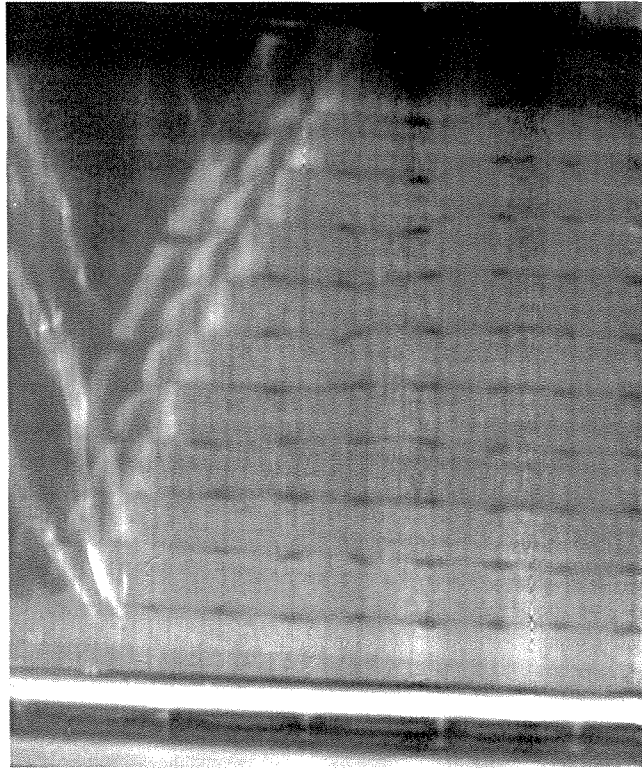


Figure 4.60 a - Initiation of failure in model D12

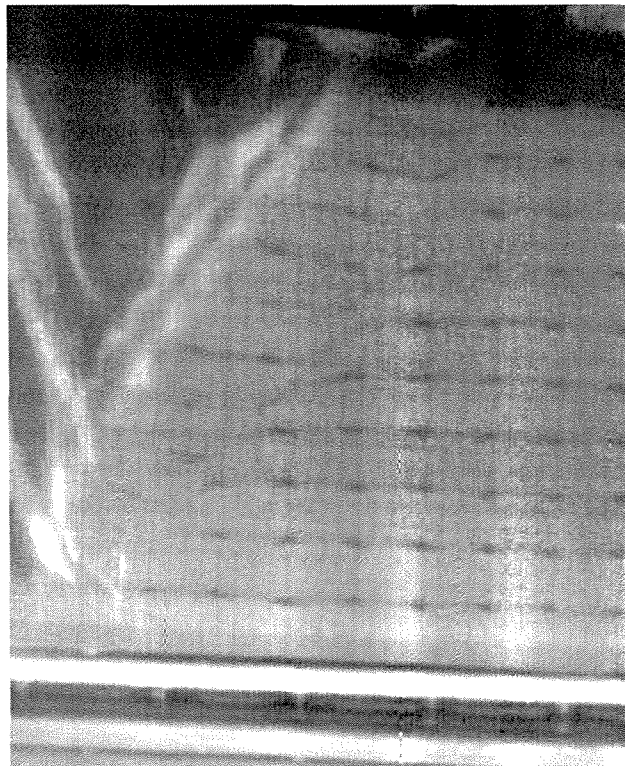


Figure 4.60 b - Final collapse of model D12

geotextiles for model D6 confirmed that failure started at the middle of the slope height. While reinforcements in the upper half of the model showed the development of tears, the reinforcements in the lower half of the model showed only evidences of straining at the location of the failure surface. At the lower layers the straining was even difficult to identify. Additional evidence that the reinforcement force distribution is not triangular, as commonly assumed in design, is the fact that the first geotextile layer (at the base of the slope) in all models did not show either tears or evidence of straining.

4.6.2.2 Location of the potential failure surfaces

The locations of the failure surfaces developed in the four centrifuge slope models from the B-series, models B18, B12, B9, and B6, are shown in Figure 4.61. For clarity, only the locations of the tears measured on the retrieved geotextile reinforcements are shown in the figure. All centrifuge models appear to have failed along approximately the same failure surface, which implies that the location of the failure surface is independent of the vertical spacing of the reinforcement layers. These results are in agreement with the results of the limit equilibrium analyses of the centrifuge slope models, discussed later in Section 4.7.3.3. They also agree with the results of variational limit equilibrium of reinforced soil slopes by Leshchinsky and Boedeker (1989) that found that the location of the critical surfaces only depends on the soil friction angle and on the angle of the reinforced slope face. Only the failure surfaces in model B6 developed slightly above the toe of the slope, within the wrapped geotextile face of the first geotextile reinforcement layer.

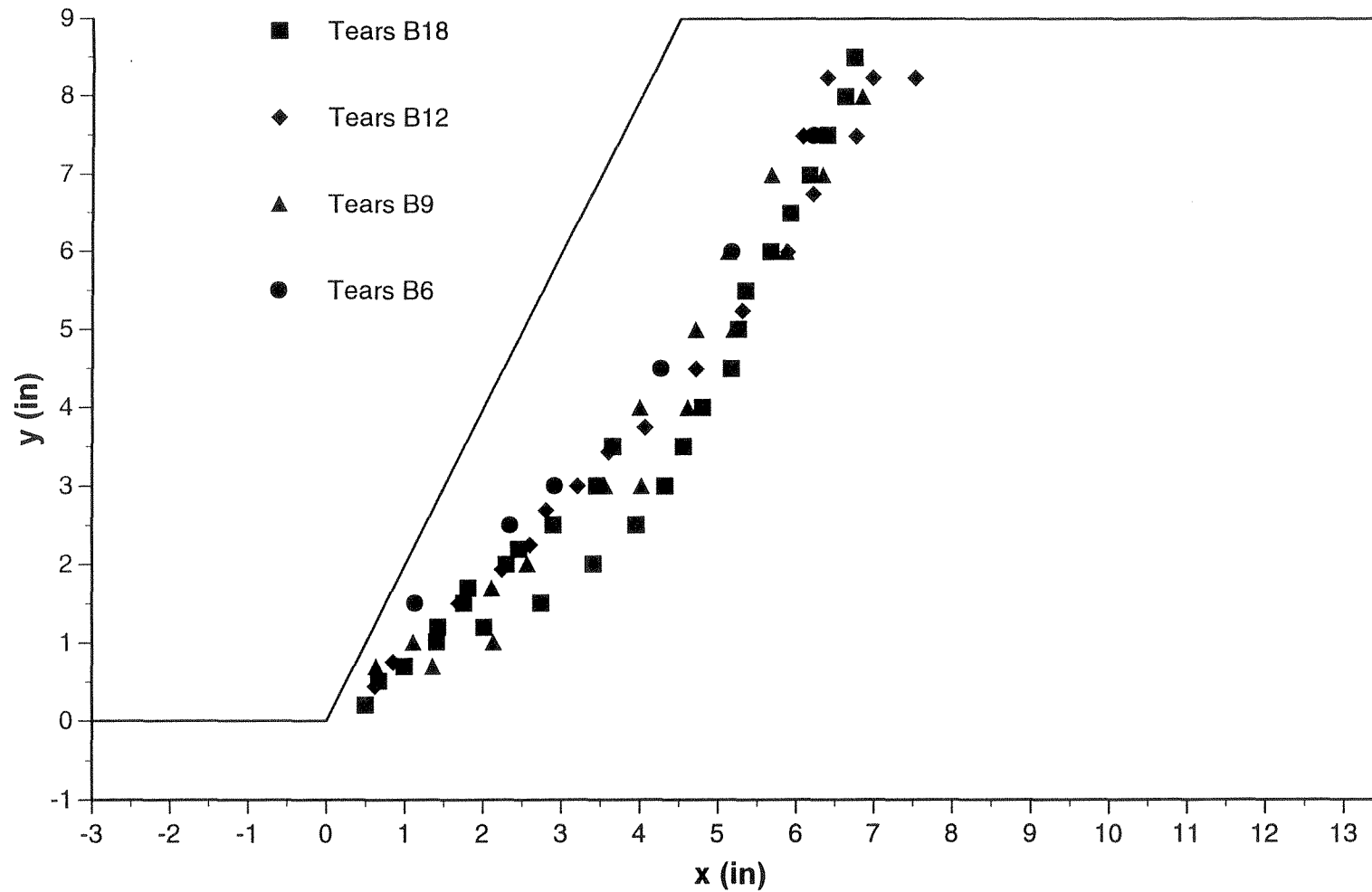


Figure 4.61 - Location of tears in reinforcements defining the failure surfaces in B-series models

The failure surfaces that developed in the two models with a denser soil, models D6 and D12, are shown in Figure 4.62. Also in this case, the two models failed along similar failure surfaces. Finally, Figure 4.63 shows the location of the failure surfaces that developed in the two centrifuge slope models from the Stronger geotextile S-series. Failure in these models developed along wider shear zones, which are indicated in the figure. However, the two models also failed along very similar failure surfaces.

Figure 4.64 shows the failure surfaces for all the centrifuge models as obtained after digitizing their location using the images of the model cross-section recorded at the moment of failure during the test. Although this source of information does not provide the location of the failure surface at the upper layers, the scatter of the data is smaller. The results in the figure clearly show that all centrifuge models failed along very similar shear surfaces. Only model B6 developed a surface that emerged slightly above the toe of the reinforced slope model.

4.6.3 Interpretation of the failure mechanisms

Interpretation of the failure mechanisms in a reinforced soil slope structure depends on a correct evaluation of the distribution of reinforcement forces with depth. From this distribution, the location of the first reinforcement that achieves its ultimate tensile strength can be identified. In the case of reinforced soil walls, for which current design methods are based on assuming the state of stress in the soil mass, reinforcement forces have been interpreted as proportional to the overburden pressure from the top of the wall (Figure 4.65). The rationale behind this assumption is that the reinforcements should resist the active earth pressure in the case of extensible reinforcement systems

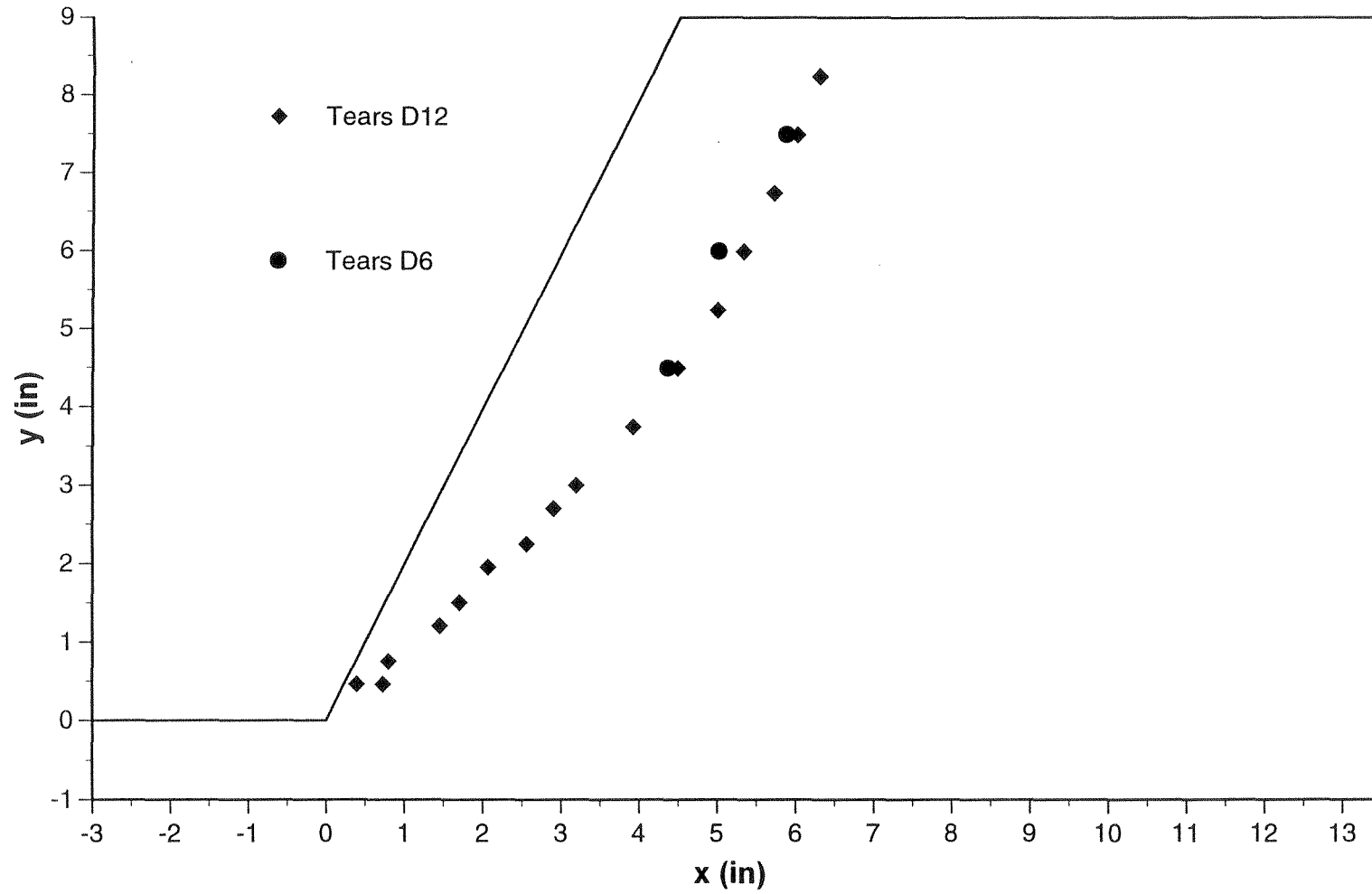


Figure 4.62 - Location of tears in reinforcements defining the failure surface in D-series models

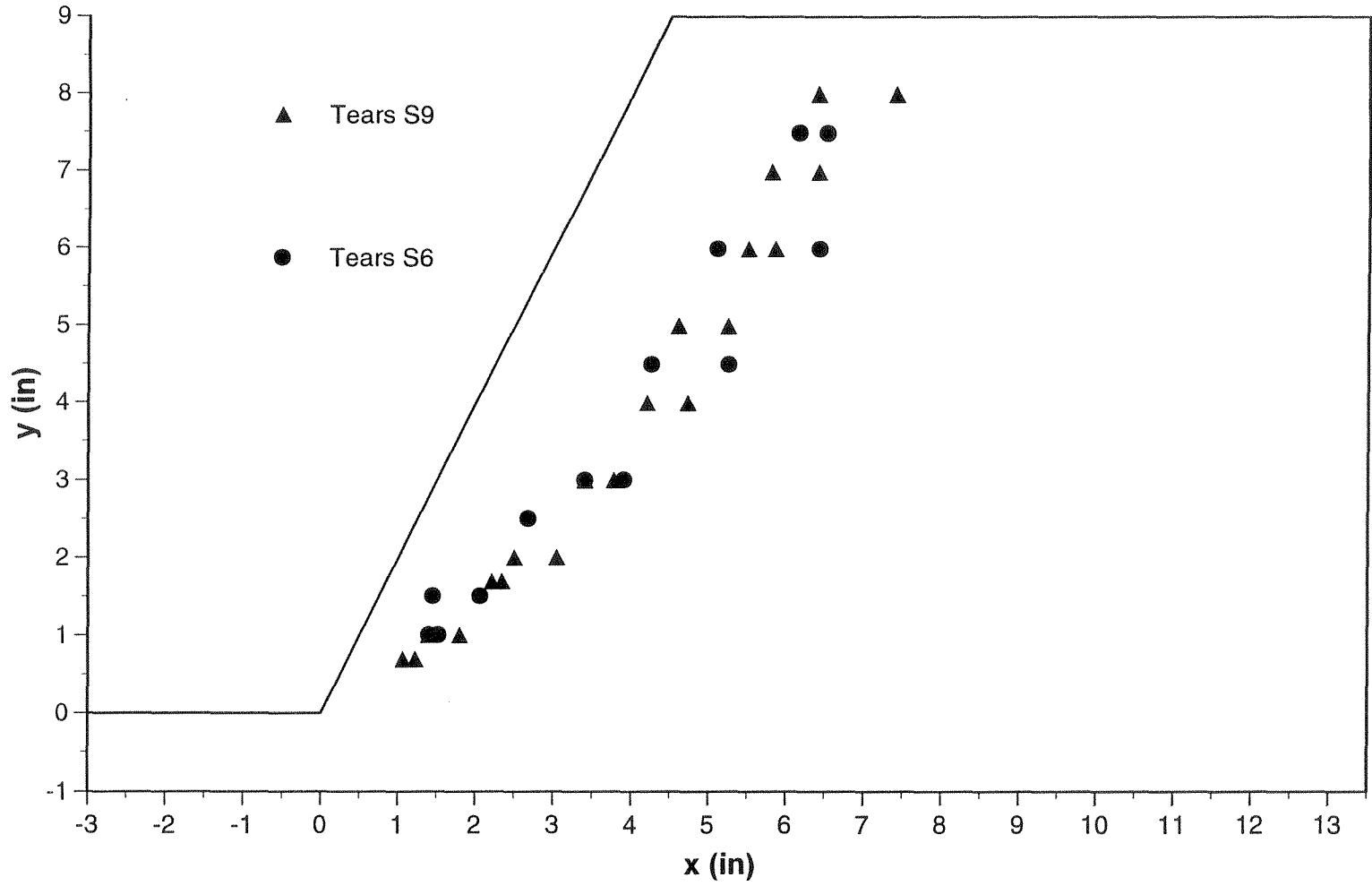


Figure 4.63 - Location of tears in reinforcements defining the failure surface in S-series models

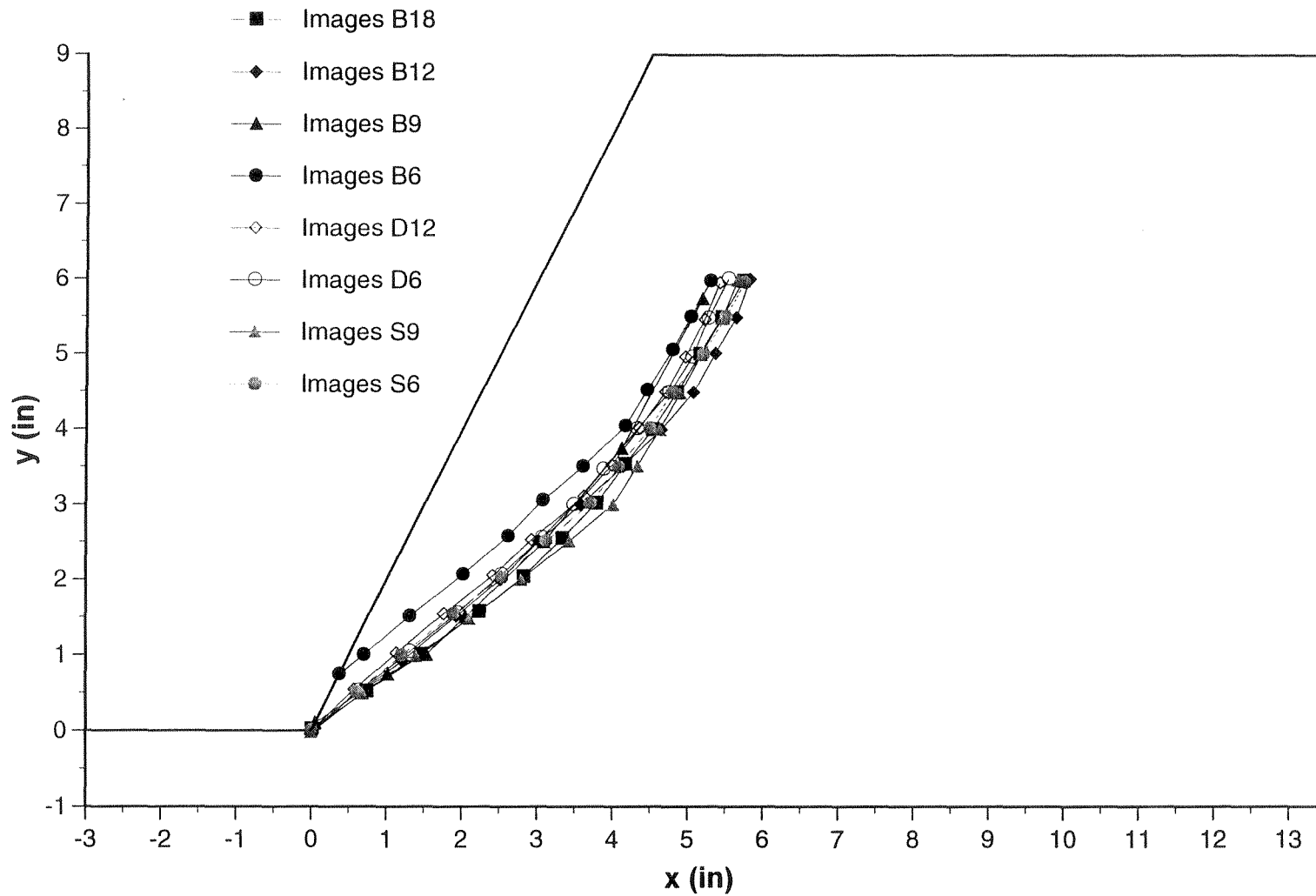


Figure 4.64 - Location of failure surface obtained from images recorded in-flight

(Mitchell and Christopher, 1990). Although foundation stiffness has been found to affect the development of force in the lower reinforcement layers, field studies have shown that maximum tensile forces are well predicted by assuming a Rankine active condition in geosynthetically reinforced walls.

In the case of reinforced soil slopes, which have their design based on limit equilibrium and not on working stress methodologies, the reinforcement force distribution with depth should also be assumed. Extending the observations gathered for the case of reinforced soil walls, triangular reinforcement tension distribution increasing proportionally with the depth below the slope crest has been assumed for reinforced soil slopes. This assumption is considered in design charts that have been implemented based on limit equilibrium analysis of geosynthetically reinforced soil slopes (Jewell, 1984; Schmertmann et al., 1987; Leshchinsky and Perry, 1987; Leshchinsky and Boedeker,

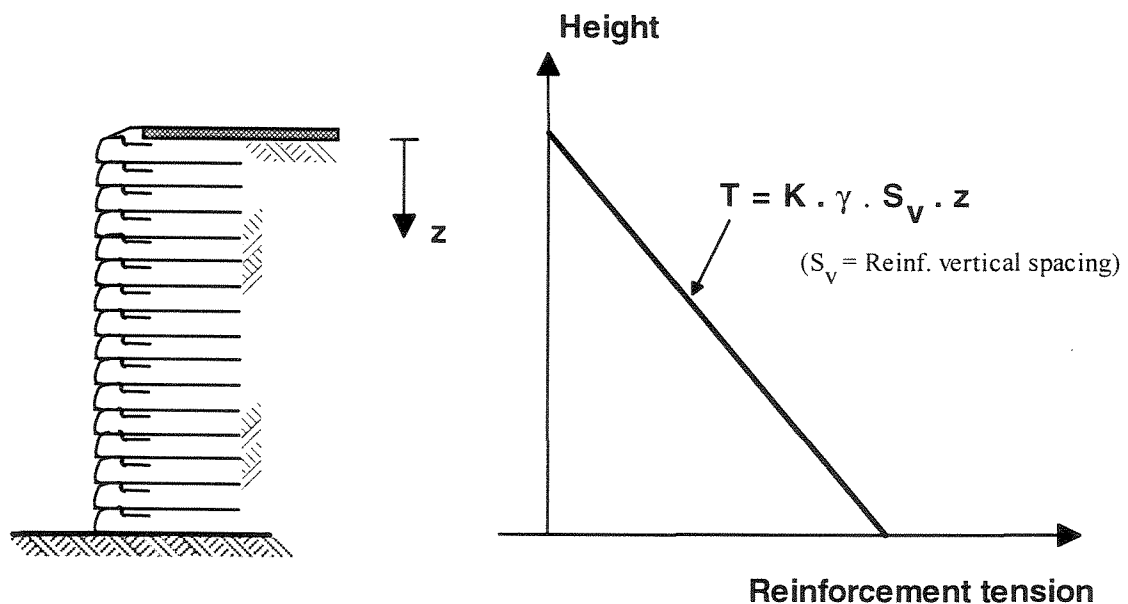


Figure 4.65 - Reinforcement force distribution with depth assumed for design of reinforced soil walls

1989; Jewell, 1991). Current FHWA design method for reinforced soil slopes also recommends tensile forces distribution directly proportional to depth below the slope crest for the case of slopes higher than 6 m (Christopher et al., 1990).

However, the conventional triangular distribution of reinforcement forces is in disagreement with the centrifuge results obtained in this study, since failure of the models did not initiate at the toe of the slope models. As previously discussed in Section 4.6.2, failure appeared to initiate at midheight of the slope in all centrifuge tests. Clarification of this issue has major implications on design, since vertical spacing and ultimate strength of the reinforcements are currently selected based on the requirements for the lower layers of reinforcements, which are considered the most critical zone.

A reassessment of the local equilibrium between reinforcement forces and working soil stresses may provide insight into the possible reinforcement force distribution for reinforced soil slopes. A rational approach for determining the reinforcement force distribution has been to consider that the reinforcements resist the horizontal stresses in the soil *at the location of the potential failure surface*. In the case of vertical reinforced soil walls, the horizontal soil stresses along the potential failure surface are proportional to the overburden pressure which increases with depth below the top of the wall. In the case of reinforced soil slopes, the horizontal soil stresses along the potential failure surface are also proportional to the overburden pressure, but they increase approximately with depth below the *slope face*. Notice that the conventional triangular distribution in reinforced slopes has been obtained by considering the overburden pressure to increase proportionally with depth below the *slope crest*.

Figure 4.66 shows a reinforced soil slope with the two reinforcement tension distributions under discussion. The triangular distribution is obtained assuming that the reinforcement forces are proportional to the overburden pressure calculated as a function of depth z below the slope crest. The alternative distribution is estimated proportionally to the depth z^* below the slope face, and the difference between z and z^* is indicated in the figure for point A along the potential failure surface. The indicated distribution is for the case of 1H:2V reinforced slopes that corresponds to the geometry of the centrifuge models in this study. As indicated in the figure, the location of the maximum force in the reinforcements is at a height h_p from the base of the slope. This height is determined by the location of the point P in the figure, which is the point along the potential failure surface directly below the slope crest. Above h_p , the reinforcement tension distribution increases proportionally with depth below the slope crest ($z=z^*$ in this case), while below h_p the reinforcement tension decreases, being proportional to z^* and becoming zero at the toe of the slope.

In the case of a slope inclined at 1H:2V, h_p is approximately equal to one half of the total height H of the slope. This is in agreement with the location of failure initiation in all centrifuge slope models in this study. In a general case, the height h_p will mostly depend on the angle of the slope face. Although, since the location of the failure surface also depends on the soil friction angle, the location of the maximum reinforcement force will also depend on ϕ . Particularly, for the case of vertical walls the point P will be at the toe of the structure and, consequently, $h_p=0$. This is in agreement with current design methods for reinforced soil walls that consider a triangular distribution of the reinforcement forces.

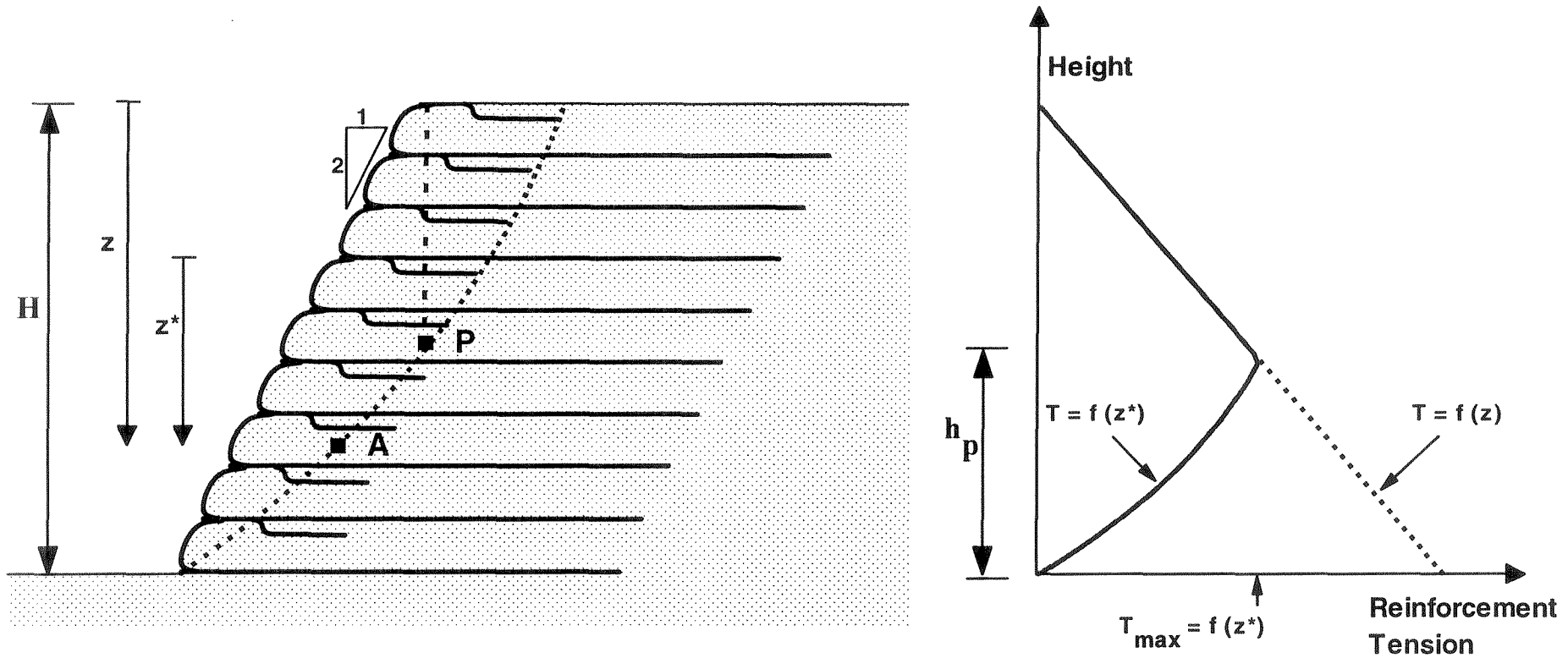


Figure 4.66 - Reinforcement force distribution with depth for reinforced soil slopes under working stresses

The proposed distribution, which is in agreement with the results obtained in the centrifuge tests, seems more consistent for reinforced soil slopes under working stresses than the conventional triangular distribution. Although additional investigation should be pursued to further evaluate the reinforcement tension distribution in reinforced slopes, the distribution of maximum reinforcement tension with depth measured from well instrumented 1H:2V geogrid- and geotextile-reinforced slopes (Adib, 1988; Christopher et al., 1992) appear to support the proposed distribution.

Figure 4.66 represents the distribution of reinforcement tensions under working stress conditions, and helps explain the failure mechanisms in the centrifuge slope models. However, substantial stress redistribution is expected to occur after the first reinforcement reaches its ultimate strength, so that the reinforcement tension distribution is approximately uniform at the moment of failure of the reinforced slope. From the results of an internally instrumented reinforced soil wall, Jaber and Mitchell (1990) noticed that stress redistribution occurred across the height of the wall before failure of the structure. Even brittle aluminum reinforcement strips were deformable enough to redistribute the stresses across the whole height of the wall and therefore take advantage of the tensile strength of all layers of reinforcement before failure. In comparison, the different distribution of reinforcement tensions in reinforced soil slopes, and the more ductile reinforcements elements used in this study, are two additional factors that may contribute to stress redistribution before failure. Consequently, it is reasonable to consider that almost all reinforcements will be acting at full capacity at the moment of failure.

Figure 4.67 shows the three reinforcement force distributions that have been discussed herein. The average tension in the reinforcements T_{ave} , which is a measure

of the reinforcement tension summation, is also indicated for each case. Figure 4.67a shows the triangular reinforcement distribution that has been conventionally assumed for design of reinforced slopes. Figure 4.67b is the estimated reinforcement tension distribution under working stresses (for a 1H:2V slope) discussed previously. For design purposes, it is probably appropriate to use this reinforcement force distribution with depth, considering the maximum tension in this distribution equal to the geotextile strength. The major difference with the distribution assumed in current design is not the amount of reinforcement (T_{ave} are approximately the same in both cases), but the location of the critical reinforced zone. Finally, as shown by the probable reinforcement force distribution in the centrifuge models at the moment of failure (Figure 4.67c), the magnitude of the average tension in the reinforcements approaches the geotextile tensile strength.

4.6.4 Additional design aspects

Besides the evaluation of internal failure mechanisms caused by reinforcement breakage, the centrifuge test results provide insight into additional issues relevant to the design of geotextile-reinforced soil slopes. They include observations on structure displacements, pullout safety, and selection of soil strength parameters for design.

4.6.4.1 Displacement evaluation

An overall discussion on the deformation characteristics of the centrifuge slope models is beyond the purposes of this study. Nevertheless, the measurements of the

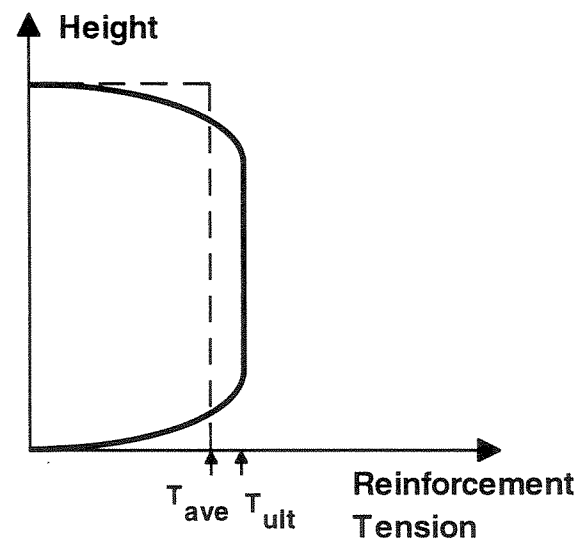
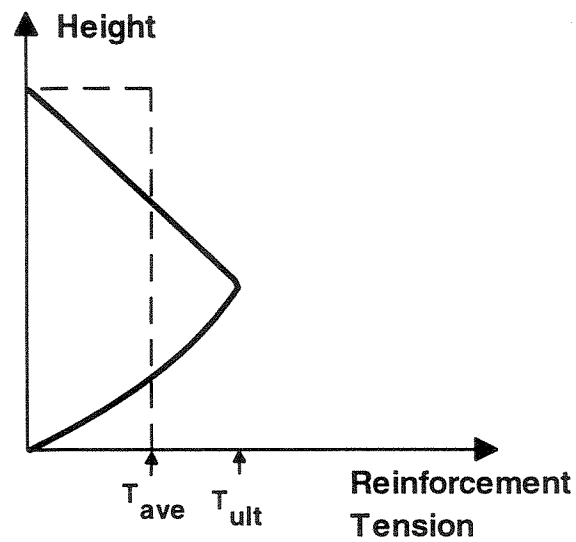
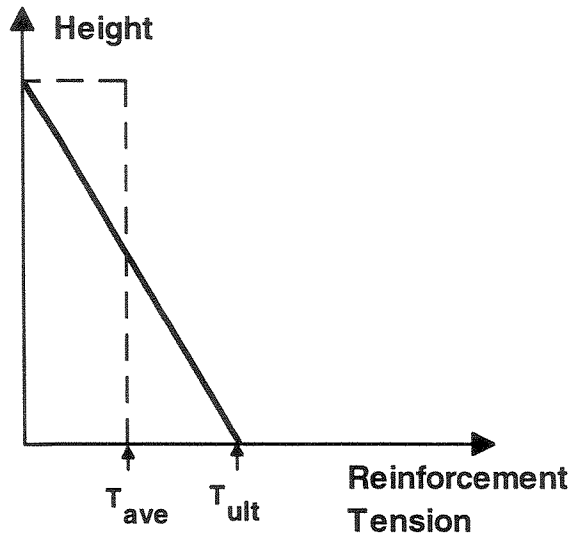


Figure 4.67 - Alternative distributions of reinforcement tension with depth in reinforced soil slopes

vertical settlements at the crest of the slope are worth discussing since they were used to specify the g-level at failure of the centrifuge tests.

Figure 4.68 shows the vertical settlement in several models, monitored by the transducer LVDT1 located 12.5 mm from the slope face. The arrows in the figure indicate the g-levels matching the initiation of failure identified by visual observation of the cross-section of the slope models. Figure 4.69 shows the vertical settlements monitored with the transducer LVDT2, which is located 63.5 mm from the slope face. The same moment of failure in each model can be identified from the settlements monitored at the two locations.

A noticeable feature of this instrumentation data is that the settlement versus g-level results for most of the models appear to follow the same curve up to the moment of failure. This is the case for models S6, S9, B12, and B18, which were built using a different number of reinforcement layers, different geotextile types, and different sand densities. However, higher settlements were measured on model B6, which had the smaller number of reinforcements (6 layers), the weaker geotextile, and the looser sand. On the other hand, smaller settlements were monitored on model D6, which was built with backfill at a higher sand relative density. The smaller settlements in D6 are better observed at the location of the transducer LVDT2.

The effect of the difference in stress paths between model and prototypes should be evaluated before drawing final conclusions from the monitored displacements. However, these results appear to indicate that the settlements of slopes reinforced with extensible inclusions are independent of the number of reinforcements and of the reinforcement strength. This seems to be true above a certain threshold of reinforcement

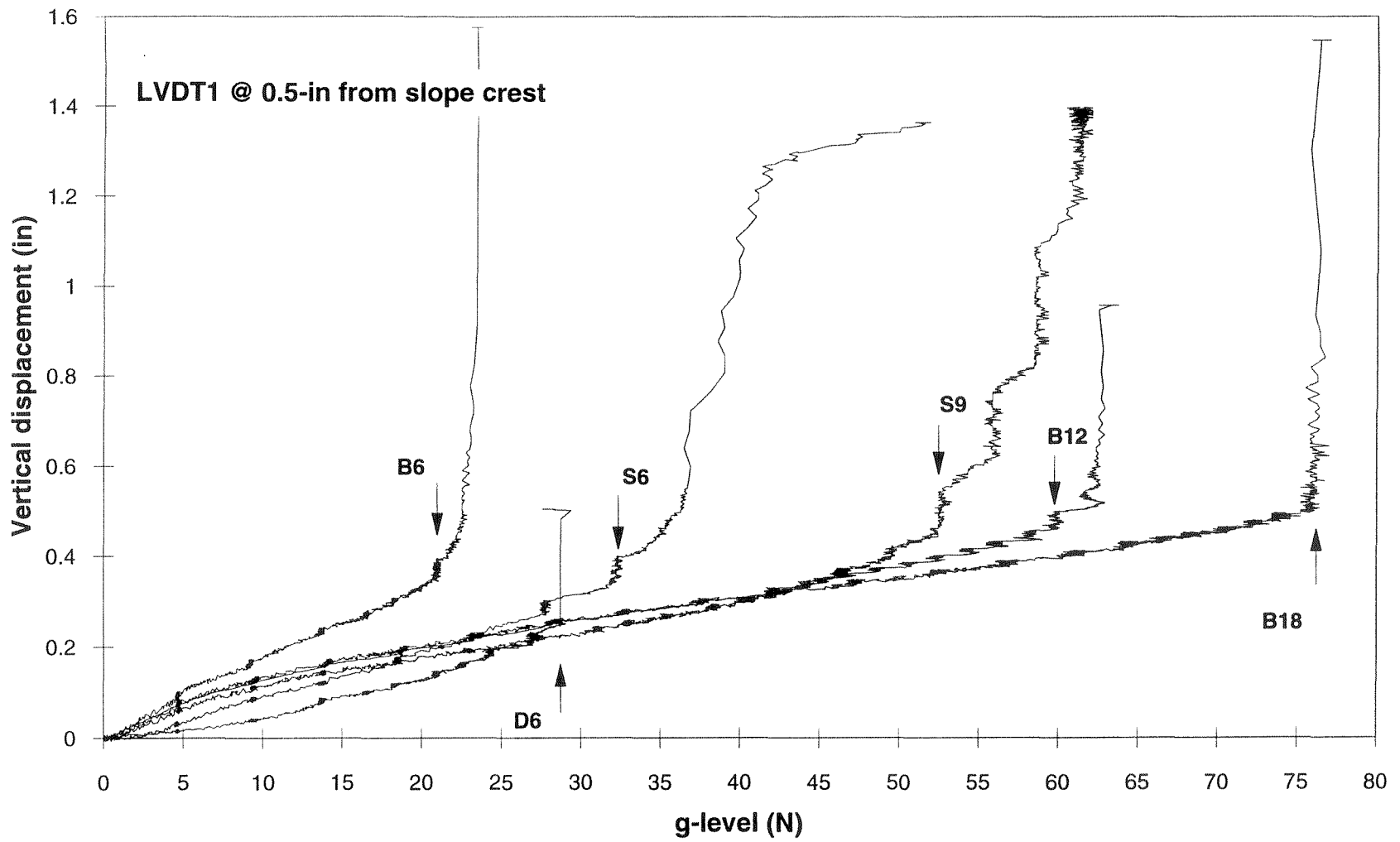


Figure 4.68 - Vertical settlements at the crest of the slope, 12.5 mm from the slope face. The moment of failure is indicated by an arrow.

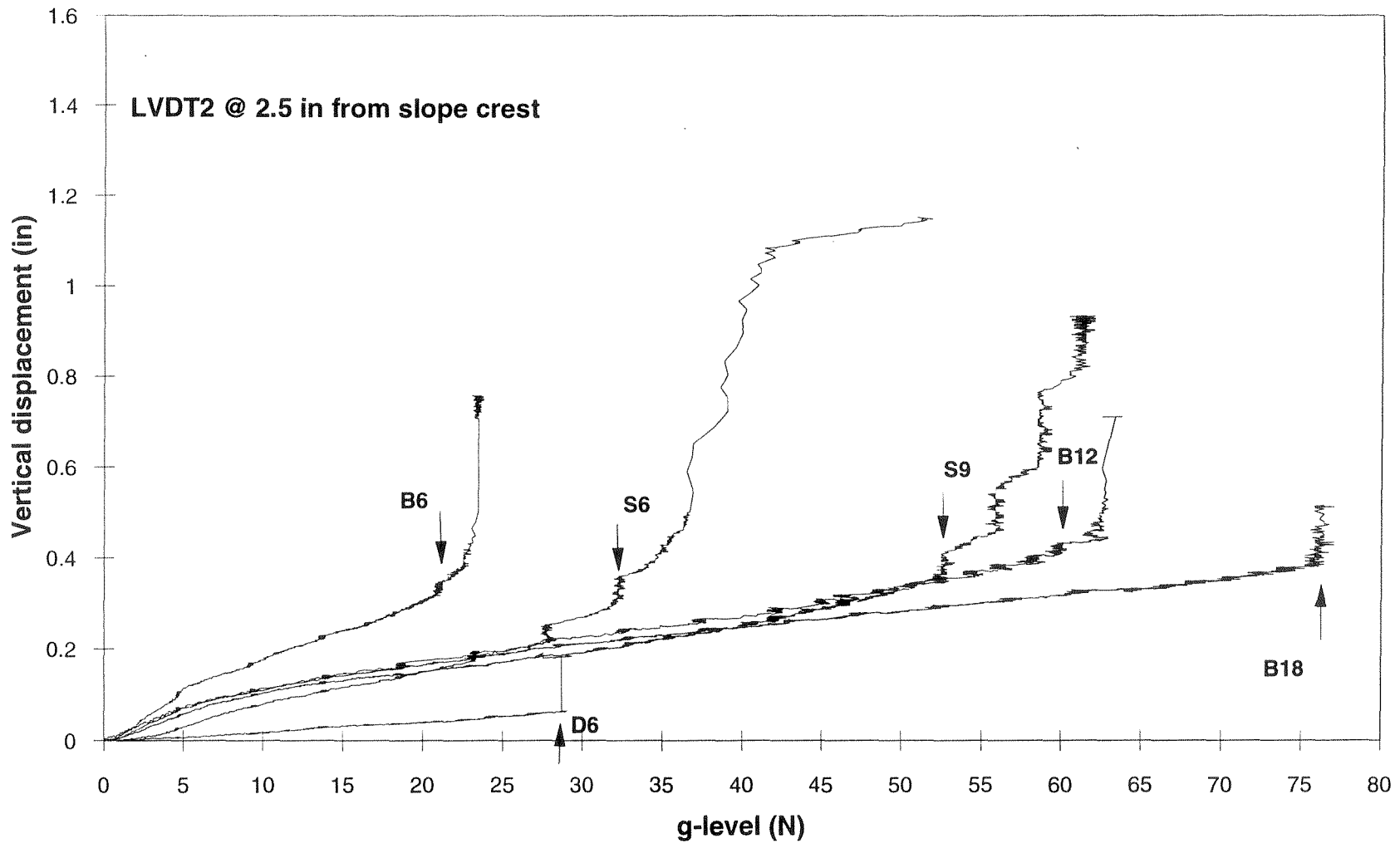


Figure 4.69 - Vertical settlements at the crest of the slope, 63.5 mm from the slope face. The moment of failure is indicated by an arrow.

density; i. e., between 6 and 9 reinforcement layers for the geometry of the models in this study. It also appears that the structure settlements strongly depend on the properties of the backfill soil. An additional variable to be investigated is the reinforcement length, which was not considered in this study.

4.6.4.2 *Evaluation of pullout safety*

Conventional design disregards the effect of geotextile overlaps on the stability of reinforced soil structures. However, the number of overlaps that failed by breakage and not by pullout indicate that this conservative practice should be reviewed. Breakage of the of the geotextile overlaps in several of the centrifuge slope models was observed in the geotextiles retrieved from the models after centrifuge testing, as already discussed in Section 4.5.3. An evaluation of the effect of overlap geotextiles on the calculated factors of safety using limit equilibrium analysis is presented in Section 4.7.2.4.

Sufficient reinforcement length was adopted in the models so that the models would fail by reinforcement breakage and not by pullout. However, it was somewhat unexpected to see no pullout failures of the geotextile overlaps, even in cases where the overlap anchorage length was less than 10 mm.

Nevertheless, a verification of the pullout safety of the geotextile overlaps does confirm that only very short overlap anchorage lengths are enough to provide adequate pullout resistance. The pullout resistance P_r of the overlaps can be estimated as:

$$P_r = 2 \sigma_v L_e \tan \delta \quad (4.29)$$

where σ_v is the effective vertical stress, L_e is the length of the overlap embedded on the resisting zone behind the failure surface, and δ is the sand/geotextile interface strength.

Figure 4.70 shows one of the geotextile overlaps that were intersected by the failure surface (second reinforcement layer for model B9), and for which the pullout resistance is evaluated herein for illustration purposes. The anchorage length for this particular overlap is approximately 13 mm, and the vertical stress is calculated considering the depth of approximately 77 mm from the slope face to the geotextile anchorage zone. Using Equation (4.29), the pullout resistance for this particular overlap at the moment of failure of model B9, that occurred at an acceleration 37 times the acceleration of gravity is estimated as:

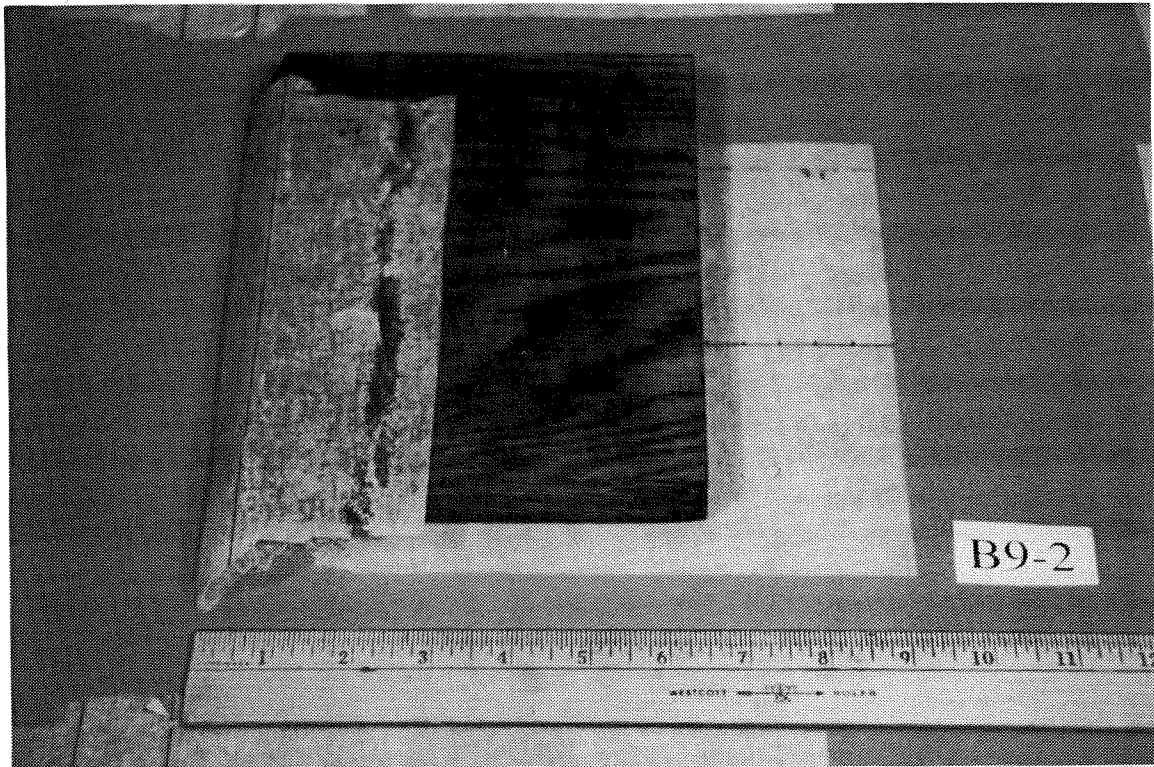


Figure 4.70 - Second reinforcement layer for model B9, showing breakage of the geotextile overlap

$$P_r = 2 (37 \times 15.64 \text{ kN/m}^3 \times 0.077 \text{ m}) 0.013 \text{ m} \tan(31^\circ) = 0.7 \text{ kN/m}$$

The calculated pullout resistance is much higher than the estimated in-soil geotextile tensile strength at which the overlap failed ($\approx 0.12 \text{ kN/m}$). In fact, for this ultimate tensile strength, enough pullout resistance would have been provided by an overlap anchorage length of only 2 mm.

It is worth noting that, in absence of nonlinearity in strength, the lateral soil stresses and reinforcement pullout capacity increase linearly with centrifugal acceleration. Consequently, a model that does not fail by pullout under its own weight during construction would not do so during centrifuge testing.

4.6.4.3 Selection of soil strength parameters

The criteria for characterizing reinforcements as extensible or inextensible can be established by comparing the horizontal strain in an element of reinforced soil subjected to a given load, to the strain required to develop an active plastic state in an element of the same soil without reinforcement (Bonaparte and Schmertmann, 1987):

- extensible reinforcement is such that the tensile strain at failure in the reinforcement is equal to or larger than the horizontal extension required to develop an active plastic state in the soil; and
- inextensible reinforcement is such that the tensile strain at failure in the reinforcement is significantly less than the horizontal extension required to develop an active plastic state in the soil.

Steel reinforcement meets the criterion for inextensible reinforcement, while most currently available geosynthetic reinforcing materials meet the criterion for extensible reinforcements in almost all practical applications.

The nonwoven geotextiles used to reinforce the centrifuge model slopes are extensible reinforcements. Consequently, the soil strength is expected to be mobilized rapidly, reaching its peak strength before the geotextile reinforcements achieve their ultimate strength. It has been speculated that the stability of a geosynthetically reinforced soil structure would then be governed by the critical state friction angle of the backfill material and not by the peak soil strength. It was with the purpose of clarifying this issue that the same sand at two different relative densities was used as backfill material for the centrifuge models in this study. Monterey No.30 sand would achieve the same critical state friction angle ($\approx 32.5^\circ$ under triaxial compression) for the models in the B- and D-series, reinforced using the same geotextile material but with sand backfill placed at different relative densities.

However, as previously shown in Figure 4.48, models in the D-series failed at higher g-levels than models in the B-series with the same number of reinforcement layers. Moreover, as will be shown in Section 4.7.3, the g-levels at failure obtained experimentally in the centrifuge tests can be predicted using the peak soil friction angles in limit equilibrium analyses. Consequently, the centrifuge tests in this study indicate that both the geosynthetic reinforcements and the soil backfill supply their maximum tensile and shear strengths, respectively, at the moment of failure.

A possible explanation for this observation is that failure of the structure is governed by the resisting forces generated in the soil *along the potential failure surface*.

Although the soil reaches an active state due to large *horizontal* strains compatible with geotextile deformations, large shear displacements (and drop in shear strength) in the soil *along the potential failure surface* does not occur until final sliding of the active reinforced wedge along the potential failure surface. Since the internal failure only occurs after breakage of the geotextile reinforcements, it is expected that both reinforcements and soil will contribute with their peak strengths to the stability of the structure.

4.7 Limit equilibrium analyses

4.7.1 General

Different techniques are available to assess the potential for collapse of a geotechnical structure. While the more rigorous plasticity solutions (limit analysis) or analyses that account for stress-strain behavior of soil and reinforcements (e.g., finite element analysis) have received increased attention, the limit equilibrium method (Terzaghi, 1956) still remains the most widely used approach to obtain approximate solutions for complex stability problems. This method assumes a failure surface and the stress distribution along that surface such that an overall equation of equilibrium in terms of stress resultants can be formulated. The purpose of the analyses presented in this section is to evaluate the suitability of the limit equilibrium approach for the analysis of geotextile-reinforced soil slopes.

Limit equilibrium analysis of unreinforced structures includes assumptions, like the shape of the failure surface, that have to be made also in the analysis of reinforced soil slopes. Moreover, additional assumptions to those already introduced in the analysis of unreinforced structures are needed for the analysis of reinforced slopes. These include

the inclination (e.g., horizontal, tangential) and distribution (e.g., linear, constant with depth) of the reinforcement tensile forces along the selected failure surface.

The limit equilibrium failure surfaces most widely used for the analysis of reinforced soil slopes include the planar wedge (Schlosser and Vidal, 1969; Lee et al., 1973; Segrestin, 1979), the bilinear wedge surface (Romstad et al., 1978; Stocker, 1979; Jewell et al., 1984; Schneider and Holtz, 1986; Bonaparte and Schmertmann, 1987; Jewell, 1991), the logarithmic spiral (Juran and Schlosser, 1978; Leshchinsky and Reinschmidt, 1985; Leshchinsky and Boedeker, 1989), and the circular surface (Phan et al., 1979; Ingold, 1982; Bangratz and Gigan, 1984; Christopher and Holtz, 1985; Gourc et al, 1986; Wright and Duncan, 1991). Several of these analysis methods have been used to develop design charts to determine the reinforcement requirements for simple slopes.

Although several different definitions for the factor of safety are currently being used, the one considered in this study is defined with respect to the shear strength of the soil:

$$FS = \frac{\text{Available soil shear strength}}{\text{Soil shear strength required for equilibrium}} \quad (4.30)$$

This definition is consistent with conventional limit equilibrium analysis, for which extensive experience has evolved for the analysis of unreinforced slopes.

A rigorous internal stability method was selected for this study. Current design practices for design of reinforced soil slopes also often consider less rigorous analyses that decouple the soil-reinforcement interaction. Such analyses neglect the influence of reinforcement forces on the soil stresses along the potential failure surface, which may result in significantly different calculated factors of safety than those obtained using more

rigorous approaches. Different rigorous methods of analysis have been developed for the analysis of geosynthetically reinforced slopes (e.g., Leshchinsky and Boedeker, 1989; Jewell, 1991; Wright and Duncan, 1991). In this study, Spencer's method for circular surfaces, as coded in the computer program Utexas3 (Wright, 1990), was selected for the analysis of the centrifuge slope models. The basis for the selection was the flexibility of the code, oriented towards analysis rather than specifically for design, and the fact that all known forces are used to satisfy horizontal force, vertical force and moment equilibrium on each slice. Additionally, as discussed in Section 4.7.4, the centrifuge test results are compared those predicted using design charts based on other rigorous limit equilibrium approaches.

4.7.2 Evaluation of modeling assumptions in limit equilibrium

The limit equilibrium analyses in this study are performed considering a search for the critical circular surface, instead of adopting a fixed circle that approximately matches the observed failure surface. Based on the observations made in Section 4.6.3, a uniform distribution of reinforcement forces with depth is considered in the analyses. The effect of geotextile tensile strength on the limit equilibrium results and the selection of the in-soil strength values are discussed in Section 4.7.2.1. In order to account for the possible effect of the increasing unit weight with the centrifuge radius, all limit equilibrium analyses were performed considering ten soil layers (Section 4.7.2.2). The orientation of the reinforcement forces are considered horizontal and the overlaps are modeled as additional geotextile reinforcements, as will be discussed in Sections 4.7.2.3

and 4.7.2.4, respectively. An evaluation of the possible effect of the method of slices selected for the analyses is discussed in Section 4.7.2.5 .

Based on the results from the soil testing program described in Section 4.4.1, the estimated friction angles from triaxial compression at 100 kPa confining pressure are $\phi_{tc}=35^\circ$ for Monterey sand at 55% relative density, and $\phi_{tc}=37.5^\circ$ for Monterey sand at 75% relative density. As shown by the triaxial test results performed at different confining pressures, there is only minor nonlinearity in the soil strength of the subrounded sand used as backfill material for the centrifuge models. Consequently, a constant friction angle was considered for the limit equilibrium analyses performed in this study. Considering the ratios between plane strain and triaxial friction angles for Monterey sand (Section 4.4.1.2), the plane strain friction angles used in the analyses are $\phi_{ps}=39.5^\circ$ for Monterey sand at 55% relative density and $\phi_{ps}=42.5^\circ$ for Monterey sand at 75% relative density.

Parametric studies, done to evaluate the variables relevant to the stability of the centrifuge slope models, are presented in this section. They are performed on model B18, which failed at 74 g. The results from the limit equilibrium analyses performed for all centrifuge models are discussed later in Section 4.7.3.

4.7.2.1 Effect of geotextile tensile strength

As discussed in Section 4.4.2, the geotextile tensile strength obtained from unconfined wide-width tests is not representative of the geotextile strength under operational conditions. The geotextile testing program performed to evaluate the effect of test boundary conditions strongly indicates that the in-soil geotextile strength is higher

than that obtained using the standard wide-width test. Although the evidence of improvement in geotextile mechanical properties is apparent, there is still no established testing procedure to accurately quantify this improvement. Consequently, the in-situ geotextile strength was evaluated by backcalculation, using limit equilibrium, of one centrifuge test reinforced with each geotextile type. Since a uniform reinforcement force with depth is assumed, the backcalculated strength value will be identified as the ultimate tension at failure T_{ult} . Although an approximately uniform reinforcement force distribution is estimated to occur at the moment of failure, the backcalculated strength would more rigorously correspond to the average reinforcement tension at the moment of failure (T_{ave} in Figure 4.67c).

The factors of safety for internal stability were calculated for model B18 using geotextile strengths T_{ult} varying from 0.3 lb/in to 1.8 lb/in (0.0525 kN/m to 0.315 kN/m). Figure 4.71 shows the calculated factors of safety for the different assumed geotextile strengths, considering increasing values of centrifuge acceleration. The results show an approximate linear increase of the calculated factors of safety with increasing reinforcement strength for each g-level N .

Of particular interest is the curve in the figure which corresponds to the analyses performed using the g-level at failure obtained experimentally in the centrifuge test ($N=N_f=76.5$). At this centrifugal acceleration, the backcalculated geotextile strength corresponds to the T_{ult} value that brings the FS to 1.00. For the Pellon Sew-in geotextile used as reinforcement in model B18, this backcalculated geotextile strength obtained is 0.6877 lb/in. Thus, a rounded value of $T_{ult}=0.7$ lb/in (0.1225 kN/m) was adopted as the in-soil tensile strength for the limit equilibrium analyses performed for models reinforced

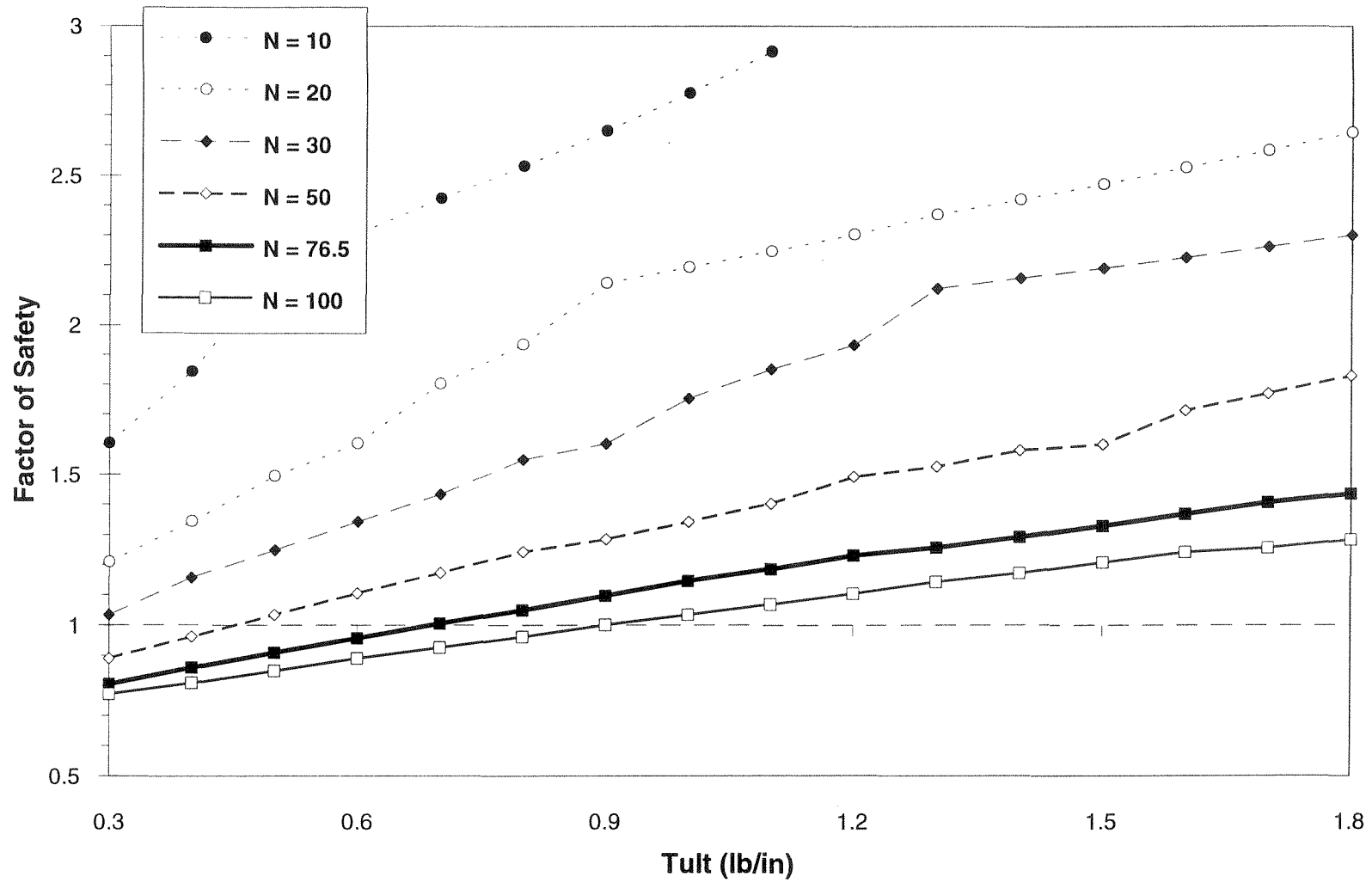


Figure 4.71 - Effect of geotextile tensile strength on the calculated factor of safety for model B18

with Pellon Sew-in geotextiles. Based on a similar backanalysis using model S9, the in-soil tensile strength for the Pellon Tru-grid geotextile was estimated as 1.05 lb/in (0.18375 kN/m).

The backcalculated in-soil strength values fit well within the range of ultimate geotextile strength values obtained from the geotextile tensile testing program (Figure 4.34). Possible interpretations for the "actual" in-soil strength were discussed in Section 4.4.2.3. More importantly, as will be discussed in Section 4.7.3.1, the T_{ult} values backcalculated from all six centrifuge models built using Sew-in fabrics and from the two models reinforced with Tru-grid fabric are essentially the same.

Figure 4.72 shows the critical circle obtained from the limit equilibrium analysis of model B18 using the ultimate geotextile strength of 0.7 lb/in at the centrifugal acceleration that brought the model to failure ($N_f=76.5$ g). The critical circle obtained after the search process matches very well the location of the failure surface as interpreted from the tears in the geotextile reinforcements, and from the location digitized from images of the model recorded at the moment of failure. The accurate prediction of the location of the potential failure surface is relevant for estimating the required reinforcement length of reinforced soil structures. Additional evidence that limit equilibrium is able to predict correctly the location of the potential failure surfaces in reinforced soil slopes is presented later in Section 4.7.3.3.

Although the in-soil geotextile strengths were eventually selected using results from two centrifuge tests, it is important to note that these values were not blindly predicted from this backcalculation. In fact, the possible range for geotextile strength values was defined from the geotextile tensile testing program, and these results were

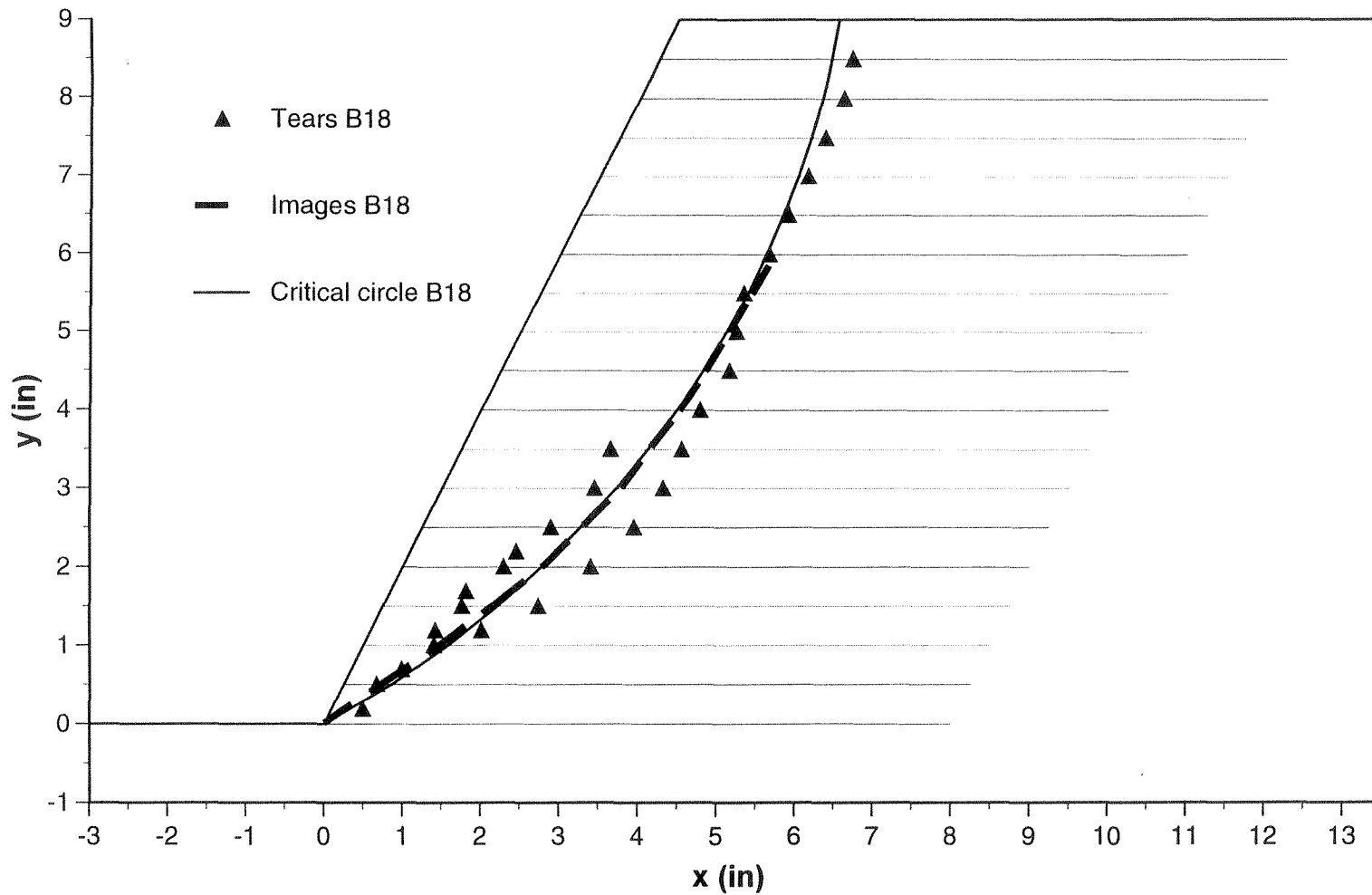


Figure 4.72 - Comparison between the failure surface measured for centrifuge model B18 and the critical circle predicted using limit equilibrium

eventually refined using information from centrifuge tests. This procedure for selecting the geotextile parameters was adopted given the inability of current standard tensile tests to evaluate the in-soil mechanical properties of geotextiles. This emphasizes the need of further research to correctly evaluate the in-soil mechanical properties of geotextiles.

4.7.2.2 Effect of nonuniform unit weight

The effect of increasing acceleration with radius in the centrifuge model slopes was investigated for the case of model B18. The factors of safety calculated considering a constant unit weight were compared to those calculated considering an increasing unit weight in the model. The uniform g -level is defined using the effective radius R_{eff} estimated in Section 4.5.2. For example, the limit equilibrium analysis at the g -level at failure obtained experimentally from the centrifuge test ($N_f=76.5$, defined using $R_{\text{eff}}=34.375$ inches) is performed using a uniform soil unit weight of 1196.5 kN/m^3 ($76.5 \times 15.64 \text{ kN/m}^3$). On the other hand, the same analysis considering nonuniform acceleration was performed by dividing the model into horizontal slices and using unit weights increasing from 1126 kN/m^3 at the top of the model to 1405.5 kN/m^3 at the base.

Figure 4.73 shows the decrease of the factors of safety against failure with increasing g -levels in model B18. The analyses are performed using $T_{\text{ult}}=0.7 \text{ lb/in}$, and a search for the critical circular failure surface is done at the different g -levels. The solid line in the figure corresponds to the analyses performed using sand layers with increasing unit weight, while the dashed line corresponds to the analyses performed with a uniform unit weight of the backfill. There is a very good agreement between the results obtained from the two type of analyses. Good agreement was also obtained for the location of the

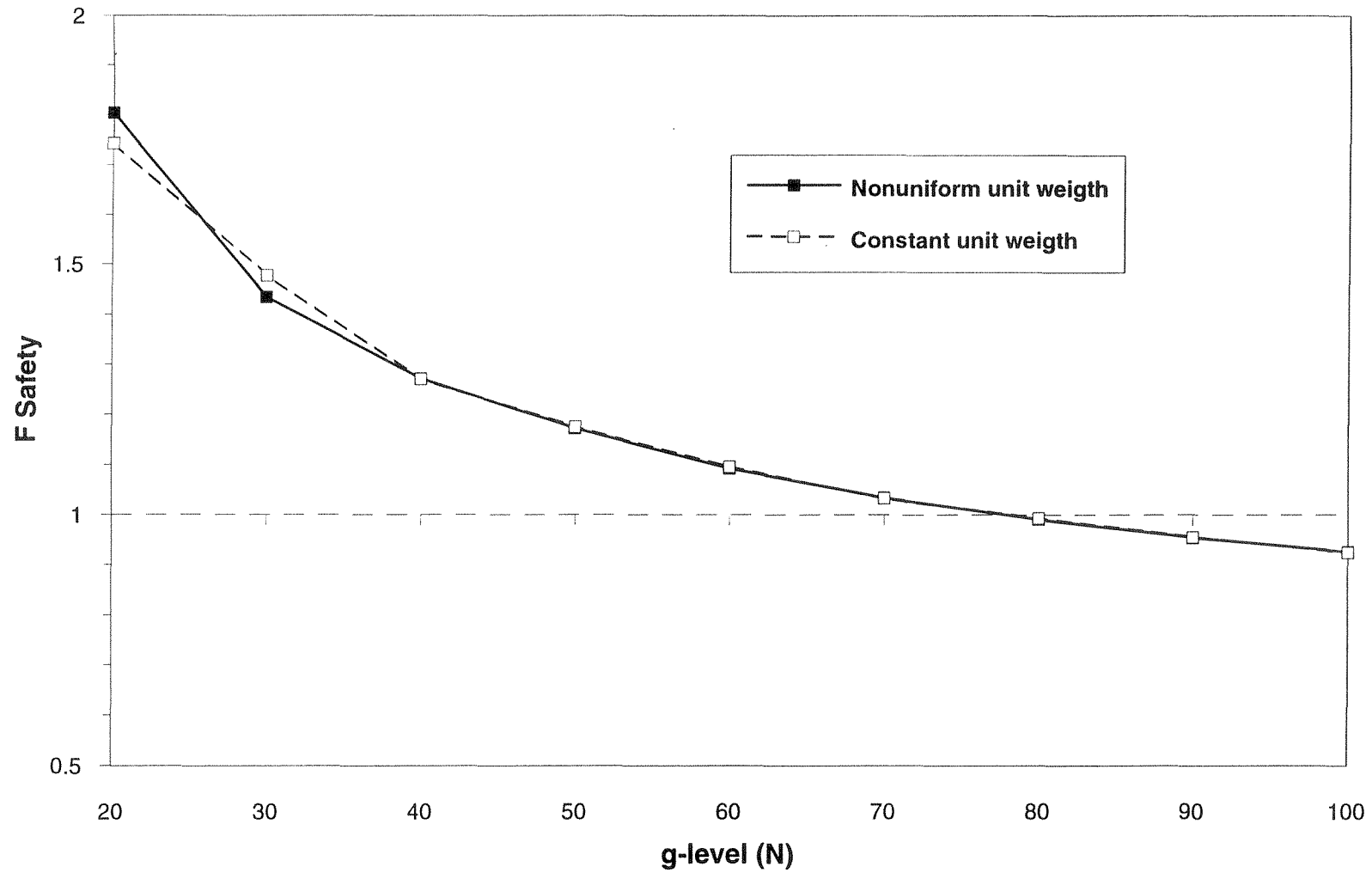


Figure 4.73 - Calculated factors of safety for model B18 with increasing centripetal acceleration: Effect of nonuniform unit weight

critical circles using the two procedures. Although the use of sand layers with increasing unit weight was finally adopted for the limit equilibrium analysis in this study, the good agreement obtained in this parametric study provides confidence in the procedure adopted to select the effective radius for the centrifuge arm. Moreover, these results justify the use of simpler interpretations of centrifuge modeling results made assuming uniform soil unit weight in the analyses.

4.7.2.3 Effect of orientation of reinforcement forces

A possible inaccuracy in limit equilibrium analyses of reinforced soil slopes is the direction in which the reinforcement forces are assumed to act. The inclination of the tensile forces has been assumed to vary between horizontal (as-installed) and tangent to the potential slip surface. Observation of the deformation of the reinforced slope models during increasing gravity accelerations suggests that the orientation of the reinforcements was not tangent to the failure surface and, most probably, remained horizontal until the moment of failure. This is consistent with results from laboratory and analytical studies of soil shear zone formation (Shewbridge and Sitar, 1989, 1992). Based on these observations, it was decided to consider the orientation of reinforcement forces horizontal in the limit equilibrium analyses performed for this study. Nevertheless, the effect of reinforcement orientation on the calculated factors of safety was evaluated.

Figure 4.74 shows the factors of safety calculated for model B18 with increasing centripetal accelerations considering either horizontal or tangential reinforcement forces. The figure shows that only small differences are obtained in the calculated factors of safety (less than 10% difference). The results of this particular analysis indicate that the

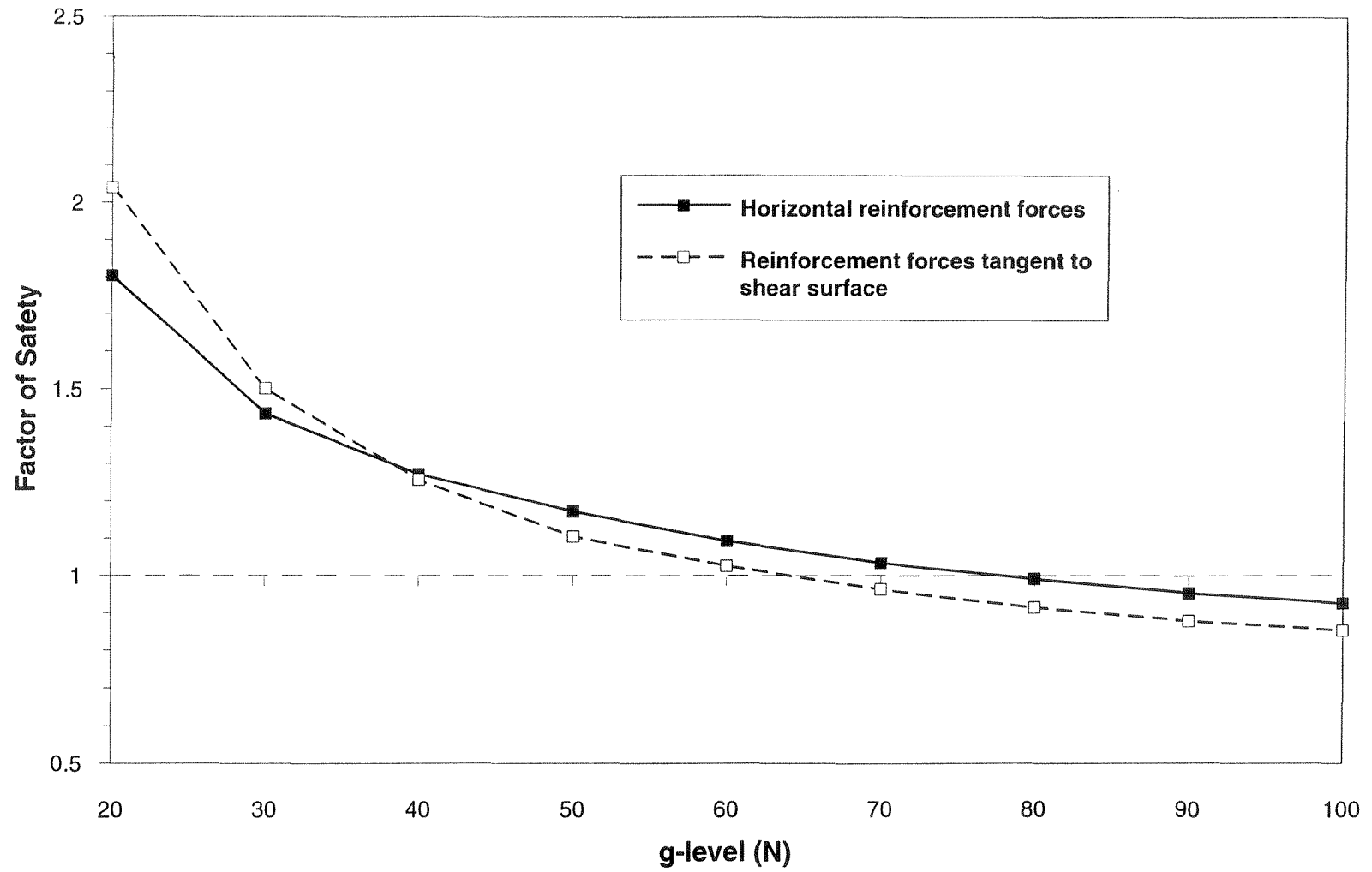


Figure 4.74 - Calculated factors of safety for model B18 with increasing centripetal acceleration: Effect of orientation of reinforcement forces

use of horizontal reinforcements would be a conservative assumption for overdesigned slopes (high FS), while it would not be conservative for the case of underdesigned structures (low FS). For factors of safety typically adopted in design (say, 1.3 to 1.5), either assumption on the orientation of the reinforcements renders similar factors of safety.

These results are in agreement with previous studies on the effect of reinforcement orientation (Leshchinsky and Volk, 1986; Leshchinsky and Boedeker, 1989; Wright and Duncan, 1991). These studies concluded that, for cohesionless fills, the orientation of reinforcement forces has little effect on the factors of safety, as long as the calculations are done using limit equilibrium methods that satisfy complete static equilibrium. Just for verification purposes, factors of safety for model B18 were also calculated using nonrigorous limit equilibrium approaches that decouple the effect of reinforcement forces and the normal stresses along the potential failure surface. In this case, the factors of safety calculated using tangential reinforcement forces were consistently higher than those estimated using horizontal forces.

A reinforcement force tangential to the failure surface tends to produce a larger moment than a horizontal force, but it has a smaller contribution to the normal forces (and shear strength) along the shear surface. Since the two effects tend to compensate for each other, the net effect of the selected reinforcement force orientation is thus small (Wright and Duncan, 1991). This rationale is corroborated by the results obtained for model B18 and indicated in Figure 4.74 for increasing g -levels. At low g -levels, the contribution of the soil resisting forces to the structure stability is penalized by a high factor of safety affecting the soil strength in the calculations. Consequently, the effect of reinforcement

moments is comparatively larger, and higher factors of safety are obtained when tangential forces are assumed in the calculations. Conversely, at high g-levels the contribution of the soil resisting forces to the structure stability is only slightly decreased or even increased (for $FS < 1.00$) in the calculations. In this case, the effect of stresses normal to the shear surface is comparatively larger, and higher factors of safety are obtained when horizontal forces are assumed in the calculations.

4.7.2.4 Effect of geotextile overlaps

Current design of geotextile-reinforced slopes does not take into account the effect that geotextile overlaps may have on the internal stability of the structure. However, the breakage of geotextile overlapping layers that are near the base of the models clearly indicates that the overlaps work as additional reinforcements. As discussed in Section 4.6.4.2, reinforcement overlaps intersected by the failure surface did fail by geotextile breakage, without signs of pullout. Based on this experimental evidence, the overlaps were modeled as additional short reinforcement layers in the limit equilibrium analyses performed in this study.

Figure 4.75 illustrates the importance of correctly modeling the geotextile overlaps. The figure shows the factors of safety calculated for model B18 using increasing centripetal acceleration. A total of eighteen reinforcement layers were used in the analyses performed without considering the overlaps and a total of 36 reinforcements (short and long ones) were considered in the analyses that accounted for the effect of overlapping layers. The figure shows that the geotextile overlaps contribute approximately by a constant value to the stability of the structure (approximately

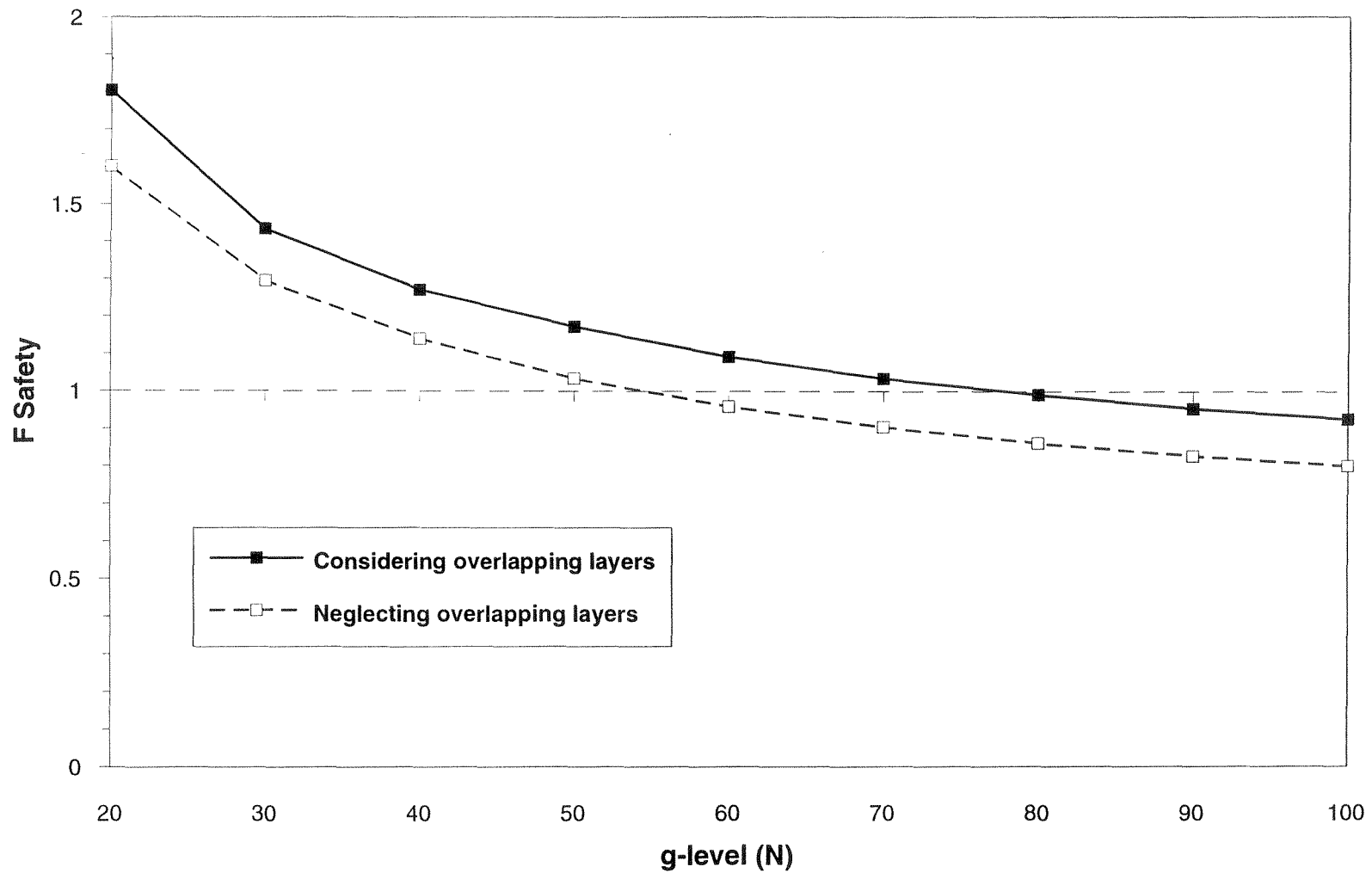


Figure 4.75 - Calculated factors of safety for model B18 with increasing centripetal acceleration: Effect of geotextile overlaps

$\Delta FS=0.12$) for the different g-levels. Although disregarding the effect of overlaps may be a conservative assumption for the design of geotextile-reinforced slopes, it is clear that this effect should be taken into account for this study in order to correctly predict the failure of the centrifuge models.

Although neglecting the effect of geotextile overlaps provides conservative results for the estimation of the internal stability factor of safety, it appears that this assumption is unconservative when estimating the location of the critical failure surface. Figure 4.76 compares the critical circles obtained from limit equilibrium analyses performed to investigate the effect of overlaps. The critical circle which matches the observed failure surface was obtained for the acceleration at failure for model B18 ($N_f=76.5$) taking the geotextile overlaps into account. In comparison, two critical circles are shown for analyses performed without modeling the overlaps: the critical circle obtained for the analysis at 60 g, which gives approximately a factor of safety of unity, and another obtained using the experimental g-level at failure ($N_f=76.5$). These results indicate that the estimated reinforcement lengths would be shorter if the analyses are performed without modeling the geotextile overlaps, providing an unconservative estimation of the pullout resistance for the reinforced soil slope.

4.7.2.5 Effect of wall friction at model boundaries

Negligible edge effects were observed in the centrifuge models as indicated by:

- (1) the breakage pattern of the geotextiles, that showed no curvature towards the edges;
- (2) the good comparison between the displacements along the plexiglass wall and those within the soil mass observed in one model wetted and dissected after testing; and (3) the

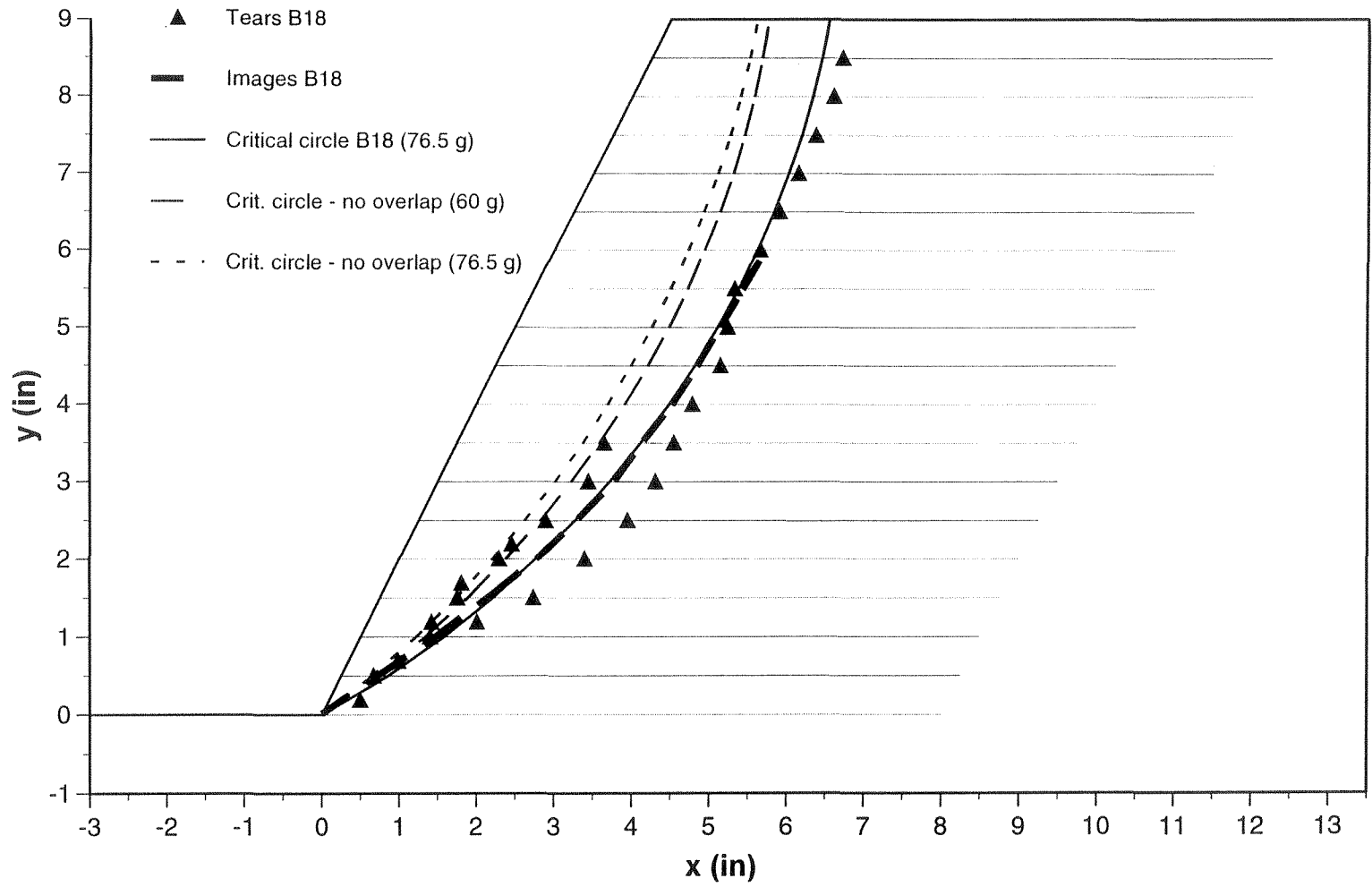


Figure 4.76 - Effect of geotextile overlaps on the predicted critical circles

agreement between the failure surface defined from the geotextile tears and from the images recorded through the plexiglass wall. However, friction angles obtained for the sand/teflon and sand/mylar interfaces were somewhat higher than expected (Section 4.4.3). Consequently, a parametric study was performed in order to investigate the possible effect of the lateral friction on the calculated factors of safety.

The lateral friction of the sand models against the walls of the centrifuge box can be considered as a three dimensional effect in a two dimensional slope stability analysis. Figure 4.77 shows a schematic representation of the lateral shear stresses τ_f caused by the lateral friction on the active reinforced soil wedge. The figure also shows one of the slices considered in the limit equilibrium analysis. Horizontal soil stresses at the moment of failure exerted against the lateral wall at a depth z from the slope surface can be estimated as:

$$\sigma_h = K \gamma z \quad (4.31)$$

where K is the earth pressure coefficient and γ is the soil unit weight. Lateral deformations in geotextile-reinforced walls are large enough to bring the soil mass into an active plastic state close to the moment of failure. Nevertheless, since plane strain condition prevails in the models, lateral stresses against the wall are probably bounded between those defined using the active (K_a) and at rest (K_0) earth pressure coefficients. After defining the lateral stresses against the wall, the lateral shear stresses τ_f along the soil/wall interface can be evaluated from:

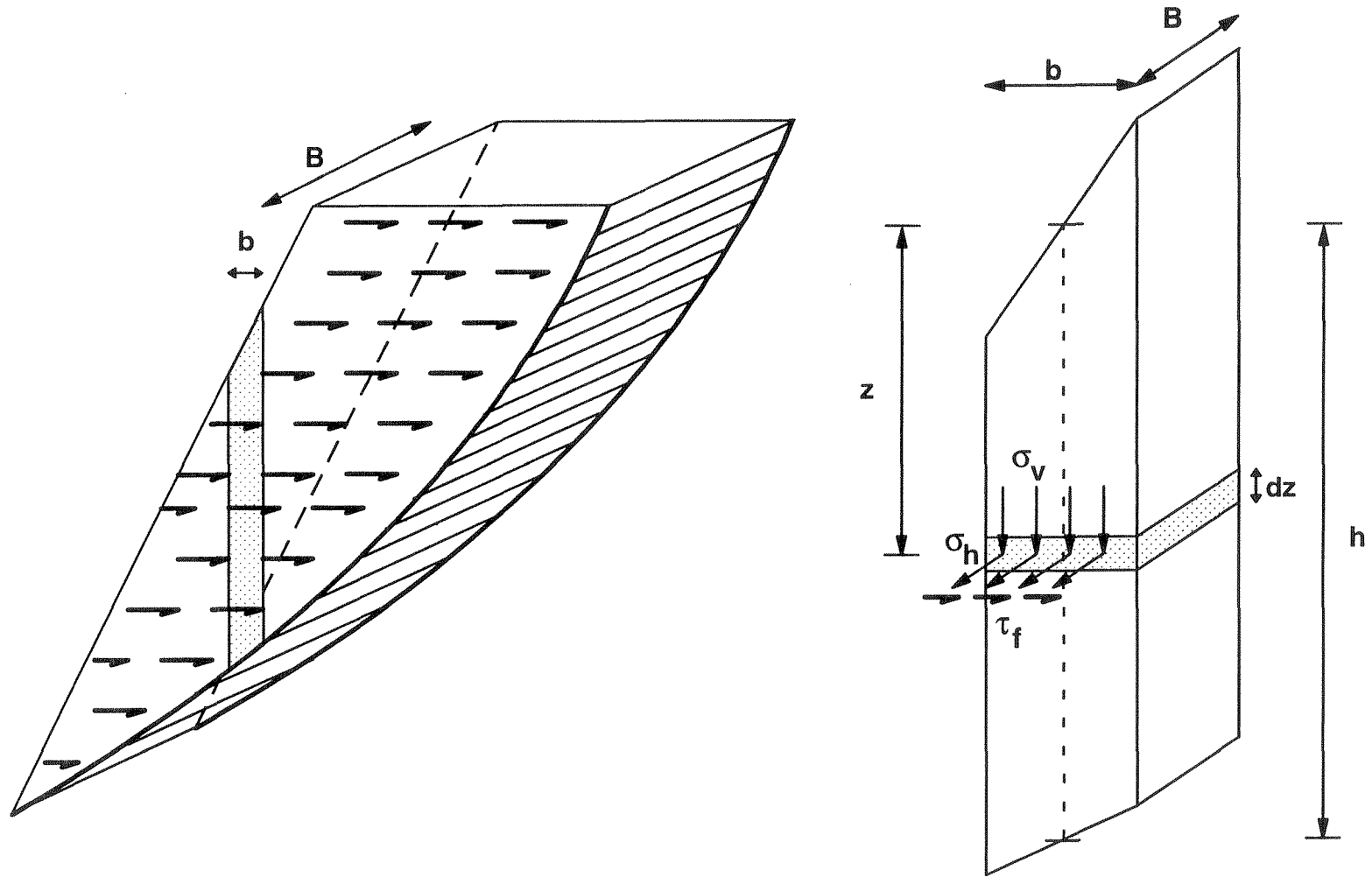


Figure 4.77 - Lateral shear stresses caused by wall friction in a centrifuge slope model

$$\tau_f = \sigma_h \tan\delta = K \gamma z \tan\delta \quad (4.32)$$

where δ is the interface friction angle. The lateral shear force dF_f exerted on a differential area of height dz , can be estimated as:

$$dF_f = (2/B) \tau_f (b \cdot dz) \quad (4.33)$$

where $(b \cdot dz)$ is the differential area, b is the width of the slice, and B is the width of the centrifuge box. The factor $(2/B)$ is considered in order to estimate dF_f as a lateral shear force per unit width (the factor 2 accounts for the two lateral walls). Using Equation (4.33), the lateral shear force F_f on the entire slice can be estimated as:

$$F_f = \int_0^h dF_f = \left(\frac{\tan\delta K}{B} \right) h (\gamma \cdot b \cdot h) \quad (4.34)$$

where h is the height of the slice. Defining the constant η as:

$$\eta = \left(\frac{\tan\delta K}{B} \right) \quad (4.35)$$

and recognizing that $(\gamma \cdot b \cdot h)$ is the slice weight W , the lateral shear force can be finally obtained as:

$$F_f = \eta h W \quad (4.36)$$

which is the lateral force that should be considered in each slice to account for the friction of the sand model against the lateral walls. Notice that the lateral shear force F_f should be applied at $h/3$ from the base of each slice in the case of homogeneous granular slopes since the distribution of lateral shear stress increases linearly with depth.

The lateral shear force F_f could be implemented in a limit equilibrium code. However, a preliminary approximation can be made by noticing the similarity between F_f and the pseudo-static seismic force F_s , which is calculated as:

$$F_s = \alpha W \quad (4.37)$$

where α is the pseudo-static seismic coefficient. By comparing (4.36) and (4.37) it may be concluded that the lateral shear force F_f could be handled as a "negative pseudo-static horizontal force" in the calculations. In this case, the equivalent seismic coefficient should be estimated as:

$$\alpha = - \eta h_{ave} \quad (4.38)$$

where η is defined by (4.36) and h_{ave} is the average height of the slices on the critical circle. The negative sign accounts for the fact that, conventionally, positive pseudo-static accelerations are assumed in the direction of the slope. It is worth noting that in this approximation, the lateral force will be applied at the center of each slice.

For the evaluation of the effect of lateral shear forces on the factors of safety calculated for model B18, the following parameters are considered:

$\delta = 14.5^\circ$: average between the residual friction angles for sand/mylar and sand/teflon.

Residual angles are assumed since large lateral displacements already occurred at the interfaces at the moment of failure.

$K = 0.222$: the active earth pressure coefficient, defined based on $\phi_{ps} = 39.5^\circ$, is considered in the calculations.

$B = 203$ mm: width of the centrifuge box

$h_{ave}=74$ mm: average height of the slices from the critical circle in Figure 4.72

Using these parameters, the "negative pseudo-static seismic coefficient" estimated from (4.36) and (4.39) is $\alpha = - 0.02093$.

Figure 4.78 shows the factors of safety for model B18 obtained using increasing centripetal accelerations, and calculated considering the resistance originated from friction on the lateral walls. These results indicate that the effect of lateral friction on the calculated factor of safety is small (on the order of 3%). Calculations were also made considering the at rest earth pressure coefficient ($K_0=0.363$), and the results also showed a small effect on the factor of safety (on the order of 5%).

Considering the small influence of the lateral wall friction on the calculated factor of safety, it was decided not to account for this effect in the analyses performed in this study. However, it should be noted that small differences in the factor of safety do not necessarily imply a negligible effect on the predicted g-level at failure. Thus, the decision of not accounting for wall friction in the analyses was not made based solely on the small influence observed in the calculations, but also on the several experimental evidences that indicated negligible edge effects on the test results. Nevertheless, it seems appropriate that future studies consider the implementation in limit equilibrium of lateral shear forces calculated using Equation (4.36), in order to account for three dimensional effects using the simplified procedure developed herein.

An additional consideration made in not accounting for the effect of lateral friction on the calculations is that the adopted plane strain friction angles were obtained from

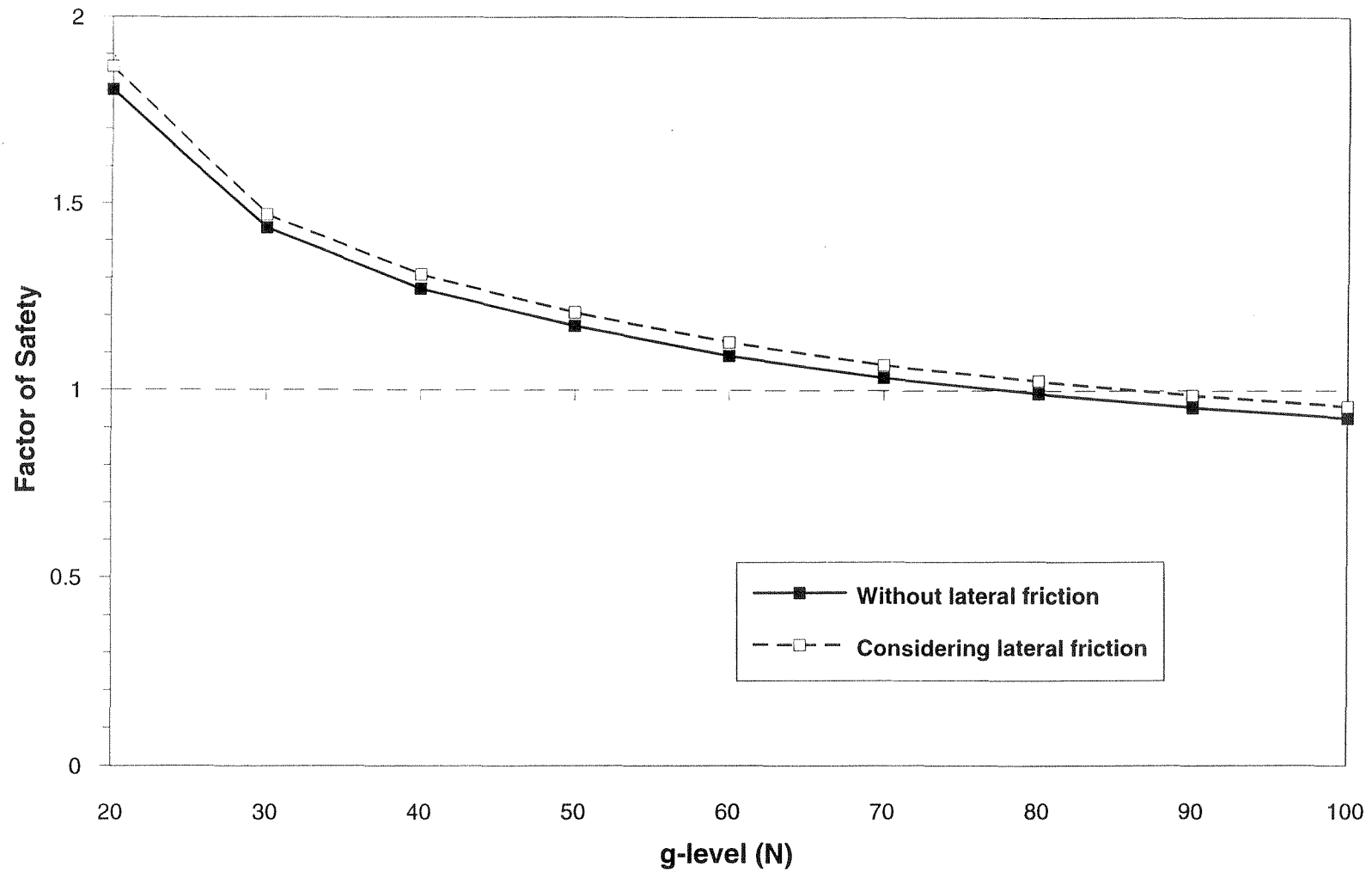


Figure 4.78 - Calculated factors of safety for model B18 with increasing centripetal acceleration: Effect of friction on lateral walls

laboratory studies which minimized, but did not eliminate lateral friction in their testing procedures. In fact, experimental studies done to investigate the plane strain friction angle of sands follow procedures to reduce the lateral friction on the plane strain cells similar to the techniques adopted in this study to minimize friction against the centrifuge lateral walls. Consequently, the effect of lateral friction is probably already accounted for in the adopted plane strain friction angles of Monterey sand.

4.7.2.6 Influence of the selected slope stability method of analysis

The factors of safety for the centrifuge models were calculated in this study using Spencer's method (Spencer, 1967). This method satisfies all conditions of equilibrium and assumes that the interslice forces are all parallel. For practical design purposes, it has been shown that methods that satisfy all conditions of equilibrium (e.g., Janbu's, Morgenstern and Price's, Spencer's) are accurate for any conditions, except when numerical problems are encountered. The factor of safety computed using any of these methods differ by no more than 12% from the factor of safety calculated by any other method that satisfies all conditions of equilibrium, and no more than about 6% from what can fairly be considered to be the correct answer (Duncan, 1992; Duncan and Wright, 1980).

However, a difference in the calculated factor of safety of 12%, which is inconsequential for design purposes, may become significant when predicting the g-level at failure in the centrifuge slope models. This is because the factor of safety versus g-level curves are highly nonlinear. Consequently, a parametric study was performed to evaluate the implication of having adopted a specific slope stability method. Since no

code was available for limit equilibrium analysis of reinforced soil slopes using the different methods, a rigorous evaluation was not possible. However, good evidence that the different limit equilibrium methods would render very similar results was obtained by simulating the reinforcement forces as pseudo-static seismic forces.

An unreinforced slope with the same geometry and soil properties as model B18 was used for this study. Using Spencer's method, the pseudo-static seismic coefficient that simulates the effect of the reinforcements in model B18 was estimated such that it will render a factor of safety of unity for the g-level causing failure in model B18. The calculated seismic coefficient is $\alpha = -0.205$. The computer program Slopas (Espinoza et al., 1992), which considers a variety of limit equilibrium methods and allows the use of pseudo-static seismic forces, was then used to compare the influence of the selected slope stability method on the calculated factors of safety.

The various limit equilibrium methods make different assumptions regarding the direction of the resultant internal forces, the height of the line of thrust, or the shape of the distribution of internal shear forces. Table 4.6 compares the factors of safety calculated by different methods using the same critical circle. The factors of safety estimated using Spencer's and Bishop's methods were calculated using both Utexas3 and Slopas, which gave identical results. The rest of the analyses were performed using Slopas. As can be seen from the results indicated in the table, all rigorous methods rendered virtually the same factor of safety. Except for Janbu's method, which gave a factor of safety very close to 1.000, all other rigorous methods yielded exactly the same result up to the third decimal figure.

Table 4.6 - Calculated factors of safety for model B18 using different methods of analysis

Method	Calculated factor of safety
<i><u>Methods that satisfy all equilibrium equations</u></i>	
Spencer (1967)	1.000
Morgenstern and Price (1965)	1.000
Sarma (1973)	1.000
Sarma (1979)	1.000
Janbu (1954)	1.026
Correia (1988)	1.000
<i><u>Methods that do not satisfy all equilibrium equations</u></i>	
Fellenius (1936)	0.780
Lowe and Karafiath (1960)	1.112
Bishop (1955)	1.000

Additionally, three methods commonly used in geotechnical practice that do not satisfy complete static equilibrium were also considered in this evaluation. The Ordinary Method of Slices (Fellenius, 1936), which only satisfies momentum equilibrium, underestimated the factor of safety by more than 20%. Lowe and Karafiath's method, which satisfies both vertical and horizontal force equilibrium but does not satisfy moment equilibrium, did not give an accurate result either, overpredicting by more than 10% the factor of safety. Bishop's modified method, which satisfies moment and vertical force

equilibrium, but does not satisfy horizontal force equilibrium, predicted the factor of safety as accurately as the rigorous methods, giving a factor of safety of exactly 1.000.

The results obtained from this evaluation provide evidence that similar results would have been obtained in the limit equilibrium analysis of the centrifuge models, using any of the indicated rigorous limit equilibrium methods or Bishop's method. All these methods considered circular surfaces using the method of slices. An evaluation of the centrifuge results using rigorous limit equilibrium methods assuming other surface shapes for the analysis of reinforced soil slopes is presented in Section 4.7.4 .

4.7.3 Comparison between predicted and experimental results

One of the objectives of the centrifuge testing program was to compare the experimental results with predictions using limit equilibrium analysis. Thus, after identifying the relevant variables for the analysis (Section 4.7.2), a discussion of the limit equilibrium predictions of failure in all the models (g-levels at failure, location of shear surface) is presented herein.

4.7.3.1 Characteristics of the analyses

As in the analyses performed in Section 4.7.2, limit equilibrium calculations were performed considering a search for the critical circular surface, instead of adopting a fixed circle that matches the observed failure surface. In this way, besides investigating the ability of limit equilibrium to predict the g-level at failure, its capability of predicting the location of the failure surface can be also assessed. As previously indicated, the plane

strain friction angles finally used in the analyses are 39.5° and 42.5° for the backfill at 55% and 75% relative densities, respectively.

The in-soil geotextile strength values were defined considering the backanalyses from the two centrifuge models discussed in Section 4.7.2.1, that are consistent with tensile strength results obtained from a geotextile tensile testing program (Section 4.4.2). Accordingly, the geotextile strengths used in the analyses are $T_{ult}=0.1225$ kN/m (0.7 lb/in) for the Pellon Sew-in geotextile and $T_{ult}=0.18375$ kN/m (1.05 lb/in) for the Pellon Tru-grid geotextile.

Considering the interpretation of the failure mechanisms discussed previously, a uniform distribution of reinforcement forces with depth is considered in the analyses. In order to account for the possible effects of nonuniform centripetal acceleration, the limit equilibrium analyses considered ten soil layers with unit weights increasing with the centrifuge radius. The orientation of the reinforcement forces was assumed horizontal and the overlapping geotextile layers were modeled as additional geotextile reinforcements. Finally, the effect of the friction of the model against the lateral centrifuge walls was considered negligible and not accounted for in the analyses. The justification for these different modeling assumptions was discussed in the parametric studies presented in Section 4.7.2.

4.7.3.2 Experimental and predicted g-levels at failure

The calculated factors of safety with increasing g-level for the centrifuge slope models in the B-series are plotted in Figure 4.79. For a given model, the factor of safety against failure decreases as the g-level increases. The calculated factors of safety curves

show similar nonlinear trends for the different centrifuge models. Figures 4.80 and 4.81 show the calculated factors of safety versus g-level for the centrifuge models from the D-series and from the S-series. Results obtained for models from the B-series with the same number of geotextile reinforcements are also included for comparison. The curves show similar patterns to those obtained for the B-series tests. The predicted g-levels at failure for each centrifuge model can be obtained from the information provided by these figures, and corresponds to the g-level that gives a factor of safety of one.

Figure 4.82 shows a comparison between the g-level at failure obtained experimentally in each centrifuge test (Table 4.5) and the predicted values obtained using limit equilibrium analysis. The results shows a very good agreement between measured and predicted g-levels at failure, with all the points falling essentially on the 45° line. Based on the very good comparison between analytic and experimental results it may be inferred that the limit equilibrium method is capable of accurately predicting the failure of the reinforced slopes. This good match also provides confidence in the selection of parameters and in the modeling assumptions made for the limit equilibrium analyses. Note that equally good comparisons between predicted and measured results are obtained for centrifuge slope models built using different reinforcement spacings, different soil densities, and geotextiles with different ultimate tensile strengths.

4.7.3.3 Experimental and predicted location of failure surfaces

Correct identification of the location of the potential failure surfaces is relevant for the design of reinforced soil structures, since it is used to define the length of the reinforcement elements. The reinforcement anchorage length required to provide enough

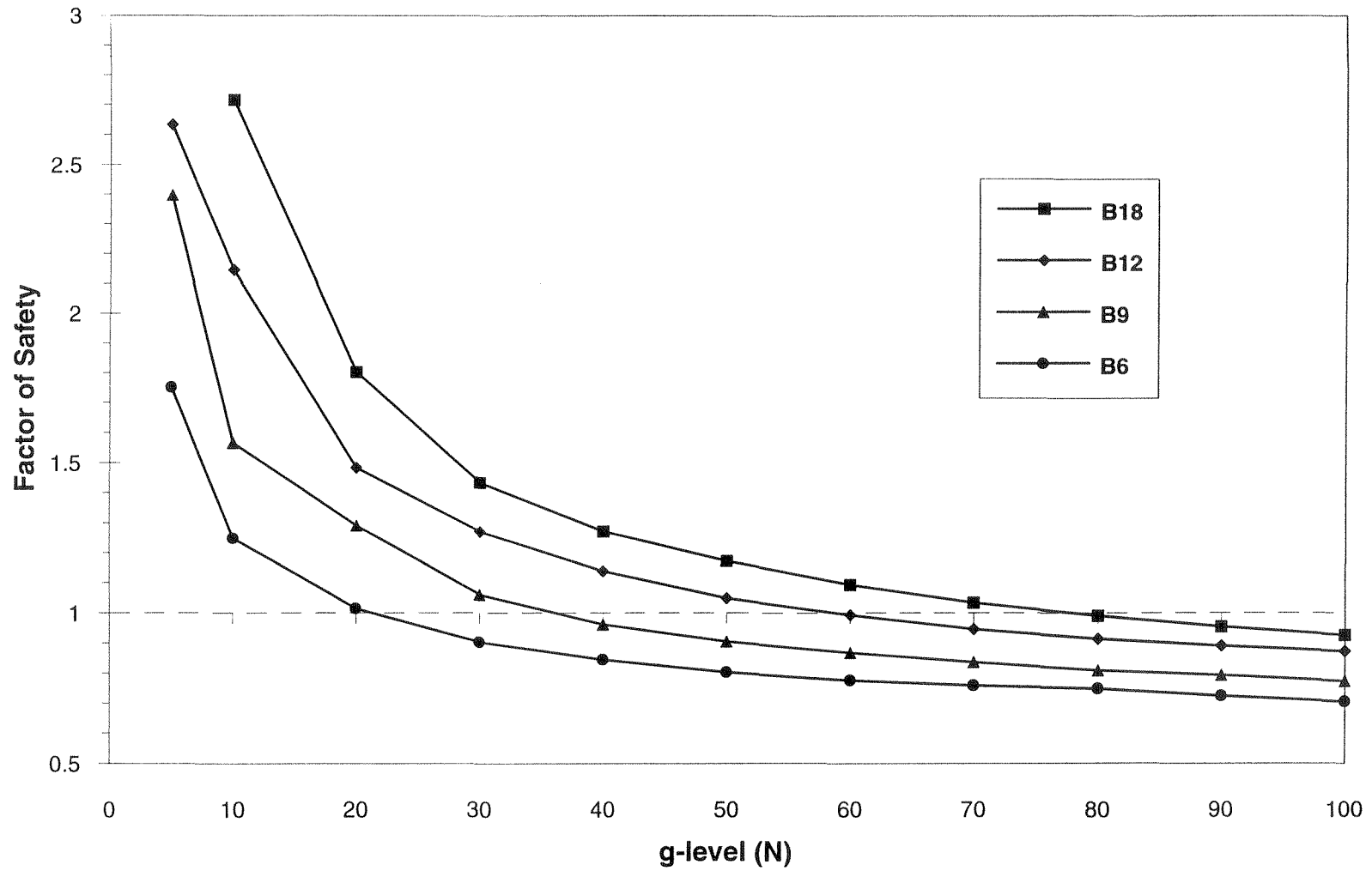


Figure 4.79 - Calculated factors of safety with increasing g-level loading for models in the B-series

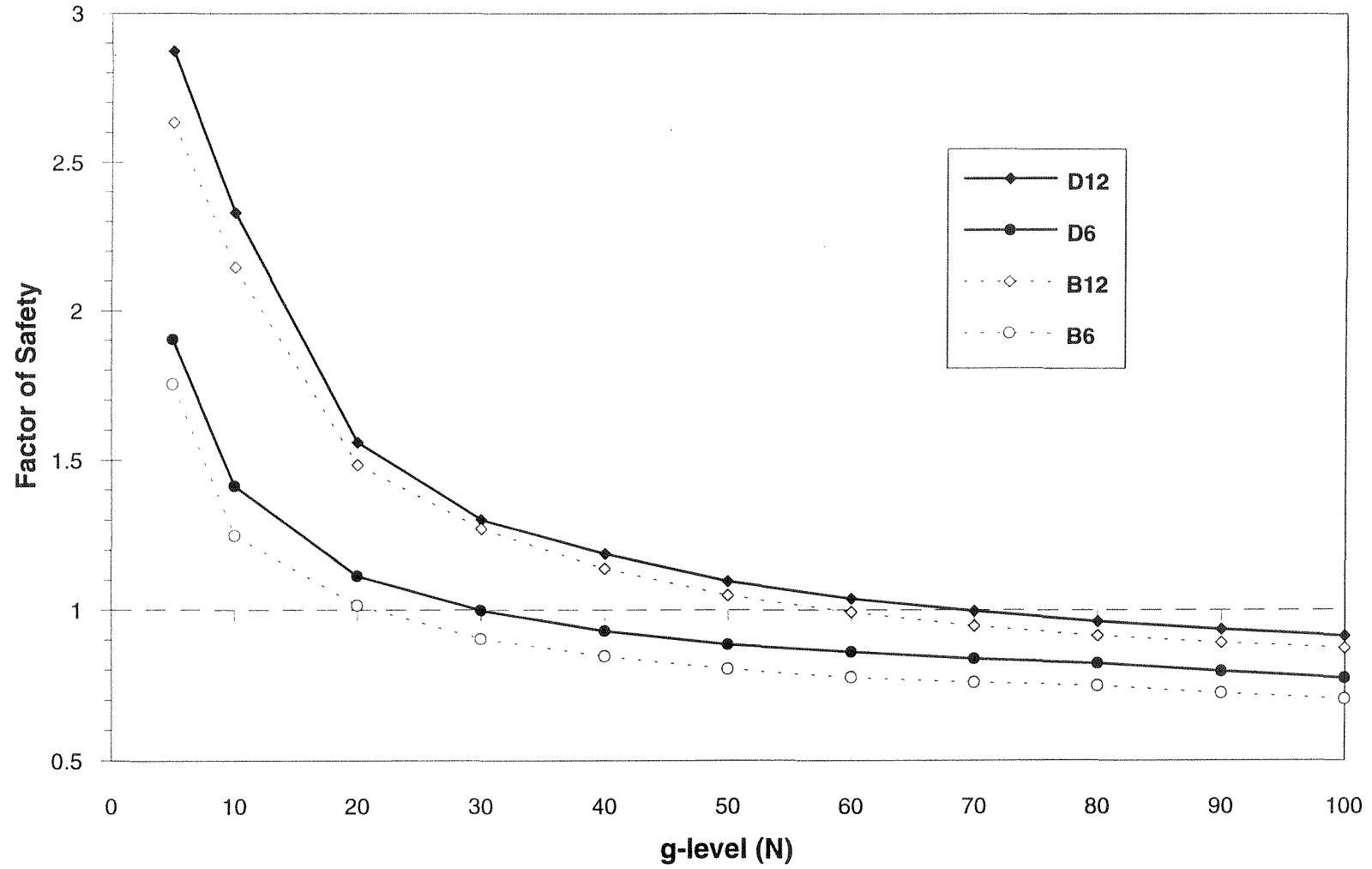


Figure 4.80 - Calculated factors of safety with increasing g-level loading for models in the D-series

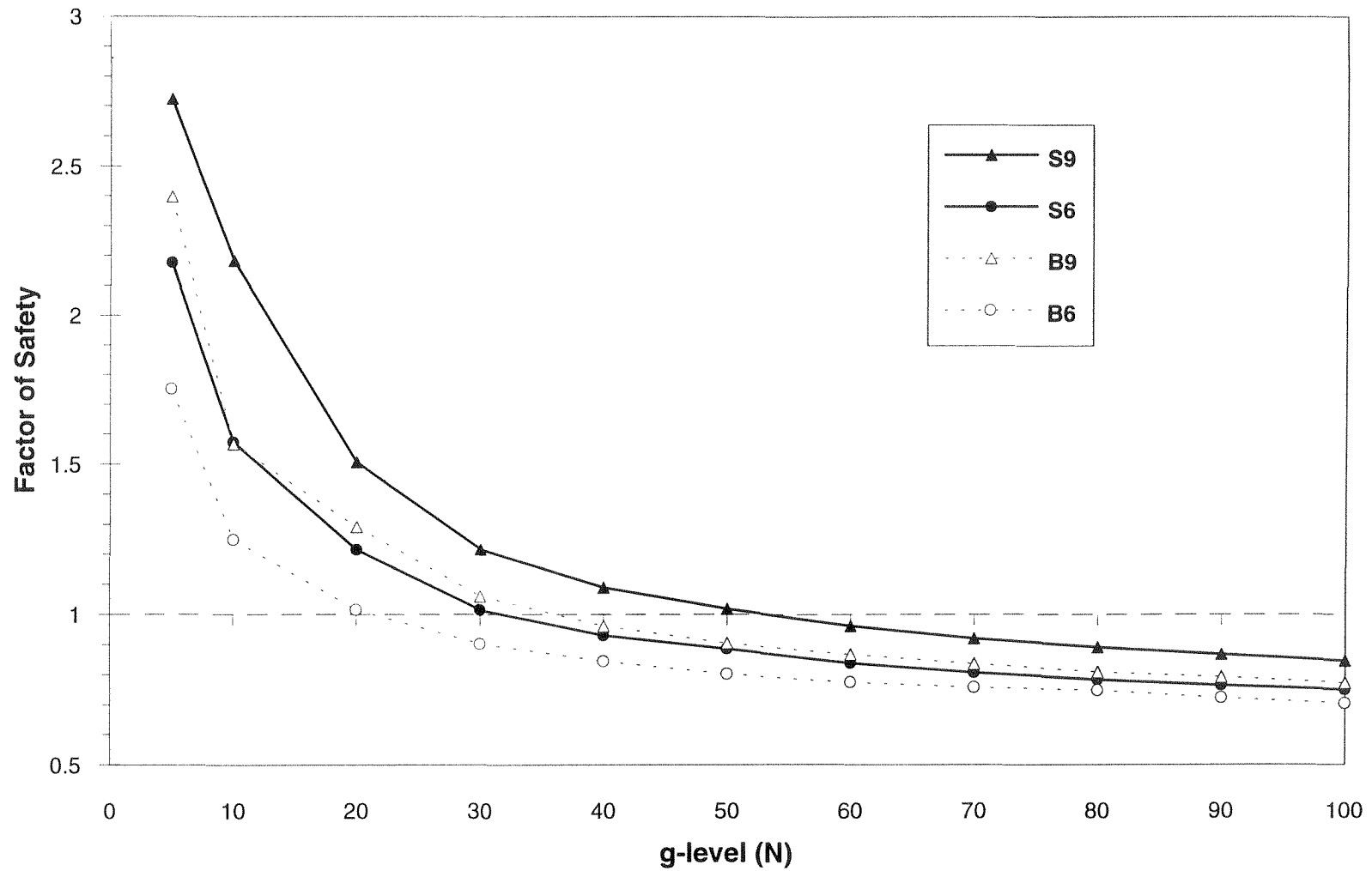


Figure 4.81 - Calculated factors of safety with increasing g-level loading for models in the S-series

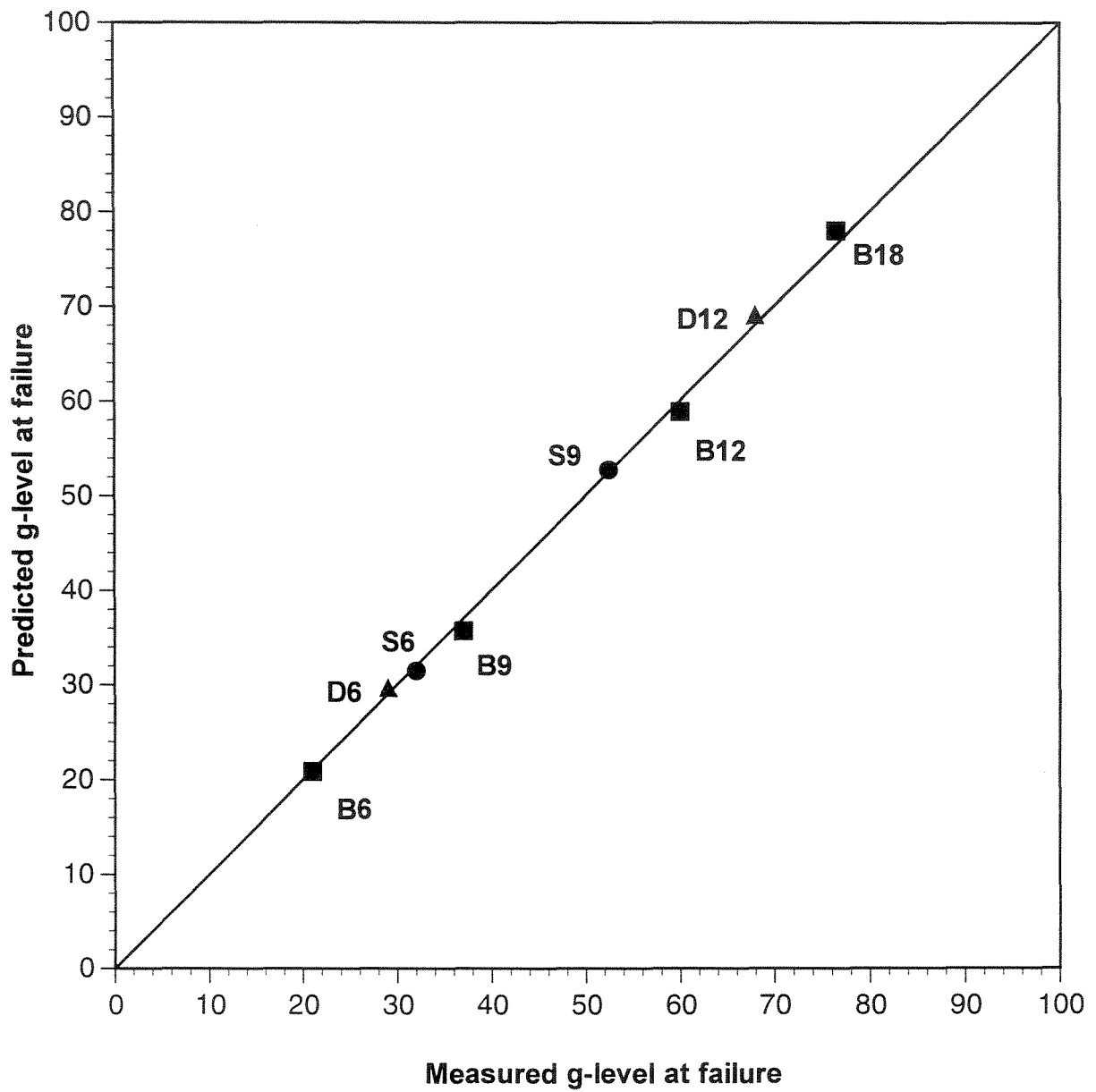
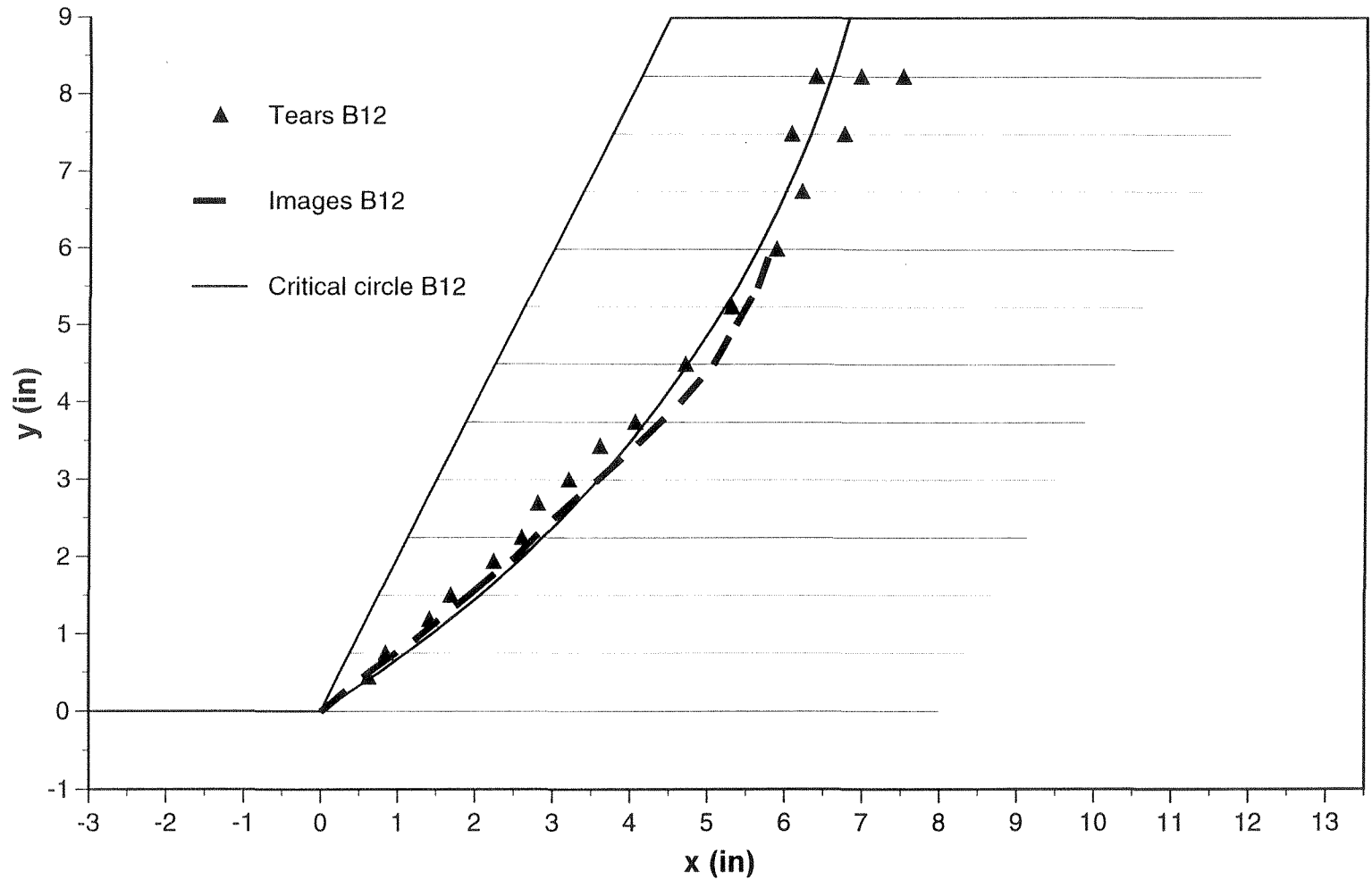


Figure 4.82 - Predicted and measured g-levels causing failure for all centrifuge models

pullout resistance is defined as the geotextile length beyond the potential failure surface. Although conventional design considers that the location of the potential failure surface can be defined from limit equilibrium analysis, experimental evidence to substantiate this design procedure is, at best, limited.

The comparison between the failure surface obtained experimentally and predicted by limit equilibrium for the case of model B18 was presented earlier in Figure 4.72. Figures 4.83 to 4.89 show the trace of the critical circular slip surfaces predicted using limit equilibrium analysis for the rest of the models from the B-series, as well as for the models from the D- and S-series. Superimposed on these figures are the location of the failure surfaces obtained experimentally from the location of the reinforcement tears, as measured from the geotextiles retrieved from the models after centrifuge testing. Moreover, the experimental location of the failure surface is also indicated as obtained from the images recorded through the plexiglass wall during testing. Overall, there is an excellent agreement between the critical circles predicted by the limit equilibrium analyses and the two different experimental sources of information.

The comparison of the experimentally obtained failure surfaces for the different models (Figures 4.61 to 4.64) indicated that all centrifuge models appeared to fail along approximately the same failure surface. This observation can be verified by the results of the limit equilibrium analyses presented in this section. Figure 4.90 shows the location of the critical circles obtained from the analyses performed at the g-levels of failure for all centrifuge models in this study. All circles define approximately the same failure surface, which is in agreement with the experimental results. As was also the case for the comparison between experimental and predicted g-levels at failure, the comparison



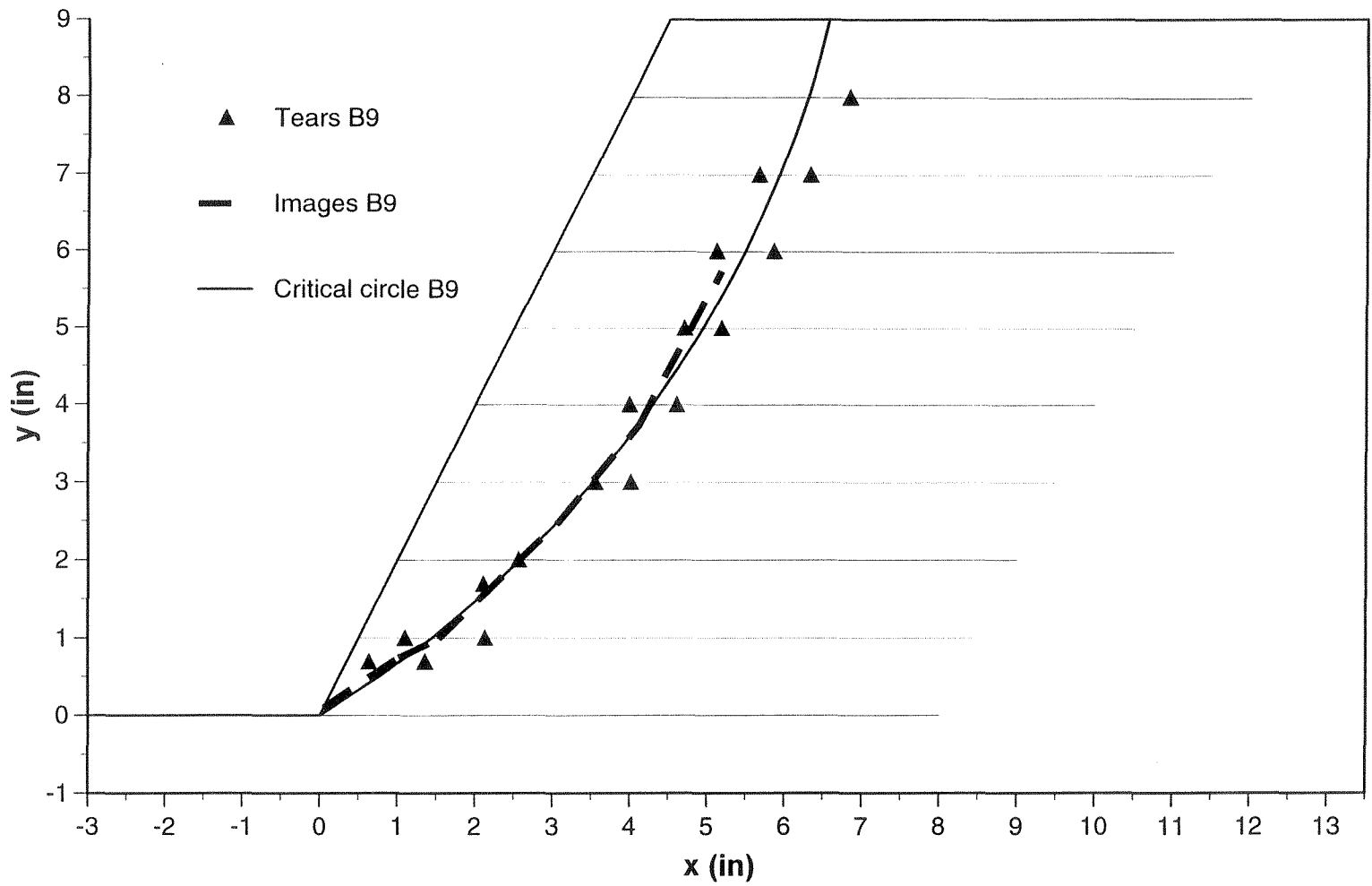


Figure 4.84 - Predicted and measured location of failure surface for model B9

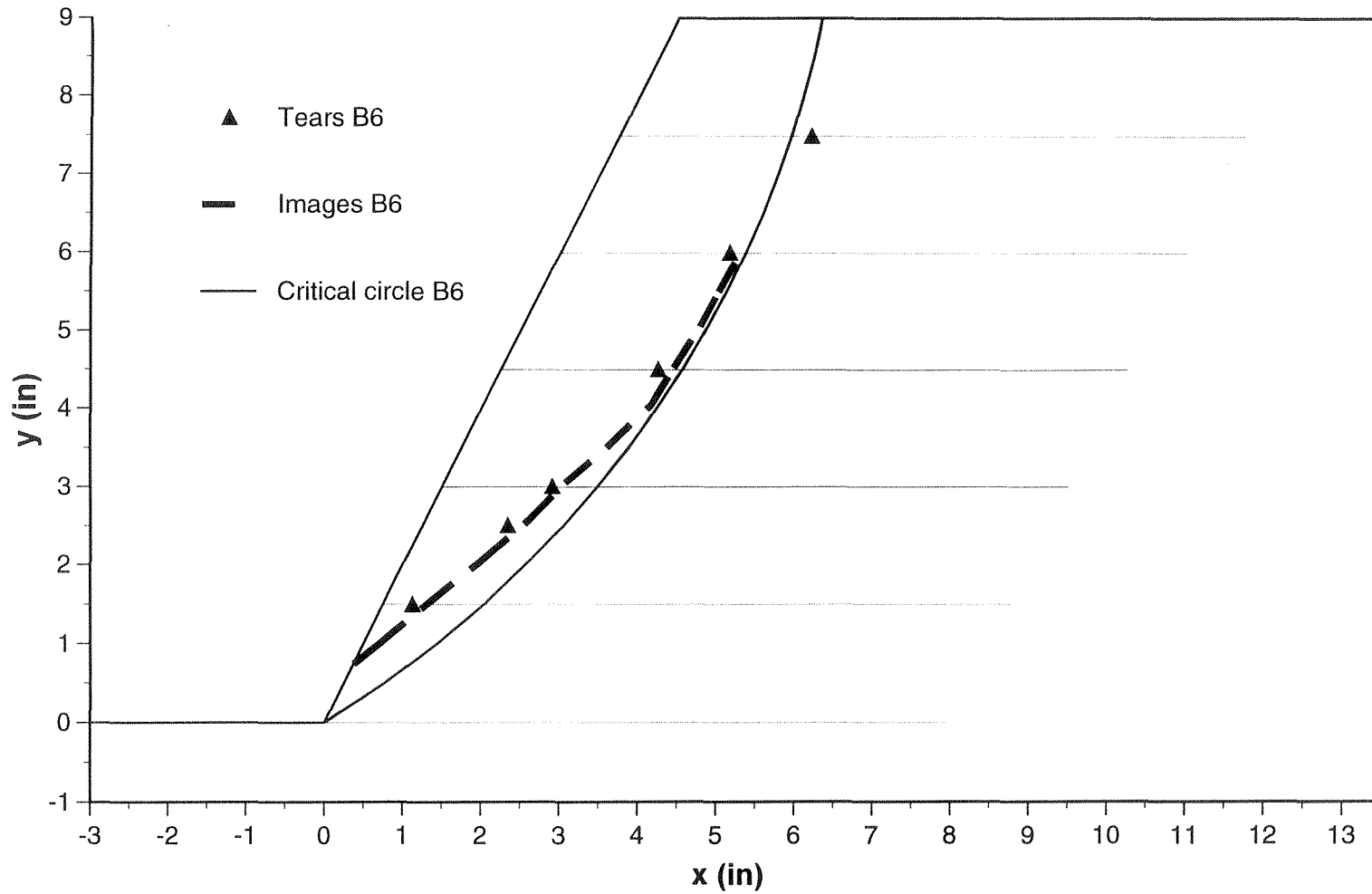


Figure 4.85 - Predicted and measured location of failure surface for model B6

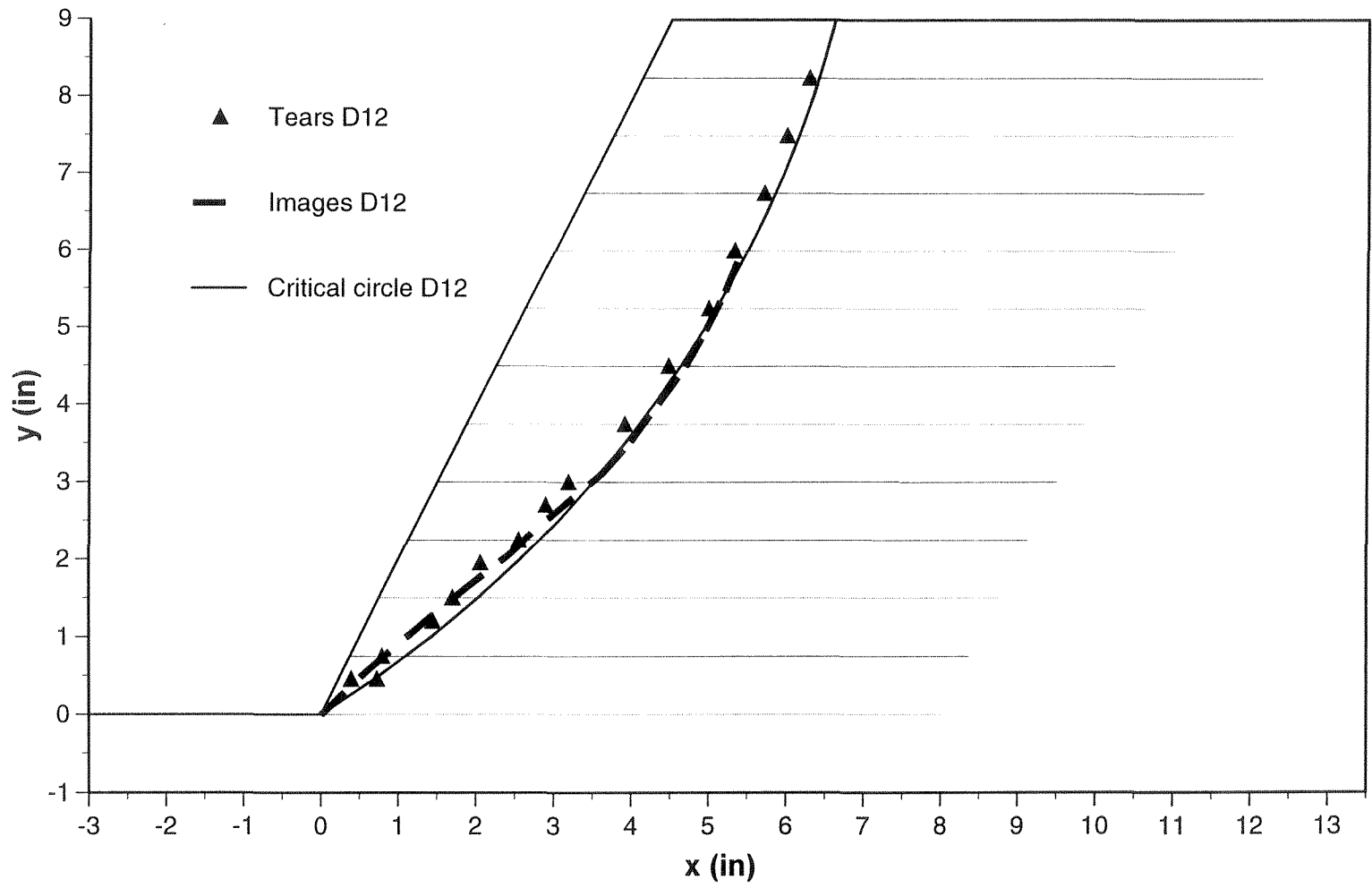


Figure 4.86 - Predicted and measured location of failure surface for model D12

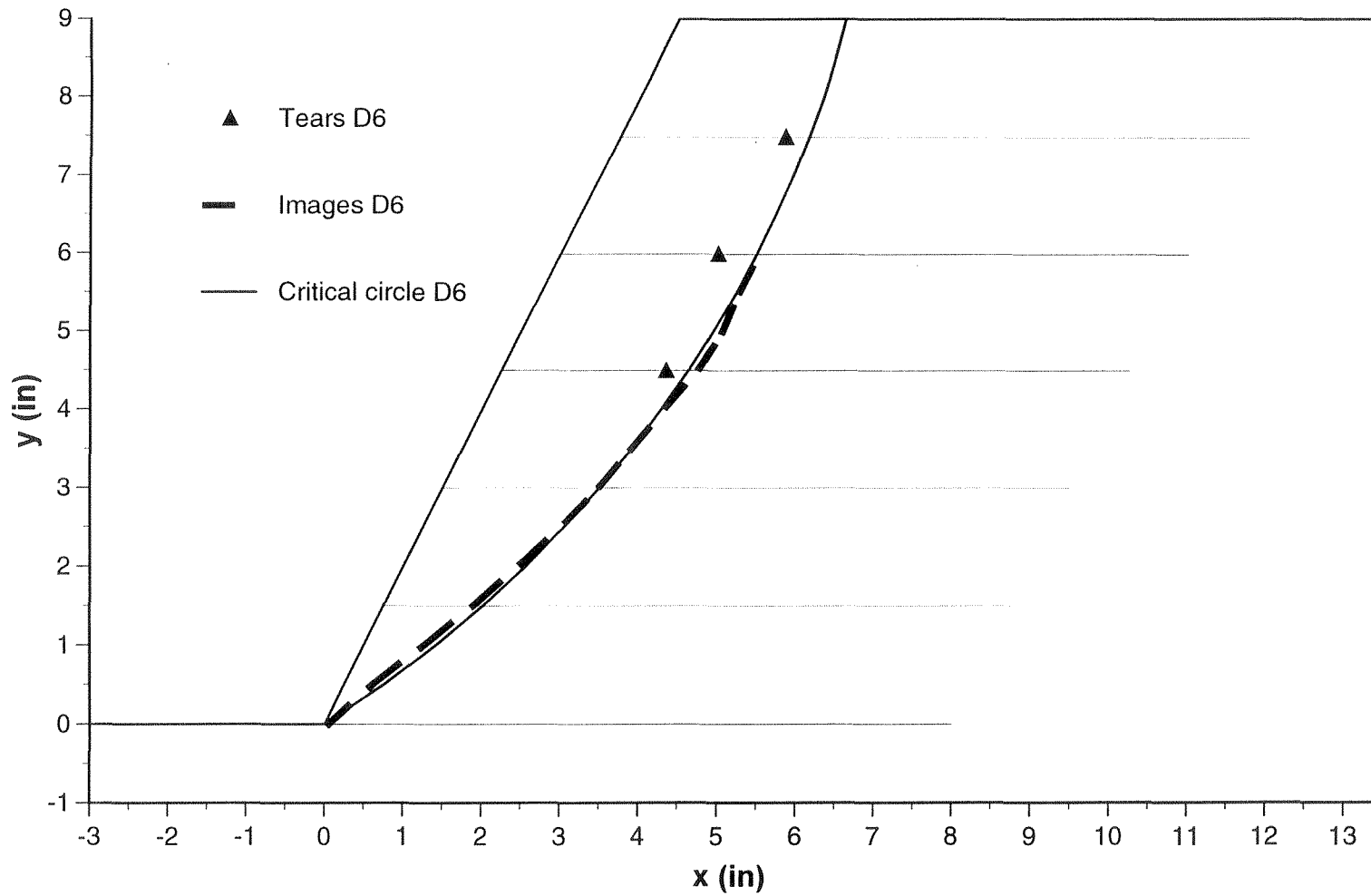


Figure 4.87 - Predicted and measured location of failure surface for model D6

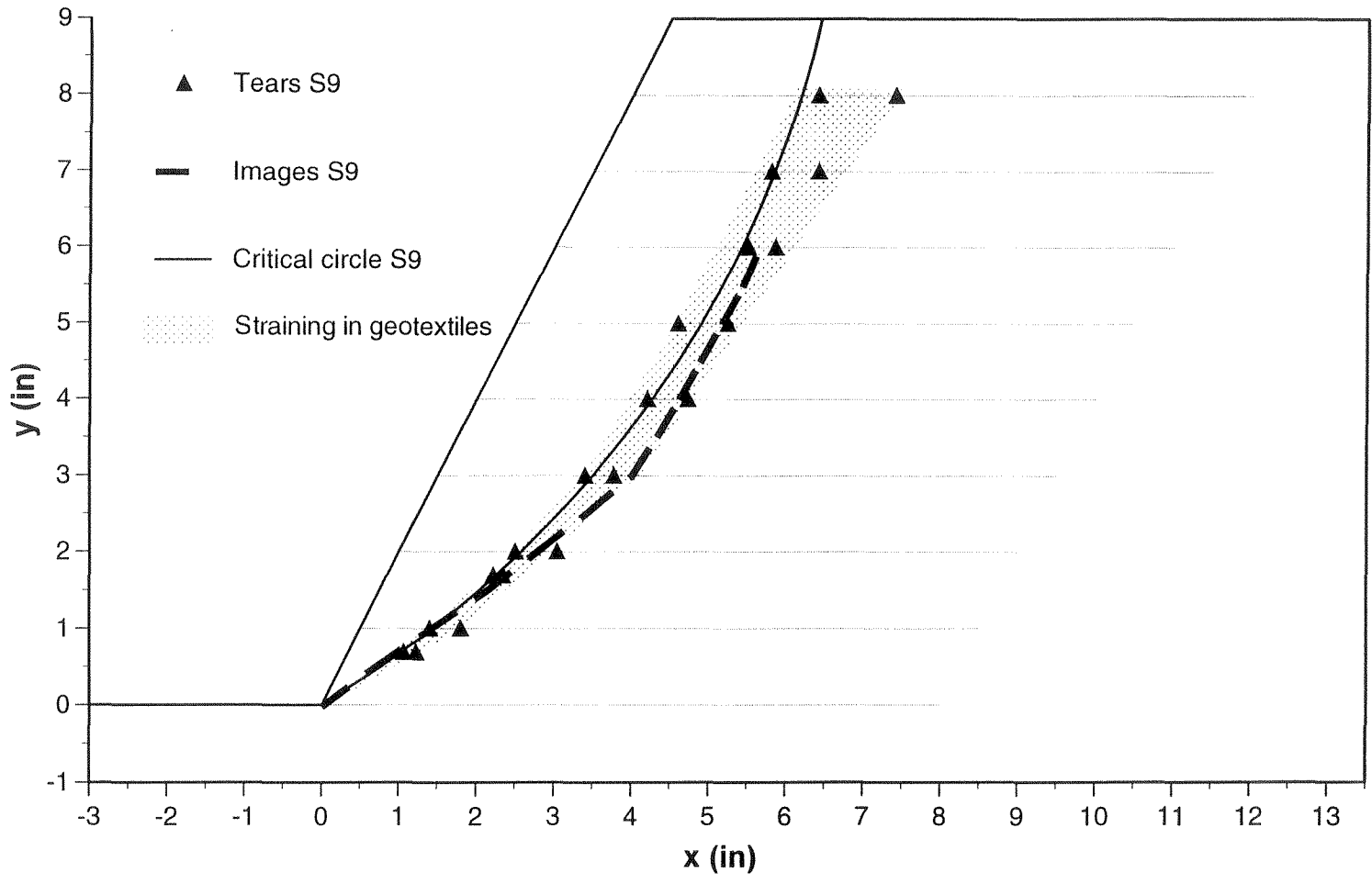


Figure 4.88 - Predicted and measured location of failure surface for model S9

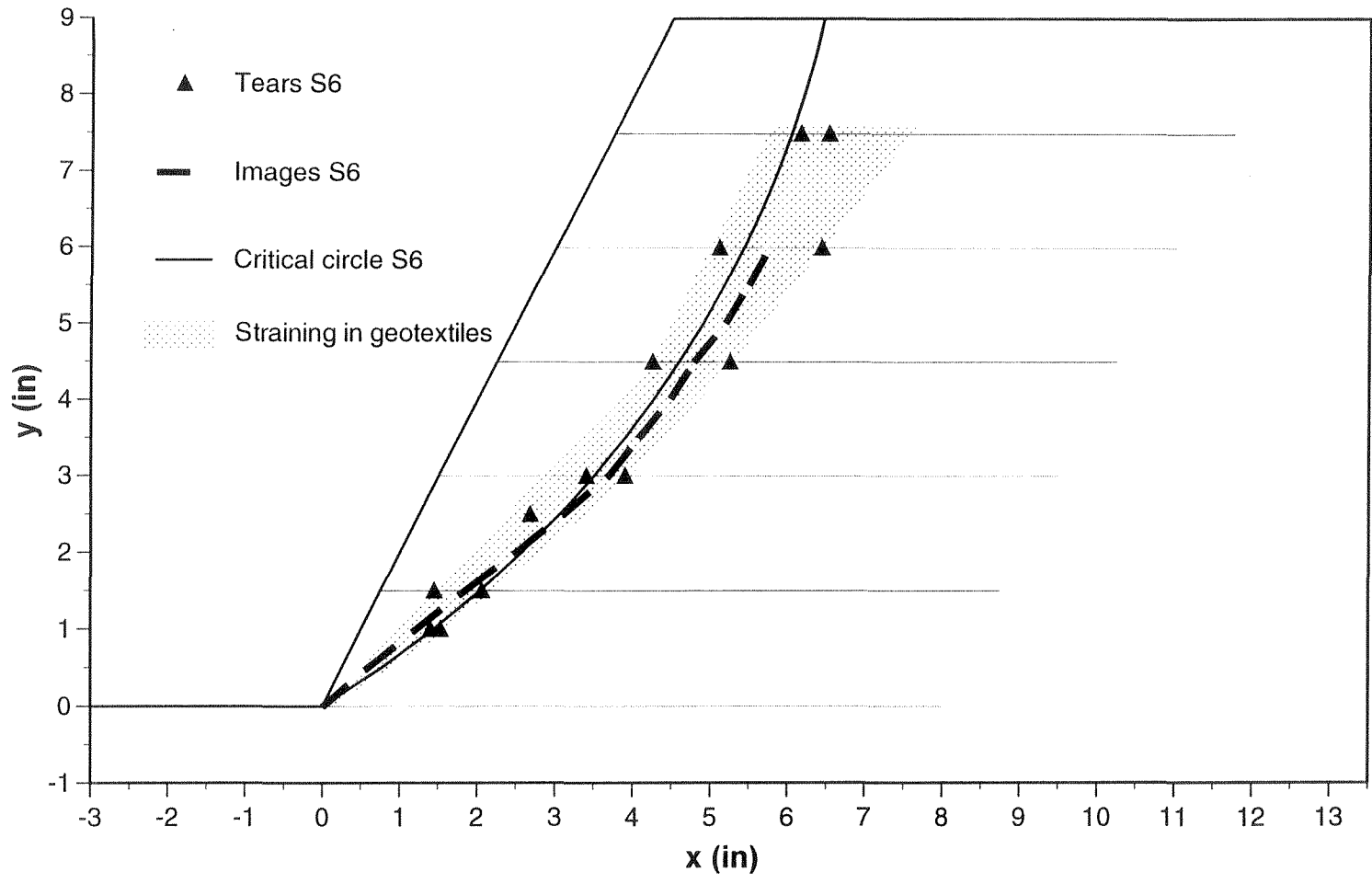


Figure 4.89 - Predicted and measured location of failure surface for model S6

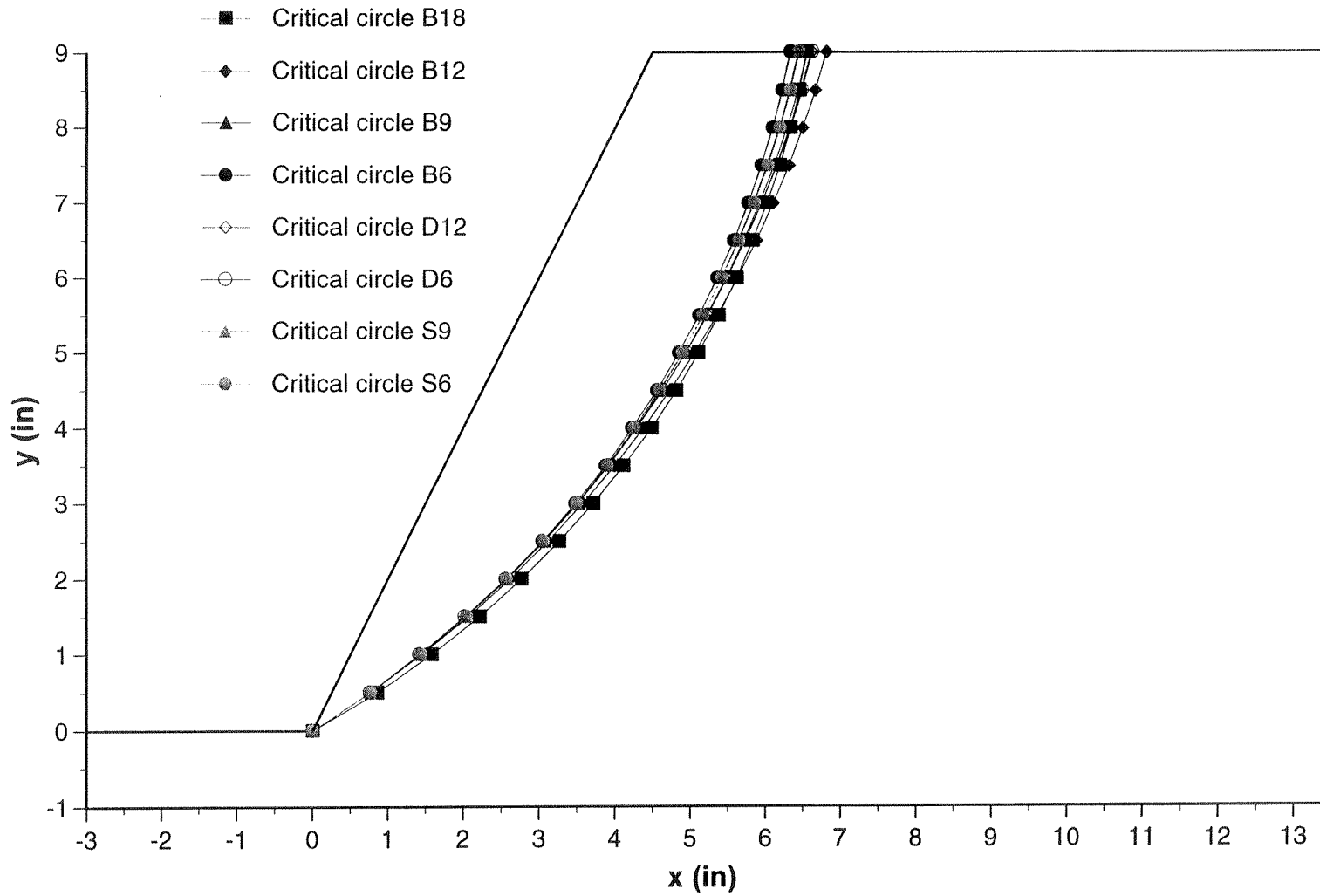


Figure 4.90 - Critical circles for all centrifuge models predicted by limit equilibrium

between predicted and experimental location of the shear surfaces is equally good for centrifuge slope models built using different reinforcement spacings, different soil densities, and geotextiles with different ultimate tensile strengths.

4.7.3.4 Evaluation of in-soil geotextile tensile strength

As previously stated, the centrifuge tests can be considered as special tests for evaluating the in-soil mechanical properties of geosynthetics, since the conditions imposed on the geotextile reinforcements duplicate the operational conditions of prototype structures. The effect of geotextile tensile strength was investigated by performing a parametric limit equilibrium study of all the centrifuge models, where the factors of safety were calculated for increasing values of geotextile strength. The analyses were performed considering a unit weight $N_f \gamma$, which is the unit weight of the sand backfill at the g-level at failure N_f obtained experimentally for each centrifuge test. Assuming a uniform distribution of reinforcement forces with depth, the in-soil geotextile strength for all models can then be estimated as the value that gives a factor of safety of one.

Figure 4.91 shows the factors of safety calculated from the analyses performed for all the centrifuge slope models. The figure shows that the results of analyses of all models built with the same type of geotextile essentially collapse onto a single curve. A unique in-soil geotextile strength can then be obtained from these results for each geotextile type. The strength values agree with those adopted for the analyses, as discussed in Section 4.7.2.1. These results confirm that the Pellon Sew-in geotextile used in the B- and D-series has an in-soil strength of approximately 0.7 lb/in (0.12 kN/m), which represents a 94% increase in relation to the strength obtained from unconfined

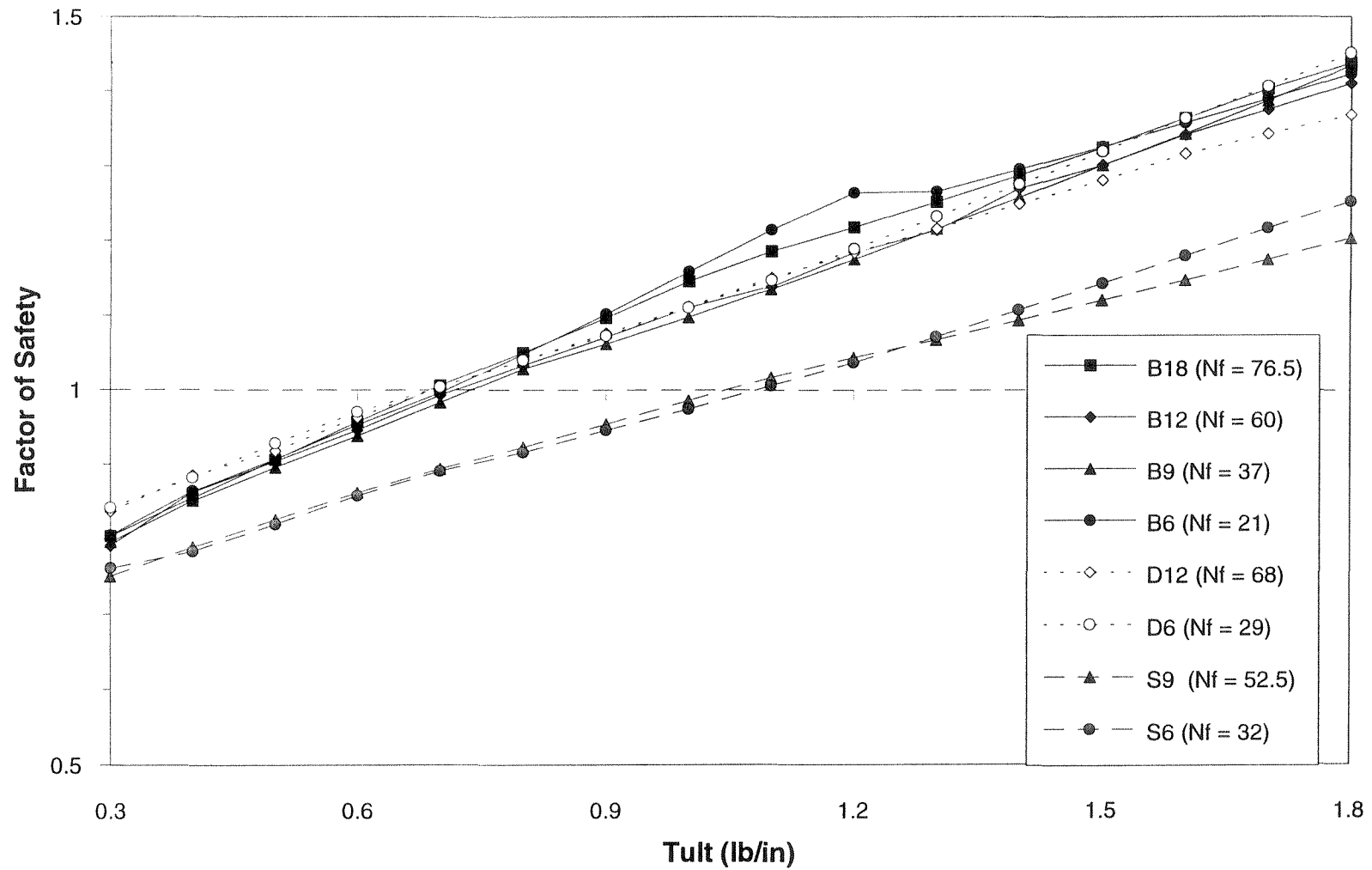


Figure 4.91 - Effect of geotextile strength on the calculated factor of safety for all centrifuge models

tensile tests. Similarly, the Pellon Tru-grid shows an in-soil strength of approximately 1.05 lb/in (0.18 kN/m), 55% higher than the unconfined strength. As previously discussed in Section 4.4.2, these values are within the expected range of in-soil strength, based on the results of a geotextile testing program that accounted for more representative testing boundary conditions.

It is worth noting that the Factor of Safety versus T_{ult} curve is very sensitive to the g-level at which the analysis is performed, as can be observed in Figure 4.71 for analyses performed at different g-levels for the same model (model B18). In Figure 4.91, however, the calculations for the different models were performed at the different g-levels that correspond to the g-level at failure N_f for each model. The sensitivity of the results to the selected g-level emphasizes the significance that the values calculated for different g-levels at failure N_f collapse into a single curve.

The results shown in Figure 4.91 indicate no evidence of changes in the in-soil geotextile strength for models failing at significantly different accelerations. This observation suggests that the strength improvement of the geotextiles when embedded in soil appears not to be sensitive to the confining pressure, at least for the range of pressures for the models in this study. This evidence supports the hypothesis presented in Section 4.4.2 that the improvement of mechanical properties of geotextiles embedded in soil is not only caused by the increase in confining stresses but, even more importantly, by the prevention of lateral geotextile deformations.

4.7.4 Remarks on the suitability of limit equilibrium for the analysis of reinforced soil slopes

Although limit equilibrium methods are commonly used for the design of geotextile-reinforced soil slopes, the predictive potential of this analysis had not yet been extensively assessed. This is mainly because there are rarely fully documented failures due to internal collapse of these structures. Current approaches to deal with this shortage of validations has been translated into conservative designs in terms of selection of material properties and factors of safety. Issues have also been raised in relation to the inability of limit equilibrium methods to deal directly with displacements and the potential incompatibility of displacements between the soil and the reinforcements. As a result, alternative analysis methodologies had been proposed in order to account for these apparent limitations of the limit equilibrium approach (e.g., Gourc et al., 1986; Beech, 1987; Juran et al., 1990).

As indicated by the good agreement between centrifuge results and analytic predictions in this study, strong evidence has been put forth that limit equilibrium is capable of accurately predicting the failure of geotextile-reinforced soil slopes. Although the analyses in this study have been performed considering a specific shape of the failure surface (circular), and a specific method (Spencer's), other rigorous limit equilibrium methods have been proposed for the analysis of geosynthetically reinforced soil slopes (e.g., Jewell et al., 1984; Schmertmann et. al., 1987; Leshchinsky and Boedeker, 1989; Jewell, 1991). In order to further evaluate the predictive capabilities of limit equilibrium methods, the centrifuge experimental results are compared to predictions based on methods proposed by Leshchinsky and Boedeker (1989) and Jewell (1991). These

methods, which respectively assume logarithmic spiral and bilinear failure surfaces, were selected since design charts have been published for the range of structure geometries and soil parameters suitable for the analysis of the model slopes. Although by using design charts the accuracy of the calculations may be sacrificed and several modeling details may not be accounted for, their use would provide additional evidence of the suitability of limit equilibrium for the analysis of reinforced soil slopes.

The different proposed design charts for reinforced soil slopes have similar characteristics: the desired overall soil factor of safety is accounted for by using a factored friction angle which, together with the angle of the slope, gives the required summation of reinforcement forces. Validation of the experimental centrifuge results can be done using the design charts in the reverse order: for a given summation of reinforcement forces the mobilized friction angle can be estimated. For the failure situation obtained experimentally, the mobilized friction angle obtained from the design charts should equal the peak strength of the soil, which would imply a predicted factor of safety of unity. Leshchinsky and Boedeker (1989) and Jewell (1991) consider a triangular distribution of the reinforcement forces, which is not in agreement with the limit equilibrium analyses performed in this study. Nevertheless, their design charts can also be used for the case of uniform reinforcement forces.

The summation of reinforcement forces at the moment of failure obtained from the centrifuge tests was discussed in Section 4.6.1, where it was shown that the reinforcement forces could be expressed in the form of a nondimensional Reinforcement Tension Summation (or earth pressure coefficient) K . For centrifuge models built using

Monterey sand at 75% relative density (D-series), the normalized Reinforcement Tension Summation (RTS) at the moment of failure was:

$$K_D = 0.062$$

Similarly, the normalized RTS for all the models built using Monterey sand at 55% relative density (B- and S-series) was:

$$K_B = K_S = 0.084$$

It is worth remembering that these coefficients incorporate the effect of the number of overlapping layers intersected by the failure surfaces.

Leshchinsky and Boedeker (1989) used a logarithmic spiral failure mechanism to obtain the minimum factor of safety for reinforced slopes, while satisfying all three global limiting equilibrium equations. They assumed that on the verge of failure the distribution of mobilized tensile resistance is linear with depth, proportional to the overburden pressure. Figure 4.92 shows the design chart for the required tensile force in the reinforcements. For the case of uniform distribution of reinforcement forces with depth, the nondimensional mobilized equivalent tensile resistance T_m in the chart equals the normalized RTS K obtained in Section 4.6.1. Using the two normalized RTS values obtained from the centrifuge tests, the mobilized friction angles ϕ_m for 1H:2V slope ($m=2$ in the chart) are:

$\phi_m \approx 39^\circ$ for the case of centrifuge models built with sand at 55% relative density; and

$\phi_m \approx 42^\circ$ for the case of centrifuge models built with sand at 75% relative density.

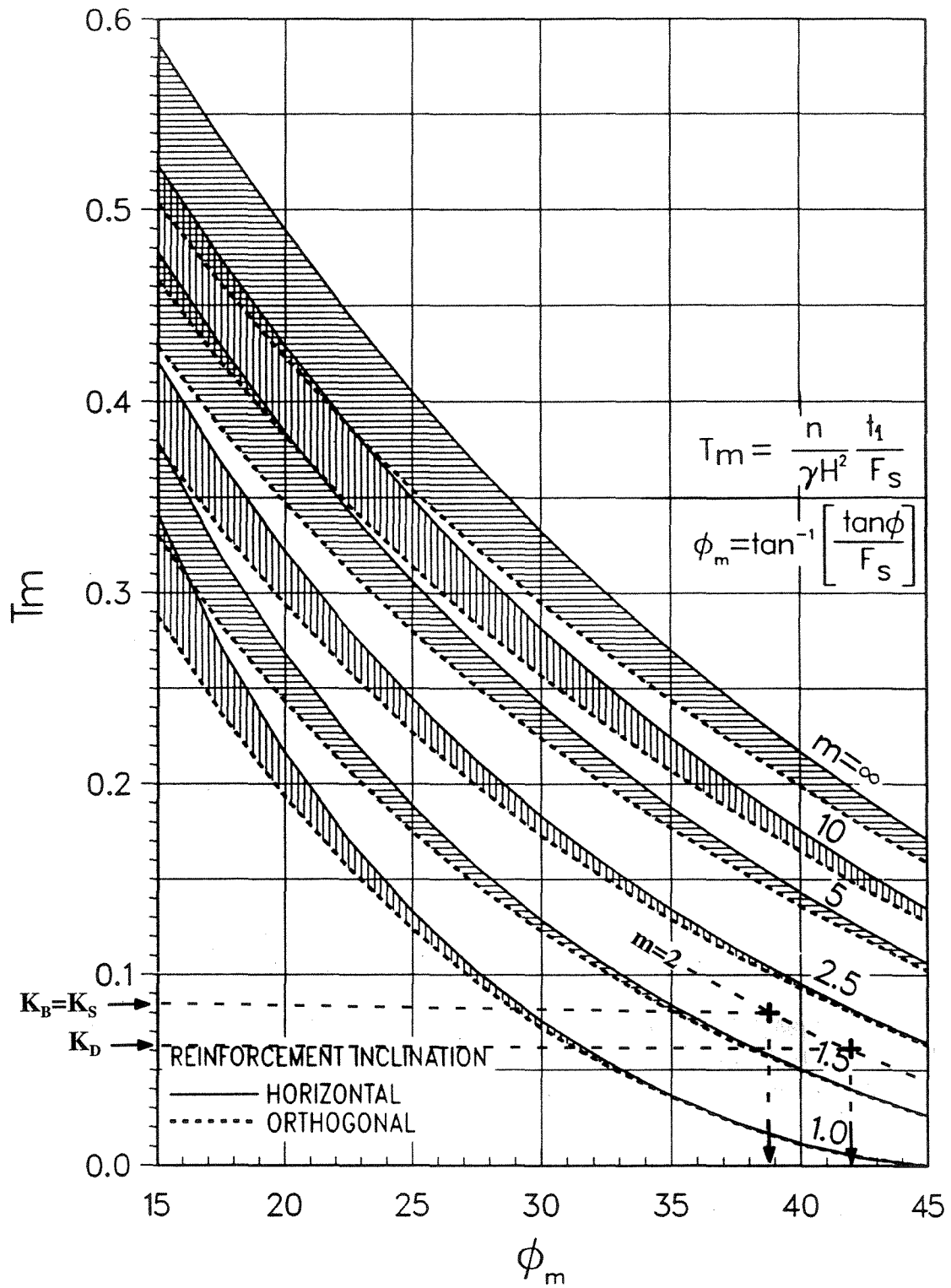


Figure 4.92 - Design chart for reinforced soil slopes (from Leshchinsky and Boedeker, 1989)

These predicted mobilized friction angles are in good agreement with the peak plane strain friction angles for Monterey sand at the relative densities used in the centrifuge models ($\phi_{ps}=39.5^\circ$ and $\phi_{ps}=42.5^\circ$). Consequently, the predicted factors of safety are approximately 1.00 which is in good agreement with the experimental results.

Jewell (1991) presented an approach for the design of geosynthetically reinforced slopes using a two-part wedge analysis. This approach is considered a "full" analysis, since it does not require assumptions to be made for its solution. The reinforcement force distribution is assumed proportional with depth, and the total required reinforcement tensile forces can be estimated from the design chart presented in Figure 4.93. The coefficient K_{req} in the design chart is equivalent to the normalized RTS value K discussed in Section 4.6.1, the parameter ϕ_d is the design friction angle of the backfill soil, and β is the angle of the reinforced slope. Using the two normalized RTS values obtained from the centrifuge tests, the design friction angles ϕ_d obtained for a slope angle $\beta=63.4^\circ$ (1H:2V) are:

$\phi_d \approx 39^\circ$ for the case of centrifuge models built with sand at 55% relative density; and

$\phi_d \approx 42.5^\circ$ for the case of centrifuge models built with sand at 75% relative density.

The predicted design friction angles agree very well with the peak plane strain friction angles for the Monterey sand at the relative densities used in the models. Consequently,

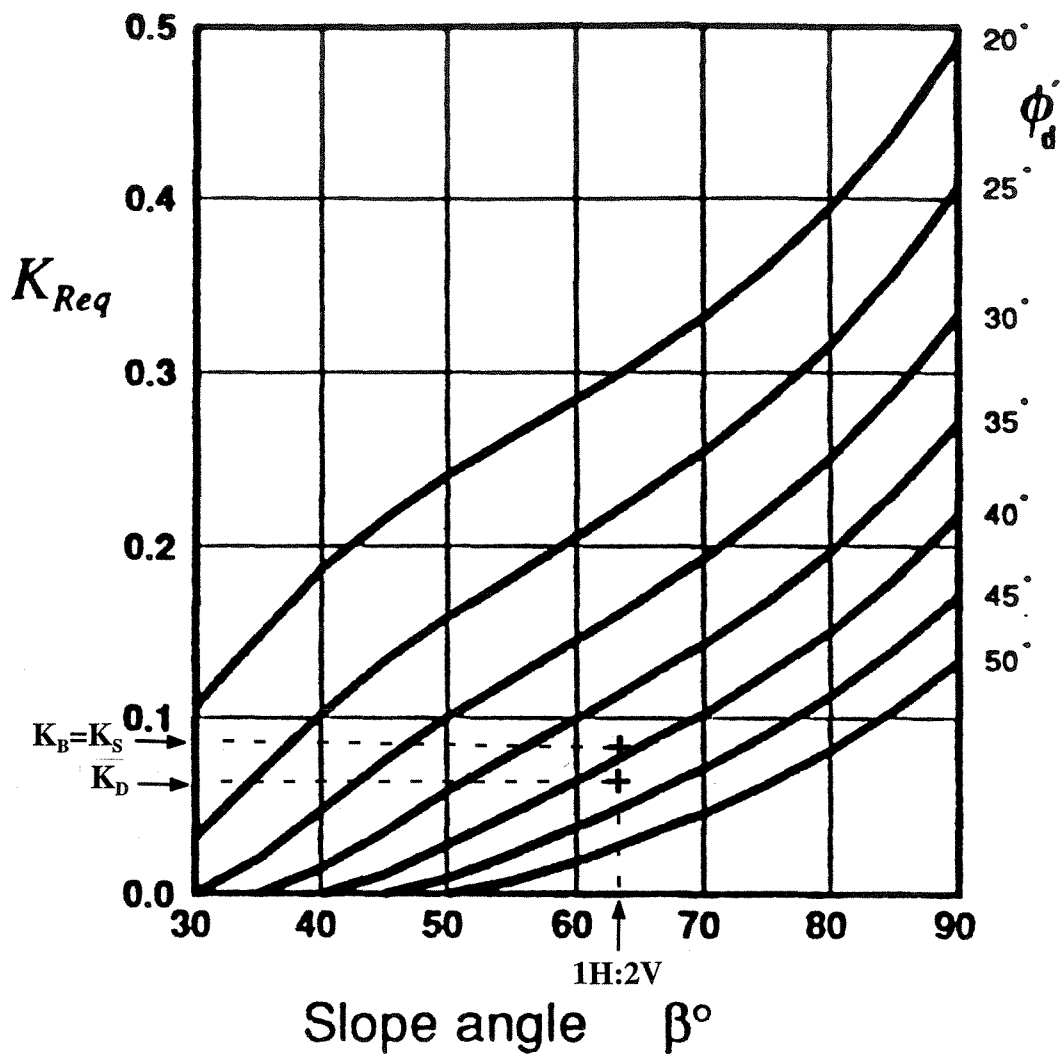


Figure 4.93 - Design chart for reinforced soil slopes (from Jewell, 1991)

Jewell's limit equilibrium design methodology also shows good agreement with the experimental results.

The good comparisons obtained between the experimental centrifuge data and predictions using different limit equilibrium methodologies, suggest that confidence can be placed on the ability of limit equilibrium methods to analyze the stability of geotextile-reinforced slopes. Although equilibrium methods of slope stability analysis had been used in the design of earth structures for about 70 years, their extension to the design of reinforced soil structures still required hard-to-get experimental validation. The centrifuge modeling performed as part of this study provided such validation. It is worth noting, however, that this study focused only on internal failure due to the breakage of the reinforcements and this constitutes only one of the criteria to be satisfied in the design of geotextile-reinforced slopes. Moreover, this study concentrated specifically on the performance of slopes reinforced using geotextile reinforcements. Consequently, although it would be appropriate to extend the validity of the conclusions to slopes reinforced with other extensible reinforcements, these conclusions should not be extrapolated to the case of slopes reinforced using inextensible inclusions without careful consideration.

4.8 Conclusions

Using the centrifuge modeling technique, a series of geotextile-reinforced soil slopes was tested in order to identify the possible failure mechanisms and to verify the ability of limit equilibrium methods to predict the experimental results. The variables considered in the centrifuge study were reinforcement spacing, reinforcement tensile strength, and soil strength, which can all be taken into account using conventional limit

equilibrium analyses. An extensive testing program was also performed in order to evaluate the strength properties of the sand used as backfill material, of the geotextile reinforcements, and of several interfaces that could influence the performance of the slope models. The geotextile tensile strength was found to depend on the testing boundary conditions, which should be selected to properly represent the in-soil operational conditions. All models were built with the same slope angle (1H:2V) using controlled construction procedures. Detailed description was given concerning the building, testing and monitoring of the centrifuge slope models.

Consistency of the centrifuge results was evidenced by the fact that all the 1H:2V centrifuge slope models built using the same backfill soil yielded a single normalized Reinforcement Tension Summation. This normalized value can be equally interpreted as an earth pressure coefficient that only depends on the soil strength and on the slope inclination. Failure of all centrifuge slope models was observed to initiate at midheight of the slopes, contradicting current design assumptions that failure should develop from the toe of the reinforced slopes. Consequently, a reinforcement force distribution with depth is proposed for reinforced soil slopes under working stresses, which is consistent with the experimental observations and which leads to an approximately uniform distribution with depth at the moment of failure. Important contribution to the stability of the models was provided by the overlapping geotextile layers, which failed by breakage instead of by pullout when intersected by the failure surfaces. Moreover, the stability of the reinforced slopes was found to be governed by the peak shear strength and not by the critical state friction angle of the backfill soil.

The suitability of limit equilibrium methods for the analysis of geotextile-reinforced slopes was evaluated by comparing the centrifuge test results with theoretical predictions. A rigorous limit equilibrium method that assumes circular failure surfaces was selected for the study. The effect of different modeling assumptions on the calculated factors of safety was initially investigated by performing a parametric study of variables relevant to the stability of the models. These studies included the effect of the in-soil geotextile tensile strength, the nonuniformity of the unit weight within the centrifuge model, the orientation of reinforcement forces, the geotextile overlapping layers, the lateral friction against walls of the centrifuge box, and the selected method of slope stability analysis. A very good agreement was obtained between the limit equilibrium predictions and the experimental results. The good agreement included both the g-level at failure and the location of the failure surfaces in the centrifuge models. Different rigorous limit equilibrium methodologies currently used for the analysis of reinforced soil slopes were also found to provide equally good results. Moreover, the centrifuge testing of reinforced slope models provided insight into the evaluation of in-soil strength properties of geotextiles.

The results have shown that centrifuge model testing is a useful tool to investigate the stability of earth structures particularly in the absence of prototype failure records. Not only does this approach provide qualitative information on prototype behavior, it also allows evaluation of the adequacy of the design methodologies. In this particular study, centrifuge testing provided much needed evidence that limit equilibrium methodologies adequately predict the performance of geotextile-reinforced soil structures at failure.

References

- Adib, M. E. (1988). *Internal lateral earth pressure in earth walls*, Thesis submitted in partial satisfaction of the requirements for the degree of Doctor of Philosophy. Department of Civil Engineering, University of California, Berkeley, California.
- American Society for Testing and Materials, *Standard test method for tensile properties of geotextiles by the wide-width strip method*. In Annual Book of ASTM Standards, Vol. 04.08, ASTM D-4595-86, 1988, . 770-780.
- Avgherinos, P. and A. Schofield. (1969). "Drawdown failures of centrifuged models." *Proc., Seventh International Conference on Soil Mechanics and Foundation Engineering*. Mexico, 497-505.
- Bangratz, J.L. and Gigan, J.P. (1984), "Methode rapide de calcul des massifs cloues," *Proc. Int. Conf. Insitu Soil and Rock Reinforcement*, Paris, 293-299.
- Beech, J.F. (1987). "The importance of stress-strain relationships in reinforced soil system design." *Proc., Geosynthetics Conference '87, I*, New Orleans, 133-145.
- Bishop, A.W. (1955) "The use of the slip circle in stability analysis of slopes," *Géotechnique* 5, No.1, 7-17.
- Blivet, J. C., P. Jouve and R. Maillot. (1986). "Numerical modelization of earth reinforcement by geotextile: hydraulic function." *Proc., Third International Conference on Geotextiles*. Vienna, 249-253.
- Bolton, M. (1986). "The strength and dilatancy of sands." *Géotechnique* 36(1), 65-78.
- Bolton, M., S. Choudhury and P. Pang. (1978). "Reinforced earth walls: a centrifugal model study." *Proc., Symposium on Earth Reinforcement, ASCE*. Pittsburgh, 252-281.

- Bolton, M. and P. Pang. (1982). "Collapse limit states of reinforced earth retaining walls." *Géotechnique* 32(4), 349-367.
- Bolton, M. and J. Sharma. (1994). "Embankments with base reinforcement on soft clay." *Proc., Centrifuge 94*. Singapore, September, 587-592.
- Bonaparte, R. and G. R. Schmertmann. (1987). "Reinforcement extensibility in reinforced soil wall design." *The application of polymeric reinforcement in soil retaining structures*, P. M. Jarrett and A. McGown, eds., Nato Advanced Research Workshop. Royal Military College of Canada, Ontario, 409-457.
- Boyle, S. and R. Holtz. (1994). "Deformation characteristics of geosynthetic-reinforced soil." *Proc., Fifth International Conference on Geotextiles, Geomembranes and Related Products*. Singapore, 361-364.
- Casey, J., D. Soon, B. Kutter and K. Romstad. (1991). "Modeling of mechanically stabilized earth systems: a seismic centrifuge study." *Geotechnical Engineering Congress*, Geotechnical Special Publication No.27, ASCE, vol. 2, 839-850.
- Christopher, B.R. and Holtz, R.D. (1985). *Geotextiles Engineering Manual*, National Highway Institute, FHWA, Washington, D.C.
- Christopher, B., C. Bonczkiewicz and R. Holtz. (1992). "Design, construction and monitoring of full scale test of reinforced soil walls and slopes." *Recent case histories of permanent geosynthetic-reinforced soil retaining walls*, F. Tatsuoka and D. Leshchinsky, eds. Tokyo, Japan: A.A. Balkema, 45-60.
- Christopher, B. R., S. A. Gill, J. P. Giroud, I. Juran, J. Mitchell, F. Schiosser and J. Dunicliff. (1990). *Design and construction guidelines for reinforced soil*

structures - Volume I, Report No. FHWA-RD-89-043. Federal Highway Administration, U.S. Department of Transportation.

- Christopher, B., R. Holtz and D. Bell. (1986). "New tests for determining the in-soil stress-strain properties of geotextiles." *Proc., Third International Conference on Geotextiles*. Vienna, 683-688.
- Cornforth, D.H. (1964). "Some experiments on the influence of strain conditions on the strength of sand," *Géotechnique*, Vol.14, No.2, pp.143-167.
- Correia, R.M. (1988) "A limit equilibrium method for slope stability analysis," *Proc., 5th Int. Symp. Landslides*, Lausanne, 595-598.
- Craig, W., R. Sapak and K. Brady. (1991). "Model studies of an anchored earth structure." *Proc., International Conference on Centrifuge*, Hon-Yim Ko and Mclean Francis, eds. Colorado, 303-311.
- Duncan, J. M. (1992). "State-of-the-Art: Static stability and deformation analysis." *Stability and Performance of Slopes and Embankments II*, Geotechnical Special Publication No.31, ASCE. Berkeley, California, June, 222-266.
- Duncan, J. and S. Wright. (1980). "The accuracy of equilibrium methods of slope stability analysis." *Engineering Geology* 16(1), 5-17.
- Espinoza, R., P. Repetto and B. Muhunthan. (1992). "General framework for stability analysis of slopes." *Géotechnique* 42(4), 603-615.
- Fellenius, W. (1936), "Calculation of the stability of earth dams," *Proc. 2nd. Congr. Large Dams*, Washington D.C., Vol.4, .445-462.
- Frydman, S., R. Baker and A. Levy. (1994). "Modelling the soil nailing - Excavation process." *Proc., Centrifuge 94*. Singapore, September, 669-674.

- Gomes, R., E. Palmeira and D. Vidal. (1994). "Soil reinforcement interaction by in-soil tensile tests and direct shear tests." *Proc., Fifth International Conference on Geotextiles, Geomembranes and Related Products*. Singapore, 395-400.
- Goodings, D. J. (1990). "Research on geosynthetics in reinforced cohesive soil retaining walls at the University of Maryland." *Geotechnical News* (June), 23-25.
- Goodings, D. J. and J. C. Santamarina. (1989). "Reinforced earth and adjacent soils: Centrifuge modeling study," Technical Note. *Journal of Geotechnical Engineering, ASCE* 115(7), June, 496-501.
- Güler, E. and D. G. Goodings. (1992). "Centrifuge models of Clay-Lime reinforced soil walls." *Grouting, Soil Improvement and Geosynthetics*, Borden R.H., R. Holtz and I. Juran, eds., Geotechnical Special Publication No.30, ASCE, vol. 2. New Orleans, 1249-1260.
- Hird, C. C., I. C. Pyrah and D. Russell. (1990). "Finite element analysis of the collapse of reinforced embankments on soft ground." *Géotechnique* 40(4), 633-640.
- Holtz, R. and B. Broms. (1977). "Walls reinforced by fabrics - Results of model tests." *Proc., International Conference on the Use of Fabrics in Geotechnics*. Paris, 113-117.
- Ingold, T.S. (1982). "An analytical study of geotextiles reinforced embankments." *Proc., 2nd Int. Conf. on Geotextiles*, Las Vegas, Vol.3, .683-688.
- Jaber, M. B. (1989). *Behavior of reinforced soil walls in centrifuge model tests*, Thesis submitted in partial satisfaction of the requirements for the degree of Doctor of Philosophy. Department of Civil Engineering, University of California, Berkeley, California.

- Jaber, M. and J. Mitchell. (1990). "Behaviour of reinforced soil walls at limit state." *Performance of Reinforced Soil Structures*, A. McGown, K. Yeo and K. Z. Andrawes, eds. London: Thomas Telford Ltd., 53-57.
- Jaber, M., J. K. Mitchell, B. R. Christopher and B. L. Kutter. (1990). "Large centrifuge modelling of full scale reinforced soil walls." *Design and performance of earth retaining structures*, Geotechnical Special Publication No.25, ASCE, 379-393.
- Janbu, N. (1954) "Applications of composite slip surface for stability analysis," *Proc., European conference on stability of earth slopes*, Stockholm, 3, 43-49.
- Jewell, R. (1990). "Strength and deformation in reinforced soil design." *Proc., Fourth International Conference on Geotextiles, Geomembranes and Related Products*. The Hague, Netherlands, 913-946.
- Jewell, R. A. (1991). "Application of revised design charts for steep reinforced slopes." *Geotextiles and Geomembranes* 10, 203-233.
- Juran, I. and B. R. Christopher. (1989). "Laboratory model study on geosynthetic reinforced soil retaining walls." *Journal of the Geotechnical Engineering Division, ASCE* 115(7), 905-926.
- Jewell, R.A., Paine, N. and Woods, R.I. (1984). "Design methods for steep reinforced embankments," *Proc. Symposium on Polymer Grid Reinforcement*, Institute of Civil Engineering, London, 18-30.
- Juran, I., H. Ider and K. Farrag. (1990). "Strain compatibility analysis for geosynthetics reinforced soil walls." *Journal of Geotechnical Engineering, ASCE* 116(2), February, 312-329.

- Juran, I. and Sclosser, F. (1978). "Theoretical analysis of failure in reinforced earth structures." *Proc. Symp. Earth Reinforcement*, ASCE Pittsburgh, pp.528-555.
- Koerner, R.M. (1994) *Designing with geosynthetics*, Third edition, Prentice hall, New Jersey
- Kulhawy, F.H., and Mayne, P.W. (1990). *Manual on estimating soil properties for foundation engineering*, Report EL-6800, Electric Power Res. Inst, Palo Alto, 306p.
- Kutter, B., J. Casey and K. Romstad. (1990). "Centrifuge modeling and field observations of dynamic behavior of reinforced soil and concrete cantilever retaining walls." *Proc., Fourth U.S. National conference on earthquake engineering*. Palm Springs, California, 663-672.
- Ladd, C., R. Foott, K. Ishihara, F. Schlosser and H. Poulos. (1977). "Stress-deformation and strength characteristics." *Proc., Ninth International Conference on Soil Mechanics and Foundation Engineering*. Tokyo, Japan, 421-494.
- Lade, P. and J. M. Duncan. (1973). "Cubical triaxial tests on cohesionless soil." *Journal of the Soil Mechanics Division Div., ASCE* 99(SM10), 793-812.
- Law, H., J. Tohda, H. Ko and T. Goddery. (1992). "Prediction of the performance of a geosynthetic-reinforced wall by centrifuge experiments." *Proc., International Symposium on Geosynthetic-Reinforced Soil Retaining Walls*, J. T. H. Wu, ed. Denver, Colorado: A.A. Balkema, August, 347-360.
- Lee, K. L., B. D. Adams and J. J. Vagneron. (1973). "Reinforced earth retaining walls." *ASCE Journal of the Soil Mechanics Division* 99(SM10), 745-764.

- Leflaive, E., J. Paute and M. Segouin. (1982). "Strength properties measurement for practical applications." *Proc., Second International Conference on Geotextiles*. Las Vegas, 733-738.
- Leshchinsky, D. and R. H. Boedeker. (1989). "Geosynthetic reinforced soil structures." *Journal of Geotechnical Engineering, ASCE* 115(10), 1459-1478.
- Leshchinsky, D. and E. Perry. (1987). "A design procedure for geotextile-reinforced walls." *Geotechnical Fabrics Report* 5(4), August, 21-27.
- Leschchinsky, D. and Reinschmidt, A.J. (1985). "Stability of membrane reinforced slopes," *Journal of Geotechnical Engineering, ASCE*, Vol.3, No.11, 1285-1300.
- Leschchinsky, D. and J. Volk. (1986). "Predictive equation for the stability of geotextile reinforced earth structure." *Proc., Third International Conference on Geotextiles*. Vienna, 383-388.
- Liang, R.K., Tse, E.C., Kuhn, M.R. and Mitchell, J.K. (1984). "Evaluation of a constitutive model for soft clay using the centrifuge." *Proc., Symposium on Recent Advances in Geotechnical Centrifuge Modeling*, University of California at Davis, 55-70.
- Ling, H. I., J. T. H. Wu and F. Tatsuoka. (1992). "Short-term strength and deformation characteristics of geotextiles under typical operational conditions." *Geotextiles and Geomembranes* Vol.11(2), 185-219.
- Liu, L., M. Wang and E. Ding. (1991). "Centrifugal tests of mechanism of geotextile-reinforced soft foundation under breakwater." *Proc., Centrifuge 91*. Boulder, 319-324.

- Lowe, J. and Karafiath, L. (1960) "Stability of earth dams upon drawdown," *Proc. 1st Panamerican Conference of Soil Mechanics*, Mexico City, 2, 537-552.
- Marachi, N., J. Duncan, C. Chan and H. Seed. (1981). "Plane-strain testing of sand." *Laboratory shear strength of soil, ASSTM STP 740*, 294-302.
- Matichard, Y., E. Balzer, P. Delmas, D. Fargeix, B. Thamm and A. Sere. (1992). "Behaviour of a geotextile reinforced soil abutment - Full scale and centrifuge models." *Proc., Earth Reinforcement Practice*, H. Ochiai, S. Hayashi and J. Otani, eds. Fukuoka, Japan: A. A. Balkema, 379-384.
- Matichard, Y., C. Blivet, J. Garnier and P. Delmas. (1988). "Etude en grandes déformations d'ouvrages de soutènement renforcés par géotextile." *Proc., International Conference on Geotechnical Centrifuge Modelling*, Jean Francois Corte, ed. Paris, 273-281.
- Matichard, Y., B. Thamm and A. Sere. (1992). "Behaviour of a geotextile reinforced earthwork under surface loading." *Recent case histories of permanent geosynthetic-reinforced soil retaining walls*, F. Tatsuoka and D. Leshchinsky, eds. Tokyo, Japan: A.A. Balkema, 117-130.
- McGown, A., K. Z. Andrawes and M. H. Kabir. (1982). "Load-extension testing of geotextiles confined in soil." *Proc., Second International Conference on Geotextiles*. Las Vegas, 793-798.
- Mitchell, J. K. and B. R. Christopher. (1990). "North American Practice in Reinforced Soil Systems." *Design and Performance of Earth Retaining Structures*, Geotechnical Special Publication No.25, ASCE, June, 322-346.

- Mitchell, J. K., M. Jaber, C. K. Shen and Z. K. Hua. (1988). "Behavior of reinforced soil walls in centrifuge model tests." *Proc., Centrifuge 88*. Paris, 259-271.
- Mitchell, J. K., R. B. Seed and H. B. Seed. (1990). "The Kettleman Hills waste landfill slope failure - I: Liner interface properties." *Journal of the Geotechnical Engineering Division, ASCE* 116(4), 647-668.
- Morgenstern, N.R. and Price, V.E. (1965) "The analysis of the stability of general slip surfaces," *Géotechnique* , 15, 70-93.
- Ovesen, N. (1975). "Centrifugal testing applied to bearing capacity problems of footings on sand." *Géotechnique* 25(2), 394-401.
- Phan, T.L., Segrestin, P., Schlosser, F., and Long, N.T. (1979). "Etude de la stabilité interne et externe des ouvrages en terre armée par deux méthodes de cercles de rupture." *Proc. Int. Conf. Soil Reinforcement*, Vol. 1, Paris, 119-123.
- Porbaha, A. and D. Goodings. (1994). "Geotextile reinforced cohesive slopes on weak foundations." *Proc., Centrifuge 94*. Singapore, September, 623-628.
- Ragheb, A. and A. Elgamal. (1991). "Effects of gradual reinforcement compromise on the behavior of mechanically stabilized earth walls." *Proc., International Conference on Centrifuge*, Hon-Yim Ko and Mclean Francis, eds. Colorado, 333-340.
- Resl, S. (1990). "Soil-reinforcing mechanisms of non woven geotextiles." *Proc., Fourth International Conference on Geotextiles, Geomembranes and Related Products*. The Hague, Netherlands, 93-96.
- Riemer, M.F., (1992) *The effects of testing conditions on the constitutive behavior of loose, saturated sand under monotonic loading*, Phd Dissertation, Department of Civil Engineering, University of California, Berkeley, California.

- Romstad, K.M., Al-Yassin, A., Hermann, L.R., and Shen, C.K. (1978). "Stability analysis of reinforced earth retaining structures," *Proc. Symp. Earth Reinforcement*, ASCE, Pittsburgh, 685-713.
- San, K., D. Leshchinsky and T. Matsui. (1994). "Geosynthetic reinforced slopes: Limit equilibrium and finite element analyses." *Soils and Foundations* 34(2), June, 79-85.
- Sarma, S.K. (1973) "Stability analysis of embankments and slopes," *Géotechnique* , 23, No.3, 423-433.
- Sarma, S.K. (1979) "Stability analysis of embankments and slopes," *J. Geotech. Engng. Am. Soc. Civ. engrs*, 105, GT2, 1511-1524.
- Schlosser, F. and Vidal, H. (1969). "La terre armée." *Bull. Liason du Laboratoire Central des Ponts et Chaussées*, Vol.41, 101-144.
- Schmertmann, G. R., V. E. Chouery-Curtis, R. D. Johnson and R. Bonaparte. (1987). "Design charts for geogrid-reinforced soil slopes." *Proc., Geosynthetics'87 Conference*. New Orleans, 108-120.
- Schneider, H.R. and Holtz, R.D. (1986). "Design of slopes reinforced with geotextiles and geogrids." *Geotextiles and Geomembranes*, Vol.3, No.1, 29-51.
- Schofield, A. (1980). "Cambridge Geotechnical Centrifuge Operations." *Géotechnique* 30(3), 227-268.
- Scott, R.F. and Morgan, N.R. (1977) *Feasibility and desirability of constructing a very large centrifuge for geotechnical studies*, Prepared for National Science Foundation

- Segrestin, P. (1979). "Design of reinforced earth structures assuming failure wedges." *Proc. Int. Conf. Soil Reinforcement*, Paris, Vol.1, 163-168.
- Shen, C., Y. Kim, S. Bang and J. Mitchell. (1982). "Centrifuge modeling of lateral earth support." *Journal of Geotechnical Engineering*, ASCE 108(GT9), September, 1150-1164.
- Shen, C., X. Li and S. Kim. (1984). "Microcomputer based data acquisition systems for centrifuge modeling." *Geotechnical Testing Journal* 7(4), December, 200-204.
- Shewbridge, S. and N. Sitar. (1989). "Deformation characteristics of reinforced sand in direct shear." *Journal of Geotechnical Engineering*, ASCE 115(8), 1134-1147.
- Shewbridge, S. and N. Sitar. (1992). "Shear zone formation and slope stability analysis." *Stability and Performance of Slopes and Embankments II*, Geotechnical Special Publication No.31, ASCE. Berkeley, California, June, 358-370.
- Shrestha, S. and J. Bell. (1982). "A wide strip tensile test of geotextiles." *Proc., Second International Conference on Geotextiles*. Las Vegas, 739-744.
- Spencer, E. (1967) "A method of analysis of the stability of embankments assuming parallel inter-slice forces," *Géotechnique* , 24, No.4, 661-665.
- Springman, S., M. Bolton, J. Sharma and S. Balachandran. (1992). "Modelling and instrumentation of a geotextile in the geotechnical centrifuge." *Proc., Earth Reinforcement Practice*, H. Ochiai, S. Hayashi and J. Otani, eds. Fukuoka, Japan: A. A. Balkema, 167-184.
- Stocker, M.F., Korber, G.W., Gassler, G., and Gudehus, G. (1979). "Soil Nailing." *Proc., Int. Conf. Soil Reinforcement*, Paris, Vol.2, 469-474.

- Taniguchi, E., Y. Koga, S. Yasuda and I. Morimoto. (1988). "A study on stability analyses of reinforced embankments based on centrifugal model tests." *Proc., Int. Geot. Symposium on Theory and Practice of Earth Reinforcement*, T. Yamanouchi, N. Miura and H. Ochiai, eds. Fukuoka Kyushu, Japan: A.A.Balkema, 485-490.
- Terashi, M. and M. Kitazume. (1988). "Behavior of a fabric reinforced clay ground under an embankment." *Proc., International Conference on Geotechnical Centrifuge Modelling*, Jean Francois Corte, ed. Paris, 243-253.
- Terzaghi, K. (1956). *Theoretical Soil Mechanics*. John Wiley and Sons, Inc., New York, N.Y.
- Tufenkjian, M. and M. Vucetic. (1992). "Seismic stability of soil nailed excavations." *Proc., Earth Reinforcement Practice*, H. Ochiai, S. Hayashi and J. Otani, eds. Fukuoka, Japan: A. A. Balkema, 573-578.
- Wright, S.G. (1990). *UTEXAS3 A Computer Program for Slope Stability Calculations*, Austin, Texas.
- Wright, S. G. and J. M. Duncan. (1991). "Limit equilibrium stability analyses for reinforced slopes." *Transportation Research Record* 1330, 40-46.
- Yoo, N. J. and H. Ko. (1991). "Centrifuge modelling of reinforced earth retaining walls." *Proc., International Conference on Centrifuge*, Hon-Yim Ko and Mclean Francis, eds. Colorado, 325-333.
- Zienkiewicz, O.C. and R.L. Taylor. (1991). *The Finite Element Method*, Fourth Edition, Volume 2, McGraw-Hill, 807p.

CHAPTER 5

PERFORMANCE OF GEOTEXTILE-REINFORCED SOIL STRUCTURES UNDER WORKING STRESS CONDITIONS: A FIELD INSTRUMENTATION STUDY



View of a 15.3 m high geotextile-reinforced slope built using high strength geotextiles and decomposed granite as backfill material.

5.1 Introduction

Field instrumentation is vital to the practice of geotechnics, in contrast to the practice of most other branches of engineering in which people have greater control over the materials with which they deal (Peck, 1988). While several reinforced soil walls have been instrumented, field experience to date has provided only a qualitative assessment of

the design variables in the case of geotextile-reinforced soil slopes. There is consequently a major need of quantitative information on the behavior of these structures. Although adequate field instrumentation is costly, examination of the performance of full-scale structures constitutes the only true confirmation that the design of reinforced soil structures is, in fact, satisfactory. A field instrumentation study to evaluate the performance of geotextile-reinforced soil slopes under working stress conditions is presented in this chapter.

As part of a highway widening project, the Federal Highway Administration designed and supervised the construction of a permanent 1H:1V geotextile-reinforced slope 15.3 m high. Several characteristics were unique to the design: the structure was higher than usual geotextile-reinforced slopes, it involved the use of both a high modulus composite and a nonwoven geotextile, and it was constructed using indigenous soils (decomposed granite) as backfill material. The reinforced structure is a 1H:1V (45°) slope located in Idaho's Salmon National Forest along U.S. Highway 93. The 172 m long and up to 15.3 m high geotextile-reinforced slope is vegetated, causing a minimum environmental impact to the Salmon National Forest. This structure, designed by the Western Federal Lands Highway Division, represents one of the higher geotextile-reinforced slopes in the U.S.

The slope was designed using geotextile reinforcements that were required to have not only adequate tensile strength, but were also expected to provide appropriate in-plane drainage capacity to allow dissipation of pore water pressures that could be generated in the fill. In this way, an additional drainage system was not necessary, even though seepage was expected from the fractured rock mass at the backslope of the reinforced

zone, which could cause a destabilizing seepage regime within the decomposed granite fill. Due to the unique characteristics of this structure, the reinforced slope was considered experimental, and an extensive program of instrumentation and construction monitoring was implemented to evaluate its performance.

As part of this instrumentation program, forty-five mechanical extensometers were placed on the geotextiles, two inclinometer tubes were installed to monitor horizontal movements within the reinforced zone, piezometers were installed to evaluate generation and dissipation of pore water pressures, and survey points were used to monitor face movements.

5.2 Design considerations

5.2.1 Site description

The project consists of a geotextile-reinforced slope designed as part of the widening of U. S. Highway 93 between Salmon, Idaho, and the Montana state line (Barrows and Lofgren, 1993). U.S. Highway 93 runs 1,860 miles from Phoenix, Arizona, to the Canadian National Railway yard in Jasper, Alberta (Figure 5.1). The specific location of the project, in Idaho's Salmon National Forest, is also indicated in the key map of Idaho. Esthetics was an important consideration in the selection of the retaining structures along scenic Highway 93, which has been recognized by a recent article in National Geographic (Parfit, 1992). The 172 m long and up to 15.3 m high geotextile-reinforced slope is vegetated, causing a minimum environmental impact to the Salmon National Forest. Other retaining structures were also designed and constructed as part of

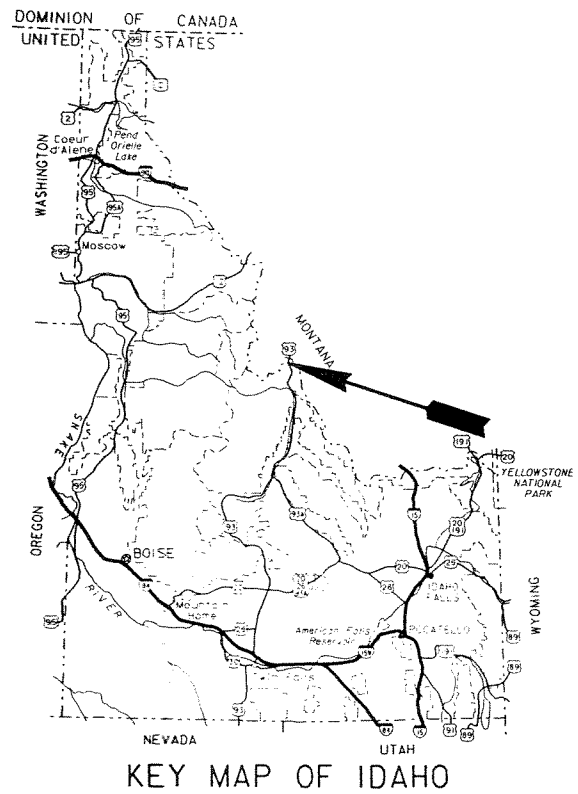
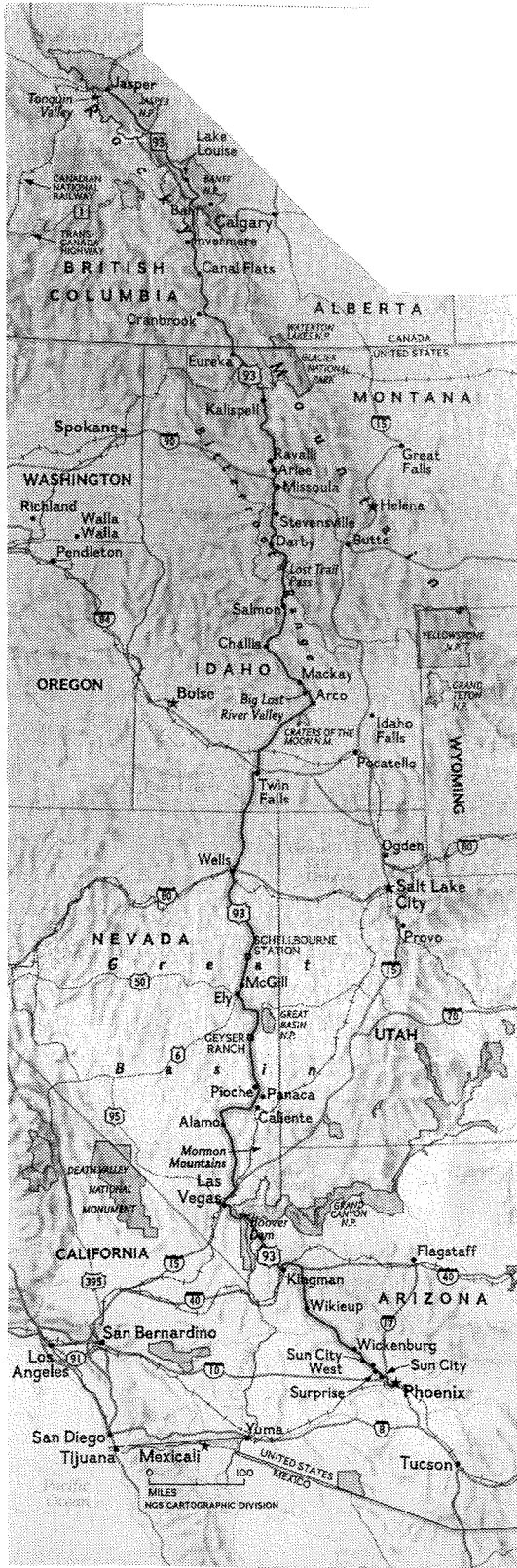


Figure 5.1 - Map showing Highway 93 and the location of the slope under study

the reconstruction of three miles of the roadway, including gabion walls and stepped gabion faced mechanically stabilized walls.

5.2.2 Use of indigenous soils

On-site soil coming from excavation of the road alignment was to be used as backfill material. Subsurface drilling revealed that the majority of subsurface material on this project is granite bedrock that varies from hard, intact rock to highly decomposed, soil-like material. Preconstruction evaluation of the cutbank soil indicated a maximum density of 18 to 21 kN/m³ and an optimum moisture content of 9.5 to 13.5%, as determined by Standard Proctor tests. Although the project specifications required the use of material with no more than 15% passing U.S. no. 200 sieve, internal drainage was a design concern. This was because of the potential seepage from the fractured rock mass into the reinforced fill, especially during spring thaw, coupled with the potential crushing of decomposed granite particles that may reduce the hydraulic conductivity of the fill. A thorough evaluation of the mechanical properties and the influence of particle breakage on decomposed granite as an embankment fill material was presented by Yapa et al. (1993).

5.2.3 Basis for geotextile selection

The decision to use a reinforced soil slope was based on the ease of construction, the anticipated lower cost as compared to more conventional structures, and the reduced environmental impact of this solution. On the other hand, the use of reinforcements with appropriate in-plane transmissivity was specified in order to deal with potential seepage

from the fractured rock mass. As mentioned, the lateral drainage provided by the reinforcements would avoid the need for a separate drainage system. Permeable geosynthetics were then specified for this FHWA project based on the experimental evidence that these reinforcements can more effectively reinforce poorly draining soils.

As discussed in Chapter 2 of this dissertation, there is no general design methodology for reinforced soil structures built with poorly draining soils. Nevertheless, since a number of this type of reinforced structures has already been constructed, many lessons can be learned from past experience. A good example that supports the selection of permeable reinforcements was provided by a 5.6 m high experimental structure built in Rouen, France, in which pore water pressures were monitored within the silt backfill (Perrier et al., 1986). The structure consisted of sections reinforced with woven geotextiles and a section reinforced with a composite nonwoven bonded to a polyester geogrid. As shown by Figure 2.24 (in Chapter 2), while positive pore water pressures were registered along the woven geotextile, negative pore water pressures were registered over the whole length of the composite reinforcement even at the end of construction. Additional evidence that good structure performance is dependent on maintaining a low water content in poorly draining backfills was provided by Tatsuoka et al. (1990), Burwash and Frost (1991), and Huang (1992), among others. However, as discussed in Chapter 2, practice has led theory in the use of poorly draining backfill for reinforced soil structures, and a number of research needs should still be addressed in order to formulate a consistent design methodology.

5.2.4 Design methodology

Design of the geotextile-reinforced slope, done according to FHWA guidelines, included analysis of the external and internal stability (Christopher et al., 1990). The external stability was evaluated by analyzing the potential for sliding and for overall deep-seated slope failure. Since a detailed subsurface investigation revealed low-strength decomposed granite zones, a reinforced rock shear key was built at the base of the reinforced slope in order to increase the external and compound stability. Methods of slope stability analysis, adapted to consider forces provided by the reinforcements, were used to determine the required geotextile layer spacing and reinforcement tensile strength. The total reinforcement length that provides adequate pullout resistance was finally calculated. The selected geotextiles were evaluated by obtaining product specific durability and creep test results and by performing a construction damage assessment (Wayne and Barrows, 1994). The partial factors of safety established based on these results were a creep reduction factor of 3.3, a durability factor of 1.1, and a construction damage factor of 1.2. Consequently, the allowable tensile strength of the geotextiles was defined considering a global reduction factor of 4.4 over the required ultimate tensile strength of the reinforcements.

5.2.5 Reinforcement layout

Widening of the original road was achieved by turning the existing 2H:1V nonreinforced slope into a 1H:1V reinforced slope. The specified geotextile strength was varied with the height of the slope to follow current design strength requirements. As shown in Figure 5.2, the final design adopted two geosynthetically reinforced zones with

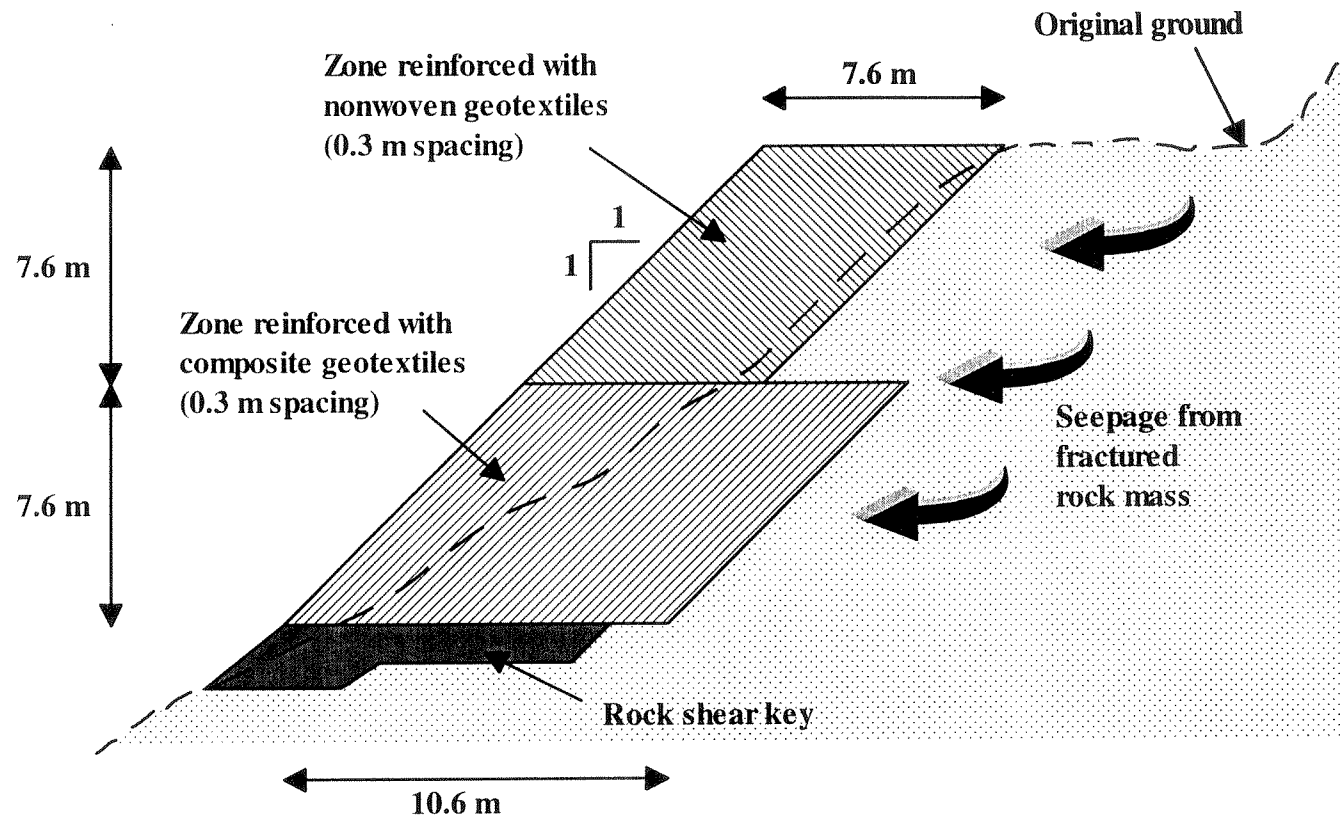


Figure 5.2 - Cross section of the geotextile-reinforced slope

a constant reinforcement spacing of 0.3 m (1 ft). At the highest cross-section of the structure, the reinforced slope has a total of 50 geotextile layers. The figure schematically shows the potential seepage from the backslope fractured rock. A nonwoven geotextile (PP-20) was selected for use in the upper half of the slope, while a high strength composite geotextile (PPC-100) was used in the lower half. Both geosynthetic reinforcements were manufactured by Polyfelt. The PP-20 material (Figure 5.3), with a nominal ultimate tensile strength of over 20 kN/m, is a polypropylene continuous filament needle punched nonwoven. The PPC-100 (Figure 5.4), with a nominal ultimate tensile strength over 100 kN/m, is a polypropylene continuous filament nonwoven geotextile reinforced by a biaxial network of high-modulus yarns. Wide width strip tensile tests ASTM D4595 were performed for quality control of the geotextile reinforcements. The ultimate strength in the machine direction obtained for the PP-20 geotextile was 24.4 kN/m, and for the PPC-100 composite was 104.7 kN/m. Both materials exhibit a typical in-plane hydraulic transmissivity of 0.006 l/s/m under a normal stress of 200 kPa. The composite geotextile was chosen for the lower half of the slope in order to provide the reinforcing benefits of a high-modulus geosynthetic and the hydraulic advantages of a nonwoven material. As indicated in section 5.2.3, minimum reinforcement requirements were defined during slope design by considering a global reduction factor of 4.4 to account for construction damage, long-term durability and creep issues. In addition, the geotextile strength required by design was lower than the tensile strength of the reinforcement finally selected for construction.

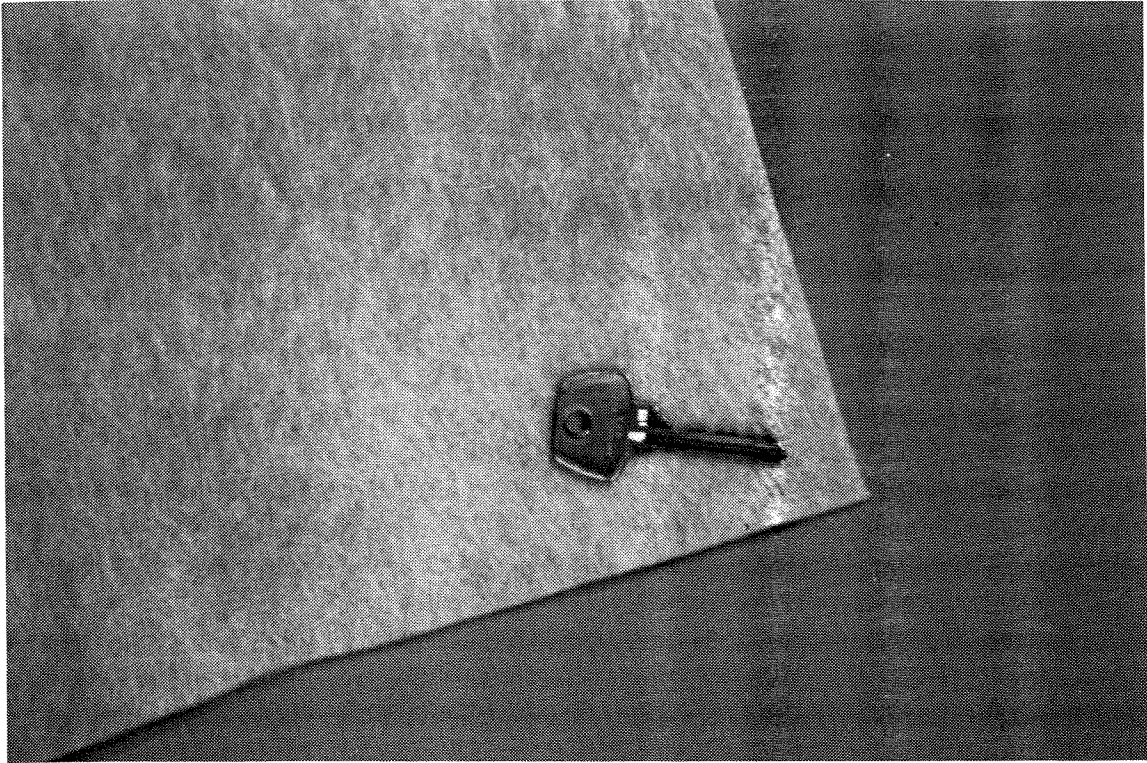


Figure 5.3: Nonwoven geotextile PP-20 used in the upper half of the slope

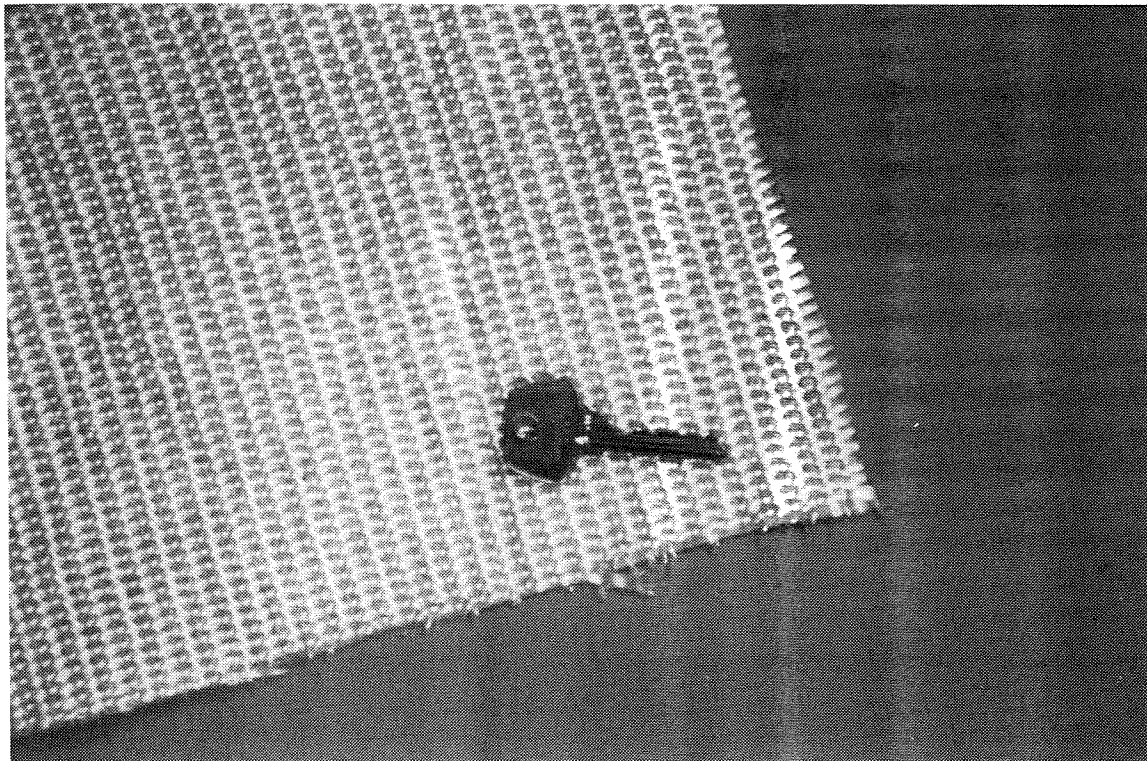


Figure 5.4: Composite geotextile PPC-100 used in the lower half of the slope

5.3 Construction

Slope construction, performed using conventional construction equipment, took place during the summer of 1993. The original slope was excavated back to a 1H:1V side slope (Figure 5.5), and the base for the embankment was graded to a smooth condition. The rock shear key was constructed by depositing, spreading, and then compacting the rock material with a vibratory roller. The rock shear key was reinforced with welded wire mesh having a vertical spacing of 0.45 m. The selection of a welded wire mesh reinforcement was based on the large openings required to accommodate the size of the rock material in the shear key (up to 380 mm). A total of 1000 cubic yards of loose rip-rap Class 3 was used for the shear key. Although construction took place during the dry summer season, seepage appearing as weeps at the base of the cut slope emerged from the fractured rock mass.

No special expertise was required for slope construction, and a crew of five members without previous experience in reinforced soil construction placed an average of three layers per day along the instrumented, 172 m long slope. Figure 5.6 shows the reinforced slope after layer 25 had been placed, with one of the inclinometer casings visible at the center of the picture. In each lift, backfill material was spread with a medium sized bulldozer and oversized rocks (greater than 100 mm) were then removed. Each layer had to be compacted to 95% of maximum density, as determined by Standard Proctor tests, and the water content of the backfill was specified to be within 3% of the optimum. These compaction requirements were easily achieved by the contractor using static compaction methods: a grid roller was used for compaction of most of the fill, and a small walk-behind compactor was used close to the facing. Figure 5.7 shows the



Figure 5.5 - Rock shear key under construction

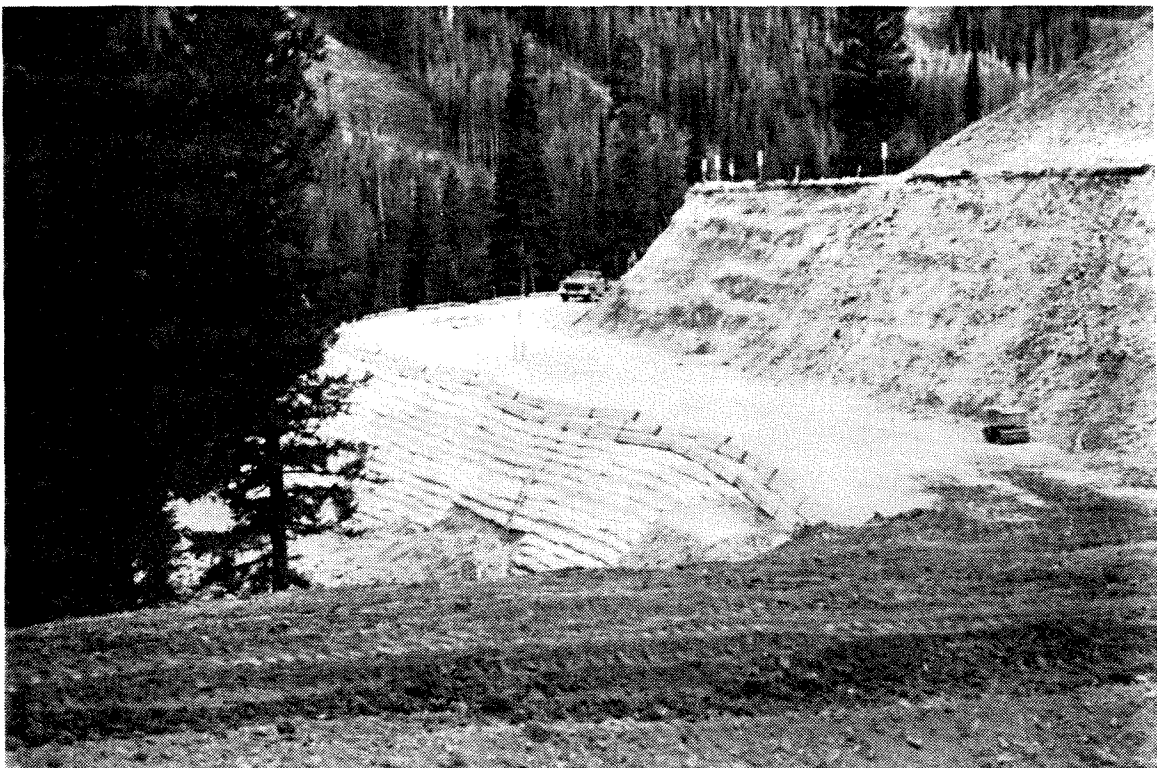


Figure 5.6 - View of the reinforced slope after placement of layer 25

compaction equipment typically used throughout construction of the geotextile-reinforced slope. Special care was required when working around the inclinometer tubes during slope construction. The geotextile at each lift level was placed with the longitudinal direction perpendicular to the slope, overlapping adjacent rolls a minimum of 0.60 m. Although initial design did not consider wrapping of the geotextiles at the slope face, the geotextiles were eventually wrapped in order to satisfy National Forest Service requirements. A single layer forming system inclined at 45° was used. In order to promote vegetation, 50 mm holes were initially cut into the fabric at 150 mm intervals. Later, propane torches were used, since they proved more efficient to create holes in the fabric.

Figure 5.8 shows the backfilling operations during placement of the top layer (layer 50), which was finished approximately one month after placement of the initial layer. An erosion control matting was subsequently placed on the slope and anchored to protect the face until vegetation is well established. Figure 5.9 shows the completed geotextile-reinforced slope after the erosion control matting has been placed. The subgrade was completed in the 1993 summer season and the reinforced slope has performed as intended since then. A considerable amount of instrumentation data has been accumulated during the construction period and until eight months after construction. Post-construction performance is still being monitored at this writing.

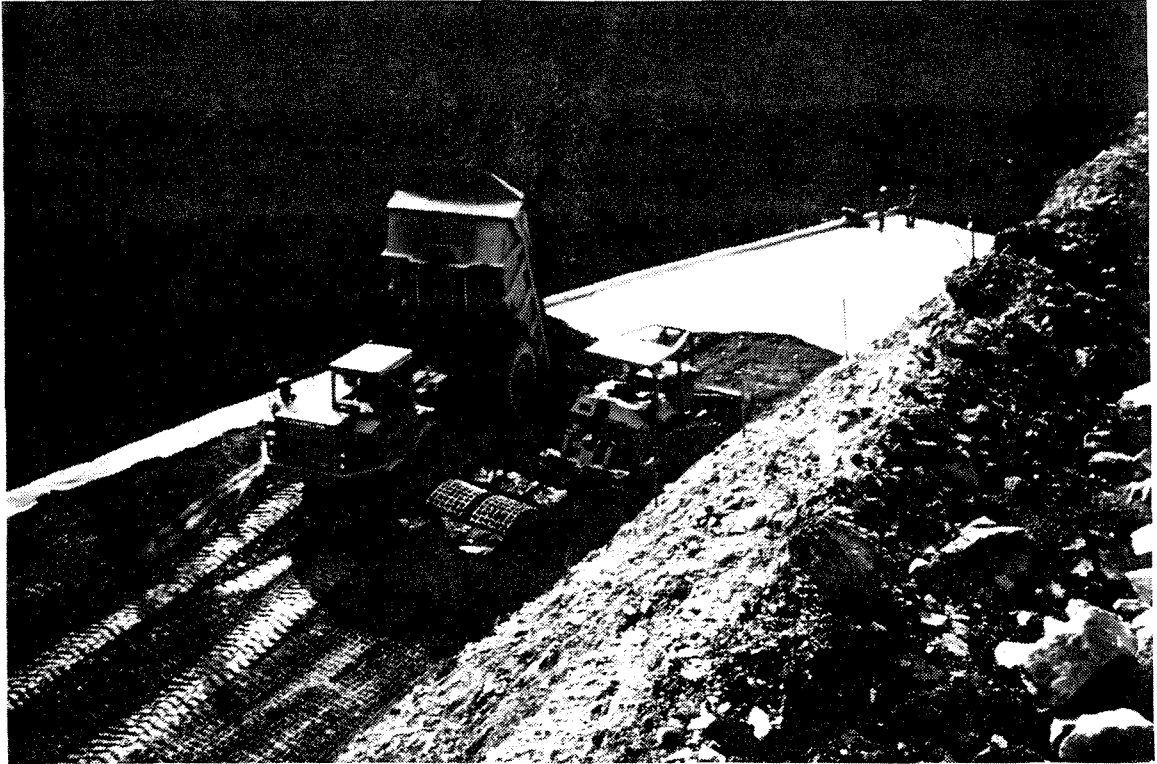


Figure 5.7 - Top view of the reinforced slope during compaction operations



Figure 5.8 - Placement of backfill during construction of the top layer

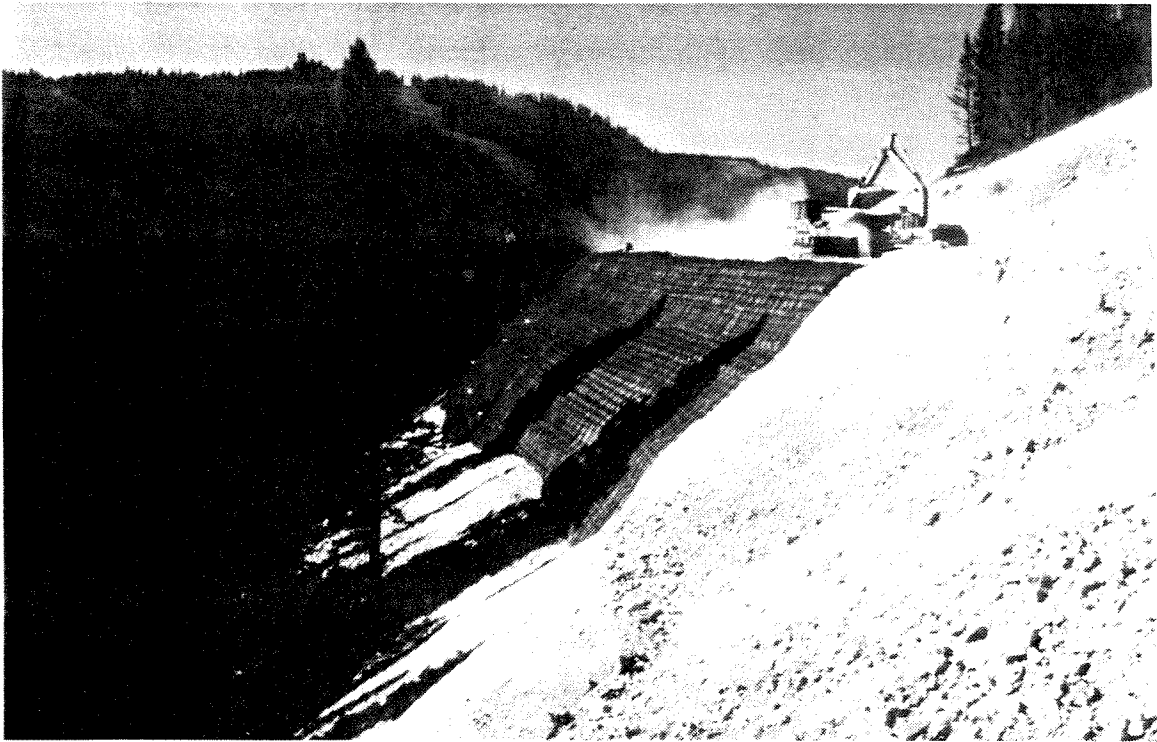


Figure 5.9 - Finished reinforced slope with erosion matting in place

5.4 Instrumentation program

A comprehensive monitoring program was designed to evaluate the performance of the reinforced soil slope during and after construction. The instruments were placed at the highest cross-section of the geotextile-reinforced structure with the objectives of:

- evaluating the deformation response of the structure;
- assessing the strain distribution within the geotextile reinforcements;
- evaluating the effect of lateral drainage provided by geosynthetics with adequate in-plane transmissivity;
- investigating the long-term performance of the geotextile-reinforced structure; and

- providing a reference base for future designs with the possibility of improving design procedures and/or reducing costs.

To achieve these goals, the parameters selected for monitoring were the global strain distribution in the geotextiles, with special attention to the magnitude and location of maximum strains, horizontal movements within the reinforced soil mass, movements in the slope face, and pore water pressures within the fill.

Figure 5.10 shows the location of the instrumentation used in the monitoring program of the geotextile-reinforced slope. Since most instruments measure conditions at only one point, a large number of measurement points was required to evaluate parameters of interest over the entire section of the structure. Instrument readings were taken during construction of the reinforced slope and were continuously taken until approximately eight weeks after the completion of the fill. Additional measurements were made after the spring thaw to evaluate the long-term performance of the structure.

As part of the instrumentation program, two inclinometer tubes were installed to monitor horizontal movements within the reinforced zone, both during and after construction. These inclinometers were installed at 7.3 m and 11.9 m from the toe of the reinforced slope, and daylighted on top of geotextile rows 24 and 39 respectively. The inclinometer tubes were grouted into the drill casings in the rock shear key for anchorage. During construction of the geotextile-reinforced slope, inclinometer casings were added in 1.52 m sections (Figure 5.11) and backfill was hand-placed and compacted around the inclinometer casings.

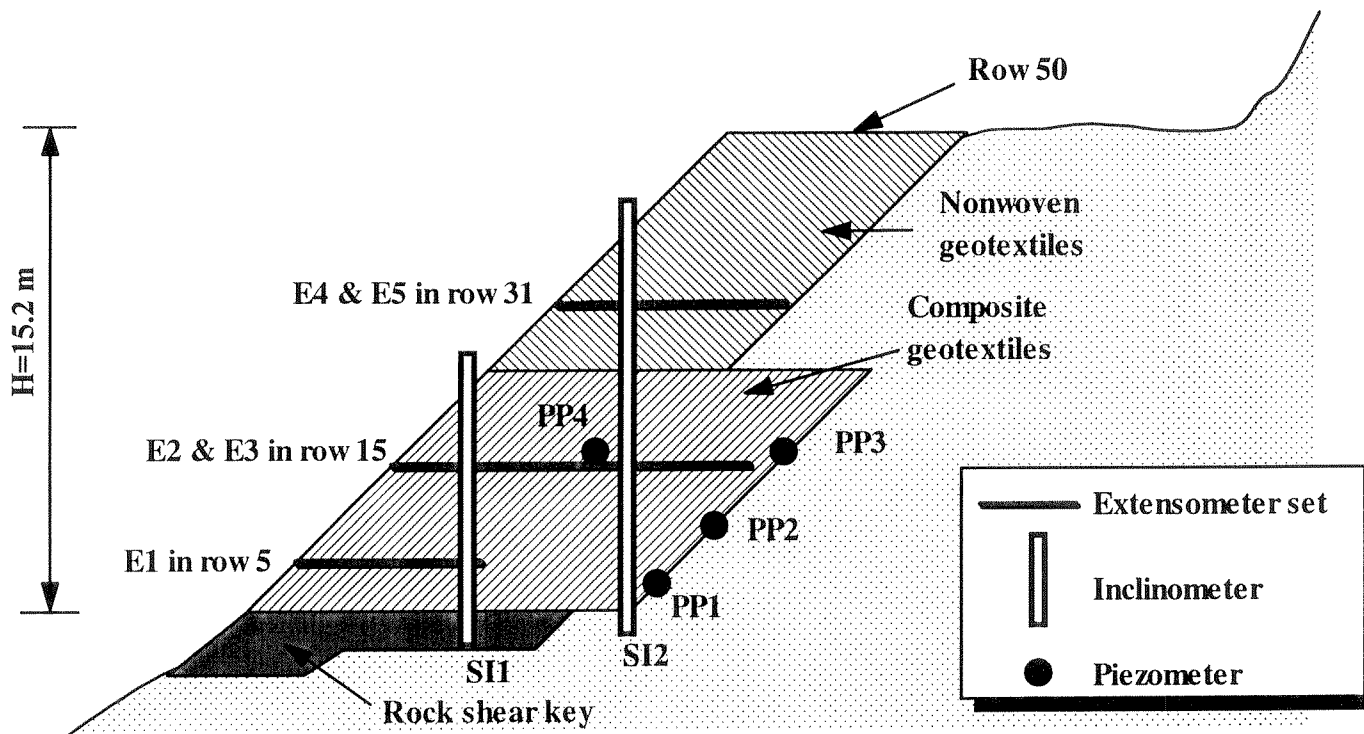


Figure 5.10 - Cross section of the reinforced slope showing the instrumentation layout

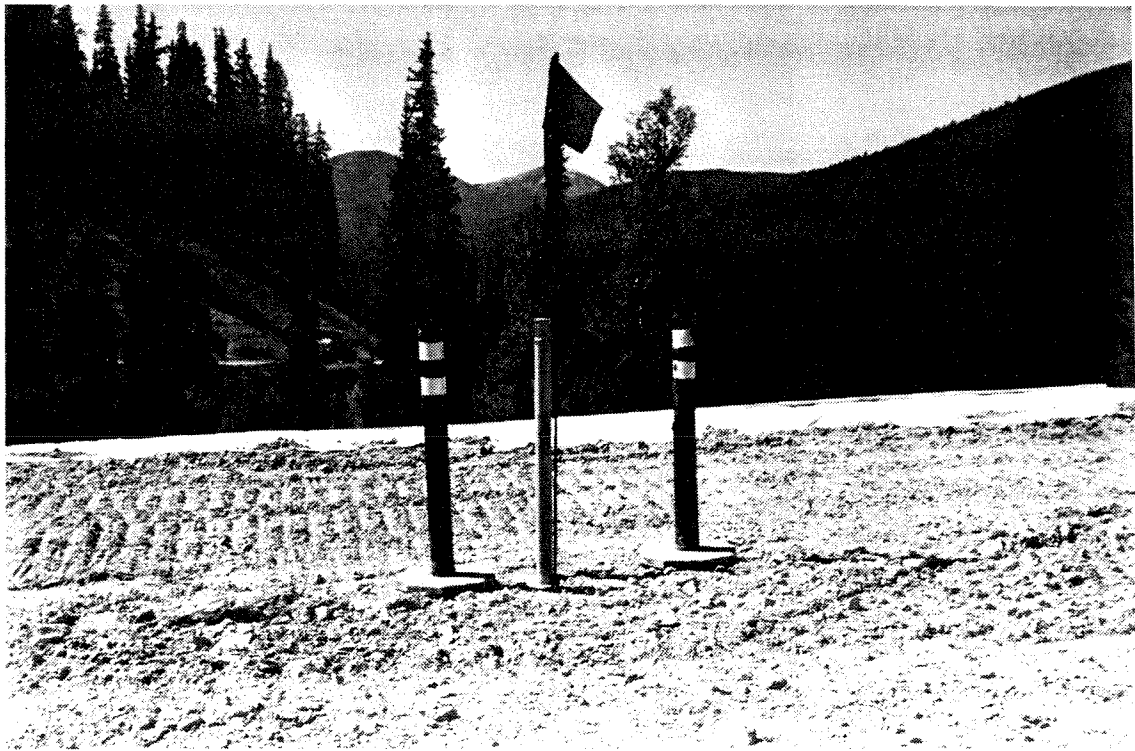


Figure 5.11 - View of inclinometer casing added during construction progress

Movements of the slope face were monitored by survey points located in four vertical rows in the vicinity of the instruments. Each survey point consisted of a short piece of rebar embedded between two reinforcing layers. Slope movements in response to increase in overburden were monitored through changes in offset distances, to the nearest 3 mm (0.01 ft), from control points at the toe of the fill to survey points on the structure face.

Forty-five single-point mechanical extensometers were placed on the geotextiles to measure local displacement of the geotextile and to evaluate the strain distribution as well as the location and magnitude of maximum tensile strains. The extensometers consisted of metal rods attached to the geotextile at increasing lengths from the slope, and extended to the front face in a stiff PVC casing to protect them from soil overburden. Figure 5.12 shows the end bearing plate of a mechanical extensometer already attached

to the nonwoven geotextile. The end bearing plates were placed at increasing distances from the wrapped around face (Figure 5.13), at nominal intervals of 610 mm between them. Relative displacements between the extensometer anchor plate and the slope face were measured to the nearest 0.025 mm (0.001 inch). The extensometers were concentrated around the predicted location of the potential failure surface, as defined by the limit equilibrium analysis used in the structure design. As indicated in Figure 5.10, the extensometers were mounted on the composite geotextile layers 5 and 15, and on the nonwoven geotextile layer 31, located at elevations 1.22 m, 4.27 m, and 9.14 m, respectively. Extensometer sets were installed at two parallel cross-sections of the reinforced structure in order to provide sufficient redundancy to explain possible anomalous data as well as to account for possible damages of some instruments during construction. Extensometer sets E1 (with five single-point extensometers), and sets E2 and E4 (ten extensometer each), were installed in one of the instrumented cross-sections. Extensometer sets E3 and E5, analogous to E2 and E4, were additionally installed in a parallel cross-section. The provision of considering redundant instruments proved to be crucial to the success of the instrumentation program, as several single-point extensometers in set E5 were lost during compaction operations.

Additionally, four electronic piezometers were installed to evaluate generation and dissipation of pore water pressures that could develop either during construction or after rainfall events. Groundwater seepage is expected from the excavation behind the fill, mainly during the spring runoff. One port on each of silicon-diaphragm transducer (Figure 5.14) is open to the water, while the back of the diaphragm is vented to the surface. The groundwater monitoring system operates unattended under extreme weather

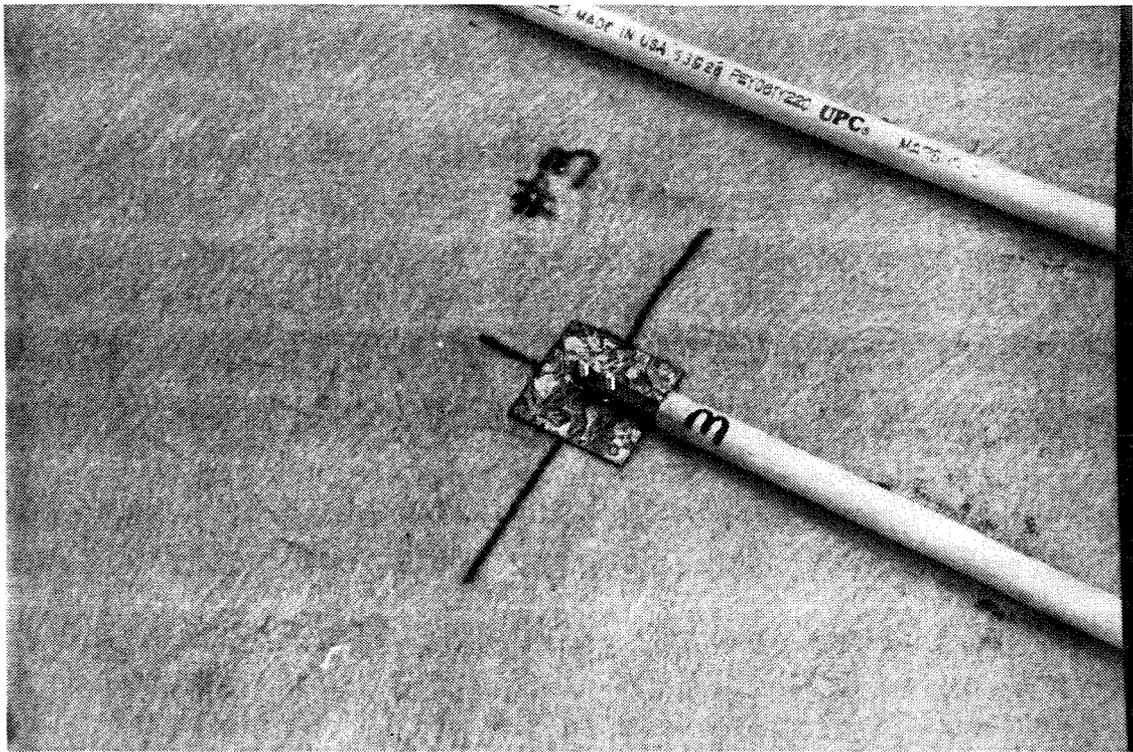


Figure 5.12 - End bearing plate of a mechanical extensometer attached to a geotextile reinforcement

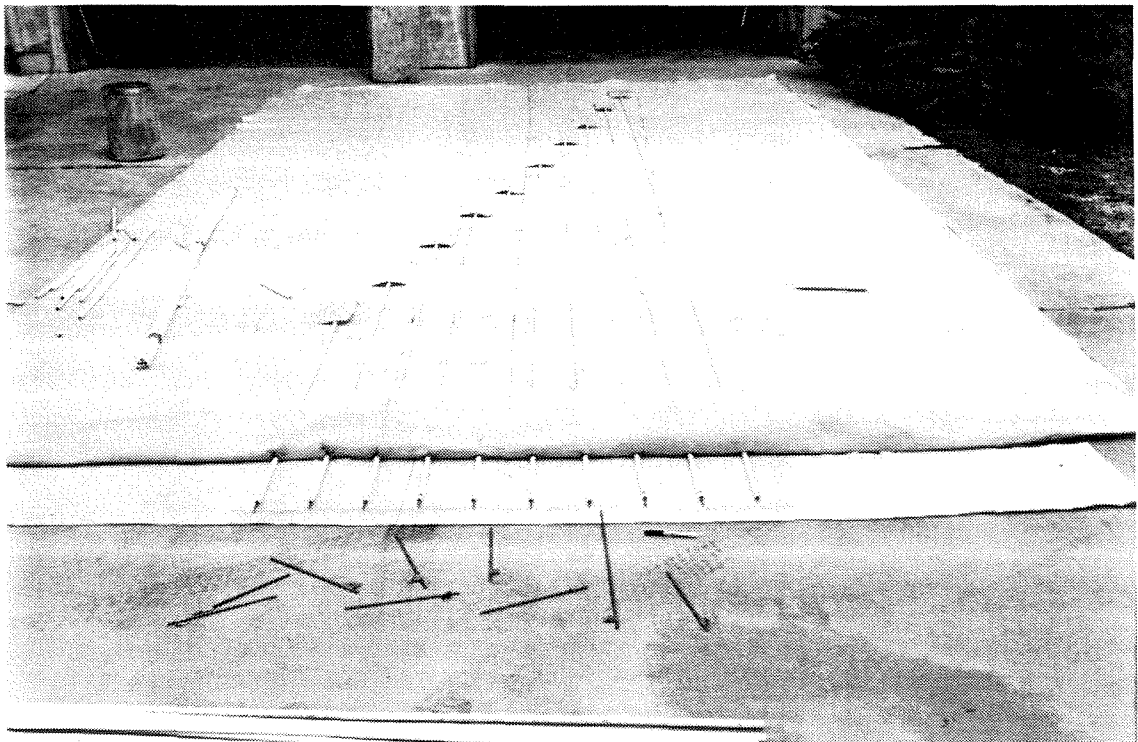


Figure 5.13 - Geotextile layer instrumented with extensometers ready for placement in the field

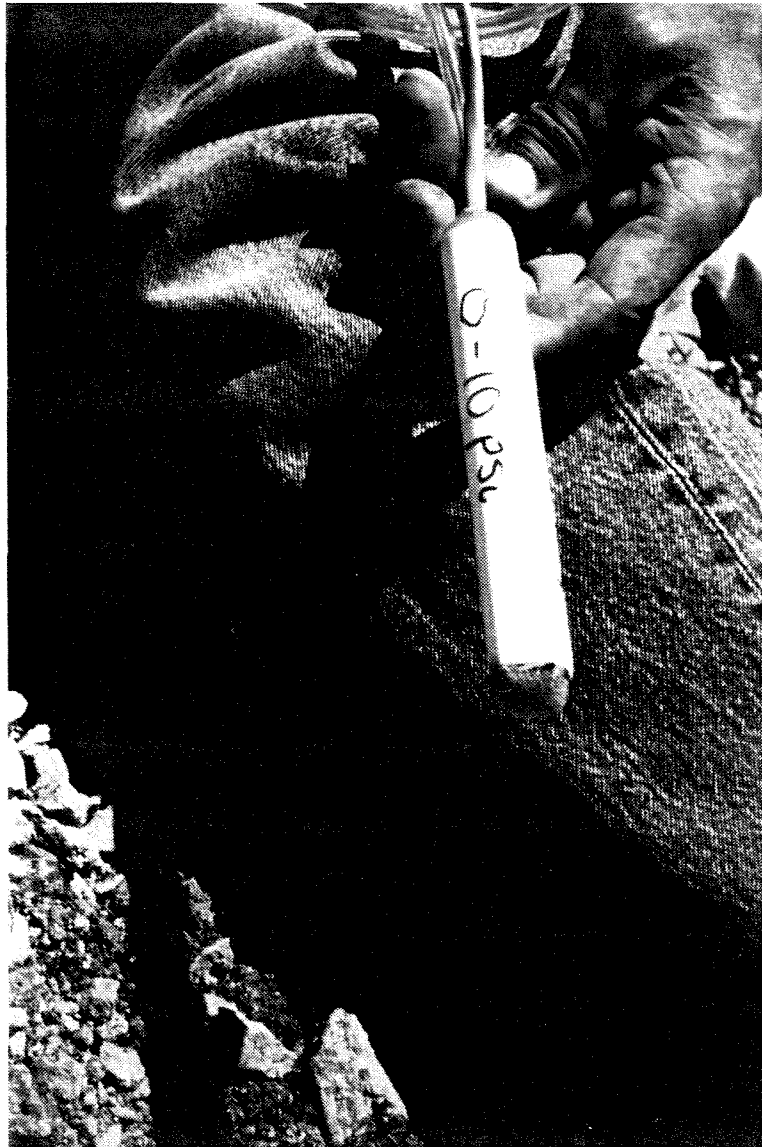


Figure 5.14 - Silicon-diaphragm transducer used to monitor pore water pressure

conditions, powered by rechargeable batteries (Prellwitz and Babbit, 1984). Three piezometers were installed at the back of reinforcement layers 2, 7, and 15 at elevations 0.3 m, 1.8 m, and 4.27 m, respectively. In order to evaluate the worst case scenario, the piezometers were placed at a cross-section that showed seepage flux from the rock mass during the construction period. A fourth piezometer was installed within the fill between geotextile rows 15 and 16 (4.4 m high) to evaluate possible pore pressure generated within the fill. However, the air venting tube of this piezometer was cut by the cat blade during construction. Although the venting tube was quickly spliced in the field before it was buried, some water or soil may be within the air-vent tube exerting pressure on the back of the differential transducer diaphragm. Pore water pressures were measured at each sensor every 30 minutes, and the maximum, minimum, and average values were stored daily using a multi-channel data logger.

5.5 Instrumentation results

The performance behavior of the reinforced slope was monitored during the construction period, with installation and measurements made concurrent with construction progress. Figure 5.15 indicates the construction progress of the geotextile-reinforced slope. Continuous monitoring continued until approximately eight weeks after construction in order to evaluate the early post-construction performance. Monitoring was interrupted during the winter, and additional measurements were made after snow melting during the spring. Additional post-construction monitoring is planned to take place at the site.

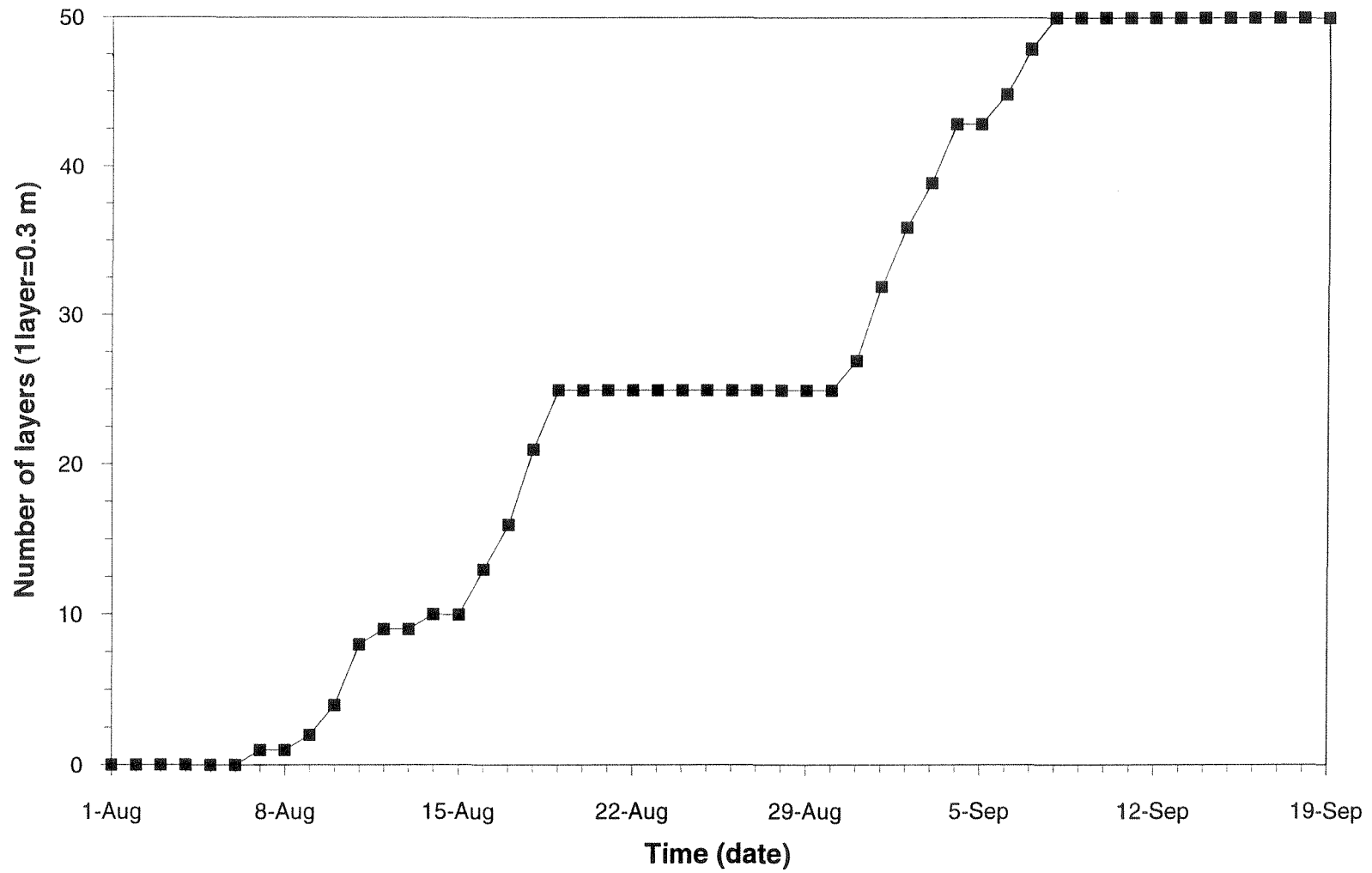


Figure 5.15 - Construction progress of the geotextile-reinforced slope

5.5.1 Global structure deformations

Global deformations of the geotextile-reinforced slope were determined from the two inclinometers installed within the reinforced zone and from the survey points located on the structure face. The inclinometers measured horizontal deflections within the reinforced fill to the nearest 0.025 mm (0.001 in), providing a precise evaluation of displacements caused by increasing overburden and of possible post-construction movements.

5.5.1.1 Construction period

Figure 5.16 shows the development of lateral displacements recorded by inclinometer SI1 at different elevations during construction of the slope. Fill elevation is indicated in the figure as the number of geotextile layers already placed (vertical spacing is 0.3 m). These data show an approximately linear increase in displacements during construction, with horizontal displacements starting when construction reached the fill elevation of approximately 3.3 m, corresponding to layer 11. The initial absence of lateral displacements is because during the initial construction stages the inclinometer is behind the theoretical stable slope surface defined by the friction angle of the fill. As indicated in Figure 5.17, the progress of lateral displacements for inclinometer SI2 shows a trend similar to that indicated for inclinometer SI1. In this case, lateral displacements at the location of SI2 started when the fill reached approximately 6.7 m, the level of layer 22. The zone of negligible initial displacements may be related to the existence of a zone of zero required reinforcement forces (Jewell, 1985), beyond which no reinforcement forces are required to maintain equilibrium.

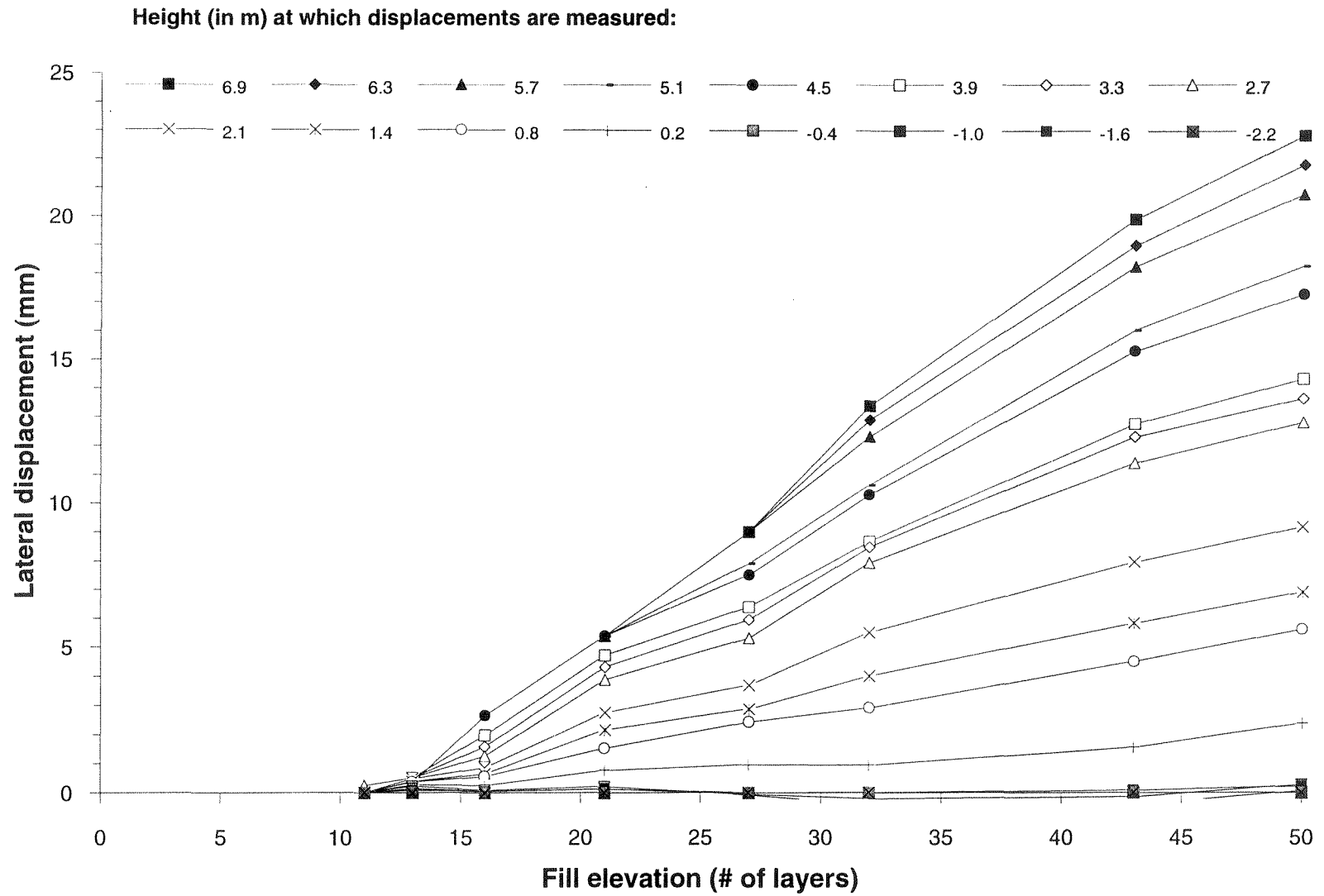


Figure 5.16 - Development of lateral displacements measured by inclinometer S11 with increase in fill height

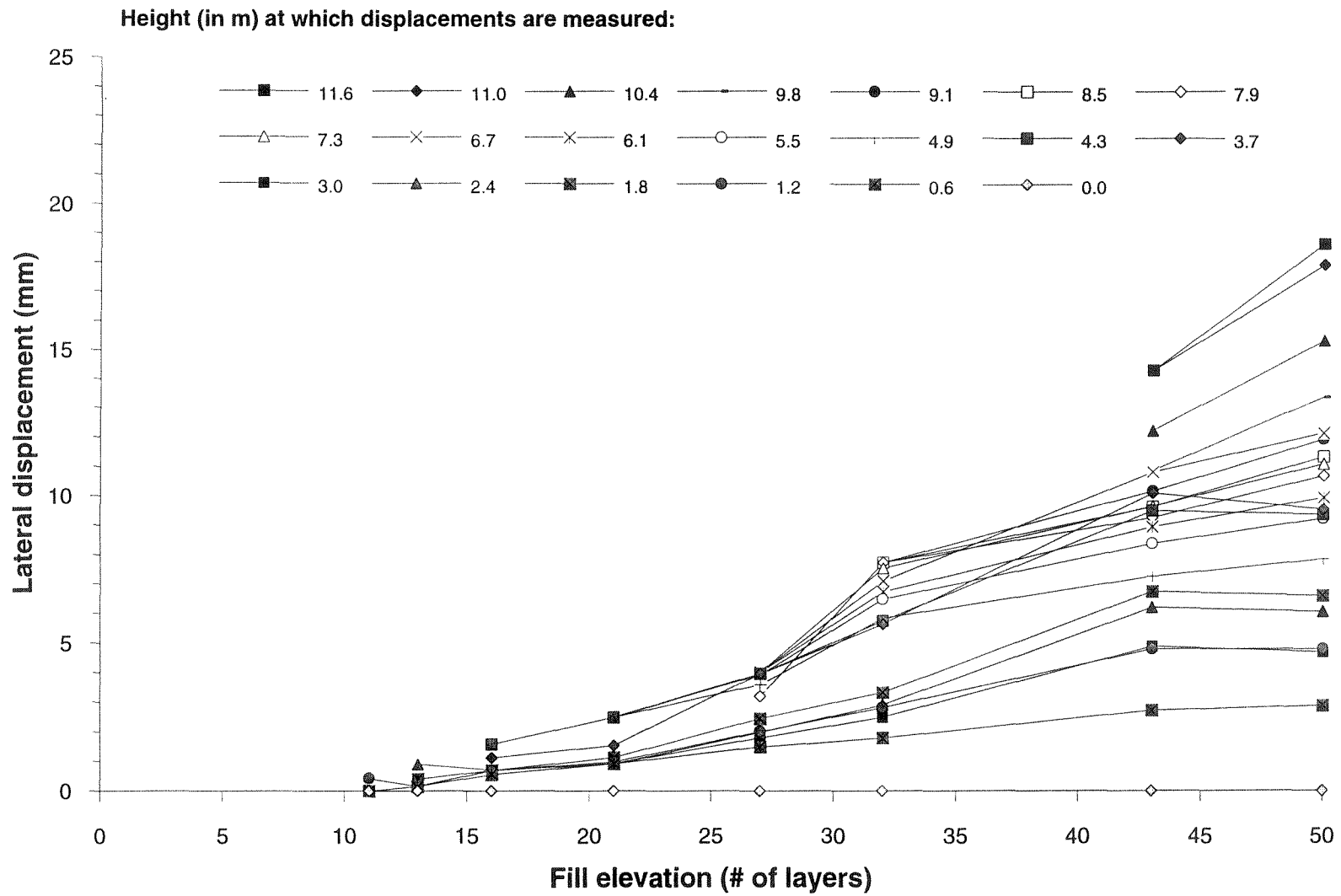


Figure 5.17 - Development of lateral displacements measured by inclinometer S12 with increase in fill height

Lateral deflections obtained from inclinometers SI1 and SI2 during the construction period are indicated in Figure 5.18. Inclinometers measure the total horizontal movement relative to the bottom of the inclinometer casing, which is a fixed reference. The displacement profile obtained for inclinometer SI1 shows a relatively uniform rotation of approximately 0.2 degrees, with a maximum horizontal displacement at the end of construction of less than 25 mm (1 inch). This ultimate horizontal displacement is very small, representing a horizontal movement on the order of 0.16% of the height of the geotextile-reinforced slope. A slight kink can be observed in the lateral displacement profile at an approximate height of 2.7 m.

For inclinometer SI2, the maximum lateral displacement obtained at the end of construction is approximately 19 mm (3/4 inch), and was located at the top of the inclinometer. This deflection corresponds to a rotation of less than 0.1 degrees, and represents a movement on the order of 0.12% of the height of the structure. The lateral displacement profile shows a peak at a height of approximately 4 m, probably caused by localized constraints in the inclinometer tube caused by oversized aggregate or local overcompaction. However, this feature is localized and appears not to affect the general displacement trend. A kink can also be observed in the inclinometer SI2 profile at an approximate height of 6.7 m.

The evaluation of face movements at various stages during fill placement was made by measuring offset distances from survey points to control points located at the toe of the structure. Face movements at the end of construction, obtained from four cross-sections, are indicated in Figure 5.19. The face movements in the figure correspond to the incremental displacements at the end of construction with initial readings taken when

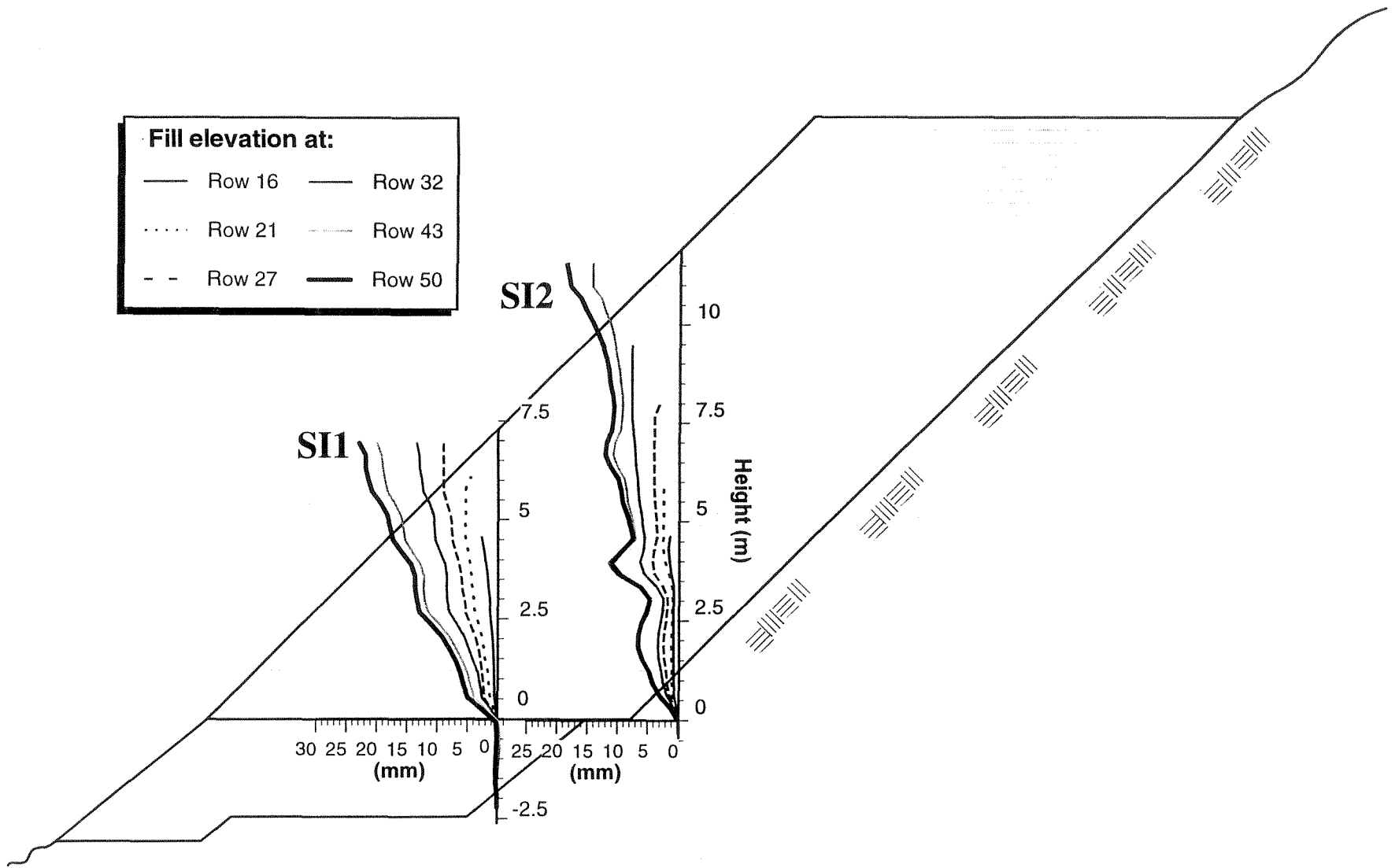


Figure 5.18 - Horizontal deflections obtained by the inclinometers during the construction period

the order of 35 mm), which is consistent with results obtained from the more accurate inclinometer and extensometer data.

5.5.1.2 Early post-construction period

The development of lateral displacements until eight weeks following the end of construction, obtained from inclinometer SI1 readings, is indicated in Figure 5.20. Although slight displacement fluctuations can be observed after the completion of the slope construction, there is clearly no increasing displacement trend, which would be indicative of time-dependent movement. Figure 5.21 shows the profiles obtained from inclinometer SI1 during the construction and early post-construction periods. The figure shows that the displacements obtained after construction of the last layer (layer 50) can be considered to remain approximately constant during the eight weeks following construction. Similarly, no apparent post-construction lateral displacements was observed from inclinometer SI2 readings as observed from the progress of lateral displacements with time (Figure 5.22) and from the inclinometer SI2 profiles (Figure 5.23). Consistent with these results, survey measurements taken during this early post-construction period showed no additional face movements in relation to those obtained at the end of construction.

5.5.1.3 Spring measurements

Fill placement was completed on September 8, 1993. After interrupting continuous monitoring during the winter, additional measurements were taken eight months after the end of construction during the spring runoff (on May 29, 1994). Figure

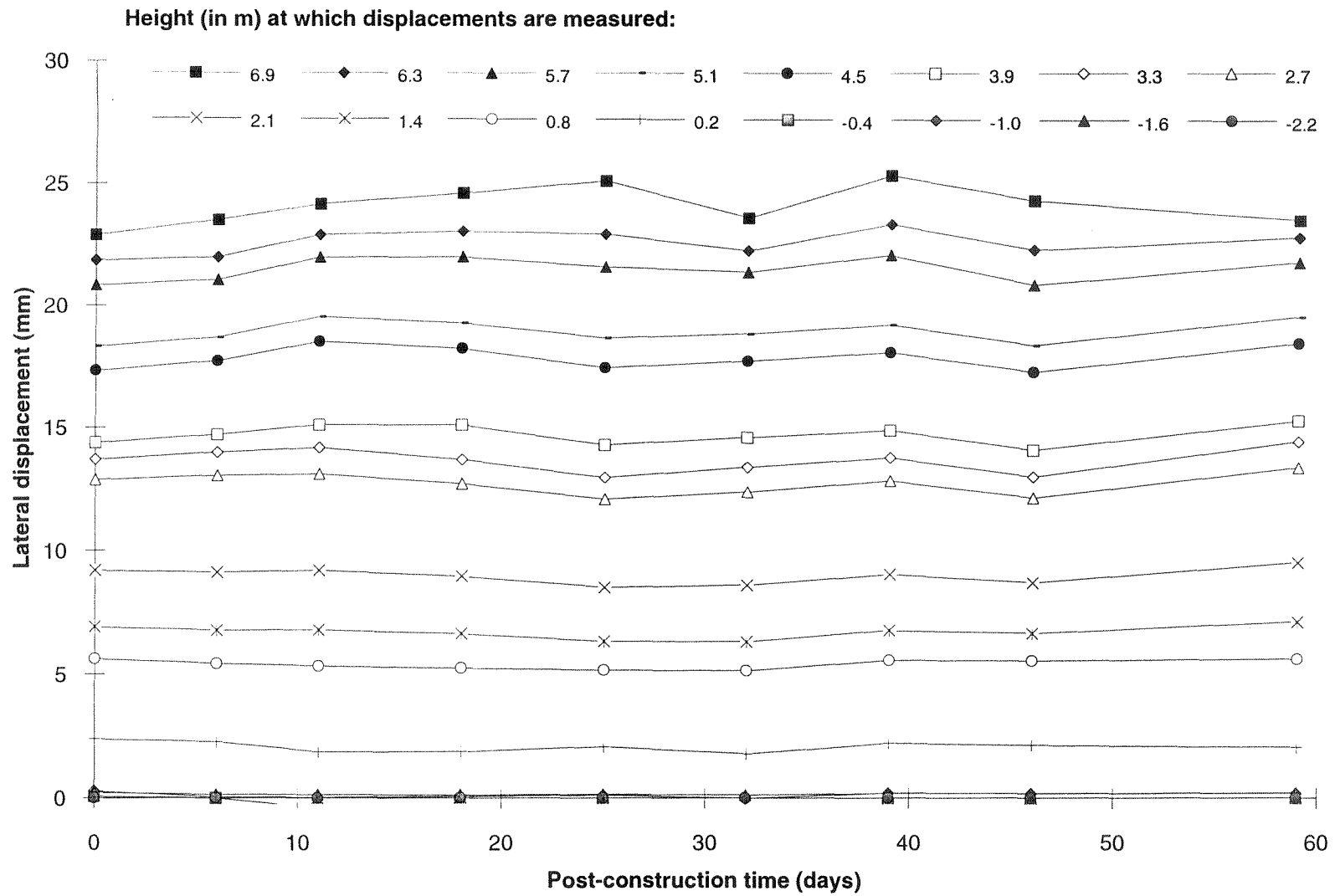


Figure 5.20 - Development of lateral displacements measured by inclinometer S11 with time after construction

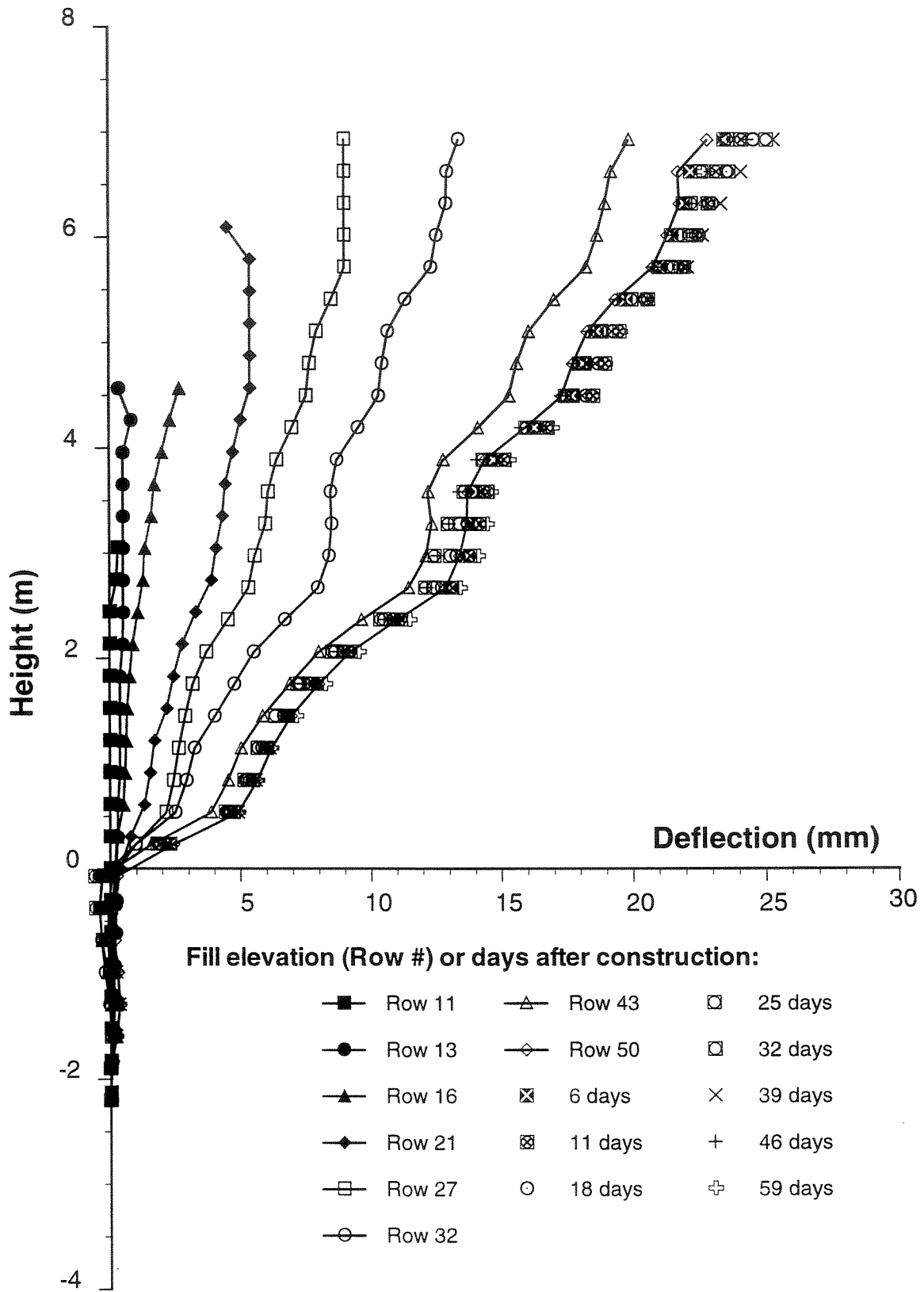


Figure 5.21 - Horizontal deflections from inclinometer SII

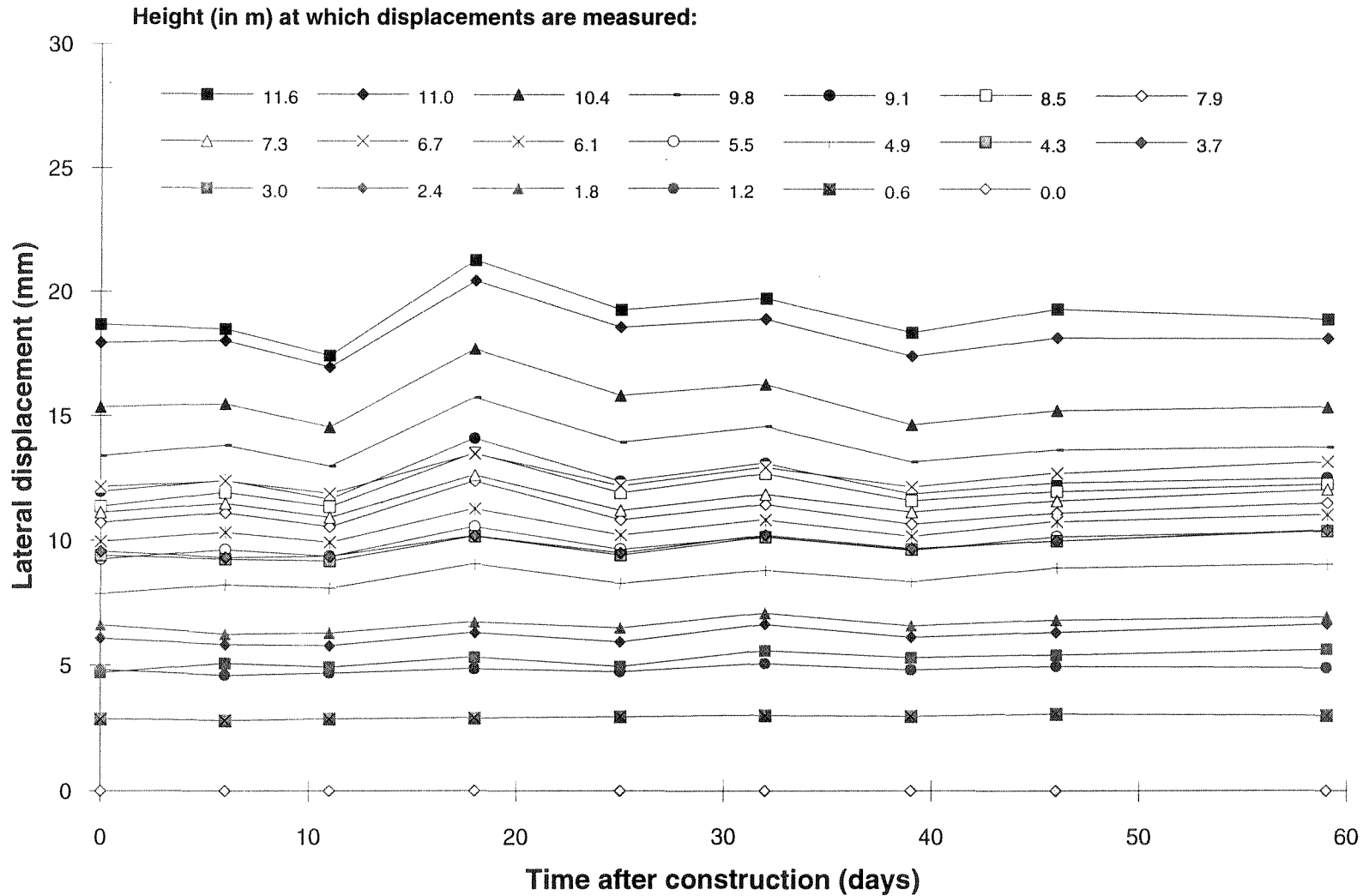


Figure 5.22 - Development of lateral displacements measured by inclinometer SI2 with time after construction

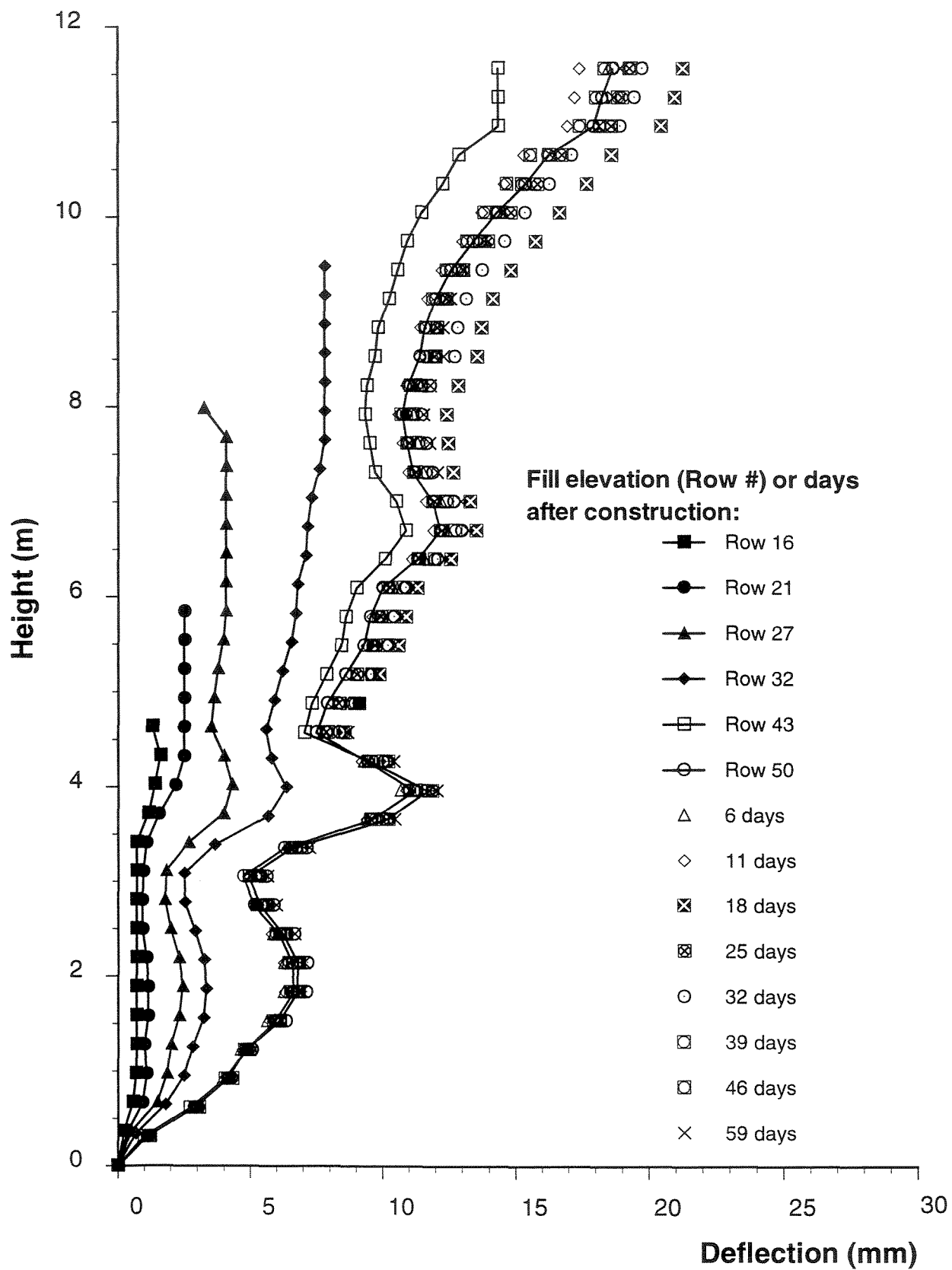


Figure 5.23 - Horizontal deflections from inclinometer SI2

5.24 shows the horizontal displacement profiles obtained during the spring from the inclinometer measurements. For comparison, the displacement profiles at the end of construction are also shown in the figure. Essentially no increase in lateral displacements can be observed in both inclinometer profiles. The only location where the increase in lateral displacements is not negligible is at the slope face where inclinometer S11 daylighted (10 mm increase approximately). These movements are smaller than anticipated, showing no evidence of time-dependent (creep) displacements or adverse effects due to the possible increase in water content within the fill during the snow melting period. Part of the observed movements may even be a consequence of the effect of freezing and thawing of the fill material.

Face movements after the winter season were also evaluated using the offset distances measured from survey points to control points located at the toe of the structure. Figure 5.25 shows the total face movements obtained using survey measurements taken during the spring. The estimated displacement profile at the end of construction is also indicated in the figure for comparison purposes. Survey measurements incorporate the effect of local movements in the wrapped around geotextile face, which may cause the scatter observed on the different cross-sections. Although survey measurements may be inaccurate, the results in the figure indicate that essentially no movements occurred in the lower half of the reinforced fill since the end of construction. On the other hand, slight, approximately uniform movements (10 and 20 mm) occurred in the upper half of the slope. Also in the spring measurements, the small movements obtained from survey measurements are consistent with the inclinometer results.

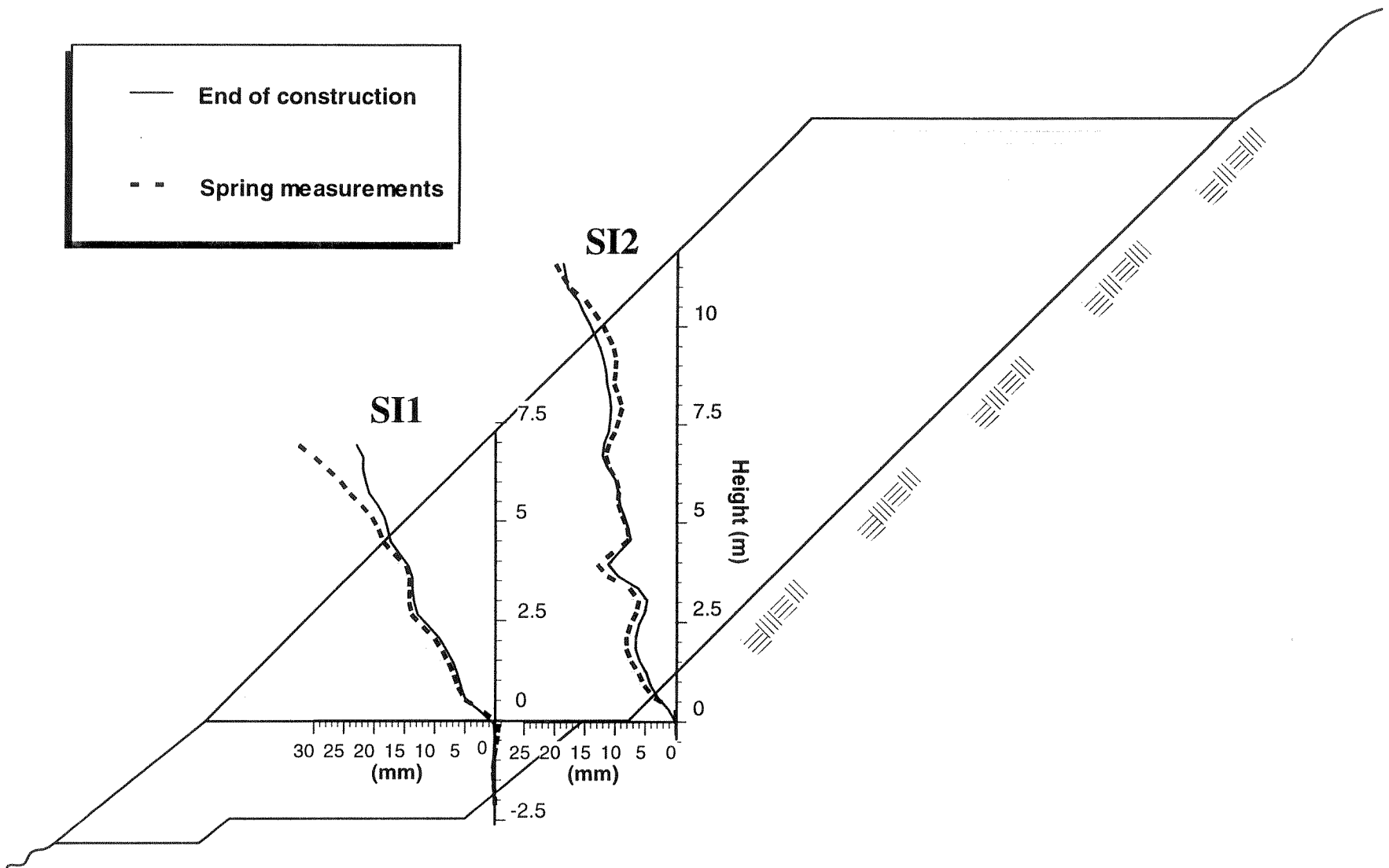


Figure 5.24 - Horizontal deflections obtained from spring measurements in each inclinometer

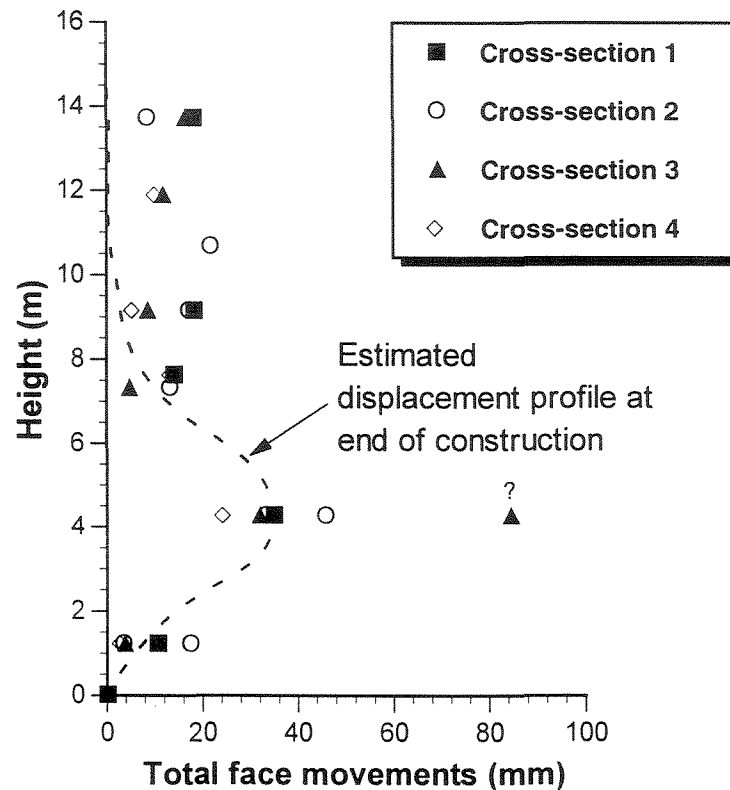


Figure 5.25 - Total face movements determined from survey measurements taken during the spring (estimated profile at end of construction also indicated)

An accurate evaluation of settlements could not be performed during the spring due to the difficulty in maintaining access to level survey points. Nevertheless, since the total face displacements measured by the offset distances incorporate possible vertical movements, only small settlements may have occurred since the end of construction. Moreover, visual inspection indicated no evidence of differential settlement, which would have been easily identified in the completed subgrade.

5.5.2 Geotextile strain distribution

Mechanical extensometers measure the relative displacements between the slope face and the extensometer plate anchored to the geotextile within the fill. Since the instruments in each extensometer set are installed at increasing distances from the face,

relative displacements between extensometer plates and, consequently, geotextile strains can be estimated.

5.5.2.1 Construction period

Since no damage during construction operations was experienced in any of the extensometers from sets E1, E2 and E4, which were installed at the same cross-section, calculations to define geotextile displacements and strains from extensometer measurements were based mainly on the results from these three instrument sets. Information from extensometer sets E3 and E5 was used to verify the correctness of individual measurements.

Of particular relevance are the measurements at the level of layer 15, since these results can be used to cross-check the inclinometer readings. Figure 5.26 shows the horizontal geotextile displacements obtained from extensometer set E2, located 4.27 m above the slope base in row 15, along with superimposed smooth curves defined by fitting of the raw data, as explained next. The figure shows displacement distributions at different fill elevations, indicated by number of rows placed during construction.

The superimposed smooth curves in Figure 5.26 were used to evaluate the geotextile strain distribution. Geotextile strain values can be obtained by calculating the relative movements between extensometers and dividing them by the distance between measuring points. However, the use of raw extensometer displacement data to perform these calculations produces unclear reinforcement strain distributions since minor scatter in the displacement trend results in major oscillations in the calculated strain distribution. Consequently, the raw extensometer displacement information was initially smoothed by

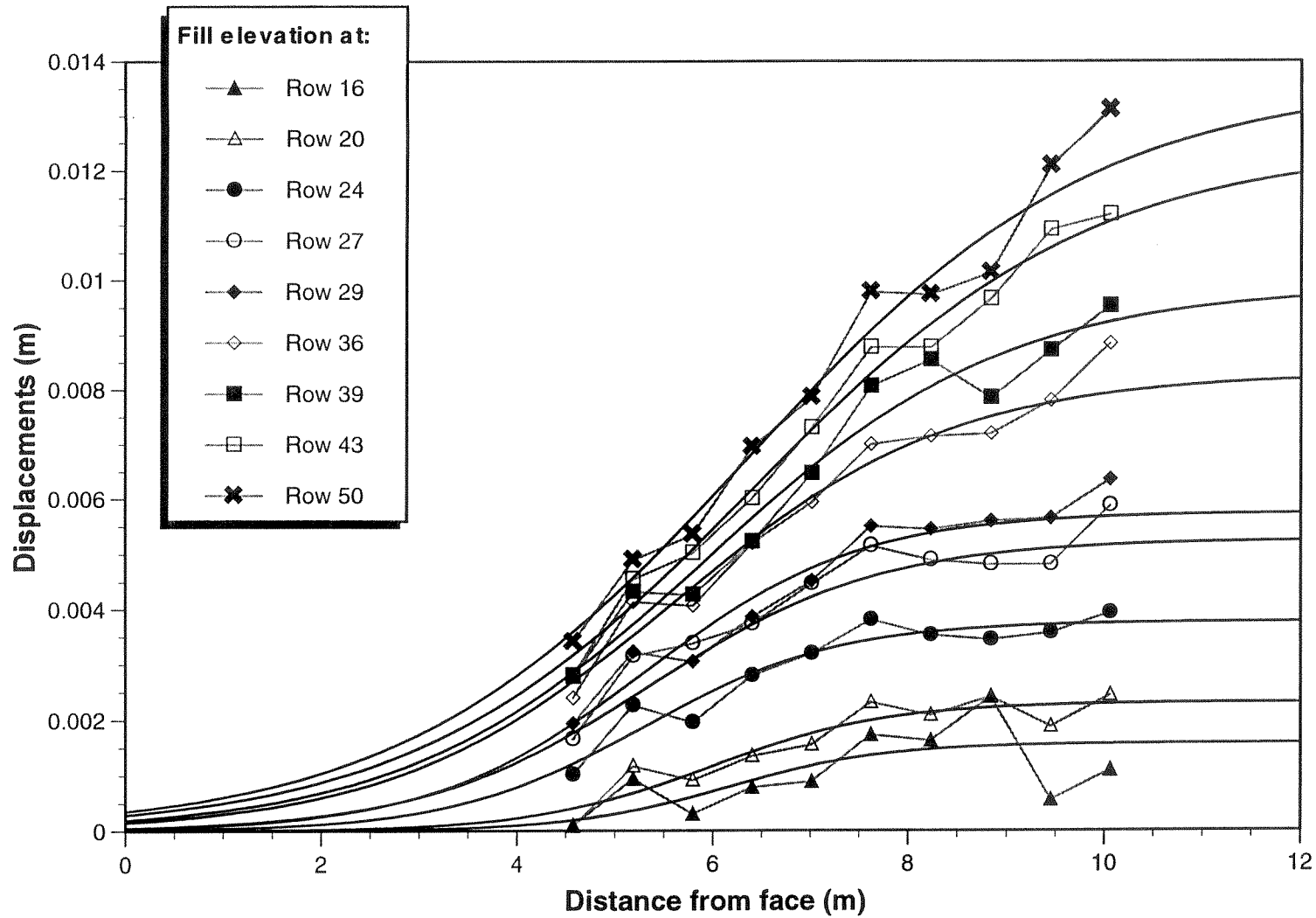


Figure 5.26 - Lateral displacements measured by extensometers attached to geotextile layer 15 (Extensometer set E2)

fitting the data to a monotonically increasing curve in order to better define the strain distribution. The expression used to fit the extensometer displacements is a sigmoid curve defined by:

$$d = \frac{1}{a + b e^{-cx}} \quad (5.1)$$

where d is the extensometer displacement, x is the distance from the structure face to the extensometer anchoring plate, and a , b , and c are parameters defined by fitting the curve to the raw data using the least squares technique.

The geotextile strain distributions at each construction stage can be obtained analytically from the derivative of the displacement function, and are indicated in Figure 5.27 for the case of extensometer set E2. The figure shows the strain distribution at different stages during the construction period.

The maximum strain ϵ_{\max} at the different construction stages and its location x_{\max} from the slope face can be determined analytically using the parameters a , b , and c that define the best-fitting curve for the extensometer data. The expressions are:

$$\epsilon_{\max} = \frac{c}{4a} \quad (5.2)$$

$$x_{\max} = -\ln\left(\frac{a}{b}\right) \cdot \left(\frac{1}{c}\right) \quad (5.3)$$

Although adding significant fluctuations to the strain distribution, calculations done using the raw relative movements between extensometer plates provide a trend similar to the one obtained by smoothing the raw data.

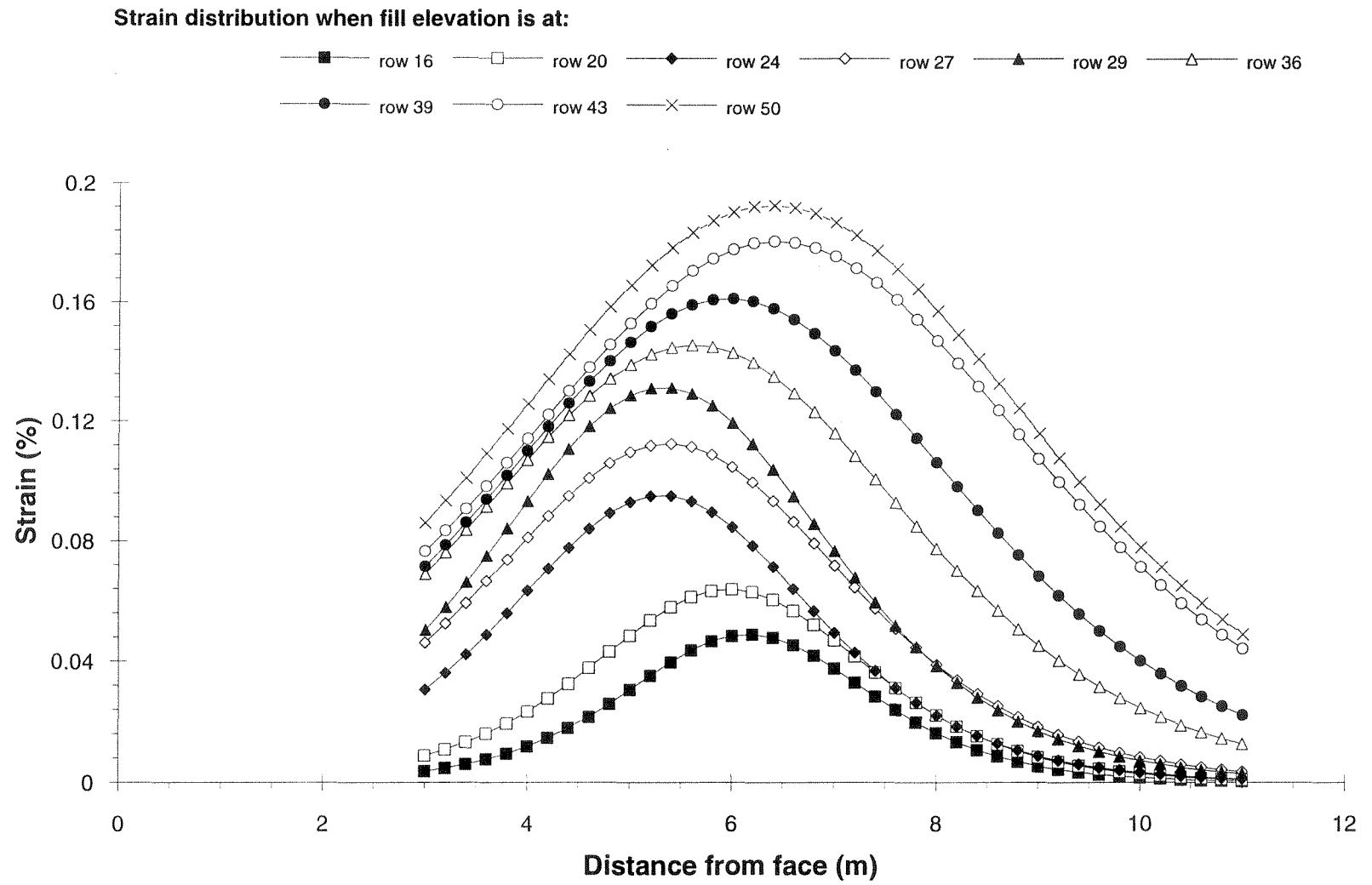


Figure 5.27 - Development of geotextile strains at geotextile layer 15 with increasing fill height

Extensometer displacement distributions similar to the one shown for extensometer set E2 were also obtained for the other extensometer sets. Figure 5.28 shows the horizontal geotextile displacements obtained from the extensometer set E1, located 1.22 m above the slope base, along with the superimposed smooth curves defined by fitting of the raw data. Figure 5.29 shows the horizontal geotextile displacements obtained for the case of extensometer set E4 located 9.14 m above the base of the slope at the level of layer 31.

Figure 5.30 shows the strain distribution in the different instrumented geotextile layers obtained from extensometer readings taken at different construction stages. A discussion on the locus of maximum reinforcement tensions indicated in the figure is discussed later in Section 5.6.1. The calculated maximum strains at the end of construction are 0.12 % for layer 5 (1.22 m high), 0.20 % for layer 15 (4.27 m high), and 0.16 % for layer 31 (9.14 m high). The strain levels in all the instrumented geotextile layers are very low.

5.5.2.2 Early post-construction period

Consistent with results obtained from inclinometer data, no post-construction movements were noticeable from the extensometer measurements taken after completion of the fill construction over the eight week monitoring period after construction. Figure 5.31 shows the progress of displacements measured by the extensometers until eight weeks following the end of construction for the case of extensometer set E2. Similar progress of extensometer readings with time was obtained for the instrument sets E1 and E4. Consequently, post-construction displacement results obtained during eight weeks

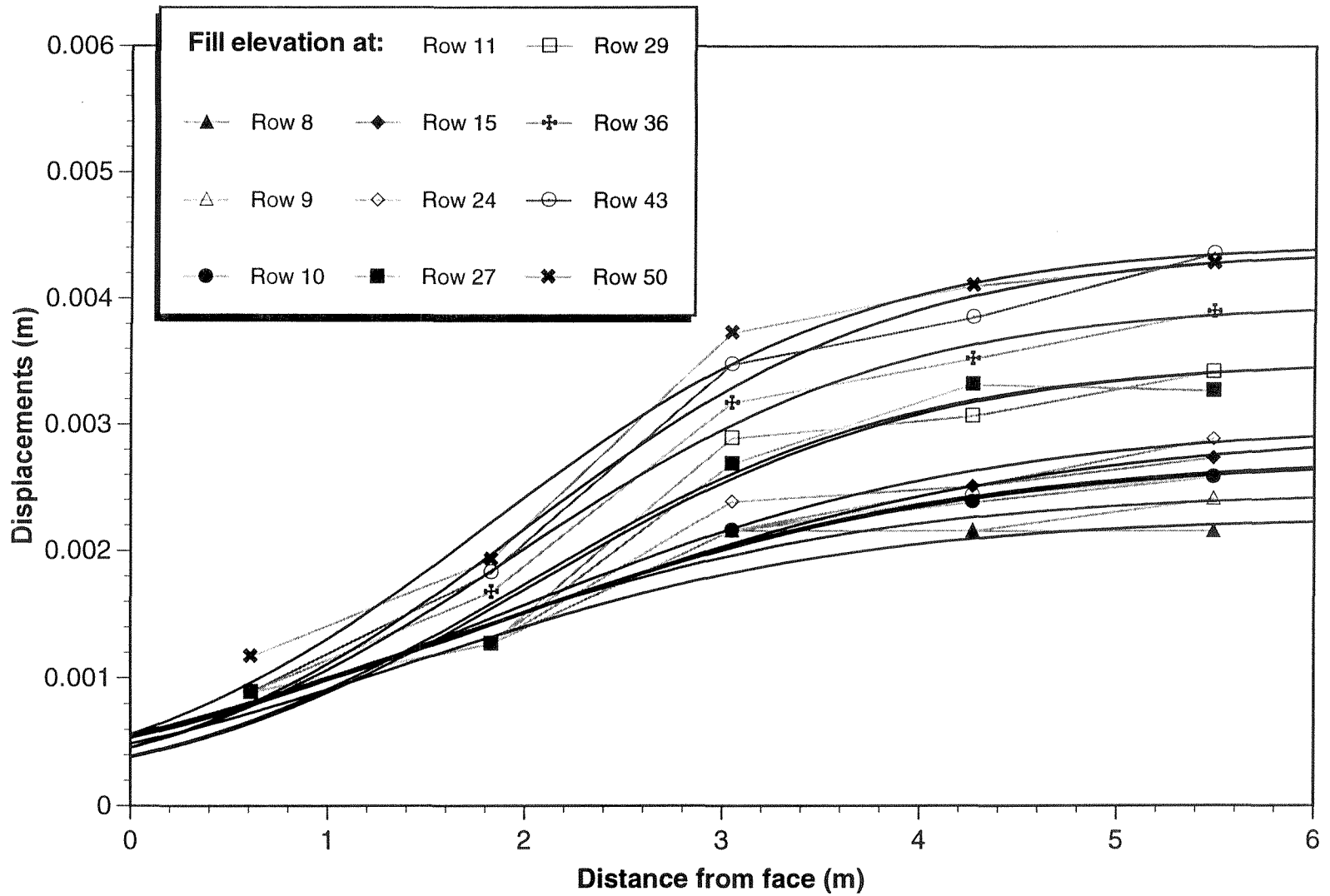


Figure 5.28 - Lateral displacements measured by extensometers attached to geotextile layer 5 (E1)

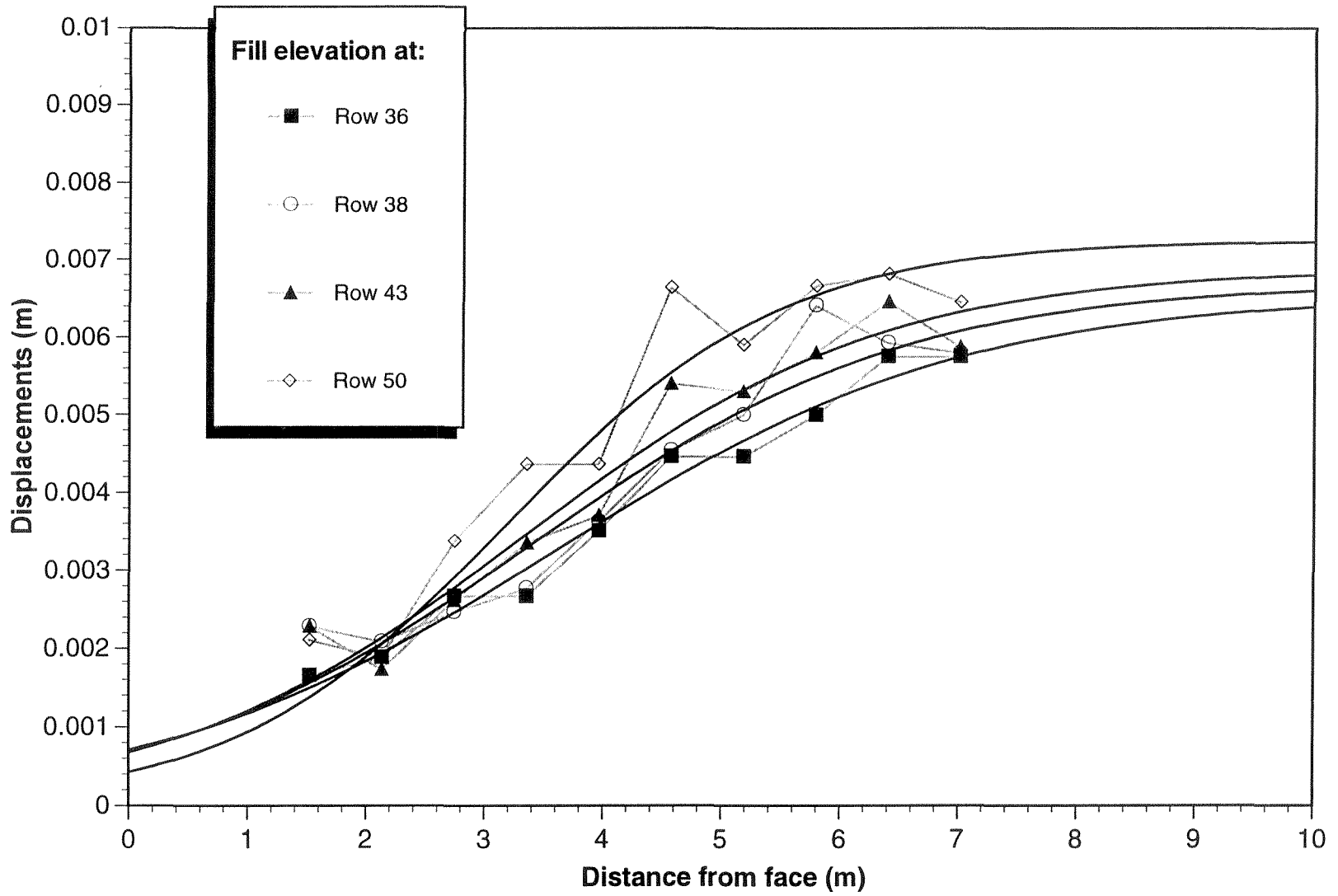


Figure 5.29 - Lateral displacements measured by extensometers attached to geotextile layer 31 (E4)

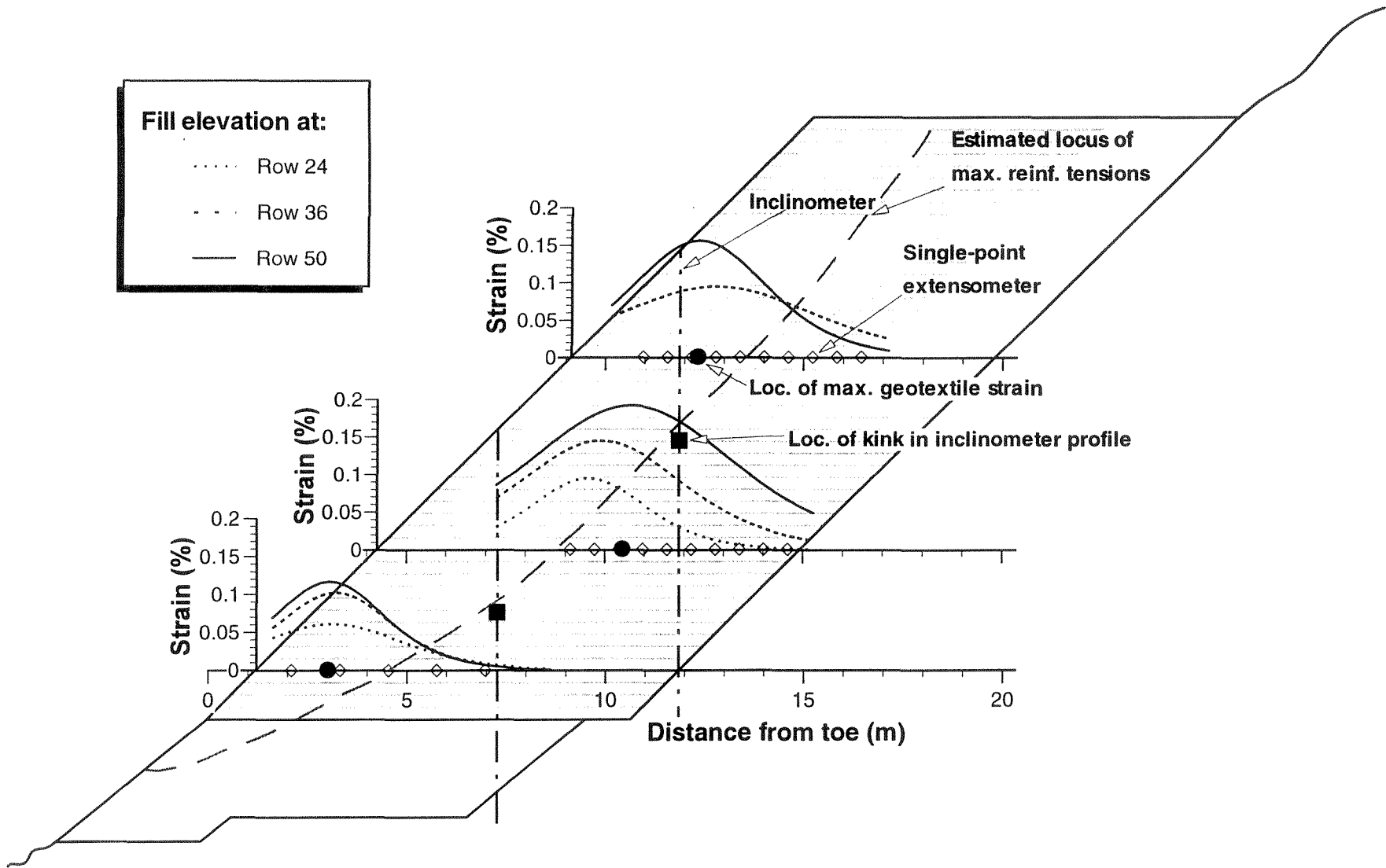


Figure 5.30 - Distribution of strains during construction in each instrumented geotextile layer

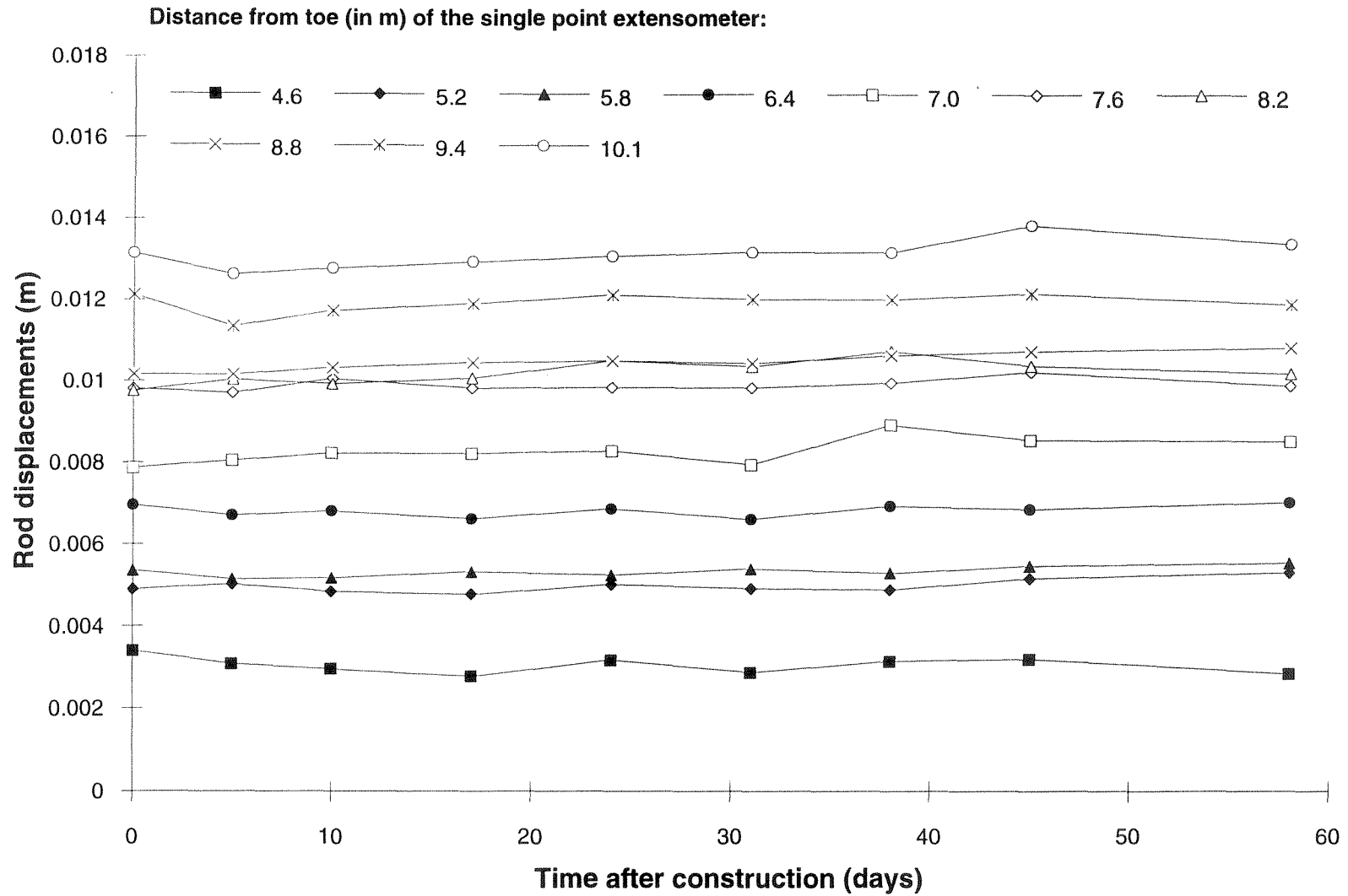


Figure 5.31 - Development of lateral displacements measured by extensometers set E2 during early post-construction

following the end of construction essentially reproduce the results obtained for at the end of construction (e.g., results for Row 50 in Figure 5.27). These displacement records resulted in almost no change in the geotextile strains during the eight weeks following the end of construction, and the strain distributions essentially reproduce the curves at the end of construction in Figure 5.30.

5.5.2.3 Spring measurements

Additional extensometer measurements were made during the spring runoff (on May 29, 1994). Slight movements were recorded by the mechanical extensometers, that resulted in small increases in the estimated strain distribution at the instrumented geotextile layers. Figure 5.32 compares the strain distribution estimated using the spring extensometer measurements with those obtained at the end of construction. The calculated maximum strains obtained from the spring monitoring results are 0.15 % for layer 5 (1.22 m high), 0.225 % for layer 15 (4.27 m high), and 0.19 % for layer 31 (9.14 m high). The increase in maximum strains is approximately of 0.03% for the three instrumented layers. Extensometer monitoring results may also incorporate small differential settlements that may have occurred in the fill during winter and spring seasons. As previously mentioned in relation to the global structure deformations, structure deformations and geotextile straining were expected to occur during the winter, but the measured values are smaller than anticipated.

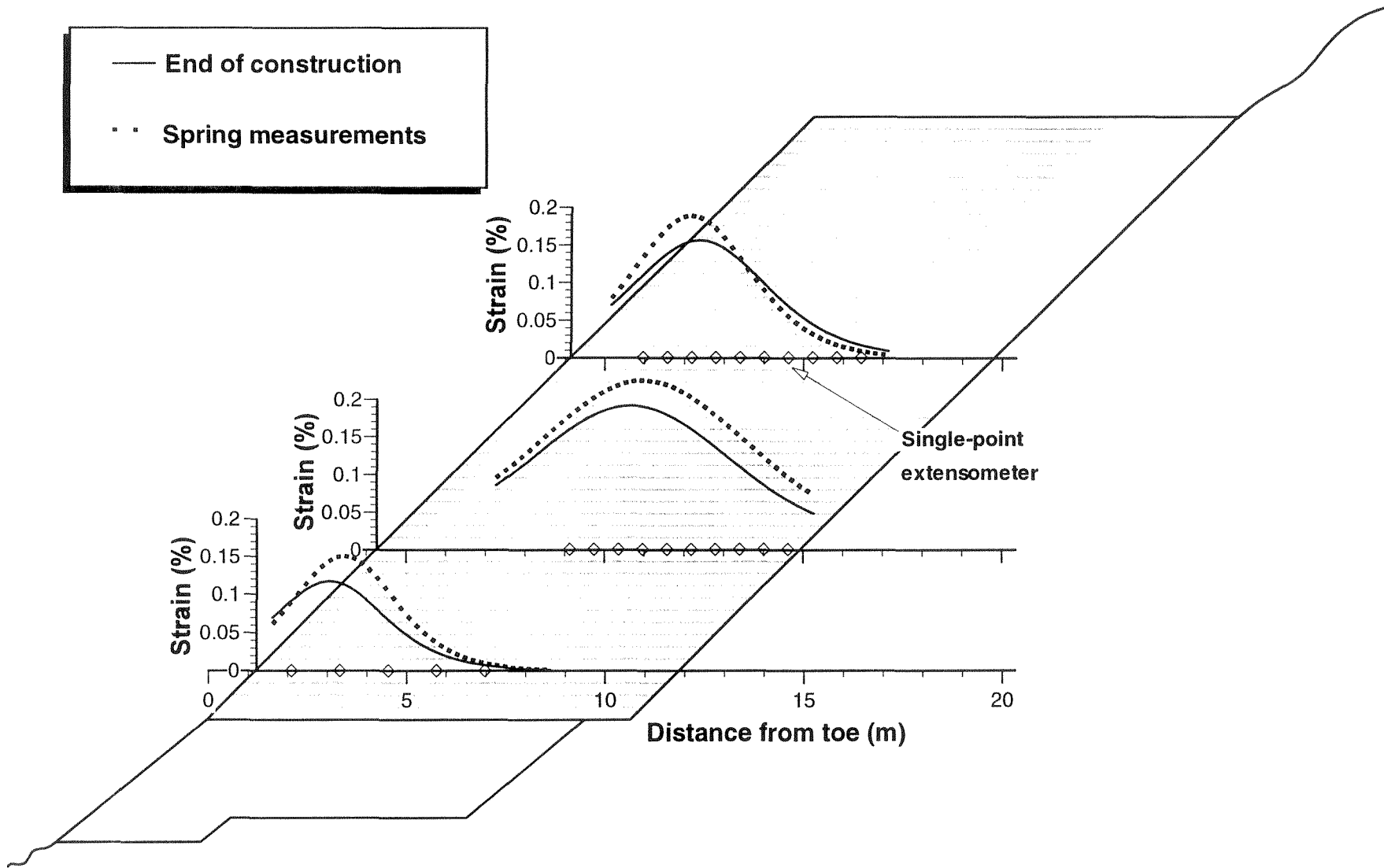


Figure 5.32 - Distribution of strains from spring measurements in each instrumented geotextile layer

5.5.3 Cross-check of displacement measurements

The pair of inclinometers installed within the reinforced zone allowed for the determination of differential soil movement between them. This was particularly useful in order to cross-check inclinometer displacements with the displacements obtained from extensometers mounted on the reinforcements. Considering the location of extensometers and inclinometers (Figure 5.10) this cross-check can be particularly useful at the level of extensometer set E2 (4.27 m high), which is at a geotextile layer that intercepts both inclinometers. Figure 5.33 shows the relative horizontal displacements between inclinometers SI1 and SI2, at the level of extensometer set E2. The progress in relative displacements with increasing fill elevation obtained from extensometer E2 readings is also indicated in the figure, and agrees very well with the displacement progress obtained from the inclinometer monitoring results. This validation supports the accuracy of the displacements interpreted from both inclinometer and extensometer measurements.

Average soil horizontal strains, obtained from inclinometer measurements between the locations of inclinometers SI1 and SI2 can also be estimated. Figure 5.34 compares the geotextile strain distribution previously obtained from the extensometer set E2 with the average horizontal soil strains defined from the inclinometer measurements. The arrows in the figure indicate the location of the inclinometers. Strain values obtained from inclinometer readings compare very well with the average strain between the two inclinometers, as estimated from the curves defined by extensometer readings. The good agreement found between the results obtained from these two different instrumentation sources, provides confidence on the estimated geotextile strains.

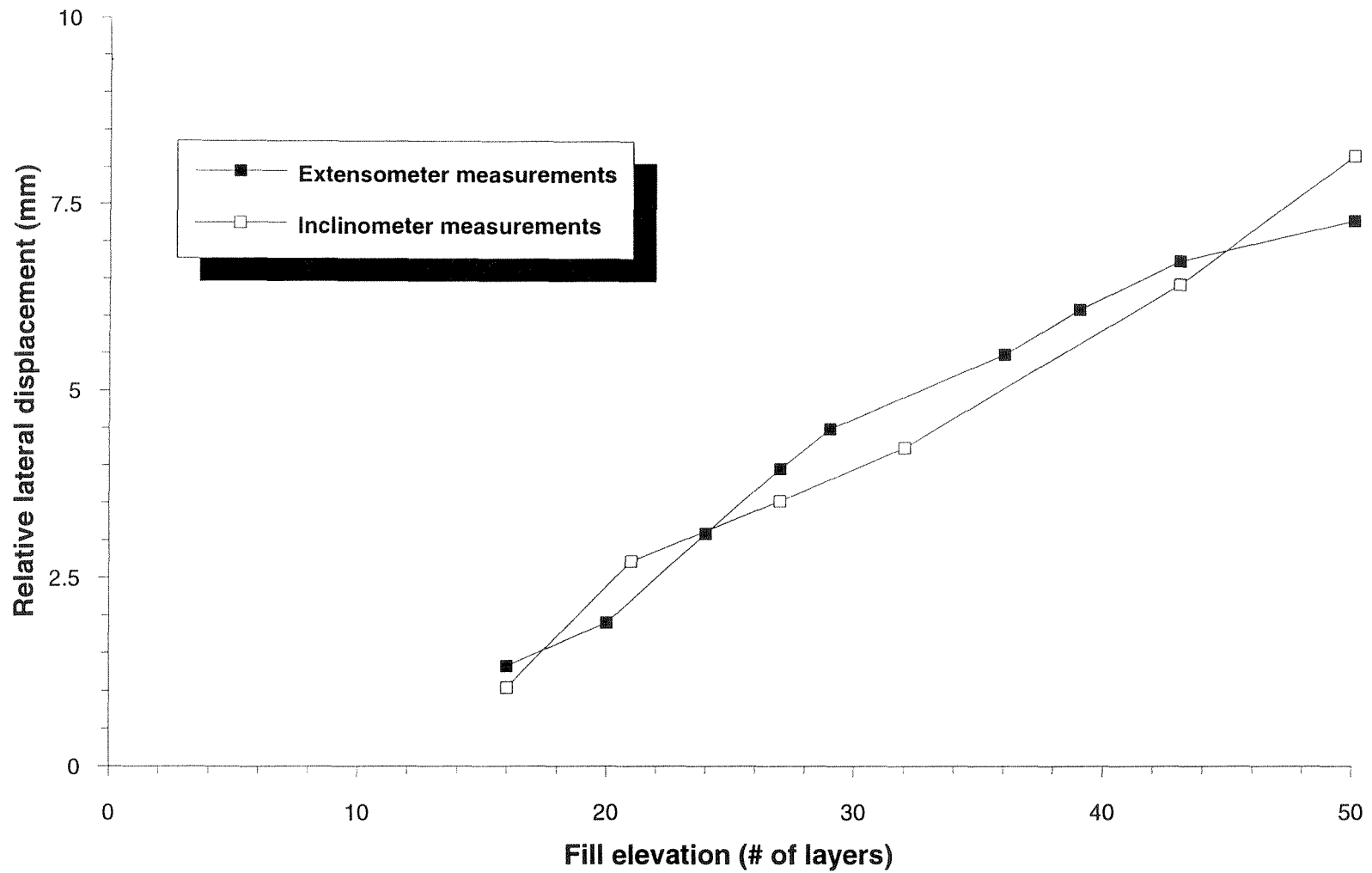


Figure 5.33 - Development of relative displacements with increase in fill height, as measured by inclinometers and extensometers (horizontal displacements between S11 and S12 at the level of E2)

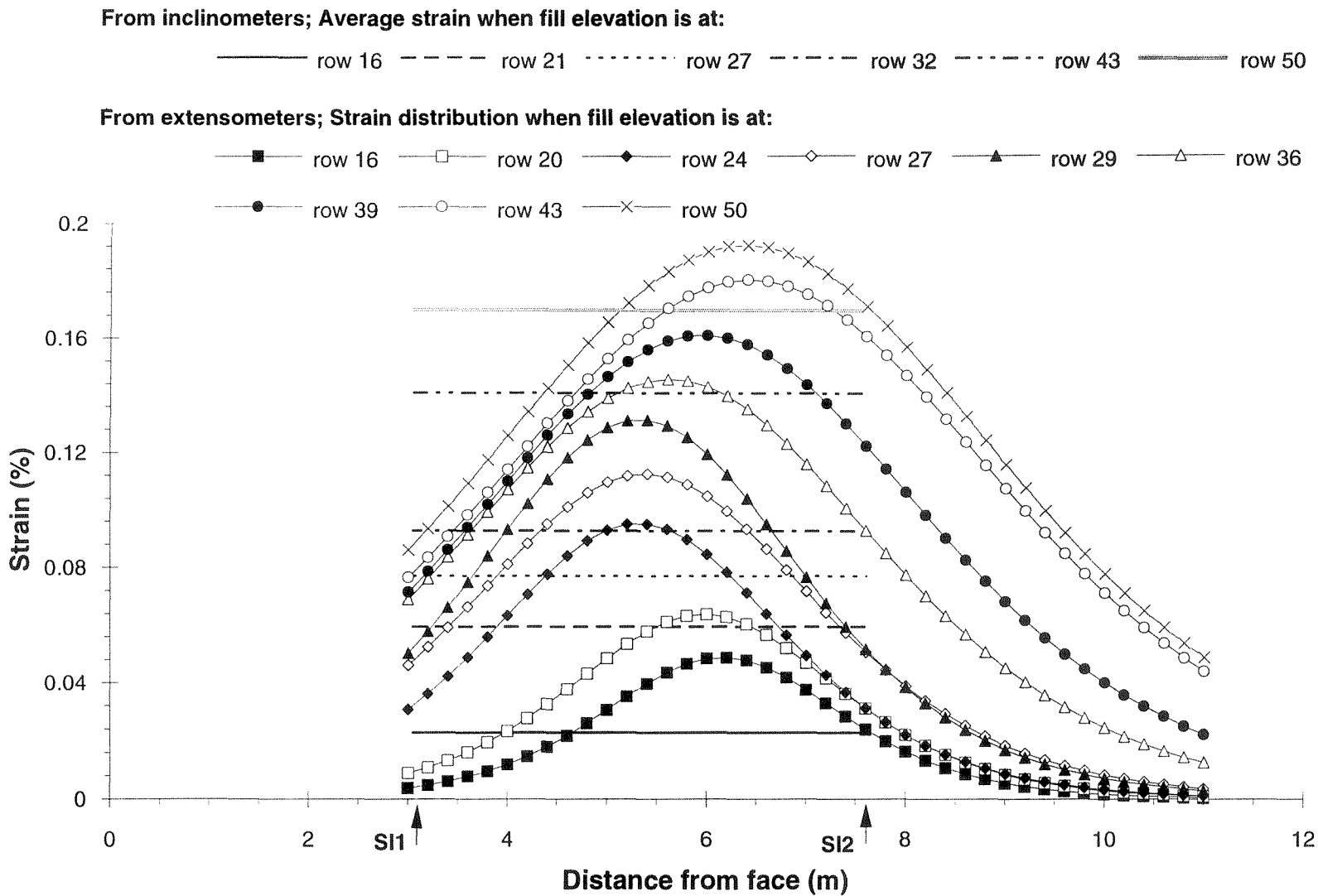


Figure 5.34 - Development of strains at geotextile layer 15 with increase in fill height (from inclinometer and extensometer measurements)

5.5.4 Pore water pressures

Recording for all pore pressure channels started on August 12, after amplifiers were calibrated. The signal-conditioning circuitry and recorder were programmed to sense the pore-water pressure at each sensor every 30 minutes in order to determine the daily minimum, maximum, and average of those readings. As previously mentioned, the air vent tube for the piezometer installed within the fill (PP4) was severed during construction. The readings from this piezometer showed that the transducer is probably not venting properly due to drops of water in the line, and the output most probably reflects atmospheric changes and/or moisture accumulation through the splice. Negative pore water pressures of almost -5 kPa were initially recorded which erratically decreased and turned positive after 200 days of recording. The other three transducers had no installation problems and appeared to work properly.

Figure 5.35 shows the pore water pressures measured in piezometers PP1, PP2, and PP3, located at the back of the reinforced fill at elevations 0.3 m, 1.8 m, and 4.27 m respectively. As expected, piezometer PP1 showed some response since it was installed in a seepage area of the backslope bedrock. Some spikes can be observed on the PP1 measurements during the fall and winter seasons, that are most probably a response to several rain storms occurred during this period. Pore water pressures from the piezometer located the base of the slope increased during the spring thaw up to an average of 5 kPa. However, these positive pore water pressures recorded during the thaw period are small (less than 10 kPa), and the bottom of the fill appears to be draining properly through the rock shear key. Piezometers PP2 and PP3 show negligible (either positive or negative) pore water pressures throughout the monitored period. These results indicate that no

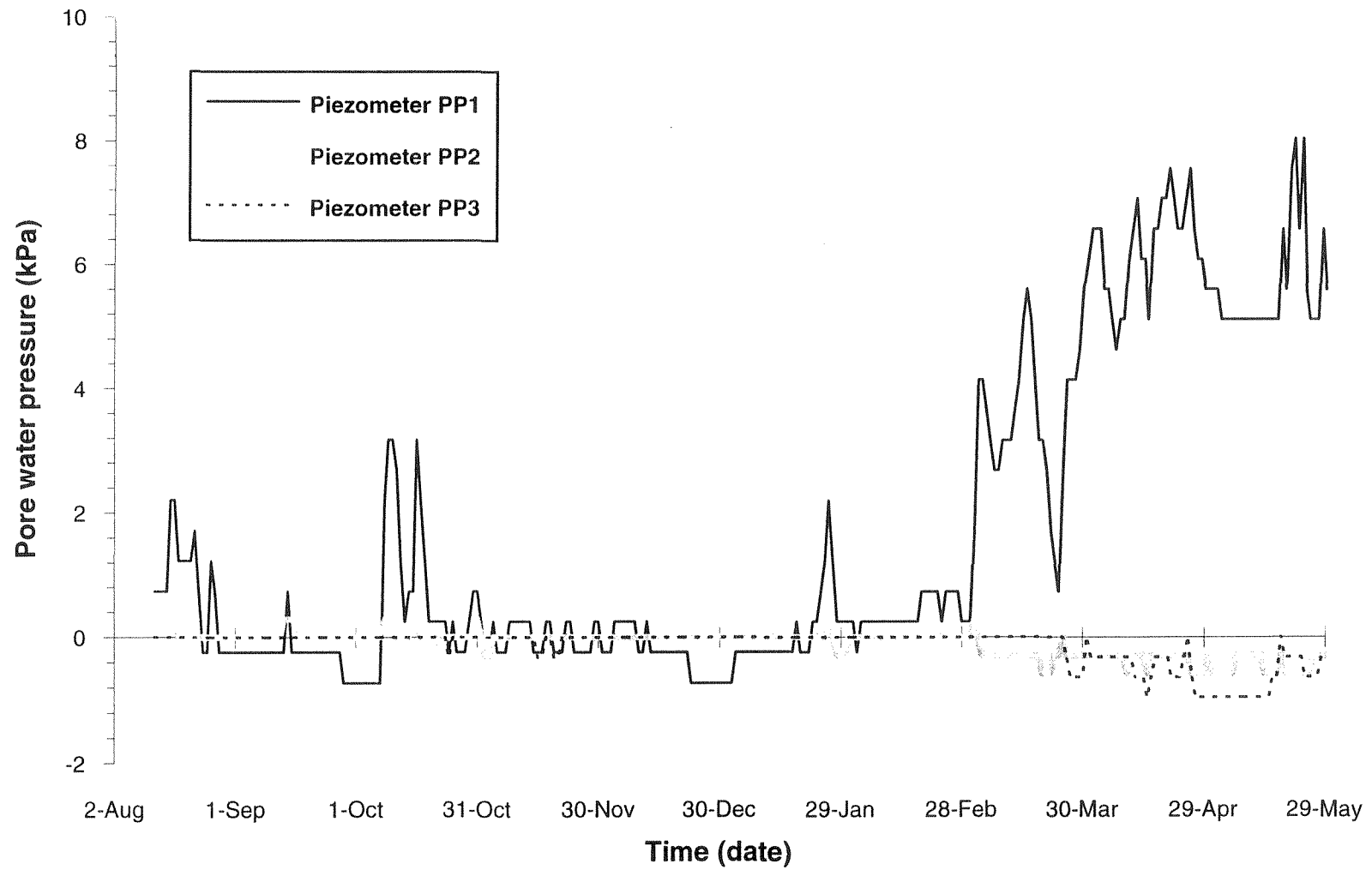


Figure 5.35 - Pore water pressure measurements

destabilizing flow configuration, originated by seepage from the backslope fractured rock, is occurring within the reinforced soil mass. The pore water pressures monitored until the first spring after construction confirm that a separate drainage system was not necessary at the back of the slope.

5.6 Implications for design

5.6.1 Suitability of current design approach

Limit equilibrium methods have been conventionally used in the analysis of reinforced soil slopes to determine the required geotextile layer spacing and reinforcement tensile strength. The suitability of these methods for predicting the failure of geotextile-reinforced slopes was evaluated in the centrifuge study presented in Chapter 4 of this dissertation. These methods are techniques for conventional slope stability analysis, adapted to take into account the stabilizing moment created by the reinforcements. Under working stress conditions, the location of the potential failure surface for internal stability verification purposes has been generally identified as the locus of the maximum stresses (or strains) in the reinforcements. In order to define this locus, Figure 5.30 indicates the location of maximum geotextile strains at the end of construction in each of the instrumented layers (solid circles). The location of the previously mentioned kinks in inclinometer profiles SI1 and SI2 (solid squares) may provide additional field evidence of the locus of maximum strains. One of the possible loci of maximum reinforcement tensions that can be inferred from these features of the instrumentation results is indicated in the figure. Although the strain levels are too low to expect a well defined line of maximum tension in the reinforcements, the indicated locus agrees with the critical

surface defined by conventional limit equilibrium analysis. The field instrumentation results appear to be consistent with the use of limit equilibrium methods as a design basis for geotextile-reinforced soil slopes.

The preceding evaluation is for internal stability purposes since the location of potential failure surfaces not crossing the instrumented reinforcements cannot be assessed from the collected data. Consequently, compound or external potential failure surfaces cannot be inferred from the information provided by the inclinometer and extensometer readings. Nevertheless, these external modes of failure should be contemplated in design. In fact, external stability considerations during design stages of the structure led to the adoption of a rock shear key at the base of the reinforced slope.

5.6.2 Geotextile strain levels

The maximum strains observed in the three instrumented geotextile layers are on the order of 0.2%. These are very low strain levels, especially if we consider that extensometers report global strains, comparable with the soil strains obtained from inclinometer readings. Global strains may be higher than the local strains that may actually occur in the geotextile layers because extensometer readings incorporate the effect of geotextile macrostructure, and local effects such as geotextile creases and folds.

These strain levels are notably lower than the relatively large geotextile strains at which the design strength would typically be developed. However, the low strain levels obtained from field monitoring in the structure under study are consistent with previous experiences of well instrumented geotextile-reinforced structures. A good example is the geotextile-reinforced wall evaluated as part of the finite element study presented in

Chapter 3 of this dissertation. That reinforced wall, 12.6 m high with a surcharge fill more than 5 m in height, has been extensively instrumented, and its performance was reported by Christopher et al. (1990) and Allen et al. (1991). Although that temporary structure was designed with low factors of safety, and it was a vertically faced wall, the maximum global strains obtained from extensometer readings were less than 1%. The strain levels in the Idaho slope are expected to be comparatively lower than those in the vertical wall since, both structures have a comparable height, and the Idaho slope is a permanent structure designed with much higher factors of safety and a 1H:1V slope face.

The maximum strain levels obtained from the extensometer measurements in this study are also in good agreement with peak strains monitored in geotextile- and geogrid-reinforced slopes built as part of a Federal Highway Administration project on the behavior of reinforced soil (Christopher et al., 1992). In that case, the maximum strain levels for 1H:1V reinforced slopes were on the order of 0.3%, while the peak strains for 1H:2V reinforced slopes were approximately 0.7%. The small maximum strains obtained from monitoring records of this and other geosynthetically reinforced slopes indicate that current design factors of safety are extremely conservative. The geotextile strain levels are much lower than those assumed in current design to define the required tensile strength of the reinforcements. The low strain level in the geotextiles show that the backfill soil, and not the geosynthetic reinforcements controls the strain in the reinforced soil mass. In order to further evaluate the performance of the structure under working stress conditions, deformation analyses should be pursued and the stress-strain relations of geotextiles at low strain levels, mainly under confined condition, should be investigated.

5.6.3 Global structure deformation and post-construction performance

As monitored by the two inclinometers installed within the fill and confirmed by survey measurements, very small lateral deflections occurred in the reinforced fill (maximum displacements of 30 mm approximately). The accuracy of these horizontal displacements was validated by cross-checking the inclinometer data with the displacements obtained from extensometers mounted on the reinforcements. Small structure displacements are also confirmed by survey measurements on the slope face.

No time-dependent deformations were observed in the geotextile reinforced slope, monitored continuously for eight weeks following the end of construction. Only small additional deformations were observed from the monitoring results taken during the spring, eight months after construction. Consequently, as shown by all extensometer and inclinometer data, the geotextile has performed without any time-dependent degradation, and no creep movements were detected. The spring measurements also indicate that apparently no relevant settlements occurred due to hydrocompression (soil structure collapse due to wetting) of the decomposed granite backfill. The global deformation results obtained for the reinforced slope under study indicate that the safety allowances used in its design resulted in a structure that meets the deformation serviceability requirements.

5.6.4 Ability of geotextile reinforcements to control pore water pressures in the fill

Based on the pore water pressures monitored since construction of the reinforced slope during the summer of 1993 and through the following spring, it can be inferred that

destabilizing flow is not occurring within the reinforced soil mass. As previously mentioned, the pore water pressure monitoring records indicate that a separate drainage system was not necessary at the back of the slope. It is worth recalling that the instrumented slope under study constitutes a permanent structure in a major roadway and, consequently, comparative approaches like constructing a second instrumented cross section reinforced using impermeable reinforcements was not possible. Nevertheless, the monitored pore water pressure results provide additional evidence that the selection of permeable reinforcements was appropriate since the reinforced slope performed as intended during the spring thaw.

5.6.5 Additional considerations

In addition to the information provided by the instrumentation monitoring results, lessons can also be learned from the construction procedures adopted for the nonconventional geotextile-reinforced soil structure described in this study. The time required for construction of the reinforced slope was substantially less than mechanically stabilized earth walls of comparable size also constructed on the widening project of U.S. Highway 93. It is worth noting that the construction crew had no previous experience on reinforced soil construction.

The contractor selected a 1:1 forming system, which allowed proper compactive effort at the face of the embankment. However, stepped vertical faces might have required less hand labor and may have been a better choice. In selecting the long term face stabilization method not only erosion control, but also esthetics were carefully evaluated at the design stages. The use of an erosion control matting and subsequent

seeding of the slope face proved very successful, as judged by the excellent vegetation of the slope face observed during the spring, which blends well with the surrounding environment. Elimination of the face wrap could have reduced the costs without compromising face stabilization of the slope.

Finally, the geotextile-reinforced slope evaluated in this study provides construction experience with the use of decomposed granite as embankment fill material. All materials required as backfill for the reinforced slope were obtained from roadway construction without processing. As previously discussed, the fill was placed approximately at the optimum water content and easily compacted using standard static compaction equipment. From the evaluation of the performance of the structure after eight months of construction, no settlements due to hydrocompression of the decomposed granite were detected even though the fill may have been wetted due to rainstorms and melting snow during the monitoring period.

5.7 Conclusions

The instrumentation program detailed herein has evaluated the performance of a 1H:1V slope 15.3 m high, constructed using decomposed granite as backfill material. High modulus composites and nonwoven geotextiles were selected as reinforcements after considering their potential in-plane drainage capacity to allow dissipation of pore water pressures that could be generated in the fill. An extensive monitoring program was implemented that included the installation of inclinometers, mechanical extensometers, piezometers and survey points.

Time required for the construction of the instrumented embankment was substantially less than for other retaining structures of comparable size constructed on the same project. Results from the instrumentation program indicate an excellent performance of the slope, with small global deflections (on the order of 30 mm) and low geotextile strain levels (on the order of 0.2%). A procedure for representation of extensometer measurements was developed, which assisted in the interpretation of the geotextile strain distributions. Cross-check of extensometer and inclinometer measurements showed very good agreement, providing confidence on the monitoring results. No time dependent movements were observed during continuous monitoring for eight weeks after completion of construction, and only slight additional movements were observed eight months after the end of construction during the spring thaw. The locus of maximum reinforcement tensions estimated from field instrumentation results is consistent with the location defined using design methods for internal stability analysis of reinforced slopes based on limit equilibrium. Pore water monitoring at the back of the reinforced slope indicates appropriate drainage of the seepage water from the backslope rock mass. The low strain levels observed in the experimental structure under study indicate that further cost reductions could be achieved by eliminating face wrap and reducing factors of safety. The monitoring results provide insight into the mechanisms that dominate the behavior of geotextile-reinforced slopes, and support the selection of reinforcement materials and the design procedures considered in this project.

References

- Allen, T. M., B. R. Christopher and R. D. Holtz. (1991). "Performance of a 12.6 m high geotextile wall in Seattle, Washington." *Proc., International Symposium on Geosynthetic-Reinforced Soil Retaining Walls*, J. T. H. Wu, eds. Denver, Colorado: A.A. Balkema, August, 81-100.
- Barrows, R. J. and Lofgren, D. C. (1993). *Salmon-Lost Trail Pass Highway Idaho Forest Highway 30 Earth Retention Structures Report*, Geotechnical Report No. 20-92, FHWA, U. S. Department of Transportation, February 1993.
- Burwash, W.J. and Frost, J.D. (1991). "Case History of a 9 m High Geogrid Reinforced Retaining Wall Backfilled with Cohesive Soil", *Proceedings of Geosynthetics '91 Conference*, Vol.2, Atlanta, USA, pp. 485-493.
- Christopher, B., C. Bonczkiewicz and R. Holtz. (1992). "Design, construction and monitoring of full scale test of reinforced soil walls and slopes." *Recent case histories of permanent geosynthetic-reinforced soil retaining walls*, F. Tatsuoka and D. Leshchinsky, eds. Tokyo, Japan: A.A. Balkema, 45-60.
- Christopher, B.R., Holtz, R.D. and Allen, T.M. (1990). "Instrumentation for a 12.6 m high geotextile-reinforced wall", *Performance of Reinforced Soil Structures*, London, pp. 73-78.
- Christopher, B. R., Gill, S.A., Giroud, J.P., Juran, I., Mitchell, J.K., Schlosser, F. and Dunncliff, J. (1990). *Design and construction guidelines for reinforced soil structures - Volume I*, Report No. FHWA-RD-89-043, Federal Highway Administration, U.S. Department of Transportation, November 1990.

- Huang, C.C. (1992). "Report on Three Unsuccessful Reinforced Walls", *Recent Case Histories of Permanent Geosynthetic-Reinforced Soil Retaining Walls*, Tatsuoka, F. and Leshchinsky, D., Eds., Balkema 1994, Proceedings of the symposium held in Tokyo, Japan, November 1992, pp. 219-222.
- Jewell, R.A. (1985). "Limit equilibrium analysis of reinforced soil walls", *Proceedings of the XI ICSMFE*, San Francisco, Vol.3, pp. 1705-1708.
- Parfit, M. (1992). "The hard ride of route 93," *National Geographic*, Vol. 182, No. 6, December 1992, pp. 42-69.
- Peck, R.B. (1988). Foreword to *Geotechnical Instrumentation for Monitoring Field Performance* by Dunnicliff, J., J. Wiley & Sons, 577 p.
- Perrier, H., Blivet, J.C., and Khay, M. (1986). "Stabilization de Talus par Renforcement tout Textile: Ouvrages Experimental et Reel", *Proceedings of the Third International Conference on Geotextiles*, Vol. 2, Vienna, pp. 313-318.
- Prellwitz, R.W. and Babbitt, R.E. (1984). "Long-term groundwater monitoring in mountainous terrain", *Transportation Research Record* 965, pp. 8-15.
- Tatsuoka, F., Murata, O., Tateyama, M., Nakamura, K., Tamura, Y., Ling, H.I., Iwasaki, K. and Yamauchi, H. (1990). "Reinforcing Steep Clay Slopes with a Non-woven Geotextile", *Performance of Reinforced Soil Structures*, McGown, A., Yeo, K. and Andrawes, K.Z., Eds., Thomas Telford Ltd., London, pp. 141-146.
- Wayne, M. H. and Barrows, R.J. (1994). "Construction damage assessment of a nonwoven geotextile," *Transportation Research Board Annual Proceedings*, paper no. 940703, January 1994.

Yapa, K.A.S., Mitchell, J.K. and Sitar, N. (1993). *Decomposed granite as an embankment fill material: Mechanical properties and the influence of particle breakage*, Geotechnical Engineering Report No. UCB/GT/93-06. Department of Civil Engineering, University of California, Berkeley.

CHAPTER 6

SUMMARY AND CONCLUSIONS

"It goes without saying that theoretical analyses, if used without judgement, are worthless and may even lead to disaster . . . the main aim in any study of fundamentals is the development of sound judgement."

D.W. Taylor (1948)

The increasing use of geotextile-reinforced systems for important earth structures requires proper understanding of their behavior and validation of the assumptions in their design. Geotextile reinforcement materials are particularly useful in reinforced soil systems built using indigenous backfill soils, which may be finer grained, more plastic and less permeable than fill materials commonly specified in soil reinforcement practice. Four aspects of the performance of geotextile-reinforced soil structures were investigated as part of this research by performing: (1) An evaluation study of the suitability of poorly draining soils for reinforced soil structures; (2) a finite element study on the deformability and design aspects of geotextile-reinforced soil walls; (3) a centrifuge study on the failure mechanisms and on the suitability of limit equilibrium methods to predict failure of

geotextile-reinforced soil slopes; and (4) a field instrumentation study to evaluate the performance of a permanent geotextile-reinforced slope built using decomposed granite as backfill material. Each analysis provides specific lessons useful for understanding the performance of the engineered composite material which is reinforced soil. Collectively, they illustrate that the behavior of reinforced soil structures (and probably of earth structures in general) may defy characterization by a single method of analysis. Instead, by complementing strengths and limitations of different approaches, good understanding of many facets in the performance of a geotechnical structure can be achieved.

Given the individual objectives and the specific background of each aspect of the research, the information in each chapter is presented in a self-contained manner. Objectives, background, conclusions, and references were separately indicated in each chapter. The main conclusions reached in each facet of this study are summarized below.

An evaluation study on the performance of reinforced soil structures with poorly draining backfills was initially undertaken. Although reported results from experimental studies on triaxial, direct shear and pullout tests have led to contradictory conclusions on the effects of impermeable reinforcement layers, there is already strong experimental evidence that permeable reinforcements can effectively reinforce poorly draining backfills. If permeable geosynthetics are used to reinforce poorly draining backfills, the geosynthetic layers can function not only as reinforcements but also as lateral drains. Although theoretical methods have been proposed to evaluate the dissipation of pore water pressures generated during construction using a saturated backfill, the hydraulic function of reinforcements has yet to be incorporated into reinforced soil design. Available data on

the long-term performance of geosynthetics in marginal soils has so far shown adequate durability and creep characteristics of the tested geotextile samples.

Benefits and applications of reinforcing poorly draining backfills were addressed, and research needs aimed at formulating a consistent design methodology for these structures were presented. The use of fine-grained poorly draining materials in reinforced soil structures could reduce the cost of projects that would otherwise require granular material to satisfy current specifications, and could broaden the range of use of soil reinforcement to new applications. No consistent design methodology for reinforced soil structures containing poorly draining backfills has been developed. Nevertheless, a number of structures has been constructed, and the performance of some of them has been reported. Reduced and full-scale reinforced soil structures with poorly draining backfills were evaluated, focusing particularly on the generation of pore water pressures in the fill, on the possible modes and causes of failure, and on the structure deformability. Analysis of these case histories shows that large movements were generally recorded in reinforced structures when pore water pressures were generated in the fill, especially in those containing metallic reinforcements. Thus, good performance strongly depends on prevention of excess pore water pressure development within the fill material. This conclusion is strengthened by the fact that the failure cases reported so far involved poorly draining backfills that became saturated due to surface run-off, and were reinforced with impermeable inclusions.

In order to reinforce marginal soils, it is apparent that new synthetic materials with both high in-plane drainage capacity and high tensile strength and stiffness will be valuable. Composite geosynthetics, that combine the hydraulic properties of nonwovens

with the mechanical characteristics of geogrids or wovens, are probably the most appropriate reinforcement for marginal soils.

A finite element study on the performance of geotextile-reinforced soil structures with sloping backfills was performed in order to evaluate the deformability and design aspects of these structures. The approach involved the initial interpretation of instrumentation results from a full-scale wall, the subsequent validation of the numerical model against the field data, and finally the numerical simulation of new design aspects. The effect of sloping backfills on the location of the potential failure surface was of particular relevance in these analyses.

The finite element analysis of a well instrumented geotextile-reinforced soil wall with a sloping backfill surcharge was initially performed, and the numerical results added useful information to the available field records. Good agreement was found between the numerical results and the different instrumented responses of the instrumented wall (geotextile tension distribution, lateral displacements, vertical stresses). Moreover, the in-situ geotextile stiffness, back calculated by matching the available instrumentation records to the finite element results, was found to vary from twice to four times the values determined from laboratory unconfined wide width tensile tests.

Using calibrated input parameters and modeling procedures obtained from the back analysis of the instrumented wall, a parametric study was performed to investigate the effect of sloping backfill surcharges on the performance of geosynthetically reinforced soil walls. The analyses showed that, for practical purposes, the location of the critical planar potential failure surface is independent of the presence of a sloping backfill surcharge on

the top of the wall. This was found to be true independently of the sloping surcharge geometry (surcharge slope and surcharge height), and of wall design characteristics (wall height and reinforcement stiffness). A Rankine failure surface was found to provide a conservative, however suitable, design basis for separation of the active and resistant zones within geosynthetically reinforced walls with sloping backfills.

A centrifuge study to investigate the performance of geotextile-reinforced soil slopes at failure was subsequently undertaken. A series of geotextile-reinforced slope models was tested in order to identify the possible failure mechanisms and to verify the ability of limit equilibrium methods to predict the experimental results. The variables considered in the study were reinforcement spacing, reinforcement tensile strength, and soil strength, which can all be taken into account using conventional limit equilibrium analyses. An extensive testing program was also performed in order to evaluate the strength properties of the sand used as backfill material, of the geotextile reinforcements, and of several interfaces that could influence the performance of the slope models. The geotextile tensile strength was found to depend on the testing boundary conditions, which should be selected to properly represent the in-soil operational conditions.

All slope models built using the same backfill soil gave a single normalized Reinforcement Tension Summation, which can be interpreted as an earth pressure coefficient that only depends on the soil strength and on the slope inclination. Failure of all centrifuge slope models was observed to initiate at midheight of the slopes, contradicting current design assumptions that failure should develop from the toe of the reinforced slopes. Consequently, a reinforcement force distribution with depth was

proposed for reinforced soil slopes under working stresses, which is consistent with the experimental observations and which leads to an approximately uniform distribution with depth at the moment of failure. An important contribution to the stability of the models was provided by the overlapping geotextile layers, which failed by breakage instead of pullout when intersected by the failure surfaces. Moreover, the stability of the reinforced slopes was found to be governed by the peak shear strength and not by the critical state friction angle of the backfill soil.

The suitability of limit equilibrium methods for the analysis of geotextile-reinforced slopes was evaluated by comparing the centrifuge test results with theoretical predictions. A rigorous limit equilibrium method that assumes circular failure surfaces was selected for the study. The effect of different modeling assumptions on the calculated factors of safety was initially investigated by performing a parametric study of variables relevant to the stability of the models. These assumptions related to the effect of the in-soil geotextile tensile strength, the nonuniformity of the unit weight within the centrifuge model, the orientation of reinforcement forces, the geotextile overlapping layers, the lateral friction against walls of the centrifuge box, and the selected method of slope stability analysis. A very good agreement was obtained between the limit equilibrium predictions and the experimental results. The good agreement included both the g-level at failure and the location of the failure surfaces in the centrifuge models. Different rigorous limit equilibrium methodologies currently used for the analysis of reinforced soil slopes were also found to provide equally good results. Moreover, the centrifuge testing of reinforced slope models provided insight into the evaluation of in-soil strength properties of geotextiles.

A field instrumentation study to investigate the performance of geotextile-reinforced soil structures under working stress conditions was finally performed. As part of a highway widening project, the Federal Highway Administration designed and supervised the construction of a permanent geotextile-reinforced slope 15.3 m high. The reinforced structure is a 1H:1V (45°) slope located in Idaho's Salmon National Forest along Highway 93. Several characteristics were unique to the design: the structure was higher than usual geotextile-reinforced slopes, it involved the use of high strength composite geotextile, and it was constructed with indigenous soils (decomposed granite) as backfill material. Consequently, the reinforced slope was considered experimental, and an extensive program of instrumentation and construction monitoring was implemented to evaluate its performance.

The slope was designed using geotextile reinforcements that were required to have not only adequate tensile strength but were also expected to provide appropriate in-plane drainage capacity to allow dissipation of pore water pressures that could be generated in the fill. The instrumentation program included mechanical extensometers to monitor geotextile strains, inclinometers to monitor horizontal movements within the reinforced zone, piezometers to evaluate possible pore water pressures, and optical survey points to monitor face movements. A considerable amount of data has been gathered both during construction of the slope and during the post-construction period.

Results from the instrumentation program revealed an excellent performance of the slope, that showed small global deflections (on the order of 30 mm) and low geotextile strain levels (on the order of 0.2%). A procedure for representation of extensometer measurements was developed, which assisted in the interpretation of the

geotextile strain distributions. Cross-check of extensometer and inclinometer measurements showed very good agreement, providing confidence on the monitoring results. No time dependent movements were observed during continuous monitoring for eight weeks after completion of construction, and only slight additional movements were observed eight months after the end of construction during the spring thaw. The locus of maximum reinforcement tensions estimated from field instrumentation results is consistent with the location defined using design methods for internal stability analysis of reinforced slopes based on limit equilibrium. Pore water monitoring at the back of the reinforced slope indicates appropriate drainage of the seepage water from the backslope rock mass. Interpretation of the instrumentation data provided both verification of the design assumptions and insight into the mechanisms that dominate the slope behavior.

Although the objectives of each study presented as part of this dissertation was specific in a technical sense, the common purpose was to contribute towards the design of safe, durable, and economical reinforced soil systems built using indigenous backfill soils. Different approaches common to the practice of geotechnical engineering (numerical and physical modeling, field instrumentation) were used in this research to address specific aspects of the performance of geotextile-reinforced soil structures. The strengths and limitations of each approach have been addressed in each corresponding chapter. An immediate continuation of the study would be to gain additional insight into the performance of geotextile-reinforced soil structures by pursuing integration between numerical modeling, physical modeling, and field instrumentation results. Such an

approach would be particularly useful for the developing a rational design methodology for reinforced soil structures with poorly draining or nonconventional fills.

Besides the general direction for future research stated above, there are research needs specific to the technical issues addressed each study presented in this dissertation. Particularly, several research areas in which additional knowledge is required for the design of reinforced soil structures with poorly draining backfills were listed in Chapter 2. Additionally, numerical analyses of well instrumented reinforced soil structures, such as the one presented in Chapter 3, could be pursued since they proved very useful to complement the information provided by field instrumentation records. The displacements of the centrifuge slope models performed in the experimental work presented in Chapter 4 have been monitored, and investigation can be pursued on the deformability of geotextile-reinforced soil structures. Moreover, the long-term performance of the permanent geotextile-reinforced slope described in Chapter 5 is still under evaluation, and the extensive monitoring records already collected can be used for validation of analytic tools. Finally, a common issue relevant to the different studies described in this dissertation is the need for correct evaluation of the mechanical properties of geotextiles under the embedment of soil. To provide actual geotextile strength properties, rather than mere quality control values, additional research should be pursued to develop tensile tests that duplicate field conditions.

Reference

Taylor, D.W. (1948) *Fundamentals of Soil Mechanics*, John Wiley & Sons